

JOURNAL OF THE MYANMAR ACADEMY OF ARTS AND SCIENCE



Chemistry, Industrial Chemistry

Vol. XXII, No.1, May, 2025

Myanmar Academy of Arts and Science

Journal of the Myanmar Academy of Arts and Science

Vol. XXII. No.1

Contents

Section (i) Chemistry

Sr.No	Title	Pages
1	Margaret Hkawn Tawng , *Characteristics of Microplastic From Surface Roadside Soil In Selected Areas of Mon State, Myanmar	1
2	Aung Than Htwe , *Synthesis and Characterization of Chitosan Based Silica Composites Derived Asparagus Stalk End Used for Removal of Chromium (Vi) Ions from Aqueous Solution	11
3	Prema , *Isolation, Identification of Phytoconstituents from the Rhizomes of Globba Sherwoodiana (Padein-Gno) and their Biological Activities	23
4	Sabai Phyu , *Preparation And Utilization Of Biosolid Fertilizer Using Municipal Sewage Sludge	35
5	Aye Aye Lwin , Neem Leaves Based Organic Fertilizer for Cultivation of Peanut Crop in Soil from Yenanchaung Township	43
6	Yin Yin Myint , Three Friedelane Triterpenoids from the Bark of <i>Salix Alba</i> L. (White Willow)	55
7	Aye Aye Thant , Structural Elucidation of an Organic Compound and Estimation of Anti-Inflammatory and Antiarthritic Activities of <i>Bacopa Monnieri</i>	67
8	Thin Wut Soe , Sun Protection Factor Evaluation of Prepared Herbal Sunscreen Creams from <i>Mansonia gagei</i> J.R. Drumm (Kalamet) Stem	79
9	Cho Lwin Lwin Khine , Sun Protection factor Evaluation of Prepared Herbal Sunscreen Gels from <i>Premna Integrifolia</i> L. (Taung-Tan-Gyi) Stem	89
10	Mi Aye Aye Aung , Screening on Cytotoxicity, Anti-Inflammatory, Antiproliferative, and Antiarthritic Activities of the <i>Stephania Venosa</i> (Blume) Spreng. (Taung-Kya) Tuber	99
11	Khin Maw Maw , A Study on the Phytochemicals, Antimicrobial Activity of Crude Extracts, and Identification of Echitamine Alkaloid of <i>Alstonia Scholaris</i> L. (Taung-Ma-Yo) Bark	109
12	Aung Kyaw Min , Isolation of Endophytic Fungi from <i>Oroxylum Indicum</i> (L.) Benth (Kyaung-Sha) Fruits and their Biological Activities	121
13	Kay Khine Win Swe , Investigation of Some Bioactivities and Phytoconstituents from the Peels of <i>Litchi Chinensis</i> Sonn. (Lychee)	131
14	Thwe Thwe Soe , Enhancing Rubber Stopper Performance: A Comprehensive Analysis of Reinforcement With Alkali Treated areca Nut Fiber	141
15	Mya Theingi , Facile Synthesis, Characterization and Optical Property of CuO Nanoparticles	153

Sr.No	Title	Pages
16	Thu Zin Tun , Characteristics of Synthesized Magnesium Oxide Nanoparticles Using Aqueous Leaf Extract of <i>Oroxylum Indicum</i> (L.) and its Bioactivities	163
17	Chit Lay Ko , Enzymic Study on Pectinase Extracted from Red Dragon Fruit Peels	175
18	May Zin Htay , Studies on Enzymatic Properties of Partially Purified Polyphenol Oxidase in Cabbage (<i>Brassica Oleracea</i> L.) and its Antimicrobial Activity	185
19	Moh Moh Htun , Purification, Biological Properties and Partial Structural Determination of Antibacterial Metabolites Produced by <i>Aspergillus Tamaris</i>	197
20	Ko Ko Aung , Treatment of Low Quality Soil with Prepared Biofertilizers and Cultivation of Cucumber, <i>Cucumis Sativus</i> L	211
21	Su Yi Mon , Extraction of Essential oil, Screening of Antimicrobial and Antioxidant Activities of <i>Citrus Medica</i> Var. <i>Acida</i> Brandis (Shauk Thakwa) Leaf	221
22	Hnin Nandar Hlaing , Antimicrobial And Amylase Activities of Isolated Soil Fungi from Taung Thar Township (Mandalay Region)	229
23	Su Swe Su , Investigation of Some Biological Activities from the Leaves of Calotropis Gigantea (L.) W.P. Aiton (Mayo Gyi)	239
24	Win Ko , Copper Extraction and Radon Examination in Selected Mine Samples	245
25	Phyu Phyu Thwin , Enzymic Study on Pectinase Extracted from White Dragon Fruit Peels	255

Section (ii) Industrial Chemistry

Sr.No	Title	Pages
1	Shunn Lei Nandar , *Conversion of Sugarcane Bagasse Into Levulinic acid by Acid-Catalyzed Hydrothermal Method	267
2	Seinn Lei Lei Phyu , Extraction and Utilization of Water-Soluble Dietary Fibre (Sdf) from Banana Peel	281
3	Naw Zar Htwe , Extraction of Ferulic Acid from Defatted Wheat Bran for Improving Antioxidant Activity	293
4	Mon Mon Maung , Physicochemical Properties and Sensory Evaluation of Processed Cognac (Grape Brandy)	303

CHARACTERISTICS OF MICROPLASTIC FROM SURFACE ROADSIDE SOIL IN SELECTED AREAS OF MON STATE, MYANMAR

Margaret Hkawn Tawng¹, Aung Than Htwe², Ye Myint Aung³, Ni Ni Than⁴

Abstract

In many nations, the widespread use of plastics represents an important environmental risk. The pollution caused by microplastics (MP) in soil settings is not well understood, yet. In this work, MP quantity and polymer type in roadside soil from Mawlamyine, Mudon, and Kyaikmaraw in Mon State were characterized. Soil samples were also separated by using density separation and the floating portions were collected. Under a microscope, the extracted microscopic fragments from the soil samples were analyzed, and then they were identified using FT IR. The concentrations of MP in roadside soils collected from Mawlamyine, Mudon, and Kyaikmaraw were 238 pieces/kg (dry weight) ($n = 143$), 147 pieces/kg ($n = 47$), and 150 pieces/kg ($n = 42$), respectively. Significant relationships between the total amount of MP in roadside soils and daily vehicle traffic were found in Mudon and Kyaikmaraw. The higher concentrations of MP in Mawlamyine compared to other collected areas may be due to the city's high population and traffic density. The analysis of soil samples showed that polyethylene and polypropylene were dominant, all of which are commonly used plastics. These findings indicate a relationship between MP profiles in roadside soil and differences in economics and populations.

Keywords: microplastics, microscope, roadside soil, polyethene, polypropylene, density separation

Introduction

There is increasing anxiety about the effects of microplastics (MP; plastics less than 5 mm in size), which have been found in the environment (Cole *et al.*, 2011). They are a widespread environmental contaminant that can be found in soil, water, and the air. Plastics are utilized in a variety of industrial applications, including packaging, construction, vehicles, textiles, electrical materials, agriculture, household goods, and products for health and safety. About 8.3 billion tons of plastic have been produced worldwide in the last 65 years, and 60% of that quantity is considered to have been dumped into the ocean (Geyer *et al.*, 2017). MP come in a variety of sizes and forms, including microbeads, fibres, fragments, film foam pellets, and filaments, to name a few (Wright and Kelley 2017). MPs are separated into primary and secondary MPs depending on where they came from. The characteristics of primary and secondary MP, such as colour, surface morphology, size, crystallinity, and density, alter as a result of continuous degradation. According to Rouillon *et al.* (2016), these changes may have an effect on their chemical and physical processes as well as on their environment and other life forms.

Globally, MP has been discovered in sources of soil, water, and air as well as in salt, beer, marine life, and, most recently, packaged drinking water (Schymanski *et al.*, 2015). According to Wright and Kelley (2017), MP exposure may accumulate and deposit in human tissue and body parts, change the immune system, or result in various clinical issues. Worldwide reports of MP contamination and plastic waste have been reported. Road dust from Asian nations and considerable MP contamination in open dumping site soils have been the subject of recent

* First Prize (2023)

¹ Department of Chemistry, Yangon University of Distance Education, Myanmar

² Department of Chemistry, University of Yangon, Myanmar

³ Department of Chemistry, University of Yangon, Myanmar

⁴ Department of Chemistry, University of Yangon, Myanmar

investigations (Tun *et al.*, 2022; Mon and Nakata, 2020). These findings imply that MPs in roadside soil may represent a significant terrestrial source in different nations. Additionally, Mon and Nakata (2020) reported the presence of microplastics in cosmetics sourced from Myanmar, but little is known about the distribution and dispersion of MPs in environmental matrices, such as road dust. The amount and distribution of MPs in roadside soil samples collected in different parts of Mon State were the focus of this study. Analysis was done on the various kinds of MP polymer and their probable sources in the environment.

Materials and Methods

Study Area

289,388 people live in Mawlamyine's urban area, compared to 197,703 in Mudon and 195,810 in Kyaikmaraw. A high car density is the effect of such a dense population. The entire study region is highly urbanized, has a high level of traffic, and has the largest quantity of land used for paving, building, and road surfaces. The historic center district, which has a lot of urban activity and frequent vehicular traffic, is at the center of the area under study.

Sample Collection

In November 2021, 30 roadside soil samples from Mon State's Mawlamyine ($n = 15$), Mudon ($n = 8$), and Kyaikmaraw ($n = 7$) districts were collected (Figure 1). By population density, Mawlamyine is the fourth-largest city in Myanmar. 30 urban and rural locations were used to collect soil samples from the side of the road. Using a clean brush and dustpan, all roadside soil samples were collected from the edge of a road and stored at $-20\text{ }^{\circ}\text{C}$ until examination.

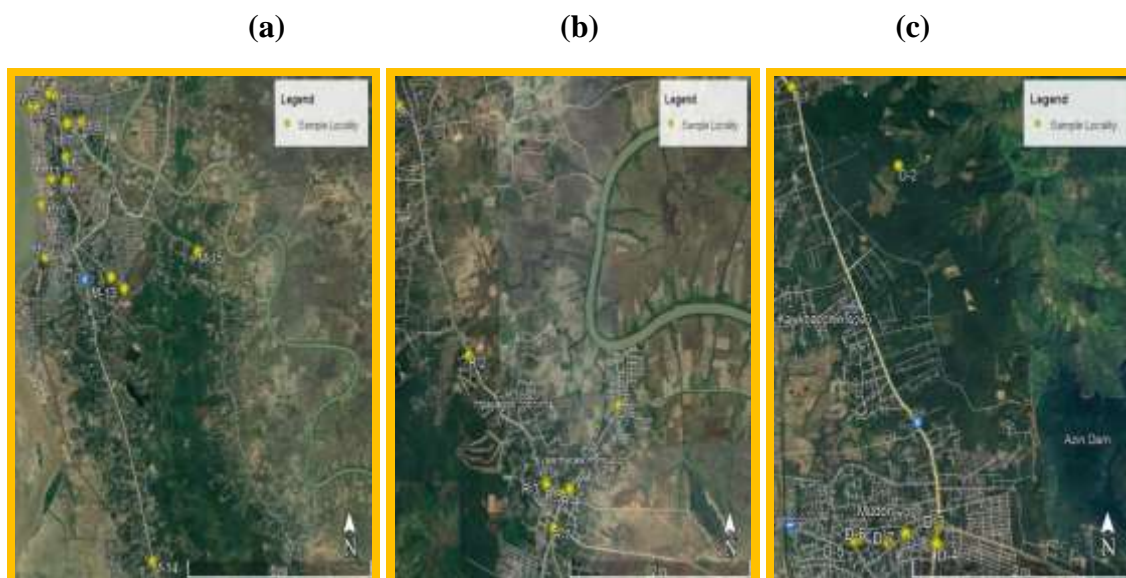


Figure 1. (a) Sampling sites of the Mawlamyine Township (b) Mudon Township (c) Kyaikmaraw Township

Determination of Physicochemical Properties of Roadside Soil

The bulk density and moisture content of the soil samples collected from the side of the road were determined using the AOAC method (AOAC, 2002). The sample's pH was measured using a pH meter according to the conventional method.

Abundance and Polymer Identification

A method developed (Ken and Nakata, 2020) was used to determine MP abundances and polymer types in the roadside soil samples. Roadside soil samples weighing 40g were first strained using stainless steel sieves with a 1 mm screen. The sieved soil samples were exposed to 30 % hydrogen peroxide for three days at room temperature in a glass beaker covered with an aluminium sheet to study the decomposition of organic materials. The recovered soil samples were dried in an oven at 50 °C with a nylon filter with a 100 μ m screen. Gravity separation was used to extract the microplastic from the dried samples. In beakers, the samples were exposed to a three-hour treatment of a 60 % sodium iodide (NaI) solution (1.8 g/cm³). The NaI solution's floating solids were removed and filtered using a nylon filter, and the residues were then dried. For reuse, the NaI solution was filtered. With the use of tweezers, each MP candidate was removed from the filter and placed into a tiny plastic bag for examination under a microscope and with an FT IR spectrometer.

A stereo microscope (S9, LEICA, Germany) was used to obtain photographs of the potential microplastic candidates. The polymer type of each piece was then determined by attenuated total reflectance (ATR) FT IR (IR Affinity 1S, Shimadzu, Japan) analysis. Before sample analysis, background spectra were examined, and isopropyl alcohol (IPA) was used to clean the instrument detector. The types of plastics were identified by comparing sample spectra with those of a reference library database, and the FT IR wavenumber employed ranged from 600 to 4000 cm⁻¹. A 75 % or better match to the reference library was required for microplastic polymer identification to pass quality standards. Due to sample handling constraints, smaller MP fibres (maximum diameter of 100–300 μ m) and rubber microplastics, such as styrene–butadiene rubber (SBR), were not examined in this work.

Results and Discussion

Aspect of Physicochemical Properties of Roadside Soil

The physicochemical characteristics of roadside soil samples from the Mon State region are shown in Table 1. pH, moisture, and bulk density are measurement parameters. In the Mawlamyine region, roadside soil samples collected at different points had a pH value in the range of 6.2-7.8, whereas those collected in the Mudon and Kyaikmaraw regions had a pH value in the range of 7.4-8.5. It could be classified as an alkaline soil type. Mawlamyine Township's roadside soil was determined to have a moisture level of 2-4.5 %. Additionally, it was found that the moisture content in Mudon Township was 2.5-4 % and Kyaikmaraw Township was 2-4 %. All roadside soil samples were found to have a bulk density of between 0.779 and 1.374 g/mL. The highest bulk density was noted in M-1 and D-5, and the highest pH values in D-2, R-5 and R-6. The Ayethayar market (M-8) and the Myineyadana market (M-9) were found to have the highest moisture percentage in soil sample. As a result, all the physical properties of the roadside soil samples exhibited acceptable values.

Table 1. Some Physicochemical Properties of Roadside Soil Samples

Sampling sites	Sample ID	pH	Moisture (%)	Bulk Density (g mL ⁻¹)
Mawlamyine (n=15)				
railway station	M-1	7.8	3.00	1.291
bus station	M-2	7.6	3.50	1.252
downtown 1	M-3	7.7	2.00	1.000
downtown 2	M-4	6.6	4.00	0.779
no.1 market	M-5	6.8	3.50	1.008
Strand road	M-6	6.7	2.00	1.271
downtown 3	M-7	6.7	2.50	0.974
ayethayar market	M-8	6.2	4.50	0.963
myineyadana market	M-9	6.6	4.50	1.013
thanlwin market	M-10	6.3	3.00	0.798
hospital	M-11	6.2	4.00	1.268
university	M-12	7.2	3.50	1.200
air port	M-13	6.5	3.00	1.255
technology university	M-14	6.5	2.00	1.000
highway	M-15	6.8	3.50	1.008
Mudon (n=8)				
highway	D-1	7.8	2.50	1.250
gateway	D-2	8.5	3.50	1.000
downtown	D-3	8.3	4.00	1.271
shwehintar market	D-4	7.5	3.00	1.268
police station	D-5	8.3	4.00	1.374
myoma market	D-6	7.4	3.50	1.317
hospital	D-7	7.8	2.50	1.078
high school	D-8	7.5	2.50	1.035
Kyaikmaraw (n=7)				
police station	R-1	8.1	4.00	1.039
gateway	R-2	7.8	3.50	0.881
hospital	R-3	7.6	2.50	1.278
downtown	R-4	8.2	2.50	0.836
high school	R-5	8.5	3.50	1.268
myoma market	R-6	8.5	2.00	1.031
highway	R-7	8.1	2.50	0.807

Abundance of Microplastics in Surface Roadside Soil

In 30 surface roadside soil samples collected from the selected area of Mon State, microplastics (MP) were found. Microplastics were present in roadside soil samples in Mawlamyine at 238 ± 137 pieces/kg dry wt., Mudon at 147 ± 90 pieces/kg dry wt., and Kyaikmaraw at 150 ± 164 pieces/kg dry wt. (Table 2). The findings on microplastic concentration are in line with data on population, industrial activity, and traffic volume compiled by other researchers (Yukioka *et al.*, 2020). With measured quantities of 150, 200, 250, and 275 pieces/kg dry weight, respectively, in D-3, D-4, D-6, and D-7 in Mudon, the abundance of microplastics was highest there (Table 2). High levels of vehicle traffic were present at these places, and D-3, D-4, and D-6 were close to commercial businesses in Mudon's downtown. The highest concentration of microplastic in roadside soils in Kyaikmaraw was found at R-6 (400 pieces/kg dry weight), followed by R-4 (375 pieces/kg dry weight). These sites are found in Kyaikmaraw's market and downtown areas. More roadside soil microplastics are present in Mawlamyine samples than in Mudon and Kyaikmaraw samples. Mawlamyine is Myanmar's fourth-largest city according to population density. This shows that there is a significant amount of microplastic contamination in the soil along the roads due to increased traffic brought on by Mawlamyine's densely populated area. The roadside soil in front of Thanlwin Market (M-10; 375 pieces/kg dry weight) had the highest concentration of microplastics, followed by No. 1 Market (M-5; 525 pieces/kg dry weight) and Railway Station (M-1; 425 pieces/kg dry weight). More than 200 pieces/kg dry wt. of microplastics were found in most Mawlamyine sample sites. These results show that microplastics are the dominant component in surface roadside soils.

Polymer Composition of Roadside Soil Microplastics

The different kinds of polymers in the microplastics isolated from roadside soils in samples collected in Mudon, Kyaikmaraw, and Mawlamyine were identified. The identification of microplastics in the surface roadside soil was carried out using FTTR. To assess the validity of different detection modes in FTIR, a confirmatory test was conducted using known standard polymers; polyethylene (PE), polypropylene (PP), polyurethane (PU), and polyethylene terephthalate (PET) (Figure 2). Following polypropylene (PP; 32 %), poly (diallyl phthalate) (PDAP; 7 %), and polyvinyl chloride (PVC; 4 %), which made up the bulk of the microplastics in Mudon (55 % of the total; $n = 47$), the subsequent order was polyethene (PE), which made up the majority of them (Figure 3). PE and PP were abundant in D-1, D-3, D-6 and D-7 (Table 2). PE was found in 7 of the 8 sampling areas, with the largest amounts occurring at sites with significant activity in the market area, D-4, D-5, and D-6 (Table 1). Additionally, PVC and PET were found in samples from Mudon's D-2 and D-3 (Table 2), this might have been caused by the damaged wire insulating layer of electrical equipment (Chai *et al.*, 2020).

Similar profile was also found in roadside soil sample from Kyaikmaraw, where PE (56%), PP (10%), PDAP (29%) and PVC (5%) (Figure 3). Every sampling site in Kyaikmaraw revealed PE, with site R-6 having the highest concentration (Table 2). PP was found in the roadside soil sample from site R-5 and R-6. Along with PDAP found at R-2, R-4, and R-5 (Table 3), they could be caused by the breakdown of urban building materials, their fragmentation, and their subsequent integration into roadside soil (Tun *et al.*, 2023).

Table 2. Summary of Abundance and Polymer Types of MPs in Roadside Soils Collected from Mon State

Sample	Sample weight analyzed (g dry)	Abundance of MPs (pieces/ g dry wt.)	Abundance of MPs (pieces/kg dry wt.)	Number of Polymer types (pieces/g)						
				PE	PP	PS	PET	PVC	PDAP	PU
Mawlamyine (n=15)										
M-1	40	17	425	13	3				1	
M-2	40	14	350	10	4					
M-3	40	6	150						1	5
M-4	40	6	150	3						3
M-5	40	21	525	13	5	1	1		1	
M-6	40	12	300	4	8					
M-7	40	6	150	4	2					
M-8	40	8	200	2	4			1	1	
M-9	40	14	350	10	4					
M-10	40	15	375	6	8		1			
M-11	40	4	100		3		1			
M-12	40	5	125	2					3	
M-13	40	6	150	6						
M-14	40	3	75		3					
M-15	40	6	150	2	3				1	
			238							
Mudon (n=8)										
D-1	40	4	100	2	2					
D-2	40	2	50				1	1		
D-3	40	6	150	2	3			1		
D-4	40	8	200	6					2	
D-5	40	5	125	5						
D-6	40	10	250	6	3				1	
D-7	40	11	275	4	7					
D-8	40	1	25	1						
			147							
Kyaitmaraw (n=7)										
R-1	40	1	25	1						
R-2	40	2	50	1					1	
R-3	40	2	50	2						
R-4	40	15	375	3				2	10	
R-5	40	4	100	1	2				1	
R-6	40	16	400	14	2					
R-7	40	2	50	2						
			150							

PE: polyethene, PP: polypropylene, PS: polystyrene, PET: polyethene terephthalates; PVC: polyvinyl chloride; PDAP: poly-diallyl phthalate; PU: polyurethane

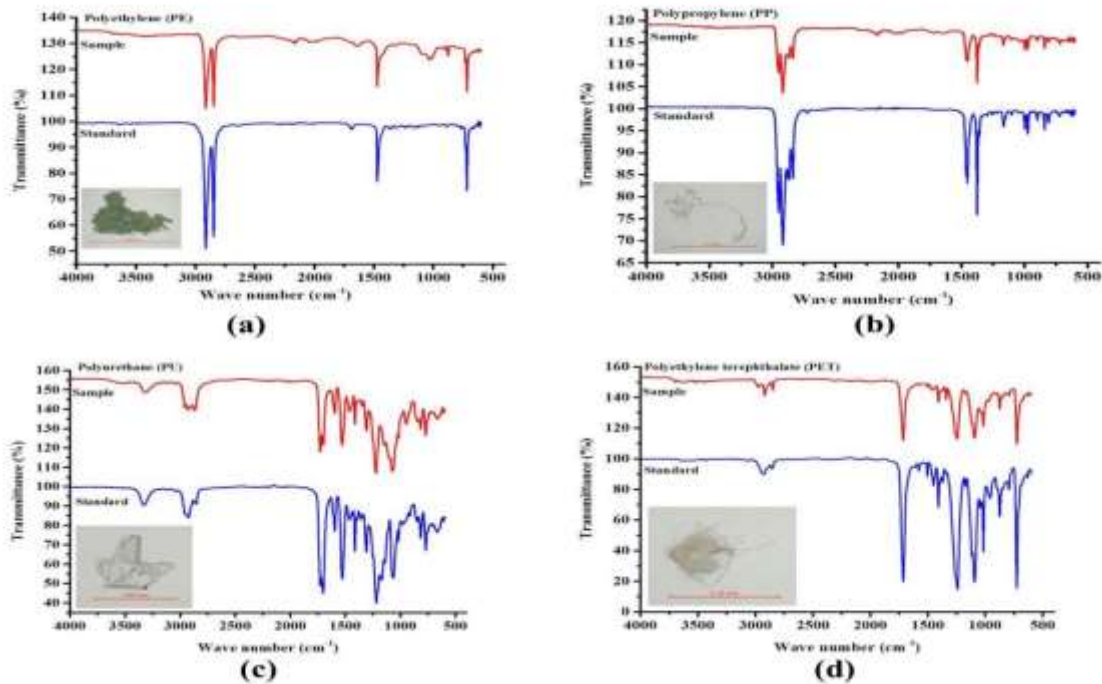


Figure 2. FT IR spectra of extracted microplastics from collected roadside soils in Mon State with reference library (a) polyethylene (PE) (b) polypropylene (PP) (c) polyurethane (PU) and (d) polyethylene terephthalate (PET)

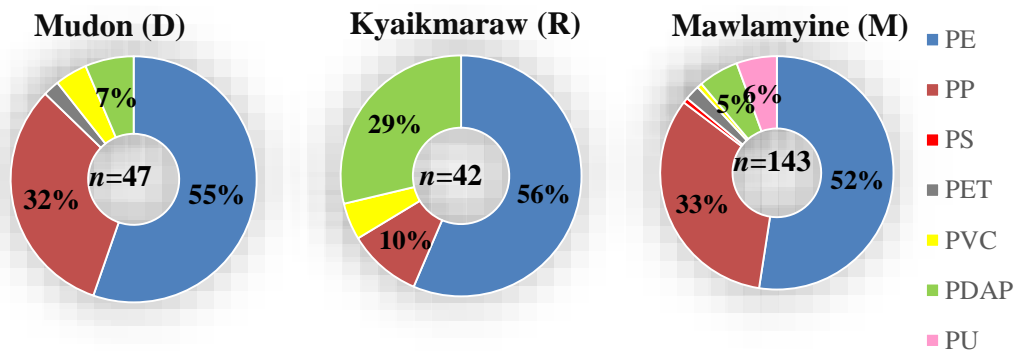


Figure 3. Pie chart diagrams of polymer compositions of microplastic in roadside soil samples from Mawlamyine, Mudon and Kyaikmaraw Townships

PE ($n = 143$) formed the majority of the MPs in Mawlamyine, accounting up 52 % of the total, followed by PP (33 %), polyurethane (PU; 6 %), and poly (diallyl phthalate; PDAP, 5 %). The M-5 sample, which was collected from an area close to a market, included large amounts of PE and PP, whereas PE and PP, which are typically found in home goods, were the main polymers found in Mawlamyine, Mudon, and Kyaikmaraw. According to Mon *et al.* (2022), PE and PP made up the majority of the MPs found in road dust collected from Myanmar, which may indicate that containers and packaging are probable sources of MPs.

Polymer Colour, Shape, and Size of Roadside Soil Microplastics

In Mawlamyine, an examination of the colour of the MP revealed that white or transparent was predominant (45 % of all the MP; $n = 143$), followed by red (26 %), green (16 %), and blue (10 %), in that order (Figure 4). The majority of MPs (30 %; $n = 47$) in Mudon were red, whereas the majority (55 %; $n = 42$) in Kyaikmaraw were blue. In Mawlamyine, Mudon, and Kyaikmaraw, the percentages of white or translucent MP were 45 %, 21 %, and 10 %, respectively (Figure 4).

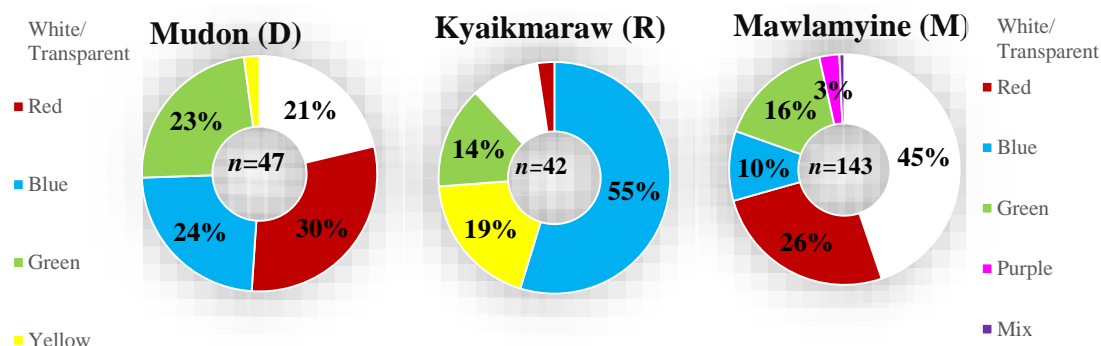


Figure 4. Pie chart diagrams of the colour of microplastic in roadside soil samples from Mawlamyine, Mudon and Kyaikmaraw Townships

Three types of MP shapes were identified: pieces, films or sheets, and lines or threads. In Mawlamyine (67 % of the total MP; $n = 143$), Mudon (91 %; $n = 47$), and Kyaikmaraw (90 %; $n = 42$), the majority of MP pieces were fragments (Figure 5).

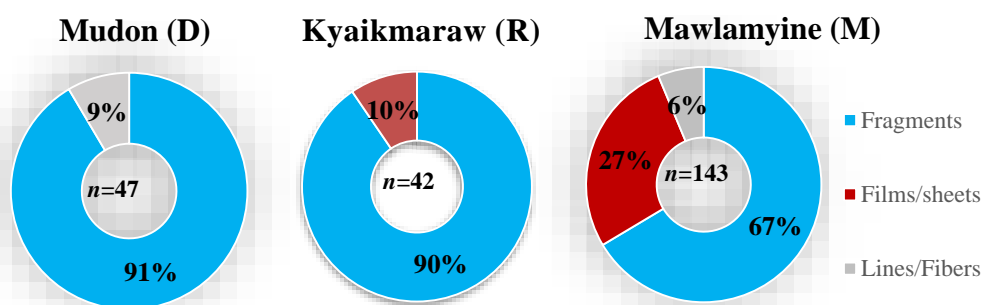


Figure 5. Pie chart diagrams of the shape of microplastic in roadside soil samples from Mawlamyine, Mudon and Kyaikmaraw Townships

Seven categories were used to categorize the size distribution of MP: 500, 500-1,000, 1,000-1,500, 1,500-2,000, 2,000-2,500, 2,500-3,000, and > 3,000 μm. For all MP in Mudon and 1000-1500 μm (33 %) in Kyaikmaraw, the most prominent distribution was 1000-1500 μm (26 %) (Figure 6). In Mawlamyine, the predominant distribution was >3,000 μm (38 %; n=143).

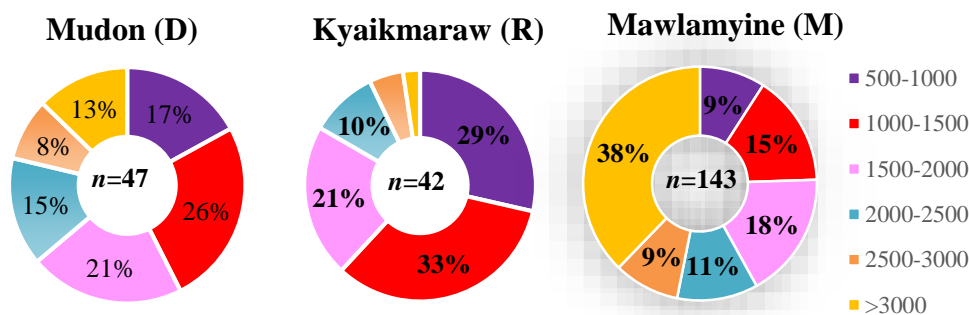


Figure 6. Pie chart diagrams of the size of microplastic in roadside soil samples from Mawlamyine, Mudon and Kyaikmaraw Townships

Conclusion

In this research, surface roadside soil samples were collected from thirty sites in Mon State, and microplastics were frequently detected. When the findings of this investigation and the literature are compared, significant levels of microplastic contamination are revealed. The highest MP abundances were detected in Mawlamyine (525 pieces/kg), Mudon (275 pieces/kg), and Kyaikmaraw (400 pieces/kg) in Mon State. Microplastic pollution of roadside soil was greater in Mawlamyine, which has the largest population and highest traffic density of all areas sampled in this study. PE and PP were the two main plastic polymers in the MPs found in the soils along the sides of the roadways, suggesting that consumer goods and road paints may be possible sources of MPs in the road dust. MPs concentrations in roadside soil were slightly correlated with population size, suggesting that human activities are a major source of MPs in roadside soils. This study showed that polyethylene plastics are the dominant component of microplastics in roadside soils. Because of this, research on microplastic contamination should be accelerated, and public awareness of the problem should be raised daily, leading to a greener environment.

Acknowledgements

The authors gently acknowledge the Myanmar Academy of Arts and Science (MAAS), Ministry of Education, Yangon, Myanmar. Dr. Tin Maung Tun, rector of the University of Yangon, as well as Drs. Khin Chit Chit, Cho Cho, and Thidar Aye, pro-rectors, deserve our sincere gratitude.

References

- Abbasi, S., B. Keshavarzi, F. Moore, A. Tumer, F. Kelly, A. Dominguez, and N. Jaafarzadeh. (2019). "Distribution and Potential Health Impacts of MPs and Microrubers in Air and Street Dusts from Asaluyeh County, Iran". *Environmental Pollution*. vol. 244, pp. 153-164
- AOAC (2002). "Official Methods of Analysis", Washington, DC:14th Ed., Association of Official Analytical Chemists, pp. 472-474

- Chai, B., Q. Wei, Y. She, G. Lu, Z. Dang, and H. Yin. (2020). "Soil Microplastic Pollution in an E-waste Dismantling Zone of China". *Waste Management*, vol. 118, pp. 291-301
- Cole, M., P. Lindeque, C. Halsband, and T. Galloway. (2011). "Microplastics as Contaminants in the Marine Environment: A Review". *Marine Pollution Bulletin*. vol. 62 (12), pp. 2588-2597
- Geyer, R., J. R. Jambeck, and K. L. Law. (2017). "Production, Use, and Fate of all Plastics Ever Made". *Science Advances*, vol. 3 (7), pp. 1-8
- Ken, K., and H. Nakata. (2020). "Plastic Additive as Tracers of Microplastic Sources in Japanese Road Dusts", *Science of The Total Environment*, vol. 736, pp. 1-8
- Mon, E. E. and H. Nakata. (2020). "Occurrence of Microplastic in Cosmetic Products Collected from Myanmar". *Earth and Environmental Science*, vol. 496, pp. 1-8
- Mon E. E., T. Z. Tun, T. Agusa, H. M. Yen, C. H. Huang, and H. Nakata. (2022). "Monitoring of Microplastics in Road Dust Samples from Myanmar and Taiwan". *Environmental Monitoring and Contaminants Research*, vol. 2, pp. 112-119
- Rouillon, C., P. O. Bussiere, E. Desnoux, S. Collin, C. Vial, S. Therias, and J. L. Gardette. (2016). "Is Carbonyl Index a Quantitative Probe to Monitor Polypropylene Photodegradation?" *Polymer Degradation and Stability*, vol. 120, pp. 200-208
- Schymanski, D., C. Goldbeck, H. U. Humpf, and P. Furst. (2018). "Analysis of Microplastics in Water by Micro-Raman Spectroscopy: Release of Plastic Particles from Different Packaging into Mineral Water". *Water Research*, vol. 129, pp. 154-162
- Tun, T. Z., T. Kunisue, S. Tanabe, M. Prudent, A. Subramanian, A. Sudaryanto, P. H. Viet, and H. Nakata. (2022). "Microplastics in Dumping Site Soils from Six Asian Countries as a Source of Plastic Additives". *Science of The Total Environment*, vol. 806, pp. 1-9
- Tun, T. Z., A. T. Htwe, N. N. Than, M. M. Khine, S. Chavanich, V. Viyakarn, A. Isobe, and H. Nakata. (2023). "Polymer Types and Additive Concentration in Single-use Plastic Products Collected from Indonesia, Japan, Myanmar, and Thailand". *Science of the Total Environment*, vol. 889, pp. 1-8
- Wright, L. and F. J. Kelly. (2017). "Plastic and Human Health: A Micro Issue?" *Environmental Science and Technology*, vol. 51, pp. 6634-6647
- Yukioka, S., S. Tanaka, Y. Mabetani, Y. Suzuki, T. Ushijima, S. Fujii, H. Takada, and S. Singh. (2020). "Occurrence and Characteristics of Microplastics in Surface Road Dust in Kusatsu (Japan), Da Nang (Vietnam), and Kathmandu (Nepal)". *Environmental Pollution*, vol. 256, pp. 1-31

SYNTHESIS AND CHARACTERIZATION OF CHITOSAN BASED SILICA COMPOSITES DERIVED ASPARAGUS STALK END USED FOR REMOVAL OF CHROMIUM (VI) IONS FROM AQUEOUS SOLUTION*

Aung Than Htwe¹, May Thazin Kyaw², Win Pa Pa Phy², Moh Moh Zaw³,
Cho Mar Kyi³, Theint Yee Mon³

Abstract

The aim of the study was to prepare and characterize a chitosan based silica composite for the removal of Cr (VI) metal ions from aqueous solutions. In the current study, chitosan and silica were combined to prepare a chitosan-based silica composite with different mass ratios. Silica (SiO₂) was obtained from the agricultural waste material of asparagus stalk ends. The prepared CS-SiO₂ composites were characterized by modern techniques like XRD, FT IR, SEM, UV-visible, and TG DTA analyses. The FT IR spectra showed the presence of new adsorption peaks (Si-O-Si bond), contributed by silica interaction with the hydroxyl group of chitosan. The study of morphology of the composite suggests that the SiO₂ particles were within the range of 2–7 nm in diameter and were uniformly dispersed in the polymer matrix. The thermal properties of these composite materials, indicated that the thermal stability of the chitosan was enhanced. Under the experimental conditions, which include pH of the solution, adsorbent dose, initial concentration, contact time the sorption properties of the CS-SiO₂ composite was observed for efficient removal of Cr (VI) ions from the aqueous solution. The adsorbent CS-SiO₂ composite showed a maximum removal percent of Cr (VI) ions of 94.65%. These findings suggested that silica obtained from asparagus stalk ends could be utilized to enhance chitosan characteristics, decrease agricultural waste dumping, and decrease Cr (VI) metal ions polluting water.

Keywords: chitosan, silica, CS-SiO₂ composite, Cr (VI) ions

Introduction

Heavy metal pollution in wastewater is becoming severe with the rapid development of industry and has become a widespread concern worldwide (Liu *et al.*, 2022). Heavy metals such as mercury, cadmium, lead, chromium, and metal-like arsenic are of major environmental concern because they are non-biodegradable and cannot be decomposed or metabolized. Several metals cause serious health and environmental problems, and chromium (Cr) compounds are one of the most toxic contaminants in wastewater due to their high solubility, and toxicity, and free transferability (Du *et al.*, 2020).

Chromium contamination is a growing issue that frequently arises in industrial effluent from processes including metalworking, tanning leather, electroplating, and pigment production. Hexavalent chromium, Cr (VI) and trivalent chromium, Cr (III) are the two primary oxidation forms of chromium found in wastewater, and Cr (VI) is more hazardous to human health due to its greater carcinogenicity, teratogenicity, and mutagenicity.

Wastewater contains a variety of Cr (VI) species, including CrO₄²⁻, Cr₂O₇²⁻, HCrO₄⁻, and H₂CrO₄. According to the World Health Organization (WHO), the maximum amount of

* Second Prize (2023)

¹ Department of Chemistry, University of Yangon, Myanmar

² Department of Chemistry, University of Yangon, Myanmar

³ Department of Chemistry, Mohnyin University, Myanmar

chromium that should be present in drinking water, is 0.05 mg/L. Therefore, it is necessary to develop effective methods to remove Cr (VI) from wastewater (Azizkhani *et al.*, 2020).

Adsorption processes can be performed through interactions between molecules of contaminants and adsorbents and mainly include hydrogen bonding, electrostatic bonding interactions, and π - π interactions (Moradi *et al.*, 2021). Chitosan (CS) is a biopolymer derivative of chitin, a polysaccharide found abundantly in nature in crustacean exoskeletons of crab, shrimp, and lobster, as well as in the cuttlebone of cuttlefish. Chitosan has a lone pair of electrons on the amino and hydroxyl functional groups, which act as active sites for the removal of heavy metal ions from aqueous solutions (Mahatmanti *et al.* 2014).

SiO₂ particles are spherical in shapes and are of special importance due to their unique properties such as high active surface area, high mechanical and thermal resistance, non-toxicity, high porosity, dispersibility in different solvents, and environmental compatibility (Moradi *et al.*, 2021). Silica contains various silanol groups (Si-OH) on its outer shell, which act as suitable nucleation and anchor points for the natural functionalization of silica (Grace *et al.*, 2022). Thus, the silicon precursor shows quick in situ development of the silica network in the presence of ethanol and water via the sol-gel route, forming glassy, homogeneous, and transparent films compatible over a wide composition range (Sagheer and Muslim, 2009).

This research work focuses on the following key contributions: synthesis of chitosan-SiO₂ composites; characterization of chitosan-SiO₂ composites using SEM, FT IR, XRD, TG-DTA, and UV-visible analyses; and investigation of the adsorption capacity of Cr (VI) ions on CS-SiO₂ composites.

Materials and Methods

Silica particles were prepared from asparagus stalk end and used after calcination at 500 °C for 4 hours. Chitosan was purchased from the British Drug House (BDH) Chemical England. All other chemicals used were of analytical reagent grade. In all investigations, the recommended standard methods and techniques involving both conventional and modern methods were provided.

Preparation of Silica (SiO₂) Derived Asparagus Stalk End Powder

Asparagus stalk end was collected, cleaned, dried and treated by thermal combustion under the controlled conditions at 500 °C for 4 h. The asparagus stalk end ash is treated with alkali extraction followed by acid treatment. The precipitate was washed several times with boiled distilled water to remove sulphate impurities and dried in a hot air oven. The powdered silica was refluxed with 1 M HCl at 80 °C for 2 h using the sand bath. Then it was dissolved in 1 M NaOH by continuous stirring for 2 h on a magnetic stirrer, and concentrated H₂SO₄ was added drop by drop to adjust the pH in about 8. The precipitated silica was washed with warm water and after the washing process silica was dried at 60 °C for 6 h in the oven.

Synthesis of Chitosan Based Silica Composite

Silica (0.1 to 0.5 g) was dissolved in each mixture of 30 mL of 1:2 (v/v) ethanol-water and 1 mL of 1M HCl solution and kept under constant stirring at 250 rpm for 30 min to obtain silica suspension. The suspended silica solution was added drop by drop into 100 mL of 1 % (w/v) chitosan solution (1g of chitosan in 100 mL of 1 % (v/v) acetic acid solution) and then was heated 60 °C at 100 rpm for 2 h. Then, 0.1 M NaOH was added dropwise to obtain gel and kept for 24 h. The precipitated CS-SiO₂ gel was centrifuged at 3000 rpm for 10 min and washed with distilled water to neutralize at pH 7. After that, the sample was dried in oven at 60 °C for 2 h and labeled as CS-SiO₂ (0.1g) (CSS 1), CS-SiO₂ (0.2 g) (CSS 2), CS-SiO₂ (0.3 g) (CSS 3), CS-SiO₂ (0.4 g) (CSS 4), and CS-SiO₂ (0.5 g) (CSS 5).

Characterization of Chitosan Based Silica Composite

The prepared SiO₂ and CS-SiO₂ composites were analysed by FT IR spectrometer in a wide range of wavelengths between 400 cm⁻¹ and 4000 cm⁻¹ with a resolution of 1 cm⁻¹ and 3 scans/sample. The surface morphology of the prepared blend films were tested by JSM-5610 LV. Scanning Electron Microscope, JEOL at 20 kV. X-ray diffraction (XRD) analyses of prepared SiO₂ and CS-SiO₂ composites were carried out with Ni filtered Cu K α X-ray radiation. UV-visible spectra of the samples were collected from 185 to 600 nm using a UV-2550 spectrophotometer (Shimadzu) at room temperature. Thermogravimetric analysis was carried out in a nitrogen atmosphere at a heating rate of 15 °C/min up to a temperature of 1400 °C on the DTG-60H thermal analyzer.

Batch adsorption experiments

The stock solution of Cr (VI) was prepared by dissolving acidified K₂Cr₂O₇ in deionized water. The solution concentrations required for the adsorption study were prepared by diluting this stock solution of Cr (VI). The pH of the prepared solutions was adjusted by using 0.1 M NaOH and 0.1 M HCl solutions. The effect of pH on the adsorption of Cr (VI) from aqueous solution on the adsorbents was investigated in different solution with a pH ranging from 3 to 7. The prepared CS, SiO₂, CS-SiO₂ composites were added to Cr (VI) solution (50 ppm, 25 mL of Cr (VI), pH 5). The adsorbent doses from 0.1 to 0.5 g were investigated. After that, the impact of contact time in optimum conditions was studied by varying the contact time from 60 to 180 min. Adsorbent-adsorbate interaction was performed with a mechanic stirrer at 200 rpm for 1 h. After adsorption process, the amount of Cr (VI) remaining in the solution was determined with UV-visible spectrophotometer (Shimadzu UV2550) at 540 nm (Altun, 2020).

Results and Discussion

Preparation and Characterization of CS-SiO₂ Composites

Formation of silica on chitosan can occur through hydrogen bonds or van der Waals. Chitosan has many hydroxyl groups which can form hydrogen bonds with silanol groups as a result of hydrolysis. Another bonding mechanism between silica and chitosan by electrostatic attraction of chitosan undergoes protonation in an amino group and a hydroxyl group dissociating of silica in solution (Figure 1).

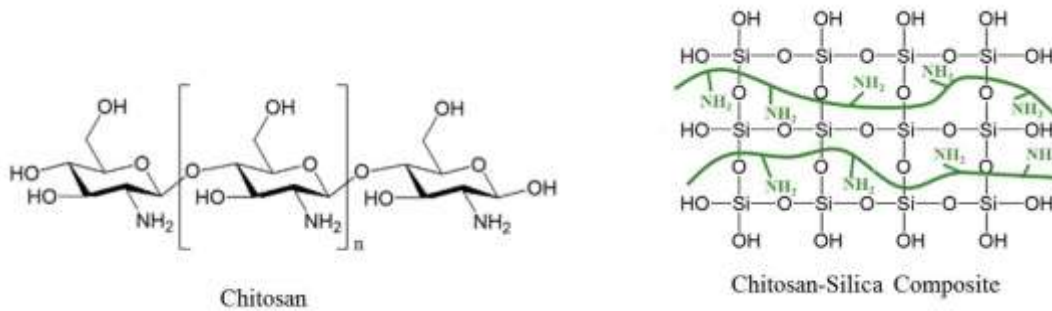


Figure 1. Chitosan and Chitosan-Silica Composite

FT IR spectra analysis

FT IR analysis was carried out in the wavenumber range $400\text{-}4000\text{ cm}^{-1}$. FT IR spectra of SiO_2 , CS, and CSS composite are displayed in Figure 2. Chitosan has a wide peak at 3294 cm^{-1} (overlap between O-H and N-H groups). The peak at 2880 cm^{-1} is C-H stretch, and amide groups can be observed at wavenumbers 1656 , 1583 and 1376 cm^{-1} . C-O stretch is also detected at 1079 cm^{-1} . The characteristics SiO_2 peak are the hydroxyl O-H of the silanol group and water that appears at wavenumbers 3386 and 1638 cm^{-1} , Si-O groups at 1095 , 970 , 802 and 466 cm^{-1} which show Si-O stretching, Si-OH stretching, Si-O stretching and Si-O-Si bending. The wavenumbers at 1413 and 1423 cm^{-1} show the presence of C-H groups (asymmetric) on chitosan- SiO_2 composite and chitosan which are not present in SiO_2 .

Figure 2 shows the FT IR spectra of the silica and silica-chitosan composite with SiO_2 amount variations. A large vibration area peak at 3424 cm^{-1} corresponds to O-H and N-H stretching. A small peak at 1638 cm^{-1} relates to the possible interaction between the hydroxyl group of silica and the amine group of chitosan. Sharp peaks at 1092 cm^{-1} and 789 cm^{-1} are attributed to asymmetric and symmetric stretching vibration Si-O-Si. The peak at 941 cm^{-1} indicates a functional group of Si-OH stretching vibration, and the peak at 457 cm^{-1} indicates the existence of O-Si-O symmetric deformation vibration (Budnyak *et al.*, 2015).

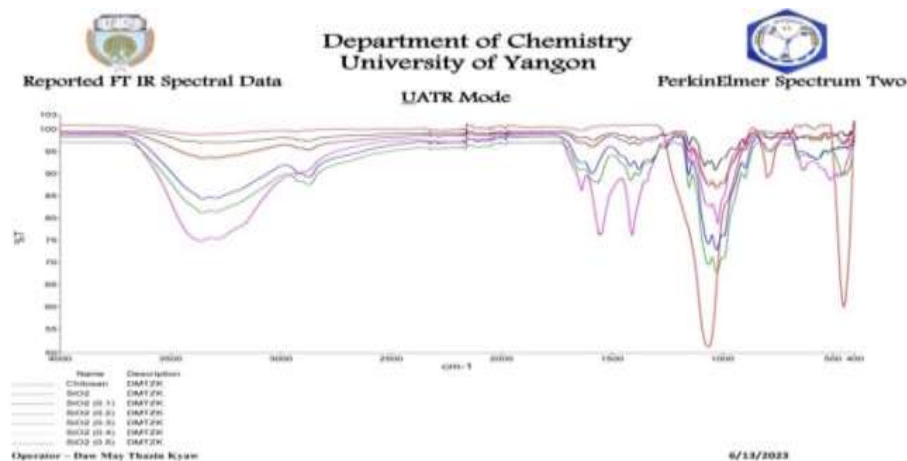


Figure 2. FT IR spectra of CS, SiO_2 and CSS composites

X-ray diffraction analysis

The XRD spectra of chitosan, SiO₂, and chitosan-SiO₂ composites are shown in Figure 3. The diffraction peaks of CS exhibit two diffraction peaks at $2\theta = 10^\circ$ and 19.65° which are the typical finger prints for chitosan powder. These two phases correspond to the hydrated crystallization and anhydrous crystallization of chitosan, respectively. The development of crystallinity in chitosan was due to the formation of hydrogen bonds between chains, and the crystalline form of chitosan changes with the conformation of chitosan (Siriprom *et al.*, 2018). The diffraction pattern of SiO₂ shows no polycrystalline peak except of the broad one centered at $2\theta = 26.24^\circ$, indicating that the SiO₂ has an amorphous-crystalline structure.

In the XRD patterns of CSS 1, CSS 2, CSS 3, CSS 4 and CSS 5, with the increase of silica content, the diffraction peak at $2\theta = 10^\circ$ disappears, the intensity of the diffraction peak at $2\theta = 20^\circ$ weakens and gradually shifts to $2\theta = 23^\circ$. The addition of silica will partially destroy the hydrogen bond between chitosan molecules and thus affect the crystal structure of chitosan. In addition, due to the presence of free amino groups and the spontaneous hydrophobic action of acids, chitosan is in an unstable state of loose double helices composed of polysaccharides asymmetric units, providing a large number of growth sites for amorphous silica formation (Zhong *et al.*, 2023).

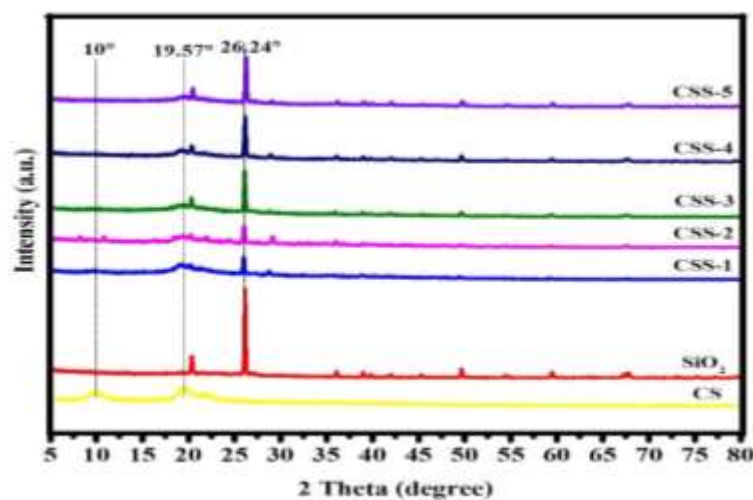


Figure 3. XRD patterns of CS, SiO₂ and CSS composites

SEM Analysis

The morphology of CS, SiO₂, CSS 1, CSS 2, CSS 3, CSS 4 and CSS 5 were observed with SEM images as shown in Figure 4. As can be seen from Figure 4(a), the surface fold of chitosan show a tight shape of polymeric fiber and accompanied by a few holes. SEM image of silica particles (Figure 4b) was distributed uniformly and tendency to arrange inhomogeneously. Silica nanoparticles are spherical in shape it is due to the even distribution during the process of composite preparation. From the SEM (Figures 4 c, d), CSS 1 and CSS 2 found many irregular spheres with obvious particles and holes. From the SEM (Figures 4 E, F) images of CSS 3 and CSS 4, it can be clearly seen porous coral-like micro/nano structure, and the pore size is in the nanometer range.

The SEM image of CSS 5 composite (Figure 4g) shows that SiO₂ is deposited tightly on the surface of chitosan, forming a uniform silica nanoparticle layer locally. In the precursor

solution, the alcohol hydroxyl group in chitosan can hydrogen-bond with SiO_2 . However, with the increase of SiO_2 content, excessive SiO_2 will continue to hydrolyze and polycondense after encountering the residual strong acid on the surface of crystal nucleus, resulting in secondary growth of primary crystal nucleus and agglomeration of nanoparticles (Zhong *et al.*, 2023).

It can be concluded that the SEM image of all CSS composites showed that the composite was uniformly distributed and interaction between the silica and chitosan (Grace *et al.*, 2022).

To reveal the particle size distribution of the chitosan, silica and CS- SiO_2 , the particle images in Figures 4(a to g) were analyzed using Image J software. Figure 4(h) shows the particle size distribution of the CS, SiO_2 , and all CSS composites. It can be seen that the silica and CS- SiO_2 tends to have a narrow particle size distribution than CS. It is also clearly noticed that the average diameter size distribution of silica is larger than that of CSS except CSS 5.

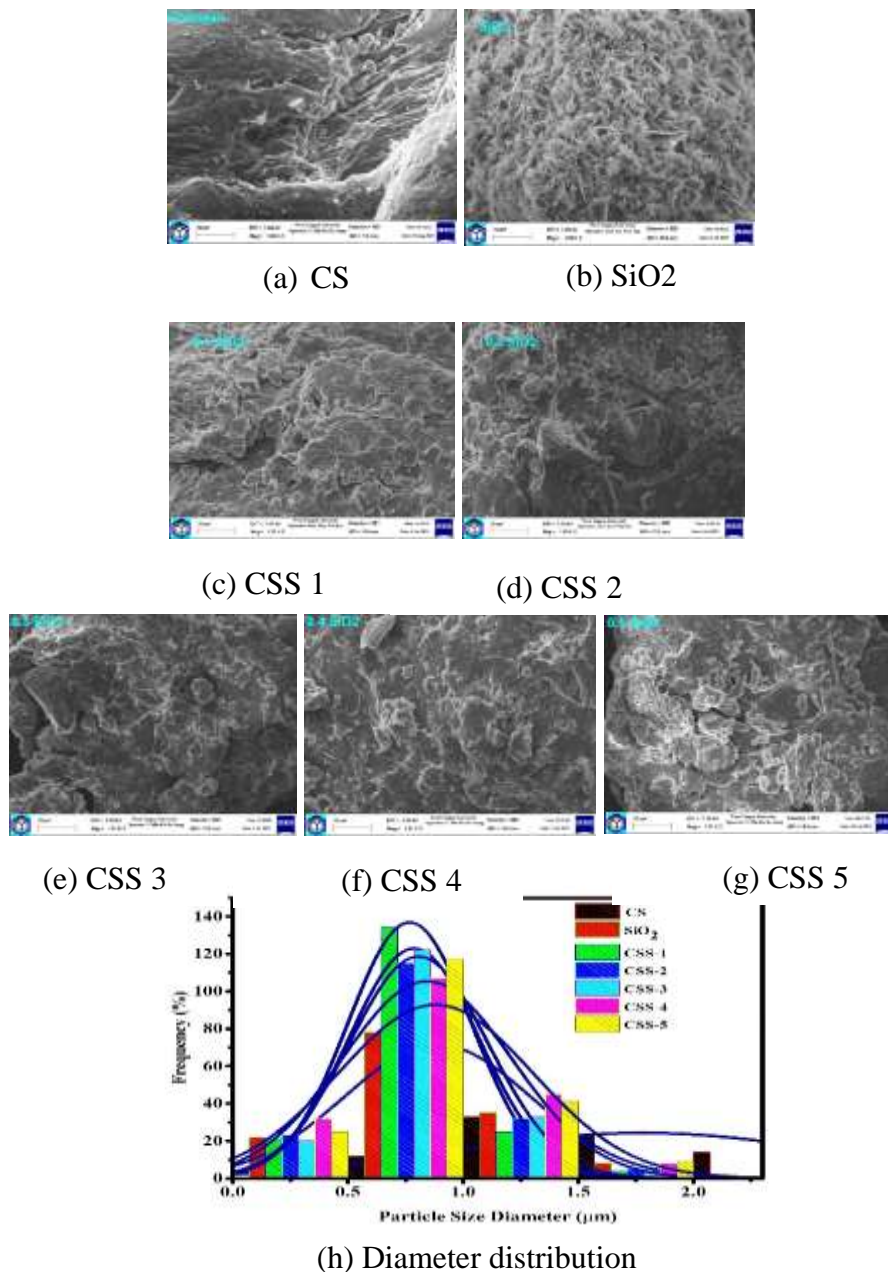


Figure 4. SEM images of (a) CS, (b) SiO_2 , (c) to (g) CSS composites and (h) particle diameter size distribution

Thermogravimetric analysis

Thermogravimetric analysis was performed to evaluate the thermal stability of materials as well as to confirm the amount of CS, SiO₂ and all prepared CS-SiO₂ composites. Thermograms of composites are shown in Figure 5(a) and DTA curves in Figure 5 (b). According to the TG thermogram profiles, CS showed three decomposition stages. The first stage has a temperature range of 38.86 °C to 252.52 °C and a weight loss of 14.70%. There is moisture evaporation upon heating. The second stage is the loss in weight 32.28 % was decomposed within the temperature range of 252.52 °C to 324.38 °C. This can be attributed to the weight loss peak of C-C single bond, C-O single bond and C-N single bond decomposition in chitosan. The third stage has a temperature range of 324.38 °C to 600 °C and a weight loss of 51.90 % with reference to the depolymerization and elimination of glycosidic units of CS, the decomposition at 100 °C is clearly observed. Thermal elimination of CS takes place above 200 °C after the residual water gets eliminated initially around 100 °C (Htwe *et al*, 2021). For SiO₂, there is no obvious weight loss between 200 °C and 600 °C, the mass loss is only about 2.45 %, which can be attributed to the weight loss of Si-O-Si bond on the silica molecule.

The thermogram of all CSS shown in Figure 5(a), having a weight loss in three stage. The first weight loss (about 15 %) appeared at around 100 °C. There is caused by the evaporation of the trace amount of free and bound water contained in the sample due to physical absorption. In the second stage, a rapid weight loss (about 36 %) from the temperature range between 236 °C to 400 °C was observed. This can be attributed to the weight loss peak of C-C single bond, C-O single bond, C-N single bond decomposition in chitosan. When the dispersible SiO₂ nanoparticles form a composite material with chitosan, the intermolecular hydrogen bonding force in the chitosan chain is weakened, and the thermal decomposition temperature of chitosan chain degradation in the composite material is reduced (Zhong *et al.*, 2023). In third stage, a slow degradation from 400 °C to 600 °C representative of thermal degradation of deposited chitosan on the surface of the SiO₂ were observed with the weight loss of about 35 %. The significant increase in the weight residues at 600 °C illustrates successful incorporation of higher amounts of silica into the chitosan-SiO₂ and ultimately increases in thermal stability.

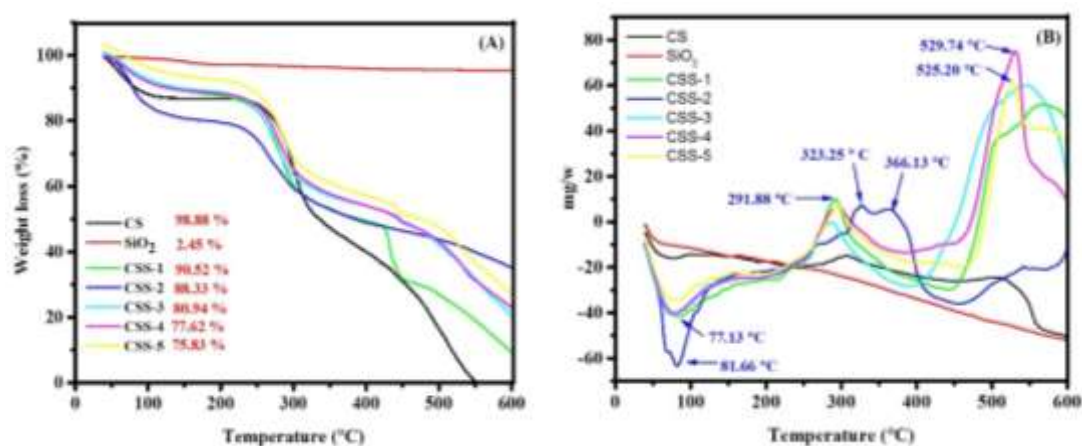


Figure 5. (a) TG curves and (b) DTA curves for CS, SiO₂ and CSS composites

UV-visible absorption spectra

The UV-visible spectrum of chitosan, silica and chitosan silica composite are show in Figure 6 showed a single peak at around 200 nm. This single peak is characteristic of silica absorption spectrum and its intensity decreases with the decrease in the concentration of silica. The CS peaks shows at 239 nm and 289 nm. The CSS composite shows 289 nm, and 295 nm. It was found that the intensity of CSS composite is lower than that of CS and SiO₂. Figure 6 shows the UV-visible absorption spectra of the suspension of naked and chitosan-coated SiO₂. According to Figure 6(C to G), chitosan coating SiO₂ change in the UV-Vis spectra, and this confirms the binding of chitosan on SiO₂ nanoparticle.

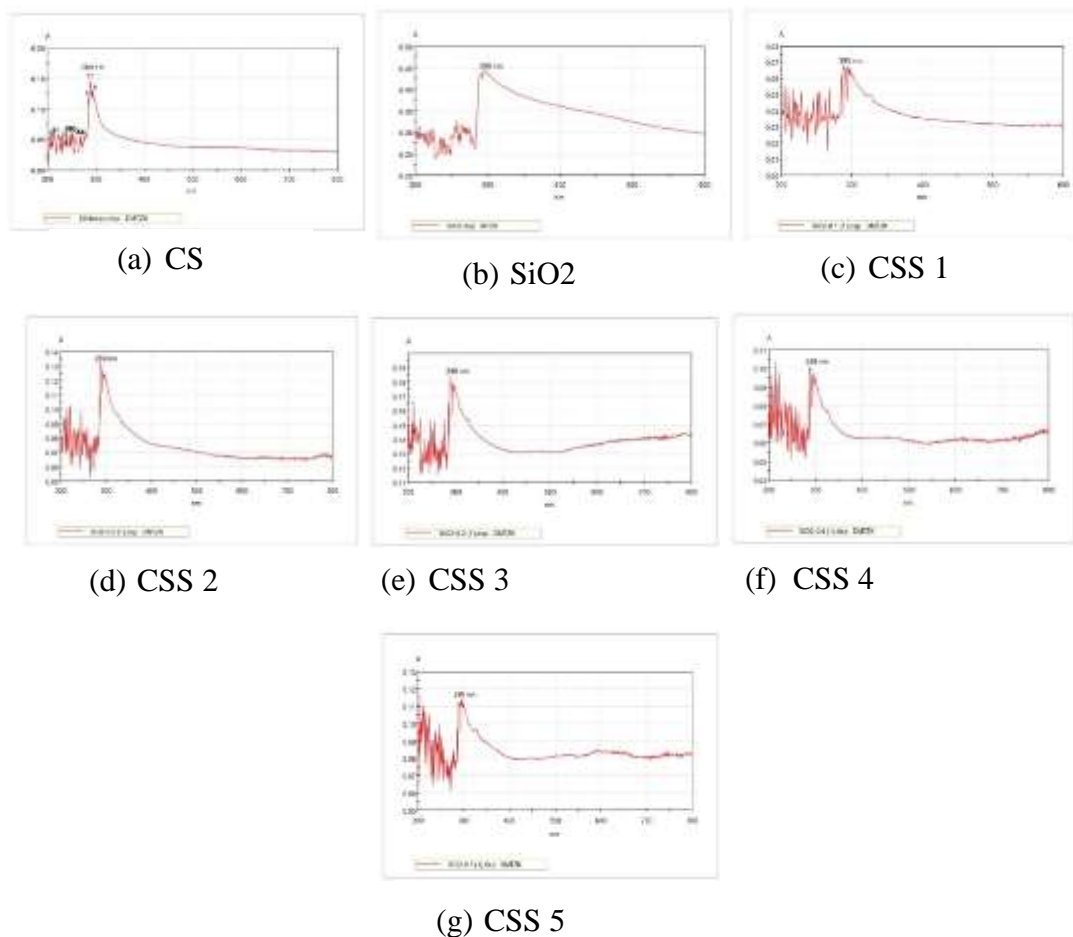


Figure 6. UV-Visible spectra of (a) CS, (b) SiO₂ and (c to g) CSS composites

Adsorption performances of Cr (VI) ion with CS, SiO₂, and CSS Composites

Effect of pH

pH is one of the important parameters in the adsorption because it affects the surface mechanism of the adsorbent, in other words, to the binding points of pollutant and the adsorbent. The influence of initial pH on adsorption was studied in the range of 3-7 for initial metals ion concentration of 50 ppm by UV-visible spectrophotometer at 540 nm. As it can be seen in Figure 7, at pH 5, while 50 ppm Cr (VI) ion was removed with 79.18 % for SiO₂, 82.98 % for CS, 87.39 % for CSS 1 and 90.89 % for CSS 5, this rate decreased to 28 % at pH 6. This situation can be attributed to the cationic structure of the adsorbent and to the presence of excess OH⁻ ions in the solution. The maximum uptake of Cr (VI) ions took place at pH 4-5,

which may be attributable to the changes in the surface charge of the adsorbent. With an increase of the pH at above pH 5, the uptake of Cr (VI) ions decreased. The optimum pH of the Cr (VI) adsorption with the all composite adsorbent was found to be approximately 5. The species of Cr (VI) in aqueous solution were in the form of the bichromate (HCrO_4^-), chromate (CrO_4^{2-}) and dichromate ($\text{Cr}_2\text{O}_7^{2-}$) ions. By increasing pH, decrease in adsorption percentage was observed. This might be due to the weakening of electrostatic force of attraction between the oppositely charged adsorbate and adsorbent that ultimately led to the reduction in sorption capacity (Baral *et al.*, 2006).

This may be attributed to the presence of free lone pair of electrons on nitrogen atoms of chitosan suitable for coordination with the metal ion to give the corresponding chitosan–metal complex (Donia *et al.*, 2008).

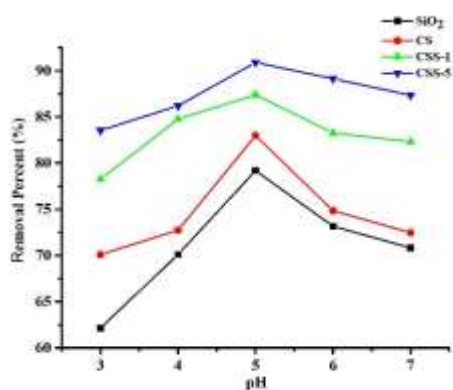


Figure 7. Effect of pH on adsorption of Cr (VI) ions onto CS, SiO₂ and CS-SiO₂ composites (condition: 0.4 g dosage /25 mL, 50 ppm of initial concentration, contact time - 120 min, 25 °C)

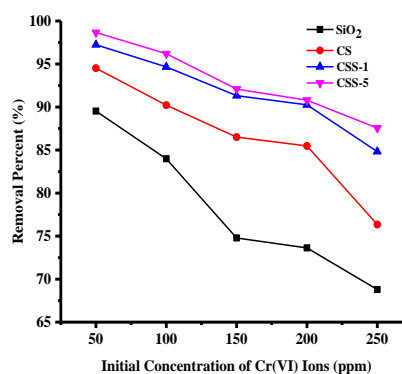


Figure 8. Effect of initial concentration of Cr (VI) ions onto CS, SiO₂ and CS-SiO₂ composites (condition: pH 5, 0.4 g dosage/ 25 mL, contact time - 120 min, 25 °C)

Effect of initial metal ions concentration

The effect of initial concentration of Cr (VI) (50-250 ppm initial concentration range) on adsorption (initial solution pH 5, and adsorbent amount of 0.4 g/25 mL for SiO₂, CS, CSS 1, and CSS 5 at 25°C) is shown in Figure 8. The results showed that the adsorption capacity decreased with the increase of initial Cr (VI) concentrations and therefore, decreased the removal percentage of Cr (VI) ions from 50 to 250 mg/L. It can be assumed that increasing initial metal concentration increases the number of collisions between Cr (VI) ions and adsorbents thus decreasing adsorption (Rahbar *et al.*, 2014). It can be concluded that the maximum removal of Cr (VI) ions (97 % by CSS 5) would occur for an initial concentration of 50 ppm.

Effect of adsorbent dose

In terms of both the efficiency and cost of the process, it is of great importance to determine the appropriate adsorbent dosage in the adsorption processes. In this study, a series of experiments were performed with 50 ppm Cr (VI) solution in varying adsorbent dosages (0.1-0.5 g) and as a result, the effect of adsorbent amount on Cr (VI) adsorption was investigated. As seen

in Figure 9, it was observed that as the adsorbent dosage increased, the metal removal percent also increased. While Cr (VI) removal was 73.54 % for SiO₂, 78.92 % for CS, 81.47 % for CSS 1 and 83.43 % for CSS 5 with 0.1 g adsorbent, it increased to 83.86 % for SiO₂, 85.14 % for CS, 93.46 % for CSS 1 and 94.63 % for CSS 5 as the adsorbent dosage was increased to 0.4 g. Therefore, 0.4 g of adsorbent was regarded as the optimum dosage for the removal of Cr (VI) in this study. A higher dose provides a larger number of binding sites, which eventually causes the enhanced removal of Cr (VI). Increasing in adsorbent dose leads to increase in active sites of metal binding which means more metal ions are adsorbed. Hence, the adsorptivity increases till saturation. Any further addition of the adsorbent beyond 0.4 g did not cause any apparent change in the adsorptivity. The decrease in adsorption capacity can be attributed to the fact that some of the adsorption sites remain unsaturated during the adsorption process (Bandaru *et al.*, 2013).

Effect of contact time

Contact time is one of the effective factors in the adsorption process. In this study, metal removal percentages were calculated in terms of contact time while all other parameters were kept constant. 0.4 g of adsorbent was mixed with 50 ppm Cr (VI) solution at pH 5 at varying time intervals and sorption percentage was drawn against contact time (Figure 10). From this investigation, adsorbed metal amount rapidly increased within a contact time of 30- 180 min, however, a significant difference was not observed for the measurements after 120 min. The effect of contact time on the adsorption of Cr (VI) were studied to determine the time taken by SiO₂, CS, CSS 1, and CSS 5 composites to remove 50 ppm Cr (VI) solution at 25 °C. Figure 10 shows the adsorption capacity of SiO₂, CS, CSS 1, and CSS 5 composites for Cr (VI) increased sharply within the first 90 min, which may be attributable to the availability of the sites on the surface of the adsorbent. It is suggested that a concentration gradient is present in both the adsorbent and adsorbate in the solution (Wu *et al.*, 2013). Then, it reached adsorption equilibrium at 120 min, and afterwards, there was no appreciable increase. Hence, the optimum contact time was taken to be 72 h for further studies. Hence, the optimal removal efficiency reached 97 % within about 120 min.

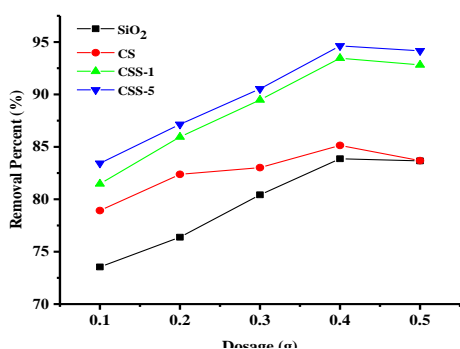


Figure 9. Effect of dosage of CS, SiO₂ and CSS composites on adsorption of Cr (VI) ions (condition: pH 5, 50 ppm of initial concentration, volume of 25 mL, contact time-120 min, 25 °C)

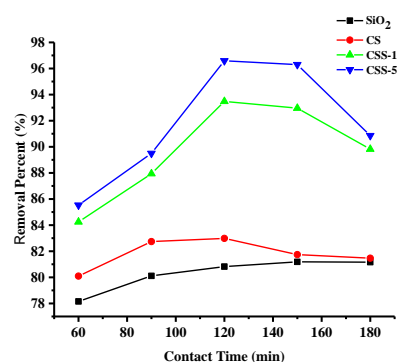


Figure 10. Effect of contact time on adsorption of Cr (VI) ions onto CS, SiO₂ and CSS composites (condition: pH 5, 50 ppm of initial concentration, 0.4 g dosage /25 mL, 25 °C)

In this study, the adsorption of heavy metal ion on chitosan based silica composite used as an adsorbent, which were derived from agricultural by-products, asparagus stalk end (silica). The CS-SiO₂ composite were prepared and characterized by FT IR, XRD, SEM, UV-visible and TG-DTA analyses. The results show that the morphology and properties of composites change with the introduction of silica. The CS-SiO₂ composite had a coral-like three-dimensional microporous, amorphous structure, and good thermal stability. The prepared CS-SiO₂ composites were used for the removal of Cr (VI) ions from an aqueous solution. The effect of several operating parameters, such as solution pH, initial Cr (VI) concentration, the dosage of adsorbents, and contact time, on the adsorption performance was examined by a batch system. When the dosage is 0.4 g/25 mL, the initial concentration of Cr (VI) ions solution is 50 mg/L, the pH of solution is 5, and the adsorption time is 120 min, the removal of Cr (VI) ions by CS-SiO₂ was observed 94.65 %.

The main contribution of the present work producing synthesis of chitosan based silica composite could promote to a certain extent of sustainable development goals and foster innovation engaging more on rural development toward and may be used for wastewater treatment.

Acknowledgements

The author feel indebted to Professor and Head Dr Nyein Nyein Htwe, Department of Chemistry, Mohnyin University, Kachin State, Myanmar, for her stimulating suggestions.

References

- Altun, T. (2020). "Preparation and Application of Glutaraldehyde Cross-Linked Chitosan Coated Bentonite Clay Capsules: Chromium(VI) Removal from Aqueous Solution". *J. Chil. Chem. Soc.*, vol. 65(2), pp. 4790-4797.
- Azizkhani, S., E. Mahmoudi, N. Abdullah, M.H.S. Ismail, A.W. Mohammad and S.A. Hussain. (2020). "Synthesis and Characterisation of Graphene Oxide-Silica-Chitosan for Eliminating the Pb(II) from Aqueous Solution". *Polymers*, vol. 12(1922), pp. 1-18.
- Bandaru, N.M., N. Reta, H. Dalal, A.V. Ellis, J. Shapter and N.H. Voelcker. (2013). "Enhanced Adsorption of Mercury Ions on Thiol Derivatized Single Wall Carbon Nanotubes". *Journal of Hazardous Materials*, vol. 261, pp. 534-541.
- Baral, S.S., S.N. Dasa and P. Rath. (2006). "Hexavalent Chromium Removal from Aqueous Solution by Adsorption on Treated Sawdust". *Biochem. Eng. J.*, vol. 31(3), pp. 216-222.
- Budnyak, T.M., I.V. Pylypchuk, V.A. Tertykh, E.S. Yanovska and D. Kolodynska. (2015). "Synthesis and Adsorption Properties of Chitosan-Silica Nanocomposite Prepared by Sol-Gel Method". *Nanoscale Research Letters*, vol. 10(87), pp. 1-10.
- Donia, A.M., A.A. Atia and K.Z. Elwakeel. (2008). "Selective Separation of Mercury(II) Using Magnetic Chitosan Resin Modified with Schiff's Base Derived from Thiourea and Glutaraldehyde". *J. Hazard. Mater.*, vol. 151, pp. 372-379.
- Du, X., C. Kishima, H. Zhang, N. Miyamoto and N. Kano. (2020). "Removal of Chromium(VI) by Chitosan Beads Modified with Sodium Dodecyl Sulfate (SDS)". *Appl. Sci.*, vol. 10(4745), pp. 1-23.
- Grace, A.S. and G.S.P.L. Malar. (2022). "Synthesis and Characterisation of Chitosan/Nanosilica Composite and Their Applications of Heavy Metal Ions Cu(II), Cr(II) and Pb(II) Removal from Aqueous Solution". *Tierärztliche Praxis*, vol. 42(3), pp. 95-107.

- Htwe, A.T., N.M. Tun, M.M. Soe, M. Gohdo, Y. Yoshida and N.N. Than. (2021). "Synthesis and Characterization of Chitosan Based Graphene Oxide Bionanocomposite". *J. Myanmar Acad. Arts Sci.*, vol. XIX(1B), pp. 213-226.
- Liu, Y., H. Shan, C. Zeng, H. Zhan and Y. Pang. (2022). "Removal of Cr(VI) from Wastewater Using Graphene Oxide-Chitosan Microspheres Modified with α -FeO(OH)". *Materials*, vol. 15(4909), pp. 1-20.
- Mahatmanti, F.W., N. Nuryono and N. Narsito. (2014). "Physical Characteristics of Chitosan Based Film Modified with Silica and Polyethylene Glycol". *Indonesian Journal of Chemistry*, vol. 14(2), pp. 131-137.
- Moradi, O., S. Mhdavi, and S. Sedaghat. (2021). "Synthesis and Characterisation of Chitosan/Agar/SiO₂ Nano Hydrogels for Removal of Amoxicillin and of Naproxen from Pharmaceutical Contaminants". *Research Square*, pp. 1-23.
- Rahbar, N., A. Jahangiri, S. Boumi and M.J. Khodayar. (2014). "Mercury Removal from Aqueous Solutions with Chitosan-Coated Magnetite Nanoparticles Optimized Using the Box-Behnken Design". *Jundishapur J. Nat. Pharm. Prod.*, vol. 9(2), pp. 1-7.
- Sagheer, F.Al. and S. Muslim. (2010). "Thermal and Mechanical Properties of Chitosan/SiO₂ Hybrid Composites". *Journal of Nanomaterials*, vol. 2010, pp. 1-7
- Siriprom, W., K. Chantarasunthon and K. Teanchai. (2018). "Physical and Thermal Properties of Chitosan". In *Advanced Materials Research*, pp. 315-318
- Wu, Y., H.J. Wang, H. Wang, C. Zhang, J. Zhang and Z.L. Zhang. (2013). "Adsorption of Hexavalent Chromium from Aqueous Solutions by Graphene Modified with Cetyltrimethylammonium Bromide". *J. Colloid Interface Sci.*, vol. 394, pp. 183-191
- Zhong, T., M. Xia, Z. Yao and C. Han. (2023). "Chitosan/Silica Nanocomposite Preparation from Shrimp Shell and Its Adsorption Performance for Methylene Blue". *Sustainability*, vol. 15(47), pp. 1-19

ISOLATION, IDENTIFICATION OF PHYTOCONSTITUENTS FROM THE RHIZOMES OF *GLOBBA SHERWOODIANA* (PADEIN-GNO) AND THEIR BIOLOGICAL ACTIVITIES*

Prema¹, Thet Thet Zaw², Hla Ngwe³, Hiroyuki Morita⁴

Abstract

The aim of the present study was to isolate and to identify the phytoconstituents from the rhizomes of *Globba sherwoodiana* (Padein-gno) and to screen their biological activities. The active CHCl_3 extract of Padein-gno was separated by silica gel column chromatography which afforded four compounds namely campest-4-en-3-one (**A**, 4 mg, colourless needle crystal), stigmasta-4,22-dien-3-one (**B**, 15 mg, colourless needle crystal), stigmast-4-en-3-one (**C**, 8 mg, colourless needle crystal), and docosyl ferulate (**D**, 1.0 g, white amorphous powder). All of the isolated compounds, **A–D** were identified by modern spectroscopic techniques including FT IR, ^1H NMR, ^{13}C NMR, and HR ESI MS as well as by comparing with the reported data. The antiproliferative activity of the crude extracts of Padein-gno rhizomes and its constituents were screened against four human cancer cell lines [human cervical cancer cell line (HeLa), human lung cancer cell line (A549), human breast cancer cell line (MCF-7), and human gastric cancer cell line (GSU)] and normal human fibroblast cells (WI) by 3-(4,5-dimethylthiazol-2-yl)-2,5-dimethyltetrazolium bromide (MTT) assay. The screening results revealed that the CHCl_3 extract showed a higher than the MeOH extract against all the tested cancer cell lines. In addition, the isolated compounds **A** to **D** also showed the potent activity with IC_{50} values ranging from 13.9 to 98.3 $\mu\text{g/mL}$. In the antibacterial activity, both of the crude extracts exhibited a moderate activity against Gram-positive bacteria *B. subtilis* and *S. aureus* with MIC values ranging from 25.0 to 100 $\mu\text{g/mL}$. The isolated compounds, **A–C** were found to show significant antibacterial activity against *B. subtilis* and *S. aureus* with MIC values ranging from 3.1 to 25.0 $\mu\text{g/mL}$, respectively.

Keywords: *Globba sherwoodiana*, antiproliferative activity, antibacterial activity, isolated compounds

Introduction

Cancer has become the second leading cause of death worldwide. For many years, chemotherapeutic agents have been developed and used to treat cancer. However, there is no drug that shows good selectivity for cancer cells. To date, about 70% of anti-cancer drugs were developed from natural resources, and world populations still rely mainly on anti-cancer drugs derived from medicinal plants. Medicinal plants are known to produce certain bioactive molecules which react with other organisms in the environment, inhibiting bacterial and fungal growth (Chopra *et al.*, 1992). Bacteria and fungi are various types of organisms. They can also cause tissue damage and hamper our body functions to the point of causing disease (Vogt and Dippold, 2005). Medicinal plants include a various types of plants used in herbalism and some of these plants have medicinal activities. These medicinal plants consider as a rich resources of ingredients which can be used in the development and synthesis of drugs. Beside that these plants play a critical role in the development of human cultures around the whole world (Hassan, 2012). Plants, especially used in Ayurveda can provide biologically active molecules and lead structures for the development of modified derivatives with enhanced activity and reduce toxicity.

* Third Prize (2023)

¹ Department of Chemistry, University of Yangon

² Department of Chemistry, University of Myitkyina

³ Department of Chemistry, University of Yangon

Globba sherwoodiana (Zingiberaceae) is a small perennial herb from 38 to 45 cm in height with rhizomes and compact and tall leafy shoots. It was identified as a new species in 2012, based on its obvious morphology. In Myanmar, it is cultivated and locally known as 'Padein-gno'. It is also cultivated in Thailand and India. The flowers of the Padein-gno are sold in markets and used for Buddhist offerings in Myanmar and Thailand. The previous phytochemical studies revealed that the genus *Globba* contains labdane diterpenoids, sesquiterpenoids, steroids, lipids, and phenolic compounds. Labdane diterpenoids were reported to possess antibacterial and antifungal activities. To the best of our knowledge, no phytochemical and biological studies have been reported from any part of *G. sherwoodiana*. Therefore, in this paper the isolation and identification of four compounds from the rhizomes of Padein-gno and the screening of their biological activities were firstly reported.

Materials and Methods

The experimental works were conducted at the Division of Natural Products Chemistry, University of Toyama, Japan. The fresh Padein-gno rhizomes (10.0 kg) were collected from Pyin Oo Lwin Township, Mandalay Region, Myanmar, in October 2018. The plant was identified as *Globba sherwoodiana* by authorized botanist at the Botany Department, University of Yangon. The rhizomes were cleaned by washed with water and air-dried at room temperature. The dried rhizomes were ground into powder and stored in air-tight container. The following instruments were used for structure elucidation of isolated compounds: Nuclear magnetic resonance (NMR) spectra were measured at 500 MHz (^1H NMR) and 125 MHz (^{13}C NMR) on a JEOL ECA500II spectrometer (Wako Pure Chemical Industries, Ltd., Osaka, Japan) in CDCl_3 . High-resolution mass spectrometry (HRESIMS) data were taken on a SHIMADZU LCMS-IT-TOF (Shimadzu, Kyoto, Japan) instrument. Normal phase silica gel (silica gel 60 N, spherical, neutral, 40–50 μm ; Kanto Chemical, Tokyo, Japan) and reversed phase silica gel (Cosmosil 75C₁₈-OPN; Nacalai Tesque, Kyoto, Japan) were used for open column chromatography (C.C.). Thin layer chromatography (TLC) was performed using silica gel GF₂₅₄ precoated (Merck) plates. The fractions were detected by visualization using a UV lamp at 254 and 365 nm, followed by spraying with 1% Ce (SO₄)₂–10% aqueous H₂SO₄, *p*-anisaldehyde stain solution and heating to 150 °C for 5–10 min in a drying cabinet. Normal-phase HPLC column chromatography with COSMOSIL 5SL-II (10 × 250 mm) columns together with an Agilent Technologies 1260 quat pump with a JEOL detector, was used for separation of the compounds. The biological assay was measured at 570 nm using a SH-1200 Microplate Reader (Corona, Hitachinaka, Japan).

Extraction and Isolation of the rhizomes of *G. sherwoodiana*

The dried rhizome powder of *G. sherwoodiana* (3.2 kg) was sonicated in chloroform (7.0 L, 90 min, × 5) at room temperature and the extract was concentrated under reduced pressure to give a residue (80.4 g). The chloroform extract (80.0 g) was subjected to silica gel C.C. eluted with *n*-hexane: EtOAc (from 9.5:0.5 to only EtOAc) and EtOAc: MeOH (9:1 and 7:3) to give 28 fractions of 500 mL each, and these fractions were combined into ten main fractions (F1-F10) after TLC profiling. Fraction F8 (7.4 g) was subjected to Cosmosil 75C₁₈ C.C., eluted with MeOH: H₂O (3:1 to 7:1) to yield three subfractions (Fr. 8-1–8-3). Subfraction 8–3 was purified by normal-phase HPLC, eluted with a linear gradient solvent system (*n*-hexane–EtOAc, 3:7 to

1:4), and monitored at the wavelength of 254 nm, to afford compound **A** (2.0 mL/min, t_R = 50.65 min, 4.0 mg), compound **B** (2.0 mL/min, t_R = 51.23 min, 15.0 mg), and compound **C** (2.0 mL/min, t_R = 57.23 min, 8.0 mg). Fraction F9 (6.9 g) was chromatographed on Cosmosil 75C₁₈ C.C. eluted with MeOH:H₂O (3:1 to 7:1) to give five main subfractions (Fr. 9-1–9-5). The subfraction 9–2 (2.5 g) was rechromatographed on silica gel C.C., using the *n*-hexane:CH₂Cl₂:EtOAc (20:20:1) isocratic solvent system to obtain compound **D** (1.0 g). All of **A–D** were isolated in this investigation for the first time from this plant species.

Structural Elucidation

The structures of isolated compounds **A**, **B**, **C**, and **D** were elucidated by modern spectroscopic techniques, namely FT IR, ¹H NMR, ¹³C NMR and HRESIMS.

Investigation of some Biological Activities of the Crude extracts of Padein-gno Rhizomes and Its Isolated Compounds

Antiproliferative activity by MTT assay

The crude extracts and isolated compounds **A** to **D** were evaluated their antiproliferative activity using the 3-(4,5-dimethyl-thiazol-2-yl)-2,5 diphenyltetrazolium bromide (MTT, Nacalai Tesque, Japan) assay, according to the published procedure. α -Minimum essential medium with l-glutamine and phenol red (α -MEM; Wako, Japan) were used to culture the HeLa, A549, MCF-7, and GSU cancer cell lines, and WI human fibroblast cell. All media were supplemented with 10% fetal bovine serum (FBS; Sigma, USA) and 1% antibiotic antimycotic solution (Sigma, USA). For the MCF-7 cells, the growth medium was supplemented with 1% 0.1 mM non-essential amino acids (NEAA; Gibco, USA) and 1% 1 mM sodium pyruvate (Gibco, USA). Each cancer cell line was seeded in 96-well plates (2×10^3 cells per well) and incubated in the respective medium at 37 °C, under 5% CO₂ and 95% air atmosphere, for 24 h. After the cells were washed with phosphate-buffered saline (PBS), different concentrations of the tested samples (1, 10, and 100 μ g/mL) were added. After 72 h incubation, the cells were washed with PBS and 100 μ L of medium containing 10 μ L of MTT solution (5 mg/mL) was added to each well and incubated for 3 h. Subsequently, the absorbance of each well was measured at a 570 nm wavelength. 5-Fluorouracil (Wako, Japan) was used as a positive control. Cell viability was calculated from the mean values of data from three wells by using the following equation, and cytotoxicity was expressed as the IC₅₀ (50% inhibitory concentration) value.

$$(\%) \text{ Cell viability} = 100 \times \left[\frac{\text{Abs (test samples)} - \text{Abs (blank)}}{\text{Abs (control)} - \text{Abs (blank)}} \right]$$

Antibacterial activity by MTT assay

Antibacterial assay was performed using the standard microdilution-MTT assay according to the published procedure with slight modifications. *B. subtilis* NBRC 13719, *S. aureus* NBRC 100910, *E. coli* NBRC 102203, and *K. pneumoniae* NBRC 14940 were utilized for this assay. The bacterial strains were inoculated on YP agar plates [1% polypeptone (Nihon Pharmaceutical Co., Ltd., Tokyo, Japan), 0.2% yeast extract (BD Difco™, USA), 0.1% MgSO₄·7H₂O, and 2% agar (Nacalai Tesque Inc., Kyoto, Japan)] and incubated at 37°C for 12 h.

A stock sample solution (crude extracts and pure compounds) were prepared in DMSO with concentration of 10 mg/mL each and further diluted to varying concentrations in 96-well plates that contained microbial strains incubated in YP medium for the bacterial strains. The plate was incubated at 37°C overnight. Ampicillin and kanamycin (Nacalai Tesque) were used as positive controls for Gram-positive and Gram-negative bacterial strains. The MIC values were visually observed by addition of 10 μ L of 3-(4,5-dimethylthiazol-2-yl)-2,5-diphenyl-tetrazolium bromide (MTT, Sigma-Aldrich, USA) solution (prepared 5 mg/mL in isopropanol-HCl) into each well, followed by 1 h incubation.

Results and Discussion

Compound **A** (4 mg, 0.0001% yield) was obtained as colourless needles. Its HRESIMS showed a quasi-molecular ion peak at m/z 421.3428 $[M+Na]^+$ compatible with the molecular formula of $C_{28}H_{46}O$ in conjunction with NMR data. The FT IR spectrum showed the absorption bands at 3100 and 1624 cm^{-1} due to the presence of alkene groups. The strong band appeared at 1742 cm^{-1} suggesting the presence of carbonyl groups. The 1H NMR spectrum of compound **A** in $CDCl_3$ (Figure 1) showed the presence of ten methylene groups, seven methine protons, one olefinic proton at δ_H 5.71 (brs, H-4), and six methyl groups at δ_H 0.69 (s, H₃-18), 0.75 (dd, $J = 1.7, 6.9$ Hz, H₃-28), 0.79 (d, $J = 6.9$ Hz, H₃-27), 0.84 (dd, $J = 1.7, 6.9$ Hz, H₃-26), 0.90 (dd, $J = 4.0, 6.9$ Hz, H₃-21), and 1.18 (s, H₃-19). The ^{13}C NMR (Figure 2) spectroscopic data revealed 28 carbon resonances, including ten methylene carbons at δ_C 35.7 (C-1), 39.7 (C-2), 32.5 (C-6), 32.1 (C-7), 38.7 (C-11), 21.1 (C-12), 20.3 (C-15), 24.0 (C-16), 33.7 (C-22), and 30.3 (C-23), six methyl carbons at δ_C 12.0 (C-18), 15.4 (C-27), 15.5 (C-28), 17.5 (C-19), 18.3 (C-26), and 18.7 (C-21), one carbonyl carbon at δ_C 199.9 (C-3), two olefinic carbons at δ_C 123.8 (C-4) and 172.0 (C-5), two quaternary carbons at δ_C 38.7 (C-10) and 42.5 (C-13), seven methine carbons at δ_C 28.2 (C-25), 33.0 (C-24), 34.0 (C-20), 35.9 (C-8), 53.9 (C-9), 55.9 (C-14), and 56.1 (C-17). The 1H and ^{13}C NMR spectroscopic data (Table 1) of compound **A** were similar to those of a campest-4-en-3-one (Seto *et al.*, 2000). Furthermore, the HRESIMS spectrum (Figure 3) of compound **A** shows the $[M+Na]^+$ peak at m/z 421 (100%) suggesting the molecular weight 398 consistent with the molecular formula, $C_{28}H_{46}O$, of the identified compound campest-4-en-3-one and its chemical structure was shown in Figure 4.

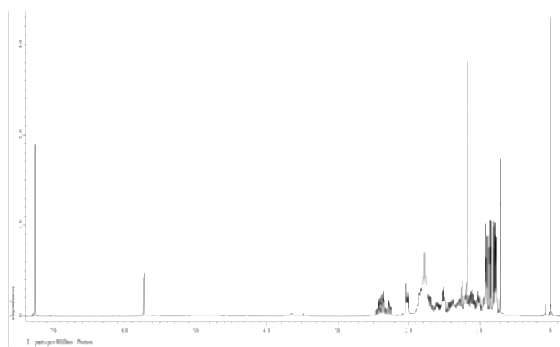


Figure 1. 1H NMR spectrum of isolated compound **A** (500 MHz, $CDCl_3$)

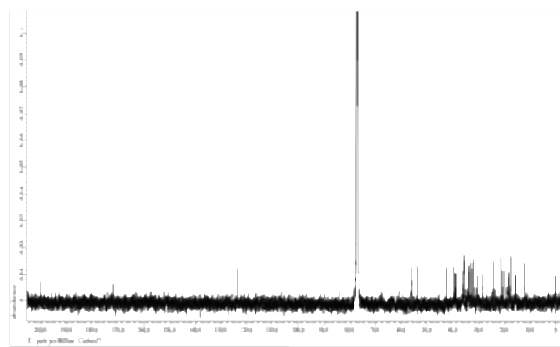


Figure 2. ^{13}C NMR spectrum of isolated compound **A** (125 MHz, $CDCl_3$)

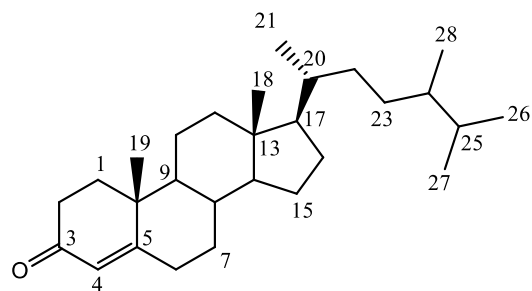
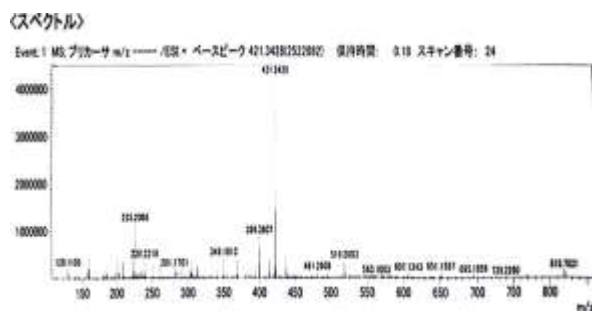


Figure 3. HRESIMS spectrum of compound A **Figure 4.** Chemical structure of campesta-4-en-3-one (C₂₈H₄₆O)

Compound **B** (15 mg, 0.005 % yield) was obtained as colourless needles. Its molecular formula was deduced as C₂₉H₄₆O from the NMR data and positive-ion HRESIMS (Figure 7) data (*m/z* 433.3425 [M+Na]⁺), which was 12 amu higher than that of compound **A**. The ¹H and ¹³C NMR spectroscopic data in CDCl₃ (Table 1 and Figures 5-6) of compound **B** showed a close structural resemblance to compound **A**, the presence of an additional olefinic group [*δ*_H 5.00 (dd, *J* = 15.5, 9.2 Hz, H-23) and 5.12 (dd, *J* = 15.5, 9.2 Hz, H-22); *δ*_C 129.5 (C-23) and 138.2 (C-22)], instead of two methylene group in compound **A**. Furthermore, the presence of one extra methylene carbon signal for C-28 (*δ*_C 25.5) in compound **B**, as compared to those of compound **A** (*δ*_C 15.5) was observed. From the above spectral data of (Figure 7) compound **B** was identified as stigmasta-4,22-dien-3-one (Rosandy *et al.*, 2017) and its chemical structure was shown in Figure 8.

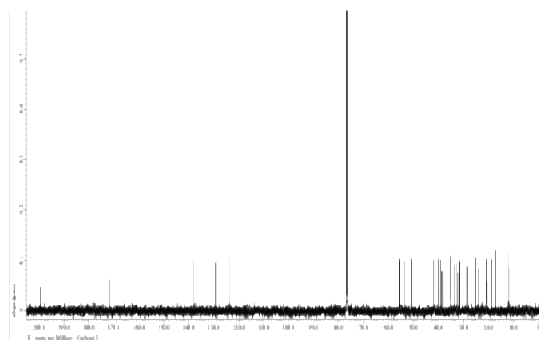
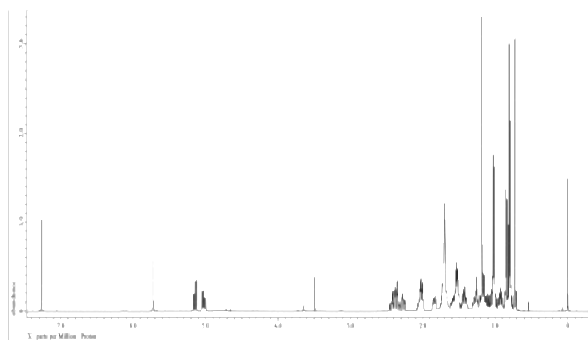


Figure 5. ¹H NMR spectrum of isolated compound B (500 MHz, CDCl₃) **Figure 6.** ¹³C NMR spectrum of isolated compound B (125 MHz, CDCl₃)

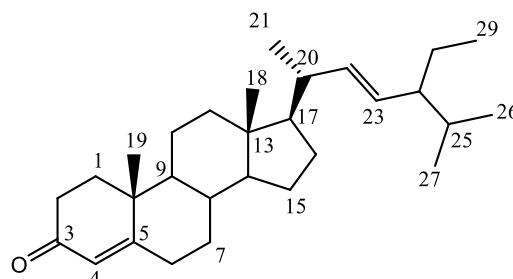
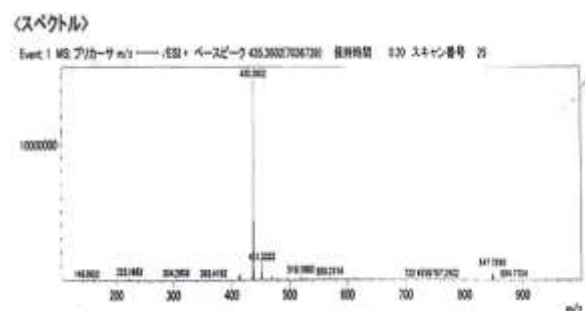


Figure 7. HRESIMS spectrum of isolated compound B (MeOH) **Figure 8.** Chemical structure of stigmasta-4,22-dien-3-one (C₂₉H₄₆O)

Compound **C** (8 mg, 0.0002% yield) was obtained as colourless needles. The HRESIMS of compound **C** (Figure 11) showed a quasi-molecular ion peak at m/z 435.3602 $[M+Na]^+$ corresponding to the molecular formula $C_{29}H_{48}O$. The 1H and ^{13}C NMR spectra of compound **C** (Figures 9 and 10) displayed the similar signals to compound **A**, except the presence of one more ethyl group at δ_C 23.1 (C-28) and 11.9 (C-29) in compound **C**, instead of methyl group at δ_C 15.5 (C-28) in compound **A**. The 1H and ^{13}C NMR spectroscopic data of compound **C** (Table 1) were essentially identical to those of stigmast-4-en-3-one (Hoa *et al.*, 2014) and its chemical structure of compound **C** was shown in Figures 11-12.

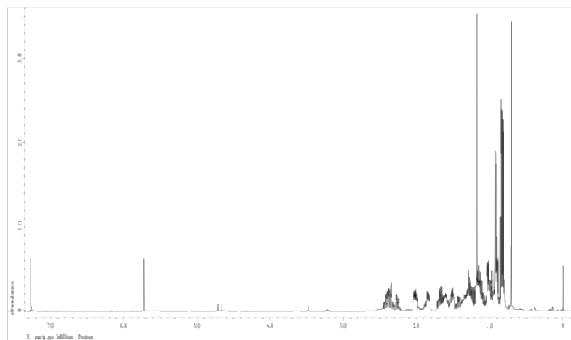


Figure 9. 1H NMR spectrum of isolated compound **C** (500 MHz, $CDCl_3$)

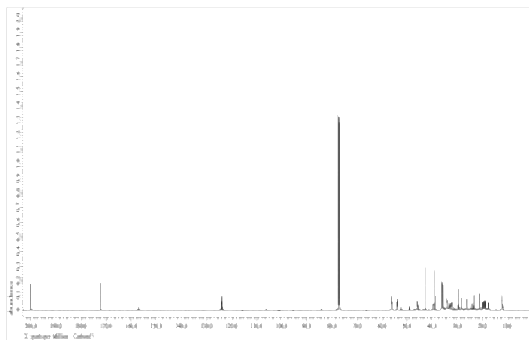


Figure 10. ^{13}C NMR spectrum of isolated compound **C** (125 MHz, $CDCl_3$)

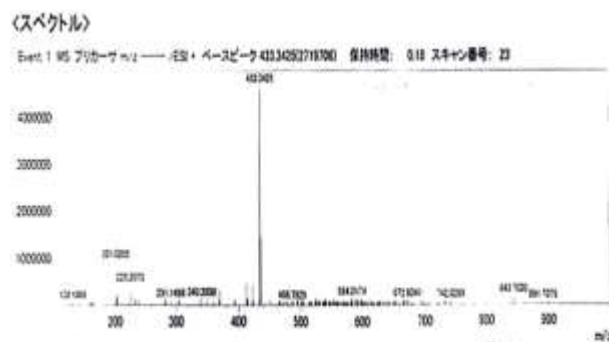


Figure 11. HRESIMS spectrum of isolated compound **C** (MeOH)

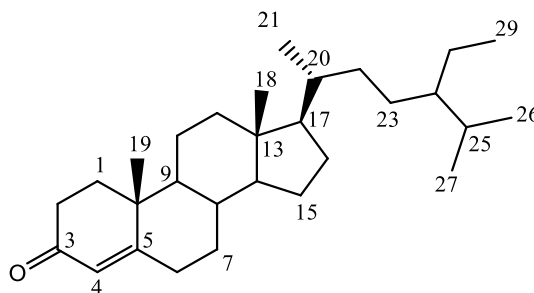


Figure 12. Chemical structure of stigmast-4-en-3-one ($C_{29}H_{48}O$)

Table 1. The ¹H and ¹³C NMR Spectral Data of Compounds A to C (500 & 125 MHz, CDCl₃)

Position	A		B		C	
	¹ H (mult, <i>J</i> in Hz)	¹³ C	¹ H (mult, <i>J</i> in Hz)	¹³ C	¹ H (mult, <i>J</i> in Hz)	¹³ C
1		35.7		35.7		35.7
2		39.7		34.0		34.0
3		199.9		199.9		199.9
4	5.71 (br.s)	123.8	5.71 (br.s)	123.8	5.71 (s)	123.8
5		172.0		171.9		172.1
6		32.5		33.0		34.0
7		32.1		32.1		33.0
8		35.9		35.7		35.7
9		53.9		55.9		53.9
10		38.7		38.7		38.7
11		21.1		21.1		21.1
12		38.9		39.6		39.8
13		42.5		42.3		42.5
14		55.9		53.9		55.9
15		20.3		24.3		24.3
16		24.0		28.9		28.3
17		56.1		56.1		56.1
18	0.69 (3H, s)	12.0	0.71 (3H, s)	12.2	0.69 (3H, s)	12.1
19	1.18 (3H, s)	17.5	1.17 (3H,s)	17.4	1.16 (3H, s)	17.5
20		34.0		40.5		36.2
21	0.90 (3H, dd, 4.0, 6.9)	18.7	1.00 (3H, d, 6.3)	21.2	0.91 (3H, d, 6.9)	18.7
22		33.7	5.12 (dd, 15.5, 9.2)	138.2		32.0
23		30.3	5.00 (dd, 15.5, 9.2)	129.5		26.1
24		33.0		51.3		45.9
25		28.2		31.9		29.2
26	0.84 (3H, dd, 1.7, 6.9)	18.3	0.84 (3H, d, 6.3)	19.1	0.82 (3H, d, 6.9)	19.9
27	0.79 (3H, d, 6.9)	15.4	0.80 (3H, d, 6.3)	21.1	0.80 (3H, d, 6.9)	19.1
28	0.75 (3H, dd, 1.7, 6.9)	15.5		25.5		23.1
29			0.79 (3H, d, 6.9)	12.3	0.84 (3H, d, 7.4)	11.9

Compound **D** (1 g, 0.0312% yield) was obtained as a white amorphous powder. Its HRESIMS showed the molecular ion peak at m/z 501.3915 [M-H]⁻ corresponding to the molecular formula of C₃₂H₅₄O₄. The FT IR spectrum (Figure 13) showed the strong vibration bands at 3685 and 1288 cm⁻¹ due to the stretching and bending vibrations showing a phenolic OH group. The stretching vibration of =CH and C=C groups appeared at 3032 and 1620 cm⁻¹. The stretching vibration of carbonyl peak appeared at 1712 cm⁻¹. The ¹H NMR spectrum of compound **D** in CDCl₃ (Figure 14 and Table 2) revealed the five aromatic proton signals at δ_H 6.29 (d, *J* = 15.9 Hz, H-2), 6.91 (d, *J* = 7.9 Hz, H-8), 7.03 (d, *J* = 7.9 Hz, H-5), 7.08 (d, *J* = 7.9 Hz, H-9), and 7.61 (d, *J* = 15.9, H-3), one oxygenated methylene signals at δ_H 4.18 (t, *J* = 6.7 Hz, H₂-1'), one methoxy group at δ_H 3.93 (s, H₃-10), twenty methylene group in the range between

δ_{H} 1.21- 1.71 (40 H, m, H-2' to H-21') and one methyl group at δ_{H} 0.88 (t, $J = 7.3$ Hz, H₃-22'). The ^{13}C NMR spectrum (Figure 15) exhibited a ester carbonyl carbon signal at δ_{C} 167.5 (C-1), three aromatic quaternary carbon signals at δ_{C} 127.1 (C-4), 146.8 (C-6) and 147.9 (C-7), five aromatic methine carbon signals at δ_{C} 109.4 (C-5), 115.8 (C-2), 144.7 (C-3), 114.8 (C-8), and 123.1 (C-9), one oxygenated methylene carbon at δ_{C} 64.7 (C-1'), one methoxy carbon at δ_{C} 56.0 (C-10), twenty methylene carbon in the range between δ_{C} 22.8 - 32.0 (C-2' to C-22') and one methyl carbon at δ_{C} 14.2 (C-22'). These NMR data of **D** were found to be similar those of docosyl ferulate which was isolated by Thongthoom *et al.* (2010) and its chemical structure was shown in Figure 16.

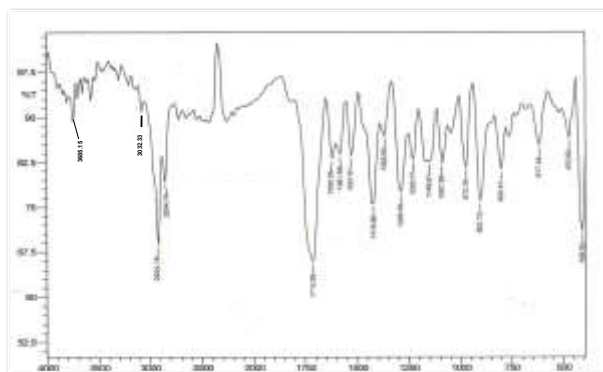


Figure 13. FT IR spectrum of isolated compound **D** (KBr)

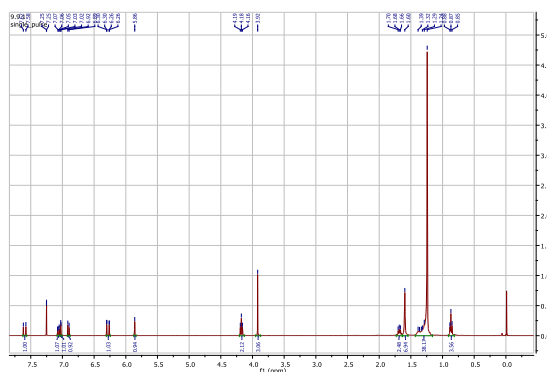


Figure 14. ^1H NMR spectrum of isolated compound **D** (500 MHz, CDCl_3)

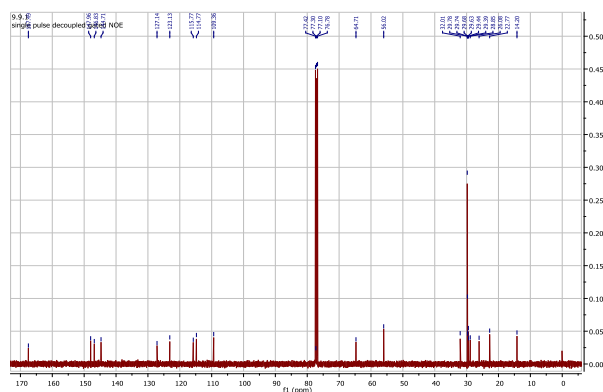


Figure 15. ^{13}C NMR spectrum of isolated compound **D** (125 MHz, CDCl_3)

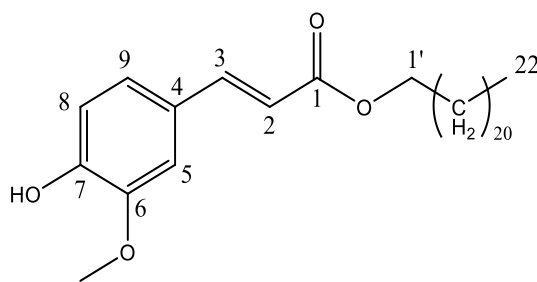


Figure 16. Chemical structure of docosyl ferulate ($\text{C}_{32}\text{H}_{54}\text{O}_4$)

Table 2. The ^1H and ^{13}C NMR Spectral Data of Compound D (500 & 125 MHz, CDCl_3)

Position	^1H (mult, J in Hz)	^{13}C
1	-	167.5
2	6.29 (d, $J = 15.9$)	115.8
3	7.61 (d, $J = 15.9$)	144.7
4	-	127.1
5	7.03 (d, $J = 7.9$)	109.4
6	-	146.8
7	-	147.9
8	6.91 (d, $J = 7.9$)	114.8
9	7.08 (d, $J = 7.9$)	123.1
10	3.93 (s)	56.0
1'	4.18 (t, $J = 6.7$)	64.7
2' - 21'	1.21-1.71 (m)	22.8-32.0
22'	0.88 (t, $J = 6.7$)	14.2
OH	5.87 (s)	

Antiproliferative Activity of Crude Extracts and Isolated Compounds

The antiproliferative activity of crude extracts and all isolated compounds (**A-D**) were tested against human cervical cancer cell line HeLa, human lung cancer cell line A549, human breast cancer cell line MCF-7, human gastric cancer cell line GSU, and normal human fibroblast cell line WI at the concentrations of 1, 10, and 100 $\mu\text{g/mL}$, using MTT assay. All of the tested samples exhibited antiproliferative activity against the four cancer cell lines. CHCl_3 and MeOH extracts exhibited moderate activity against all tested cell lines with the IC_{50} values in the range of 19.3 to 93.7 $\mu\text{g/mL}$. On the other hand, isolated compounds **A** to **C** showed the most potent activity against GSU cancer cell line with IC_{50} values 14.4, 15.5, and 13.9 $\mu\text{g/mL}$. This is the first time that the antiproliferative activity of the crude extract of Padein-gno rhizomes and its constituents were screened. IC_{50} values of all the tested samples are shown in Figure 17. Furthermore, these results suggest that the combination of sterol moiety was crucial for increasing the cytotoxic activities against all tested cancer cell lines.

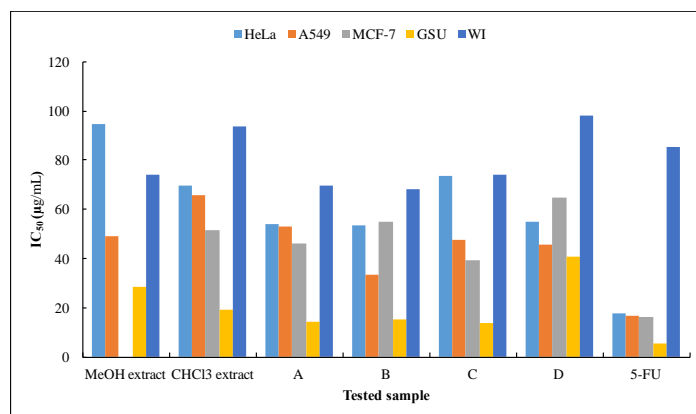


Figure 17. A bar graph of IC₅₀ values of crude extract and isolated compounds

Antibacterial activity of Crude Extracts and Isolated Compounds

All tested were also evaluated for their antibacterial activities against the gram positive bacteria, *B. subtilis* and *S. aureus*, and the gram negative bacteria, *K. pneumonia* and *E. coli*. The MeOH and CHCl₃ extracts exhibited moderate antibacterial activities against the two Gram positive bacteria: *B. subtilis*, *S. aureus* with MIC values ranging between 25–100 µg/mL but did not show the any activity on the Gram-negative bacteria: *E-coli*, *K. pneumoniae*. Compounds **A**, **B**, and **C** possessed stronger antibacterial activities against *B. subtilis*, *S. aureus* with MIC values ranging from 3.12 to 25 µg/mL than compound **D**. Notably, the antibacterial activity was investigated for the first time with the crude extracts of Padein-gno rhizomes sample and its constituents.

Table 3. Antibacterial Activities of Crude Extracts and Isolated Compounds from Padein-gno

Samples	Minimum Inhibitory Concentration (MIC) (µg/mL)			
	<i>Bacillus subtilis</i>	<i>Staphylococcus aureus</i>	<i>Klebsiella pneumoniae</i>	<i>Escherichia coli</i>
MeOH extract	50	25	>100	>100
CHCl ₃ extract	100	25	>100	>100
A	25	12.5	>100	>100
B	6.2	3.1	>100	>100
C	6.2	3.1	>100	>100
D	>100	>100	>100	>100
Ampicillin ^a	3.1	3.1	–	–
Kanamycin ^b	–	–	3.1	6.3

^a positive control for Gram-positive bacteria. ^b positive control for Gram-negative bacteria.

Conclusion

By the silica gel column chromatographic separation, three steroid compounds and one phenolic compound were isolated from the CHCl₃ extract of the Padein-gno rhizomes. The isolated compounds were identified to be campest-4-en-3-one, stigmasta-4,22-dien-3-one, stigmast-4-en-3-one, and docosyl ferulate. The MeOH and CHCl₃ extracts of Padein-gno and its constituents were found to possess antiproliferative activity against all the tested cancer cell lines. Similarly, Padein-gno rhizomes could be applicable as broad-spectrum antibacterial agents especially on Gram positive bacteria. Thus, the present biological investigation contributed to the medicinal importance of the plant, Padein-gno, especially with respect to its potential use in treating diseases related to bacterial infection, and cancer.

Acknowledgements

The authors acknowledge the Department of Higher Education, Ministry of Education, Myanmar, for allowing us to carry out this research programme.

References

- Chopra, R. N., S. L. Nayer, and I. C. Chopra. (1992). “*Glossary of Indian Medicinal Plants*”. New Delhi: 3rd Edn., Council of Scientific and Industrial Research, pp. 7-246
- Hasan, M. M. U., I. Azhar, Muzammil, S. Ahmed, and Ahmed. SW (2012). “Anti-Emetic Activity of some Leguminous Plants”. *Pak. J. Bot.*, vol. **44** (1), pp. 389 – 391
- Hoa, N. T., P. H. Dien, and D. N. Quang. (2014). “Cytotoxic Steroids from the Stem Barks of *Pandanus tectorius*”. *Research Journal of Phytochemistry*, vol. **8** (2), pp. 52-56
- Rosandy, A. R., N. M. Kamal, N. Talip, R. Khalid, and M.A. Bakar. (2017). “Isolation of Four Steroids from the Leaves of Fern *Adiantum latifolium* Lam”. *Malaysian Journal of Analytical Sciences*, vol. **21**(2), pp. 298 - 303
- Seto, H., S. Fujioka, S. Takatsuto, H. Koshino, T. Shimizu, and S.Yoshida. (2000). “Synthesis of 6-oxy Functionalized Campest-4-en-3-ones: Efficient Hydroperoxidation at C-6 of Campest-5-en-3-one with Molecular Oxygen and Silica Gel”. *Journal of Steroids*, vol. **65** (8), pp. 443-449
- Thongthoom, T., U. Songsiang. C. Phaosiri, and C. Yenjai. (2010). “Biological Activity of Chemical Constituents from *Clausena harmandiana*. Arch”. *Pharm. Res.*, vol. **33** (5), pp. 675-680
- Vogt, R. L. and L. Dippold. (2005). “*Escherichia coli* O157:H7 Outbreak Associated with Consumption of Ground Beef, June–July 2002”. *Public Health Rep.*, vol. **120** (2), pp. 174–178

PREPARATION AND UTILIZATION OF BIOSOLID FERTILIZER USING MUNICIPAL SEWAGE SLUDGE*

Sabai Phyu¹, Khin Cho Thant², Ni Ni Than³

Abstract

In the present work, biosolids were prepared from municipal sewage sludges. Municipal sewage sludge was treated to form biosolids by processes such as dewatering, sludge pasteurization, anaerobic digestion, aerobic digestion, composting, and storage. The different sewage sludge fertilizers, S1 and S2 were prepared. S1 contained only biosolid and S2 contained in the weight ratios of (1:1:1) of biosolid, rice husk ash and cocopeat. And then, some physicochemical properties and micro-macro nutrients of biosolids fertilizers were qualitatively and quantitatively characterized by EDXRF, AAS methods, and other conventional methods. By using biosolids fertilizer, a field experiment was conducted to test with mung beans. These mung bean seeds were collected from Yezin Agricultural University, Pyinmana Township, Naypyidaw. The field experiment was laid out using a randomized complete block design (RCBD), with six treatments (T1-T6). Physicochemical parameters and micro-macro nutrients of soil samples before sowing and after harvesting were analyzed. The results from the study indicated that the prepared biosolid fertilizers can effectively reduce the use of chemical fertilizers for the growth and production of mung beans. To know the presence of beneficial or non-beneficial microbes in biosolids, microbial tests were studied by total plate count methods.

Keywords: biosolids fertilizer, sewage sludge, mung beans, micro-macro nutrients

Introduction

Farmers have known for centuries that animal manures spread on pastures and cropland can improve soil fertility (Gupta, 2000). They began to use sludge from municipal wastewater treatment plants as a fertilizer. "Sewage Sludge" refers to the solids separated during the treatment of municipal waste water. "Biosolids" refers to treated sewage sludge that meets the EPA pollutant and pathogen requirements for land application and surface disposal (Adamtey, *et al.*, 2010).

The scientific and agricultural communities have come to understand that municipal sludge or "biosolids" contain valuable nutrients and organic matter that improve the soil in a way similar to animal manures (Kone *et al.*, 2007). Biosolids are organic solids that have been treated to stabilize organic matter and reduce disease-causing organisms or pathogens. The greatest advantage is a reduction in fertilizer costs (Nikiema *et al.*, 2013). Biosolids also contain nitrogen, phosphorus and many micronutrients that can be beneficial to crop growth (Cofie *et al.*, 2009). Other advantage is the addition of organic matter to the soil (Nair, 2008). Organic matter reduces surface runoff, reduces erosion and improves the water holding capacity and nutrient of the soil. Mung beans are a nutritionally various food that belongs to the legume family. Other names for mung beans include green gram, maash, moong, monggo, or munggo. They are mainly cultivated in Asia, Africa, and South America, but mung beans are enjoyed by people all around the world.

* Special Award (2023)

¹ Department of Chemistry, University of Yangon

² Department of Chemistry, West Yangon University

³ Department of Chemistry, University of Yangon

Mung beans are a rich source of plant-based protein, complex carbohydrates, fiber, and other nutrients. Mung beans that are usually green, but can also be yellow or black. Add them to soups, salads, and casseroles (Sayed, 2020). They are widely used in India to make curries. In Myanmar, mung beans are among the types of bean that are exported abroad. The aim of the research work is to prepare effective biosolid fertilizers using municipal sewage sludge for agricultural productivity.

Materials and Methods

Sample Collection, Preparation and Application

The sewage sludges were collected from Yangon City Development Committee (YCDC), Botahtaung Township, Yangon Region. The raw materials (cocopeat and rice husk ash) were collected from Hlaing Thar Yar Industrial Zone, Yangon Region. Municipal sewage sludge was treated by processes that included dewatering, sludge pasteurization, anaerobic digestion, aerobic digestion, composting and storage. The fertilizers were packaged in bags, stored in a cool place. By using biosolids fertilizers, the trials were carried out during the 2022 winter season in Kha Yaung Village, Hlegu Township, Yangon Region. The average maximum and minimum temperatures of the experimental sites were 34 and 19 °C, respectively. The experiment was laid out using a randomized complete block design (RCBD). The area of each plot was (30×24) sq ft. The row spacing and plant spacing were 10 and 6 inches in six treatments, respectively. The treatments used in this research were

T1 = control,

T2 = compound fertilizer (NPK 15:15:15) [50 kg/ac],

T3 = biosolid [200 kg/ac],

T4 = biosolid: cocopeat: rice husk ash (1:1:1) [Used 200 kg in 1 ac],

T5 = biosolid [200 kg/ac] + compound fertilizer [33.3 kg/ac],

T6 = biosolid [200 kg/ac] + compound fertilizer [25 kg/ac].

Determination of Physicochemical properties, Nutrient Values, Elemental Analysis and Microbial Analysis of Prepared Fertilizers

Some physicochemical properties (pH, moisture content, electrical conductivity, NPK contents) of biosolids (S1) were determined. Measurement of pH was carried by a pH meter and the moisture content was determined by moisture analyzer. The electrical conductivity of biosolids fertilizers was determined by conductivity meter. The nitrogen content was determined by Kjeldahl's method. The potassium content was determined by Flame photometric technique and the phosphorus content was determined by UV-visible spectrophotometric technique (The Su Min, 2018). Elemental contents of raw materials and biosolids fertilizer were semi-quantitatively determined by using EDXRF technique and also quantitatively determined by AAS technique. Six treatments T1 to T6 were analyzed by conventional and modern techniques before sowing and after harvesting. Soil texture was determined by international pipette method. Available potassium, exchangeable calcium, magnesium and potassium in the soil were

determined by AAS. In the analytical procedures of the experiment, recommended methods and technique were applied (AOAC, 2000). Microbial population in S1 was determined by total plate count method. Figure 1 shows the photographs of sewage sludge and biosolid (treated sewage sludge).



Figure 1. Photograph of (a) sewage sludge (b) biosolid (treated sewage sludge)

Results and Discussion

Some Physicochemical Properties, Nutrients and Microbial Analysis of Biosolids

Table 1 represents the moisture content, electrical conductivity, pH, bulk density, organic carbon content, humus and C: N ratio of biosolids. It was found that acceptable value of moisture content, electrical conductivity, and pH. The pH value (7.70) of biosolids are found to be suitable for the preparation of biosolid fertilizer. The bulk density was found to be 0.87. So, it has high porosity. Both bulk density and porosity give a good indication of the suitability for root growth, and soil permeability is vitally important for the soil-plant atmosphere system and medium organic carbon and humus percent. The C: N were calculated at the value of 32.50. Total organic matter plays a very important and sometimes spectacular role in the maintenance and improvement of soil properties.

Table 2 shows that biosolid contains 1.26 % nitrogen, 2.10 % phosphorus, and 0.04 % potassium. It was found that the amount of nitrogen and phosphorus is high in biosolids. From these data, biosolids contained the macronutrients (NPK) for plants and soil fertility. Therefore, biosolid was used for the preparation of biosolid fertilizers.

Table 3 shows the determination of microbes in biosolids. It was found that yeast and mould population were found to be 5×10^5 cfu/g and *Bacillus subtilis* was 5×10^3 cfu/g. The complex plant-microbe could be beneficial for both crop productivity and the well-being of soil microbiota. The harmful bacteria such as, *E. coli*, *Coliform*, and *Salmonella* were not detected.

Table 1. Some Physicochemical Properties and Nutrients of Biosolid

Parameters	Content
moisture (%)	19.15
electrical conductivity (μ S/cm)	158.00
pH	7.70
bulk density (g/mL)	0.87
organic carbon (%)	40.95
humus (%)	70.59
C:N	32.50

Table 2. N, P and K Content of Biosolid

Nutrient	Content (%)
Nitrogen	1.26
Phosphorus	2.10
Potassium	0.04

Table 3. Microbial Analysis of Biosolid

Microbes	Population (cfu/g)
yeast and mold	5×10^5
<i>E. coli</i>	ND
<i>Coliform</i>	ND
<i>Salmonella</i>	ND
<i>Bacillus subtilis</i>	5×10^3

Relative Abundance of Some Elemental Contents in Biosolid

The relative abundance of some elements in biosolid from sewage sludges was determined by EDXRF technique. It was observed that biosolids contained fourteen elements (Si, K, Ca, Mn, Fe, Zn, Cu, S, Ti, Pb, Zr, Sr, Ni and Cr) as shown in Table 4. It can be said that biosolid can supply, multi nutrients to soil and plants. And then, the exact amount of some nutrient elements determined by AAS method. Fe (5.64 ppm) Cu (1.13 ppm) and K (1.04 ppm). The sufficient amount of macro-and micro nutrients were found to be present in biosolid fertilizers. So, it can be summarized that biosolids may be a good source of elemental nutrients for plants.

**Figure 2.** EDXRF spectrum of treated sewage sludge (Biosolid)

Table 4. Relative Abundance of Some Elements in Biosolid by EDXRF

Element	Relative abundance (%)
	Biosolid
Si	28.28
K	4.47
Ca	6.69
Mn	1.47
Fe	49.14
Zn	2.96
Cu	1.25
S	2.22
Ti	2.97
Pb	0.45
Zr	0.42
Sr	0.36
Ni	0.19
Cr	0.15

Table 5. Elemental Contents of Biosolid by AAS

Element	Content (ppm)
Ca	0.17
Cu	1.13
Cr	0.02
K	1.04
Zn	0.51
Fe	5.64
Mn	0.67
S	17.00
Pb	ND

Analysis of Five Treated Soil and Control before Sowing

The physicochemical properties of treated soils before sowing of the mung bean plant were studied. These soils were subjected to five different treatments (T2 – T6) by using cocopeat, rice husk ash, and chemical fertilizer. The soil without any fertilizers treatment (T1) was kept as a control. These trial farm soils were analyzed for their physical and chemical properties. The results are shown in Table 6. From these results, based on the soil texture diagram, all farm soils (before sowing) falls in the loam. The pH values of treated soils were found to be in the range of 5.99 to 6.86, slightly acidic type of soil. Soil pH may influence nutrient absorption and plant growth.

Table 6. Analysis Data of the Soil before Sowing

Analytical Item	Content					
	T1	T2	T3	T4	T5	T6
texture- sand (%)	43.40	43.75	40.91	39.62	41.00	41.68
silt (%)	36.90	36.85	40.95	39.98	39.87	39.00
clay (%)	19.70	19.40	18.14	20.40	19.13	19.32
moisture (%)	4.89	5.00	3.45	3.00	3.20	2.55
pH	6.86	6.10	6.14	6.09	5.99	6.00
electrical conductivity ($\mu\text{S}/\text{cm}$)	51.00	75.00	70.90	82.1	70.00	69.20
organic Carbon (%)	0.75	2.00	1.50	1.76	1.75	1.40
humus (%)	1.29	3.45	2.59	3.03	3.02	2.41
total N (%)	0.16	0.30	0.20	0.23	0.38	0.25
C/N ratio	4.69	6.67	7.50	7.65	4.60	5.60
available P (ppm)	20.00	36.00	33.35	31.35	32.50	31.95
available K_2O (mg/100 g)	15.60	19.00	17.75	18.10	18.23	18.00
exchangeable Ca (meq/100 g)	11.31	18.00	15.45	14.50	14.80	15.00
exchangeable Mg (meq/100 g)	0.67	0.50	0.39	0.49	0.52	0.55
exchangeable K (meq/100 g)	0.33	1.60	0.70	0.85	1.50	1.10

Analysis of Soil after Harvesting Mung Bean

Based on the soil texture diagram, all types of soils (T1- T6) are loam and so they cannot be changed before and after harvesting. The pH values of these soils were increased from 6.40 to 7.00. In addition, the amounts of total N, available P and K, and exchangeable Ca. Mg, K in all treatments(T1-T6) were reduced as compared to treated soil (T1-T6) before sowing. It can be said that, the mung bean plants consumed the necessary nutrients from treated soils (T1-T6).

Table 7. Analysis Data of Soil after Harvesting Mung Bean

Analytical item	Content					
	T1	T2	T3	T4	T5	T6
texture-sand (%)	43.00	43.10	40.76	39.54	40.31	41.11
silt (%)	36.40	36.50	40.00	39.76	39.47	38.31
clay (%)	20.60	20.40	19.24	21.20	20.22	20.58
moisture (%)	3.15	4.95	2.38	2.35	2.85	2.25
pH	7.00	6.40	6.50	6.40	6.50	6.70
electrical Conductivity ($\mu\text{S}/\text{cm}$)	47.20	74.20	75.70	55.30	59.50	62.50
organic Carbon (%)	0.72	1.90	1.20	1.50	1.70	1.32
humus (%)	1.24	3.78	2.06	2.59	2.93	2.28
total N (%)	0.10	0.22	0.16	0.17	0.20	0.19
C/N ratio	7.20	8.64	7.50	8.82	8.50	6.94
available P (ppm)	16.00	30.00	27.05	25.00	28.90	27.45
available K_2O (mg/100 g)	14.00	16.50	15.98	15.36	15.42	15.33
exchangeable Ca (meq/100 g)	10.00	14.00	13.65	13.00	14.21	14.10
exchangeable Mg (meq/100 g)	0.50	0.49	0.34	0.40	0.42	0.45
exchangeable K (meq/100 g)	0.33	1.50	0.68	0.80	1.20	0.92

Effect of Biosolid Fertilizer on Growth and Yield of Mung Beans

The time interval from transplanting to harvesting was 82 days. The growth factors of the mung bean were evaluated in terms of the plant height (cm), number of branch, number of pod/plant, number of seed/pod, 100 seed weight (g), yield (g/m²) yield (basket/ac) and shown in Table 8. It was significantly different in plant height, number of pod/plant, number of seed/pod between (T2- T6) soil and control (T1). It was slightly different in branch and 100 seeds weight for all treatments. From this research, it was clearly observed that the yields of mung beans (T2- T6) were higher than control (T1). The yield of mung beans in T2 was the highest. The second and third highest yields were observed in T5 and T6. So, it can be said that sewage sludge (biosolid) can be used to reduce the use of chemical fertilizers in mung beans planting.



Figure 3. Photographs of (a) field of mung beans and (b) growth of mung beans

Table 8. Effect of Biosolid Fertilizer on Growth and Yield of Mung Bean

Treatment	Plant height (cm)	No. of branch	No. of pod/plant	No. of seed/pod	100 seed weight (g)	Yield (g/m ²)	Yield (basket/ac)
T1	53.6	1.0	9.1	9.2	2.18	63	7.70
T2	63.3	1.2	14.3	10.8	2.24	91	11.12
T3	64.1	1.2	13.5	11.0	2.21	79	9.53
T4	61.4	1.2	17.8	11.6	2.25	75	9.17
T5	65.6	1.4	16.4	11.2	2.30	90	11.00
T6	62.6	1.2	14.1	12.0	2.26	86	10.51

Conclusion

In this research, municipal sewage sludge was treated to prepare biosolid by processing such as dewatering, sludge pasteurization, anaerobic digestion, aerobic digestion, composting and storage. The three different fertilizers (T4 -T6) were prepared using biosolids from sewage sludge, chemical fertilizer (compound 15:15:15). In addition, T1 (control), T2 (only compound 15:15:15) and T3 (only biosolid) were also used to study. According to the physicochemical properties and micro- and macro-nutrients, it can be said that, all fertilizers are suitable for plant growth. In this work, field experiments using (T1-T6) were conducted to know the effect of biosolid on plant growth and yield of mung bean. From the results, the yield of T2, T5 and T6 are leading runners (11.12, 11.00, 10.51 basket/ac). The yields of T5 and T6 (Biosolid plus

compound fertilizers) are not significantly different compared to T2 (compound fertilizer). So, it can be concluded that biosolid obtained from sewage sludge can effectively be used as a partial substitute for chemical fertilizer in mung bean planting fields. Moreover, the biosolid from sewage sludge only contains beneficial microbes; but non-beneficial microbes are absent.

Acknowledgement

The authors would like to express their profound gratitude to the Department of Higher Education, Ministry of Education, Yangon Myanmar for provision of opportunity to do this research and Myanmar Academy of Arts and Science for allowing to present this paper.

References

- Adamtey, N., O. Cofie, K. G. Ofosu-Budo, J. Ofosu-Anim, K. B. Laryea and D. Forster. (2010). "Effect of N-enriched co-compost on Transpiration Efficiency and Water-use Efficiency of Maize (*Zeamays L.*) Under Controlled Irrigation". *Agric. Wat. Manag.*, vol. 97, pp. 995–1005.
- AOAC. (2000). *Official Methods of Analysis of the Association of Official Analytical Chemists*. H. Willam, Virginia: 17th Ed., AOAC Inc. pp. 42-49.
- Cofie, O., D. Kone, D. S. Rothenberger, S. D. Moser and C. Zurbrügg. (2009). "Co-composting of Faecal Sludge and Organic Solid Waste for Agriculture Process Dynamics". *Wat. Res.*, vol. 43, pp. 4665–4675.
- Gupta, C. R. and S. S. Sengar. (2000). Response of Tomato (*Lycopersico esculentum* Mill.) to Nitrogen and Potassium Fertilization in Acidic Soil of Bastar". *Vegetable Sci.*, vol. 27(1), pp. 94-95.
- Koné, D., O. Cofie, C. Zurbrügg, K. Gallizzi, D. Moser, S. Drescher, and M. Strauss. (2007). "Helminthes Eggs Inactivation Efficiency by Faecal Sludge Dewatering and Co-composting in Tropical Climates". *Wat. Res.*, vol. 41, pp. 4397–4402.
- Nair, A., A. A. Juwarkar, and S. Devotta. (2008). "Study of Speciation of Metals in an Industrial Sludge and Evaluation of Metal Chelators for their Removal". *J Hazard Matter*, vol. 152, pp. 545-53.
- Nikiema, J., O. Cofie, R. Impraim, and N. Adamtey. (2013). "Processing of Fecal Sludge to Fertilizer Pellets Using a Low-cost Technology in Ghana". *Environ. Pollut.*, vol. 24, pp. 70- 80.
- Sayed, M. N. K. (2020). *Crop Production Manual*. Food and Agriculture Organization (FAO), pp. 1-30.
- Thet Su Min. (2018). *Efficacy of Biofertilizer with Bioinoculant Trichoderma Harzianum on some Solanaceous Cops*. PhD Dissertation, Department of Chemistry, University of Yangon, Myanmar, pp.25-46.

NEEM LEAVES BASED ORGANIC FERTILIZER FOR CULTIVATION OF PEANUT CROP IN SOIL FROM YENANCHAUNG TOWNSHIP

Aye Aye Lwin¹, Kay Thi Moh Moh Win², Yin Yin Htun³, Akayi Chan Nyein Oo⁴,
Phyu Phyu Aye⁵, Tin Oo Kyi⁶

Abstract

This research is concerned with the investigation of the preparation, and characterization of organic fertilizer from neem leaves, cow dung, and peanut shell. The raw materials were collected from the Yenanchaung Township. The organic fertilizers (OF) were prepared by three different weight ratios of neem leaves, cow dung, and peanut shell (100 kg: 100 kg: 100 kg) for OF-1, (125 kg:75 kg: 100 kg) for OF-2, and (150 kg:50 kg: 100 kg) for OF-3 respectively. The organic fertilizers were prepared by compost heap layer method. Field experiments were conducted in Kyawe-Pone Village, Yenanchaung Township, Magway Region to test the effect of organic fertilizer on the growth of peanuts with three treatments (T-1, T-2, and T-3) and a control. The highest yield of T-3 was 725.58 kg/ha, and the lowest yield of peanut in control was 543.49 kg/ha. In this work, the soil before cultivation and after harvesting was analyzed with regards to soil parameters. After harvesting nitrogen content, available phosphorus, and available potassium were higher in organic fertilizer-treated soil than before cultivation soil to maintain and sustain the soil fertility.

Keywords: organic fertilizer, neem leaves, cow dung, peanut shell, soil fertility

Introduction

Soil is essential to life, and it is a non-renewable, dynamic natural resource. Soil plays a vital role in sustaining life on the planet (Schoonover and Jackie, 2015). Soil texture influences nutrient retention, and has an important role in nutrient management. Soil organic matter is a primary source of carbon, which gives energy and nutrients to soil organisms (Bissonnais, 1996). The amount of organic matter depends not only on soil microorganisms, but also on the type of soil, vegetation, and environmental conditions such as moisture and temperature (Antil and Singh, 2007). Soil acidity, or alkalinity, can be measured by soil pH. It is an important indicator of soil health. It affects crop yields, crop suitability, plant nutrient availability, and soil microorganisms activity, which influence key soil processes (Dai *et al.*, 1998). Plants require 16 essential elements. Carbon, hydrogen, and oxygen are derived from the atmosphere and soil water (Jones, 1998). Nitrogen is biologically combined with C, H, O, and S to create amino acids, which are the building blocks of proteins (Hungria and Vagas, 2000). Phosphorus aids in root development, flower initiation, and seed and fruit development (Hansch and Mendel, 2009). The primary function of phosphorus is the transfer of energy from plant leaves to their storage in sugars and starches (Epstein and Bloom, 2005). The presence of potassium is vital for plant growth because it is known to be an enzyme activator that promotes metabolism (Barber, 1995). Calcium is an activator of several enzyme systems in protein synthesis and carbohydrate transfer (Barker and Pilbeam, 2010). The essential micronutrients are zinc (Zn), iron (Fe), manganese

¹ Department of Chemistry, Yenanchaung University

² Department of Chemistry, Yenanchaung University

³ Department of Chemistry, Yenanchaung University

³ Department of Chemistry, Yenanchaung University

⁴ Department of Chemistry, Yenanchaung University

⁵ Department of Chemistry, Yenanchaung University

⁶ Department of Chemistry, Yenanchaung University

(Mn), boron (B), chlorine (Cl), copper (Cu), molybdenum (Mo), cobalt (Co), vanadium (V), sodium (Na), and silicon (Si) (Chan and Ma, 2013).

Fertilizers are materials containing one or more nutrient elements in the form of chemical compounds of organic and inorganic nature (Bhatt *et al.*, 2019). Organic fertilizers are natural materials from plant or animal sources, such as manure, green manures, crop residues, household waste, and compost, which directly and indirectly influence the properties of soil. Organic fertilizer increases root growth due to enhanced soil structure, promotes soil aggregates, and enhances cation exchange capacity (Bhatt *et al.*, 2019). Raw materials such as crop residues, animal wastes, municipal wastes, and industrial wastes were applied as a fertilizing resources (Sawhney, 1976). Neem can grow in tropical and subtropical regions with semi-arid to humid climates. Neem leaves are cheap and useful fertilizers. Neem leaves improve the efficiency of fertilizer utilization in crop production through the gradual release of nitrogen to crops (Fathima, 2004). Cow dung is the most important source of bio-fertilizer but at the same time, cow's urine, cow's horn, and the dead body of a cow can be used for preparing effective bio-fertilizer (Hlaing, 2021). Peanut (*Arachis hypogaea* L.), or groundnut, is an annual herbaceous plant of the Fabaceae or Legume family.

Materials and Methods

Sample Collection

In this research, three raw materials of neem leaves, cow dung, and peanut shells were used for the preparation of organic fertilizer. Neem leaves, cow dung, and peanut shells were collected from the Industrial Zone in Yenanchaung Township, Magway Region.

Physicochemical Determination of Neem Leaves, Cow Dungs, Peanut Shells, and Prepared Organic Fertilizers

The pH of neem leaves, cow dung, peanut shells, and prepared organic fertilizers was determined by a pH meter. The moisture was determined by the oven-dry method. The total nitrogen content was determined by Kjeldahl's method, the phosphorus content was determined by the same UV-visible spectrophotometric method, the potassium content was determined by the flame spectrophotometric technique, and the organic carbon and humus percent were determined by the titration method.

Determination of Some Elemental Compositions in Raw Materials and Prepared Organic Fertilizers

The elements present in raw samples (neem leaves, cow dung, and peanut shells) and prepared organic fertilizers were determined by the EDXRF technique at the Department of Chemistry, Monywa University.

Preparation of Organic Fertilizer from Neem leaves, Cow dung, and Peanut Shells

The three composted piles were prepared with plastic sheets, and the size of each pile was approximately 1.5 m in length, width, and height. The prepared organic fertilizers were made in three different ratios. The organic fertilizers (OF) were prepared by three different weight ratios of neem leaves, cow dung, and peanut shell (100 kg: 100 kg: 100 kg) for organic fertilizers-1(OF-1), (125 kg: 75 kg: 100 kg) for organic fertilizers-2 (OF-2), and (150 kg: 50 kg: 100 kg) for

organic fertilizers-3 (OF-3) respectively. Organic fertilizers were prepared by the compost heap layer method. The temperature gradually rises and reaches its optimum within 7 days. The mixture maintained its optimum temperature for several days and then dropped gradually.

After three months, the compost-making material became black in colour. Then, organic fertilizers were obtained. Part of the fertilizer was kept in an airtight container and used for chemical analysis. Figure 1 shows a photograph of organic fertilizer piles.



Figure 1. Photograph of organic fertilizer piles

Application of Organic Fertilizers on Peanut Plants in Yenanchaung Township

A field experiment was carried out on sandy loam soil during (the rainy season) in 2022 at the farm, in Kyawe Pone village, Yenanchaung Township, Magway Region in Myanmar. The experiments were conducted in organic fertilizer-treated soil and control cultivation. The field experiments were carried out by the following.

Control	=	Untreated soil
Treatment 1 (T-1)	=	Soil treated with organic fertilizer-1 (OF-1)
Treatment 2 (T-2)	=	Soil treated with organic fertilizer-2 (OF-2)
Treatment 3 (T-3)	=	Soil treated with organic fertilizer-3 (OF-3)

Measurements of Plants

Plants measured were taken 15 days, 45 days, 75 days, and 120 days after cultivation. The plant height, plant width, number of leaves, number of flowers, and yield of components were measured for six randomly selected plants from each experiment.

Analysis of the Farm Soil Samples

Soil samples were collected from a farm in Yenanchaung Township, Magway Region. Soil samples were taken at a depth of about 20 cm from the surface in a zigzag manner, mixed thoroughly, and dried in the shade before sieving. Then the soil samples were stored in polythene bags and clearly labeled.

The soil samples were subjected to physical and chemical analyses using conventional and modern techniques. Some of this work was done in the laboratory of the Analysis Department of the Land Use and Seed Division, Ministry of Agriculture and Irrigation. The soil samples taken before cultivation and after harvesting were analyzed.

Results and Discussion

In this study, organic fertilizers were prepared from organic waste materials such as neem leaves, cow dung, and peanut shells. The effect of organic fertilizers on soil fertility was analyzed.

Sampling

In this research, three raw materials (neem leaves, cow dung, and peanut shells) were used in the preparation of organic fertilizer. The photographs of these samples are shown in Figure 2.

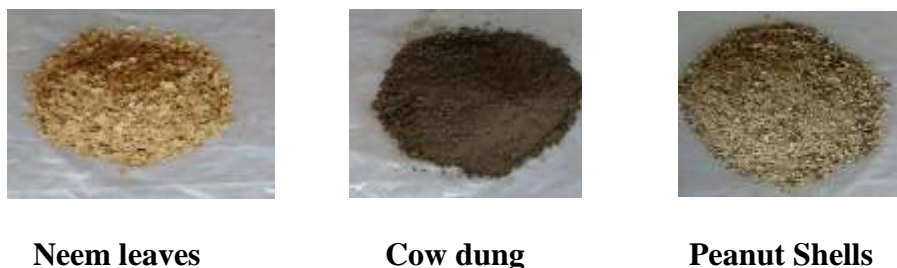


Figure 2. Photographs of neem leaves, cow dung, and peanut shells

Physicochemical Properties of Neem Leaves, Cow Dung, and Peanut Shells

The pH values of neem leaves, cow dung, and peanut shells are 6.2, 7.5, and 6.5 respectively. The pH values of cow dung are higher than those of neem leaves and peanut shells. The pH values of all waste materials are found to be suitable for the preparation of organic fertilizer. The results are presented in Table 1, and Figure 2. Among the three samples, the cow dung sample found the least amount of moisture content, whereas the peanut shell samples showed the highest amount of moisture content. In the present work, it was found that the nitrogen contents of neem leaves, cow dung, and peanut shells were 3.118 %, 1.575 %, and 0.88 % respectively. The amounts of phosphorus in neem leaves, cow dung, and peanut shells were 0.379 %, 1.720 %, and 0.028 % respectively. The amounts of potassium in neem leaves, cow dung, and peanut shells were 1.162%, 0.422 %, and 0.29 %, respectively. It can be seen that the neem leaf sample contained the highest amount of nitrogen and potassium. The amount of phosphorous in cow dung was contained in all three samples. From these data, the waste materials contained the appropriate amounts of NPK needed for plants and soil fertility. So, these waste materials (neem leaves, cow *dung*, and peanut shells) were used for the preparation of organic fertilizers. Table 1 shows the results of some physicochemical properties of neem leaves, cow dung, and peanut shells.

Table 1. Physicochemical Properties of Neem Leaves, Cow Dung, and Peanut Shells

Sample	Parameters					
	pH	Available N (%)	Available P (%)	Available K (%)	Organic Carbon (%)	C: N
Neem leaves	6.2	3.118	0.379	1.162	53.9	44.1
Cow dungs	7.5	1.575	1.720	0.422	10.26	23.51
Peanut shells	6.5	0.88	0.028	0.29	55.8	63.41

Relative Abundance of Elements in Neem Leaves, Cow Dung, and Peanut Shells

The presence of elements (calcium, potassium, sulphur, iron, strontium, manganese, copper, titanium, and zinc) in neem leaves, cow dung, and peanut shells is shown by EDXRF spectra represented in Figures 3 (a), (b), and (c). It can be observed that the relevant elements (macronutrients and micronutrients) for plants were contained in neem leaves, cow dung, and peanut shell samples.

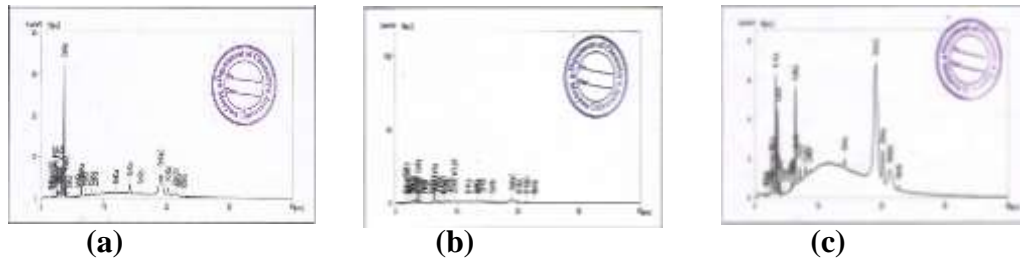


Figure 3. EDXRF spectra of (a) neem leaves, (b) cow dung, and (c) peanut shell

Preparation of Composted Organic Fertilizer

Temperature changes of compost pile during the composting process

In composting operations, temperature is a key parameter. The temperature profiles of three different ratios of composting organic fertilizers are shown in Figure 4. During the composting process, the temperature of three different compost piles was measured at (10 a.m, and 5 p.m) daily. The daily temperature of compost was recorded for up to 120 days. In the process, the temperature of the compost began at 41°C, and then the temperature was gradually increased to ~ 62°C after 30-31 days. The increase in temperature during the composting process is caused by the heat generated from the respiration and decomposition of sugar, starch, and protein by the population of microorganisms. The temperature pattern showed that there is a rapid process from the initial mesophilic phase to the thermophilic phase for this treatment. The temperature slightly decreased at 65-67 days because of the depletion of food sources, overall microbial activity decreased, and the temperature fell to ambient (Cobb and Rosenfield, 1991). The highest temperature of 70°C was observed at 65-62 days, and the temperature dropped gradually again to reach 51°C at 86-90 days. The parameter for the temperature showed that the decomposition of organic matter occurs during the 90 days. After three months later, the compost was ready to use on the field. The photographs of prepared organic fertilizer are shown in Figure 5.

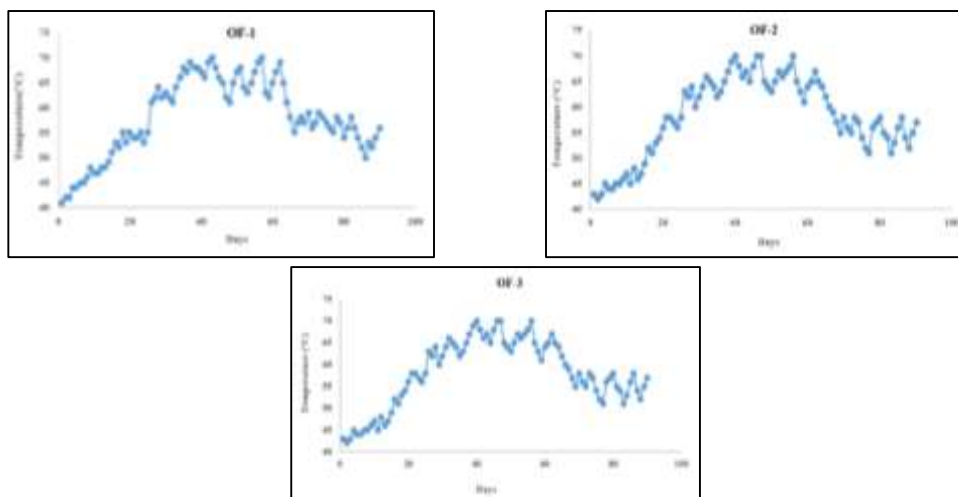


Figure 4. Temperature changes of organic fertilizers (OF-1, OF-2 and OF-3)

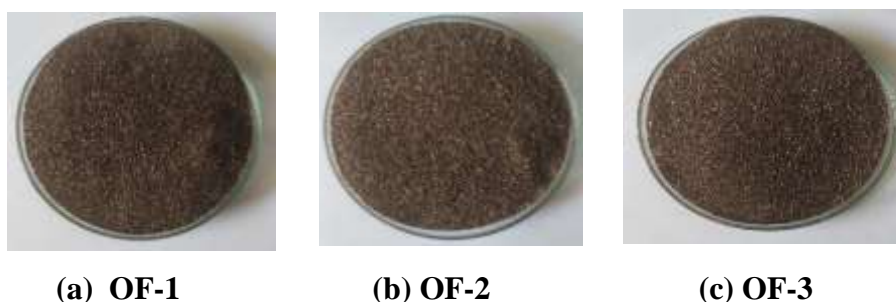


Figure 5. Photographs of organic fertilizers (OF-1, OF-2 and OF-3)

Physicochemical Properties of Composted Organic Fertilizers

The pH, moisture content, organic carbon content, C/N ratio, total nitrogen content (N), phosphorus content (P_2O_5), and potassium content (K_2O) of organic fertilizers are specified. Therefore, chemical analyses were carried out by standard methods to know their specifications. The pH values of organic fertilizers were found to be in the range of 8.31-8.38.

The moisture content of organic fertilizers (OF-1, OF-2, and OF-3) was found to be 11.26 %, 22.41 %, and 18.79 % respectively. The organic carbon contents of OF-1, OF-2, and OF-3 were 18.01 %, 15.56 %, and 13.24 % respectively. In these results, the organic carbon contents were observed in the range of 13.24-18.01, and OF-1 had the highest organic matter content.

The C/N ratio of organic fertilizers was 17.83, 19.95, and 15.58. Although a C/N ratio of 10 to 20 normally indicates being in the range of mature enough, total organic matter plays a very important and sometimes spectacular role in the maintenance and improvement of soil properties. The results are reported in Table 2.

Table 2. Physicochemical Properties of Compost Organic Fertilizers

Fertilizers	pH	Moisture (%)	Organic carbon (%)	Total N (%)	Total P (%)	Total K (%)	C/N ratio
OF-1	8.38	11.26	18.01	1.01	0.145	1.06	17.83
OF-2	8.36	22.41	15.56	0.78	0.131	0.77	19.95
OF-3	8.31	18.79	13.24	0.85	0.096	0.53	15.58

Relative Abundance of Elements in Organic Fertilizers by EDXRF Method

The EDXRF spectra of prepared organic fertilizers are shown in Figures 6 (a), (b), and (c). The presence of silicon, calcium, potassium, iron, sulphur, titanium, manganese, zinc, strontium, copper, chromium, rubidium, zirconium, vanadium, and yttrium. It was observed that each spectrum indicated the presence of relevant elements for plant growth in organic fertilizers. The content of silicon, calcium, and potassium is higher than other elements in these organic fertilizers. These organic fertilizers have the highest content of silicon.

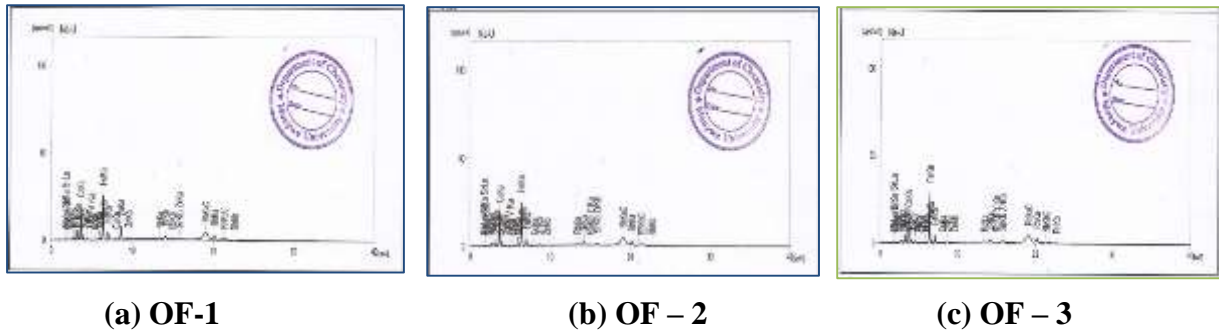


Figure 6. EDXRF spectra of organic fertilizer (OF-1, OF-2, and OF-3)

Application of Organic Fertilizers by Cultivation of Peanuts

The field experiments were carried out on the farm at Kyawe Pone village, Yenanchaung Township, Magway Region Myanmar. From 23rd July, 2022, to 27th October, 2023, to study the effect of organic fertilizers on the growth of peanuts. The field was well prepared since good tillage is required for raising a good crop.

The size of each experimental plot design was (16 x 3) square feet for treatments. Each plot has one row. The row and plant spacing was 18 inches. Weeding and pest control were carried out whenever necessary. The use of fertilizers may affect, either directly or indirectly, the availability of soil nutrients. The application of fertilizer, particularly moisture, is one of the most important factors for the growth of plants.

Fertilizers observed in general stimulate early crop growth. Fertilizers may also have little effect on the rate of growth of certain crops, but at harvest, a decided increase in yield is noted (Rahman, 1991).

In this research, plant height, leaf length, number of seeds, and yield of peanut (*Arachis hypogaea* L.) were measured. The fieldwork did not only measure the rate of growth of peanuts, but also yield production. The results are shown in Figures 7 and 8, which show photographs of peanut plant growth on the farm.

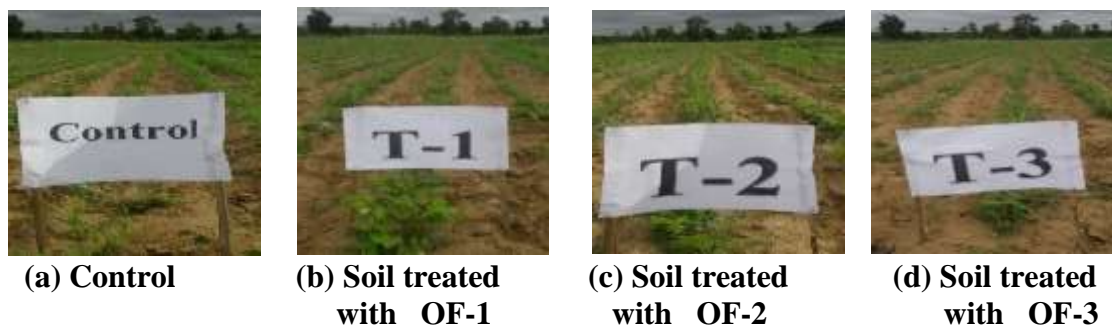


Figure 7. The photographs of peanut plant growth on the farm



Figure 8. Peanut plants grown on soil treated with organic fertilizers

Measurement of growth of peanut

From the time of cultivation to the harvested time, the time frame for peanuts is 120 days. The growth factors of the peanut were evaluated in terms of the plant height (cm) and the number of peanuts. Plants were measured for eighteen randomly selected plants from the sample area. The sample plants were measured after 15 days of cultivation until maturity. The effect of organic fertilizer on plant height, plant width, and leaves of peanut is shown in Figure 9. Indicates a progressive increase in plant height with the age of the crop. The plant height of peanuts at (15, 45, 75, and 120) days after cultivation was recorded in treatments with organic fertilizers. The time frame was 120 days from the time of cultivation to the harvested time for peanuts. During this time frame, the growth and yield of peanuts are shown in Table 4. The growth characteristics of the peanut were analyzed in terms of the plant height (cm) and yield. The plant height was found to be 7.4 cm in control and T-1, 8.9 cm in T-2, and 9.9 cm in T-3 at 15 days. The plant height of peanuts increased with the increase in the growth period. After 120 days, the peanut plant height was found 43.18 cm in control and T-1, 45.72 cm in T-2, and 50.8cm in T-3. From these results, the highest plant was found to be in T-3. The plant height of control and T-1 was found to be shorter than the others.

Yield of peanuts

The yield of peanuts in T-3 was significantly higher than of control, T-1, and T-2. The highest yield of T-3 was 5.22 kg and the lowest yield of control was 3.91 kg in fresh weight on 100 plants. The highest yield of peanut in T-3 was 725.58 kg/ha, and the lowest yield of control and T-1 was 543.49 kg/ha. From these results, it was observed that the yield of peanuts applied with organic fertilizer was greater than that of these plants without the application of organic fertilizer. Thus, it can be reported that organic fertilizer can increase the growth and productivity of peanuts. Figure 10 shows the yield of peanuts.

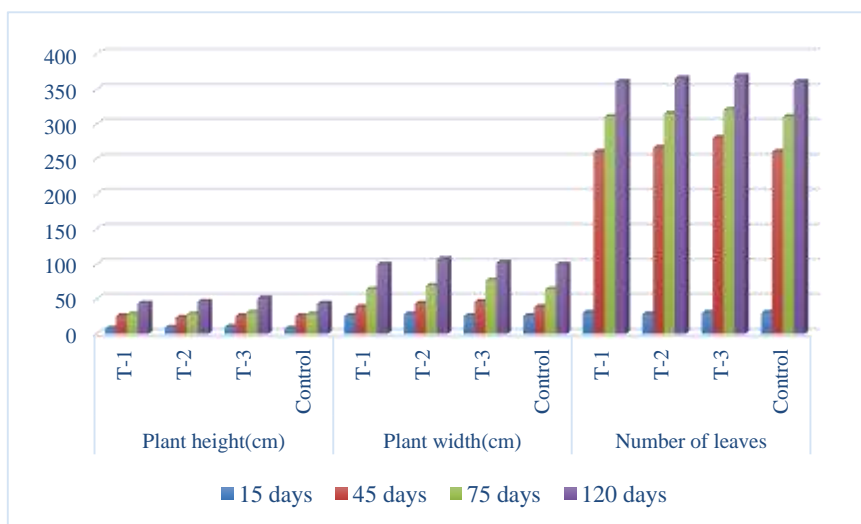


Figure 9. Plant height, plant width, and number of leaves of peanut plant on different days during cultivation

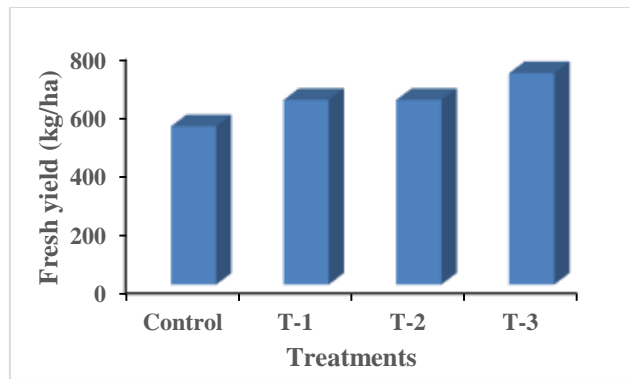


Figure 10. Yields of peanut plants

Analysis of the Farm Soil Before and After Cultivation

Soil is the most essential natural nutrient for vegetable and crop productivity. The fertility of soil can be assessed by the quality and stand of crop growth and yield. After cultivation of the plants, the texture, pH, electrical conductivity, organic matter, total N, available P_2O_5 , available K_2O , exchangeable Ca^{2+} , exchangeable Mg^{2+} , exchangeable Na, and C/N ratio of soil treated with organic fertilizers (OF-1, OF-2, and OF-3) were investigated. The prepared organic fertilizers treated soils were compared with the control soil and the before cultivation soil.

The farm soil samples 1 (control), T-1 (soil treated with OF-1), T-2 (soil sample treated with OF-2), and T-3 (soil sample treated with OF-3) were composed of sand (83.90 %, 83.92 %, 84.64 %, and 84.13 %), silt (7.02 %, 6.89 %, 7.10 %, and 6.01 %) and clay (9.08 %, 9.19 %, 8.26 %, and 9.86 %) respectively. These farm soils were classified as loamy sand soil. According to the results, OF-2 treated soil (T-2) has the highest sand percentage 84.64 %. The clay content of T-3 was higher than that of soil samples T-1 and T-2, and the silt content of T-2 was higher than that of T-1, T-3, and other soil samples. The increase in sand content and decrease in silt content are indicative of the translocation of the three phases of sand, silt, and clay which may have taken place. It includes the mineralization of silt accompanied by aggregation into the sand phase (Orellana *et al.*, 1990).

The pH of these soils is slightly alkaline. The pH values of the soil samples before and after cultivation (control, T-1, T-2, and T-3) are 8.05, 8.01, 8.38, 8.36, and 8.3, respectively. Alkaline soil has a pH of 7.5 to 8.5, and acidic soil has a pH of 4.0 to 6.5. Several essential elements tend to become less available as the pH is raised from 5 to 7.4 or 8.0. At pH values below about 5, aluminum, iron, and manganese are often soluble in sufficient quantities to be toxic to the growth of some plants. The pH of the soil affects the root system and its capacity to absorb other nutrients (Srikanth, 1997).

The values of electrical conductivity of soil samples before and after cultivation (control, T-1, T-2, and T-3) were 0.07, 0.06, 0.05, 0.06, and 0.05 dS/m. The electrical conductivity of soil samples is similar in all three samples. The electrical conductivity is the most important measure of soil salinity and is indicative of the ability of the aqueous solution to carry an electric current.

The organic matter of soil samples before and after cultivation (control, T-1, T-2, and T-3) was 0.54, 0.42 %, 0.59 %, 0.78 %, and 0.62 %. Soil sample T-2 had the highest organic matter content. It releases nutrients for plant growth, promotes the structure, biological, and physical health of the soil, and is a buffer against harmful substances (Reijneveld, 2013).

The nitrogen content of soil samples before and after cultivation (control, T-1, T-2, and T-3) was 36, 51, 53, 55, and 56 % for each sample. The available phosphorous content of soil samples before and after cultivation (control, T-1, T-2, and T-3) was 1.72, 1.40, 1.70, 1.71, and 1.82 mg/kg, respectively. The content of soil sample T-3 was higher than control, T-1, and T-2. The available potassium content of soil samples (control, T-1, T-2, and T-3) were 78.66, 88, 109.9, 99, and 97 mg/kg. The available potassium content of soil sample T-1 was highest in these soil samples and the lowest was before the cultivation soil sample. The organic carbon content, pH, electrical conductivity, and exchangeable cations of control, T-1, T-2, and T-3 soils were permanently slightly changed under cultivation because most of them were removed from the soil by the crop produced. After harvesting, nitrogen content, available phosphorus, and available potassium were observed to be higher in organic fertilizer-treated soil than before cultivation soil to maintain and sustain soil fertility. The exchangeable Ca^{2+} , Mg^{2+} , and Na amounts were found to be lower before the cultivation of peanuts. The results of Ca^{2+} contents before cultivation and after cultivation (control, T-1, T-2, and T-3) were 10.3, 9.50, 13.21, 11.72, and 11.83 Cmol/kg, respectively. The amounts of Mg^{2+} contents were 3.95, 2.55, 2.86, 2.59, and 2.83 Cmol/kg. The exchangeable amounts of Na were 0.20, 0.12, 0.13, 0.15, and 0.16, respectively. According to these data, it was found that applying organic fertilizers can improve soil fertility and crop production.

Conclusion

This research is concerned with the investigation of the preparation, and characterization of organic fertilizer from neem leaves, cow dung, and peanut shell. The physicochemical properties of pH in neem leaves, cow dung, and peanut shells were (6.2, 7.5, and 6.5). According to these data, the raw materials were used as the main ingredients for the preparation of organic fertilizer. The organic fertilizers (OF) were prepared by three different weight ratios of neem leaves, cow dung, and peanut shell (100 kg: 100 kg: 100 kg) for OF-1, (125 kg: 75 kg: 100 kg) for OF-2, and (150 kg: 50 kg: 100 kg) for OF-3 respectively. pH values of organic fertilizer were observed to be slightly alkaline. Field experiments conducted to test the effect of organic fertilizer on the growth of peanuts with four treatments: control, T-1 (soil treated with OF-1), T-2 (soil treated with OF-2), and T-3 (soil treated with OF-3). The yield percent of peanuts in T-3 had significantly higher values than those of control, T-1, and T-2. The highest yield of T-3 was 725.58 kg/ha, and the lowest yield of peanut in control was 543.49 kg/ha. The result of this work showed that organic fertilizer increases the growth and productivity of peanuts. The soil parameters viz the organic carbon content, pH, electrical conductivity, and exchangeable cations of control, T-1, T-2, and T-3 soil showed slight changes under the cultivation of peanuts. After harvesting, nitrogen content, available phosphorus, and available potassium were higher in organic fertilizer-treated soil than on the soil untreated. The application of organic fertilizer is one of the local needs of farmer, cultivating cash crop. This research shows some contributions to the theme of rural area development.

Acknowledgements

We would like to express our heartfelt thanks to Dr. Cho Cho Myint, Rector, Yenanchaung University for her encouragement to do this research. We are also thankful to our research group for their effort. We are also thankful to the Department of Higher Education for the necessary supplement.

References

- Antil, R. S. and M. Singh. (2007). "Effects of Organic Manures and Fertilizers on Organic Matter and Nutrients Status of the Soil". *Archives of Agronomy and Soil Science*, vol. 53, pp.519-528.
- Barber, S. A. (1995). *Soil Nutrient Bioavailability. A Mechanistic Approach*. New York: 2nd Ed., Wiley
- Barker, A.V. and D. J. Pilbeam. (2010). *Handbook of Plant Nutrition*. Boca Raton, FL: CRC Press
- Bhatt, M. K., R. Labanya and H. C. Joshi. (2019). "Influence of Long-term Chemical Fertilizers and Organic Manures on Soil Fertility - A Review". *Universal Journal of Agricultural Research*. vol. 7(5), pp.177-188.
- Bissonnais, Y. (1996). "Aggregate Stability and Assessment of Soil Crustability and Erodibility. Theory and Methodology". *J. Soil Sci.* vol. 47, pp.425-437.
- Chen, Z. C. and J. F. Ma. (2013). "Magnesium Transporters and their Role in Al Tolerance in Plants". *Plant Soil*, vol. 368, pp.51-56.
- Cobb, K. and J. Rosenfield. (1991). *Municipal Compost Management*. Cornell University Waste Management Institute
- Dai, Z., Y. Liu., X. Wang and D. Zhao. (1998). "Changes in pH, CEC and Exchangeable Acidity of Some Forest Soils in Southern China during the Last 32-35 years". *Water Air Soil Pollut.*, vol. 108, pp.377-390.
- Epstein, E. and A. J. Bloom. (2005). *Minerals Nutrition of Plants: Principles and Perspectives*. Second Edition. Sunderland, MA: Sinauer Associates
- Fathima, S. K. (2004). *Investigations on the Biology and Management of Phomopsis Azadirachtae on Neem*. Mysore, India: Ph.D. thesis, University of Mysore
- Hansch, R. and R. R. Mendel. (2009). "Physiological Functions of Mineral Micronutrients (Cu, Zn, Mn, Fe, Ni, Mo, B, Cl)". *Curr. Opin. Plant Biol*, vol. 12, pp.259-266.
- Hlaing, T. T. (2021). *Preparation of Organic Fertilizer from Banana Leaf with Cow Dung for Cultivation of Chilli (Capsicum annuum L.)*. Maubin: MSc Thesis, Department of Chemistry, Maubin University.
- Hungria, M. and M. A. T. Vargas. (2000). "Environmental Factors Affecting N₂ Fixation in Grain Legumes in the Tropics, with an Emphasis on Brazil". *Field Crops Research*, vol. 65, pp.151-164.
- Jones, Jr. (1998). *Plant Nutrition Manual*. Boca Raton, FL: CRC Press. p.149.
- Orellana, M., R. G. Barber and O. Diaz. (1990). "Effects of Deep Tillage and Fertilization on the Population, Growth, and Yield of Soya During an Exceptionally Wet Season on a Compacted Sandy Loam". *Research Soils and Tillage*, vol.17, pp.47-61.
- Rahman, S. (1991). "Influence of Organic Matter on the Yield and Mineral Nutrition of Modern Rice and Soil Properties". *Bangladesh: Bangladesh Rice Journal*, vol. 2, pp.107-112
- Reijneveld, J. A. (2013). *Unraveling Changes in Soil Fertility of Agricultural Land in the Netherlands*. Wageningen: Wageningen University, pp.201-214
- Sawhney, B. L. (1976). "Leaf Compost for Container-grown Plants". *Journal of Hortscience*. vol.11(1): pp.34-35
- Schoonover, J. E. and F. Jackie. (2015). "An Introduction to Soil Concepts and the Role of Soils in Watershed Management". *Journal of Contemporary Water Research & Education*. vol.154: pp.21-47
- Srikanth, K. 1997. *Enrichments of Compost and its Effect on Soil Properties and Crop Growth*. Bangalore: Ph.D Thesis, University of Agricultural Sciences

THREE FRIEDELANE TRITERPENOIDS FROM THE BARK OF *SALIX ALBA* L. (WHITE WILLOW)

Yin Yin Myint¹, Naw Li Li Yan², Mya Thandar Aung³, Ni Ni Than⁴

Abstract

White willow (*Salix alba* L.) grows throughout Africa, North America, Europe, and Asia. The genus *Salix* has traditionally been used in folk medicine for different kinds of pain due to the presence of salicylic acid. This paper highlights the isolation of three friedelane triterpenoids: 3-oxo friedelane (L-1, 0.006 %, m.pt 258-260 °C), 3- β -hydroxyl friedelane (L-2, 0.04 %, m.pt 275-277 °C) and 3-oxofriedelan-21-acetate (L-3, 0.046 %, m.pt 303-305 °C) from the pet ether extract of the bark of *Salix alba* L. These compounds were isolated using column chromatographic method and identified by FT IR, ¹H NMR, and ¹³CNMR,

Keywords: *Salix alba* L., 3-oxo friedelane, 3- β -hydroxyl friedelane, 3-oxofriedelan-21-acetate

Introduction

Terpenes are the most extensive and varied class of secondary metabolites produced by plants. Numerous scholars have detailed the wide uses of terpenoids (derivatives of terpene containing different functional groups) for the treatment of many diseases due to their broad range of biological activities. More than 400 naturally occurring friedelane triterpenoids have been identified. Friedelin and 3 β -friedelinol are pentacyclic triterpenoids commonly distributed in plants and are found in edible fruits, vegetables and frequently coexist with each other. Friedelin and its derivative 3 β -friedelinol are reported to have significant pharmacological potential, including antibacterial, anti-viral, and cytotoxic properties. Friedelane triterpenoids could be considered as promising candidates in drug development against human coronaviruses, including SARS-CoV-2 (Radi, *et al.*, 2023). The aim of this paper is structural identification, physicochemical properties and spectral data of the isolated organic constituents from the bark extract of *Salix alba* L. The bark of *Salix alba* L. is particularly used to treat many different types of pain including rheumatic pain, back pain, toothache and menstrual cramps. *Salix alba* L., commonly known as white willow, is the original source of salicin. It belongs to Salicaceae, and its Myanmar name is Moe-ma-kha.

The genus *Salix* have been reported to possess altogether 322 secondary metabolites including flavonoids, phenolic glycosides, organic acids, non-phenolic glycosides, sterols and terpenes, lignins, and non volatile fatty acids (Tawfeek *et al.*, 2021).



Figure 1. Photographs of plant of *Salix alba* L. and stem bark

¹ Department of Chemistry, Hinthada University

² Department of Chemistry, Hpa-An University

³ Department of Chemistry, University of Yangon

⁴ Department of Chemistry, University of Yangon

Materials and Methods

Sample Collection and Preparation

The bark of *Salix alba* L. was collected from Yankin township, Yangon Region, in April, 2016. The scientific name of this plant was verified at the Department of Botany, Dagon University. The sample was washed thoroughly with water and air dried at the room temperature. The dried samples were cut into small pieces and ground into fine powder by using a grinder.

Chemicals and Reagents

All the solvents and chemical reagents were used of the laboratory grade.

Apparatus and Instruments

Gallenkamp melting point apparatus, FT IR (8400) spectrophotometer (Shimadzu, Japan), and NMR spectrometer (JEOL, USA) with 500 MHz for ^1H NMR spectra and 125 MHz for ^{13}C NMR spectra were used. The NMR spectra were run on the CDCl_3 solution of the sample.

Isolation of Friedelane Triterpenoids from the Bark of *Salix alba* L.

Three compounds; L-1, L-2 and L-3 (friedelane triterpenoids) were isolated from the petroleum ether extract of the dried powder of bark of *Salix alba* by column chromatographic method. Firstly, the dried powder (300 g) *Salix alba* bark was directly soaked with 1 L of petroleum ether (PE) (60- 80 °C) at room temperature, for one week and filtered. This procedure was repeated three times. The combined filtrates were evaporated under reduced pressure by means of a rotatory evaporator. The petroleum ether (1.27 g) extract were fractionated on a glass column (60 cm \times 1.5 cm) packed with 150 g of silica gel (40-60 μm , Merck). Elution was carried out by 100% petroleum ether, followed by gradient elution with petroleum ether and ethyl acetate (EA) mixtures; 90:1 to 40:1 v/v. The flow rate was adjusted to about one drop per five seconds. Six main fractions F-I, F-II, F-III, F-IV, F-V, and F-VI were collected after combination of different fractions on the basis of their behaviors on TLC. The isolated compound L-1 (20 mg, 0.006%, as colourless needle shape crystals) was purified from fraction F-II by washing with pet ether and followed by crystallization with chloroform. The compound L-2 (120 mg, 0.04%, colourless powder) was obtained by rechromatography of fraction F-IV, on a silica gel column (60 x 0.75 cm), using 30 g of silica gel and gradient elutions with 100% petroleum ether and petroleum ether: ethyl acetate (80:0.1 to 80:1 v/v) mixtures. Compound L-3 (138 mg, 0.046%) in the form of needle shaped crystals, was obtained through rechromatography of fraction F-VI, using silica gel column and gradient elution with 100% petroleum ether, petroleum ether:ethyl acetate (90:0.1 to 40:1 v/v) mixtures. All the isolated compounds; L-1, L-2 and L-3 were treated with colour reaction tests and recorded the R_f values. The melting point of each isolated compound was measured using Gallenkamp melting point apparatus. FT IR and NMR spectra were recorded on FT IR (8400) and NMR (JEOL, USA) spectrometers.

Results And Discussion

Physicochemical Characterization and Identification of Isolated Compounds

All the isolated compounds; L-1, L-2 and L-3 were UV inactive under UV lamp (254 nm and 365 nm) and the type of compounds were preliminary checked by colour reaction tests as well as their R_f values (0.48, 0.33 and 0.28) with PE: EA (15: 1 v/v) eluent as presented in Table 1 and Figure 2. These compounds were soluble in petroleum ether, chloroform, ethyl acetate, and

methanol but insoluble in water. The melting points of L-1, L-2 and L-3 were found to be 258-260 °C, 275 -277 °C and 303- 305 °C, respectively.

Compound L-1: The FT IR spectrum of compound L-1 indicated the strong absorption band of carbonyl functional group at 1713 cm^{-1} which appeared due to the C=O stretching vibration of carbonyl group of cyclohexane. The absorption bands at 2917 cm^{-1} and 2848 cm^{-1} were assigned to symmetric and asymmetric C-H stretching in $-\text{CH}_2$ and $-\text{CH}_3$ groups. The absorption bands at 1461 cm^{-1} and 1388 cm^{-1} correspond to the bending vibration of $-\text{CH}_2$ and $-\text{CH}_3$ groups. The absorption band at 719 cm^{-1} corresponds to rocking of $-\text{CH}_2$ group. In ^1H NMR spectra of compound L-1 indicated that it contained totally 50 protons. It provided eight methyl proton signals at δ_{H} 0.87 ppm (H-23, d, J 6.4 Hz), 0.72 ppm (H-24, s), 0.88 ppm (H-25, s), 1.00 ppm (H-26, s), 1.05 ppm (H-27, s), 1.18 ppm (H-28, s), 1.00 ppm (H-29, s) and 0.95 ppm (H-30, s). In addition, the numerous methylene signals appeared at δ_{H} 1.23 ppm to 2.41 ppm.

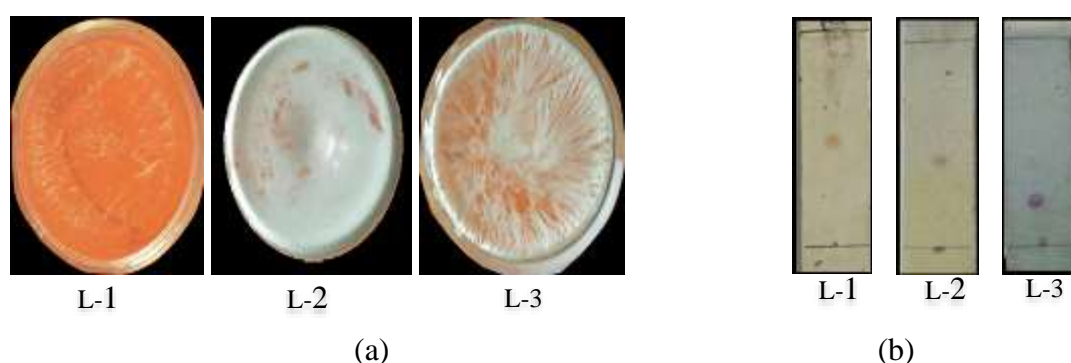


Figure 2. (a) Photograph of crystals, and (b) thin layer chromatograms of isolated compounds L-1, L-2 and L-3 (PE: EA, 15:1 v/v, sprayed with 5% H_2SO_4 , Δ)

Table 1. Results of Physicochemical Properties of the Isolated Compounds

Reagent	Observation			Remark
	L-1	L-2	L-3	
5 % H_2SO_4 , Δ	Brown colour	Brown colour	Brown colour	Presence of organic compound
10 % FeCl_3	No colour change	No colour change	No colour change	Absence of phenolic OH
Bromocresol green	No colour change	No colour change	No colour change	Absence of organic acid
Liebermann-Burchard, Δ	Light pink colour	Light pink colour	Pale pink colour	Terpenoid compound
Anisaldehyde/ H_2SO_4 , Δ	Pale violet colour	Violet colour	Purple colour	Terpenoid compound
R_f , (PE:EA 15:1 v/v)	0.48	0.33	0.28	

*Randerath, 1966

The ^{13}C NMR (125 MHz, CDCl_3) of compound L-1 indicated the presence of eight methyl carbons, eleven methylene carbons, four methine carbons and six quaternary carbons and one carbonyl carbon. The carbon signals for eight methyl carbons were observed at δ_{C} 7.1 ppm (C-23), 15.0 ppm (C-24), 18.3 ppm (C-25), 20.6 ppm (C-26), 19.0 ppm (C-27), 32.4 ppm (C-28), 35.4 ppm (C-29) and 32.1 ppm (C-30) whereas eleven methylene carbons were assigned at δ_{C} 22.6 ppm (C-1), 41.9 ppm (C-2), 41.7 ppm (C-6), 18.6 ppm (C-7), 36.0 ppm (C-11), 30.9 ppm

(C-12), 32.8 ppm (C-15), 36.4 ppm (C-16), 35.7 ppm (C-19), 33.1 ppm (C-21) and 39.6 ppm (C-22). And also four methine carbons appeared at δ_c 58.6 ppm (C-4), 53.5 ppm (C-8), 59.9 ppm (C-10) and 43.2 ppm (C-18). Moreover, six quaternary carbons appeared at δ_c 42.5 ppm (C-5), 37.8 ppm (C-9), 40.1 ppm (C-13), 38.7 ppm (C-14), 30.4 ppm (C-17) and 28.5 ppm (C-20). The one carbonyl group was found as δ_c 213.4 ppm (C-3). According to the results, the molecular formula of compound L-1 is C₃₀H₅₀O.

Table 2. NMR Spectral Data of Isolated Compound L-1 with 3-oxo Friedelane (Friedelin)

C Position	C-Type	Observed (δ in ppm, CDCl ₃)		3-oxo Friedelane * (δ in ppm, CDCl ₃)	
		¹ H	¹³ C	¹ H	¹³ C
		(500 MHz)	(125 MHz)	(400 MHz)	(100MHz)
1	CH ₂	1.97	22.6	1.97,1.57	22.3
2	CH ₂		41.9	2.30, 2.29	41.5
3	C=O		213.4		213.3
4	CH	2.25(m)	58.6	2.25	58.3
5	C		42.5		42.2
6	CH ₂		41.7	1.74	41.3
7	CH ₂		18.6	1.38	18.3
8	CH		53.5		53.1
9	C		37.8	1.53	37.5
10	CH		59.9	1.47	59.5
11	CH ₂		36.0		35.6
12	CH ₂		30.9		30.5
13	C		40.1		39.7
14	C		38.7		38.3
15	CH ₂		32.8	1.59	32.5
16	CH ₂		36.4		36.0
17	C		30.4		30.0
18	CH		43.2		42.9
19	CH ₂		35.7		35.4
20	C		28.5		28.2
21	CH ₂		33.1	1.53,1.38	32.3
22	CH ₂		39.6	0.94	39.3
23	CH ₃	0.87 (<i>d</i> , <i>J</i> =6.4 Hz)	7.1	0.87(<i>d</i>)	6.9
24	CH ₃	0.72(<i>s</i>)	15.0	0.71(<i>s</i>)	14.2
25	CH ₃	0.88(<i>s</i>)	18.3	0.86(<i>s</i>)	18.1
26	CH ₃	1.00(<i>s</i>)	20.6	1.06(<i>s</i>)	20.3
27	CH ₃	1.05(<i>s</i>)	19.0	1.04(<i>s</i>)	18.7
28	CH ₃	1.18(<i>s</i>)	32.4	1.17(<i>s</i>)	32.1
29	CH ₃	1.00(<i>s</i>)	35.4	0.99(<i>s</i>)	35.1
30	CH ₃	0.95(<i>s</i>)	32.1	0.94(<i>s</i>)	31.8

* Odeh, *et al.*, 2016

¹H NMR and ¹³C NMR spectral data of compound L-1 matched with the reported compound 3-oxofriedelane see in Table 2 and Figures 3 and 5 (Odehl, *et al.*, 2016). Quintansa, *et al.*, 2014 reported that melting point of 3-oxofriedelane is 258-260°C. Therefore, compound L-1

was finally proved to be 3-oxofriedelane by comparison of its ^1H NMR and ^{13}C NMR spectral data and melting point. The structure of 3-oxofriedelane is shown in Figure 3(a).

Compound L-2: In the FT IR spectrum of compound L-2, the absorption band at 3466 cm^{-1} corresponds to the O-H stretching and frequencies at 1448 cm^{-1} and 1384 cm^{-1} which were indicative of bending O-H. The absorption bands at 1257 cm^{-1} , 1172 cm^{-1} , 1020 cm^{-1} and 1000 cm^{-1} were observed for C-O stretching vibration of alcohol. The absorption bands at 2930 cm^{-1} and 2869 cm^{-1} represent the asymmetric and symmetric C-H stretching vibration of $-\text{CH}_2$ and $-\text{CH}_3$ groups. Besides, in plane bending of O-H of primary and secondary alcohols which was coupled with C-H bending vibration of $-\text{CH}_2$ and $-\text{CH}_3$ group occurred at $1420\text{--}1330\text{ cm}^{-1}$ (Silverstein, *et al.*, 2009). The ^1H NMR spectrum indicated eight methyl protons signals at δ_{H} 1.01 ppm (H-23, d, $J = 7.5\text{ Hz}$), 1.02 ppm (H-24, s), 0.87 ppm (H-25, s), 0.96 ppm (H-26, s), 0.98 ppm (H-27, s), 1.18 ppm (H-28, s), 0.94 ppm (H-29, s) and 1.02 ppm (H-30, s). In addition, one singlet signal of methine proton attached with one -OH appeared at δ_{H} 3.73 ppm.

Table 3. NMR Spectral Data of Isolated Compound L-2 and 3- β -hydroxyl Friedelane (3- β - Friedelinol)

C Position	C-Type	Observed (ppm)		3- β -hydroxyl Friedelane* (ppm)	
		^1H (δ) (500 MHz, CDCl_3)	^{13}C (δ) (125MHz, CDCl_3)	^1H (δ) (400 MHz, CDCl_3)	^{13}C (δ) (100 MHz, CDCl_3)
1	CH_2		16.2	1.69(<i>dt</i> ,13,3, H_{ax}) 1.45(H_{eq})	16.2
2	CH_2		35.7	1.99(<i>qd</i> ,13,3, H_{ax}) 0.99(H_{eq})	36.1
3	CH-OH	3.73	73.1	3.81(<i>q</i> like,2, H_{eq})	71.6
4	CH		49.6		49.6
5	C		38.2		38.1
6	CH_2		42.1	1.76(<i>td</i> ,12,3, H_{eq}) 0.99(H_{ax})	41.9
7	CH_2		17.9	1.41,1.39	17.7
8	CH		53.6	1.28(H_{ax})	53.3
9	C		37.5	1.25(H_{ax})	37.2
10	CH		61.8	0.93(<i>dd</i> ,12, 2, H_{ax})	61.7
11	CH_2		35.6	1.42, 1.24	35.7
12	CH_2		31.0	1.34, 1.31	30.7
13	C		38.7		38.4
14	C		40.1		39.7
15	CH_2		33.2	1.53, 1.28	32.3
16	CH_2		36.5	1.46, 1.18	35.9
17	C		30.0		30.1
18	CH		43.2	1.56(<i>dd</i> ,11,6, H_{ax})	42.9
19	CH_2		35.9	1.37, 1.21	35.4
20	C		28.7		28.2
21	CH_2		32.7	1.49,1.28	32.9
22	CH_2		39.7	0.93(<i>dd</i> ,12,2, H_{ax}) 1.49(H_{eq})	39.3
23	CH_3	1.01 (<i>d</i> , $J=7.5\text{ Hz}$)	12.0	1.02 (<i>d</i> , $J=7.0\text{ Hz}$)	12.1

C Position	C-Type	Observed (ppm)		3- β -hydroxyl Friedelane * (ppm)	
		^1H (δ) (500 MHz, CDCl_3)	^{13}C (δ) (125MHz, CDCl_3)	^1H (δ) (400 MHz, CDCl_3)	^{13}C (δ) (100 MHz, CDCl_3)
24	CH_3	1.02(s)	16.8	1.10(s)	16.6
25	CH_3	0.87(s)	18.6	0.89(s)	18.4
26	CH_3	0.96(s)	19.0	0.99(s)	18.6
27	CH_3	0.98(s)	20.5	1.02(s)	20.1
28	CH_3	1.18(s)	32.5	1.18(s)	32.1
29	CH_3	0.94(s)	35.4	0.97(s)	35.0
30	CH_3	1.02(s)	32.2	1.02(s)	31.9

*Salazar, *et al.*, 2000

The ^1H NMR spectrum of compound L-2 indicated totally 52 protons. The ^{13}C NMR spectrum indicated the presence of eight methyl carbons, eleven methylene carbons, five methine carbons and six quaternary carbons. The carbon signals for eight methyl carbons were observed at δ_c 12.0 ppm (C-23), 16.8 ppm (C-24), 18.6 ppm (C-25), 19.0 ppm (C-26), 20.5 ppm (C-27), 32.5 ppm (C-28), 35.4 ppm (C-29), 32.2 ppm (C-30) whereas eleven methylene carbons were assigned at δ_c 16.2 ppm (C-1), 35.7 ppm (C-2), 42.1 ppm (C-6), 17.9 ppm (C-7), 35.6 ppm (C-11), 31.0 ppm (C-12), 33.2 ppm (C-15), 36.5 ppm (C-16), 35.9 ppm (C-19), 32.7 ppm (C-21) and 39.7 ppm (C-22). And also four methine carbons appeared at δ_c 49.6 ppm (C-4), 53.6 ppm (C-8), 61.8 ppm (C-10) and 43.2 ppm (C-18). Moreover, six quaternary carbons appeared at δ_c 38.2 ppm (C-5), 37.5 ppm (C-9), 38.7 ppm (C-13), 40.1 ppm (C-14), 30.0 ppm (C-17) and 28.7 ppm (C-20). One hydroxyl group was found that it attached to C-3 at δ_c 73.1 ppm. The NMR spectral data of the isolated compound L-2 agree with the previously reported NMR spectral data of 3- β -hydroxyl friedelane (friedelinol), Table 3 and Figures 3 and 6 (Salazar, *et al.*, 2000). Thus, compound L-2 is suggested to be 3- β -hydroxyl friedelane, with the molecular formula of $\text{C}_{30}\text{H}_{52}\text{O}$, as confirmed by its spectral data and physicochemical properties. Figure 3(b) shows the structure of 3- β -hydroxyl friedelane.

Compound L-3: In the FT IR spectrum of isolated compound L-3, the two strong absorption bands at 1715 cm^{-1} and 1726 cm^{-1} are due to stretching $\text{C}=\text{O}$ of carbonyl group of hexacyclic ketone and ester, because the carbonyl group of ester has higher frequency than a normal ketone (Silverstein, *et al.*, 2009). The two strong absorption bands at 1245 and 1027 cm^{-1} show the C-O stretching of an ester. The absorption bands at 2923 cm^{-1} and 2862 cm^{-1} show symmetric and asymmetric C-H stretching vibration of $-\text{CH}_2$ and $-\text{CH}_3$ groups. The absorption band at 1453 cm^{-1} and 1388 cm^{-1} are due to C-H bending vibrations of $-\text{CH}_2$ and $-\text{CH}_3$ groups. Moreover, ^1H NMR spectral data of compound L-3 revealed the presence of 52 protons. It showed one secondary methyl signal at δ_H 0.87 ppm (3H, d, $J=6.5$ Hz, H-23), six tertiary methyl proton signals at 0.71 ppm (3H, s, H-24), 0.86 ppm (3H, s, H-25), 0.94 ppm (3H, s, H-26), 1.07 ppm (3H, s, H-27), 1.27 ppm (3H, s, H-28), 1.09 ppm (3H, s, H-29), 0.94 ppm (3H, s, H-30) and one methyl proton signal at 2.02 ppm (3H, s) of acetate ($-\text{OCOCH}_3$), the remaining methylene and methine signals showed chemical shifts between 1.27 - 1.95 ppm. A methine proton signal at 4.9 ppm (1H, dd, $J=15, 5$ Hz) is indicative of an attached acetate group. Its chemical shift and multiplicity suggest that this may correspond to a ring methine carbon. The isolated compound L-3 revealed that it has eight methyl carbons: at δ_c 6.9 ppm (C-23), 14.6 ppm (C-24), 18.0 ppm (C-25), 18.7 ppm (C-26), 18.9 ppm (C-27), 32.6 ppm (C-28), 30.3 ppm (C-29), and 26.1 ppm

(C-30); one methyl carbon of acetate ($-\text{OCOCH}_3$) at δ_{C} 21.2 ppm; two carbonyl carbons: at δ_{C} 213.2 ppm (C-3) for cyclic ketone and 171.3 ppm suggested the presence of another carbonyl carbon of acetate attached at ring carbon; four methine carbons: at δ_{C} 58.2 ppm (C-4), 52.2 ppm (C-8), 59.4 ppm (C-10) and 43.3 ppm (C-18); six quaternary carbons: at δ_{C} 42.1 ppm (C-5), 37.4 ppm (C-9), 39.2 ppm (C-13), 38.8 ppm (C-14), 31.8 ppm (C-17), and 33.4 ppm (C-20); and ten methylene carbons: at δ_{C} 22.2 ppm (C-1), 41.5 ppm (C-2), 41.2 ppm (C-6), 18.2 ppm (C-7), 34.6 ppm (C-11), 30.5 ppm (C-12), 31.5 ppm (C-15), 36.5 ppm (C-16), 35.8 ppm (C-19), and 43.6 ppm (C-22). ^{13}C NMR spectral data of compound L-3 was presented alongside the NMR spectral data of 3-oxofriedelane (compound L-1) and 3- β -hydroxy friedelan-21 α -acetate in Table 4 (Patra and Chaundhuri, 1987 and Anjaneyulu *et al.*, 1993). By comparing ^{13}C NMR spectral data, the upfield shift of $\text{C}=\text{O}$ at δ_{C} 213.2 ppm may be considered that same chemical shift of 3-position of 3-oxo friedelane. The chemical shift δ_{C} 171.3 ppm for $\text{C}=\text{O}$ of acetate group, it may be attached on ring D or E of pentacyclic triterpenoid of friedelane type that can be seen in Figure 3. The chemical shift 76.4 ppm for methine carbon (C-21) revealed the attachment of acetate. Furthermore, the comparable chemical shifts of L-1 (3-oxo friedelane) and L-3 indicated the downfield shift at δ_{C} 33.4 ppm for C-20 and 43.6 ppm for C-22 and upfield shift at 30.3 ppm for C-29 and 26.1 ppm for C-30 see in Table 4, Figures 5 and 7. Moreover, when a ring carbon atom is attached to an acetate group, the presence of carbonyl group induces a β -effect at the β -position carbon, leading to a downfield shift (higher ppm). At the same time, the electron donating methyl group in the acetate induces γ -effect at the γ -position carbon, leading to an upfield shift (lower ppm). In compound L-3, since an acetate group would attach at 21 position that caused β -effect on C-20 (+ 4.9 ppm) and C-22 (+ 4.0 ppm) and γ -effect on C-29 (-5.1 ppm) and C-30 (-6.0 ppm) were comparatively observed with 3-oxo friedelane (L-1) see in Table 4.

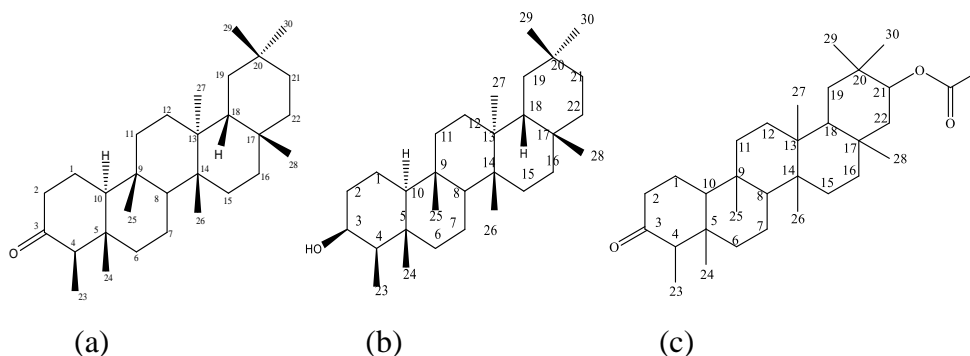


Figure 3. The possible chemical structure of isolated compounds

- (a) 3-oxofriedelane, L-1, (b) 3- β -hydroxyl friedelane, L-2 and
(c) 3-oxofriedelan-21-acetate. L-3

NMR spectral data of L-3 provided evidence of agreement and consistency with an acetate group attached at 21-position of 3-oxofriedelane. Thus, the possible chemical structure of isolated compound L-3 may be considered as 3-oxofriedelan-21-acetate see in Figure 3(c).

Table 4. NMR Spectral Data of Isolated Compound L-3 and 3-oxofriedelane and 3 β -OH friedelan-21 α - acetate

Carbon position	Observed data of L-3 (δ value ppm, CDCl ₃ <i>J</i> value in Hz)		3-oxofriedelane (δ value ppm, CDCl ₃)	*3 β -OH friedelan-21 α - acetate (¹³ CNMR, δ value ppm, CDCl ₃ , 50.32 MHz)
	¹ H NMR, 500MHz	¹³ CNMR, 125MHz	¹³ CNMR, 125MHz	
1		22.2	22.6	15.7
2		41.5	41.9	34.9
3		213.2	213.4	72.5
4		58.2	58.6	49.0
5		42.1	42.5	37.7
6		41.2	41.7	41.6
7		18.2	18.6	17.4
8		52.2	53.5	52.2
9		37.4	37.8	37.0
10		59.4	59.9	61.2
11		34.6	36.0	35.2
12		30.5	30.9	30.3
13		39.2	40.1	39.1
14		38.8	38.7	38.5
15		31.5	32.8	31.0
16		36.5	36.4	36.3
17		31.8	30.4	31.8
18		43.3	43.2	43.2
19		35.8	35.7	35.8
20		33.4	28.5	33.4
21	4.9 (dd, <i>J</i> =15, 5)	76.4	33.1	76.6
22		43.6	39.6	43.6
23	0.87 (<i>d</i> , <i>J</i> =6.5)	6.9	7.1	11.5
24	0.71 (<i>s</i>)	14.6	15.0	16.2
25	0.86 (<i>s</i>)	18.0	18.3	18.3
26	0.94 (<i>s</i>)	18.7	20.6	18.6
27	1.07 (<i>s</i>)	18.9	19.0	18.9
28	1.27 (<i>s</i>)	32.6	32.4	32.5
29	1.09 (<i>s</i>)	30.3	35.4	30.7
30	0.94 (<i>s</i>)	26.1	32.1	26.1
OCOCH ₃		171.3		171.4
OCOCH ₃	2.02(<i>s</i>)	21.2		21.1

*Patra and Chaundhuri 1987 and **Anjaneyulu, *et al.*, 1993

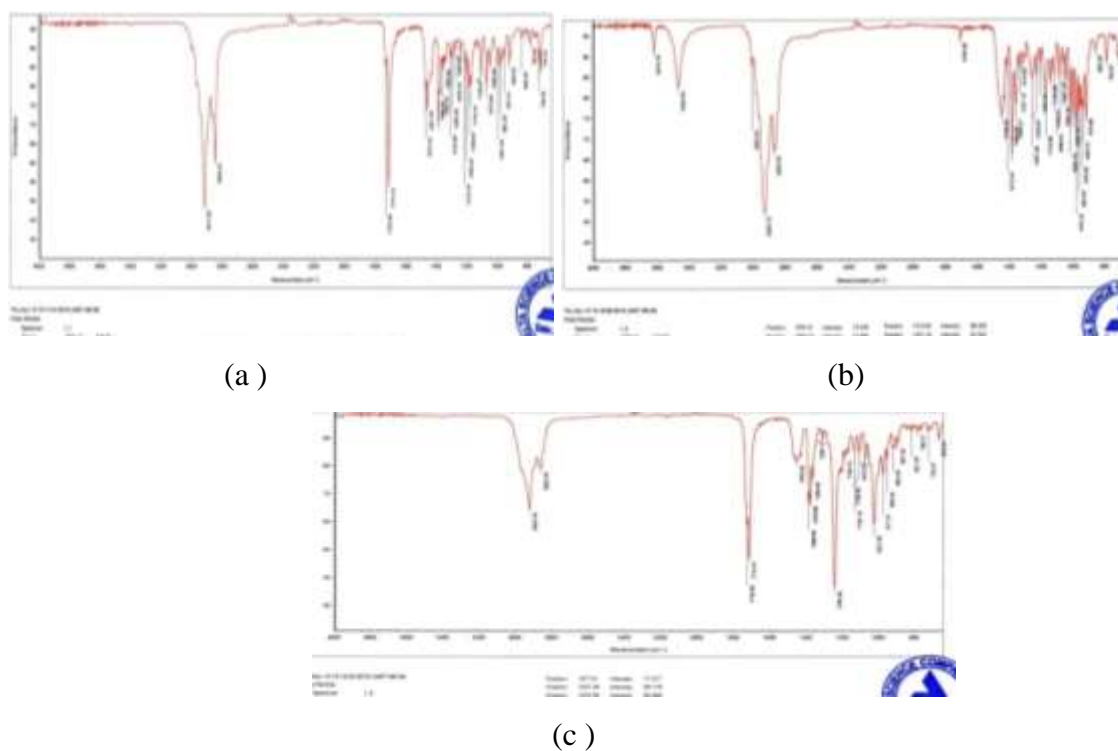


Figure 4. FT IR spectra of isolated compounds; (a) L-1, (b) L-2, and (c) L-3

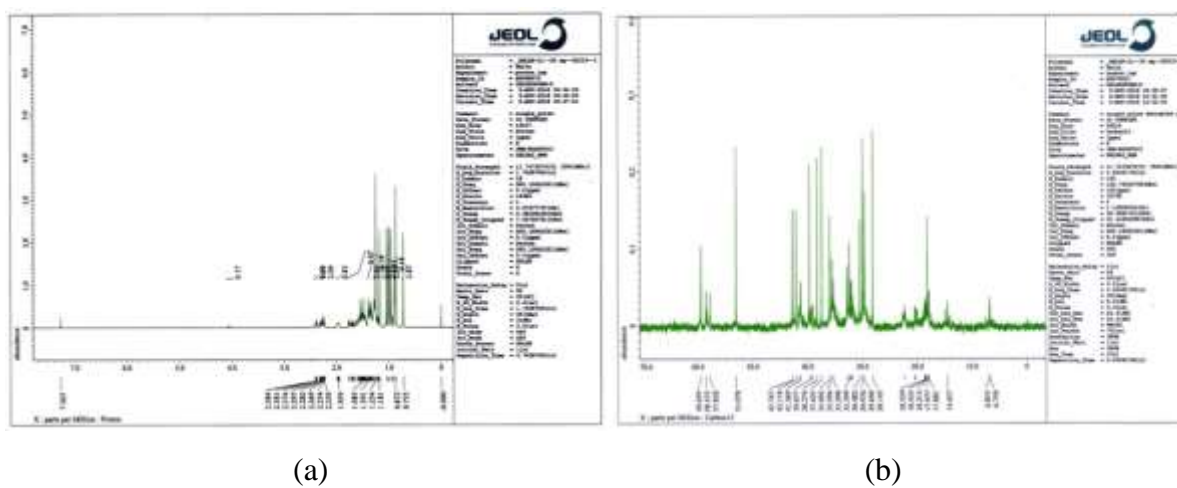


Figure 5. (a) ^1H NMR spectra of isolated compound L-1 (500 MHz, CDCl_3) and (b) ^{13}C NMR spectra of isolated compound L-1 (125 MHz, CDCl_3)

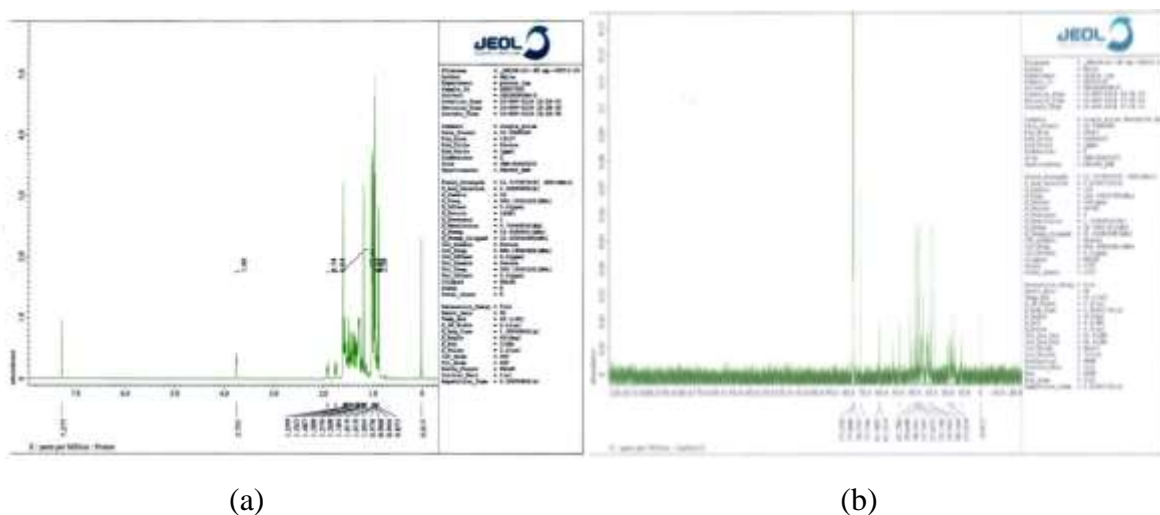


Figure 6. (a) ^1H NMR spectra of isolated compound L-2 (500 MHz, CDCl_3) and (b) ^{13}C NMR spectra of isolated compound L-2 (125 MHz, CDCl_3)

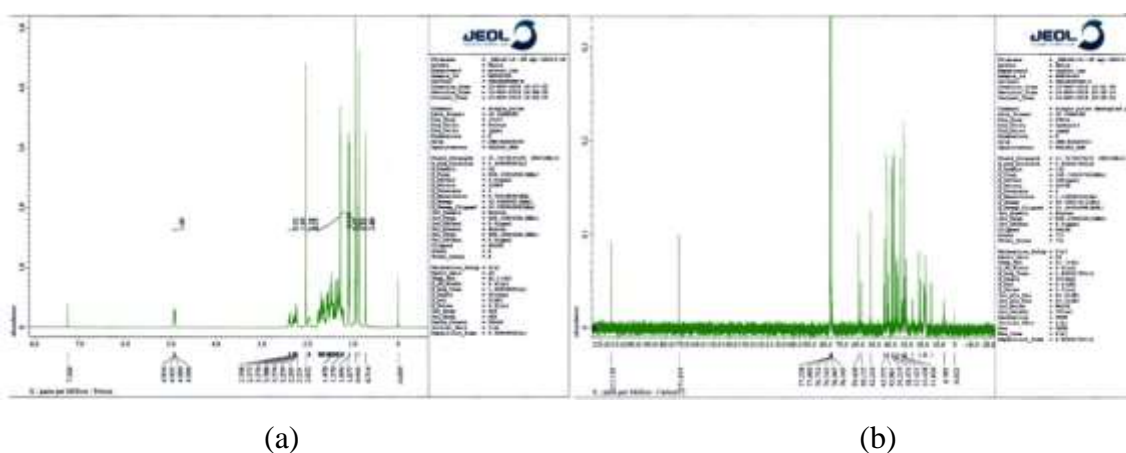


Figure 7. (a) ^1H NMR spectrum of isolated compound L-3 (500 MHz, CDCl_3) and (b) ^{13}C NMR spectrum of isolated compound L-3 (125 MHz, CDCl_3)

Conclusion

Three friedelane triterpenoids were isolated from the bark of *Salix alba* L., and their structures were elucidated as 3-oxofriedelane, 3- β -hydroxyl friedelane and 3-oxofriedelan-21-acetate by ^1H and ^{13}C NMR and FT IR, in combination with the reference data. According to numerous scientific studies, friedelane compounds have shown antioxidant, anticancer and anti-inflammatory properties. Thus, *in vitro* and *in vivo* studies should be conducted in the future to explore these properties.

Acknowledgements

The author would like to thank Dr. Ni Ni Than (Professor and Head, Department of Chemistry, University of Yangon) and the colleagues for their valuable support and contributions throughout this research.

Reference

- Anjaneyulu, V., J. S. Babu, H. Babu, K. Raw and J. D. Connolly. (1993). "Two D: A-Friedo- OleananeDerivatives from *Euphorbia tortills*". *Phytochemistry*, vol 33 (3), pp.647- 649
- Odeh, I.C., T.A. Tor-Anyiin, J.O. Igoli and J.V. Anyam. (2016). "In Vitro Antimicrobial Properties of Friedelin -3-one from *Pterocarpus Santalinoides* L.Herit, ex D C". *African Journal of Biotechnology*, vol.15 (14), pp.531-538
- Patra, A. and S. K. Chaudhuri. (1987). "Assignment of Carbon -13 Nuclear Magnetic Resonance Spectra of some Friedelanes". *Magnetic Resonance in Chemistry*, vol. 25 (2), pp. 95-100
- Quintansa, J.S.S., E.V. Costab, J.F. Tavaresc, T.T. Souzaa, S.S. Araujoa, C.S. Estevama, A. Barisonc, A.G.S. Cabrald, M.S. Silvad, M.R. Serafinia, and L.J. Quintans-Juniora. (2014). "Phytochemical Study and Antinociceptive Effect of the Hexanic Extract of Leaves from *Combretum Duarceanum* and Friedelin, a Triterpene Isolated from the Hexanic Extract, in Orofacial Nociceptive Protocols". *Brazilian Journal of Pharmacognosy*, vol 24 (1), pp.60-66
- Randerath, K. (1966). "Thin Layer Chromatography". Weinheim: 2nd Ed., Verlag Chemie, GmbH, Weinheim/Bergstr., pp. 1-291
- Radi, M.H. R. A. El-Shiekh, A. M. El-Halawany, and E. A. Sattar. (2023). "Friedelin and 3 β -Friedelinol: Pharmacological Activities". *Brazilian Journal of Pharmacognosy*, Springer Nature, pp.1-15
- Salazar, G.C.M., G.D.F. Silva, L.P. Duarte, S.A. Vieira Filho and I.S. Lula. (2000). "Two Epimeric Friedelane Triterpenes Isolated from *Maythenus Truncata* Reiss: ¹H and ¹³C Chemical Shift Assignment". *Magnetic Resonance in Chemistry*, vol.38 (11), pp. 977-980
- Silverstein, R.M. and F.X. Webster. (2005). "Spectrometric Identification of Organic Compounds". New York:6th Ed., John Willey and Sons Inc., pp.99-164
- Tawfeek, N., M. F. Mahmoud, D. I. Hamdan, M. Sobeh, N.I. Farrag, M. Wink, and A. M. El- Shazly. (2021). "Phytochemistry, Pharmacology Medicinal Uses Plants of the Genus *Salix*: An Updated Review". *Frontiers in Pharmacology*, vol. 12, pp.1-30

STRUCTURAL ELUCIDATION OF AN ORGANIC COMPOUND AND ESTIMATION OF ANTI-INFLAMMATORY AND ANTIARTHRITIC ACTIVITIES OF *BACOPA MONNIERI*

Aye Aye Thant¹, Yi Yi Win², Myint Myint Khine³, Ni Ni Than⁴

Abstract

The present research deals with the analysis to isolate and elucidate an organic compound and to assess the antiarthritic and anti-inflammatory activities of the aerial parts of *Bacopa monnieri* that were collected from Twantay Township, Yangon Region. By column and thin layer chromatography separation, the isolated compound structure was elucidated by physicochemical properties and modern spectroscopic techniques such as FT IR, ¹H NMR, ¹³C NMR spectroscopy, and ESI-MS spectrometry, as well as by comparing it with their reported data. *In vitro*, the anti-inflammatory activity of ethanol and watery extracts was evaluated by a nitric oxide inhibition assay. These results did not significantly affect cellular nitric oxide production or cell viability because of cytotoxicity. The ethanol, watery extract, and an isolated compound (bacosine) were assessed for antiarthritic activity. Diclofenac sodium was used as the reference drug. In the egg albumin method, the bacosine compound (IC₅₀ = 105.23 µg/mL) had a more significant antidenaturation effect than the ethanol extract (IC₅₀ = 162.44 µg/mL) and watery extract (172.71 µg/mL). In the bovine serum albumin method, the bacosine compound (IC₅₀ = 118.73 µg/mL) had a more significant antidenaturation effect than ethanol extract (IC₅₀ = 180.58 µg/mL) and watery extract (299.24 µg/mL) compared with diclofenac sodium (IC₅₀ = 73.44 µg/mL), respectively.

Keywords: *Bacopa monnieri*, antiarthritic activity, anti-inflammatory activity, bacosine

Introduction

Bacopa monniera (Figure 1) is a plant of the Scrophulariaceae family that is commonly known as Brahmi, thyme-leaved gratiola, water hyssop, herb of grace, and Indian pennywort. *Bacopa* has been used in traditional Ayurvedic treatments for epilepsy and asthma. It is one of the ingredients in many Ayurvedic formulations used for ulcers, tumours, ascites, splenomegaly, inflammatory disorders, leprosy, anaemia, and gastroenteritis. *B. monnieri* also exhibits potent antioxidant, anticancer, antiulcer, calcium antagonist, vasodilatory, mast cell stabilizing, anti-inflammatory, and antistress (Kishore *et al.*, 2017). The ethanol extract of *B. monniera* exhibited marked anti-inflammatory activity against carrageenan-induced paw oedema in mice and rats, an acute inflammatory model. To assess the possible mechanism of anti-inflammatory action against carrageenan, the ethanol extract was used to treat the chemical mediator-induced histamine, selectively inhibited prostaglandin E2-induced inflammation (Channa *et al.*, 2006). The current study estimates the anti-inflammatory potential of crude extracts. For the antiarthritic property, the crude extracts and an isolated compound of *B. monnieri* were examined.

¹ Department of Chemistry, University of Yangon

² Department of Chemistry, Mawlamyine University

³ Myingyan University

⁴ Department of Chemistry, University of Yangon



Figure 1. Photograph of *Bacopa monnieri*

Materials and Methods

Plant Material

The aerial parts of the plant were collected from the Twantay Township, Yangon Region, Myanmar, in May 2019 and identified as *B. monnieri*, by the authorized botanist at the Department of Botany, University of Yangon. The sample was dried in the shade for a week, cut into very small pieces, and then ground into a purely fine powder using an electric motor grinder. The powdered sample was stored in airtight containers to prevent moisture changes and contamination.

Extraction and Isolation of Pure Compounds

The dried powdered sample (500 g) was extracted with 95 % ethanol in an air-tight bottle for three days, and then filtered and concentrated by using a rotary evaporator at 70 °C under reduced pressure. This similar procedure was repeated three times until 40 g of the crude ethanol extract was obtained. The ethanol extract was extracted with petroleum ether, followed by ethyl acetate. The ethyl acetate extract (10 g) was subjected to column chromatography on a normal-phase silica gel GF₂₅₄ adsorbent increasing the polarity of the eluent solvent system (PE: EA), and five main fractions (F I to F V) were obtained. Fraction F II (PE: EA 7:1) was subjected to column chromatography with a PE-EtOAc gradient system. It was obtained in six fractions (fractions F-1 to F-6). Fraction F-2 gave an isolated compound (colourless crystals, 65 mg, 0.13 % yield based on the dried sample). The isolated compound was structurally identified by modern spectroscopic methods, including FT IR, ¹H NMR, and ¹³C NMR. The FT IR spectrum was measured at the University of Yangon and ¹H NMR, ¹³C NMR and ESI-MS were measured at Department of Chemistry, Faculty of Science and (NUS) National University of Singapore.

Anti-inflammatory Activity of Ethanol and Watery Extracts by Nitric Oxide Inhibition Assay

The nitric oxide (NO) inhibition assay was used to assess the anti-inflammatory effects of crude ethanol and watery extracts at Toyama University in Toyama, Japan. RAW 264.7 cells were expanded in-MEM supplemented with 10% incubated fetal bovine serum, 1% penicillin

(1000 U/mL), and streptomycin (10 mg/mL). The cells were harvested with a cell scraper and diluted to a suspension in fresh media, after the cell growth reached around 70 % confluent. A 100 μ L portion of RAW 264.7 (1×10^4 /well) was seeded in 96 well plates and incubated at 37 °C for 24 h. The sample was then treated with 50 μ L of each LPS (100 ng/mL) and different concentrations on the cell after a 24 h period of 37 °C incubation. Briefly stated, a fresh plate cell was created and filled with 100 μ L of each supernatant from 96 wells. After that, a fresh plate cell was put to an equivalent volume of Griess reagent (0.5% sulphanilamide, 0.05 % naphthylenediamide dihydrochloride, 2.5 % H₃PO₄) (Schmidt, 1996) and allowed it to stand for 10 min at room temperature. A microplate spectrophotometer was used to measure the absorbance at 540 nm. A positive control was employed, which was L-NMMA monoacetate. 100 μ L of each 10 % MTT solution (5 mg/mL) in the medium was added to the wells, after the residual medium from the initial plate was removed. The formazan crystal was dissolved with 100 μ L each of DMSO after 3 h of incubation, and the absorbance was measured at 570 nm with a microplate reader Jin *et al*, (2012). The following formulae were used to calculate the percentages of NO inhibition and cell viability:

$$\text{NO inhibition (\%)} = \left[\frac{A_{\text{control}} - A_{\text{sample}}}{A_{\text{control}}} \right] \times 100$$

$$\text{Cell viability (\%)} = 100 \times \left[\frac{(A_{\text{test sample}} - A_{\text{blank}})}{(A_{\text{control}} - A_{\text{blank}})} \right]$$

where, A_{control} = the absorbance of the control group treated by LPC alone,

A_{blank} = the absorbance of the samples.

Assessment of *in vitro* Antiarthritic Activity

The *in vitro* antiarthritic activity was studied using the bovine serum protein denaturation method and the egg albumin denaturation method. The egg albumin denaturation assay is based on the idea that substances with anti-inflammatory qualities may be able to stabilize protein structures and prevent denaturation, which is frequently linked to inflammation and tissue damage. Most biological proteins lose their biological function when denatured.

Protein Egg Albumin Denaturation Inhibition Assay

The assay was performed according to the previous method with slight modifications (Madhuranga and Samarakoon, 2023). The reaction mixture (5 mL) consisted of 0.2 mL of egg albumin (EA) from fresh hen's eggs, 2.8 mL of PBS (pH 6.4), and 2 mL of plant extract at various concentrations. Distilled water, or DMSO, was used as a control. In standard control, diclofenac sodium solutions were used in place of extract solutions. The control and test solutions were incubated at 37 °C for 0.25 h followed by heating at 70 °C for 5 min. After cooling to 37 °C, the absorbance of test and control solutions was determined at 660 nm. The percentage inhibition in protein denaturation was calculated.

$$\% \text{ Inhibition} = \frac{A_{\text{control}} - (A_{\text{sample}} - A_{\text{blank}})}{A_{\text{control}}} \times 100$$

where, A_{sample} = absorbance of the sample,

A_{blank} = absorbance of blank (without egg albumin),

A_{control} = absorbance of control (without test sample).

50 % inhibition concentration (IC₅₀) value were calculated by linear regressive excel program.

Protein Bovine Serum Albumin Denaturation Inhibition Assay

The assay was carried out following the previous method with slight modifications Saleem *et al*, (2019). A 0.45 mL of 5 % bovine serum albumin (BSA) was added to 0.5 mL of distilled water to prepare the test control solution. The control solution was prepared by replacing water with an equal volume of extract solution. The test solution (0.5 mL) was composed of 0.45 mL of BSA and 0.05 mL of test extract at 50-1600 mg/mL concentrations. Ethanol and watery extracts, and an isolated compound (bacosine) were dissolved in DMSO in place of water. DMSO served as a control for these extracts and an isolated compound in all *in vitro* antiarthritic assays. The standard drug solution (0.5mL) was comprised of 0.45 mL of BSA and 0.05 mL of diclofenac sodium. The pH of all solutions was set to 6.4. All solutions were incubated at 37 °C for 20 min and then at 60 °C for 3 min in an oven. Solutions were cooled to 37 °C, and 2.5 mL of PB (pH 6.4) was incorporated into each solution. The absorbance of test and control solutions was determined at 660 nm. The assay was performed in triplicate, and the percentage inhibition in protein denaturation was determined.

$$\% \text{ Inhibition} = \frac{A_{\text{control}} - (A_{\text{sample}} - A_{\text{blank}})}{A_{\text{control}}} \times 100$$

where, A_{sample} = absorbance of the sample,

A_{blank} = absorbance of blank (without BSA),

A_{control} = absorbance of control (without test sample).

50 % inhibition concentration (IC₅₀) value were calculated by linear regressive excel program.

Results and Discussion

Phytoconstituents Present in Aerial parts of *B. monnieri*

Primary phytochemical screening of *B. monnieri* was performed using the appropriate methods. The phytochemical tests revealed the presence of metabolites such as alkaloids, carbohydrates, glycosides, saponins, organic acids, phenolic compounds, flavonoids, tannins, steroids, and terpenoids. Cyanogenic glycosides and reducing sugar were absent in the sample. These results are summarized in Table 1.

Table 1. Preliminary of Phytochemical analysis on the Aerial Parts of *B. monnieri*

No.	Tests	Extract	Test reagents	Observation	Results
1.	alkaloid	1% HCl	dragendorff's reagent	orange ppt	+
2.	flavonoids	EtOH	EtOH, Mg turning and conc. HCl	pink colour solution	+
3.	glycosides	H ₂ O	10 % lead acetate	white ppt	+
4.	carbohydrates	H ₂ O	10 % α -naphthol and conc. H ₂ SO ₄	red ring	+
5.	cyanogenic glycosides	H ₂ O	sodium picrate	no brick red colour	-

No.	Tests	Extract	Test reagents	Observation	Results
6.	organic acids	H ₂ O	bromocresol green	green colour	+
7.	phenolic compounds	H ₂ O	10 % FeCl ₃	Dark green colour	+
9.	reducing sugars	H ₂ O	benedict's solution	no brick red ppt	-
10.	saponins	H ₂ O	distilled water	frothing	+
11.	tannins	H ₂ O	1% gelatin	white ppt	+
12.	steroids	pet-ether	Ac ₂ O and conc.H ₂ SO ₄	green colour	+
13.	terpenoids	(CHCl ₃)	Ac ₂ O and conc. H ₂ SO ₄	pink colour	+

(+) = presence (-) = absence ppt = precipitation

Characterization and Identification of an Isolated Compound

A compound has been isolated from the EtOAc extract of the aerial parts of *B. monnieri* and obtained as colourless crystals with a melting point of 240 °C. It was soluble in chloroform, ethanol, and methanol, but insoluble in pet ether and ethyl acetate. Its R_f value was found to be 0.45 on silica gel TLC with PE: EtOAc (5:1, v/v). It is UV-inactive and according to chemical tests, it did not contain a carbonyl group because the reaction did not give yellow ppt with 2,4-DNP solution. No reaction with a 5 % FeCl₃ solution indicated that it was not a phenolic compound. Since an isolated compound gave a pink colour spot when heated along with 5 % sulphuric acid. The pure compound must be a terpenoid compound. The isolated compound also changed the colour of bromocresol to green, indicating that it is an organic acid.

Structure Elucidation of the Isolated Compound

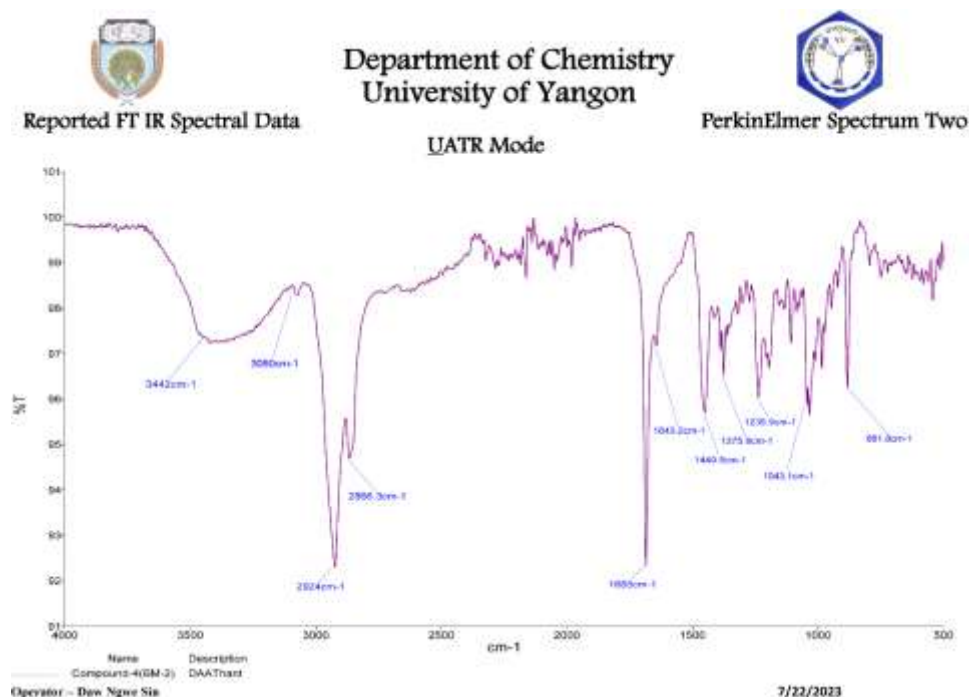


Figure 2. FT IR spectrum of the isolated compound

Table 2. FT IR Spectral Data of the Isolated Compound with Reported Data of Bacosine

Wavenumber (cm ⁻¹)		Band assignment
Compound	Bacosine*	
3442	3440	$\nu_{\text{O-H}}$ of alcoholic O-H group
3080	-	$\nu_{\text{=CH}}$ of vinylidene group
2924, 2866	2930, 2850	$\nu_{\text{C-H}}$ of asym and sym CH ₃ and CH ₂ group
1685	1680	carbonyl group of esters
1643	1640	$\nu_{\text{C=C}}$ of olefinic group
1449	1452	$\delta_{\text{C-H}}$ of CH ₃ and CH ₂ group
1375	1368	CH ₃ deformation of isopropyl group
1236	1240	$\nu_{\text{C-O}}$ of carboxylic acid
1043	1040	$\nu_{\text{C-O}}$ of alcoholic group
882	890	Olefinic C-H out of plane bending

*Ahmed and Rahman, 2000

In FT IR spectrum, the peaks at 3442 cm⁻¹, 3080 cm⁻¹, 1236 cm⁻¹, 1043 cm⁻¹ reveals the presence of O-H stretching, C=C bond stretching of alkene, C-O stretching vibrations, commonly found in carboxylic acid, alcohol or esters. (Table 2, Figure 2). The special data are in accordance with reported data of bacosine.

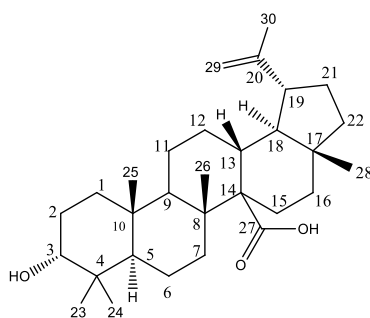
¹H NMR and ¹³C NMR Spectral Data of the Isolated Compound

¹H NMR (500 MHz, DMSO-*d*₆) spectral data is illustrated in Table 3. There are a total of 48 protons, including a double proton at δ 4.27, which indicates the hydroxyl group at C-3. The presence of two signals at δ 4.68 (d, $J = 6.5$ Hz, α -H-29) and 4.55 (dd, $J = 1.4, 6.5$ Hz, β -H-29) were attributed to two exocyclic methylene protons that established the lupane skeleton for the compound (Figures 3 & 4). Six-methyl signals were resonated at δ 0.76 (Me-23), 0.86 (Me-24), 0.92 (Me-25), 0.87 (Me-26), 0.65 (Me-28) and 1.64 (Me-30). In the ¹³C NMR spectra, it can be clearly observed in Figure 5 and Table 3 that there are a total of 30 carbons, consisting of one carbonyl carbon, six quaternary carbons, six methine carbons, eleven methylene carbons, and six methyl carbons. one carbinol carbon due to the peak at δ 76.80 (C-3), two olefinic carbons due to the peaks appearing at δ 150.30 and 109.6, and one carboxylic acid group due to the peak at δ 177.2 for the -C=O group (Figure 5). The ¹H and ¹³C NMR values for all the protons and carbons were observed to be identical with the reported data for bacosine (Ahmed and Rahman, 2000), except that some proton chemical shifts (δ_{H}) were slightly different, which may be due to the solvent effect.

Table 3. ^1H and ^{13}C NMR Data of Isolated Compound Compared with Literature Data

Position	Isolated compound (DMSO- d_6 , 500 MHz)		*Bacosine (CDCl $_3$, 300 MHz)		Isolated compound δ_c	*Bacosine δ_c
	δ_H (α)	δ_H (β)	δ_H (α)	δ_H (β)		
1	1.34 m	1.79 m	1.35 m	1.70 m	33.90	34.00
2	1.42 m	1.43 m	1.41 m	1.44 m	25.10	25.16
3	-	-	-	-	76.80	76.86
4	-	4.27 m	-	4.27 m	38.70	38.76
5	0.95 m	-	0.97 m	-	48.50	48.61
6	1.48m	1.23 m	1.47 m	1.23m	18.00	18.05
7	1.40 m	1.27 m	1.40 m	1.27 m	36.30	36.42
8	-	-	-	-	40.20	40.43
9	1.53 dd (10, 5Hz)	-	1.53dd (7, 4.5Hz)	-	49.90	50.01
10	-	-	-	-	37.60	37.67
11	2.10 m	1.60	2.08 m	1.59 m	20.50	20.54
12	1.09 m	1.80 m	1.09 m	1.82 m	27.10	27.24
13	2.92 m	-	2.92 m	-	38.50	38.58
14	-	-	-	-	55.40	55.50
15	2.10 m	2.24 m	2.07 m	2.28 m	30,10	30.18
16	1.80 m	2.97 m	1.83 m	2.97 m	31.70	31.79
17	-	-	-	-	42.00	42.08
18	2.12d (10)	-	2.13d (4.5)	-	46.60	46.70
19	2.95 m	-	2.95 m	-	54.90	54.97
20	-	-	-	-	150.30	150.40
21	1.57 m	2.19 m	1.56 m	2.18 m	29.20	29.29
22	2.24 m	1.54 m	2.23 m	1.54 m	36.70	36.81
23	0.76 s	-	0.76 s	-	28.10	28.19
24	0.86 s	-	0.86 s	-	15.70	15.81
25	0.92 s	-	0.93 s	-	15.90	16.04
26	0.86 s	-	0.87 s	-	15.80	15.9
27	-	-	-	-	177.20	177.33
28	0.64 s	-	0.65 s	-	14.40	14.47
29	4.68d (6.5)	4.55d(1.4)	4.68 d (3)	4.5d (1.5)	109.60	109.74
30	1.64 s	-	1.64 s	-	18.90	19.03

*Ahmed and Rahman, 2000

**Figure 3.** Structure of bacosine

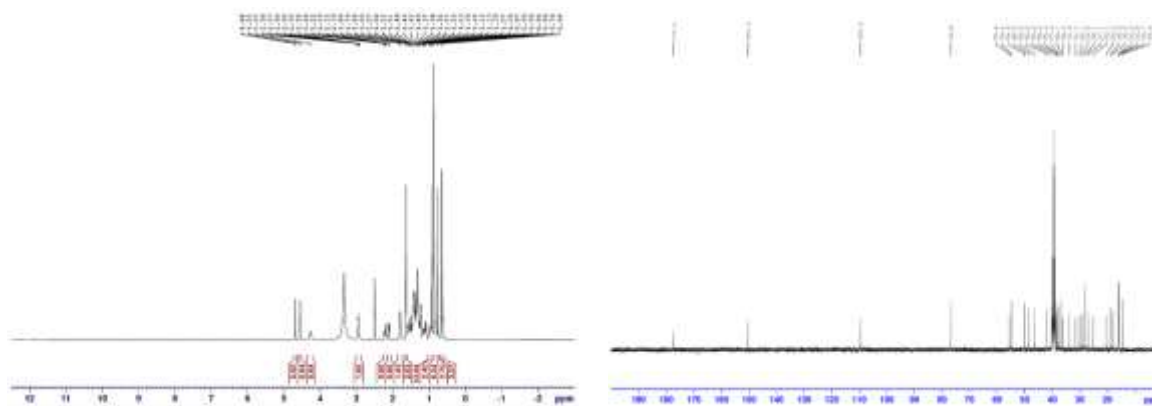


Figure 4. ^1H NMR (DMSO- d_6 , 500 MHz) and ^{13}C NMR (DMSO- d_6 , 125 MHz) spectra of the isolated compound

From the ESI-MS spectrum, $[\text{M}+4\text{H}+9\text{Na}]^+$ was observed, at m/z 667 (positive ion mode) (Figure 5a). Consequently, from all of the spectral data analyses, an isolated compound was identified as bacosine with the molecular formula $\text{C}_{30}\text{H}_{48}\text{O}_3$. From the ESI-MS spectrum (Figure 5 b), the molecular mass of the compound depicted the molecular formula $\text{C}_{30}\text{H}_{48}\text{O}_3$, which was deduced from molecular ion peak $[\text{M}-\text{H}]^-$ at m/z 455 (negative ion mode). From all the information, it could be inferred that compound was bacosine with the following structure:

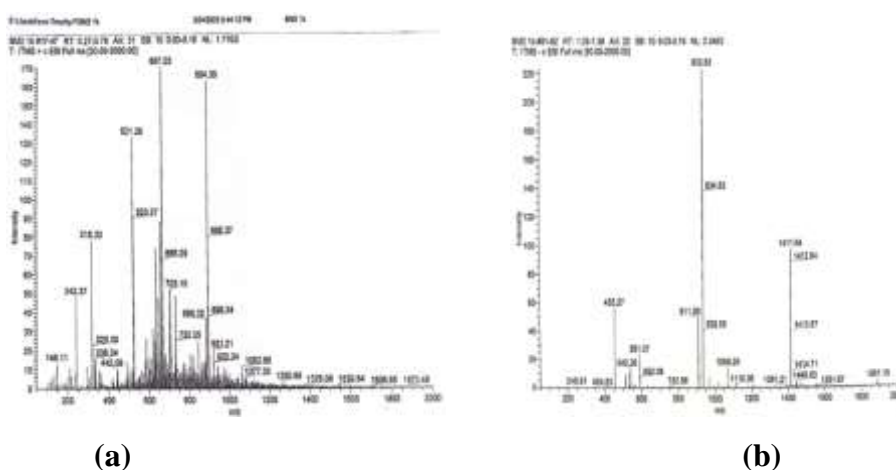


Figure 5. ESI-MS spectra of isolated compound (a) positive ion mode (b) negative ion mode

Anti-inflammatory Activity of *B. monnieri*

Inflammation is a protective or healing response to tissue injury in the body. It is a complex cascade of reactions that can be prompted by several agents, including toxic compounds, microbes, impaired cells, and accumulated exudates (Adegbaaju *et al.*, 2020). Macrophages are large, specialized cells, present in virtually all tissues. *In vitro* anti-inflammatory activity of the ethanol and watery extracts of BHA was determined by inhibition of NO production against LPS-induced RAW 264.7 cells. NO production is a typical phenomenon that occurs in LPS-stimulated macrophages. It is used as an indicator of a typical inflammatory response. The anti-inflammatory effect of the tested extracts was estimated in comparison with the IC_{50} values of NO inhibition and cell viability. The results of the tested samples are shown in Table 4.

During the 24 h incubation with LPS of tested extracts of *B. monnieri*, the inhibition of NO production in RAW 264.7 cells was dramatically increased at 10 µg/mL and 100 µg/mL concentrations. However, EtOH and watery extracts had higher IC₅₀ values of % NO inhibition than IC₅₀ values of % cell viability above the 10 µg/mL. Therefore, concentration above 10 µg/mL of two extracts in the sample did not show antiinflammatory activity because of cytotoxicity.

Table 4. % NO Inhibition, % Cell Viability and IC₅₀ of Crude Extracts of *B. monnieri* by Inhibition of Cellular NO Production

Sample	Anti-inflammatory activity					
	% NO inhibition			% Cell viability		
	10 µg/mL	100 µg/mL	IC ₅₀ (µg/mL)	10 µg/mL	100 µg/mL	IC ₅₀ (µg/mL)
ethanol extract	10.21	60.38	81.38	66.75	60.38	> 100
watery extract	2.82	32.57	> 100	88.20	94.48	< 10
L-NMMA	18.49	50.35	98.25	100.32	92.01	> 100

***In vitro* Assessment Antiarthritic Activity**

Arthritis comprises varieties of joint disorders such as rheumatoid arthritis (RA), osteoarthritis (OA), etc., that affect one joint or multiple joints. Denaturation of tissue proteins is one of the well-documented causes of inflammatory and arthritic diseases. The increments in absorbances of test samples (isolated compounds) with respect to control indicated stabilization of protein, inhibition of heat-induced protein (albumin), denaturation and the reference drug diclofenac sodium. Phytochemical constituents are responsible for maximum protection against protein denaturation and albumin denaturation (Kaushik *et al.*, 2021).

Ethanol and watery extracts and isolated compound bacosine were screened for antiarthritic activity by denaturation of egg albumin and bovine albumin proteins (Tables 5 and 6). Diclofenac sodium was used as the reference drug. In the egg albumin method, the bacosine compound (IC₅₀ = 105.23 µg/mL) was more significant anti denaturation effect than ethanol extract (IC₅₀ = 162.44 µg/mL) and watery extract (172.71 µg/mL) and in the bovine serum albumin method, the bacosine compound (IC₅₀ = 118.73 µg/mL) was more significant anti denaturation effect than ethanol extract (IC₅₀ = 180.58 µg/mL) and watery extract (299.24 µg/mL) compared with diclofenac sodium (IC₅₀ = 73.44 µg/mL). The present findings exhibited a concentration-dependent inhibition of protein and albumin denaturation.

Table 5. Inhibition at Egg Albumin Denaturation of Crude Extracts and Isolated Compound of *B. monnieri*

Sample	% Inhibition at different concentration ($\mu\text{g/mL}$)						IC ₅₀ ($\mu\text{g/mL}$)
	50	100	200	400	800	1600	
ethanol extract	28.87	36.50	58.12	63.82	74.98	78.32	162.44
watery extract	24.65	31.04	38.89	54.17	61.04	73.37	272.71
bacosine	42.33	49.60	57.24	63.04	78.23	86.38	105.23
diclofenac sodium	45.63	54.95	63.65	72.80	84.53	92.18	73.44

Table 6. Inhibition at Bovine Serum Albumin Denaturation of Crude Extracts and Isolated Compound of *B. monnieri*

Sample	% Inhibition at different concentration ($\mu\text{g/mL}$)						IC ₅₀ ($\mu\text{g/mL}$)
	50	100	200	400	800	1600	
ethanol extract	40.36	42.32	51.85	63.16	66.67	73.69	180.58
watery extract	26.32	38.08	47.37	52.64	56.15	64.92	299.24
bacosine	38.17	47.37	61.41	64.16	68.43	81.93	118.73
diclofenac sodium	45.63	54.95	63.65	72.80	84.53	92.18	73.44

Conclusion

The preliminary phytochemical analysis showed the presence of bioactive secondary metabolites in this plant sample. In this study, the isolation of bacosine ($\text{C}_{30}\text{H}_{48}\text{O}_3$) from the ethyl acetate fraction of *B. monnieri* was accomplished by modern spectroscopic techniques: FT IR, ^1H NMR (500 MHz), and ^{13}C NMR (125 MHz). The compound was elucidated as a known compound, in agreement with reference data. The ethanol extract had a higher IC₅₀ of NO inhibition than that of cell viability because of cytotoxicity, watery extracts had higher IC₅₀ of NO inhibition and cell viability above 100. The ethanol extract exhibited significant inhibitory inflammation however; it can be exhibited less concentration 100 $\mu\text{g/mL}$. The inhibition of protein denaturation and albumin denaturation was studied to estimate the antiarthritic activity of isolated compounds, ethanol, and watery extracts of the aerial parts *B. monnieri*. The present findings demonstrate the significant antiarthritic activity compared with the standard drug diclofenac sodium.

Acknowledgements

The authors would like to express their profound gratitude to the Department of Higher Education, Ministry of Education, Yangon, Myanmar, for giving them the opportunity to do this research and the Myanmar Academy of Arts and Science for allowing them to present this paper.

References

- Adegbaju, O. D., G. A. Otunola, and A. J. Afolayan. (2020). "Anti-inflammatory and Cytotoxic Evaluation of Extracts from the Flowering Stage of *Celosia argentea*". *BMC Complementary Medicine and Therapies*, vol. 20 (152), pp 1-7.
- Ahmed, B. and A. Rahman. (2000). "Basosterol, a New 13, 14-seco-steroid and Bacosine, a New Triterpene from *Bacopa monniera*". *Indian Journal of Chemistry*, vol.39 B, pp 620-625.
- Channa, S., A. Dar, S. Anjum, M. Yaqoob, and A. Rahman. (2006). "Anti-inflammatory Activity of *Bacopa monniera* in Rodents". *Journal of Ethnopharmacology*, vol. 104, pp 286–289.
- Jin, S. E., Y. K. Son, B. S. Min, H. A. Jung, and J. S. Choi. (2012). "Anti-inflammatory and Antioxidant Activities of Constituents Isolated from *Pueraria lobata* Roots". *Arch Pharm Res*: vol.5, pp. 823-837.
- Kaushik, S., P. Jain, and T. Satapathy. (2021). "Perna Purabiyal and Amit Roy Evaluation of Anti-arthritis and Anti-inflammatory Activities of *Martynia annua* L. Ethanolic Extract". *Clinical Phytoscience*, vol.7 (7), pp.1-11.
- Kishore, L., N. Kaur, and R. Singh. (2017). "Bacosine Isolated from Aerial Parts of *Bacopa monnieri* Improves the Neuronal Dysfunction in Streptozotocin-induced Diabetic Neuropathy". *Journal of Functional Foods*, vol.34, pp 237–247.
- Madhuranga, H. D. T., and D. N. A. W. Samarakoon. (2023). "In vitro Anti-Inflammatory Egg Albumin Denaturation Assay: An Enhanced Approach". *Nat Ayurvedic Med.*, vol. 7(3), pp. 1-7.
- Saleema, A., M. Saleema, and M. F. Akhtar. (2020). "Antioxidant, Anti-inflammatory and Antiarthritic Potential of *Moringa oleifera* Lam: An Ethnomedicinal Plant of Moringaceae Family". *South African Journal of Botany*, vol.128, pp.246-256.
- Schmidt, H. and M. Kelm. (1996). *Determination of Nitrite and Nitrate by the Griess Reaction*. In Feelisch, M. and J. Stamler (Eds.) *Methods in Nitric Oxide Research*. Chichester (UK): John Wiley & Sons, vol. 12, pp.491-497.

SUN PROTECTION FACTOR EVALUATION OF PREPARED HERBAL SUNSCREEN CREAMS FROM *Mansonia gagei* J.R. DRUMM (KALAMET) STEM

Thin Wut Soe¹, Cho Lwin Lwin Khine², May Zin Oo³, Su Su Aung⁴, Myat Myat Thaw⁵

Abstract

In this project, *Mansonia gagei* J. R. Drumm (Kalamet) stem in the tropics of Myanmar is investigated for sunscreen creams preparation. The sample was collected from Kaunghmudaw Pagoda Market, Sagaing Region, in June 2023. The preliminary phytochemical tests revealed the presence of α -amino acids, carbohydrates, glycosides, flavonoids, phenolic compounds, and saponins in the stem of *M. gagei*. In addition, sunscreen creams were prepared by maxing ingredients with water and ethanol extracts from selected sample for the protection of skin from UV radiation. Prepared herbal sunscreens were evaluated for physicochemical characteristics such as color, odor, appearance, homogeneity, consistency, washability, viscosity, skin irritancy, pH, and sun protection factor (SPF). Results showed that both herbal sunscreen creams had good consistency, easy washability, were within the permitted viscosity range, and contained no irritants. The pH values of the prepared sunscreen creams were observed not to be significantly changed during testing, and those were in the range of 6.4 to 6.6. SPF values of prepared sunscreen creams were observed to be 15.17 (cream-H₂O) and 17.91 (cream-EtOH). The antibacterial activity of the prepared sunscreen creams against *Staphylococcus aureus* in topic therapy was investigated using the agar-well diffusion method. The inhibition zone diameters were found to be 11 mm (cream-H₂O) and 14 mm (cream-EtOH). In comparison to prepared creams, cream-EtOH was shown to be more stable, effective, with a high SPF, and potent antibacterial activity. It can enhance and effectively contribute to the UV-absorbing properties of conventional sunscreen. It could also have the greatest advantage of avoiding the adverse and undesired effects of synthetic sunscreen compounds.

Keywords: *Mansonia gagei* J.R. Drumm, sunscreen creams, water and ethanol extracts, sun protection factor, antibacterial activity

Introduction

Sunscreens are formulations for skin application that contain substances that can absorb, reflect, or disperse solar radiation, reducing its biological effects on the skin. Most active sunscreen ingredients have been used globally for more than 15-30 years and are considered to be safe for humans (Hanrahan, 2012). Herbal cosmetics are formulated by using different cosmetic ingredients to form a base in which one or more herbal ingredients are used to treat various therapeutic skin elements. Cosmeceuticals have medicinal benefits that affect the biological functioning of the skin, depending on the type of functional ingredients they contain. These are modern trends in the fields of beauty and fashion (Pandey *et al.*, 2021).

Mansonia gagei is a medium-sized evergreen tree with a bole that can be up to 70 cm in diameter. Leaves are simple, faintly dentate, sometimes with domatia. Flowers are mostly

¹ Department of Chemistry, Sagaing University of Education

² Department of Chemistry, Sagaing University of Education

³ Department of Chemistry, Sagaing University of Education

⁴ Department of Chemistry, Sagaing University of Education

⁵ Department of Chemistry, Sagaing University of Education

hermaphroditic, zygomorphic, fragrant, and have two stamens per staminal bundle. It is a common flowering shrub native to Myanmar, India, and tropical West Africa. (Kubitzki and Bayer, 2013). It has been used for many traditional uses, such as to treat cardiac stimulants, antiemetics, antidepressants, tonic reagents, urinary disorders, and anemia (Nishina *et al.*, 2018). The paste is also applied topically to the body for a cooling effect and to alleviate itches (DeFilipps and Krupnick, 2018). Pharmacological studies suggest that the plant possesses antifungal, antibacterial, antioxidant, antiestrogenic, and antitumor properties (Li, *et al.*, 2018) thus lending scientific support to the plant's ethnomedicinal uses. Therefore, in this research, we have a plan to investigate the sun protection factor of herbal sunscreen creams from the various extracts of stem of *Mansonia gagei* J.R. Drumm (Kalamet).

Botanical Description

Family name	: Sterculiaceae
Botanical name	: <i>Mansonia gagei</i> J.R. Drumm (Kress <i>et al.</i> , 2003)
Myanmar name	: Kalamet
Part used	: Stem
Distribution	: Myanmar, India, tropical West Africa



Figure 1. Photographs of plant, stem and powder of *Mansonia gagei* J.R. Drumm (Kalamet)

Materials and Methods

Sample Collection

The sample of *Mansonia gagei* J.R. Drumm (Kalamet) stem was collected from Kaunghmudaw Pagoda Market, Sagaing Region, in June 2023. The dried sample was made into powder by using a grinding machine. The dried powder sample was stored in an airtight container to prevent moisture changes and other contaminations. The dried powdered samples were used to investigate their chemical and biological activities. The identification of the sample was conducted with the Department of Biology at Sagaing University of Education.

Preliminary Phytochemical Tests of *M. gagei* (Kalamet) Stem

A preliminary phytochemical tests of the selected sample were carried out using standard methods (Harborne, 1984, M-Tin-Wa, 1972 and Marini-Bettoto *et al.*, 1981). The results are shown in Table 1.

Preparation of Extracts of *M. gagei* (Kalamet) Stem

The dried powdered sample (10 g) was percolated with ethanol (200 mL) for three days and then filtered. The same procedure was repeated three times. The combined filtrate was concentrated in a water bath. The dried filtrate was transferred to a weighed porcelain basin and

evaporated to dryness in a water bath to obtain ethanol extract. For water extract, a dried powdered sample (10 g) was boiled with distilled water (200 mL) for 1 h. The extract was then filtered, transferred to a weighed porcelain basin, and evaporated to dryness in the water bath. The two extracts were stored in a desiccator containing dry silica gel prior to use in each experiment.

Preparation of Herbal Sunscreen Creams from *M. gagei* (Kalamet) Stem

The oil phase of cream was prepared by heating the ingredients (coconut oil, stearic acid, lanolin, and glycerin) at 75 ± 2 °C with constant stirring using a hot plate, while for the preparation of the aqueous phase, purified water was heated separately in a 50 mL capacity beaker at 80 ± 2 °C. Methylparaben and propyl paraben were added, to the above mixture and dissolved with occasional stirring, at 75 ± 2 °C. The two phases (oil and aqueous) were mixed together with vigorous stirring for about 1-2 min. Finally, the stem extracts (water and ethanol) were individually added with constant stirring until a thick cream was formed. The temperature was further reduced to around 45 °C using a cold-water bath. The cream was collected in a wide-mouthed airtight glass container, and stored in a dry place. And then, the prepared herbal cream were characterized by instrumental methods (Mamillapalli *et al.*, 2018).

Determination of Physicochemical Parameters of Prepared Herbal Sunscreen Creams

Prepared herbal sunscreen creams were evaluated for physicochemical characteristics (color, odor, appearance, homogeneity, consistency, washability, and pH) by visual and instrumental methods. The viscosity of the prepared herbal sunscreen creams was measured using a rotor spin type (L-4) at 250 rpm in an ATAGO viscometer at the Physical Research Room, Department of Chemistry, University of Yangon. The viscosity value of the prepared creams was recorded directly from the instrument display.

Determination of Skin Irritancy Test

For the skin irritancy test, we selected 10 volunteers who met the following inclusion criteria: age ≥ 18 years old, physically and mentally healthy, skin free from lesions, and no history of allergy. All volunteers provided informed consent. According to the skin patch test description, the student volunteers were divided into two groups. Group A volunteers were applied cream-H₂O, and Group B volunteers were applied cream-EtOH. Firstly, a marked area (5 cm²) on the right-hand dorsal surface and their left-hand dorsal surface were used as control. The cream was applied to the specified area at twice (between 9:00-12:00 am and 1:00–3:00 pm) a day for one week. Irritancy, erythema, and edema were checked if any, for regular intervals up to 24 h and reported (Hiremath *et al.*, 2008).

Determination of Sun Protection Factor (SPF)

The photoprotective activity of tested samples was measured by the determination of sun protection factor (SPF). The tests were measured at the Pharmaceutical Research Laboratory, Department of Biotechnology Research (DBR), Kyaukse Township, Mandalay Region, Myanmar. Sample (2 mg) was diluted in 1 mL of methanol to obtain a concentration of 2 mg/mL. Spectrophotometric scanning was performed at wavelengths between 290 and 320 nm, with intervals of 5 nm, using a 96-well microplate reader. The SPF value was obtained according to the equation developed by? (Mansur *et al.*, 1986).

$$\text{SPF} = \text{CF} \times \text{EE}(\lambda) \times \text{I}(\lambda) \times \text{Abs}(\lambda)$$

Where, CF = correction factor (= 10),

EE (λ) = erythmogenic effect of radiation with wavelength λ ,

I (λ) = solar intensity spectrum,

Abs (λ) = spectrophotometric absorbance values of sunscreen product at wavelength λ (Mansur *et al.*, 1986)

EE x I = constant is determined by (Sayre *et al.*, 1979)

Screening of Antibacterial Activity of Prepared Herbal Sunscreen Creams

The antibacterial activity of prepared herbal sunscreen creams of *M. gagei* were determined against the gram-positive bacteria *Staphylococcus aureus*, was used as the tested microorganism for this experiment (Schlegel and Zaborosch, 1993). The tests were screened at the Pharmaceutical Research Laboratory, Department of Biotechnology Research (DBR), Kyaukse Township, Mandalay Region, Myanmar.

The tested microorganism was inoculated in Muller Hinton broth at 37 °C for overnight. On the next day, the overnight broth culture was diluted with normal saline to obtain the OD₆₀₀ at 0.08 to 0.1 with an approximate cell density of 1.5 x 10⁸ CFU/mL. Muller Hinton agar plates were prepared and sterilized by autoclaving at 121 °C for 15 min. The broth inoculums were evenly spread out with sterile cotton swabs on the Muller Hinton agar plates to obtain the uniform inoculums. After the plate was inoculated, 8 mm diameter wells were made on the agar medium by using a sterile cork borer. Each 50 μ L (0.2 g/mL) of samples was introduced into each well labelled. Chloramphenicol (30 μ g/well) was used as the positive control. Then, the plates were placed in an incubator at 37 °C for 16 to 18 h. After incubation, the plates were examined, and zone diameters of complete inhibition were measured and recorded to the nearest millimeter.

Results and Discussion

The sample of *M. gagei* (Kalamet) stem was cleaned and dried at room temperature for two weeks. The dried sample was made into powder by using a grinding machine. The dried powdered sample was stored in an airtight container to prevent moisture changes and other contaminations. The dried powdered sample was used to investigate for their chemical and biological activities. *M. gagei* stem was rich in organic constituents such as α -amino acids, glycosides, phenolic compounds, saponins, carbohydrates, and flavonoids, except alkaloids, reducing sugar, starch, steroids, and tannins.

Table 1. Results of Phytochemical Constituents of *M. gagei* (Kalamet) Stem

No.	Test	Extract	Test reagent	Observation	Result
1	alkaloids	1 % HCl	Dragendorff's reagent	no orange ppt.	–
			Mayer's reagent	no white ppt.	–
			Wagner's reagent	no reddish brown ppt.	–
2	α -Amino acids	H ₂ O	Ninhydrin reagent	violet colour	+

No.	Test	Extract	Test reagent	Observation	Result
3	carbohydrates	H ₂ O	10 % α -Naphthol, conc. H ₂ SO ₄	red ring	+
4	flavonoids	EtOH	Mg turning, conc. HCl	pink colour	+
5	glycosides	H ₂ O	10 % Lead acetate solution	white ppt.	+
6	phenolic compounds	EtOH	1 % FeCl ₃ solution	dark blue colour	+
7	reducing sugars	H ₂ O	Benedict's solution	no brick-red ppt.	-
8	saponins	H ₂ O	Distilled water	frothing	+
9	starch	H ₂ O	1 % Iodine solution	no blackish blue	-
10	steroids	PE	Acetic anhydride, conc. H ₂ SO ₄	no greenish blue	-
11	tannins	H ₂ O	1 % Gelatin	no white ppt.	-

(+) = presence, (-) = absence, (ppt.) = precipitate

Preparation of Herbal Sunscreen Creams from *M. gagei* (Kalamet) Stem

The herbal sunscreen creams were prepared by using the watery and ethanol extract of the stem of *M. gagei*. The ingredients used in the formulation were described as in Table 2.

Table 2. Composition of Prepared Herbal Sunscreen Creams of *M. gagei*

No.	Ingredients	Components (% w/w)
1.	stearic acid	40
2.	lanolin	50
3.	glycerin	156.6
4.	coconut oil	35
5.	methylparaben	4
6.	propylparaben	0.4
7.	plant extract	10
8.	distilled water	6.95

Determination of some Physicochemical Parameters

Prepared herbal sunscreen creams were evaluated for their physicochemical characteristics: color, odor, appearance, homogeneity, consistency, washability, viscosity, and pH. The results of various tests for the evaluation parameters of herbal sunscreen cream formulations using watery and ethanol extracts indicated that it exists in yellowish brown and pale brown colors with a pleasant odor and smooth appearance with homogeneity and good

consistency. Homogeneity was confirmed by visual appearance and touch. All the prepared creams were found to have good homogeneity.

Viscosity governs many properties of the product, such as the spreadability and pourability of the product from the container. The viscosities of the prepared creams were found to be in the range of >5000 cP, which indicated that the cream was easily spreadable by small amounts of shear. The pH of creams was determined to examine the possible side effects of acidic or alkaline pH, which can lead to irritation of the skin. Acidic or alkaline pH may cause irritation to the skin and influence the rate of hydration of polymers. The cream in general has a pH of 6-9 for sunscreen (Donglikar and Deore, 2017). The pH values were found to be 6.4 (cream-H₂O) and 6.6 (cream-EtOH).

Results of Skin Irritation Test

Safety testing is essential before raw materials or end products can be sold to consumers. Therefore, in this test, selected 10 volunteers who provided informed consent and were divided into two groups. One group is used for cream-H₂O and another is for cream-EtOH. During the assessment, the prepared herbal sunscreen creams indicated that they did not irritate the skin.

Determination of SPF value

The well-known UV Vis spectrophotometric method can be used for the determination of SPF values in many cosmetic formulations. The efficiency of the sunscreen products depends on the sun protection factor (SPF) value. The higher the SPF, the more protection a sunscreen offers against UV light. The calculated SPF values of prepared herbal sunscreen were found to be 15.17 (cream-H₂O), 17.91 (cream-EtOH), and 34.48 for commercial sunscreen. The prepared cream with ethanolic extract offered more sun protection than the aqueous extract compared with the commercial sunscreen, which may be attributed to the presence of a high flavonoid content. The SPF values of each prepared creams were calculated by applying the Mansur equation, e.g., for the prepared herbal sunscreen cream-EtOH, as given in Tables 3, 4, and Figure 2.

Table 3. Calculation of the Sun Protection Factor Value of the Prepared Herbal Sunscreen Cream-EtOH of *M. gagei*

Sample	Wavelength	Absorbance	EE x I	Abs x EE x I
cream-EtOH of <i>M. gagei</i>	290	2.98±0.16	0.0150	0.0447
	295	2.35±0.08	0.0817	0.1919
	300	2.01±0.09	0.2874	0.5777
	305	1.80±0.09	0.3278	0.5900
	310	1.46±0.10	0.1864	0.2721
	315	1.18±0.05	0.0839	0.0990
	320	0.83±0.09	0.0180	0.0149
				1.791±0.65

$$\begin{aligned}
 \text{SPF} &= \text{CF} \times \sum_{290}^{320} \text{EE}(\lambda) \times \text{I}(\lambda) \times \text{Abs}(\lambda) \\
 &= 10 \times 1.791 \\
 &= \mathbf{17.91}
 \end{aligned}$$

Table 4. The Sun Protection Factor Values of the Prepared Herbal Sunscreen Creams

No.	Prepared Sample	SPF	UV protection rate (%)
1	cream-H ₂ O	15.17	93
2	cream-EtOH	17.91	94
3	commercial Sunscreen	34.48	97

*Sunblock 27 from Nature Republic (Korea)

SPF(Reference): 2-12 = minimum sun protective activity, 12-30 = moderate sun protective activity

≥ 30 = high sun protective activity, ≥ 50 = very high sun protective activity (Ratnasooriya *et al.*, 2014)

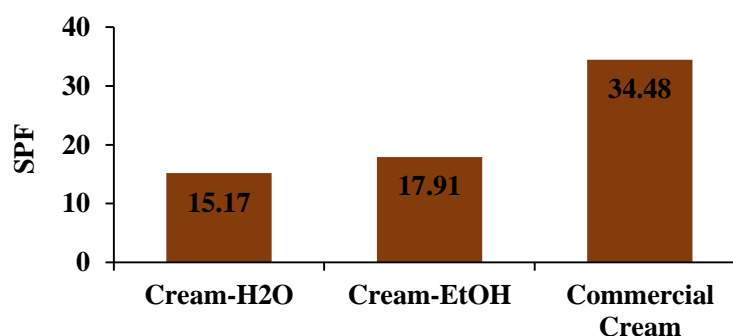


Figure 2. Comparison of SPF values of the prepared herbal sunscreen creams of *M. gagei*

Screening of Antibacterial Activity of Prepared Herbal Sunscreen Creams

In this present work, the antibacterial activity of prepared herbal sunscreen creams (H₂O, EtOH) obtained from the stem of *M. gagei* was investigated on *S. aureus* by the agar- well diffusion method. The measurable zone diameter, including the well diameter, shows the degree of antibacterial activity. The well diameter is 8 mm in this experiment. The larger the zone diameter, the more activity there is in the test organisms. The results of antibacterial activity were shown in Table 5 and Figure 3. It was found to have moderate antibacterial activity in both prepared creams (inhibition zone diameter = 11~14 mm).

Table 5: Results of Inhibition Zone Diameter of Prepared Herbal Sunscreen Creams

Microorganism	Inhibition Zone Diameter (mm)			
	70 % EtOH	Kalamet Cream-H ₂ O	Kalamet Cream-EtOH	Chloramphenicol
<i>Staphylococcus aureus</i>	0	11	14	22

Well size = 8 mm, 10-12 mm = weak activity, 13-18 mm = high activity, >18 mm = very high activity

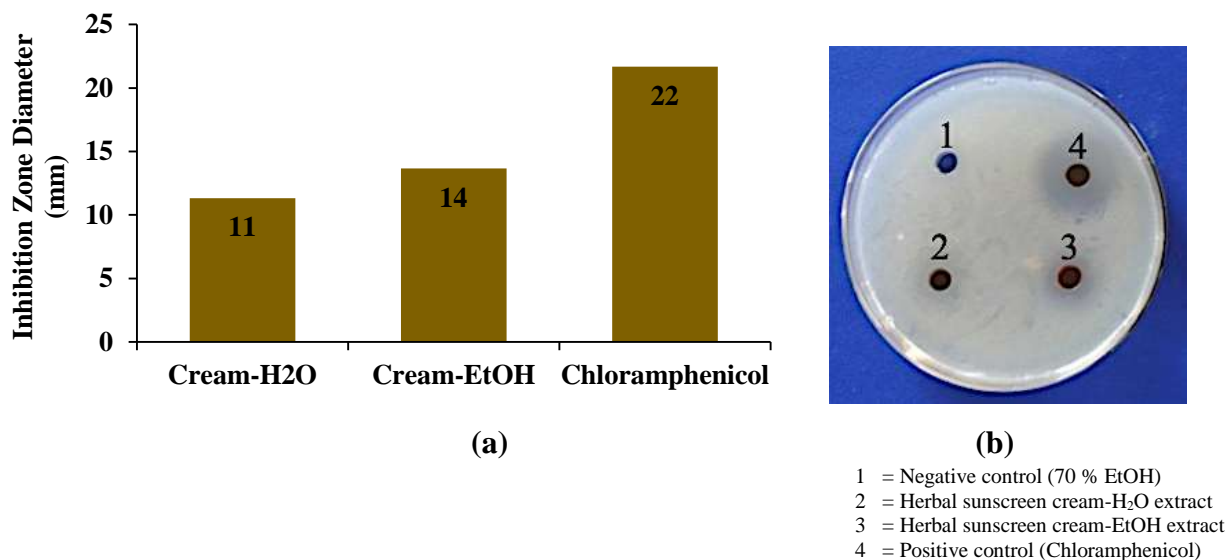


Figure 3. (a) A bar graph of antibacterial activity and (b) culture plates showing zone of inhibition of prepared herbal sunscreen creams against *S. aureus*

Conclusion

In this study, the investigation of phytochemical constituents, preparation of herbal sunscreen creams, physicochemical parameters, skin irritancy test, SPF values, and antibacterial activity from the stem of *M. gagei* (Kalamet) were reported. The results of preliminary phytochemical screening of different crude extracts revealed the presence of α -amino acids, carbohydrates, glycosides, flavonoids, phenolic compounds, and saponins. However, alkaloids, reducing sugars, starch, steroids, and tannins were found to be absent. The results of various tests for the evaluation parameters of herbal sunscreen creams using water and ethanol extracts indicated that they exist in yellowish-brown and pale brown colors with a pleasant odor and smooth appearance with homogeneity and good consistency. They were easily washable with a spread ability time of 5 sec, the viscosity in both creams were >5000 cP, and the pH values were found to be within a permissible range. The skin irritation results for all volunteers in this study showed that they do not irritate the skin. According to mild SPF results, they can be used on normal skin to prevent sunburns. It will also help in broadening the UV protection ability of conventional sunscreen formulations. From this results of antibacterial activity test, it was found that the moderate antimicrobial activity with inhibition zone diameters between 11~14 mm against *S. aureus*. Therefore, the selected sample may be useful as a related disease to alleviate itches. It can be concluded that the present research might hopefully bring advancements in the treatment of sunburns caused by exposure to UV rays. Further, the study reveals that UV spectroscopy is the most rapid, acceptable, and reproducible method for evaluating the efficacy of herbal sunscreens.

Acknowledgements

The authors would like to express their profound gratitude to the Department of Higher Education, Ministry of Education, Myanmar for providing of the opportunity to do this research, Thanks are also extended to Dr Khin Hnin Yee (Pro-Rector), and Dr Cho Kyi Than (Pro-Rector), Sagaing University of Education for their kind encouragement and nice suggestions for this research paper.

References

- DeFilippis, R. A. and G. A. Krupnick. (2018). "The Medicinal Plants of Myanmar". *Phytokeys*, vol. 102, pp. 1-341.
- Donglikar, M. M. and S. L. Deore. (2017). "Development and Evaluation of Herbal Sunscreen". *Pharmacgn*, vol. 9, pp. 83-97.
- Hanrahan, J. R. (2012). "Sunscreens". *Australian Prescriber*, vol. 35(5), pp. 148-151.
- Harborne, J. B. (1984). *Phytochemical Methods, A Guide to Modern Techniques of Plant Analysis*. New York: 2nd Ed., Chapman and Hall, pp. 120-126.
- Hiremath, S. S. P., F. S. Dasankoppa, A. Nadaf, V. G. Jamakandi, J. S. Mulla, S. A. Sreenivas, H. N. Sholapur, A. Ahmed and N. G. Nanjunda Swamy. (2008). "Formulation and Evaluation of a Novel in Situ Gum Based Ophthalmic Drug Delivery System of Linezolid". *Sci Pharm.*, vol. 76, pp. 515-532.
- Kress, W. J., R. A. Defilippis, E. Farr and Yin Yin Kyi. (2003). *A Checklist of the Trees, Shrubs, Herbs, and Climbers of Myanmar*. Department of Systematic Biology-Botany National Museum of Natural History, Washington DC.
- Kubitzki, K. and C. Bayer. (2013). "The Families and Genera of Vascular Plants". *Springer-Verlag Berlin Heidelberg*, pp. 130-135.
- Li, T., D. Zhang, Thaug Naing Oo, Myint Myint San, Aye Mya Mon, Pyae Phyo Hein, Y. Wang, C. Lu and X. Yang. (2018). "Investigation of Traditional Myanmar Medicinal Plants". *Evidence-Based Complementary and Alternative Medicine*, vol. 2018, pp. 1-13.
- M-Tin-Wa. (1972). "Phytochemical Screening Methods and Procedures". *Phytochemical Bulletin of Botanica Society of America*, vol. 5(3), pp. 4-10.
- Mamillapalli, V., P. L. Khantamneni, S. Koleti, K. Ghanta, H. M. Yakkali, K. M. Puli, and G. Kolusu. (2018). "Phytochemical and in Vitro Sun Protection Factor Evaluation of Peltophorum Leaf Extracts". *Int. J. Pharm. Sci. Rev. Res.*, vol. 48(2), pp. 49-58.
- Mansur, J. S., M. N. R. Breder, M. C. A. Mansur and R. D. Azuly. (1986). "Determinação Do Fator De Proteção Solar Por Espectrofotometria". *An. Bras. Dermatol.*, vol. 61, pp. 121-124.
- Marini-Bettolo, G. B., M. Nicolettic, and M. Patamia. (1981). "Plant Screening by Chemical and Chromatographic Procedure Under Field Conditions". *J. Choursomato.*, vol. 45, pp. 121-123.
- Nishina, A., A. Miura, M. Goto, K. Terakado, D. Sato, H. Kimura, Y. Hirai, H. Sato and Nyunt Phay. (2018). "Mansonone E from *Mansonia Gagei* Inhibited α -MSH-Induced Melanogenesis in B16 Cells by Inhibiting CREB Expression and Phosphorylation in the PI3K/Akt Pathway". *Biol Pharm Bull*, vol. 41, pp. 770-776.
- Pandey, A., M. K. Yadav and P. Yadav. (2021). "Formation of Cosmetic from Medicinal Plants". *International Journal of Pharmaceutical Research and Applications*, vol. 6(5), pp. 842-847.
- Ratnasooriya, W. D., J. R. A. C. Jayakody, S. R. D. Rosa and C. D.T. Ratnasooriya. (2014). "In Vitro Sun Screening Activity of Sri Lankan Orthodox Black Tea (*Camellia sinensis* linn)". *World Journal of Pharmaceutical Sciences*, vol. 1, pp. 144-148.
- Sayre, R. M., P. P. Agin, G. J., Le Vee and E. Marlowe. (1979) "A Comparison of in Vivo and in Vitro Testing of Sunscreen Formulas". *Photochem. Photobiol.*, vol. 29(3), pp. 559-566.
- Schlegel, H. G. and C. Zaborosch. (1993). *General Microbiology*. Cambridge: 7th Edition University Press.

SUN PROTECTION FACTOR EVALUATION OF PREPARED HERBAL SUNSCREEN GELS FROM *PREMNA INTEGRIFOLIA* L. (TAUNG-TAN-GYI) STEM

Cho Lwin Lwin Khine¹, Thin Wut Soe¹, Su Su Aung², Myat Myat Thaw³

Abstract

The present study focused on the preparation of herbal sunscreen gels from *P. integrifolia* stems. The qualitative preliminary phytochemical investigation was carried out by the reported chemical methods. The prepared herbal sunscreen gels by using watery and ethanol extracts were examined for evaluation parameters such as colour, odour, appearance, consistency, homogeneity, washability, pH, viscosity and sun protection factor (SPF). The prepared herbal sunscreen gels had a pleasant odour, smooth appearance, acceptable consistency, great homogeneity, ease of removal and brown for watery extract and yellowish brown for ethanol extract containing prepared gels. The pH of prepared gels was near skin pH, found to be 6.3 and 6.2 for watery and ethanol extracts containing gels. The viscosity results indicated that both of the two extracts using gels had > 5000 cP revealing the easy spreadability of gel application on the skin. The *in vitro* SPF values were found to be 16.16 and 13.89 for watery and ethanol extracts containing prepared gels, respectively, compared to marketed products (34.48) by using the UV spectrophotometric method. *In vitro* screening of antibacterial activity showed a mild antibacterial effect against *Staphylococcus aureus* by the agar well diffusion method. Skin irritation tests exhibited no redness, edema, inflammation, or irritation in 10 volunteers (male/female) using patch tests. The prepared herbal sunscreen gels containing watery and ethanol extracts from *P. integrifolia* stem were effectively utilized as sunscreen with significant sun protection properties and were safe with respect to skin irritation and allergic sensitization. The result can form the basis for the development of novel broad-spectrum sunscreen formulations.

Keywords: antibacterial activity, herbal sunscreen gels, *Premna integrifolia* L., skin irritation test, SPF

Introduction

Sunlight is composed of various wavelengths ranging from ultraviolet light through infrared to visible light. The solar spectrum radiation of the sun is divided into five regions: Ultraviolet C or UV-C (from 100 nm to 290 nm), Ultraviolet B or UV-B (from 290 nm to 320 nm), Ultraviolet A or UV-A (from 320 nm to 400 nm), visible range or light (from 380 nm to 780 nm) and infrared (from 780 nm to 10⁶ nm) (Mamillapalli *et al.*, 2018). Overcome the bad effects of ultraviolet rays or sunlight, one of which is using sunscreen. This sunscreen is a cosmetic ingredient that physically and real or chemically can inhibit and penetrate UV light into the skin (Yusnelti *et al.*, 2018). A sunscreen is a photoprotective agent against direct UV radiation and is used as the skin's defense against the harmful effects of UV radiation. Its ability is to absorb or reflect the sun's UV radiation on the skin from over exposure to UV radiation. They help to prevent sunburn, skin damage and skin cancer (Jangde and Daharwal, 2011). Synthetic photoprotective agents can be potentially toxic and carcinogenic and therefore phytoconstituents are becoming popular as essential ingredients of cosmetic formulations (Eff *et al.*, 2019). Today people are showing more interest towards herbal cosmetics comparatively

¹ Department of Chemistry, Sagaing University of Education

¹ Department of Chemistry, Sagaing University of Education

² Department of Chemistry, Sagaing University of Education

³ Sagaing University of Education

synthetic cosmetic products. The best thing about herbal cosmetics is that they are purely made from herbs and shrubs, so they are side-effect free and free from harmful chemicals. The main benefits reported for herbals, used in skincare and cosmetics include antioxidant, anti-inflammatory, antiseptic, and antimicrobial properties (Roy and Sahu, 2014).

Premna integrifolia L. (Figure 1) (Taung-tan-gyi in Myanmar) belongs to the Verbenaceae family and it comprises 200 species of which 30 are available in India. Its hypolipidemic, anti-diabetic, anti-inflammatory and immuno-modulatory activities were reported. Various parts of plants, like leaves, stem, stem barks, root, root barks and wood are used to treat different diseases (Chitra *et al.*, 2018). To improve the sun protection activity of the prepared herbal sunscreen gels, the incorporation of watery and ethanol extracts of *P. integrifolia* stem was conducted according to Grace *et al.* (2014) with some modifications.

Botanical Description of *Premna integrifolia* L. (Taung-tan-gyi)



Family name	: Verbenaceae
Genus	: <i>Premna</i>
Specie	: <i>integrifolia</i>
Botanical name	: <i>Premna integrifolia</i> L. (Kress <i>et al.</i> , 2003)
Myanmar name	: Taung-tan-gyi
Part used	: Stem
Distribution	: the plant prefers warm and humid climate

Figure 1. Photograph of *Premna integrifolia* L.

Materials and Methods

Sample Collection and Identification

In this research, the stem of *P. integrifolia* was collected from a local market in Tanintharyi Region, Myanmar. After cleaning, the sample was air-dried at room temperature for one week and the dried sample was ground into powder by a grinder. The dried powdered sample was stored separately in air-tight containers to prevent moisture changes and other contamination. The sample was identified by an authorized botanist of the Department of Biology, Sagaing University of Education, Myanmar.

Preliminary Phytochemical Tests

The preliminary phytochemical tests of the selected sample were carried out using the standard methods (Harborne, 1984; Marini-Bettoto *et al.*, 1981 and M-Tin Wa, 1972).

Preparation of Extracts

After performing the preliminary phytochemical tests of the selected sample, it is required to obtain watery and ethanol extracts for the preparation of herbal sunscreen gels according to the reported methods.

Preparation of Herbal Sunscreen Gels

Herbal sunscreen gels were prepared according to Grace *et al.* (2014) with some modifications. For 100 g herbal sunscreen gel, the preservatives methylparaben (0.1 %) and propylparaben (0.1 %) were dissolved in a few mL of distilled water and the gelling agent carbopol 940 (2 %) was added to the above solution. Then the solution was kept under constant stirring using a magnetic stirrer for complete dissolution of the contents. After complete dissolution, humectant glycerine (2 %) and neutralizer triethanolamine (2 %) were added under constant stirring until a uniform mixture. The active ingredient extract (1 %) and sufficient amount of distilled water were then carefully added to the above mixture and stirred continuously until a smooth and homogeneous gel was obtained.

Evaluation of some Parameters of Herbal Sunscreen Gels

The colour and odour of the samples were evaluated both visually and manually. The appearance of the samples was judged by their colour, roughness, and grade.

The consistency of the samples was evaluated by manually. The homogeneity of the samples was evaluated by visual appearance and touch. The washability of the samples was applied to the hand and washed by keeping the hand with tap water.

About 0.5 g of the sample was weighed and dispersed in 50 mL of distilled water to determine the pH using the pH paper and pH meter (Model HI-9812 HANNA instruments). The viscosity of the sample was measured using a rotor spin type (L-4) at 100 rpm with an ATAGO viscometer (BASE Series L, Japan) in Physical Research Room, Department of Chemistry, University of Yangon. The viscosity values of the samples were recorded directly from the instrument display.

Determination of Sun Protection Factor (SPF)

Determination of SPF of prepared herbal sunscreen gels was carried out by UV-vis spectrophotometer and Mansur mathematical calculation method at the Medical Biotechnology Laboratory, Department of Biotechnology Research (DBR), Kyaukse Township, Mandalay Region, Myanmar.

The photoprotective activity of tested samples was measured by the determination of sun protection factor (SPF) (Mansur *et al.*, 1986). Sample (2 mg) was diluted in 1 mL of methanol to obtain a concentration of 2 mg/mL. Spectrophotometric scanning was performed at wavelengths between 290 and 320 nm, with intervals of 5 nm using a 96-well microplate reader. SPF value was obtained according to the equation developed by (Mansur *et al.* 1986) and Kumar *et al.* (2016). The SPF value was calculated using the following equation.

$$\text{SPF} = \text{CF} \times \sum_{290}^{320} \cdot \text{EE}(\lambda) \times \text{I}(\lambda) \times \text{Abs}(\lambda)$$

CF = correction factor (= 10)

EE (λ) = erythemogenic effect of radiation with wavelength λ

I (λ) = solar intensity spectrum

Abs (λ) = spectrophotometric absorbance values of sunscreen product at wavelength λ

EE \times I = constant is determined by Sayre *et al.* (1979) **Skin Irritancy Test on Human**

Skin

The skin irritancy test was performed on 10 selected adults (male/female) from Sagaing University of Education, Myanmar. According to the patch test description, the student volunteers were divided into two groups. Each group contained five student volunteers who were physically and mentally healthy, skin free from lesions and no history of allergies. Groups (A) and (B) volunteers were marked with an area of 3 cm² on their left-hand dorsal surface applied with 0.5 g prepared herbal sunscreen gel containing watery and ethanol extracts and their right-hand dorsal surface was used as control (without applied gels). Then, irritancy, erythema, and edema were checked if any, at regular intervals up to every 24 h for fourteen days, and irritation reactions were recorded.

Investigation of Antibacterial Activity

Screening of the antibacterial activity of prepared herbal sunscreen gels were carried out against Gram-positive bacteria (*Staphylococcus aureus*) as the tested microorganism for this experiment. The tests were screened at the Pharmaceutical Research Laboratory, Department of Biotechnology Research (DBR), Kyaukse Township, Mandalay Region, Myanmar.

The agar well diffusion method was used for antibacterial activity evaluation by modifying the previous method (Schlegel and Zaborosch, 1993). Tested microorganisms were inoculated in Muller Hinton Broth at 37 °C for overnight. On the next day, the overnight broth culture was diluted with normal saline to obtain the OD₆₀₀ at 0.08 to 0.1 with an approximate cell density of 1.5 × 10⁸ CFU/mL. Muller Hinton agar plates were prepared and sterilized by autoclaving at 121 °C for 15 min. The broth inoculums were evenly spread out with sterile cotton swabs on the Muller Hinton agar plates to obtain the uniform inoculums. After the plate was inoculated, 8 mm diameter wells were made on the agar medium by using a sterile cork borer. Each 50 µL (0.2 g/mL) of samples was introduced into each labelled well. Chloramphenicol (30 µg/well) was used as the positive control. Then, the plates were placed in an incubator at 37 °C for 16 to 18 h. After incubation, the plates were examined and zone diameters of complete inhibition were measured and recorded to the nearest millimeter.

Results and Discussion

Phytochemicals Present in the *P. integrifolia* Stem

The qualitative preliminary phytochemical screening of *P. integrifolia* stem revealed the presence of alkaloids, amino acids, carbohydrates, flavonoids, glycosides, phenolic compounds, reducing sugars, saponins and starch in the sample. However, steroids and tannins were not detected in the sample (Table 1). Therefore, to improve the sun protection activity of prepared herbal sunscreen gels, a good combination of phytoconstituents was conducted, and thus confirming the SPF value in this research.

Table 1. Results of Phytochemical Investigations of *Premna integrifolia* Stem

No	Test	Extract	Test reagent	Observation	Result
1	alkaloids	1% HCl	Dragendorff's reagent Mayer's reagent Wagner's reagent	orange ppt. white ppt. reddish brown ppt.	+ + +
2	α -Amino acids	H ₂ O	Ninhydrin reagent	violet colour	+
3	carbohydrates	H ₂ O	10 % α -Naphthol, conc. H ₂ SO ₄	red ring	+
4	flavonoids	EtOH	Mg turning, conc. HCl	pink colour	+
5	glycosides	H ₂ O	10 % lead acetate	white ppt.	+
6	phenolic compounds	EtOH	1 % FeCl ₃ solution	dark blue colour	+
7	reducing sugars	H ₂ O	Benedict's solution	brick-red ppt.	+
8	saponins	H ₂ O	distilled water	frothing	+
9	starch	H ₂ O	1 % iodine solution	blackish blue	+
10	steroids	PE	acetic anhydride, conc. H ₂ SO ₄	no greenish blue	-
11	tannins	H ₂ O	1 % gelatin	no white ppt.	-

(+) = presence, (-) = absence, (ppt.) = precipitate

Herbal Sunscreen Gels Prepared from Plant Extracts

After performing the preliminary phytochemical tests, it is required to obtain watery and ethanol extracts for the preparation of herbal sunscreen gels. Plant extracts containing a wide range of phenolic acids, flavonoids and high molecular weight polyphenols usually cover the full range of UV wavelengths. These bioactive components have the capability to absorb UV radiation (Bambal *et al.*, 2011). To improve the sun protection activity of prepared herbal sunscreen gels, the incorporation of watery and ethanol extracts of *P. integrifolia* stem was conducted.

Some Parameters of Herbal Sunscreen Gels

The observed colour of the prepared herbal sunscreen gel containing watery extract was brown, and the ethanol extract was yellowish brown. Both of the prepared gels had a pleasant odour.

The prepared herbal sunscreen gels had smooth and good consistency and had no gritty particles. The homogeneity test confirms the uniform distribution of extracts in the prepared gels and shows the absence of granules. So, from the prepared gels, it can be said that they had great homogeneity. The prepared herbal sunscreen gels exhibited a non-greasy effect, after application to the skin. The gels were easily removed by washing them with tap water.

The pH of the prepared herbal sunscreen gels containing watery extract was found to be 6.3 and 6.2 for ethanol extract. These pH values agree with the specification (4.5-8.0) of the

Sunscreen Preparations National Standardization Agency (SNI, 1996), corresponding to the human skin pH (4.5-7.0). So, the prepared herbal sunscreen gels were safe to use on the skin. The viscosity of the prepared herbal sunscreen gels was found to be > 5000 cP, meeting the requirements of sunscreen preparations (2000-50000 cP) (SNI, 1996).

Sun Protection Factor of the Prepared Herbal Sunscreen Gel

The results of the SPF determination of the prepared herbal sunscreen gels indicated that watery extract possesses a higher SPF value 16.16 than ethanol extract 13.89. The SPF value of the prepared sample is very appreciative when it is compared with that of other herbal extracts reported by various authors (Bambal *et al.*, 2011; Mamillapalli *et al.*, 2018; Yanti Eff *et al.*, 2019). The SPF of the standard marketed product was found to be 34.48. The prepared herbal sunscreen gels were found to have sun protection activity of 94 % for watery extract and 93 % for ethanol extract. Thus, prepared gels exhibit significant sun protection activities and may be effectively utilized as herbal sunscreen gels preferred by users with oily skin (Tables 2, 3, 4, 5 and Figure 2).

Table 2. SPF Value of Prepared Herbal Sunscreen Gel-H₂O

Sample	Wavelength	Average Absorbance	EE × I	Abs × (EE × I)
Gel-H ₂ O	290	1.96 ± 0.21	0.0150	0.0294
	295	1.85 ± 0.05	0.0817	0.1511
	300	1.78 ± 0.01	0.2874	0.5116
	305	1.68 ± 0.01	0.3278	0.5507
	310	1.32 ± 0.01	0.1864	0.2460
	315	1.26 ± 0.01	0.0839	0.1057
	320	1.19 ± 0.01	0.0180	0.0214

$$\begin{aligned} \text{SPF} &= \text{CF} \times \sum_{290}^{320} \cdot \text{EE}(\lambda) \times \text{I}(\lambda) \times \text{Abs}(\lambda) \\ &= 10 \times 1.6159 \\ &= 16.16 \end{aligned}$$

Table 3. SPF Value of Prepared Herbal Sunscreen Gel-EtOH

Sample	Wavelength (nm)	Average Absorbance	EE × I	Abs × (EE × I)
Gel-EtOH	290	2.28 ± 0.20	0.0150	0.0342
	295	1.96 ± 0.02	0.0817	0.1601
	300	1.78 ± 0.02	0.2874	0.5116
	305	1.25 ± 0.02	0.3278	0.4098
	310	1.13 ± 0.02	0.1864	0.2106
	315	0.64 ± 0.02	0.0839	0.0537
	320	0.51 ± 0.01	0.0180	0.0092

$$\begin{aligned} \text{SPF} &= \text{CF} \times \sum_{290}^{320} \cdot \text{EE}(\lambda) \times \text{I}(\lambda) \times \text{Abs}(\lambda) \\ &= 10 \times 1.3892 \\ &= 13.89 \end{aligned}$$

Table 4. SPF Value of Marketed Product

Sample	Wavelength(nm)	Average Absorbance	EE × I	Abs × (EE × I)
sunblock 27 from Nature Republic (Korea)	290	3.49 ± 0.01	0.0150	0.0524
	295	3.50 ± 0.00	0.0817	0.2860
	300	3.49 ± 0.03	0.2874	1.0030
	305	3.50 ± 0.00	0.3278	1.1473
	310	3.41 ± 0.09	0.1864	0.6356
	315	3.16 ± 0.11	0.0839	0.2819
				3.4482 ± 0.26

$$\begin{aligned}
 \text{SPF} &= \text{CF} \times \sum_{290}^{320} \cdot \text{EE}(\lambda) \times \text{I}(\lambda) \times \text{Abs}(\lambda) \\
 &= 10 \times 3.4482 \\
 &= 34.48
 \end{aligned}$$

Table 5. Comparison of SPF Values of Prepared Gels and Marketed Product

No	Sample	SPF Calculated Value	UV Protection Rate (%)
1	Gel-H ₂ O	16.16	94
2	Gel-EtOH	13.89	93
3	*Marketed product	34.48	97

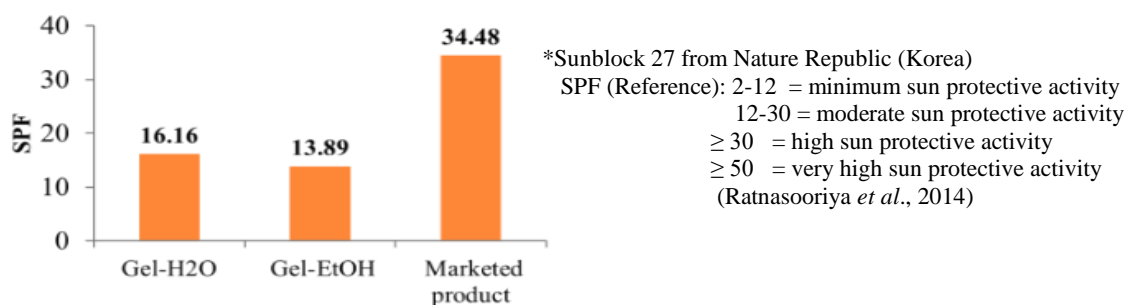


Figure 2. Comparison of SPF values of prepared gels and *marketed product

Irritancy Test on Human Skin

Evaluation of the efficacy of sunscreen for a long time has been assessed through skin test, which was performed with human volunteers. After two weeks of the applied part with prepared gels, a skin irritation study exhibited no redness, edema, inflammation, irritation, sensitivity, or minor or patchy erythema. The prepared herbal sunscreen gels were safe to use on the skin and provided complete protection from skin irritation.

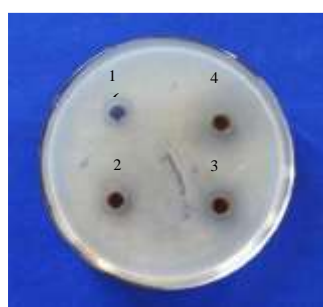
Antibacterial Activity of Prepared Herbal Sunscreen Gels

The prepared gel showed only mild antibacterial activity on *S. aureus* (Table 6 and Figure 3). *S. aureus* mainly causes skin infections and thrives best at pH 7.5, while at pH 5 to 6, they grow poorly (Tiwari *et al.*, 2022). The pH values of prepared gels were found to be 6.3 for watery extract and 6.2 for ethanol extract. The results of the pH determination indicated an appropriate pH range for inhibition of *S. aureus* skin infection.

Table 6. Antibacterial Activity of Prepared Herbal Sunscreen Gels on *S. aureus*

No.	Sample	Inhibition zone diameters (mm)
1	70 % EtOH	0
2	Gel-H ₂ O	12
3	Gel-EtOH	11
4	Chloramphenicol	22

Agar well = 10 mm	10 mm ~ 14 mm Activity weak	15 mm ~ 19 mm high activity	20 mm above very high activity
-------------------	--------------------------------	--------------------------------	-----------------------------------



- 1 = Negative control (70 % EtOH)
 2 = Herbal sunscreen cream-H₂O extract
 3 = Herbal sunscreen cream-EtOH extract
 4 = Positive control (Chloramphenicol)

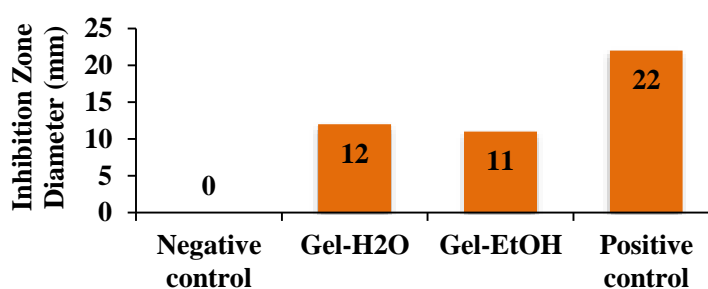


Figure 3. Antibacterial activity of prepared gels on *S. aureus*

Conclusion

Herbal sunscreen gels were successfully prepared using watery and ethanol extracts from *Premna integrifolia* L. (Taung-tan-gyi) stem in this research. From the results obtained in the study, it can be concluded that the prepared herbal sunscreen gels meet the requirements for sunscreen evaluation parameters such as colour, odour, appearance, consistency, homogeneity, washability, pH, viscosity and SPF value. In addition, the prepared herbal sunscreen gels did not irritate the skin, according to the antibacterial activity investigation and skin irritancy study. Incorporating herbal extracts into sunscreen gel preparation, SPF values showed 16.16 (94 % sun protection activity) for watery extract and 13.89 (93 % sun protection activity) for ethanol extract, which were found to have not much different sun protection properties in this research.

Acknowledgements

The authors would like to express their profound gratitude to the Department of Higher Education, Ministry of Education, Myanmar, Pro-Rectors Dr Khin Hnin Yee and Dr Cho Kyi Than (Sagaing University of Education) for provision of opportunity to do this research. Special thanks are extended to the specialists from Medical Biotechnology Laboratory, Department of Biotechnology Research (DBR), Kyaukse, Mandalay Province, Myanmar and Department of Chemistry, University of Yangon for their cooperation.

References

- Bambal, V., N. Wyawahare, A. Turaskar, and M. Mishra. (2011). "Study of Sunscreen Activity of Herbal Cream Containing Flower Extract of *Nyctanthes arbortristis* L. and *Tagetes erecta* L.". *International Journal of Pharmaceutical Sciences Review and Research*, vol. 11(1), pp.142-146
- Chitra, S., C. H. V. Narasimhaji, S. Susikumar, G. Nartunai, C. Arunachalam, R. Ilavarasan, G. Sudesh, and K. S. Dhiman Vd. (2018). "Pharmacognostical and Phytochemical Evaluation of Root Bark of *Premna integrifolia* Linn". *Journal of Pharmacognosy and Phytochemistry*, vol. 7(1), pp. 1181-1186
- Eff, A. R. Y., S. T. Rahayu, H. Saraswati and A. Mun'im. (2019). "Formulation and Evaluation of Sunscreen Gels Containing Mangiferin Isolated from *Phaleria macrocarpa* Fruits". *Int. J. Pharm. Investigation*, vol. 9(3), pp. 141-145
- Grace, F. X., J. R. Vijetha, R. S. Raj, S. Shanmuganathan and D. Chamundeeswari. (2014). "Formulation, *In-Vitro* Evaluation and UV Protective Study of Polyherbal Sunscreen Gel". *World Journal of Pharmaceutical Research*, vol. 3(4), pp. 2196-2203
- Harborne, J. B. (1984). *Phytochemical Methods, A Guide to Modern Techniques of Plant Analysis*. New York: 2nd Ed., Chapman and Hall, pp. 120-126
- Jangde, R. and S. J. Daharwal. (2011). "Herbal Sunscreen: An Overview". *Research J. Topical and Cosmetic Sci.*, vol. 2(2), pp. 35-39
- Kress, W. J., R. A. Defilippis, E. Farr and Yin Yin Kyi. (2003). *A Checklist of the Trees, Shrubs, Herbs, and Climbers of Myanmar*. Washington D C, Department of Systematic Biology-Botany National Museum of Natural History.
- Kumar, D., G. Rajora, O. Parkash, Himanshu, M. Antil and V. Kumar. (2016). "Herbal Cosmetics : An overview". *Int'l J. of Advanced Scientific Research*, vol. 1(4), pp. 36-41
- Mamillapalli, V., P. L. Khantamneni, S. Koleti, K. Ghanta, H. M. Yakkali, K. M. Puli and G. Kolusu. (2018). "Phytochemical and *In Vitro* Sun Protection Factor Evaluation of *Peltophorum Pterocarpum* Leaf Extracts". *Int. J. Pharm. Sci. Rev. Res.*, vol. 48(2), pp. 49-58
- Mansur, J. S., M. Breder, M. Mansur, R. D. Azulay. (1986). "Determination of Sun Protection Factor by Spectrophotometry". *An. Bras. Dermatol.*, vol. 61(3), pp. 121-124
- Marini-Bettolo, G. B., M. Nicolettic and M. Patamia. (1981). "Plant Screening by Chemical and Chromatographic Procedure Under Field Conditions". *J. Chromato.*, vol. 45, pp. 121-123
- M-Tin Wa. (1972). "Phytochemical Screening Methods and Procedures". *Phytochemical Bulletin of Botanical Society of America*, vol. 5(3), pp. 4-10
- Ratnasooriya, W. D., J. R. A. C. Jayakody, S. R. D. Rosa and C. D. T. Ratnasooriya. (2014). "*In Vitro* Sun Screening Activity of Sri Lankan Orthodox Black Tea (*Camellia sinensis* Linn)". *World Journal of Pharmaceutical Sciences*, pp.144-148
- Roy, A. and R. K. Sahu. (2014). "Formulation and Development of Herbal Sunscreen Cream". *Research J. Topical and Cosmetic Sci.* vol. 5(1), pp. 12-14
- Sayre, R. M., P. P. Agin, G. J. Le Vee and E. Marlowe. (1979). "A Comparison of *In Vivo* and *In Vitro* Testing of Sunscreen Formulas". *Photochem. Photobiol.*, vol. 29(3), pp. 559-566

- Schlegel, H. G. and C. Zaborosch. (1993). *General Microbiology Cambridge*, Cambridge University Press
- SNI. (1996). Sunscreen Preparations SNI 16-4399-1996. Jakarta. National Standardization Agency, pp. 1-3
- Tiwari, R., I. Singh, M. Gupta, L. P. Singh and G. Tiwari. (2022). "Formulation and Evaluation of Herbal Sunscreens: An Assessment Towards Skin Protection from Ultraviolet Radiation". *Pharmacophore*, vol. 13(3), pp. 41-49
- Yusnelti, R. Asra and M. Aina. (2018). "Formulation of Sunscreen Cream from Tengawang Oil (Shorea Sumatrana)". *International Conference on Pharmaceutical Research and Practice*, Universitas Islam Indonesia, pp. 196-200

SCREENING ON CYTOTOXICITY, ANTI-INFLAMMATORY, ANTIPROLIFERATIVE, AND ANTIARTHRITIC ACTIVITIES OF THE *STEPHANIA VENOSA* (BLUME) SPRENG. (TAUNG-KYA) TUBER

Mi Aye Aye Aung¹, Kay Khine Nyunt², Myint Myint Khine³, Ni Ni Than⁴

Abstract

Stephania venosa (Blume) Spreng. (Taung-kya) belongs to the family Menispermaceae and is a rich source of alkaloids. The research focused on the screening of the cytotoxicity, anti-inflammatory, antiproliferative, and antiarthritic activities of the tuber of *S. venosa*. The cytotoxicity activity of the watery and ethanol extracts determined by a brine shrimp lethality bioassay showed LD₅₀ values > 1000 µg/mL, a non-toxic effect. The anti-inflammatory activity of the methanol and watery extracts of *S. venosa* was determined by inhibition of nitric oxide (NO) production against LPS-induced RAW 264.7 cells. The IC₅₀ value of nitric oxide inhibition was found to be less than the IC₅₀ value of cell viability. The watery extract showed mild antiproliferative activity against the A549 cell line with an IC₅₀ value of 144.86 µg/mL. The watery extract was found to possess significant antiproliferative activity against the HeLa (Cervix cancer) cell line, with the IC₅₀ value less than 20 µg/mL. Additionally, the methanol extract had significant antiproliferative activity against the A549 (Lung cancer) cell line, with an IC₅₀ value of less than 20 µg/mL. But the methanol extract possessed weaker antiproliferative activity for HeLa (Cervix cancer) cell line, with IC₅₀ values >200 µg/mL than the standard 5 FU (IC₅₀ =19.06 µg/mL against Lung cancer cell line and IC₅₀ =15.84 µg/mL Cervix cancer cell line). The antiarthritic activity of ethanol and watery extracts was determined by using fresh hen's egg albumin denaturation method in different concentrations ranging from 50 to 1600 µg/mL. According to the results, the IC₅₀ values of ethanol and watery extracts were found to be 743 µg/mL and > 1600 µg/mL, respectively. Therefore, the two extracts showed lower antiarthritic activity than the standard drug diclofenac sodium (IC₅₀ = 266 µg/mL).

Keywords: *Stephania venosa* (Blume) Spreng., cytotoxicity, anti-inflammatory, antiproliferative and antiarthritic activities

Introduction

Stephania venosa (Blume) Spreng. is an herbaceous perennial vine growing to around four metres tall with a large tuber on the ground. It belongs to the Menispermaceae family and is known as Taung-kya in Myanmar (Figure 1). It is widely distributed in East and South Asia and Australia. Its leaves are spirally arranged on the stem, with the leaf petiole attached near the centre of the leaf. It is a plant rich in alkaloids. Its tubers have been used in traditional medicine as nerve tonics, aphrodisiacs, and appetizers. Moreover, it is also used for the treatment of asthma, hyperglycemia, antimalarial activities, microbial infections, and cancer. *S. venosa* leaves have been used to treat ringworm, tinea versicolor, chronic cancer, and acne. It has been reported to have a range of biological effects (Moongkarndi *et al.*, 2004). The phytochemical screening from the tuber of the plant showed the presence of a wide variety of isoquinoline and aporphine alkaloids with different structural types including tetrahydropalmatine, crebanine, *O*-methylbulbocapnine, and *N*-methyltetrahydropalmatine. *S. venosa* possesses various pharmacological activities reported by Ingkaninan *et al.* (2006). The aim of the present work is to

¹ Department of Chemistry, West Yangon University

² Department of Chemistry, Dagon University

³ Myingyan University

⁴ Department of Chemistry, University of Yangon

screen the cytotoxicity, anti-inflammatory, antiproliferative, and antiarthritic activities of the tuber of *S. venosa*.



Figure 1. The photograph of tuber of *Stephania venosa* (Blume) Spreng.

Materials and Methods

Collection and Identification of Plant Samples

The tuber of *S. venosa* (Blume) Spreng. was collected from Thanlyin Township, Yangon Region, Myanmar, in June, 2019. The plant was identified at the Department of Botany, Hpa-an University. The sample was washed, dried in the shade for a week, cut into very small pieces, and then ground into a fine powder using an electric grinder. The powdered sample was stored in an air-tight container.

Chemicals

Phosphate buffer saline (PBS) powder, fetal bovine serum (FBS, Sigma 172012), trypsin, alcohol (MeOH and EtOH), Minimum Essential Medium α (MEM, Wako 135-15735), 0.1 mM Non-Essential Amino Acid (NEAA, Gibco 11140-050), Lipopoly saccharide (LPS), (naphthyl)ethylenediamine dihydrochloride, sulphanilamide, 1mM sodium pyruvate (SM, Gibco-11360-170) and MTT reagent, dimethyl sulfoxide (DMSO), distilled water, bovine serum albumin (BSA), sodium chloride (NaCl), disodium hydrogen phosphate (Na_2HPO_4), monosodium dihydrogen phosphate (NaH_2PO_4), diclofenac sodium, potassium dichromate, caffeine, artificial seawater (37 %)

Instruments

Quartz cuvette (4 mL), UV-visible spectrophotometer (UV-7504), a stirrer, an autoclave (Tomy Seiko Co., Ltd, Tokyo, Japan), a constant temperature bath (Yamato Scientific Co., Ltd, Japan), sterile Petri-dish, spirit burner, polyethylene plastic bag, a refrigerator and an incubator, multipipette, 96 well plate, aluminum foil, centrifuge tube, Haemocytometer, microscope and vibrator, syringe (3 mL, 5 mL), beakers, chambers, Pasteur pipette, lamp and water bottles (1.5 mL)

Preparation of Extracts from the *S. venosa* Tuber

Each 50 g of air-dried powder sample was percolated with ethanol (100 mL), methanol (100 mL), and water (100 mL) for one week at room temperature, and then the filtrate was individually evaporated under reduced pressure by a rotatory evaporator to yield different solvent extracts.

Determination of Cytotoxicity of *S. venosa* by Brine Shrimp Lethality Bioassay

The cytotoxicity of ethanol and watery extracts of *S. venosa* was investigated by a brine shrimp lethality bioassay, according to the procedure described by Olowa *et al.* (2013). The brine shrimp (*Artemia salina*) was used in this bioassay (Ali *et al.*, 2013). The sample solution was prepared by dissolving 5 mg of the respective crude extract in 5 mL of distilled water. The stock solution was tenfold diluted serially with distilled water to get the sample solutions with concentrations of 1000, 100, 10, and 1 $\mu\text{g/mL}$. Artificial seawater (9 mL) was mixed with the sample solution (1 mL) and placed in the chamber of the ice cup. Alive brine shrimp (10 nauplii) were taken with a Pasteur pipette and then placed into each chamber, which was kept at room temperature for about 24 h. After 24 h incubation, the number of surviving brine shrimp was counted, and a 50 % lethal dose (LD_{50}) was calculated. Cytotoxic effect of control solutions ($\text{K}_2\text{Cr}_2\text{O}_7$ and caffeine) was also determined according to the above procedure.

Determination of *in vitro* Anti-inflammatory Activity of Crude Extracts from Tuber of *S. venosa*

In vitro anti-inflammatory activity of methanol and watery extracts of the tuber of *S. venosa* was evaluated by a nitric oxide (NO) inhibition assay against LPS-induced RAW cells according to the method (Jin *et al.*, 2012) modified by Win *et al.* (2015). These tests were done at the Department of Natural Products Chemistry, the Institute of Natural Medicine, and the University of Toyama, Japan. When the cell proliferation reached about 70 % confluence, the cells were harvested using a cell scraper and diluted to a suspension in fresh medium. The 100 μL of cells ($1 \times 10^4/\text{well}$) were seeded in the 96 well plates, and then, they were incubated for 24 h at 37 $^\circ\text{C}$. The cells were treated with 50 μL each of LPS (100 ng/mL) and 100 $\mu\text{g/mL}$ and 10 $\mu\text{g/mL}$ of different doses of samples for 24 h. After incubation at 37 $^\circ\text{C}$ for 24 h, 100 μL each of the supernatants from 96 well was mixed with an equal volume of Griess reagent (0.5 % sulphanilamide and 0.05 % naphthylenediamide dihydrochloride in 2.5 % H_3PO_4) in the new 96 well plates and allowed to stand for 5 min at room temperature. The resulting colour was assayed for absorbance at 540 nm using a microplate reader. L-NMMA monoacetate was used as a positive control. On the other hand, the effect of the samples on cell proliferation was evaluated by the MTT reagent. The 100 μL of MTT (5 mg/mL) in the medium was added to the remaining 96 wells. After 2 h incubation, the medium was discarded and 100 μL each of DMSO was added to dissolve the formazan crystals, and the absorbance at 570 nm was recorded by a microplate spectrophotometer. The percentage of NO inhibition and that of cell viability were calculated as follows:

$$\text{NO inhibition (\%)} = [(\text{Abs}_{(\text{control})} - \text{Abs}_{(\text{sample})})/\text{Abs}_{(\text{control})}] \times 100$$

where, $\text{Abs}_{(\text{control})}$ = the absorbance of LPS treated control group,

$\text{Abs}_{(\text{sample})}$ = the absorbance of the sample

$$\text{Cell viability (\%)} = [(\text{Abs}_{(\text{test sample})} - \text{Abs}_{(\text{blank})})/(\text{Abs}_{(\text{control})} - \text{Abs}_{(\text{blank})})] \times 100$$

where, $\text{Abs}_{(\text{test sample})}$ = absorbance of test sample solution,

$\text{Abs}_{(\text{control})}$ = absorbance of DMSO solution,

$\text{Abs}_{(\text{blank})}$ = absorbance of MTT reagent.

IC₅₀ (50 % inhibitory concentration) in % NO inhibition should be less than IC₅₀ in % cell viability if the extract exhibits only an anti-inflammatory effect.

Determination of *in vitro* Antiproliferative Activity of Watery and Methanol Extracts Against Human Cancer Cell Lines

The antiproliferative activity of watery and methanol extracts from the tuber of *S. venosa* was tested against two human cancer cell lines, A549 (lung cancer) and HeLa (cervical cancer). The antiproliferative activity was assessed using the MTT (3-(4,5-dimethylthiazol-2-yl)-2,5-diphenyltetrazolium bromide) assay (Win *et al.*, 2015). These tests were done at the Department of Natural Products Chemistry, the Institute of Natural Medicine, and the University of Toyama, Japan. This assay detects the reduction of MTT by mitochondrial dehydrogenase to a blue formazan product, indicating the normal function of mitochondria and cell viability. A minimum essential medium with L-glutamine and phenol red (α -MEM, Wako) was used for cell cultures. All media were supplemented with 10 % fetal bovine serum (FBS, Sigma) and 1 % antibiotic antimycotic solution (Sigma). From the above medium solution, 100 mL of this supplemented medium was mixed with 1 mL of non-essential amino acid (NAA) for A549. The antiproliferative activity of the crude extracts was determined by the procedure described by Win *et al.* (2015). The assay was carried out using MTT dye and measuring the absorbance at 570 nm with a SH-1200 microplate reader (Corona, Hitachinaka, Japan). Briefly, each cell line was seeded in 96-well plates (2×10^3 per well) and incubated in the respective medium at 37 °C under 5 % CO₂ and 95 % air for 24 h. After that, the cells were treated with serial dilutions of the tested samples. After 72 h of incubation, the cells were washed twice with PBS, and 100 μ L of MTT reagent solution was added to the wells. After 3 h incubation, the medium will be aspirated, followed by the addition of 100 μ L of DMSO to the 96 well plates. The concentrations of the crude extracts were 200, 20 μ g/mL, and 20, 10, and 2 mm for the positive control prepared by serial dilution. Cell viability was calculated from the mean values of the data from three wells using the equation below. The antiproliferative activity was expressed as the IC₅₀ (50 % inhibitory concentration) value compared to the 5-fluorouracil (5 FU) as a positive control.

$$\text{Cell viability (\%)} = \frac{(\text{Abs}_{(\text{test sample})} - \text{Abs}_{(\text{blank})})}{(\text{Abs}_{(\text{control})} - \text{Abs}_{(\text{blank})})} \times 100$$

where, Abs_(test sample) = absorbance of test sample solution,

Abs_(control) = absorbance of DMSO solution,

Abs_(blank) = absorbance of MTT reagent.

Determination of *in vitro* Antiarthritic Activity of Watery and Ethanol Extracts by Protein Denaturation Method

The *in vitro* antiarthritic activity was studied by the protein denaturation method using fresh hen's egg albumin and bovine serum albumin (Rahman *et al.*, 2012). The reaction mixture consisted of test solutions with different concentrations (1600, 800, 400, 200, 100, and 50 μ g/mL), 0.2 mL of fresh hen's egg albumin, and 2.8 mL of phosphate buffered saline (pH 6.3) were mixed to form a total volume of 5 mL. An equal volume of distilled water served as the control solution. The test samples and standard were incubated at 37 °C in an incubator for 15 min, and then, followed by heating at 70 °C for 5 min. The absorbance of these solutions was

measured at 660 nm using a UV-visible spectrophotometer. The percentage inhibition of protein denaturation was calculated by the following formula:

$$\% \text{ Inhibition} = \frac{A_{\text{control}} - (A_{\text{sample}} - A_{\text{blank}})}{A_{\text{control}}} \times 100$$

where, A_{sample} = absorbance of the sample (with egg albumin),

A_{blank} = absorbance of blank (only sample? without egg albumin),

A_{control} = absorbance of control (only egg albumin).

Standard deviation (SD) and 50 % inhibition concentration (IC_{50}) value were calculated by linear regressive excel program.

Results and Discussion

Cytotoxicity of Ethanol and Watery Extracts from the Tuber of *Stephania venosa*

The cytotoxic activity of ethanol and watery extracts of tuber of *Stephania venosa* (Blume) Spreng. was evaluated by a brine shrimp lethality bioassay. The nauplii were exposed to different concentrations of plant extracts for 24 h. The number of motile nauplii was calculated to determine the effectiveness of the extract. The cytotoxic effect was expressed as LD_{50} values (50 % lethal dose). The potassium dichromate ($K_2Cr_2O_7$) and caffeine were chosen as a positive control and a negative control, respectively, because $K_2Cr_2O_7$ is a toxic agent in this assay and caffeine is a natural product. From the results, the LD_{50} values of ethanol and watery extracts were found to be $> 1000 \mu\text{g/mL}$, and the standard potassium dichromate and caffeine were $509 \mu\text{g/mL}$ and $> 1000 \mu\text{g/mL}$, respectively. In the presence study, the two extracts did not exhibit cytotoxic effects comparable to those of the standard potassium dichromate. Therefore, ethanol and watery extracts of *S. venosa*, were relatively safe to be consumed as antioxidants for cancer chemoprevention. After 24 h, it could be deduced that the two extracts were not cytotoxic to the brine shrimp up to the maximum dose of $1000 \mu\text{g/mL}$ compared with the Deciga-Campos criteria. For the standard potassium dichromate, the LD_{50} was $509 \mu\text{g/mL}$, and for caffeine, it was $> 1000 \mu\text{g/mL}$. The experimental data are shown in Table 1 and Figure 2.

Table 1. Cytotoxicity of Ethanol and Watery Crude Extracts from the Tuber of *S. venosa*

Sample	No. of dead of brine shrimp (Mean \pm SD) at various concentrations ($\mu\text{g/mL}$)				
	1	10	100	1000	LD_{50}
EtOH extract	6 ± 0.1	6 ± 0.1	6 ± 0.1	18 ± 0.1	>1000
watery extract	0 ± 0	0 ± 0	18 ± 0.1	34 ± 0.1	>1000
* $K_2Cr_2O_7$	0 ± 0	0 ± 0	17 ± 0.5	90 ± 0.3	509
** caffeine	3 ± 0.5	10 ± 0.9	20 ± 0.3	27 ± 0.9	>1000

* positive control, ** negative control

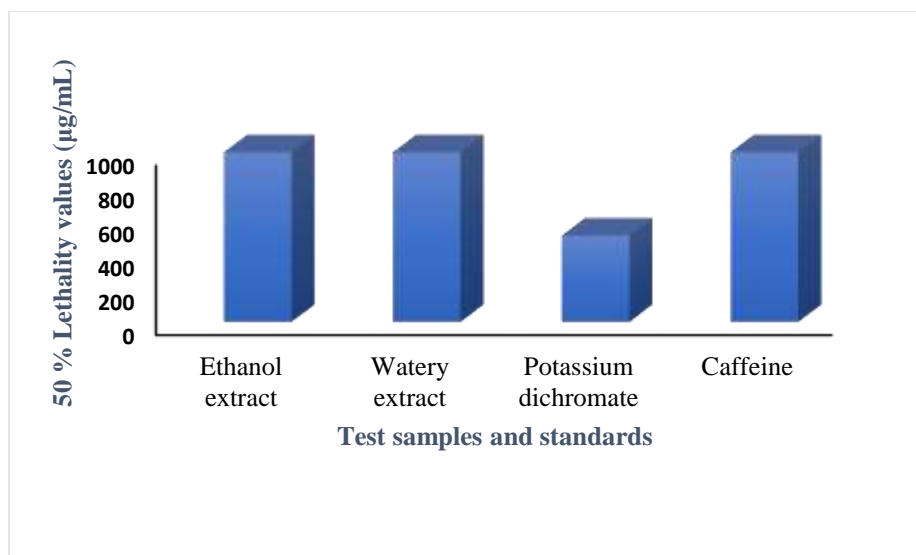


Figure 2. Brine shrimp lethality of crude extracts from the tuber of *S. venosa*

Anti-inflammatory Activity of Crude Extracts from the Tuber of *S. venosa*

In vitro anti-inflammatory activity of crude extracts (methanol, and watery extracts) of the tuber of *S. venosa* was determined by the inhibition of NO production against LPS-induced RAW 264.7 cells. NO production is a typical phenomenon that occurs in LPS-stimulated macrophages and is used as an indicator of a typical inflammatory response. The anti-inflammatory effect of tested extracts can be estimated by comparing the IC₅₀ values of the % NO inhibition and cell viability. If the percentage of cell viability is greater than that of NO inhibition, both extracts will have an anti-inflammatory effect; the ethanol and watery extracts of *S. venosa* showed significant inhibition of cellular NO production at cytotoxic concentrations. According to the results, they exhibited anti-inflammatory activity because the IC₅₀ value of % NO inhibition was less than the IC₅₀ value of cell viability. The watery and methanol extracts showed lower IC₅₀ values (79.82 and 76.86 µg/mL) than the standard (98.25 µg/mL) in % NO inhibition. So, *S. venosa* can potentially be used as a natural anti-inflammatory ingredient for the treatment of arthritis. The experimental data are shown in Table 2 and Figure 3.

Table 2. Anti-inflammatory Activity of Various Crude Extracts of Tuber of *S. venosa*

Sample	% NO inhibition (µg/mL)		IC ₅₀ (µg/mL)	% NO inhibition (µg/mL)		IC ₅₀ (µg/mL)
	10	100		10	100	
	methanol extract	20.99		60.03	76.86	
watery extract	20.99	58.37	79.82	106.10	93.16	>100.00
^a L-NMMA	18.49	50.35	98.25	100.32	92.01	>100.00

^aL-NMMA positive control

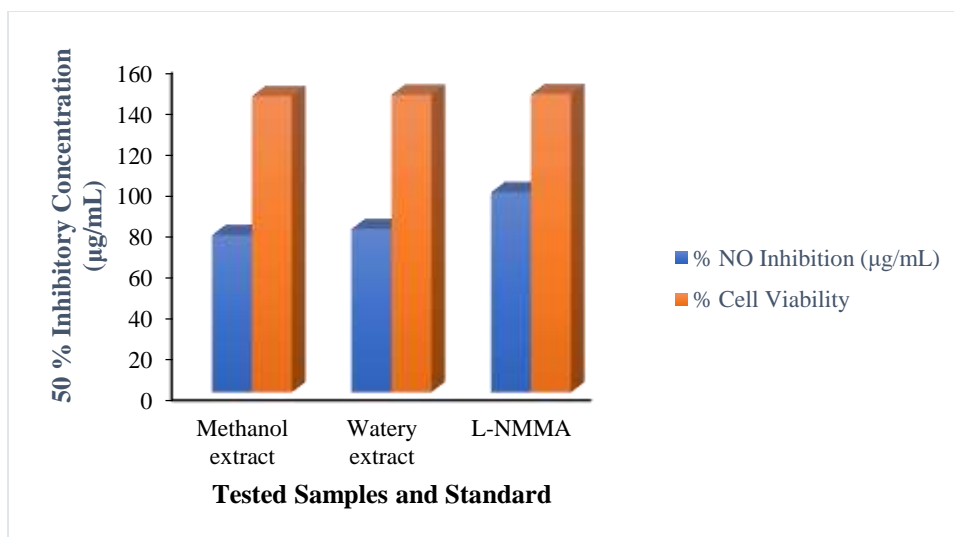


Figure 3. A bar graph diagram for anti-inflammatory activity of crude extracts of tuber of *S.venosa*

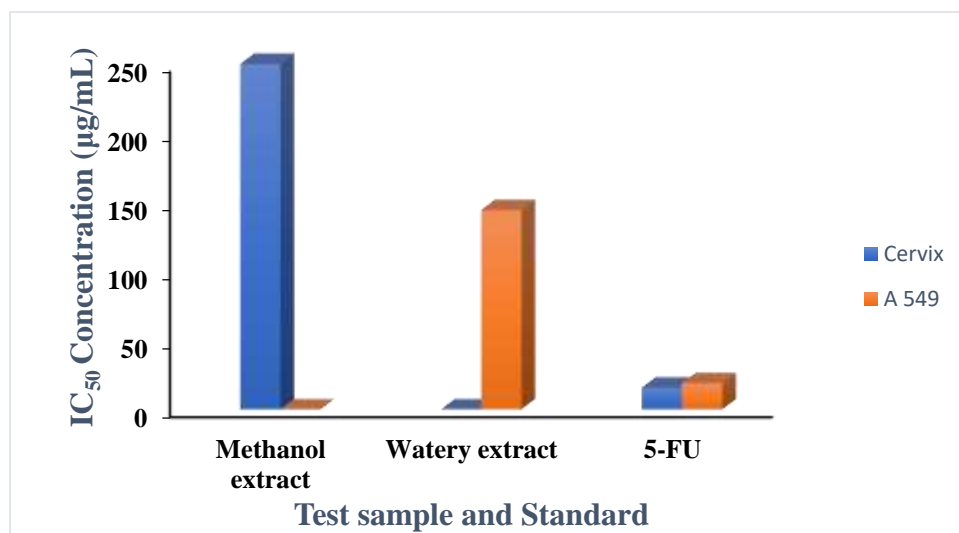
Antiproliferative Activity of Crude Extracts from the Tuber of *S. venosa*

In vitro antiproliferative activities of methanol, and watery extracts of the tuber of *S. venosa* were evaluated by MTT assay on two human cancer cell lines, such as A549 (lung cancer) and HeLa (Cervix cancer) cell lines. The antiproliferative effect was expressed as IC_{50} values (50 % inhibitory concentration). The lower the IC_{50} values, the higher the antiproliferative activity. According to these results, the H_2O extract showed mild antiproliferative activity against the A549 cell line with IC_{50} value of 144.86 $\mu\text{g/mL}$. The H_2O extract had significant antiproliferative activity against the HeLa (Cervix cancer) cell line, with an IC_{50} value of less than 20 $\mu\text{g/mL}$. But the methanol extract possessed weaker antiproliferative activity for HeLa (Cervix cancer), which was compared with watery extracts because of their IC_{50} values of > 200 $\mu\text{g/mL}$. However, the methanol extract had significant antiproliferative activity against the A549 (lung cancer) cell line, with an IC_{50} value of less than 20 $\mu\text{g/mL}$. The test samples had weaker antiproliferative activity compared with the standard 5 FU. The experimental data is shown in Table 3 and Figure 4.

Table 3. Antiproliferative Activity of Various Crude Extracts of tuber of *S. venosa* Against Two Human Cancer Cell Lines

Test Sample	Antiproliferative activity					
	Cervix (HeLa)			Lung (A549)		
	20 µg/mL	200 µg/mL	IC ₅₀ µg/mL	20 µg/mL	200 µg/mL	IC ₅₀ µg/mL
watery extract	47.66± 9.40	47.32± 0.07	<20	100.65± 6.65	27.63± 0.14	144.86
methanol extract	65.86± 1.56	53.36± 0.00	>200	78.87± 6.43	98.57± 4.88	<20

Positive control	2 µg/mL	10 µg/mL	20 µg/mL	IC ₅₀ µg/mL
5- Fluorouracil (lung cancer cell line)	136.24±12.94	70.45± 5.59	47.89± 8.21	19.06
5- Fluorouracil (cervix cancer cell line)	91.44±24.93	85.22± 4.95	24.93± 0.28	15.84

**Figure 4.** IC₅₀ values of crude extracts of the tuber of *Stephania venosa* against two human cancer cell lines***In vitro* Antiarthritic Activity of Ethanol and Watery Extracts from the Tuber of *S. venosa***

Protein denaturation is one of the primary causes of arthritis. *In vitro* antiarthritic activity of EtOH and watery extracts from the tuber of *Stephania venosa* was investigated by using the protein denaturation method (using egg albumin). According to the results of the egg's albumin denaturation, the IC₅₀ values of ethanol and watery extracts were found to be 743 µg/mL and >1600 µg/mL. Therefore, the two extracts were found to be mild activity comparable with the

standard drug diclofenac sodium (IC₅₀ value: 266µg/mL). The results of the antiarthritic activity of EtOH and watery extracts are shown in Table 4 and Figure 5.

Table 4. Antiarthritic Activity of EtOH and Watery Extracts from the Tuber of *S. venosa*

Sample	% Inhibition (mean± SD) at different concentrations (µg/mL)						IC ₅₀ (µg/mL)
	50	100	200	400	800	1600	
ethanol extract	33.42 ± 0.03	41.16 ± 0.03	41.55 ± 0.03	48.59 ± 0.05	53.14 ± 0.03	61.51 ± 0.07	743
watery extract	10.47 ± 0.05	12.20 ± 0.03	16.17 ± 0.03	21.55 ± 0.05	27.62 ± 0.03	29.86 ± 0.03	>1600
diclofenac sodium	42.73 ± 0.03	43.09 ± 0.03	48.61 ± 0.03	53.48 ± 0.03	61.79 ± 0.05	63.63 ± 0.08	266

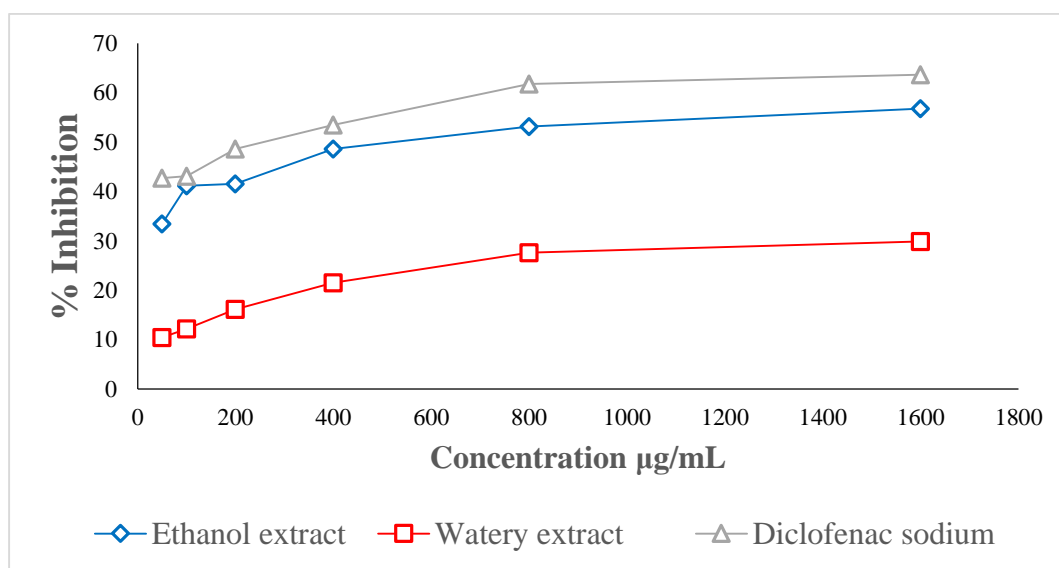


Figure 5. Antiarthritic activities of crude extracts from the tuber of *S. venosa*

Conclusion

In this research work, the screening of cytotoxicity, anti-inflammatory, antiproliferative, and antiarthritic activities based on ethanol, methanol, and watery extracts from the tuber of *S. venosa* is carried out. The cytotoxicity activity of the watery and ethanol extracts was (LD₅₀ values >1000), indicating a non-toxic effect, by a brine shrimp lethality bioassay. Methanol and watery extracts exhibited anti-inflammatory activity because their IC₅₀ values (data) of % NO inhibition against LPS-induced RAW 264.7 cells are less than the IC₅₀ values (data) of cell viability. The watery extract showed mild antiproliferative activity against the A549 cell line with an IC₅₀ value of 144.86 µg/mL, and significant antiproliferative activity against the HeLa (Cervix) cell line with an IC₅₀ value less than 20 µg/mL. However, the methanol extract had significant antiproliferative activity against the A549 (lung cancer cell line), with an IC₅₀ value of

less than 20 µg/mL, but weaker antiproliferative activity for the HeLa (Cervix) cell line, with an IC₅₀ value greater than 200 µg/mL, comparable to the standard 5 FU (IC₅₀ =19.06 µg/mL for lung cancer cell line and IC₅₀ =15.84 µg/mL for cervix cancer cell line). According to the results of ethanol and watery extracts tested by the fresh egg's albumin protein denaturation, the IC₅₀ values of ethanol and watery extracts were found to be 743 µg/mL and >1600 µg/mL, respectively. Therefore, the two extracts showed lower antiarthritic activity than the standard drug diclofenac sodium (IC₅₀ value = 266 µg/mL). From the above results, it could be concluded that the tuber of *Stephania venosa* (Blume) Spreng. possessed potential pharmacological activities such as cytotoxicity, anti-inflammatory, antiproliferative, and antiarthritic activities. This finding provided potential for the tuber of *S. venosa* as a therapeutic drug for traditional medicinal areas.

Acknowledgements

The authors would like to thank the Department of Higher Education, Ministry of Education, Myanmar, for permission to do this research and the Myanmar Academy of Arts and Science-for allowing to submit this paper.

References

- Ali, N., U. Alien, S. W. A. Shaha, M. Junaid, G. Ahmed, W. Ali, and M. Ghias. (2013). "Acute Toxicity, Brine Shrimp Cytotoxicity, Anthelmintic and Relaxant Potentials of Fruits of *Rubus fruticosus* Agg". *BMC Complement Altern. Med.*, vol.13, pp.136-143.
- Deciga-Campos, M., I. Rivero-Cruz, M. Arriaga-Alba, G. Castaneda-Corral, and G. E. Angeles-Lopez (2007). "Acute Toxicity and Mutagenic Activity of Mexican Plants Used in Traditional Medicine". *J Ethnopharmacol.*, vol.110, pp.334-342.
- Ingkaninan, K., P. Phengpa, S. Yuenyongsawad, and N. Khorana. (2006). "Acetylcholinesterase Inhibitors from *Stephania venosa* tuber". *J. Pharmacy Pharmacol.*, vol.58, pp.695-700.
- Jin, S. E., Y. K. Son, B. S. Min, H. A. Jaung, and J. S. Choi. (2012). "Anti-inflammatory and Antioxidant Activities of Constituents Isolated from *Pueraria lobata* Roots". *Arch. Pharm. Res.* vol.35, pp.823-837.
- Moongkarndi, P., N., Kosem, O., Luanratana, S., Jongsomboonkusol, and N., Pongpon. (2004). "The Antiproliferative Activity of Thai Medicinal Plant Extracts on Human Breast Adenocarcinoma Cell Line". *Fitoterapia*, vol.75, pp.375-377.
- Olowa L.F. and M. N. Olga. (2013). "Brine Shrimp Lethality Assay of the Ethanolic Extract of Three Selected Species of Medicinal Plants from Iligan City, Philippines". *Int Res J Biol Sci.*, vol.2, pp., 4-77.
- Rahman, H., M. C. Eswaraiah, and A. M. Dutta. (2015). "In Vitro Anti-inflammatory and Anti-Arthritic Activity of *Oryza sativa* Var. Joha Rice (An Aromatic Rice of Assam)". *American-Eurasian J. Agric. And Environ*, vol.15(1), pp. 115-121.
- Win, N. N., T. Ito, S. Aimaiti, H. Imagawa, H. Ngwe, I. Abe, and H. Morita. (2015). "Kaempulchraols A–H, Diterpenoids from the Rhizomes of *Kaempferia pulchra* Collected in Myanmar". *J. Nat. Prod.*, vol.78, pp. 1113–1118.

A STUDY ON THE PHYTOCHEMICALS, ANTIMICROBIAL ACTIVITY OF CRUDE EXTRACTS, AND IDENTIFICATION OF ECHITAMINE ALKALOID OF *ALSTONIA SCHOLARIS* L. (TAUNG-MA-YO) BARK

Khin Maw Maw¹, Swe Zin Myint², Saw Hla Myint³

Abstract

Alstonia scholaris (L.) R. Br., commonly known as Taung-ma-yo, is a traditional plant renowned for its diverse range of biological activities. The present research work focused on the investigation of phytochemical constituents, screening of the antimicrobial activity of crude extracts, and the isolation and identification of echitamine alkaloid of *A. scholaris* bark. Preliminary phytochemical tests revealed the presence of alkaloids, α -amino acids, carbohydrates, flavonoids, glycosides, phenolic compounds, reducing sugars, saponins, tannins, steroids, and terpenoids in the bark. The antimicrobial activity of the ethyl acetate, 70 % ethanol, and watery extracts of the bark of *A. scholaris* was evaluated using the agar well diffusion method against six different microorganisms. Both ethyl acetate and 70 % ethanol extracts exhibited significant antimicrobial activity, with inhibition zone diameters ranging from 18 to 24 mm on all the tested microorganisms. The watery extract showed inhibition zone diameters of 12-17 mm against four microorganisms but it was not active against *Pseudomonas aeruginosa* and *Escherichia coli*. One of the alkaloids, echitamine, was isolated from the ethyl acetate extract of the bark sample using column chromatography, and it was identified by FT IR, ¹H NMR, and ¹³C NMR spectral data. This study also demonstrates that *A. scholaris* has high source of phytochemicals. Reported literatures showed that the isolated alkaloid, echitamine, does not protoplasmic poison and is used as an astringent herb.

Keywords: *Alstonia scholaris* bark, phytochemicals, antimicrobial activity, echitamine, agar well diffusion method

Introduction

Plants are not only a dietary source for both human beings and animals but also safer phytomedicines. Traditionally, phytomedicines have been used to treat various ailments and Ayurvedic systems of therapy (Twaij and Hasan, 2022). The ethnomedical information of medicinal plants has great potential for researchers to provide a scientific basis for their properties (Hassan, 2009). *Alstonia scholaris* (L.) R.Br. (Taung-ma-yo) has also long been used as a traditional medicine to cure human and livestock ailments. The plant, *A. scholaris*, attracts the attention of researchers worldwide for its pharmacological activities ranging from antimalarial to anticancer activities (Bhanu *et al.*, 2013). *A. scholaris* possesses the family Apocynaceae and genus *Alstonia*; the English name is Devil tree or Dita bark, the Myanmar name is Taung-ma-yo (Figure 1). It has a wide occurrence in the Asia-Pacific region, from India and Sri Lanka through mainland Southeast Asia and China, throughout Malaysia to Northern Austria and the Salomon Islands (Anubha and Yashwant, 2015). Alkaloids, coumarins, flavonoids, leucoanthocyanins, reducing sugars, simple phenolics, steroids, saponins, and tannins were documented as the chief chemical constituents in the plant (Pankti *et al.*, 2012). Various biological and pharmacological activities such as antimicrobial, antidiarrheal, antioxidant, antidiabetic, anticancer, analgesic, anti-inflammatory, hepato protective, CNS, wound healing, immune modulatory, antiasthmatic, antifertility, and cytotoxicity properties of *A. scholaris* have

¹ Department of Chemistry, Yangon University of Education

² Department of Chemistry, Patheingyi University

³ Department of Chemistry, University of Yangon

been reported by Khyade *et al.* (2014). The bark is also traditionally used by many ethnic groups in North East India and other parts of the world as a source of cure against bacterial infection, malarial fever, toothache, rheumatism, snakebite, dysentery, bowel disorder, etc. Also, the latex is used in treating coughs, sores, and fever (Bhattacharjee, 2004). The aim of this research work is to investigate some phytochemical constituents, to determine antimicrobial activity, and to isolate echitamine alkaloid from the bark of *A. scholaris*. The isolated compound was then identified by FT IR, ^1H NMR, and ^{13}C NMR.

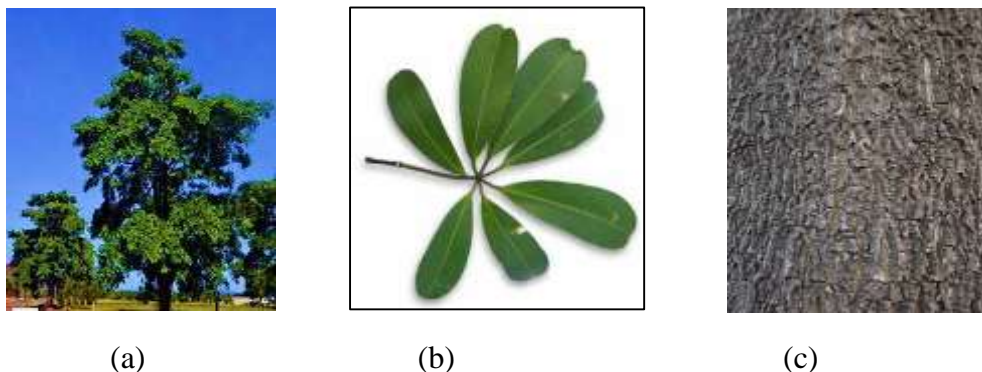


Figure 1. Photographs of *A. scholaris* (a) trees (b) leaf and (c) trunk bark

Materials and Methods

Sample Collection and Preparation

In this research work, the bark of *A. scholaris* (Taung-ma-yo) was collected from Kamayut Township, Yangon Region, in March 2018. The scientific name of this selected plant was confirmed by the Department of Botany, Dagon University. The collected bark sample was washed with water and dried in the air at room temperature. The dried bark sample was cut into small pieces and then ground into powder using a grinding machine. The powdered samples were stored in air-tight containers to prevent moisture changes and other contamination.

Preparation of Crude Extracts

Various crude extracts of ethyl acetate, 70 % ethanol, and water were prepared for screening antimicrobial activity using the percolation method in their respective solvents. The following crude extracts were also prepared for the isolation of some constituents from the bark sample. The dried powdered sample (500 g) was percolated in petroleum ether (60–80 °C) for 5 days, followed by filtration. This procedure was repeated four more times. The combined petroleum ether extracts were evaporated under reduced pressure by means of a rotary evaporator to get petroleum ether crude extract. The defatted marc was then extracted with ethyl acetate for 3 days and filtered. This procedure was also repeated four more times. The defatted ethyl acetate extract was obtained by concentrating the filtrate using a rotary evaporator. The remaining marc was then percolated with ethanol for five days and filtered. Ethanol percolation was repeated four times until the extract became faint. Ethanol crude extract was concentrated by using a rotary evaporator. The crude extracts: petroleum ether, ethyl acetate (EA-1), and ethanol crude extracts were obtained. A portion of the ethanol crude extract was then dissolved in 1 M hydrochloric acid and partitioned with further ethyl acetate. After evaporating the solvent, an **ethyl acetate** extract (**EA-2**) was obtained. Crude extracts were kept for separation.

Investigation of Phytochemical Constituents

In order to classify the types of organic constituents present in the sample, preliminary phytochemical tests for alkaloids, α -amino acids, carbohydrates, flavonoids, glycosides, phenolic compounds, reducing sugars, saponins, starch, steroids, tannins, and terpenoids on the bark sample were carried out according to the appropriate reported methods (Marini-Bettolo *et al.*, 1981; Shriner *et al.*, 1980; Robinson, 1983; Raymond, 1982; Vogel, 1966; Harborne, 1994).

Screening of Antimicrobial Activity

In vitro antimicrobial activity of ethyl acetate, 70 % ethanol, and watery extracts from the bark of *A. scholaris* was investigated by using the agar well diffusion method (Anibijuwon and Udeze, 2009) at the Pharmaceutical Research Department (PRD), Ministry of Industry, Yangon Region. The test microorganisms were *Bacillus subtilis*, *Staphylococcus aureus*, *Pseudomonas aeruginosa*, *Bacillus pumilus*, *Candida albicans*, and *Escherichia coli*. The inhibition zone (clear zone) appeared around the agar well (10 mm diameter), indicating the presence of antimicrobial activity. The antimicrobial activity of crude extracts was determined by the diameter of inhibition zone.

Isolation and Purification of Isolated Organic Compound

The isolation of the pure compound was carried out from 3 g of ethyl acetate crude extract (EA-2) of the bark of *A. scholaris* by column chromatography. Column chromatography was performed by successive gradient elution with *n*-hexane (150 mL), followed by *n*-hexane:ethyl acetate (9:1 v/v, 150 mL), *n*-hexane: ethyl acetate (1:1 v/v, 150mL), ethyl acetate (150 mL), ethyl acetate: methanol (9:1 v/v, 150 mL), ethyl acetate: methanol (1:1 v/v, 150 mL), and methanol (300 mL) solvent systems. The eluate was collected with 150 mL per fraction to provide a total of seven fractions (F₁-F₇). A colourless solid was observed in the fraction F₆. After decantation of F₆, the remaining solid was washed with *n*-hexane and then methanol. The solid compound was purified by recrystallization using ethyl acetate: methanol (1:1) solvent system. Then the purified crystal (51 mg, 0.01 %) was isolated from EA-2 extract.

Thin-layer chromatography Screening of Isolated Compound

The isolated compound was subjected to TLC analysis, and the R_f value was determined. Silica gel GF₂₅₄ percolated aluminium plate (Merck, England) was employed, and the chromatogram was developed in the appropriate solvent system. The chromatogram was viewed under UV-254 nm and UV-365 nm light, and treated with visualizing agents. The observed R_f value for the isolated compound was then recorded.

Identification of Isolated Compound by Modern Spectroscopic Techniques

The Fourier Transform Infrared Spectrum of isolated compound was recorded by an FT IR (8400) spectrophotometer (Shimadzu, Japan), at the Chemistry Department, University of Mandalay, in order to identify the functional groups. The nuclear magnetic resonance NMR spectra for the isolated compound were recorded to examine the types and numbers of hydrogen and carbon present. The NMR spectra of the isolated compound were recorded by a Bruker NMR spectrophotometer with 400 MHz for ¹H NMR spectra and 100 MHz for ¹³C NMR spectra at the Institute of Natural Medicine, University of Toyama, Japan. The spectra of the isolated compound were measured using pyridine-d₆ solvent.

Results and Discussion

Phytochemical Constituents of the *A. scholaris* Bark

Phytochemical constituents of the bark of *A. scholaris* investigated by chemical test method were alkaloids, α -amino acids, carbohydrates, flavonoids, glycosides, phenolic compounds, reducing sugars, saponins, steroids, tannins, and terpenoids. The results are shown in Table 1.

Table 1. Phytochemical Constituents in the Bark of *A. scholaris*

No.	Tests	Extracts	Reagents used	Observation	Remark
1	alkaloids	1 % HCl	Dragendorff's reagent	brick red ppt.	+
			Wagner's reagent	white ppt.	+
			Mayer's reagent	yellow ppt.	+
			Sodium picrate	yellow ppt.	+
2	α -amino acids	H ₂ O	Ninhydrin reagent	purple colour spot	+
3	carbohydrates	H ₂ O	10 % α -naphthol, conc. H ₂ SO ₄	red ring	+
4	flavonoids	EtOH	Mg ribbon, conc. HCl	pink colour	+
5	glycosides	H ₂ O	10 % lead acetate solution	white ppt.	+
6	phenolic compounds	EtOH	5 % FeCl ₃ solution, 1 % K ₄ Fe(CN) ₆	dark blue colour	+
7	reducing sugars	2 M H ₂ SO ₄	Benedict's solution	brick red ppt	+
8	saponins	H ₂ O	distilled water	frothing	+
9	starch	H ₂ O	I ₂ solution	no deep blue colour	-
10	steroids	pet ether	acetic anhydride, conc.H ₂ SO ₄	red colour solution	+
11	tannins	EtOH	1 % Gelatin, 5 % FeCl ₃ solution	green colour solution	+
12	terpenoids	CHCl ₃	acetic anhydride, conc.H ₂ SO ₄	pink colour	+

(+) presence (-) absence (ppt) precipitate

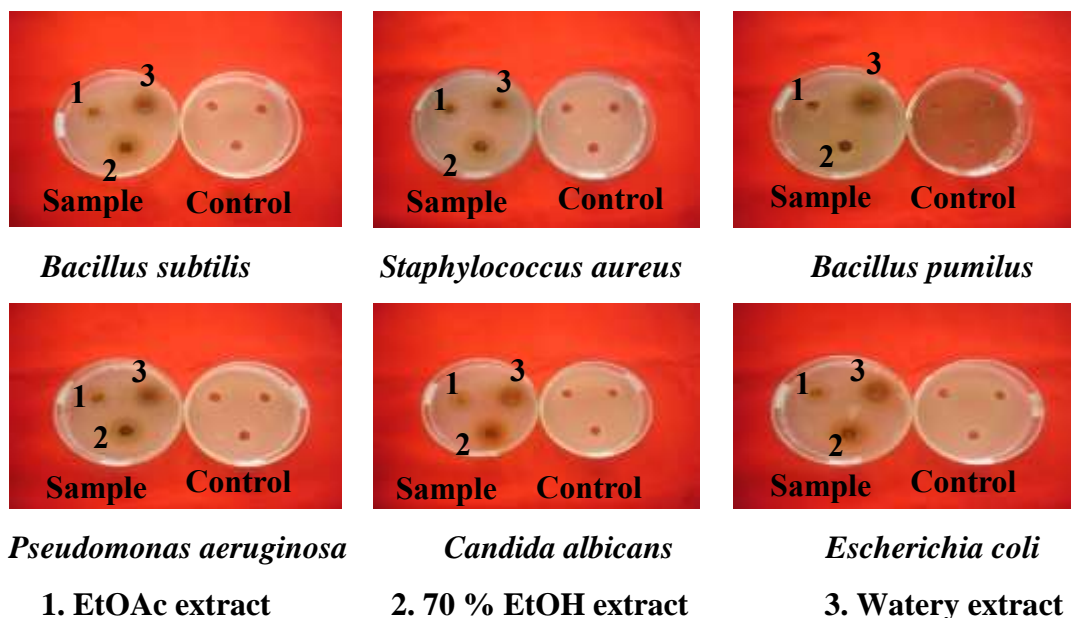


Figure 2. Antimicrobial activity of various crude extracts of bark of *A. scholaris* L. against six test microorganisms

Table 2. Antimicrobial Activity of Crude Extracts from Bark of *A. scholaris* L. by Agar Well Diffusion Method

Organisms used	Diameter of inhibition zone (mm) in various crude extracts		
	EtOAc	70 % EtOH	H ₂ O
<i>B. subtilis</i>	21	24	17
<i>S. aureus</i>	18	20	14
<i>P. aeruginosa</i>	20	22	-
<i>B. pumilus</i>	18	20	14
<i>C. albicans</i>	19	19	12
<i>E. coli</i>	21	20	-

agar well diameter 10 mm
 lower activity 10 - 14 mm
 moderate activity 15 - 19 mm
 highest activity 20mm - above

Screening of Antimicrobial Activities

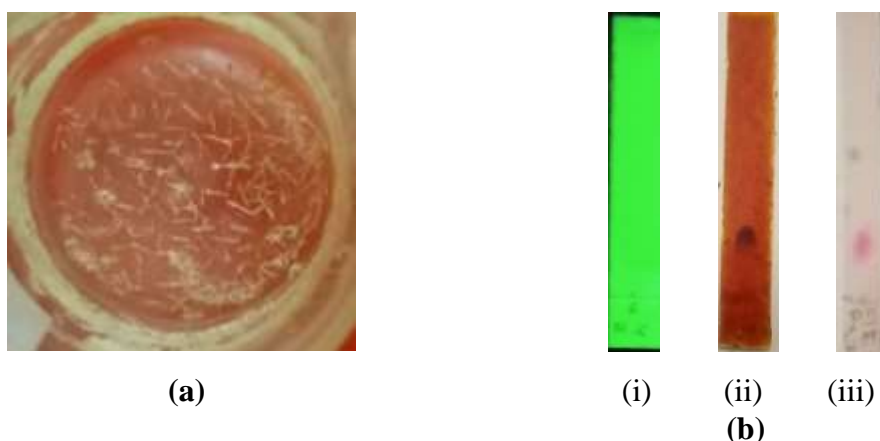
Antimicrobial activities of various crude extracts such as ethyl acetate, 70 % ethanol, and watery of bark were investigated by employing the agar well diffusion method. The advantages of this method are simplicity and low cost that have contributed to its common use for the antimicrobial screening of plant extracts. In this study, the samples were tested on six different strains of microorganisms, namely, *B. subtilis*, *S. aureus*, *P. aeruginosa*, *B. pumilus*, *C. albicans* and *E. coli*. This method is based on inhibition zone diameter that shows the degree of the antimicrobial activity. The larger the zone diameter, the more effective against tested microorganisms. The antimicrobial studies of various crude extracts of bark are shown in Figure 2. The results showed that a larger zone of inhibition was observed in ethyl acetate and

70 % ethanol extracts (inhibition zone diameter ranged from 18 to 24 mm) against six different strains of microorganisms. The watery extract exhibited lower activity (inhibition zone diameter ranged from 12 to 17 mm) than the other extracts, and it exhibited antimicrobial activity only for four types of microorganisms except *P. aeruginosa* and *E. coli*. The observed data are described in Table 2.

Isolation and Identification of an Alkaloid from Ethyl Acetate Extract

In this study, the crude extracts of bark samples were successively percolated with different solvents: pet ether, ethyl acetate, and ethanol. A dried bark sample (500 g) was extracted by the percolation method with pet ether to get pet ether crude extract (8.4 g), containing non-polar constituents. Then all of the polar components were extracted with ethyl acetate from the defatted residue to obtain moderately polar constituents. A 5.1 g of ethyl acetate extract was obtained from the extraction. The remaining marc was successively percolated with ethanol, so 8.2 g of ethanol extract was obtained. Some of the ethanol extracts were partitioned again with ethyl acetate to obtain more ethyl acetate extracts containing more polar chemical compounds.

One of the polar compounds from ethyl acetate extract, an alkaloid, was isolated by column chromatography and purified by a suitable solvent system. A colourless needle-shaped crystal of compound (51 mg, 0.01 %) was formed after evaporating the solvent. It was soluble in methanol, ethanol, ethyl acetate and chloroform but insoluble in pet ether and *n*-hexane. It was UV inactive under UV lamp (254 nm and 365 nm) and the R_f value was found to be 0.18 in EtOAc : MeOH : H₂O (150 : 26 : 19 v/v). The photograph of the isolated compound and the TLC chromatograms are shown in Figure 3. The isolated compound gave brown colouration on TLC after spraying and heating with 5 % H₂SO₄ solution. Besides, it showed an orange spot on TLC by spraying with Dragendorff 's reagent. It also provided a light pink colour on TLC when treated with anisaldehyde-sulphuric acid reagent followed by heating. From the observed TLC behaviour, and the FT IR spectral data as shown in Figure 4 and Table 3, the isolated compound may be an alkaloid.



Solvent system = EtOAc: MeOH: H₂O (150:26:19 v/v), $R_f = 0.18$

(i) Under UV₂₅₄ nm (ii) Spraying Dragendorff's Reagent (iii) Spraying Anisaldehyde

Figure 3. (a) Crystal of isolated compound from ethyl acetate extract

(b) Thin layer chromatograms of isolated compound

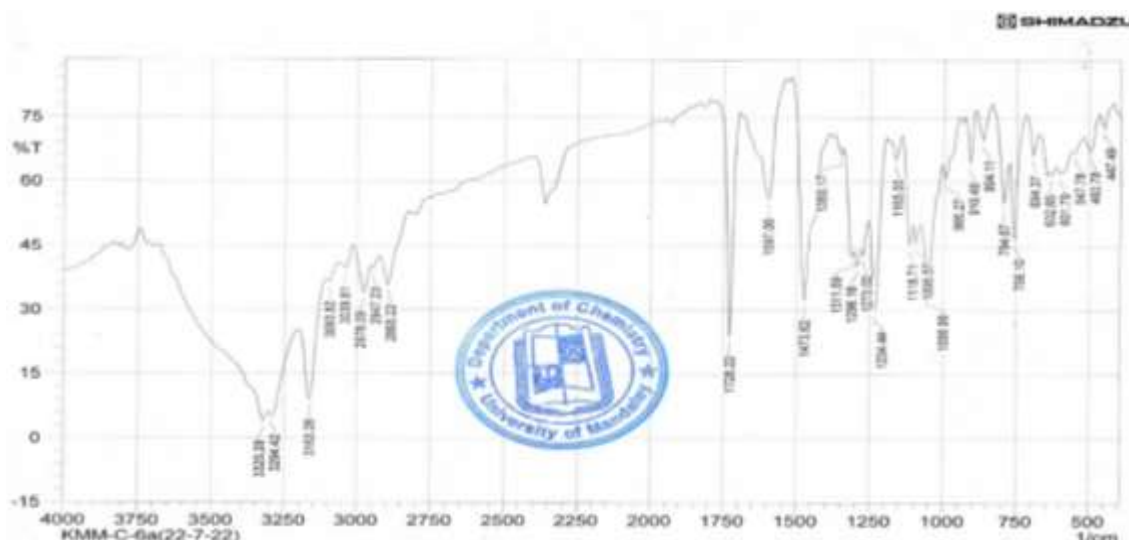


Figure 4. FT IR spectrum of isolated compound from the bark of *A. scholaris*

Table 3. FT IR Spectral Data of Isolated Compound

Wavenumber (cm ⁻¹)	Vibrational mode	Remark
3325, 3294	O-H stretching	OH group
3163	N-H stretching	-NH in heterocyclic ring
3093, 3039	=C-H stretching	<i>sp</i> ² CH group
2978, 2947, 2893	C-H as- and s-stretching	<i>sp</i> ³ CH group (-CH ₃ , -CH ₂ -)
1728	C=O stretching	Carbonyl group stretching
1620	C=C stretching	C-C in aromatic compound
1473, 1375	C-H bending	-CH ₂ , -CH ₃ group
1254	C-O stretching	COO group
794, 756	=CH oop bending	aromatic ring and alkene

Identification of Isolated Compound by NMR

The ¹H NMR spectrum (400 MHz, pyridine) of the compound was compared with the ¹H NMR spectrum (600 MHz) of echitamine predicted by the ACD (Advanced Chemistry Development) Lab. In the ¹H NMR spectrum of the isolated compound, there is a solvent effect at chemical shift values of 5.1, 7.2, 7.6, and 8.7 ppm. The remaining signals of the ¹H NMR spectrum of the isolated compound were matched with the ¹H NMR spectrum of echitamine. Chemical shift values at 3.625 ppm showed the proton signals from N-H, O-H at positions 1, 19, and 21. These chemical shift values were found to be similar to those of the predicted values of echitamine.

¹³C NMR spectrum (100 MHz, pyridine-d₆) of the isolated compound indicated that it contained 22 carbons. The ¹³C NMR spectrum of this compound was also matched with the ¹³C NMR spectrum (150 MHz) of echitamine predicted by ACD Lab. Chemical shifts near 120, 135, and 150 ppm in the compound were solvent peaks due to solvent pyridine. The chemical

shift values in the ^{13}C NMR spectral data of the compound were nearly the same as those of the predicted data of echitamine. Comparative NMR spectra are illustrated in Figures 5 and 6, and comparative NMR spectral data are also shown in Table 4. Thus, the isolated compound was confirmed to be an alkaloid, namely echitamine (molecular formula $\text{C}_{22}\text{H}_{29}\text{N}_2\text{O}_4$), based on these results.

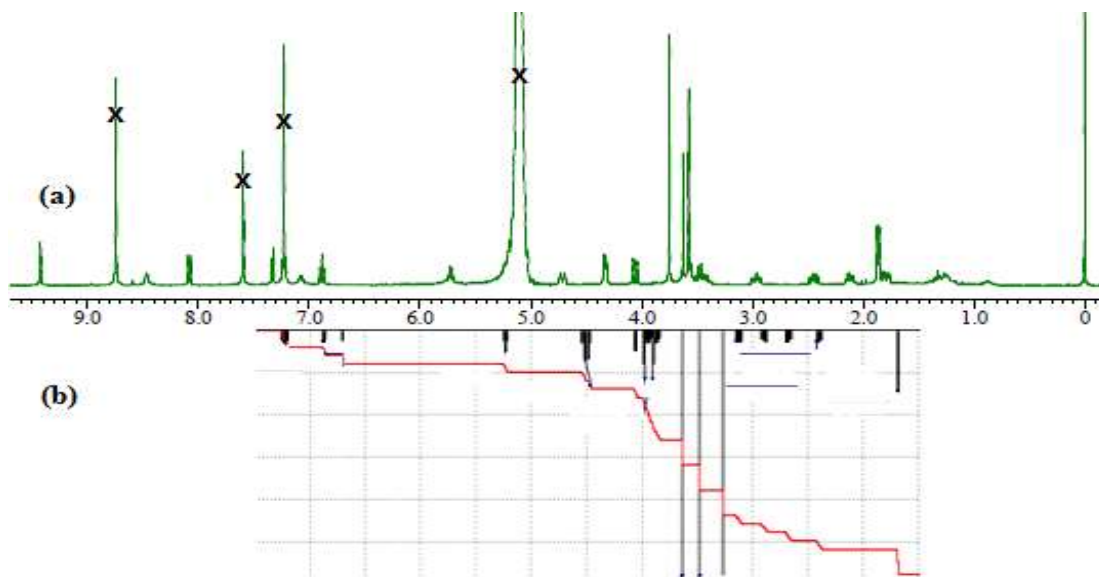


Figure 5. Comparison of (a) ^1H NMR spectrum of isolated compound (400 MHz, pyridine- d_6) and (b) the predicted ^1H NMR (600 MHz) spectrum of echitamine by ACD Lab

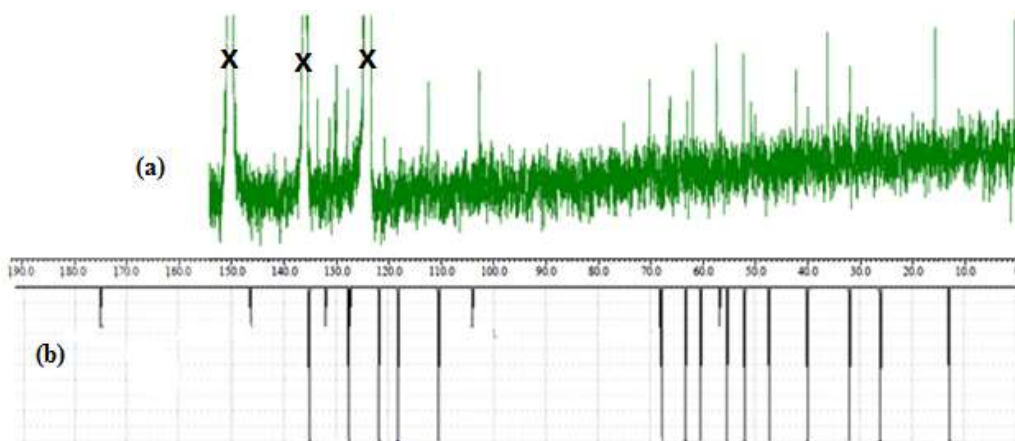


Figure 6. Comparison of (a) ^{13}C NMR spectrum of compound (100 MHz, pyridine- d_6) and (b) the predicted ^{13}C NMR (150 MHz) spectrum of echitamine by ACD Lab

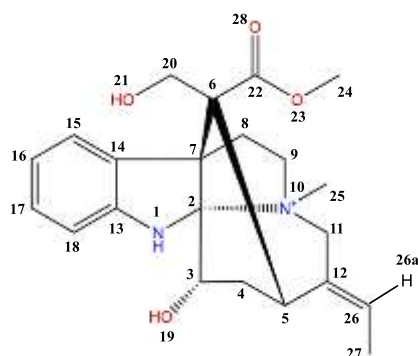


Figure 7. Structure of echitamine

Table 4. Comparison of ^1H and ^{13}C NMR Spectral Data of Isolated Compound and Echitamine*

Position	Chemical Shift (δ_{H}) (ppm)		Chemical Shift (δ_{C}) (ppm)	
	Compound	Echitamine	Compound	Echitamine
1	3.625	3.479	-	-
2	-	-	102.706	103.91
3	-	-	62.986	60.41
4	-	-	36.278	31.99
5	-	-	42.333	40.01
6	-	-	70.288	68.12
7	-	-	62.031	56.78
8	-	-	32.007	26.12
9	-	-	57.465	55.27
11	-	-	75.117	63.23
12	-	-	127.760	127.19
13	-	-	147.356	146.22
14	-	-	131.260	131.9
15	-	-	120.762	121.71
16	-	-	117.729	118.11
17	-	-	129.860	127.52
18	-	-	112.421	110.39
19	3.625	3.479	-	-
20	-	-	66.255	67.82
21	3.625	3.479	-	-
22	-	-	-	174.93
24	3.750	3.639	52.354	-
25	3.575	3.265	50.855	47.28
26	-	-	133.515	135.08
27	1.865	1.683	15.750	12.93

*Predicted by ACD (Advanced Chemistry Development) Lab

Conclusion

The preliminary phytochemical tests on the bark of *A. scholaris* revealed the presence of alkaloids, α -amino acids, carbohydrates, flavonoids, glycosides, phenolic compounds, reducing sugars, saponins, tannins, steroids, and terpenoids. The antimicrobial activity of EtOAc and 70 % EtOH extracts. Exhibits to the (inhibition zone diameter ranged from 18 mm to 24 mm) against six different strains of microorganisms. The result showed the efficiency of plant extracts as natural antimicrobial compounds against microorganisms and suggested the possibility of employing them in drugs for the treatment of infectious diseases caused by the tested microorganisms. A compound from the ethyl acetate extract of bark sample was isolated by column chromatographic technique. It was structurally identified by FT IR, ^1H NMR and ^{13}C NMR techniques. This isolated compound (0.01% yield) was found to be one of the alkaloids according to TLC and FT IR results and was identified as echitamine from ^1H NMR and ^{13}C NMR results. The isolated compound has also pointed to effective natural product herbal medicines which could be contributed to the health programme with the scientific evidence for Myanmar indigenous medicinal plants.

Acknowledgements

The authors would like to thank the Department of Higher Education, Ministry of Education, Yangon, Myanmar, for the permission of doing this research and for allowing to write this paper. Our deepest gratitude is expressed to Dr Kay Thwe Hlaing, Rector, Yangon University of Education, for her encouragement and Dr Nay Mar Soe, Professor and Head, Department of Chemistry, Yangon University of Education for her helpful advice, valuable suggestions and provision of research facilities at the Department of Chemistry, Yangon University of Education.

References

- Anibijuwon, I. I. and A. O. Udeze. (2009). "Antimicrobial Activity of *Carica papaya* on Some Pathogenic Organisms of Clinical Origin from South Western Nigeria". *Journal of Ethanol Leaflets*, vol. 13, pp. 850- 864.
- Anubha, A. and R.Yashwant. (2015). "Review: Phytochemistry, Ethanobotanical and Pharmacological Activities of *Alstonia scholaris* R. Br (Apocynaceae)". *International Journal of Advanced Research*, vol. 3 (8), pp.584 – 590.
- Bhanu P., G. S. Chakraborty, and N. Mogha. (2013). "Complete Aspects of *Alstonia scholaris*". *International Journal of Pharm. Tech. Research*, vol. 5(1), pp.17-26.
- Bhattacharjee, S. K. (2004). *Hand books on Medicinal Plant*. Jaipur: 4th Rev. ed., Pointer, pp. 569-575.
- Harborne, J. B. (1994). *Phytochemical Methods. A Guide to Modern Techniques of Plant Analysis*. New York: 2nd ed., Chapman and Hall, pp. 120-126.
- Hassan, A., S. Rahman., F. Deeba, and S. Mahmud. (2009). "Antimicrobial Activity of Some Plant Extracts having Hepatoprotective Effect". *Journal of Medicinal Plant Research*, vol. 3(1), pp. 20-23.
- Khyade, M.S., D. M. Kasote, and N. P. Vaikos. (2014). "*Alstonia scholaris* (L.) R. Br. and *Alstonia macrophylla* Wall.ex G. Don: A Comparative Review on Traditional Uses". *Journal of Ethnopharmacology*, vol. 153, pp. 1-18.
- Marini-Bettolo, G.B., M. Nicoletti, and M. Patamia. (1981). "Plant Screening by Chemical and Chromatographic Procedure Under Field Conditions". *J. Chromatography*, vol. 213, pp. 113-127.

- Pankti, K., G. Payal. C. Manodeep. and K. Jagadish. (2012). "A Phytopharmacological Review of *Alstonia scholaris*: A Panoramic Herbal Medicine". *IJRAP*, vol. 3(3), pp. 367-371.
- Raymond, E. (1982). *Encyclopedia of Chemical Technology*. New York: 3rd ed., Reinhold Pub., Corp., vol. 13, pp. 705-710.
- Robinson, T. (1983). *The Organic Constituents of Higher Plants*. North America: 5th ed., Cordus Press, pp. 285-286.
- Shriner, R.L., R. C. Fuson., D. Y. Curtin, and T. C. Morrill. (1980). *The Systematic Identification of Organic Compounds: A Laboratory Manual*. New York: John Wiley and Sons Inc., pp. 385-435.
- Twaij, B.M. and N. Md. Hasan. (2022). "Bioactive Secondary Metabolites from Plant Sources: Types, Synthesis and their Therapeutic Uses". *International Journal of Plant Biology*, vol. 13 (1), pp. 4-14.
- Vogel, A. I. (1966). *A Quantitative Organic Analysis*. London: 2nd ed., Longman group Ltd., pp. 89-92.

ISOLATION OF ENDOPHYTIC FUNGI FROM *OROXYLUM INDICUM* (L.) BENTH (KYAUNG-SHA) FRUITS AND THEIR BIOLOGICAL ACTIVITIES

Aung Kyaw Min¹, Tin Aung Kyaw², War War May Zin³, San San Aye⁴, Cho Cho Than⁵

Abstract

This research focuses on the chemical and biological aspect of crude extracts of endophytic fungi isolated from *Oroxylum indicum* (L.) Benth (Kyaung sha) fruits. The endophytic fungi have been isolated from *O. indicum* (Kyaung sha) fruit by the direct method, followed by cultured in potato agar medium (PGA). Four endophytic fungi (EFK1, EFK2, EFK3, and EFK4) have been isolated from *O. indicum* (Kyaung sha) fruit. Preliminary phytochemicals, total phenolic contents (TPC) and total flavonoid content (TFC) have been carried out as chemical investigations. Showing the presence of alkaloids, α -amino acids, carbohydrates, flavonoids, glycosides, organic acids, phenolic compounds, reducing sugars, saponins, steroids, tannins, and terpenoids, and the absence of starch in all tested samples. The total phenol contents of isolated fungi were determined by the Folin-Ciocalteu reagent (FCR) method. Gallic acid (3,4,5-trihydroxy benzoic acid), was used to construct a standard calibration curve for total phenol. TPC were expressed as a microgram of gallic acid equivalent per milligram of crude extract ($\mu\text{g GAE/mg}$). TPC ($\mu\text{g GAE/mg}$) were found to be highest in EFK2 (216.86 ± 0.66). The total flavonoids content (TFC) of isolated fungi were determined by using spectrophotometric method with aluminum chloride. The content of flavonoids was expressed in term of quercetin equivalent, mg of QE/g of extract. TFC (mg QE/g) was found to be highest in EFK3 (67.47 ± 1.40). The four isolated fungi were observed to possess antioxidant capacity by the DPPH assay method. Among them, EFK 2 has more potent antioxidant activity ($\text{IC}_{50} = 12.15 \mu\text{g/mL}$) than other tested samples. Moreover, anti-diabetic activity (expressed in terms of α -amylase inhibitory) indicated that EFK 3 and EFK 4 possessed higher anti-diabetic activity ($\text{IC}_{50} = 4.94 \mu\text{g/mL}$) than other tested samples. The four endophytic fungi were found to possess high activity against all tested microorganisms with the inhibition zone diameters ranging between 20 mm ~ 30 mm. All endophytic fungi have more portent antioxidant, antidiabetic and antimicrobial effects.

Keywords: endophytic fungi, *Oroxylum indicum* (L.) Bent, phytochemical constituents, biological activities

Introduction

Natural products and their derivatives have been recognized for many years as a valuable source of therapeutic agents and structural diversity. Recently, there has been renewed interest in the bioprospecting for natural products with potential therapeutic applications due to the failure of alternative drug discovery methods to deliver lead compounds in therapeutic areas such as immunosuppression, anti-infectives and metabolic diseases (Deka *et al.*, 2013). Endophytes are microorganisms that live within plants for at least a part of their life cycle without causing any visible manifestation of disease. Bioprospection of endophytes is considered a new frontier for the discovery of useful natural products as endophytes have been shown to produce a broad variety of bioactive secondary metabolites with potential agricultural, pharmaceutical and industrial applications (Newman and Cragg, 2020). The number of secondary metabolites produced by fungal endophytes is larger than that of any other group of endophytic

¹ Department of Chemistry, Patheingyi University

² Department of Chemistry, Patheingyi University

³ Department of Chemistry, Patheingyi University

⁴ Department of Chemistry, Panglong University

⁵ Department of Chemistry, Patheingyi University

microorganisms and to date the vast majority of microbes isolated as endophytes have been fungi. Fungal metabolites have served as lead compounds for the development of anticancer, antifungal and antibacterial agents (Calixto, 2019).

Family	<i>Bignoniaceae</i>
Botanical name	<i>Oroxylum indicum</i> (L.) Benth
English name	midnight horror, Indian trumpet flower
Myanmar name	Kyaung sha
Part used	Fruits



Figure 1. Photographs of *Oroxylum indicum* (L.) Benth (Kyaung-sha) Fruits

The main aim of this research was to investigate some phytochemical constituents from crude extracts of endophytic fungi isolated from the fruits of *Oroxylum indicum* (L.) Benth (Kyaung-sha) and to evaluate some biological activities such as antimicrobial activity, antioxidant activity and antidiabetic activity.

Materials and Methods

Sample Collection

The fruits sample of *O. indicum* (L.) Benth (Kyaung-sha) was collected from Patheingyi Township, Ayeyarwady Region in October, 2020. After being collected, the scientific name of the sample was identified by authorized botanists at Botany Department, Patheingyi University.

Tissue preparation

Endophytic fungi were isolated from the different tissues collected from *O. indicum* (L.) Benth (Kyaung-sha) fruits using a modified surface sterilization procedure (Ando *et al.*, 2004) Briefly, the plant tissue samples were removed from storage and thawed by briefly putting them under running tap water and then washed using 0.1% (v/v) for 15 minutes followed by another wash for 1 30 min using running water. The cleaned plant tissues were then transferred to a laminar airflow cabinet. The plant tissue samples were dipped in 70% ethanol; 30 sec for leaf samples and 2 min for stem samples. The ethanol was drained out after the required amount of time and the plant tissue was then washed using a 2% sodium hypochlorite solution for 15 min which was then followed by four washes using double distilled water after which the samples were dried using sterile paper towels. The effectiveness of the sterilization procedure was tested by plating 0.1 mL of the final sterile water rinse onto Petri dishes containing potato dextrose agar (PDA) and by rolling the sterilized sample onto Petri dishes containing PDA.

Isolation of endophytic fungi

The surface sterilized tissues were cut into smaller segments (1-2 cm) using sterile razor blades and placed onto Petri dishes containing PDA supplemented and incubated at 28 ± 2 °C until fungal growth was initiated. The growing hyphal tips which grew out of the samples were isolated and sub cultured onto Petri dishes containing PDA. The cycle of sub culturing was repeated until pure cultures of the isolates were obtained (Chandra, 2012).

Preparation of crude extracts by direct extraction methods

The culture was centrifuged (20 minutes, 4 °C, 3500 rpm). The cell-free supernatant was extracted with ethyl acetate for 10 times to get the ethyl acetate soluble compounds by liquid-liquid partition between ethyl acetate and the culture solution 1:1 v/v. This process was done according to the ultrasound-assisted extraction to give ethyl acetate extract which was applied to investigate the chemical constituents and some biological activities. (Ando and Inaba, 2004).

Preliminary Phytochemical Test

A few gram of crude extract of selected sample was subjected to the tests of alkaloids, α -amino acids, carbohydrates, flavonoids, glycosides, organic acids, phenolic compounds, reducing sugars, saponins, starch, tannins, steroids, terpenoids according to the standard procedure. (Harborne, 1984)

Chemical Constituents of the Ethyl Acetate Extract of Endophytic Fungi Isolated from *Oroxylum indicum* (L.) Benth (Kyaung-sha) Fruits

(a) Determination of total phenol content assay

The total phenolic content (TPC) of ethyl acetate extract of endophytic fungi isolated from *O. indicum* (L.) Benth (Kyaung-sha) fruits was estimated by Folin-Ciocalteu (FC) method according to the procedure described by (Song *et al.*, 2010). The extract solution (1000 $\mu\text{g/mL}$) was mixed with 5 mL of F-C reagent (1:10) in a test tube and incubated for about 5 min. To each test tube, 4 mL of 1 M sodium carbonate was added and the test tubes were kept at room temperature for 15 min and UV absorbance of reaction mixture was read at λ_{max} 765 nm. The blank solution was prepared as the above procedure by using distilled water instead of sample solution. Total phenol content was estimated as milligram gallic acid equivalent per gram (mg GAE/g) of extract.

(b) Determination of total flavonoid content assay

The total flavonoid content (TFC) of ethyl acetate extract of endophytic fungi isolated from *O. indicum* (L.) Benth (Kyaung-sha) fruits was estimated by Aluminium Chloride method according to the procedure described by (Song *et al.* 2010). The extract solution (1000 $\mu\text{g/mL}$) was mixed with 1.5 mL of methanol, 0.2 mL of 1 % AlCl_3 solution and 2.8 mL of distilled water. The absorbance of reaction mixture was at λ_{max} 415 nm. The blank solution was prepared as the above procedure by using distilled water instead of sample solution. Total flavonoid content was estimated as milligram quercetin equivalent per gram (mg QE/g) of extract.

Biological Activities of Ethyl Acetate Extracts of Endophytic Fungi

(a) Investigation of antioxidant activity assay

In this experiment, DPPH (2 mg) was thoroughly dissolved in EtOH (100 mL). This solution was freshly prepared in the brown coloured reagent bottle and stored in the fridge for no longer than 24 h. The crude extracts of *O. indicum* (2 mg) and 10 mL of EtOH were thoroughly mixed by shaker. The mixture solution was filtered and the stock solution was obtained. By adding with EtOH, the sample solutions in different concentrations of 200, 100, 50, 25, 12.5, 6.25 and 3.125 µg/mL were prepared from the stock solution. The effect on DPPH radical was determined by using the method of Marinova and Batchvarov (2011). The control solution was prepared by mixing 1.5 mL of 50 µM DPPH solution and 1.5 mL of EtOH using shaker. The test sample solution was also prepared by mixing thoroughly 1.5 mL of 50 µM DPPH solutions and 1.5 mL of each sample solution. The mixture solutions were allowed to stand at room temperature for 30 min. Then, the absorbance of each solution was measured at 517 nm by using UV-1650 spectrophotometer. Absorbance measurements were done in triplicate for each concentration and then mean values so obtained were used to calculate percent inhibition of oxidation (Basma *et al.*, 2011). The capability to scavenge the DPPH radical was calculated by using the following equation:

$$\% \text{ RSA} = \frac{A_{\text{control}} - (A_{\text{sample}} - A_{\text{blank}})}{A_{\text{control}} \times 100}$$

Where, %RSA = Radical Scavenging Activity

A_{control} = absorbance of the control (DPPH only) solution

A_{blank} = absorbance of the blank (EtOH + Test sample solution) solution

A_{sample} = absorbance of the test sample solution

(b) Determination of antidiabetic activity by α -amylase inhibition assay

In alpha amylase assay, the starch-iodine was used. First 2 mL of (0.5%) substrate starch solution and 1 mL of tested solution (Acarbose standard drug and crude) of seven different concentration such as 200, 100, 50, 25, 12.5, 6.25 and 3.125 µg/mL were added in a bottle and this mixture was incubated for 3 min at room temperature. To start the reaction, 1 mL of α -amylase was added in above solution followed by incubated for 15 min at room temperature. To stop the reaction, 4 mL of 0.1M HCl was added in this mixture and to detect the reaction, 1 mL of Iodine-iodide indicator (1 mM) was added in the mixture. Absorbance was read at 650 nm by UV spectrophotometer in the visible region. The control solution was prepared as above procedure by using phosphate buffer (0.02M, pH 6.5) instead of drug solution.

All the experiments were done in triplicate. Percent inhibition of each sample solution was calculated by using the following formula. Standard deviation (SD) and 50% inhibition concentration (IC_{50}) value in µg/mL were calculated by computer excel program.

$$\% \text{ Inhibition} = \frac{A_{\text{Sample}} - A_{\text{Control}}}{A_{\text{Sample}}} \times 100$$

Where,

A_{control} = the absorbance of the control solution

A_{sample} = the absorbance of sample solution

(c) Determination of antimicrobial activity of ethyl acetate extracts of endophytic fungi

The antimicrobial activity of ethyl acetate extracts of endophytic fungi isolated from *O. indicum* (L.) Benth (Kyaung-sha) fruits was determined against eight strains of microorganisms such as *Agro tumefaciens* (NITE 09678), *Bacillus pumilus* (IFO 12092), *Bacillus subtilis* (IFO 90517), *Candida albicans* (NITE 09542), *Escherichia coli* (AHU 5436), *Micro luteus* (NITE 83297), *Pseudomonas fluorescens* (IFO 94307) and *Staphylococcus aureus* (AHU 8465) by employing agar well diffusion method. To prepare the agar plate, firstly, peptone (0.5 g) and sodium chloride (0.25 g) were mixed in distilled water and made up to 100 mL with distilled water. The pH of this solution was adjusted at 7.2 with 0.1 M sodium hydroxide solution and 1.5 g of agar was added. Nutrient agar was prepared according to method described by (Ando and Inaba, 2004). Briefly nutrient agar was boiled and 20-25 mL of the medium was poured into a test tube and plugged with cotton wool and autoclaved at 121 °C for 15 minutes. Then the tubes were cooled down to 60 °C and poured into sterilized petri-dish and 0.1 mL of spore suspension was also added into the dishes. The agar was allowed to set for 30 minutes after which 10 mm plate agar well was made with the help of sterilized cork border. After that, about 0.1 mL each of the prepared extract solution was introduced into the agar well and incubated at 37 °C for 24 h. The inhibition zone (clear zone) appeared around the agar well indicating the presence of antimicrobial activity. The extent of antimicrobial activity was measured from the zone of inhibition diameter.

Results and Discussion

The four endophytic fungi (EFK 1, EFK 2, EFK 3 and EFK 4) have been isolated from *O. indicum* (L.) Benth (Kyaung-sha) fruits by the direct method, followed by cultured in potato agar medium (PGA). The phytochemical tests revealed that alkaloids, α -amino acids, carbohydrates, flavonoids, glycosides, organic acid, phenolic compounds, reducing sugars, saponins, steroid, tannins and terpenoids were found to be present but and starch was absent in selected sample. The total phenol content of the ethyl acetate extract of four endophytic fungi isolated from *O. indicum* (L.) Benth (Kyaung-sha) fruits was determined with spectrophotometric method by using Folin-Ciocalteu reagent. TPC ($\mu\text{g GAE}/\text{mg}$) were found to be highest in EFK-2 (216.86 ± 0.66). The total flavonoid content of sample was determined with spectrophotometric method by aluminum chloride reagent and was found to be highest in EFK-3 ($67.47 \pm 1.4 \text{ mg QE}/\text{g}$). The results are shown in Table1.

Table 1. Total Phenol and Total Flavonoid Contents of Four Endophytic Fungi

Fungi	Total Phenol Content (mg GAE \pm SD)/g of extract	Total Flavonoid Content (mg QE \pm SD)/g of extract
EFK-1	16.95 ± 0.28	14.68 ± 0.22
EFK-2	126.86 ± 0.14	59.77 ± 0.11
EFK-3	44.79 ± 0.21	67.47 ± 1.40
EFK-4	52.90 ± 0.14	34.61 ± 0.22

According to the experimental results, phenol and flavonoid compounds were detected in all endophytic fungi. Besides their established antioxidant activity, many phenolic compounds may exhibit significant antimicrobial activity. Since many plant extracts are rich in phenolic compounds, this is of particular interest for the development of natural alternatives to synthetic preservatives in food and cosmetic applications. Flavonoids are also present as a potent water-soluble antioxidant and free radical scavengers, which prevent from the oxidative cell damage and also have strong anticancer activity. It also helps in managing diabetes induced oxidative stress.

The antioxidant activity was measured in terms of hydrogen donating or radical scavenging ability of the four endophytic fungi by using the stable radical DPPH. The results are shown in Figure 2 and Table 2. The EFK-2 was found to be the low (IC_{50}) value 12.15 $\mu\text{g/mL}$ than the other endophytic fungi, low IC_{50} value indicate the more potent antioxidant activity. However, the selected sample was weaker activity than the standard ascorbic acid ($IC_{50} = 4.22 \mu\text{g/mL}$).

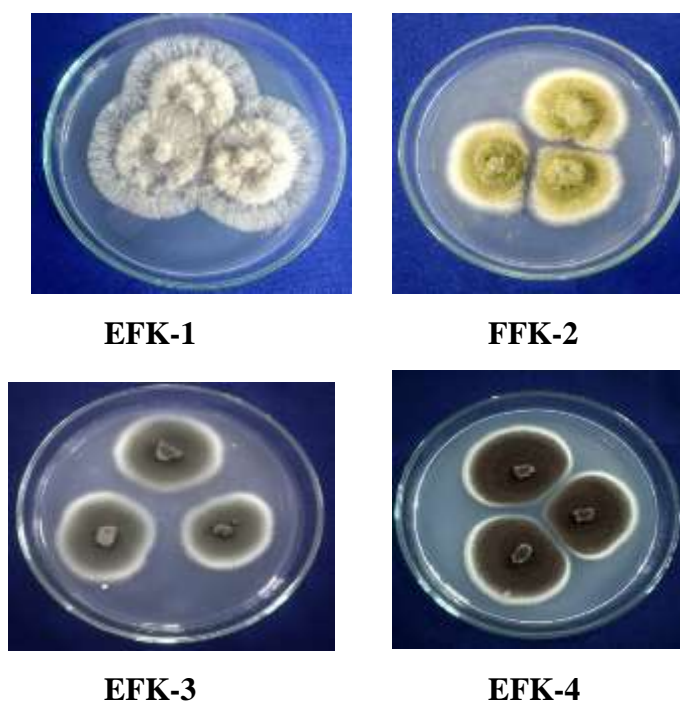


Figure 2. Colony characteristic of endophytic fungi from (Kyaung sha) fruit

Hyperglycemia has been a classical risk in the development of diabetes and the complications associated with diabetes. Therefore, control of blood glucose levels is critical in the early treatment of diabetes mellitus and reduction of macro and microvascular complications. One therapeutic approach is the prevention of carbohydrate absorption after food intake, which is facilitated by inhibition of enteric enzymes including α -glucosidase and α -amylase present in the brush borders of intestine. In this study, the α -amylase inhibitory activity of *O. indicum* (L.) Benth (Kyaung-sha) fruit was investigated. The inhibitory effect of crude extracts of four isolated fungi were analyzed. The percentage inhibition of α -amylase by crude extract were studied in a concentration range of 3.125-200 $\mu\text{g/mL}$. The percentage inhibition of the samples on α -amylase enzyme activity increased with increasing the concentrations. From the percentage inhibition, the respective IC_{50} values for the crude extracts were calculated and the results are respectively

tabulated in Table (3). The four endophytic fungi isolated from *O. indicum* (L.) Benth (Kyaungsha) fruit also explored for the *in vitro* α -amylase inhibition and their activity was compared with standard anti-diabetic drug, acarbose. The 50% α -amylase inhibition potency (IC_{50}) of crude extracts of the four endophytic fungi was ranging between 4.97-12.36 $\mu\text{g/mL}$, indicating that crude extracts possessed potent α -amylase inhibition activity. However, the selected sample was weaker activity than the standard acarbose ($IC_{50} = 3.47 \mu\text{g/mL}$).

Table 2. Antioxidant Activity of Four Endophytic Fungi by DPPH Assay

Samples	% RSA (mean \pm SD) in different concentrations ($\mu\text{g/mL}$)							IC_{50} ($\mu\text{g/mL}$)
	3.125	6.25	12.5	25	50	100	200	
EFK-1	34.63	42.83	46.72	57.94	79.36	91.19	99.83	16.15
	\pm	\pm	\pm	\pm	\pm	\pm	\pm	
	0.54	0.91	0.79	1.82	1.56	0.26	0.75	
EFK-2	32.82	45.60	50.26	51.73	70.55	77.29	80.83	12.15
	\pm	\pm	\pm	\pm	\pm	\pm	\pm	
	0.40	0.26	0.26	1.82	0.75	0.15	0.69	
EFK-3	44.30	46.98	49.48	55.96	57.69	67.01	80.14	13.5
	\pm	\pm	\pm	\pm	\pm	\pm	\pm	
	0.26	0.30	0.26	0.52	0.40	0.40	0.15	
EFK-4	34.72	37.31	45.85	47.93	57.08	66.49	72.11	30.66
	\pm	\pm	\pm	\pm	\pm	\pm	\pm	
	0.45	0.52	0.26	0.26	0.54	0.15	0.54	
Ascorbic acid	45.05	56.35	68.42	73.13	81.95	88.18	97.40	4.22
	\pm	\pm	\pm	\pm	\pm	\pm	\pm	
	0.82	0.35	0.45	0.33	0.12	0.23	0.65	

Table 3. Antidiabetic Activity of Four Endophytic Fungi by α -Amylase Inhibition Assay

Samples	% Inhibition in different concentrations ($\mu\text{g/mL}$)							IC_{50} ($\mu\text{g/mL}$)
	3.125	6.25	12.5	25	50	100	200	
EFK-1	27.64	35.66	65.23	75.82	80.85	83.79	85.48	9.28
	\pm	\pm	\pm	\pm	\pm	\pm	\pm	
	0.59	0.54	0.60	0.07	0.02	0.03	0.02	
EFK-3	33.86	41.45	50.19	52.58	54.95	60.60	64.71	12.36
	\pm	\pm	\pm	\pm	\pm	\pm	\pm	
	0.25	0.13	0.09	0.08	0.12	0.09	0.07	
EFK-3	37.47	59.05	60.96	70.06	75.88	77.89	81.40	4.97
	\pm	\pm	\pm	\pm	\pm	\pm	\pm	
	0.15	0.06	0.06	0.05	0.02	0.03	0.05	
EFK-4	20.61	52.12	58.73	60.39	65.99	72.34	77.33	4.97
	\pm	\pm	\pm	\pm	\pm	\pm	\pm	
	0.49	0.10	0.06	0.06	0.04	0.04	0.03	
Acarbose	48.03	58.11	72.49	81.22	89.11	91.30	98.19	3.74
	\pm	\pm	\pm	\pm	\pm	\pm	\pm	
	0.12	0.30	0.39	0.32	0.26	0.41	0.59	

Screening of antimicrobial activity of four endophytic fungi isolated from *O. indicum* (L.) Benth (Kyaung-sha) fruits was done by agar well diffusion method (Table 4 and Figure 3). In this study, the samples were tested on eight pathogenic microorganisms such as *Agro tumefaciens*, *Bacillus pumilus*, *Bacillus subtilis*, *Candida albicans*, *Escherichia coli*, *Micro luteus*, *Pseudomonas fluorescens* and *Staphylococcus aureus*. From these results, it was found that selected sample exhibit antimicrobial activity against all tested microorganisms. The four endophytic fungi exhibited inhibition zone diameters ranged between in 23 mm ~ 30 mm respectively against all tested microorganisms.

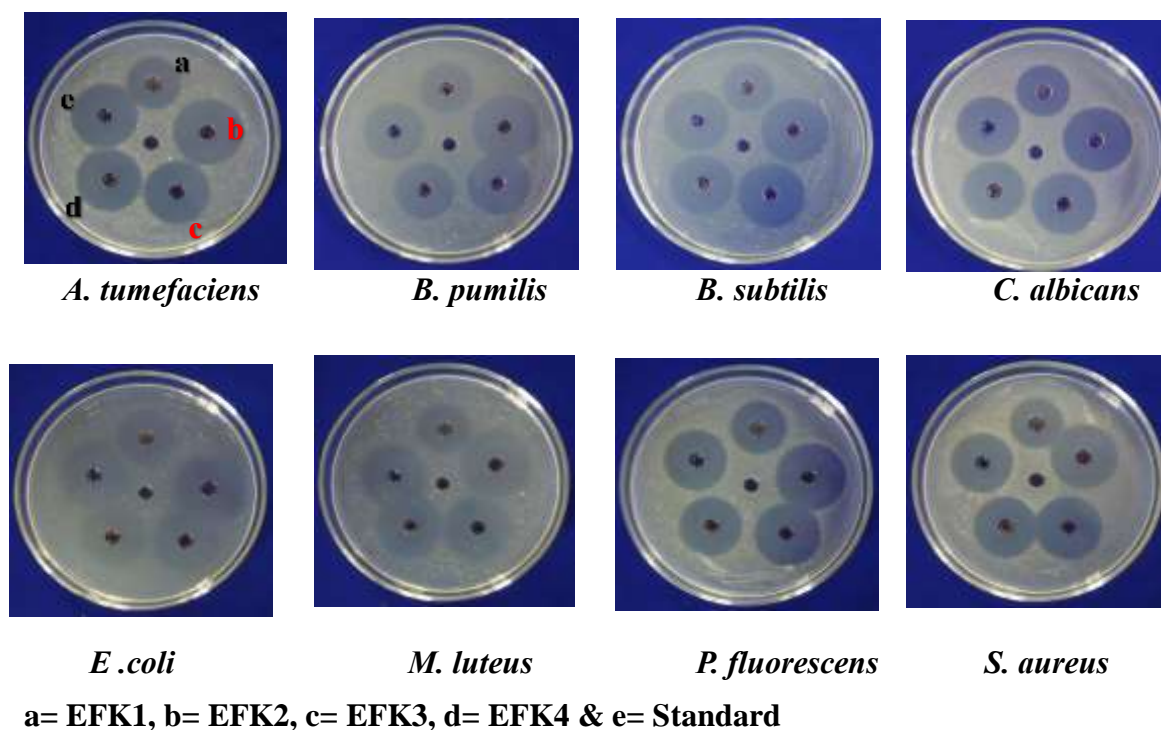


Figure 3. Screening of antimicrobial activity of the crude extracts by agar well diffusion method

Table 4. Inhibition Zone Diameters of Crude Extracts Against Eight Microorganisms by Agar Well Diffusion Method

Microorganism	Inhibition zone diameters (mm)				
	EFK-1	EFK-2	EFK-3	EFK-4	STD
<i>A. tumefaciens</i>	23.29	29.20	26.47	27.41	29.29
	±	±	±	±	±
	0.12	0.08	0.11	0.12	0.03
<i>B. pumiliu</i>	23.77	30.21	29.39	29.07	29.48
	±	±	±	±	±
	0.17	0.31	0.37	0.08	0.01
<i>B. subtilis</i>	24.13	32.79	31.26	31.16	28.89
	±	±	±	±	±
	0.08	0.02	0.25	0.03	0.05
<i>C. albicans</i>	24.51	30.17	29.53	28.51	30.34
	±	±	±	±	±
	0.16	0.25	1.19	0.43	0.09

Microorganism	Inhibition zone diameters (mm)				
	EFK-1	EFK-2	EFK-3	EFK-4	STD
<i>E. coli</i>	24.55	30.81	29.42	29.23	29.29
	±	±	±	±	±
	0.10	0.26	0.07	0.06	0.03
<i>M. luteus</i>	24.50	29.85	29.25	29.36	29.48
	±	±	±	±	±
	0.04	0.12	0.06	0.04	0.01
<i>P. fluorescens</i>	23.73	29.43	28.90	29.37	28.89
	±	±	±	±	±
	0.01	0.36	0.12	0.51	0.05
<i>S. aureus</i>	25.09	30.00	29.66	29.42	30.34
	±	±	±	±	±
	0.05	0.03	0.03	0.04	0.09

Agar well diameter (8 mm)

10 mm – 14 mm = weak activity (+)

15 mm – 19 mm = moderate activity (++)

20 mm and above = potent activity (+++)

STD = chloramphenicol

Conclusion

The four endophytic fungi isolated from *O. indicum* (L.) Benth (Kyaung-sha) showed. Phytochemical results, such as alkaloids, α -amino acids, carbohydrates, flavonoids, glycosides, organic acid, phenolic compounds, reducing sugars, saponins, steroid, tannins and terpenoids were found to be present and starch was absent. The ethyl acetate extract of EFK-2 contains significant high TPC (126.86 ± 0.14 mg GAE/g) and EFK-3 contains significant high TPC (67.47 ± 1.40 mg QE/g). It showed high antimicrobial activity (23 mm ~ 30mm) against *Agrotumefaciens*, *Bacillus pumilus*, *Bacillus subtilis*, *Candida albicans*, *Escherichia coli*, *Micro luteus*, *Pseudomonas fluorescens* and *Staphylococcus aureus* due to presence the flavonoids and phenols. The crude extracts of four isolated fungi also showed DPPH free radical scavenging activity assay ($IC_{50} = 16.15$ μ g/mL, 12.15 μ g/mL, 13.50 μ g/mL and 30.66 μ g/mL respectively) has antioxidant activity. The antidiabetic activity due to its α -amylase inhibitory effect ($IC_{50} = 9.28$ μ g/mL, 12.36 μ g/mL and 4.97 μ g/mL respectively). The results from this research strongly indicated that tested crude extracts of four endophytic fungi isolated from *O. indicum* (L.) Benth (Kyaung-sha) fruit may play a role as medicinal constituents.

Acknowledgements

The authors would like to express their profound gratitude to the Department of Higher Education, Ministry of Education, Yangon, Myanmar, for provision of opportunity to do this research.

References

- Ando, K., M. Suto and S. Inaba. (2004). *Sampling and Isolation Methods of Fungi*. Workshop at University of Patheingyi, Ayeyarwady Region
- Ando, K. and S. Inaba. (2004). *Taxonomy and Identification of Fungi*. Workshop at Patheingyi University Biotechnology Development Centre
- Basma, A. A., Z. Zakaria, L. Y. Latha and S. Sasidharan. (2011). "Antioxidant Activity and Phytochemical Screening of the Method Extracts of *Euphorbia hirta* L.", *Journal of Tropical Medicine*, 8(8), 386-390

- Calixto, J. B. (2019). "The Role of Natural Products in Modern Drug Discovery". *An. Acad. Bras. Cienc.*, 2, 91-95
- Chandra, S. (2012). "Endophytic fungi: Novel Sources of Anticancer Lead Molecules". *Appl. Microbiol. Biotechnol.*, 95, 47-59
- Deka, D. C., K. Vimal, P. Chandan and K. Kamal. (2013). "Oroxylum indicum a Medicinal Plant of North East India: An Overview of Its Nutritional, Remedial, and Prophylactic Properties". *Journal of Applied Pharmaceutical Science.*, 3 (1),104-112
- Harborne, J. B. (1984). *Phytochemical methods and A Guide to Modern Technique of Plant Analysis*. London: Chapman and Hall, 37-222
- Marinova, G. V. and Batchvarov, V. (2011). "Evaluation of the Methods for Determination of the Free Radical Scavenging Activity of DPPH". *Bulgarian Journal of Agricultural Science*, vol. 17, pp. 11-24.
- Newman, D.J. and G.M. Cragg. (2020). "Natural Products as Sources of New Drugs Over the Nearly Four Decades from 01/1981 to 09/2019". *J. Nat. Prod.*, vol. 83, 770-803
- Song, F. L., Gan, R. Y., Zhang, Y., Xiao, Q., Kuang, L. and Li, H. B. (2010). "Total Phenolic Contents and Antioxidant Capacities of Selected Chinese Medicinal Plants". *Int. J. Mol. Sci.*, vol.11, pp- 2367-2372.

INVESTIGATION OF SOME BIOACTIVITIES AND PHYTOCONSTITUENTS FROM THE PEELS OF *LITCHI CHINENSIS* SONN. (LYCHEE)

Kay Khine Win Swe¹, Prema², Ni Ni Than³

Abstract

The aim of the present work is to investigate the phytoconstituents, the total phenolic contents, antioxidant activity, cytotoxicity, antiarthritic activity, and anti-diabetic activity of *Litchi chinensis* Sonn. (Lychee) peels. Preliminary phytochemical screening by test tube methods revealed that alkaloids, α -amino acids, carbohydrates, glycosides, organic acids, phenolic compounds, reducing sugars, saponins, starch, steroids, tannins, terpenoids and flavonoids are present and cyanogenic glycosides is absent in the sample. The total phenolic content of ethanol and watery extracts from Lychee peels was determined by the Folin-Ciocalteu Reagent (FCR) method. Total phenolic content was found to be the highest in ethanol extract (114.86 ± 0.14 $\mu\text{g/mL}$). *In vitro* antioxidant activity of ethanol and watery extracts of Lychee peels was assessed by the DPPH free radical scavenging assay. IC_{50} values were found to be 86.21 $\mu\text{g/mL}$ for the watery extract and 31.03 $\mu\text{g/mL}$ for the ethanol extract of Lychee peels. The cytotoxicity of the watery and ethanol extracts was evaluated by a brine shrimp lethality bioassay. From these results, the LD_{50} values of watery and ethanol extracts were found to be non-toxic at the 1000 $\mu\text{g/mL}$ concentration. *In vitro* antiarthritic activity of watery and ethanol extracts was screened by the egg albumin method. According to the data, ethanol extract ($\text{IC}_{50} = 60.56$ $\mu\text{g/mL}$) has more potent antiarthritic activity than the watery extract ($\text{IC}_{50} = 86.39$ $\mu\text{g/mL}$). *In vitro* α -amylase inhibitory effect was determined by the starch-iodine method. The IC_{50} values were found to be 6.66 $\mu\text{g/mL}$ for the watery extract and 5.83 $\mu\text{g/mL}$ for the EtOH extract of the lychee peels.

Keywords: *Litchi chinensis* Sonn., phytochemicals, total phenolic contents, antioxidant activity, cytotoxicity, antiarthritic activity, antidiabetic activity

Introduction

Over 60 % of the world's population, including about 80 % in developing nations, still rely exclusively on medicinal plants for their health requirements, making traditional medicine the preferred main healthcare system in many communities. This is because of a variety of factors, including cost effectiveness, accessibility, and affordability. There is a long history of using plants to treat many human ailments. Different plant parts, including leaf, stem, bark, root, and others, are utilized to prevent, alleviate symptoms, or restore abnormalities to normal. Approximately 80 % of the active chemicals used in modern medicine today, which include active substances separated from higher plants, show a positive association between their current therapeutic uses and their historic usage (Shehri *et al.*, 2022). One of the significant fruit plants, lychee, contains a number of bioactive chemicals with pharmacological effects. The lychee (*Litchi chinensis*), a fruit belonging to the Sapindaceae family, originated in China and is now a common sight across the tropical and subtropical parts of the world. In the subtropics, one of the best fruit trees is the lychee. It comes with numerous health advantages, including anticancer,

¹ Department of Chemistry, University of Yangon

² Department of Chemistry, University of Yangon

³ Department of Chemistry, University of Yangon

hepatoprotective, antioxidant, antiplatelet, antiviral, antimutagenic, antimicrobial, antihyperlipidemic, antipyretic, and anti-inflammatory effects (Deshwal *et al.*, 2022).

Materials and Methods

Plant materials

Lychee fruits were collected from July to August, 2021 in Myitkyina township, Kachin State, Myanmar. The collected sample was identified as *Litchi chinensis* Sonn. (Lychee) fruits at the Botany Department, University of Yangon. The sample was cleaned by washing thoroughly with water and peeled off. Then the fresh peel was cut into small pieces and air-dried at room temperature. The dried sample was ground into powder by a grinding machine, sieved and stored in an airtight container for further use.

Phytochemical Investigation of Lychee Peels

Phytochemical tests of lychee peels were carried out according to the standard methods (Geetha *et al.*, 2014 and Harbone, 1984) which were investigate the presence or absence of alkaloids, α -amino acids, carbohydrates, cyanogenic glycosides, glycosides, organic acids, phenolic compounds, reducing sugars, saponins, starch, steroids, tannins, terpenoids, and flavonoids. The observed results are shown in Table 1.

Preparation of Crude Extracts for Biological Activities

About 20 g of dried powder sample was extracted three times with 95 % ethanol for six hours and then filtered, reduced the volume by rotary evaporator to obtain ethanol extract. To obtain watery extract, 20 g of dried powder samples was boiled in 100 mL of distilled water and filtered. It was then concentrated by evaporating the solvent on a water bath to get a watery extract. The crude extracts were dried and kept in a refrigerator for a few weeks.

Determination of Total Phenolic Contents by Folin-Ciocalteu Method

The total phenolic content was determined by the Folin-Ciocalteu (FC) method. Each extracted sample solution (0.5 mL) was added into 5 mL of FC reagent (1:10) and incubated for 5 min. To each tube, 4 mL of 1 M sodium carbonate solution was added, the tubes were kept at room temperature for 15 min, and the UV absorbance of reaction mixture was read at λ_{\max} 765 nm. Total phenolic content as $\mu\text{g GAE/mg}$ of crude extract was estimated from the gallic acid standard calibration curve (Hishamuddin *et al.*, 2020).

Determination of Antioxidant Activity by DPPH Free Radical Scavenging Assay

DPPH free radical scavenging activity was determined by a spectrophotometric method. The control solution was prepared by mixing 1.5 mL of DPPH solution and 1.5 mL of ethanol in the brown bottles. The sample solution was also prepared by mixing thoroughly 1.5 mL of DPPH solution and 1.5 mL of different concentrations of each test sample solution (3.91, 7.81, 15.63, 31.25, 62.50, and 125.00 $\mu\text{g/mL}$). These bottles were incubated at room temperature and were

shaken on the shaker for 30 min. After 30 min, the absorbance of each solution was measured at 517 nm by spectrophotometer (Hishamuddin *et al.*, 2020). Absorbance measurements were done in triplicate for each solution.

Determination of Cytotoxicity by Brine Shrimp Lethality Bioassay

The brine shrimp (*Artemia salina*) was used in this study for the cytotoxicity bioassay. Artificial sea water [3.8 % (w/v) NaCl] was prepared by dissolving (38 g) of sodium chloride in 1 L of distilled water. Brine shrimp cysts (0.5 g) were put into 1 L of artificial sea water in a bottle. This bottle was placed near a lamp. Light is essential for the cysts to hatch. Brine shrimp cysts required to hatch constant supplied oxygen and 24 h incubation at room temperature. 9 mL of artificial seawater and 1 mL of different concentrations of each sample (1000, 100, 10, 1 $\mu\text{g}/\text{mL}$) and each standard solution (caffeine and $\text{K}_2\text{Cr}_2\text{O}_7$) were added to each chamber. Alive brine shrimp (10 nauplii) were then taken with a pasteur pipette and placed into each chamber. They were incubated at room temperature for about 24 h. After 24 h, the number of dead or survival brine shrimps were counted and the estimation of cytotoxicity was done by 50 % lethality dose (LD_{50}) (Singh *et al.*, 2015). The control solution was prepared as in the above procedure by using distilled water instead of the sample solution.

Determination of Antiarthritic Activity by Egg Albumin Method

The reaction mixture (5 mL) consisted of 0.2 mL of egg albumin from fresh hen's egg, 2.8 mL of phosphate buffered saline (PBS, pH 6.4) and 2 mL of different (100, 200, 400, 800, and 1000 $\mu\text{g}/\text{mL}$) concentrations of each crude extract of lychee. Similar volume of double-distilled water served as control. Then the mixtures were incubated at 37 °C in an incubator for 15 min and then heated at 70 °C for 5 min. After cooling, their absorbance values were measured at 660 nm. Diclofenac sodium was used as a reference drug (Sunmathi *et al.*, 2016).

Determination of Antidiabetic Activity by α -Amylase Inhibition Assay

α -Amylase inhibitory activity was determined by starch-iodine method. 10 μL of α amylase solution (0.025 mg/mL) was mixed with 390 μL of phosphate buffer (0.02 M containing 0.006 M NaCl, pH 7.0) containing different concentrations (1.96, 3.91, 7.81, 15.63, 31.25, 62.50, and 125.00 $\mu\text{g}/\text{mL}$) of each extract. After incubation at 37 °C for 10 min, 10 μL of starch solution (1 %) was added, and the mixture was reincubated for 15 min. Next, 0.1 mL of 1 % iodine solution was added, and after adding 5 mL distilled water, the absorbance was taken at 565 nm (Ganapaty *et al.*, 2013).

Results and Discussion

Phytochemical Investigation of Lychee Peels

The preliminary phytochemical investigation was carried out to know the different types of phytoconstituents present in the sample. The investigation results revealed that the presence of alkaloids, α -amino acids, carbohydrates, glycosides, phenolic compounds, reducing sugars, saponins, starch, steroids, tannins, terpenoids, and flavonoids but cyanogenic glycoside was found to be absent (Table 1). The lychee peels can be employed as antioxidant, antidiabetic, and

anti-inflammatory drugs due to the presence of phenolic compounds, steroids, tannins, terpenoids, and flavonoids components.

Table 1. Results of Preliminary Phytochemical Investigation of the Lychee Peels

No.	Test	Extracts	Test reagents	Observation	Results
1	alkaloids	1 % HCl	(i) Dragendorff's reagent	orange ppt	+
			(ii) Mayer's reagent	white ppt	+
			(iii) sodium picrate	yellow ppt	+
			(iiii) Wagner's reagent	brown ppt	+
2	α -Amino acids	H ₂ O	Ninhydrin reagent	purple spot	+
3	carbohydrates	H ₂ O	10 % α -naphthol and H ₂ SO ₄	red ring	+
4	cyanogenic glycosides	H ₂ O	H ₂ SO ₄ + sodium picrate solution	no brick red	-
5	glycosides	H ₂ O	10 % lead acetate	white ppt.	+
6	organic acids	H ₂ O	bromocresol green	yellow ppt	+
7	phenolic compounds	H ₂ O	K ₃ Fe(CN) ₆ + FeCl ₃	deep blue colour	+
8	reducing sugars	H ₂ O	Benedict's solution	yellow ppt.	+
9	saponins	H ₂ O	distilled water	frothing	+
10	starch	H ₂ O	iodine solution	deep blue colour	+
11	steroids	PE	acetic anhydride + conc: H ₂ SO ₄	greenish blue colour	+
12	tannins	H ₂ O	5 % FeCl ₃ solution	bluish black ppt	+
13	terpenoids	CHCl ₃	acetic anhydride + conc: H ₂ SO ₄	red colour	+
14	flavonoids	EtOH	conc: HCl + Mg turning	pink colour	+

(+) = presence (-) = absence ppt = precipitate

Total Phenolic Content of Crude extracts of Lychee Peels

In the present investigation, the total phenolic contents (TPC) of watery and ethanol extracts were estimated by the Folin-Ciocalteu method. Gallic acid (3,4,5-trihydroxybenzoic acid) was used to construct a standard calibration curve for total phenol estimation. TPC was expressed as microgram of gallic acid equivalent (GAE) per milligram of crude extract ($\mu\text{g GAE/mg}$).

According to the results, the TPC of ethanol extract (114.86 ± 0.14) $\mu\text{g GAE/mg}$ was found to be higher than that of watery extract (71.66 ± 0.00) $\mu\text{g GAE/mg}$ (Figure 1).

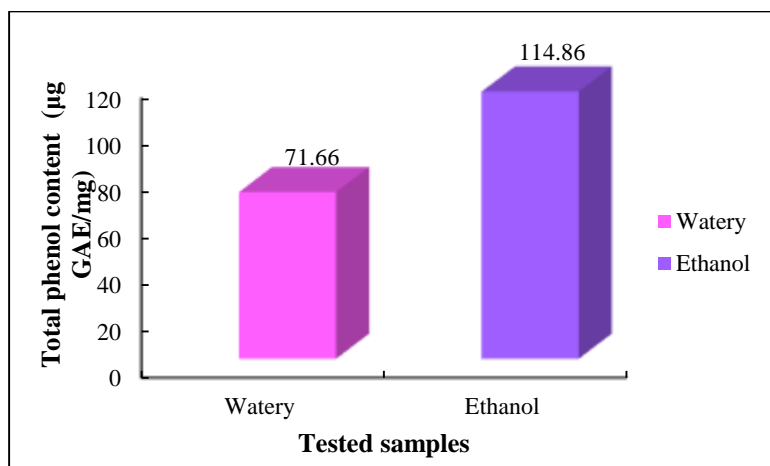


Figure 1. Histogram of total phenolic content of ethanol and watery extracts of lychee peels

Antioxidant Activity of Crude Extracts of Lychee Peels by DPPH Free Radical Scavenging Assay

Lychee peels are a good source of phenolic compounds as their potential antioxidant and antioxidant activity depend on the total phenolic contents. The antioxidant activity of ethanol and watery extracts of lychee peels was studied by the DPPH free radical scavenging assay. IC₅₀ values were observed to be 131.48 µg/mL for watery extract and 60.99 µg/mL for ethanol extract. The largest scavenging activity to scavenge the DPPH radical was observed in ethanol extract, which inhibited 50 % of free radicals at the concentration (IC₅₀) of 60.99 µg/mL. Because of the higher phenolic content, the ethanol extract is more effective than watery extract. The results are shown in Table 2 and Figures 2 and 3. The ethanol extract possessed the antioxidant activity less than the standard ascorbic acid.

Table 2. Average % Inhibition and IC₅₀ Values of Crude Extracts of Lychee Peels

Tested samples	% RSA ± SD							IC ₅₀ (µg/mL)
	of different concentrations (µg/mL)							
	3.91	7.81	15.63	31.25	62.5	125	250	
watery extract	8.90 ±0.27	13.29 ±0.00	26.58 ±0.33	35.55 ±0.44	40.85 ±0.65	48.66 ±0.55	74.47 ±0.03	131.48
ethanol extract	17.65 ±0.27	19.46 ±0.41	20.81 ±0.41	21.46 ±0.60	51.46 ±0.04	74.98 ±0.00	83.99 ±0.24	60.99
Std. ascorbic acid	46.15 ±0.03	75.81 ±0.28	79.12 ±0.16	85.93 ±0.32	87.37 ±0.37	87.62 ±0.00	87.75 ±0.07	4.41

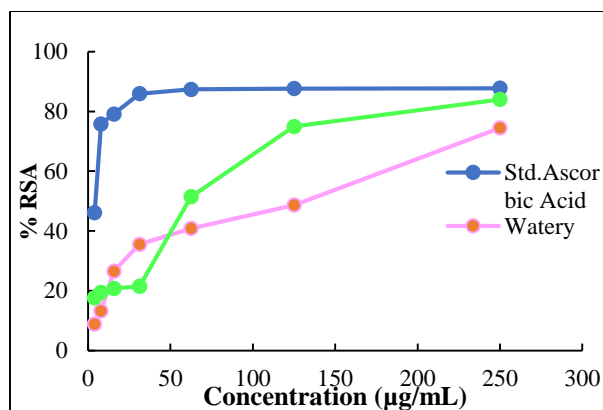


Figure 2. % RSA versus concentration of watery and ethanol extracts of lychee peels

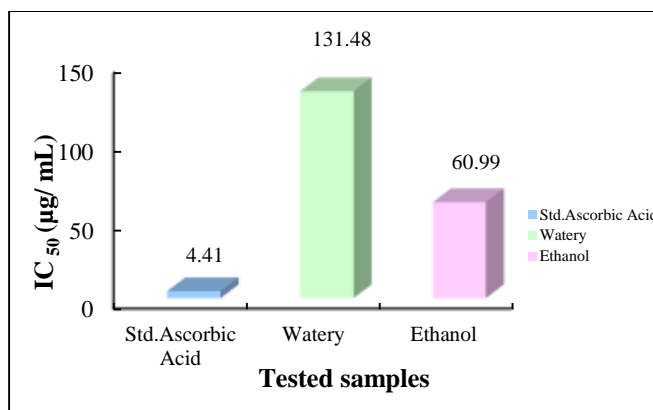


Figure 3. IC₅₀ values of standard ascorbic acid and watery and ethanol extracts of lychee peels

Cytotoxicity of Crude Extracts of Lychee Peels

The cytotoxicity of watery and ethanol extracts of lychee peels were evaluated by the brine shrimp lethality bioassay. The organisms used were brine shrimp, *Artemia salina*. Potassium dichromate and caffeine were used as the positive and negative controls. The cytotoxicity of watery and ethanol extracts of selected plant is shown in Table 3. From the results, LD₅₀ values of watery and ethanol extracts were found to be greater than 1000 µg/mL. LD₅₀ values of crude extracts, less than 1000 µg/mL was toxic (active) and greater than 1000 µg/mL was non-toxic (inactive). Therefore, watery and ethanol extracts have no cytotoxic effect.

Table 3. Cytotoxicity of Different Concentrations of Crude Extracts of Lychee Peels against *Artemia salina* (Brine Shrimp)

Tested samples	D of dead brine shrimp Presents in different concentrations of sample (µg/mL)				LD ₅₀ (µg/mL)
	1	10	100	1000	
watery extract	23.33±0.33	30.00±0.00	33.33±0.58	36.67±0.00	> 1000
ethanol extract	16.67±0.00	26.67±0.33	36.67±0.00	43.33±0.00	> 1000
*Std. K ₂ Cr ₂ O ₇	43.33±0.58	46.67±0.58	76.67±0.58	100±0.00	19.99
**Std. Caffeine	0.00±0.00	13.33±0.58	23.33±0.58	33.33±0.58	>1000

*Std. K₂Cr₂O₇ = Positive control

**Std. Caffeine = Negative control

Antiarthritic Activity of Crude Extracts of Lychee Peels

One of the well-documented causes of inflammatory and arthritic diseases is denaturation of tissue proteins. The effect of watery extract (58.81 µg/mL) and ethanol extract (31.31 µg/mL) of lychee peels was evaluated against denaturation of egg albumin (Table 4). According to the results, the IC₅₀ value of the ethanol extract of lychee peels is lower than those of watery and standard diclofenac sodium. Since, the lower the IC₅₀ value, the higher antiarthritic activity, the ethanol extract of lychee peels has more antiarthritic potency than standard and watery extract (Figures 4 and 5). So, it can be concluded that ethanol extract of lychee peels can serve as an antiarthritic agent.

Table 4. Average % Protein Denaturation and IC₅₀ Values of Crude Extracts of Lychee Peels

Tested samples	% Protein denaturation of different concentrations (µg/mL)						IC ₅₀ (µg/mL)
	31.25	62.5	125	250	500	1000	
watery extract	38.88 ± 0.27	51.49 ±0.00	62.59 ±0.33	77.03 ±0.00	77.90 ±0.11	82.83 ±0.04	58.81
ethanol extract	49.99 ±0.06	56.31 ±0.09	56.34 ±0.06	61.25 ±0.02	63.30 ±0.07	79.09 ±0.00	31.31
*Std. diclofenac sodium	34.87 ±0.03	52.84 ±0.34	54.65 ±0.10	60.57 ±0.03	65.20 ±0.07	78.83 ±0.00	57.57

*Std. diclofenac sodium = positive control

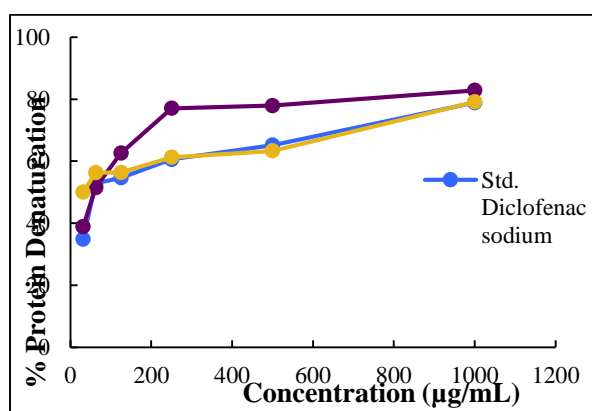


Figure 4. % Protein denaturation versus concentration of watery and ethanol extracts of lychee peels

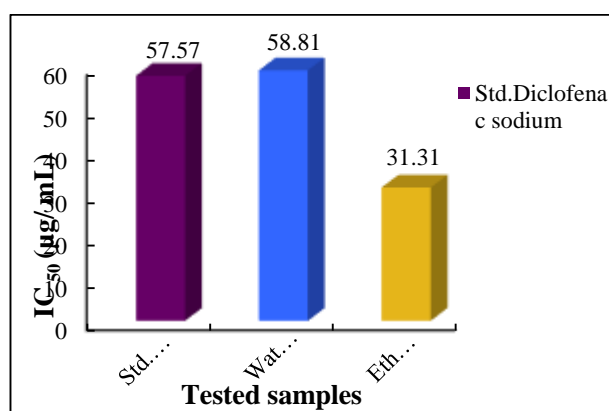


Figure 5. IC₅₀ values of watery and ethanol extracts of lychee peels

Antidiabetic Activity of Crude Extracts of Lychee Peels

The antidiabetic effect of ethanol and water extracts of lychee peels was studied by the α -amylase inhibitory assay. Acarbose was used as a standard. According to the results, the IC_{50} values were found to be 6.66 $\mu\text{g/mL}$ for the watery extract and 5.83 $\mu\text{g/mL}$ for the EtOH extract of the lychee peels. From this observation, the EtOH extract was more potent than the watery extract in antidiabetic activity, comparable with standard acarbose ($IC_{50} = 5.22 \mu\text{g/mL}$). The results are shown in Table 5 and Figures 6 and 7

Table 5. Average % Inhibition and IC_{50} Values of Crude Extracts of Lychee Peels

Tested samples	% RSA \pm SD							IC_{50} ($\mu\text{g/mL}$)
	of different concentrations ($\mu\text{g/mL}$)							
	1.96	3.91	7.81	15.63	31.25	62.5	125	
watery	41.28 ± 0.08	41.66 ± 0.04	53.49 ± 0.00	58.99 ± 0.00	64.31 ± 0.04	67.56 ± 0.09	75.49 ± 0.21	6.66
ethanol	39.83 ± 0.04	41.32 ± 0.06	58.99 ± 0.17	72.21 ± 0.42	79.69 ± 0.20	81.22 ± 0.03	85.98 ± 0.21	5.83
*Std. acarbose	45.48 ± 0.00	47.49 ± 0.03	54.99 ± 0.58	62.03 ± 0.00	64.40 ± 0.09	71.29 ± 0.10	74.01 ± 0.00	5.22

*Std. Acarbose = positive control

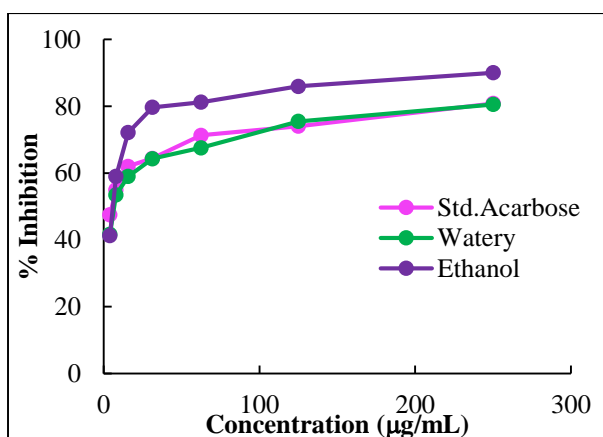


Figure 6. Mean % inhibition versus concentration of watery and ethanol extracts lychee peels

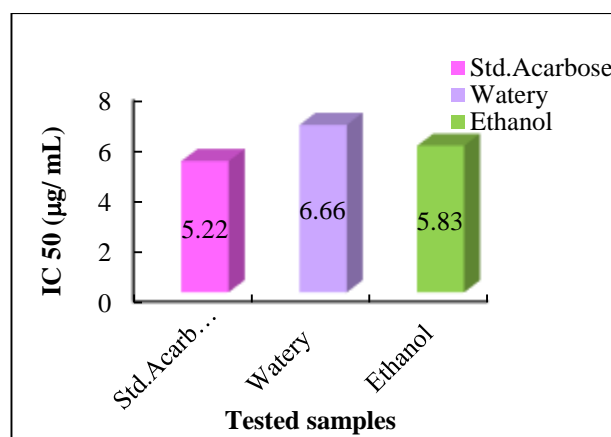


Figure 7. IC_{50} values of crude extracts of crude of lychee peels

Conclusion

The present research work deals with the first report for the investigation of phytoconstituents, total phenol contents, antioxidant, cytotoxicity, and antiarthritic and antidiabetic activities of *Litchi chinensis* Sonn. (Lychee) peels. From the preliminary phytochemical test, the secondary metabolites are present in the lychee samples. Based on the data, EtOH extract ($114.86 \pm 0.14 \mu\text{g GAE/mg}$) was found to possess a higher total phenol content than watery extract ($71.66 \pm 0.00 \mu\text{g GAE/mg}$). The antioxidant activity of the ethanol extract ($\text{IC}_{50} = 60.99 \mu\text{g/mL}$) was more effective than that of the watery extract. According to the cytotoxic effect, ethanol and watery extracts from lychee peels were observed to be free from toxic effect up to $1000 \mu\text{g/mL}$ dose. In antiarthritic activity, ethanol extract ($\text{IC}_{50} = 31.31 \mu\text{g/mL}$) was more effective than the watery extract and the standard diclofenac sodium ($\text{IC}_{50} = 57.57 \mu\text{g/mL}$). In antidiabetic activity, watery ($\text{IC}_{50} = 5.83 \mu\text{g/mL}$) and ethanol ($\text{IC}_{50} = 6.66 \mu\text{g/mL}$) extracts effectively inhibited α -amylase. As the results, this sample could be useful in the treatment of anti-aging, antiarthritic, and diabetes.

Acknowledgements

The authors would like to express their profound gratitude to the Ministry of Education, the Department of Higher Education, for providing the opportunity to do this research, and the Myanmar Academy of Arts and Science for allowing them to present this paper.

References

- Deshwal, V. K., K. Vig, S. B. Singh, and P. D. Devi (2012). Evaluation of the Antibacterial Activity of Bark of *Litchi chinensis* against *Escherichia Coli*, A UTI Causing Organism". *Journal of Plant Development Sciences*, vol. 4, pp. 101–103
- Dipak, G., P. Axay, C. Manodeep, and K. Jagdish. (2012). "Phytochemical and Pharmacological Profile of *Punica granatum*: An Overview". *International Research Journal of Pharmacy*, vol. 3(2), pp. 65–68
- Ganapaty, S., R. Nandeesh, V. P. Veerapur, B. S. Thippeswaamhy, and D. Shivasharan. (2013). "In Vivo and In Vitro Anti-diabetic Effects of *Madhuca indica* Roxb., in Alloxan-Induced Diabetic Rats". *International Journal of Advances in Pharmacy, Biology and Chemistry*, vol. 2(2), pp. 282–290
- Geetha, T. S and N. Geetha. (2014). "Phytochemical Screening, Quantitative Analysis of Primary and Secondary Metabolites of *Cymbopogon citratus* (DC) Stapf, Leaves from Kodaikanal Hills, Tamilnadu". *International Journal of PharmTech Research*, vol. 6(2), pp. 521–529
- Harbone, J. B. (1984). "Phytochemical Methods, A Guide to Modern Techniques of Plant Analysis", New York: 2nd Ed., Chapman and Hall, 120–126
- Hishamuddin, S. N. A., Q. Q. Amir, A. H. Mohamed, and N. R. Said. (2020). "Extraction of Bioactive Compounds from Longan Peel by Using Solvent Extraction Method and its Antioxidant Activity". *ASM Science journal*, vol. 13(6), pp. 60–65
- Shehri, S. H. A., R. A. Alhadlaq, K. I. BinMuhanna, N. S. Aldosri, and M. A. Alghamdi. (2022). "A Review of Medicinal Plants, their Definition, Uses, Active Ingredients and Prevalence in the Kingdom of Saudi Arabia". *International Journal of Science and Research*, vol. 11(12), pp. 1183–1188
- Singh, M. P., J. Singh, and R. Rajesh. (2015). "Brine Shrimp Cytotoxic Assay for Polyherbal Formulation of *Moringa oleifera*, *Viola odorata*, *Allium sativum*". *International Journal of Innovative Pharmaceutical Sciences and Research*, vol. 3(12), pp. 1639–1643
- Sunmathi, D., R. Sivakumar, and K. Ravikumar. (2016). "In Vitro Anti-inflammatory and Antiarthritic Activity of Ethanolic Leaf Extract of *Alternanthera sessilis* (L.) R.Br. ex DC and *Alternanthera philoxeroides* (Mart.) Griseb". *International Journal of Advances in Pharmacy, Biology and Chemistry*, vol. 5(2), pp. 109–115

ENHANCING RUBBER STOPPER PERFORMANCE: A COMPREHENSIVE ANALYSIS OF REINFORCEMENT WITH ALKALI TREATED ARECA NUT FIBER

Thwe Thwe Soe¹, Saw Hla Myint²

Abstract

The abundant availability of areca nut husks in Mone, Kyauk-kyi Township, Bago Region, as a byproduct from areca nut farming presents an opportunity for creating value-added materials of national significance. In this current research endeavor, the extracted fibers from these areca nut husks were subjected to a thorough washing followed by treatment them with a 5 % NaOH solution. Additionally, a portion of the resulting product underwent a separate treatment with permanganate to enhance the fiber's surface characteristics. The mechanical properties of the alkali-treated areca nut fiber-rubber composite, intended for use in stoppers, exhibited impressive values, including hardness (52.6 IRHD), specific gravity (0.98), tensile strength (6.8 MPa), elongation at break (737.3 %), and tear strength (23.8 kN/m). These properties outperformed those of rubber alone, which had a hardness of 30.0 IRHD and a specific gravity of 0.97. Detailed analyses, such as scanning electron microscopy (SEM) for assessing fiber dispersion in the composite, Fourier-transform infrared spectroscopy (FT IR) for confirming composite formation, and thermogravimetric-differential thermal analysis (TG-DTA) for evaluating thermal behavior, conducted on the stopper composites show favorable results. Furthermore, chemical resistance tests demonstrated the stopper's compatibility with various substances, including water, alcohol, concentrated hydrochloric acid (HCl), and moderately concentrated base solutions like 10 % NaOH and 10 % NH₄OH. These findings strongly suggest that areca nut fibers are suitable for reinforcing natural fiber-rubber composites. This study successfully transforms biowaste areca nut husks into a valuable material, specifically stoppers, through composite fabrication with natural rubber.

Keywords: Areca nut fiber-rubber composite, rubber, surface modification, mechanical properties

Introduction

Increasing environmental awareness to minimize the pollution and depletion of resources made researchers all over the world to develop composites using most environmental friendly agro-wastes (lignocellulosic materials) as reinforcing agent and thermoplastic polymers as a matrix (Kumar, 2008). The benefits offered by lignocellulosic materials include making the final product light, decreasing the wear of the machinery used, low cost, biodegradability and absence of residues or toxic byproducts. Composite is defined as the material consisting of binder which is a continuous phase and the fibrous filler as reinforcement which is the discontinuous phase (Sakshi *et al.*, 2017).

This research highlights the use of areca nut fiber as new type filler in natural rubber composites. Areca nut fiber is a commercially available and cheap natural fiber; furthermore, it has high cellulose content. To use these lignocellulosic fibers in polymeric composites, removal of the lignin and other amorphous materials is necessary to allow a better separation of the fibrils (Ahmed *et al.*, 2014). Alkali treatment procedure using a 5 % solution of sodium hydroxide was employed to remove these materials; further treatment with potassium permanganate solution or

¹ Department of Chemistry, Banmaw University

² Department of Chemistry, University of Yangon

benzoyl chloride solution was also carried out as surface treatment of the fiber, to modify the interfacial adhesion between the fiber and rubber, which has profound influence on the mechanical properties of the composites (Li *et al.*, 2007).

The applications of natural fiber-polymer composites are growing rapidly in numerous fields such as commercial, industrial, chemical and scientific applications. One of the most common applications of fiber-rubber stopper is the chemical ones. Some of the chemicals that are widely used in manufacturing are hazardous and can potentially cause grave bodily harm. Therefore, the containers holding these chemicals must be secure and tightly sealed, both for storing and handling them.

A laboratory stopper is mainly used in chemical laboratory in combination with flasks, test tube and also for fermentation in winery. Generally, in laboratory, the size of stopper can be varied up to approximately 16 sizes and each of it is specific to certain type of container. As the stopper is used in many experiments, some specific experiment requires a specific material. Most of the stoppers are oftentimes cylindrical with one tapered end. These parts have three distinct types:

1. The solid stopper: this rubber stopper is the most common one as it finds many applications in our everyday lives. Moreover, this rubber plug is also used in tube tube, wineries and breweries etc.
2. The one-hole stopper: this type of rubber part is very common in laboratories. The hole allows the scientists to insert thermometers and other devices in the container, without having to open it. This kind of rubber cork is manufactured in all of the sizes.

The aim of the present work is to fabricate the solid stopper and one-hole stopper for use in the chemistry laboratories and comparative study on the morphology and characterization of the rubber only and alkali treated areca nut fiber-rubber stopper.

Materials and Methods

Preparation of Areca Nut Fiber

The areca nut husks were collected from the local area, Mone, Kyauk-kyi Township, Bago Region.

The areca nut husks were taken directly from the areca nut fields containing a lot of dirt and dust. The dirt, dust, individual fiber and coarse fiber were removed by washing with distilled water. The selected areca fruit husks were soaked in distilled water for about five days. This process is called retting; allowing the fiber to be removed from the husk easily. Then areca nut fiber was manually separated from the husk. The resulting fiber was dried in the condition (temperature 30 °C) for four days before the alkali treatment (Joseph *et al.*, 1996). The dried fiber was designated as untreated fiber.

Alkali treatment

Areca nut fiber is amenable to chemical modification due to the presence of hydroxyl groups. One of the methods used commonly to treat the fiber is alkaline treatment method. Alkaline treatment or mercerization is used to modify the hydrogen bonding in the network structure, increasing the surface roughness of the fiber and exposing the microfibrils resulting in better mechanical interlocking.

The clean and dried areca nut fiber was soaked in a stainless-steel vessel containing 5 % NaOH at room temperature (30-32 °C) for three hours (Sampathkumar *et al.*, 2014). The alkali treated fiber was immersed in the distilled water for 24 h in order to remove the residual NaOH. Final washing was done with distilled water containing a small amount of acetic acid for neutralization. Subsequently, the fiber was dewatered and dried under sun light for five days.

Preparation of Natural Rubber Composites Reinforced by Areca Nut Fiber

Natural rubber smoked sheets for the experiments were procured from Myanmar Gone Yee Rubber Plantation, Bago Region. The areca nut fiber-rubber composites were prepared and their mechanical characteristics were measured at Rubber Research and Development Centre in Yangon.

Natural rubber smoked sheet was first rolled for 5 min on a Two Roll Mill to break out the fibrous bond of rubber polymer chain. This step is called mastication. Then mercapto benzothiazole (MBT) was mixed on rolling. After 30 s, zinc oxide and stearic acid were added simultaneously and rolled for 2 min. And then petroleum oil was added and rolled for one minute. Sulphur was added and rolled about 3-4 min until thick sheet was obtained. Vulcanized rubber was obtained. Some vulcanized rubber was used for preparation of rubber stoppers, and the remaining vulcanized rubber was mixed with the alkali-treated fiber of 10 mm fiber length at the rate of 5 % fiber loading on roller. The fiber loadings were in weight based on 100 g of vulcanized rubber. Total mixing duration was 10 to 15 min. During mixing whenever the roller becomes hot, water was sprayed on the roller. The composite preparation obtained was allowed to age for 24 h.

Preparation of rubber and alkali treated areca nut fiber-rubber composite stoppers

The molded plates of the aged composite were compressed for shaping by Hand Press Machine. Firstly, the plates were hot pressed at 153-160 °C (solid stopper for 6 min and one-hole stopper for 8 min) under 1000 lb in⁻² loading. (Figure 1 and 2)



Figure 1. Preparation of alkali treated areca nut fiber-rubber composite for stopper



Figure 2. Making of alkali treated areca nut fiber-rubber stopper

Determination of Chemical Resistance for the Rubber and the Alkali Treated Areca Nut Fiber-Rubber Stoppers

Chemical resistance of areca nut fiber reinforced natural rubber hybrid composites was determined according to ASTM D 543-87 method (Mathew *et al.*, 2006). The effect of some solvents, such as water, methanol and pet-ether, and some acids, such as conc. HCl, acetic acid and alkalies, such as 10 % NaOH and 10 % NH₄OH were studied on the hybrid composite (Jawaid *et al.*, 2011). For chemical resistance tests, the three pre weighed samples (1.50 g) (with 35 mm length fiber x 25 mm dimension x 3 mm thick) were dipped in the respective chemical reagents at different intervals time for (24-96 h). They were then removed and dried by pressing them on both sides with a filter paper at room temperature. And then, the final weight of the samples and the percentage weight gain/loss were determined. The chemical test has been done

for three samples in each case and the average value is reported (Rajulu *et al.*, 1998). The percentage chemical resistance was determined.

Comparative Study on the Surface Morphology of the Rubber and Alkali Treated Areca Nut Fiber-Rubber Stoppers

The difference in surface morphology between the rubber and the alkali-treated areca nut fiber-rubber stopper were studied using Evol 18 Zeiss scanning electron microscope (SEM) at Yadanabon University. The resulting SEM micrographs of the samples were recorded.

Comparative Study on Chemical Composition of the Rubber and Alkali Treated Areca Nut Fiber-Rubber Stopper

The changes of chemical constitution of the rubber-and the alkali treated areca nut fiber-rubber stopper were examined by infrared absorption spectra recorded on a Tracer 100 Shimadzu, Japan FT IR spectrometer at University of Yangon.

Comparative Study on the Thermal Properties of the Rubber and Alkali Treated Areca Nut Fiber-Rubber Stoppers

The difference in thermal properties between the rubber and the alkali treated areca nut fiber-rubber stoppers were studied using a TG-DTA instrument (Hi-TGA 2950 model) (Yadanabon University), at the temperature range, 0 °C to 600 °C under air.

Results and Discussion

Extraction of Areca Nut Fiber

After soaking and drying, 4.6 kg (2.8 viss) of fiber was extracted from 16.2 kg (10 viss) of raw areca husk. This is the mixture of coarse and fine fibers. (Figure 3)



Figure 3. Extracted areca nut fiber

Surface Modification of the Areca Nut Fiber

Alkali treatment

The extracted areca nut fiber was treated with 5 % NaOH solution. The resulting fiber have yellowish brown color. The colour of untreated fiber was paler than alkali treated areca nut fiber. (Figure 4)



Figure 4. Alkali treated areca nut fiber

Potassium permanganate treatment

After potassium permanganate treatment, as a result, areca fiber surface becomes darker, physically rough, bristly and this reduces hydrophilic nature of the areca fibers (Figure 5). This could improve chemical interlocking at the interface and provides better adhesion with the polymeric matrix.



Figure 5. Potassium permanganate treated areca nut fiber

Natural Rubber

Natural rubber used for the study was grade-1 (light colour) obtained from Myanmar Gone Yee Rubber Plantation, Bago Region. The results and specifications (reference with ISO) of the grade-1 rubber used at Rubber Research and Development Center in Yangon were summarized.

Table 1. Quality Specifications of the Grade-1 Natural Rubber

No.	Test	Results	Reference*
1	Plasticity number	32.50	ISO 2007 (30.0-32.5)
2	Plasticity retention index	85.00	ISO 2930 (71.05-85.00)
3	Volatile matter content (%)	0.27	ISO 248-1 (0.25-0.4)
4	Dirt content (%)	0.02	ISO 249 (0.01-0.04)
5	Ash content (%)	0.27	ISO 247 (0.25-0.5)
6	Nitrogen content (%)	0.45	ISO 1656 (0.23-0.7)
7	Mooney viscosity	63.00	ISO 289-1 (60.0-70.0)

*International Standards Organization (ISO) for Rubber

Chemical Resistance of the Alkali Treated Areca Nut Fiber-Natural Rubber Composites

Chemical resistance tests were used to study the interfacial adhesion in areca nut fiber reinforced natural rubber composites. The presence of bonding agent increased the interfacial adhesion between the fiber and matrix. The composites containing bonding agents were less prone to solvent sorption. The chemical resistance of the prepared fiber-rubber composites was also investigated in various solvents such as water, methanol, pet-ether, various acids such as conc. HCl, acetic acid, and bases such as 10 % NaOH, 10 % NH₄OH. It was observed that the swelling behavior of rubber-alkali treated areca nut fiber composites in different solvents follows: pet-ether > methanol > water. Different acids it follows the trend: acetic acid > conc. HCl and then for the various alkalis it follows: 10 % NH₄OH > 10 % NaOH. The percent chemical resistance of the composite was found to be high. This is due to the increased hindrance exerted by the fibers at higher fiber loadings and also due to the good fiber-rubber interactions. Maximum absorption of solvent was observed with pet-ether, which may be due to the diffusion of hydrocarbons. The second highest absorption was observed with acetic acid; this may be due to acetylation of some hydroxyl groups of areca nut fiber.

The chemical resistance tests of these hybrid composites were performed in order to find out whether these composites can be used for making stoppers. The weight gains for fiber reinforced natural rubber composites with different chemicals are shown in Table 2 and Figure 6. From the results, it is clearly seen that for areca nut fiber-natural rubber composite in all cases a slight weight gain (swelling property) is observed after immersion, except for the large weight gains with petroleum ether and acetic acid. This indicates that the composites did not lose weight, and therefore it does not seem as any erosion occurred. The weight increase of the composites for aqueous solutions is a result of the hydrophilicity of the fiber. Based on the findings of this study, these rubber stoppers can effectively seal reagent bottles, flasks, test tubes, and other laboratory containers requiring chemical resistance.

Table 2. Chemical Resistance of Alkali Treated Areca Nut Fiber-Natural Rubber Composites

Dipping time (h)	Chemical resistance in various solvent (%)						
	Water	Methanol	Pet-ether	Conc. HCl	Acetic acid	10% NaOH	10% NH ₄ OH
24	0.67	1.33	62.67	0	8.00	1.33	1.33
48	2.00	2.00	75.33	0	11.33	1.33	3.33
72	2.00	2.00	82.00	0	16.67	1.33	3.33
96	2.00	2.00	62.00	0	17.33	1.33	4.67

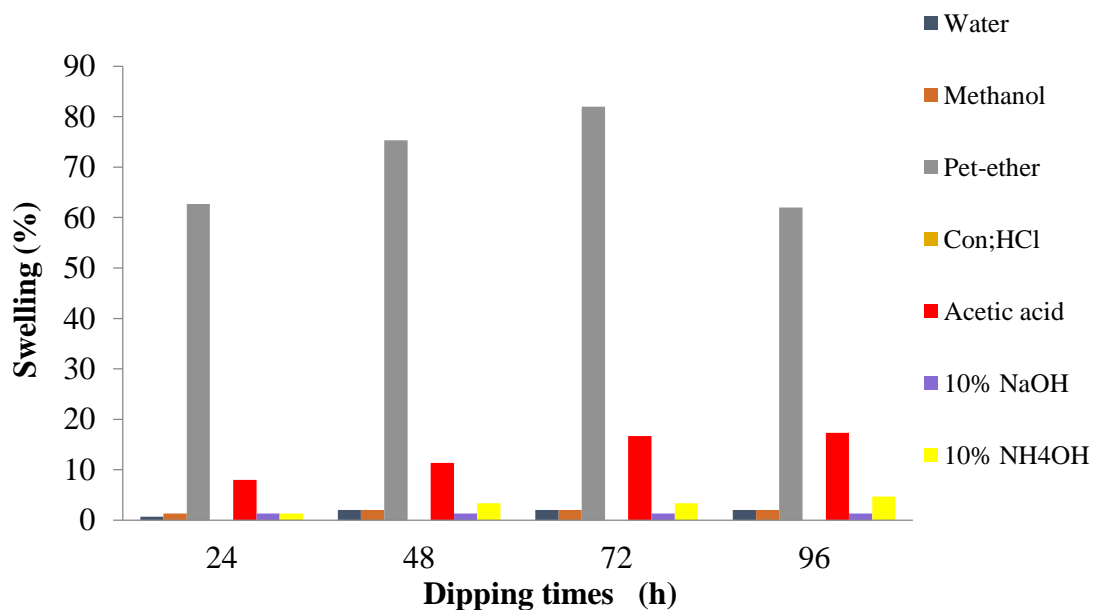


Figure 6. Swelling property of areca nut fiber-natural rubber composites towards the various solvents at different dipping time

Mechanical Properties of Rubber and Alkali Treated Areca Nut Fiber-Rubber Composite for Stopper

Based on the findings, it is evident that the composite, with alkali-treatment, featuring a 10 mm fiber length and a 5 % fiber loading, exhibited superior characteristics when compared to the rubber material. Notably, hardness and elongation at break were significantly enhanced in the composite, surpassing the performance of the rubber material (Table 3).

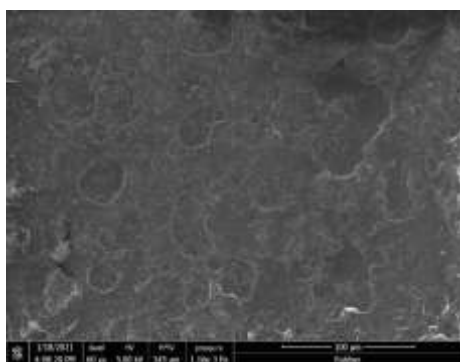
Although specific gravity and tear strength remained relatively consistent between the two materials, it is essential to emphasize that laboratory stoppers demand specific attributes. In this context, the desired attributes for laboratory stoppers include high values of hardness, specific gravity, and elongation at break. Consequently, the alkali-treated composite with a 10 mm fiber length and 5 % fiber loading emerges as the most suitable choice for fabricating laboratory stoppers based on these criteria.

Table 3. Physicomechanical Properties of Rubber and Alkali Treated Areca Nut Fiber-Rubber Composite Stoppers

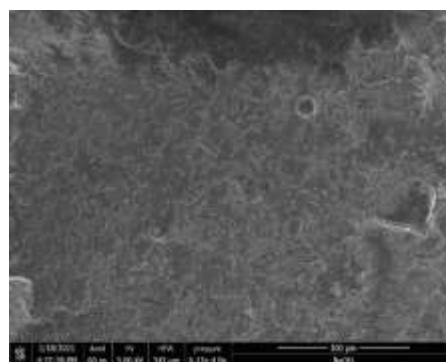
Materials	Hardness (IRHD)	Specific gravity	Tensile strength (MPa)	Elongation at break (%)	Tear strength (kN/m)
Alkali-treated	52.6	0.98	6.8	737.3	23.8
Rubber	30.0	0.97	10.6	680	24.1

Surface Morphology of Rubber and Alkali Treated Areca Nut Fiber-Rubber Stoppers

The better adhesion at the interface between the areca nut fiber surface and the rubber matrix resulted from good compatibility between the rubber-alkali treated fiber and rubber only. In this study, a good adhesion was obtained between alkali treated areca nut fiber and rubber matrix and fine dispersion of applied alkali treated areca nut fiber filler in rubber matrix was depicted in Figure 7 by SEM analysis.



(a) Rubber only material



(b) Alkali treated fiber-rubber composite

Figure 7. SEM images of fracture surface of (a) rubber only material and (b) alkali treated areca nut fiber-rubber composite for stopper

Chemical Composition of Rubber Only and Alkali Treated Areca Nut Fiber-Rubber Stopper

In this study, comparison of the FT IR spectra before and after alkali-treated composite formation (Figure 8) shows notable changes of the absorption bands, namely shift to a higher frequency of the sp^2 C-H stretching band just above 3000 cm^{-1} in region (i), intensification of C-O stretching band in region (iv) which may indicate ether, more pronounced bands assignable to sp^2 C-H out-of-plane bending in the region (v), sharper bands in the region (iii), and also the change in shape of the bands in the region (ii) for C-H bending and C=C stretching. These changes are rubber only and the alkali-treated fiber, and thus evidences of the formation of a composite.

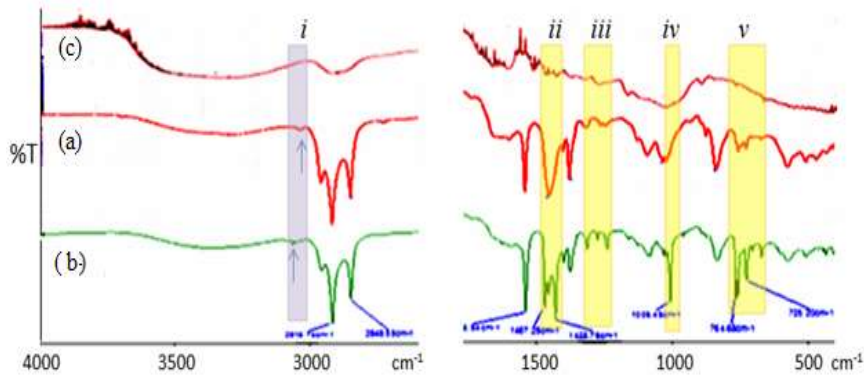


Figure 8. FT IR spectra showing (a) rubber (b) alkali treated areca nut fiber-rubber composite, and (c) alkali-treated areca nut fiber

Thermal Properties of Rubber and Alkali Treated Areca Nut Fiber-Rubber Stoppers

According to the results (Figure 9 and Table 4), the temperature of 363.35 °C was observed as the onset temperature of thermal degradation for the rubber and the temperature of 365.49 °C was observed as the onset temperature of thermal degradation for the alkali treated areca nut fiber-rubber sample. Thus, the alkali-treated areca nut fiber-natural rubber stopper showed higher onset temperature than rubber stopper, which supported the effectiveness of the alkali-treated fiber. It indicated that the thermal stability of the alkali-treated areca nut fiber-rubber stopper was higher than the rubber stopper.

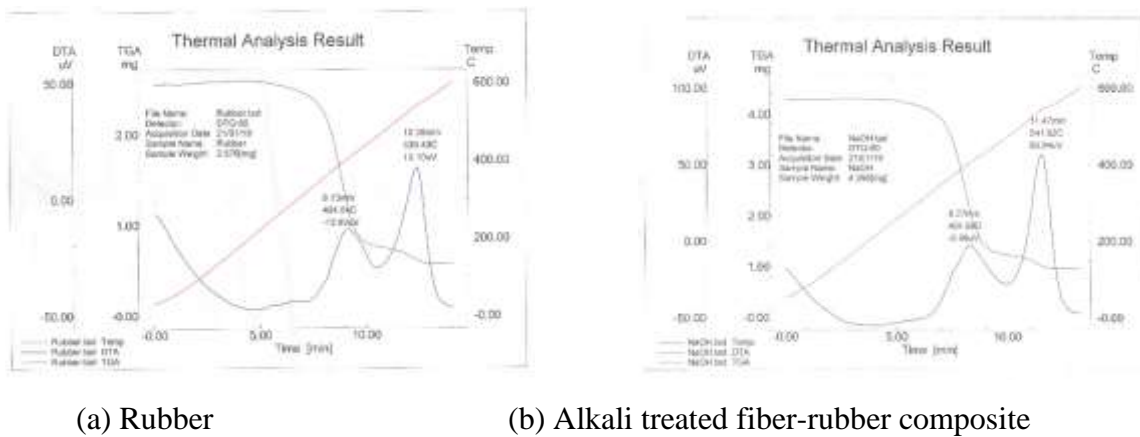


Figure .9 TG-DTA thermograms of (a) rubber and (b) alkali treated areca nut fibre-rubber composite stoppers

Table 4. Initial Decomposition and Maximum Decomposition Temperatures of Rubber and Alkali Treated Areca Nut Fiber-Rubber Stoppers

Stoppers	Temperature range of initial decomposition (°C)	Weight loss (%)	Temperature range of final decomposition (°C)	Weight loss (%)
Rubber	363.35 - 421.57	34.41	450.91 - 569.43	65.10
Alkali treated fiber-rubber	365.49 - 427.27	34.45	453.37 - 571.92	65.21

Conclusion

In conclusion, this research has successfully addressed the primary objective of enhancing the performance of rubber stoppers through the reinforcement of natural rubber with areca nut husk fiber. The utilization of areca nut husk, an abundant and underutilized biowaste material from the areca nut industry, has not only contributed to environmental sustainability but has also led to the development of a composite material. The surface treatment of areca nut husk fiber, involving treatments with 5 % NaOH and potassium permanganate, was enhanced the fiber's surface properties. These treatments improved the adhesion between the fiber and the rubber matrix, ultimately leading to the creation of a composite material (alkali treated) suitable for producing rubber stoppers for reagent bottles.

The incorporation of alkali-treated areca nut fiber into the natural rubber matrix resulted in increased rigidity, making the composite an ideal choice for stopper applications. Scanning electron microscopy (SEM) analysis confirmed the strong adhesion between the fiber and rubber matrix, along with the even dispersion of the fiber within the composite-essential factors contributing to enhanced mechanical properties. Further characterizations through FT IR spectra, as suggested by changes in position, intensity, and shape of IR bands. The successful formation of areca nut husk fiber-natural rubber composites was suggested by FT IR, where band shifts, appearance of new bands and changes in the forms of bands were observed after the composite formation. TG-DTA studies provided compelling evidence and improved thermal stability. TG-DTA study also showed better thermal stability of the fiber by the treatments than rubber.

Moreover, the composite rubber stoppers exhibited robust resistance to various acids, bases, and organic solvents, highlighting their durability and suitability for laboratory use.

Acknowledgements

The authors would like to express their gratitude to the Department of Higher Education, Ministry of Education, Myanmar, for the permission to do this research and also to the Myanmar Academy of Arts and Science for giving the opportunity to read this paper.

References

- Ahmed, K., S. S. Nizami, and N. Z. Riza. (2014). "Reinforcement of Natural Rubber Hybrid Composites Based on Marble Sludge/Silica and Marble Sludge/Rice Husk Derived Silica". *Journal of Advanced Research*, vol. 5 (2), pp. 165-173.
- Jawaid, M., H. A. Khalil, and A. A. Bakar. (2011). "Woven Hybrid Composites: Tensile and Flexural Properties of Oil Palm-Woven Jute Fibres Based Epoxy Composites". *Materials Science and Engineering: A*, vol. 528 (15), pp. 5190-5195.
- Joseph, K., S. Thomas, and C. Pavithran. (1996). "Effect of Chemical Treatment on the Tensile Properties of Short Sisal Fibre-Reinforced Polyethylene Composites". *Polymer*, vol. 37 (23), pp. 5139-5149.
- Kumar, G.M. (2008). "A study of Short Areca Fiber Reinforced PF Composites". *Proceedings of the World Congress on Engineering.*, vol. 2, pp. 2-4.
- Li, X., L. G. Tabil, and S. P. Anigrahi. (2007). "Chemical Treatments of Natural Fiber for use in Natural Fiber-Reinforced Composites: A Review". *Journal of Polymers and the Environment*, vol.15 (1), pp. 25-33.
- Mathew, L., K. U. Joseph, and R. Joseph. (2006). "Swelling Behaviour of Isora/Natural Rubber Composites in Oils used in Automobiles". *Bulletin of Materials Science*, vol. 29 (1), pp. 91-99.
- Rajulu, A. V., S. A. Baksh, G. R. Reddy, and K. N. Chary. (1998). "Chemical Resistance and Tensile Properties of Short Bamboo Fiber Reinforced Epoxy Composites". *Journal of Reinforced Plastics and Composites*, vol. 17 (17), pp. 1507-1511.
- Sakshi S. K., S. Dhanalakshmi, and B. Basavaraju. (2017). "A Review on Natural Areca Fiber Reinforced Polymer Composite Materials". *Ciencia and Tecnologia dos Materiais*, vol. 29, pp.106-128.
- Sampathkumar, D., R. Punyamurthy, B. Bennehalli, R. P. Ranganagowda, and S. C. Venkateshappa. (2014). "Natural Areca Fiber: Surface Modification and Spectral Studies". *Journal of Advances in Chemistry*, vol. 10 (10), pp. 227-229.

FACILE SYNTHESIS, CHARACTERIZATION AND OPTICAL PROPERTY OF CuO NANOPARTICLES

Mya Theingi¹

Abstract

The synthesis of the cubic-like CuO nanoparticles was achieved by a green method using starch as the capping agent. Starch was extracted from avocado seed, and pH and moisture content of the extracted starch were determined. The extracted starch was then used to prepare CuO- starch composites by using a facile process. The aqueous solutions of 10, 20, and 30 % (w/v) CuCl₂ were used not only as a precursor solution for the formation of CuO- starch composites but also as a solvent. The method involves first dissolving the starch in the three different concentrations of CuCl₂ aqueous solutions, then adding NaOH to achieve a final pH value of 8.4. When the prepared composites were calcined at 500 °C for 4 h, CuO nanoparticles (CuO NP1, CuO NP2, and CuO NP3) were obtained. The prepared CuO nanoparticles were characterized by different techniques, including XRD, SEM, and FT IR. The average crystallite sizes of CuO nanoparticles were in the range of 33-42 nm. FT IR spectra exhibited only the Cu-O stretching vibrational mode. The CuO nanoparticles were used to investigate the optical property by UV-vis spectrophotometry. According to the UV-Vis spectra of the prepared CuO nanoparticles, the optical band gaps were found to be 3.8 eV for CuO NP1, 3.4 eV for CuO NP2, and 3.3 eV for CuO NP3.

Keywords: avocado seed, CuO-starch composites, CuO nanoparticles, facile synthesis, optical property

Introduction

Nanocrystalline wide-band gap semiconductor particles have drawn considerable interest in recent years due to their interactive properties, such as their large surface-to-volume ratio and distinctive electronic and optical properties as compared to bulk materials (Kidowaki *et al.*, 2012). Moreover, copper oxide nanoparticles have attracted considerable attention due to their unique properties compared to bulk materials. Copper oxide nanoparticles are widely used as gas sensors, catalysts, batteries, high-temperature superconductors, solar energy conversion, surfactants, and antimicrobial and anticancer agents (Alishah *et al.*, 2017). A variety of techniques, including sonochemical, photolytic, chemical reduction, and microemulsion techniques (Hsieh *et al.*, 2003), have been reported for the synthesis of copper oxide nanoparticles. However, the majority of these methods are accompanied by many problems, such as dealing with various toxic and hazardous chemicals. It should be noticed that the development of a green method for the synthesis of copper oxide nanoparticles is an important aspect of current research. That is why, recently, the synthesis of copper oxide nanoparticles using bio-reducing and bio-stabilizing agents produced by different biological systems such as microorganisms, enzymes, and plant or plant extract (Fang *et al.*, 2006) has received increasing attention due to its environmentally benign nature. The ability of plant material to reduce metal ions has been known since the early 1900s. Due to its simplicity, the use of plant materials for reducing metal salts to metal nanoparticles has attracted considerable attention in previous years, and one of these plant materials is starch. The starch has a polymer structure and can cover the surface of the nanoparticles with hydroxyl groups as a capping agent (Cornelia and Christianti, 2017). The main aim of the research is to synthesize CuO nanoparticles by using starch as a capping agent and investigate their structural and optical properties.

¹ Department of Chemistry, Shwebo University

Materials and Methods

Extraction of Starch from Avocado Seed

Firstly, 100 g of avocado seed was cut into small pieces, then 200 mL of distilled water was added and blended by a blender and filtered by a filter cloth, and the filtrate was obtained. The filtrate was dried in an oven at 100 °C for 8 h. It was ground and sieved with a 100 µm sieve. The yield percent of extracted starch was calculated. The pH and moisture content of the extracted starch were determined.

Synthesis of CuO-Starch Composites

In brief, 15 g of the starch extracted from avocado seed was dissolved in 10 %, 20 %, and 30 % (w/v) of CuCl₂ aqueous solution while heating at 60 °C with constant stirring. Then a 15 % (w/v) NaOH aqueous solution was added dropwise to the solution, and the solution was stirred with constant stirring to achieve a final pH value of 8.4. After the composites were aged for 30 min with constant stirring at 60 °C, CuO-starch composites were sterilized in an autoclave at 121 °C for 50 min. These were dried in an oven at 80 °C. When it was almost dried, CuO-starch composites were obtained. The composites were characterized by XRD and FT IR for comparison studies.

Preparation of CuO Nanoparticles

The synthesized CuO-starch composites were calcined at 500 °C for 4 h in a muffle furnace. The CuO nanoparticles were washed with distilled water several times to make them free from impurities, and then dried in an oven at 80 °C. The CuO nanoparticles (designated as CuO NP1, CuO NP2, and CuO NP3) were characterized by XRD, SEM, and FT IR.

Optical Properties of CuO Nanoparticles

The optical properties of CuO nanoparticles were studied by UV-vis absorption spectroscopy in the wavelength range of 190-800 nm. The absorption coefficient ($\alpha = 2.303 (A/t)$, where $A = -\log T$, $T =$ transmittance and $t =$ thickness of the cell) was calculated from the observed absorption spectra, and the optical band gap of CuO NP1, CuO NP2, and CuO NP3 were calculated from the Tauc's plot of $(\alpha h\nu)^2$ vs $h\nu$ (Tauc *et al.*, 1966).

Results and Discussion

Syntheses of CuO-Starch Composites and CuO Nanoparticles

The yield percent of starch extracted from avocado seed was found to be 10.5 %. The pH and moisture content of the extracted starch were observed as 7.17 and 18.25 %, respectively.

The extracted starch was subjected to synthesize CuO-starch composite using 10 %, 20 %, and 30 % CuCl₂ solutions giving three CuO-starch composites (composites 1, 2, and 3). By calcination of the composites at 500 °C, three CuO nanoparticles (CuO NP1, CuO NP2, and CuO NP3) were obtained.

XRD Analysis of the Synthesized CuO-Starch Composites and CuO Nanoparticles

X-ray diffraction patterns of CuO-starch composites 1, 2, and 3 are shown in Figures 1 (a), (b), and (c). It was found that all composites show mixed Cu₂Cl(OH) phases and CuO

phases. X-ray diffractograms of CuO NP1, CuO NP2, and CuO NP3 are shown in Figures 2 (a), (b), and (c). It was found that XRD patterns show pure CuO peaks.

The average crystallite sizes of samples were calculated from the dominant peaks of X-ray line broadening planes using the Scherrer equation, $D_{Sch} = \frac{0.9\lambda}{\beta \cos \theta}$, where D_{Sch} is the average crystallite size, θ is the Bragg angle, λ is the wavelength of the X-ray, β is the full width at half maximum. The average crystallite sizes of the CuO nanoparticles decrease with increase amount of $CuCl_2$ (Tables 1, 2, and 3).

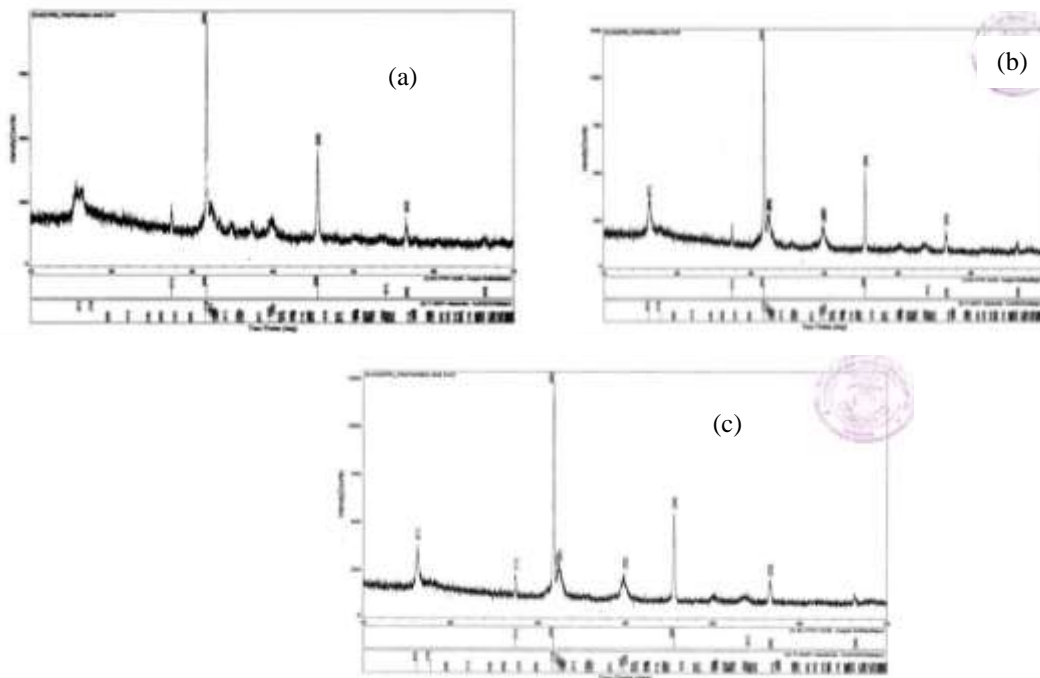


Figure 1. X-ray diffractograms of CuO-starch (a) composite 1, (b) composite 2, and (c) composite 3

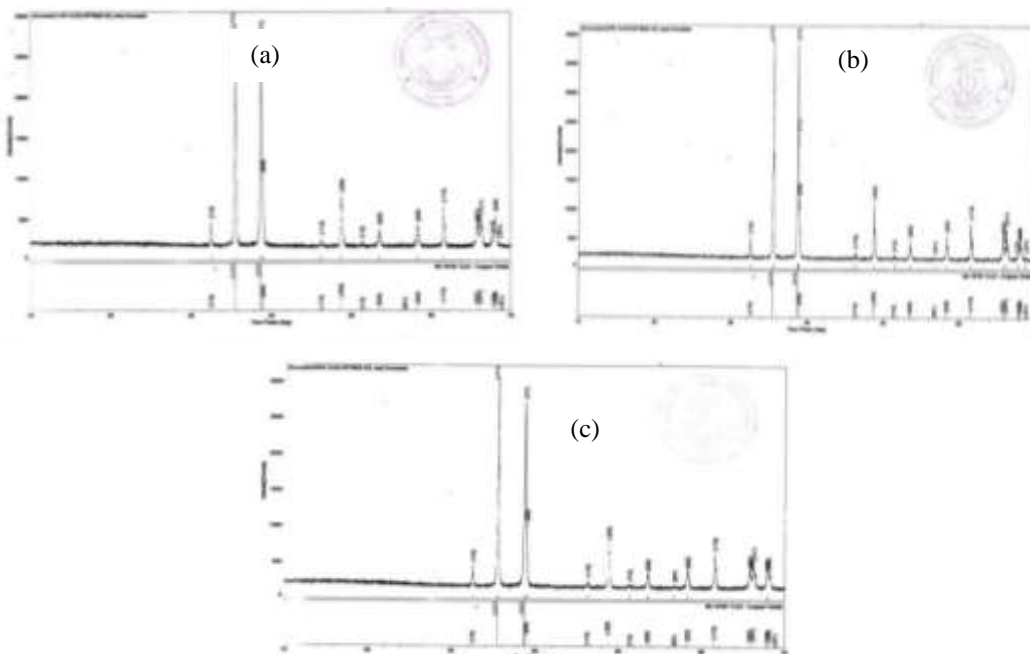


Figure 2. X-ray diffractograms of CuO nanoparticles (a) CuO NP1, (b) CuO NP2, and (c) CuO NP3

Table 1. Average Crystallite Size of the CuO NP1

Sample	2-Theta (degree)	(h k l)	FWHM (degree)	Crystallite size (nm)
CuO NP1	32.503	(1 1 0)	0.172	53.609
	38.727	(1 1 1)	0.170	54.239
	38.892	(2 0 0)	0.356	25.901
	53.459	(0 2 0)	0.219	42.104
	58.317	(2 0 2)	0.195	47.286
Average crystallite size (nm)				42.489

Table 2. Average Crystallite Size of the CuO NP2

Sample	2-Theta (degree)	(h k l)	FWHM (degree)	Crystallite size (nm)
CuO NP2	32.512	(1 1 0)	0.182	50.663
	38.720	(1 1 1)	0.238	38.742
	38.910	(2 0 0)	0.423	21.798
	53.476	(0 2 0)	0.251	36.736
	58.299	(2 0 2)	0.307	30.035
Average crystallite size (nm)				34.319

Table 3. Average Crystallite Size of the CuO NP3

Sample	2-Theta (degree)	(h k l)	FWHM (degree)	Crystallite size (nm)
CuO NP3	32.512	(110)	0.179	51.512
	38.729	(111)	0.241	38.260
	38.950	(200)	0.232	39.744
	53.440	(020)	0.329	28.026
	58.260	(202)	0.360	25.613
Average crystallite size (nm)				33.611

SEM Analysis of CuO Nanoparticles

SEM micrographs of CuO NP1, CuO NP2, and CuO NP3 are shown in Figures 3 (a), (b), and (c). It was found that all samples have agglomerate, porous, and cubic-like crystal structures. CuO NP2 and CuO NP3 particles have more significant crystalline nature than CuO NP1 particles. It can be said that CuO NP2 and CuO NP3 particles were formed from the suitable ratios of starting material (CuCl_2) and capping agent (starch).

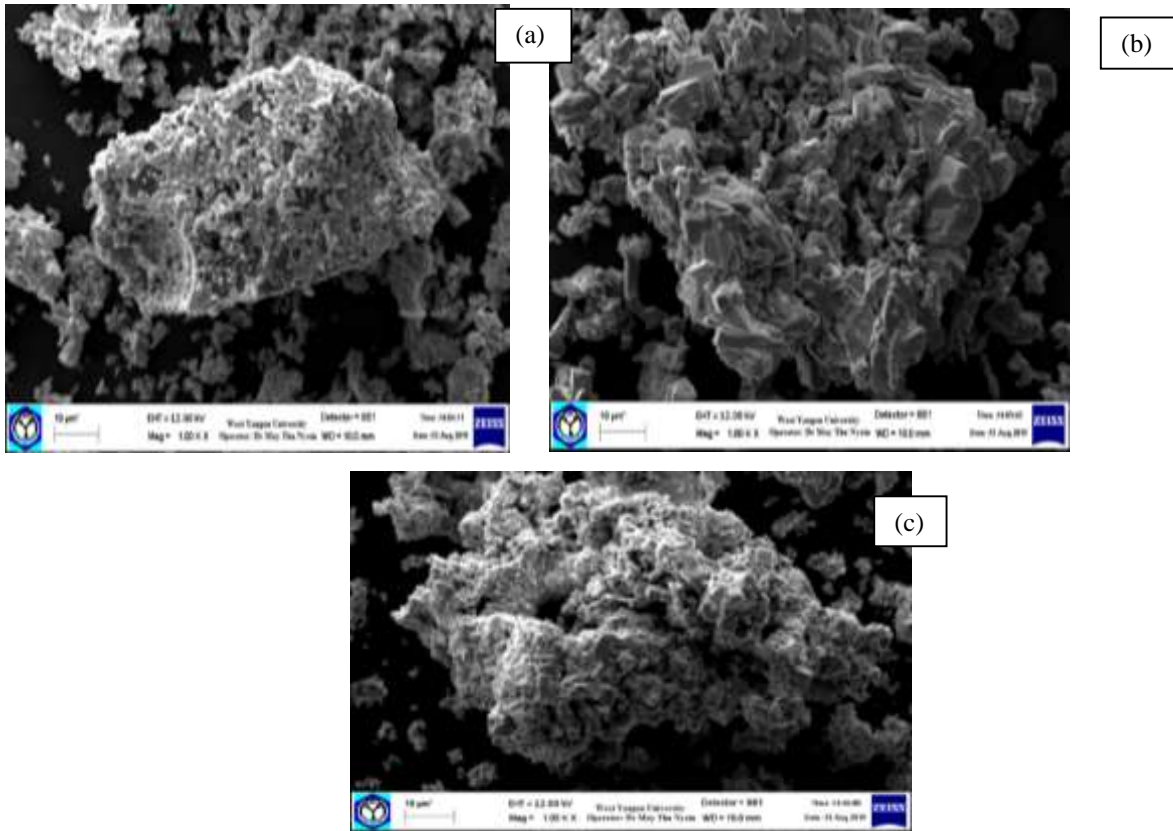


Figure 3. SEM micrographs of CuO nanoparticles (a) CuO NP1, (b) CuO NP2, and (c) CuO NP3

FT IR Analysis of CuO-Starch Composites and CuO Nanoparticles

Figures 4 (a), (b), (c), and Table 4 show the FT IR spectra and assignment data of CuO starch composites 1, 2, and 3.

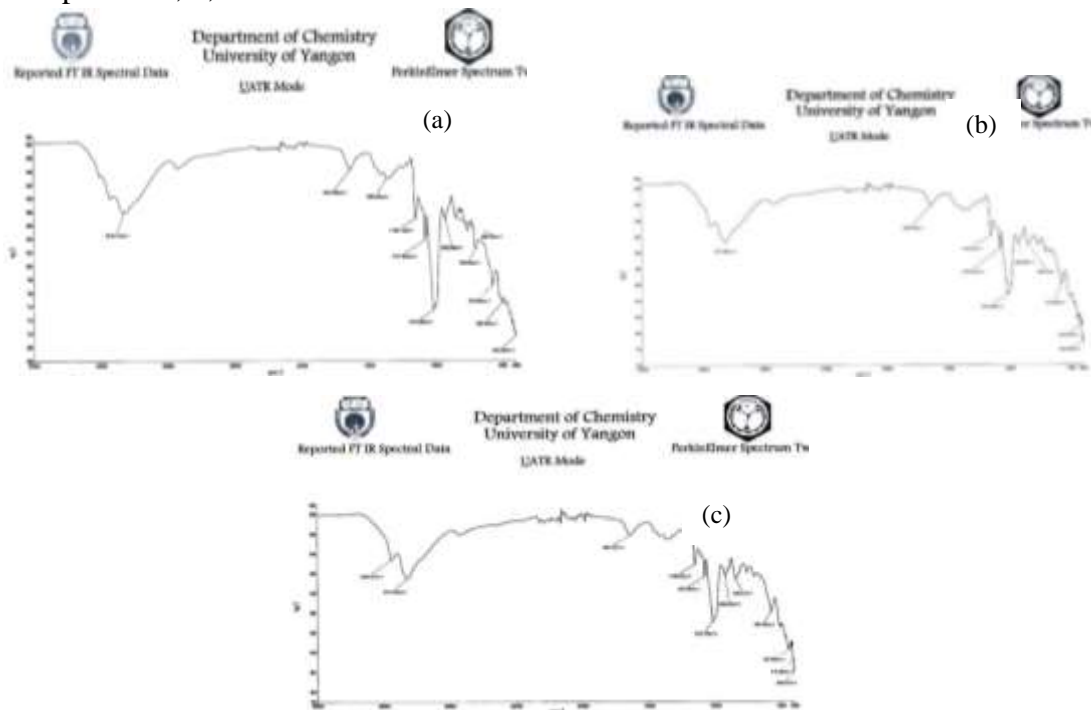


Figure 4. FT IR spectra of CuO-starch (a) composite 1, (b) composite 2, and (c) composite 3

Table 4. FT IR Spectral Data of CuO-Starch Composites

Observed wavenumber (cm ⁻¹)			*Literature wavenumber (cm ⁻¹)	Band assignment
Composite 1	Composite 2	Composite 3		
3319	3313	3314	3600-3260	O-H stretching
1634	1640	1637	1630-1690	O-H bending vibration of absorbed water molecules
1150	1150	1150	1149	C-O-C asymmetric stretching
1077	1078	1077	1200-800	C-O stretching
1015	1015	1015		
926	923	920	960-910	C-OH deformation
850	844	844	850-790	C-H out of plane bending
573	572	572	400-650	Cu-O stretching
506	419	437		
402	402	410		
		402		

*Silverstein *et al.*, 2014

The bands around 3300 cm⁻¹ indicate the stretching vibration of the O-H group of CuO-starch composites. The bands around 1630 cm⁻¹ are assigned to the O-H bending vibration of absorbed water molecules, particularly in the amorphous region of starch (Alemu *et al.*, 2022). The peaks around 1150 and 1000-1100 cm⁻¹ show the presence of C-O-C asymmetric stretching and C-O stretching vibration, respectively. The band observed around 920 cm⁻¹ is assigned to the C-OH deformation of composites. The bands observed around 850 cm⁻¹ correspond to C-H out of plane bending of the samples. Cu-O stretching vibration was observed at 400-650 cm⁻¹. Figures 5 (a), (b), (c), and Table 5 show the FT IR spectra and assignment of CuO NP1, CuO NP2, and CuO NP3. All three samples show Cu-O stretching vibration at 400-650 cm⁻¹, which indicates the presence of CuO.

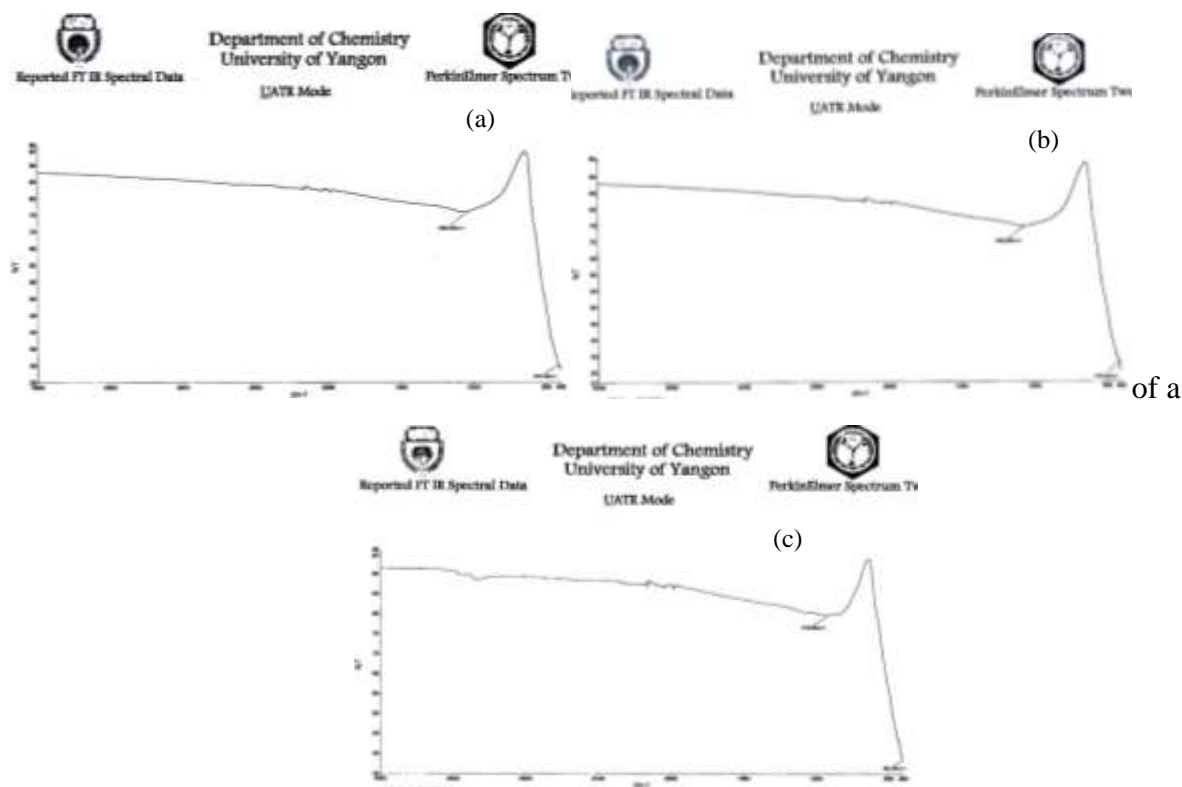


Figure 5. FT IR spectra of CuO nanoparticles (a) CuO NP1, (b) CuO NP2, and (c) CuO NP3

Table 5. FT IR Spectral Data of CuO Nanoparticles

Observed wavenumber (cm ⁻¹)			*Literature wavenumber (cm ⁻¹)	Band assignment
CuO NP1	CuO NP2	CuO NP3		
419	415	403	400-650	Cu-O stretching vibration

*Silverstein *et al.*, 2014

The Optical Properties of CuO Nanoparticles

The optical properties of CuO nanoparticles (CuO NP1, CuO NP2, and CuO NP3) were studied by UV-Vis absorption spectroscopy in the wavelength range of 190-800 nm. The absorption coefficient (α) was calculated from the observed absorption spectra, and the optical band gaps of CuO nanoparticles were calculated from Tauc's plot of $(\alpha h\nu)^2$ vs $h\nu$. Figures 6 (a), (b), and (c) show the optical band gaps of CuO nanoparticles, CuO NP1, CuO NP2, and CuO NP3, which were found to be 3.8 eV, 3.4 eV, and 3.3 eV, respectively. The band gap decreases with an increase in the amount of CuCl₂ in the constitutional ratio. According to this band gap, CuO nanoparticles are found within the wide-band gap semiconductor range. Materials can be distinguished by band gap values. Band gap values that lie between 0 and 1 eV are metals, those that lie between 1 and 4 eV are semiconductors, and those that are greater than 4 eV are insulators (Khalaji *et al.*, 2020). Wide-band gap semiconductors permit devices to operate at much higher voltages, frequencies, and temperatures than conventional semiconductors, and they are the key component used to make short-wavelength (green-

UV) LEDs or lasers and are also used in certain radio frequency applications (Yoshikawa *et al.*, 2007).

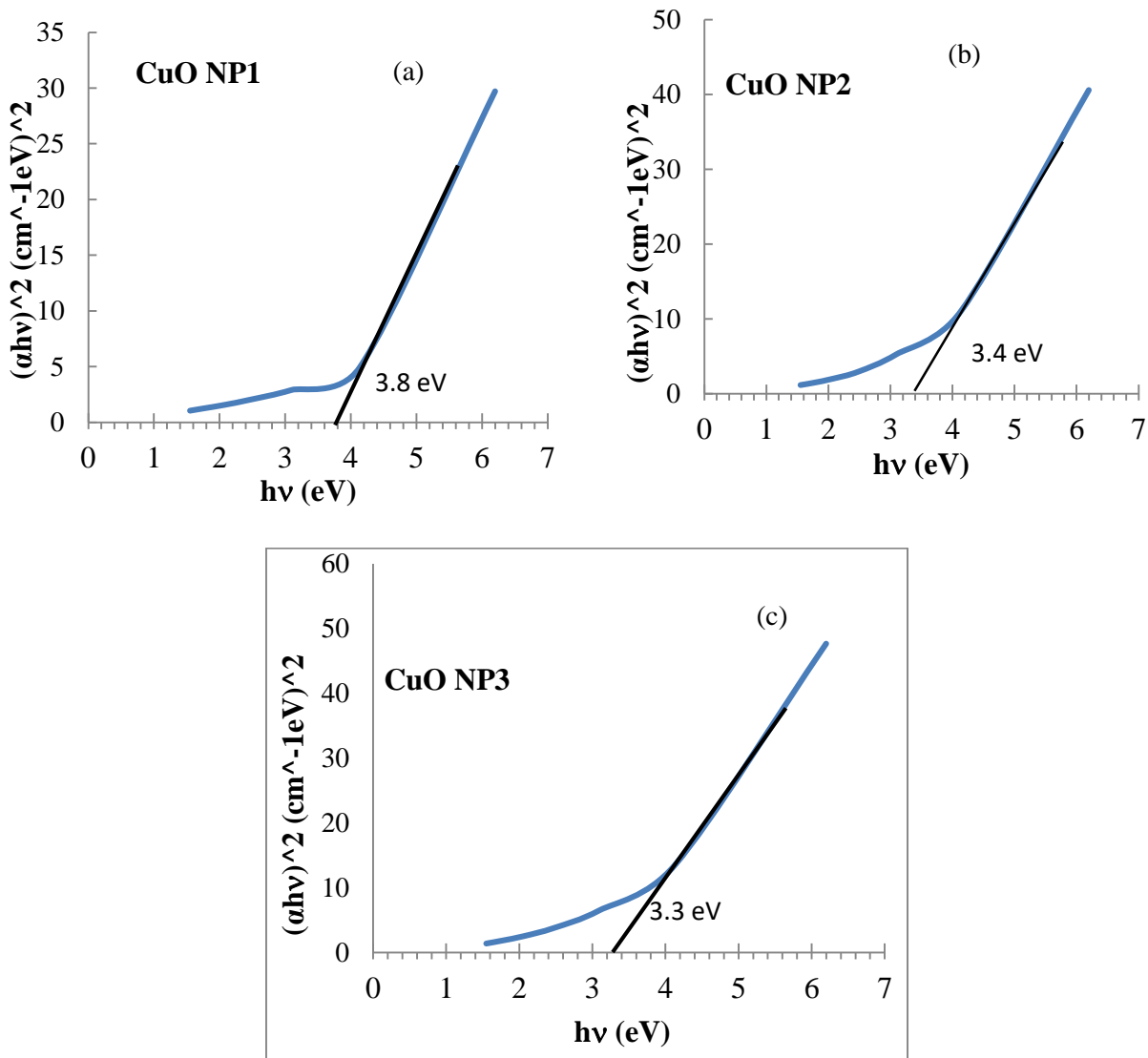


Figure 6. Plot of $(\alpha h\nu)^2$ against $h\nu$ of (a) CuO NP1, (b) CuO NP2, and (c) CuO NP3

Conclusion

The present study indicates that copper oxide nanoparticles can be prepared by using starch extracted from avocado seed. The method used is low-cost, fast, and simple. From XRD analysis, the average crystallite sizes of CuO NP1, CuO NP2, and CuO NP3 are 42.489 nm, 34.319 nm, and 33.611 nm, respectively. SEM microphotographs of CuO nanoparticles show that all samples have agglomerate, porous, and cubic-like crystalline natures. From FT IR analysis, only the Cu-O stretching vibration band can be observed. The band gap values of CuO nanoparticles indicate a semiconductor band gap range (3.8 eV, 3.4 eV, and 3.3 eV). It can be concluded that the prepared CuO nanoparticles possess wide-band gap values and exhibit good optical properties. Therefore, CuO nanoparticles synthesized by using the avocado seed starch as a capping agent can be used as optical devices, including light-emitting diodes, laser diodes,

photodiodes, photoconductive sensors, electro-modulation devices, and optical-optical modulation devices.

Acknowledgements

The author would like to thank the Department of Higher Education, Ministry of Education in Myanmar, for giving the opportunity to do this research. The author's deepest gratitude is expressed to Dr Myo Myo, Rector, Shwebo University, for her encouragement and kind guidance. The author wishes to thank Dr Tin Tin Yi, Pro-Rector, Shwebo University, for her invaluable advice and encouragement. Thanks are also extended to Dr Thi Thi Aung (Professor and Head), Department of Chemistry, Shwebo University, for her precious suggestions.

References

- Alemu, N., S. Balakrishnan, and B. Debtera. (2022). "Extraction and Characterisation of Avocado Seed Starch, and Its Blend with Enset Cellulosic". *Advances in Materials Science and Engineering*, vol. 2022, pp. 1-10.
- Alishah, H., S. Pourseyedi, S. Y. Ebrahimipour, S. E., Mahani, and N. Rafiei. (2017). "Green Synthesis of Starch-mediated CuO Nanoparticles: Preparation, Characterization, Antimicrobial Activities and *in vitro* MTT Assay against MCF-7 Cell Line". *Rend. Lincei*, vol. 28(1), pp. 65–71.
- Cornelia, M. and A. Christiani. (2017). "Utilization of Modified Starch from Avocado (*Persea americana* Mill.) Seed in Cream Soup Production". *Inter. Symp. on Food & Agro-biodiversity*, vol. 102, pp. 1-8.
- Fang, M., J. H. Chen, X. L. Xu, P. H. Yang, and H. F. Hildebrand. (2006). "Antibacterial Activities of Inorganic Agents on Six Bacteria Associated with Oral Infections by Two Susceptibility Tests". *Int. J. Antimicrob. Agents.*, vol. 27 (6), pp. 513-517.
- Hsieh, C. T., J. M. Chen, H. H. Lin, and H. C. Shih. (2003). "Synthesis of Well-ordered CuO Nanofibers by a Self-catalytic Growth Mechanism". *Apply Phys. Lett.*, vol. 82, pp. 3316-3318.
- Khalaji, A. D., Z. Pazhand, K. Kiani, P. Macheh, M. Jarosova, and R. Mazandarani. (2020). "CuO Nanoparticles: Preparation, Characterization, Optical Properties, and Antibacterial Activities". *Journal of Materials Science in Electronics*, vol. 31, pp.11949–11954.
- Kidowaki, H., T. Oku, T. Akiyama, A. Suzuki, B. Jeyadevan, and J. Cuya. (2012). "Fabrication and Characterization of CuO-based Solar Cells". *J. Mater. Sci. Res.* vol. 1 (1), pp. 138–143.
- Silverstein, R. M., F. X. Webster, D. J. Kiemle, and D. L. Bryce. (2014). *Spectrometric Identification of Organic Compounds*. New York: 8th ed., John Wiley and Sons, Inc. pp. 71-125.
- Tauc, J., R. Grigorovici and A. Vancu. (1966). "Optical Properties and Electronic Structure of Amorphous Germanium". *Physica Status Solidi*, vol.15 (2), pp. 627–637.
- Yoshikawa, A., H. Matsunami, and Y. Nanishi. (2007). *Development and Applications of Wide Bandgap Semiconductors*. In: Wide Bandgap Semiconductors. Takahashi, K., A. Yoshikawa, and A. Sandhu, (Eds), Berlin: Springer-Verlag, pp. 1-24.

CHARACTERISTICS OF SYNTHESIZED MAGNESIUM OXIDE NANOPARTICLES USING AQUEOUS LEAF EXTRACT OF *OROXYLUM INDICUM* (L.) AND ITS BIOACTIVITIES

Thu Zin Tun¹, Yee Mun Than², Ye Myint Aung³

Abstract

The biological method to synthesize magnesium oxide nanoparticles with therapeutic and medicinal potential is a significant challenge in nanotechnology. In this study, to examine the efficacy of the aqueous leaf extract of *Oroxylum indicum* as stabilizing agents, they were mixed with MgSO₄·7H₂O (Epsom salt) precursor solution, followed by NaOH solution to form a precipitate of magnesium hydroxide. Then, the precipitates were calcined for 5 h, to synthesize MgO NPs. Modern techniques such as XRD, SEM-EDX, FT IR, Raman, UV-visible and TG-DTA were employed to characterize the synthesized MgO NPs. The produced nanoparticles were identified as pure MgO with a cubic structure and a spherical in shape, and ranged in size from 16 to 21 nm. Furthermore, this study has reported that the synthesized MgO NPs have excellent bioactivities (antioxidant, antidiabetic, and anti-inflammatory) and revealed good results for biomedical applications.

Keywords: MgO NPs, *O. indicum*, green synthesis, Epsom salt, bioactivities

Introduction

Nanotechnology can be defined as the synthesis, characterization, exploration, and application of nanosized materials for the development of science. Nanoparticles are materials with at least one dimension and an average size of 1–100 nm with an extraordinary surface area. The evolution of the "Nano" field has led to tremendous growth in various areas such as food and agriculture, pharmaceuticals, material science, biotechnology, medicine, energy, and the environment (Amrulloh *et al.*, 2021). The nanoparticles are synthesized based on two approaches, namely, top-down and bottom-up, by various methods that are categorized into physical, chemical, and biological methods. Among biological methods, plants are preferred over bacteria for the green synthesis of nanoparticles because they are nonpathogenic, infinitely available, non-biohazardous, and have numerous well-studied pathways. Biomolecules present in plant extracts act as reducing and capping agents, forming stable nanoparticles. Thus, the properties of the obtained nanoparticles depend on the properties of the various phytochemicals present in the plant extracts from which they were synthesized. (Kandasamy and Prema, 2015; Zhang *et al.*, 2020)

The *Oroxylum indicum* (L.) Kurz (green source) used in the present work for the environmentally friendly preparation of MgO NPs is a species of flowering plant belonging to the family of *Bignoniaceae*, has a long history of traditional medicinal uses, and modern research shows that it contains a number of medically active compounds. *Oroxylum indicum* has a specific aromatic odour because of the presence of essential oils. The aromatic essential oil mainly contains phenols, fatty acids, and aldehydes. Besides oils, the plant also contains polyphenolics, flavonoids, and alkaloids (Sowjanya *et al.*, 2019). The plant *O. indicum* contains a number of compounds like tannins, phenols, alkaloids, flavonoids, and saponins. The main chemical

¹ Department of Chemistry, University of Yangon

² Department of Chemistry, University of Yangon

³ Department of Chemistry, University of Yangon

constituents of *O. indicum* are baicalein and scutellarein. The maximum number of phenolic compounds is present in leaf extract, followed by root, bark, and stem extract (Bhardwaj *et al.*, 2018).

Magnesium oxide nanoparticles are currently popular among researchers due to their exclusive biological, electrical, and thermal properties. Magnesium oxide nanoparticles are multipurpose metal oxide nanoparticles that provide a variety of functions. In biomedical applications, there are evident reports showing MgO NPs have antioxidant, antibacterial, antifungal, and anticancer activities. In agriculture fields, they are also used in seed germination for growth, performance, chaining quality of the plant, and crop improvement, and in rice fields to increase productivity due to their antimicrobial activity. MgO NPs are also used in dietary supplements for humans and animals. In medicine, magnesium oxide is used for the relief of heartburn and sour stomach, as an antacid, as a magnesium supplement, and to improve symptoms of indigestion (Essien *et al.*, 2020; Jag tap *et al.*, 2021).

In this study, the synthesis, characterization, and some bioactivities of MgO NPs utilizing aqueous leaf extract of *Oroxylum indicum* by green method was closely focused and studied with modern techniques.

Materials and Methods

Materials

The samples of *O. indicum* leaves were collected from the plants that grow naturally around Htaw Ka Loh Village, Nyaung Done Township, Ayeyarwady Region. The commercial magnesium sulphate heptahydrate (Epsom salt) was purchased from Zi-Wa-Ka Pharmacy, Hlaing Township.

Preparation of magnesium oxide nanoparticles

The collected fresh *O. indicum* leaves were washed using tap water, and then they were allowed to air-dry for a few weeks before being ground into powder and stored at room temperature. A dried powdered sample of *O. indicum* leaves (5 g) was weighed and mixed with 100 mL of distilled water. The mixture was then heated to 60 °C for 30 min with stirring until all the samples were evenly mixed. After heating, the solution was allowed to cool and filtered with filter paper (Whatman No. 1), and the filtrate was collected. The resulting filtrate was used for the synthesis of magnesium oxide nanoparticles (fresh extract was used for each synthesis and testing process).

Magnesium oxide nanoparticles were synthesized with the aqueous extract of *O. indicum* leaves powder using the method of Fatiqin *et al.*(2021), with slight modifications. In the synthesis process, 100 mL of *O. indicum* leaves extract solution was added dropwise by burette to MgSO₄.7H₂O solution (0.2 M, 200 mL) with stirring at 600 rpm. After the two solutions were evenly mixed, 2 M NaOH was added dropwise to the mixture to get about pH 10, and then the obtained mixture was left for 3 h at 90 °C in order to optimize the formation of the magnesium hydroxide precipitate. The precipitate formed was separated from the mixture by centrifugation with a rotation of 7500 rpm at room temperature for 20 min, and the precipitate was washed three times using distilled water and once using ethanol again. The precipitate was dried in an oven to

remove any residual water and ethanol. After drying, the precipitate was ground using a mortar and pestle to form powder and calcined at 800 °C for 5 h.

Characterization

The green synthesized MgO nanoparticle formation was confirmed using a UV-visible spectrophotometer (UV-1800, Shimadzu). The diffraction patterns, crystalline nature and purity of MgO NPs were identified by an X-ray Diffractometer System, MultiFlex 2kW Type, Rigaku, D/max 2200, Japan. The morphological study and elemental composition of MgO NPs were performed under a scanning electron microscope equipped with an energy-dispersive X-ray (SEM-EDX) analyzer (JSM-6701F/JED 2300, JEOL, Japan). A Fourier transform infrared (FT IR) spectrometer (PerkinElmer, Spectrum Two) was employed to assess the functional groups present in MgO NPs. The crystallinity and phase identification of MgO NPs were characterized by a Raman spectrometer (PerkinElmer) to support the XRD results. To study the thermal stability of MgO NPs, a TG-DTA (DTG-60H) thermal analyzer (SHIMADZU, Japan) was used.

Determination of antioxidant activity

The antioxidant activity of synthesized MgO NPs was determined using the DPPH radical scavenging method using the UV-visible spectrophotometric technique. The sample solution was prepared by thoroughly mixing 1.5 mL of 20 μM DPPH solution with 1.5 mL of MgO NPs (125 to 1.95 μg/mL) in methanol and DMSO solution. Before measuring the absorbance at 517 nm against a blank, the mixture was violently mixed and allowed to stand for 30 min in the dark. The control absorbance was read without test samples. Then, the radical scavenging ability was estimated using the given formula:

$$\% \text{ RSA} = \frac{A_{\text{Control}} - (A_{\text{Sample}} - A_{\text{Blank}})}{A_{\text{Control}}} \times 100$$

Determination of antidiabetic activity

A test that inhibits the production of α-amylase was used to measure the anti-diabetic activity of MgO NPs. The UV-visible spectrophotometric method was used to assess the test samples' ability to inhibit α-amylase. In separate test tubes, 1 mL of the test sample solutions and 1 mL of the α-amylase solution were mixed together to make the different concentrations of the sample solutions (125 to 1.95 g/mL). Utilizing 1 mL of sodium phosphate buffer, the reaction mixture was then brought to pH 6.9. The reaction mixture was incubated at room temperature for 10 min to increase the α-amylase inhibitory activity, and then 400 μL of 1% starch solution was added. This combination was then incubated at room temperature for another 10 min. Before being heated in a water bath for 10 min at 85–90 °C, 500 μL of DNSA reagent was added. The absorbance at 540 nm was then measured after the tubes had been cooled. Without test samples, the control reading was taken.

$$\% \text{ inhibition} = \frac{A_{\text{Control}} - A_{\text{Sample}}}{A_{\text{Control}}} \times 100$$

Determination of anti-inflammatory activity

The egg albumin denaturation inhibitory activity of the test samples was employed to study the possible mechanisms for the anti-inflammatory impact of MgO NPs using the UV-visible spectrophotometric technique according to (Naveed *et al.*, 2022). The sample solution was prepared by mixing 400 μL of the test sample solutions and 300 μL of egg albumin solution in separate test tubes. The reaction mixture was then adjusted to pH 6.4 using sodium phosphate buffer (2.9 mL). To elicit the denaturation of egg albumin, the reaction mixture was incubated at RT for 20 min before being heated in a water bath for 15 min at 65–70 $^{\circ}\text{C}$. After that, the tubes were cooled, and the absorbance was measured at 660 nm. As a control, the solution without test samples was used. The percentage inhibition was estimated using the given formula:

$$\% \text{ inhibition} = \frac{A_{\text{Control}} - A_{\text{Sample}}}{A_{\text{Control}}} \times 100$$

Results and Discussion

Green synthesis of magnesium oxide nanoparticles

The synthesized MgO NPs obtained from commercial Epsom salt ($\text{MgSO}_4 \cdot 7\text{H}_2\text{O}$) via phytochemicals in *O. indicum* leaf extract were white in colour, powdery, crystalline, and insoluble in water (Figure 1).



Figure 1. Magnesium oxide nanoparticles

Characterization of synthesized MgO NPs

X-ray diffraction analysis

The crystalline nature and the phase purity of the synthesized MgO NPs were analyzed by the X-ray diffractometer. Figure 2 represents the diffraction patterns of MgO NPs obtained at 800 $^{\circ}\text{C}$. It indicated the sharp peaks with no impurities. The characteristic peaks were observed at 2θ degree values of 36.94, 42.92, 62.32, 74.72, and 78.68 in the crystal planes of (111), (200), (220), (311), and (222), corresponding to the XRD patterns of MgO NPs. All peaks of the Miller indices of the MgO NP samples were matched with the International Crystal Structure Data (ICSD) no.642712 of MgO. The axial lengths of a, b, and c coordinates are 4.2128 \AA . All three interaxial angles α , β , and γ of 90° suggested the formation of the perfect cubic-shaped crystal of MgO NPs. The average crystallite size of the synthesized MgO NPs was calculated by the Scherrer equation and was found to be 23.19 nm.

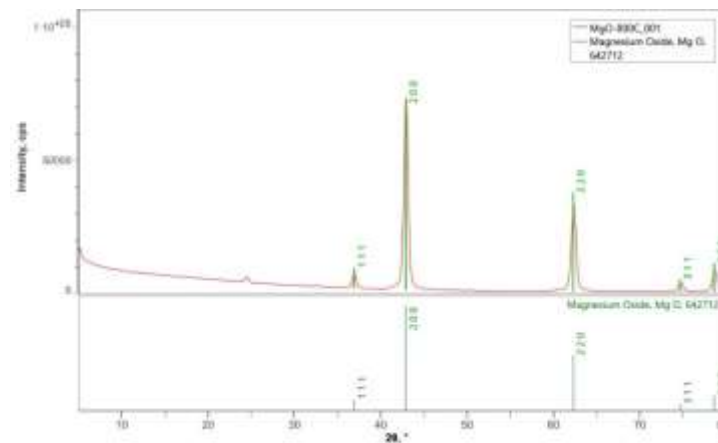


Figure 2. X-ray diffractogram of MgO NPs using an aqueous extract of *O. indicum* leaves

SEM-EDX analysis

Morphological analysis of the synthesized MgO NPs was carried out using SEM. The SEM image (Figure 3) of MgO NPs shows that the resulting MgO NPs are in the form of a spherical shape with particle sizes between 16 and 21 nm. The SEM image of MgO NPs shows good surface properties with uniform distribution of the particles however, the majority of them was clumped together. The calculated magnesium oxide nanoparticles have an average particle size of 18.5 nm in SEM images. In addition, EDX analysis confirmed the elemental composition of synthesized MgO NPs, which revealed the presence of Mg^{2+} ions and O^{2-} ions at high intensity with a weight ratio of 2:1 in the sample (Figure 4).

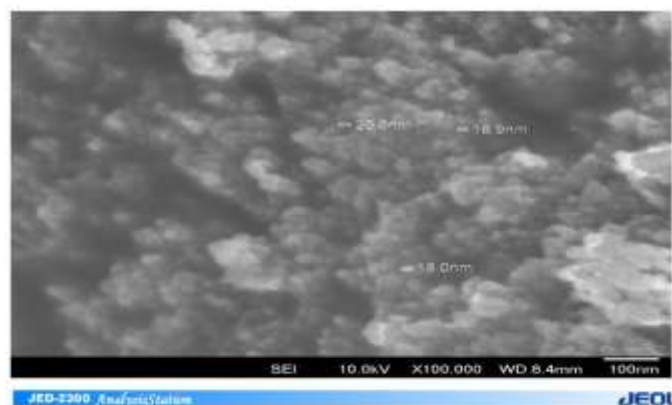


Figure 3. SEM image of MgO NPs using an aqueous extract of *O. indicum* leaves

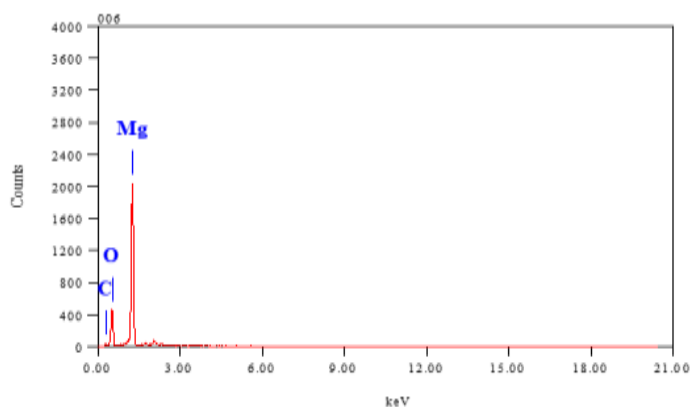


Figure 4. EDX image of MgO NPs using an aqueous extract of *O. indicum* leaves

FT IR spectroscopic analysis

Figure 5 represents the FT IR spectrum of the synthesized MgO NPs using an aqueous extract of *O. indicum* leaves after calcination at 800 °C. From this spectrum, it can be observed that the main peak at 846 cm^{-1} corresponds to the stretching vibration of the Mg-O bond, which indicates the formation of Mg-O linkage in MgO NPs as well as the stabilization of MgO NPs (Jeevanandam *et al.*, 2020; Balakrishnan *et al.*, 2020). There are no other peaks in the spectrum, indicating the influence of the Mg-O bond in the composition of MgO NPs in agreement with the SEM-EDX result.

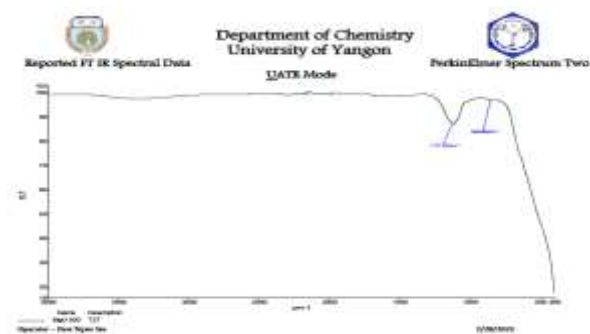


Figure 5. FT IR spectrum of MgO NPs using an aqueous extract of *O. indicum* leaves

Raman spectroscopic analysis

The Raman spectrum of the synthesized MgO NPs at 800 °C was determined to support the XRD findings, and the outcomes are expressed in Figure 6. The spectrum shows strong peaks at various regions, indicating the cubic structure as designated to the tangential modes of MgO in the amorphous phase (Athar *et al.*, 2012).

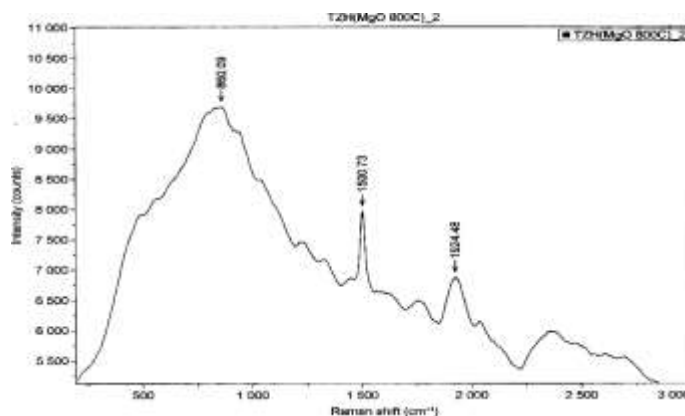


Figure 6. Raman spectrum of MgO NPs using an aqueous extract of *O. indicum* leaves

UV-visible spectroscopic analysis

UV-visible absorption spectroscopy is widely used to examine the optical properties of nanosized particles. The optical properties of metal nanoparticles strongly depend on the size, shape, and interaction between the particles present on the surface of the nanoparticles. The UV-visible absorption spectrum (Figure 7) of MgO NPs showed the absorption peak at 261 nm, which confirmed the formation and stability of MgO NPs.

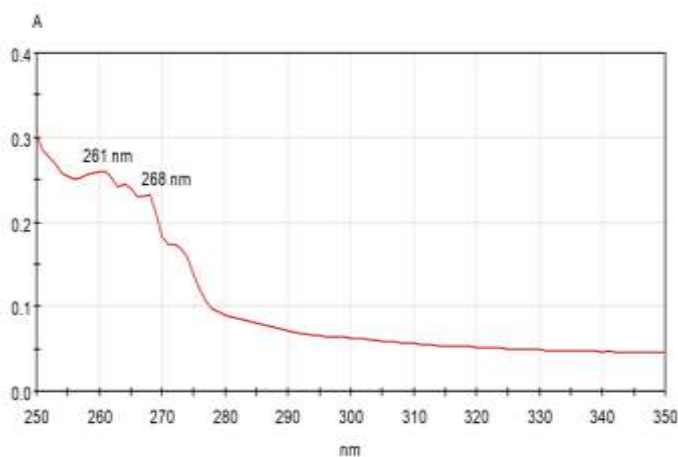


Figure 7. UV-visible spectrum of MgO NPs using an aqueous extract of *O. indicum* leaves

TG-DTA thermographic analysis

TG-DTA analysis was used to assess the thermal observation of synthesized MgO NPs using an aqueous leaf extract of *O. indicum* after calcination at 800 °C. The thermogram (Figure 8) of MgO NPs indicated only one endothermic peak at 71.41 °C, which was due to the elimination of physically absorbed water from the sample surface. The absence of any other peaks indicated that no other organic constituents were left in the nanoparticles.



Figure 8. TG-DTA thermogram of MgO NPs using an aqueous extract of *O. indicum* leaves

Screening of the Biological Properties of MgO NPs

Antioxidant activity of MgO NPs

A change in the colour of the DPPH solution serves as a marker for the screening of antioxidant activity. The synthesized MgO NPs changed the colour of the DPPH solution from violet to light yellow, indicating that they might be antioxidants. The antioxidant activity is shown by the 50% inhibitory concentration (IC_{50}). The lower the IC_{50} values, the higher the free radical scavenging activity, i.e., the higher the percentage of antioxidant properties. From these results, the IC_{50} values of the standard ascorbic acid and the synthesized MgO NPs were observed at 1.94 $\mu\text{g/mL}$ and 1.04 $\mu\text{g/mL}$, respectively. These results revealed that the synthesized MgO NPs have more potent antioxidant activity than the standard ascorbic acid, as shown in Table 1 and Figure 9.

Table 1. Antioxidant Activity (% Inhibition) and IC_{50} Values of Synthesized MgO NPs and Standard Ascorbic Acid

Samples	% Radical Scavenging Activity (\pm SD)							IC_{50} $\mu\text{g/mL}$
	62.5 $\mu\text{g/mL}$	31.25 $\mu\text{g/mL}$	15.63 $\mu\text{g/mL}$	7.81 $\mu\text{g/mL}$	3.91 $\mu\text{g/mL}$	1.95 $\mu\text{g/mL}$	0.98 $\mu\text{g/mL}$	
Ascorbic acid	75.74 \pm 0.001	75.51 \pm 0.000	75.28 \pm 0.001	75.06 \pm 0.002	72.79 \pm 0.001	50.11 \pm 0.002	42.18 \pm 0.002	1.94
MgO NPs	56.15 \pm 0.003	54.23 \pm 0.002	53.90 \pm 0.001	52.25 \pm 0.002	51.26 \pm 0.001	50.44 \pm 0.003	49.97 \pm 0.003	1.04

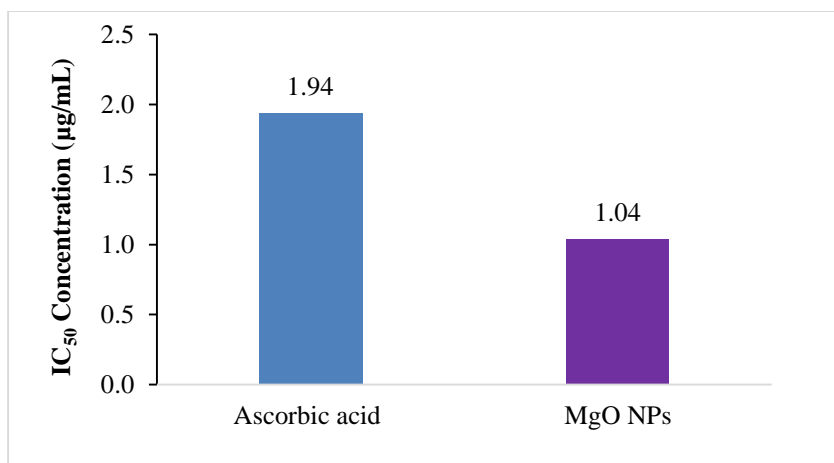


Figure 9. A bar graph of IC₅₀ values of the antioxidant activity of synthesized MgO NPs and standard ascorbic acid

Antidiabetic activity of MgO NPs

The antidiabetic activity of the synthesized MgO NPs using an aqueous extract of *O. indicum* leaves was assessed by using α -amylase inhibitory assay. The percentage of inhibition (42.80–59.09 %) increased with increasing the MgO NP concentration (1.95–125 µg/mL), indicating the antidiabetic effect in a dose-dependent manner. The greatest inhibition of MgO NPs was 59 %, whereas at the same dose (125 µg/mL), the common medication metformin showed 60 % inhibition. As shown in Table 2 and Figure 10, the IC₅₀ values of MgO NPs and the standard metformin drug were 4.78 µg/mL and 3.79 µg/mL, respectively. So, it can be seen that the green synthesized MgO NPs using the aqueous leaf extract of *O. indicum* have the potential to reduce diabetes about the same as the standard medication.

Table 2. Antidiabetic Activity (% Inhibition) and IC₅₀ Values of Synthesized MgO NPs and Standard Metformin Drug

Samples	% α -Amylase inhibition activity (\pm SD)							IC ₅₀ µg/mL
	125 µg/mL	62.5 µg/mL	31.25 µg/mL	15.625 µg/mL	7.8125 µg/mL	3.91 µg/mL	1.95 µg/mL	
Metformin drug	59.94 \pm 0.000	59.09 \pm 0.000	58.81 \pm 0.000	57.39 \pm 0.000	52.27 \pm 0.001	50.28 \pm 0.001	45.74 \pm 0.001	3.79
MgO NPs	59.09 \pm 0.001	55.97 \pm 0.000	55.40 \pm 0.001	52.84 \pm 0.000	51.99 \pm 0.001	49.43 \pm 0.001	42.80 \pm 0.000	4.78

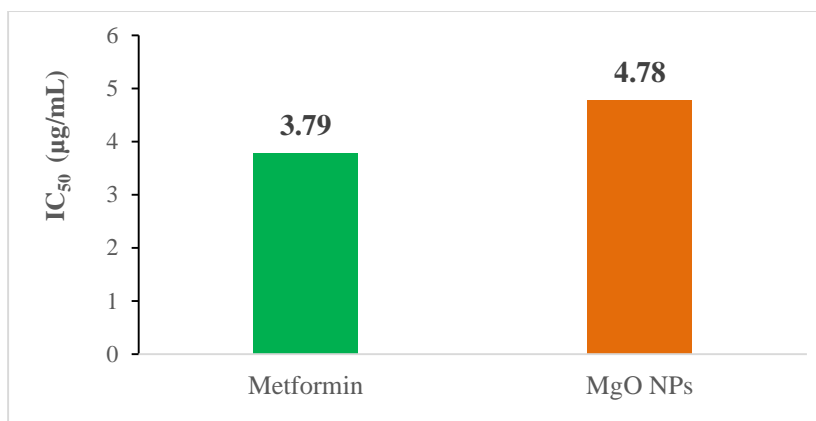


Figure 10. A bar graph of IC₅₀ values of antidiabetic activity of synthesized MgO NPs and standard metformin drug

Anti-inflammatory activity of MgO NPs

MgO NPs were discovered to prevent the denaturation of albumin by heat based on *in vitro* tests. When heated, the reaction mixture containing MgO NPs exhibited no cloudy appearance or precipitation, but egg albumin without MgO NPs produced white precipitation. The results were contrasted with those of diclofenac sodium, a common anti-inflammatory drug. According to the findings, the standard diclofenac sodium drug (10.56 to 84.39 %) demonstrated less inhibition than MgO NPs (34.25 to 84.57 %) at the same concentrations (1.95-125 µg/mL). The IC₅₀ values were found to be 4.52 µg/mL for MgO NPs and 6.77 µg/mL for standard diclofenac sodium, indicating that the synthesized MgO NPs have more effective anti-inflammatory activity than the medication (Table 3 and Figure 11).

Table 3. Anti-inflammatory Activity (% Inhibition) and IC₅₀ Values of Synthesized MgO NPs and Standard Diclofenac Sodium Drug

Samples	% Inhibition of Albumin Denaturation Activity							IC ₅₀ µg/mL
	(±SD)							
	125 µg/mL	62.5 µg/mL	31.25 µg/mL	15.625 µg/mL	7.8125 µg/mL	3.91 µg/mL	1.95 µg/mL	
Diclofenac sodium drug	84.39± 0.001	83.84± 0.000	81.91± 0.001	76.68 ± 0.002	56.20± 0.001	33.06± 0.001	10.56± 0.003	6.77
MgO NPs	84.57± 0.000	83.93± 0.001	82.74± 0.000	82.00± 0.001	70.52± 0.000	46.19± 0.002	34.25± 0.002	4.52

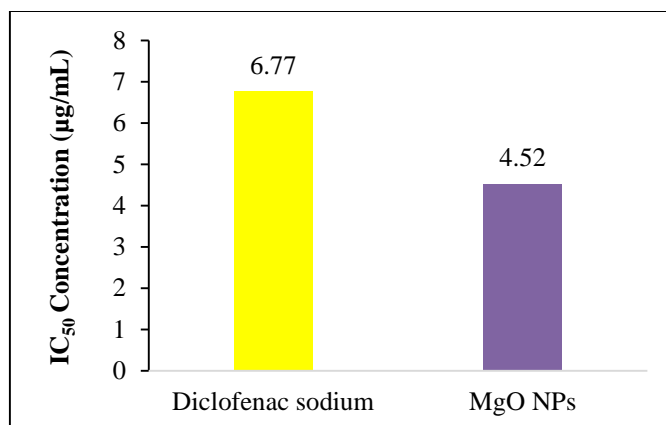


Figure 11. A bar graph of the IC₅₀ values of the anti-inflammatory activity of synthesized MgO NPs and standard diclofenac sodium drug

Conclusion

In this investigation, an inexpensive and safe method was used for the synthesis of MgO NPs using an aqueous leaf extract of *O. indicum*. The existence of a maximal absorption wavelength at 261 nm in the UV-visible spectrum suggested the formation of MgO NPs. XRD and SEM-EDX confirmed the cubic MgO NPs with a spherical form and an average particle size of 23.19 nm by XRD and 18.5 nm by SEM. The lack of any additional functional groups using FT IR analysis indicated the higher purity of MgO NPs. The TG-DTA analysis only detected one endothermic peak at 71.41 °C, proving the purity of MgO NPs and their thermal stability. Additionally, the synthesized MgO NPs exhibited excellent antioxidant, antidiabetic, and anti-inflammatory potentials. Therefore, it can be concluded that the synthesized MgO NPs using an aqueous extract of *O. indicum* leaves have the potential to be used as an agent for biochemical applications.

Acknowledgements

The authors would like to express their profound gratitude to the Myanmar Academy of Arts and Science for giving permission to submit this paper and to Professor and Head, Dr Ni Ni Than, Department of Chemistry, University of Yangon, for her kind encouragement. Special thanks to the Department of Chemistry, University of Yangon for providing the research facilities and to the National University of Singapore for SEM-EDX imaging.

References

- Amrulloh, H., A. Fatiqin, W. Simanjuntak, H. Afriyani, and A. Annissa. (2021). "Antioxidant and Antibacterial Activities of Magnesium Oxide Nanoparticles Prepared Using Aqueous Extract of *Moringa oleifera* Bark as Green Agents". *Journal of Multidisciplinary Applied Natural Science*, vol. 1 (1), pp. 44-53.
- Athar, T., A. Hakeem, and W. Ahmed. (2012). "Synthesis of MgO Nanopowder via Non-aqueous Sol-gel Method". *Advanced Science Letters*, vol. 5, pp. 1-3.
- Balakrishnan, G., R. Velavan, K. M. Batoo, and E. H. Raslan. (2020). "Microstructure, Optical and Photocatalytic Properties of MgO Nanoparticles". *Elsevier*, vol. 16, pp. 1-4.

- Bhardwaj, A., A. Pathak, D. Bhatia, J. Sahoo, U. Batra, M. Tripathi, T. Mishra, and P. Choudhary. (2018). "A Phyto-pharmacological Overview on *Oroxylum indicum* (Linn.) Vent.". *International Journal of Advanced Research*, vol. 6 (8), 291-297.
- Essien, E. R., V. N. Atasie, A. O. Okefor, and D. O. Nwude. (2020). "Biogenic Synthesis of Magnesium Oxide Nanoparticles Using *Manihot esculenta* (Crantz) Leaf Extract". *International Nano Letters*, vol. 10, pp. 43-48.
- Fatiqin, A., H. Amrulloh and W. Simanjuntak. (2021). "Green Synthesis of MgO Nanoparticles using *Moringa oleifera* Leaf Aqueous Extract for Antibacterial Activity". *Bulletin of the Chemical Society of Ethiopia*, vol. 35 (1), pp. 161-170.
- (MgO) Nanoparticles in various domains". *Advanced Materials Letters*, vol. 11 (8), pp. 1-10.
- Jagtap, K. R., S. R. Hore, P. S. Patil, S. A. Patil, and N. V. Awati. (2021). "Synthesis of Magnesium Oxide Nanoparticles by Using Green Method". *International Journal of Research in Engineering and Science*, vol. 9 (6), pp. 7-14.
- Jeevanandam, J., Chan, Y. S., Wong, Y. J., and Hii, Y. S. (2020). "Biogenic Synthesis of Magnesium Oxide Nanoparticles using *Aloe barbadensis* Leaf Latex Extract". *IOP Conference Series: Materials Science and Engineering*, vol. 943 (12030), pp. 1-14.
- Kandasamy, S., and R. S. Prema. (2015). "Methods of Synthesis of Nanoparticles and its Applications". *Journal of Chemical and Pharmaceutical Research*, vol. 7 (3), pp. 278-285.
- Naveed, M., H. Batool, S. U. Rheman, A. Javed, S. I. Makhdoom, T. Aziz, A. A. Mohamed, M. Y. Sameeh, M. W. Alruways, A. S. Dabool, A. A. Almalki, A. S. Almari, and M. Alhomrani. (2022). "Characterization and Evaluation of the Antioxidant, Antidiabetic, Anti-inflammatory, and Cytotoxic Activities of Silver Nanoparticles Synthesized using *Brachychiton populneus* Leaf Extract". *Processes*, vol. 10 (1521), pp. 1-18.
- Sowjanya, K., S. Swati, M. Manasa, S. Srilakshmi, and K. Mahima. (2019). "Review on *Oroxylum indicum*". *Journal of Pharmaceutical Sciences and Research*, vol. 11 (8), pp. 2905-2909.
- Zhang, D., X-L. Ma, Y. Gu, H. Huang, and G-w. Zhang. (2020). "Green Synthesis of Metallic Nanoparticles and their Potential Applications to Treat Cancer". *Frontiers in Chemistry*, vol. 8 (799), pp. 1-18.

ENZYMIC STUDY ON PECTINASE EXTRACTED FROM RED DRAGON FRUIT PEELS

Chit Lay Ko¹, Jue Jue Khin², Myat Kyaw Thu³, Ye Myint Aung⁴

Abstract

The extraction of pectinase enzyme from red dragon fruit peels was done by using ammonium sulphate precipitation (20–80 %) method, and then the purification of the enzyme was done by using the gel filtration chromatographic method on Sephadex G-100. The enzyme activity was measured by utilizing DNS method to detect the release of the reducing sugar group. Specific activity, protein recovery, and degree of purification were measured in each purification step. The pectinase enzyme was purified 6.49-fold over crude extract, and protein recovery was found to be 8.43 %. The K_m values of the crude and partially purified pectinase enzymes were found to be $0.1992 \times 10^{-2} \text{ g mL}^{-1}$ and $0.358 \times 10^{-2} \text{ g mL}^{-1}$, respectively. The reaction order (n) of the pectinase-catalyzed reactions was found to be first order. The activation energy (E_a) of the partially purified pectinase-catalyzed reaction was lower than that of the crude pectinase-catalyzed reaction. Both crude and partially purified pectinase enzymes were used in the clarification of apple juice, and good results were observed.

Keywords: pectinase, gel filtration chromatography, ammonium sulphate precipitation method, DNS method, clarification, apple juice

Introduction

The primary source of industrial enzymes is microorganisms, out of which 50 % originate from fungi and yeast, 35 % from bacteria, and the remaining 15 % are either of plant or animal origin (Anisa and Girish, 2014). Today, pectinases are one of the most important enzymes in the commercial sector. Pectinases are responsible for the degradation of the long and complex molecules called pectin. Pectin occurs as structural polysaccharides in the middle lamella and the primary cell walls of young plant cells (Kashyap *et al.*, 2001). Pectinases are classified into three groups according to the following criteria: hydrolytic (hydrolases) or trans-eliminative (lyases) cleavage of the glycosidic bonds; endo (randomic) or exo (from the molecule end) mechanism of action; and preference for substrate, pectic acid, or pectin. The three main types of pectinases are pectinesterase, depolymerizing enzymes, and protopectinases (Kumar, 2015). Pectinases have crucial industrial significance in improving juice yields, scouring of cotton, degumming of plant fibres, wastewater treatment, vegetable oil extraction, and so on. It plays an important role in the food and wine industry in the processing of fruit juices (Pauldas and Jain, 2018). This study aims to extract pectinase from red dragon peels and study its kinetic properties and efficiency in apple juice clarification.

Materials and Methods

Red dragon fruit (*Selenicereus costaricensis* (F. A. C. Weber) S. Arias & N. Korotova) samples were collected from Hledan Market, Kamayut Township, Yangon Region. Then, identification of the sample was done at the Department of Botany, University of Yangon. Sample extraction and purification were performed at the Analytical Chemistry Research

¹ Department of Chemistry, University of Yangon

² Department of Chemistry, University of Yangon

³ Department of Chemistry, Mohnyin University

⁴ Department of Chemistry, University of Yangon

Laboratory, Department of Chemistry, University of Yangon. 3,5-Dinitrosalicylic acid (DNS) and all other chemicals used in this work were of analytical grade and were products of BDH Chemical Limited (England).

Sample Preparation and Extraction of Pectinase

Red dragon fruit samples were washed with distilled water and dried at room temperature. Then the red dragon fruits were peeled and cut into small pieces. Peels (20 g) were homogenized with 160 mL of 0.1 M sodium acetate buffer (pH 5.0) for 5 min using a blender. After homogenization, the resulting slurry was filtered through cheesecloth. The filtrate was centrifuged for about 20 min at 6000 rpm to obtain the extract. Solid ammonium sulphate was added to this extract to obtain 20-80 % saturation and stored at 4 °C. After standing overnight, the protein precipitate containing the pectinase was collected by centrifugation for 20 min at 6000 rpm.

Enzyme Purification

The crude pectinase enzyme was dissolved in 0.1 M sodium acetate buffer (pH 5.0). Then it was put into the column filled with Sephadex G-100 equilibrated with sodium acetate buffer. The flow rate was adjusted to 1.5 mL per 5 min. A 1.5 mL fraction was collected per tube using a fraction collector. After collection, each fraction was checked for protein content by measuring the absorbance at 280 nm and enzyme activity by 3,5-dinitrosalicylic acid (DNS) method. The fraction with the highest enzyme activity was pooled to obtain a partially purified enzyme and stored at 4 °C.

Assay of the Crude and Partially Purified Enzymes

The enzyme activity was determined by measuring the release of sugar groups using the 3,5-dinitrosalicylic acid (DNS) method. In brief, 0.5 mL of enzyme solution was incubated with 0.5 mL of 1 % pectin substrate in 0.1 M acetate buffer (pH 5.0) at 45 °C for 10 min. Then, 1 mL of DNS solution was added, and this mixture was kept at 90 °C in a boiling water bath for 5 min. 1 mL of 1 M sodium-potassium tartrate was added in order to stop the reaction, and 2 mL of distilled water was added to the mixture. The absorbance of the mixture was measured at 591 nm by using a UV-visible spectrophotometer. One unit of enzyme was defined as one micromole of glucose that was liberated per minute.

Protein content in each purification step was determined by the Biuret method at 550 nm

Kinetic Studies of the Crude and Partially Purified Pectinase Enzymes

The Michaelis-Menten constant (K_m), maximum velocity (V_{max}), and the reaction order of crude and partially purified enzymes were determined using pectin as a substrate in the range of 2 mg mL⁻¹ to 16 mg mL⁻¹. The activation energy of the pectinase-catalyzed reaction was also evaluated by using different temperatures of 20 °C, 25 °C, 30 °C, 35 °C, 40 °C, and 45 °C.

Application of the Crude and Partially Purified Pectinase Enzymes in Apple Juice Clarification

Apple fruits purchased from the local market were washed carefully and chopped into small pieces with a sharp knife. Firstly, 40 g of chopped samples were mixed with 40 mL of distilled water and blended for 2 min in a blender. After that, apple fruit juice was filtered through cheesecloth to remove insoluble materials. Next, 8 mL of apple fruit juice was taken in a

test tube and warmed in a water bath at 45 °C for 10 min to inactivate any natural fruit enzymes or bacteria present. Then, crude and partially purified pectinase solutions (2 mL each) was added to 8 mL of apple fruit juice. After a 4-h incubation period, the sample was heated for 3 min at 45 °C. The juice was centrifuged for 20 min at 3000 rpm, and the supernatant was filtered out with filter paper. The clarity of the apple juice was calculated by measuring the absorbance at 660 nm (Maznila *et al.*, 2008) with a UV-Vis spectrophotometer. Similarly, the above procedure was carried out by using (i) 10 mL of apple juice without enzyme and (ii) 8 mL of apple juice and 2 mL of distilled water. The clarity was expressed in percentages.

Results and Discussion

Purification of Pectinase from Red Dragon Fruit Peels

Enzyme purification is essential for various industrial applications of enzymes. The impurities present in the enzyme solution can affect the enzyme's stability, activity, and specificity, which can, in turn, affect the final product's quality and yield. Purified enzymes are more stable and active, and their specificity is higher, making them more efficient and effective in industrial processes (Pawar, 2023). Figure 1 shows the chromatogram of pectinase on Sephadex G-100 gel. The protein content of the eluate was checked spectrophotometrically at 280 nm, and the enzyme activity was determined at 591 nm. The fractions with the highest activity (47–61 fractions) were pooled. The partially purified pectinase enzyme was purified up to 6.49 folds with a specific activity of 0.851 U/mg over crude extract. The pectinase activity, specific activities of the enzyme solutions, and purity of the enzyme were described in Table 1.

Effect of Substrate Concentration on Pectinase-catalyzed Reaction

The effect of substrate concentration on the velocity of the pectinase-catalyzed reaction was studied. It was found that velocity increases with an increase in substrate concentration from 0.2×10^{-2} to 1.6×10^{-2} g mL⁻¹. However, at higher concentrations of pectin, the enzyme becomes saturated with substrate and reaches V_{\max} , the enzyme's maximum velocity. Further increasing the concentration of substrate does not increase the velocity significantly. The results are shown in Tables 2 and 3 for crude and partially purified pectinase, respectively. Michaelis-Menten, Lineweaver-Burk, and Eadie-Hofstee plots for crude and partially purified pectinase enzymes are depicted in Figures 2, 3, 4, 5, 6, and 7, respectively. In this study, linear regression method was used to obtain V_{\max} and K_m from experimental results. These values are shown in Table 4 in comparison with the V_{\max} and K_m values obtained by Lineweaver-Burk and Eadie-Hofstee plots, which are not much different from each other, implying that they are comparable on the basis of quantitative aspects. The K_m and V_{\max} values of the pectinase were found to be 0.1992×10^{-2} g mL⁻¹ and 0.5839×10^{-2} mM min⁻¹, respectively, for the crude enzyme, and 0.358×10^{-2} g mL⁻¹ and 28.389×10^{-2} mM min⁻¹ for the purified enzyme.

Reaction Order for Pectinase-catalyzed Reaction

Depending on the substrate concentrations, the kinetics of an enzyme-catalyzed reaction may be described by the first-order rate equation (Bergmeyer, 1983). In this research, the reaction order (n) value was determined from the plot of $\log V/(V_{\max} - V)$ vs. $\log [S]$ using the linear regression method (Table 5 and Figure 8). The reaction order (n) for the crude and purified pectinase-catalyzed reactions was calculated to be first order.

Activation Energy for Pectinase-catalyzed Reaction

Enzymes are regarded as lowering the activation energy of a system by making it energetically easier for the transition state to form. In the presence of an enzyme catalyst, the formation of the transition state is energetically more favourable, thereby accelerating the rate at which the reaction will proceed but not fundamentally changing the energy levels of either the reactant or the product (Robinson, 2015). Table 6 shows the relationship between the velocity of the pectinase-catalyzed reaction and temperature. Figure 9 shows a plot of Log V as a function of 1/T for the determination of activation energy and Arrhenius constants. The Arrhenius constants of the crude and purified pectinase-catalyzed reactions were found to be 3.211×10^6 and 0.136×10^6 , respectively. The activation energy (E_a) values of crude and partially purified pectinase-catalyzed reactions were determined to be $5.339 \text{ kcal mol}^{-1}$ and $4.121 \text{ kcal mol}^{-1}$ from linear regression and $5.491 \text{ kcal mol}^{-1}$ and $4.290 \text{ kcal mol}^{-1}$ from the graph, respectively, for temperatures between 20 and 45 °C.

Application of Crude and Partially Purified Pectinase Enzymes in Apple Juice Clarification

Pectinase plays an important role in the process of extracting and purifying the juice (Berutu *et al.*, 2017). In this research, the effect of pectinase on the clarification of apple juice was studied. The clarity of the apple juice was determined by measuring the absorbance at 660 nm with a spectrophotometer and expressed in terms of percent transmittance. A lower absorbance value i.e., a higher transmittance value indicated clearer juice. The clarity of treated apple juice improved because of the removal of colloidal and suspended particles in the juice, especially pectinaceous material (Joshi *et al.*, 2011). The juice became clearer, as did the increase in colour and appearance. The percents transmittance of crude and purified enzymes in apple juice were 74.47 % and 96.38 %, respectively, compared to 50.69 % and 96.30 % for apple juice without enzymes (Table 7).

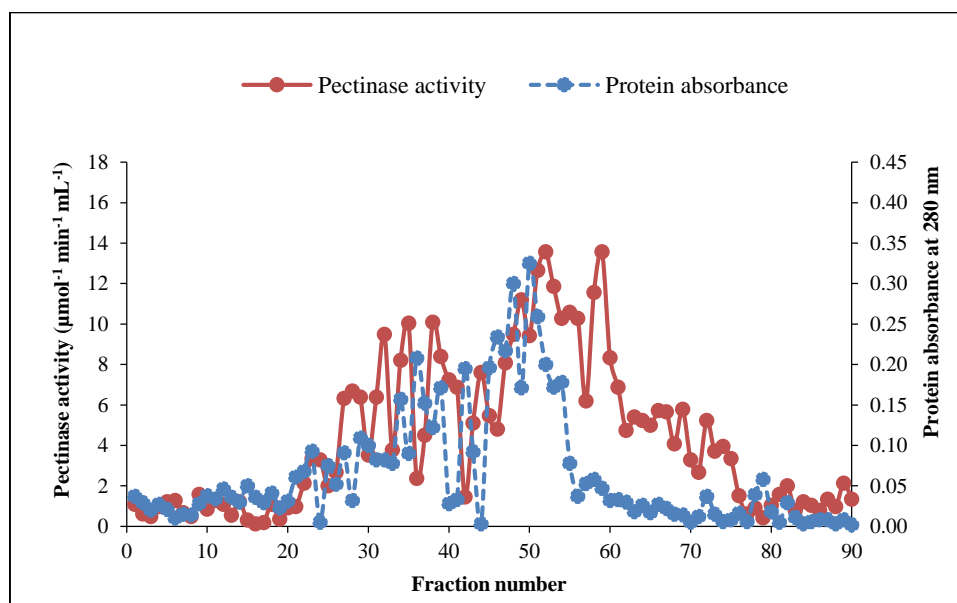


Figure 1. Chromatogram of crude pectinase enzyme on Sephadex G-100 column

Table 1. Pectinase Enzyme Activities, Protein Contents and Specific Activities of the Enzyme Solution at Different Purification Steps

Fraction	Total volume (mL)	Total enzyme activity (unit)	Total protein content (mg)	Specific activity (unit/mg)	Protein recovery (%)	Degree of purity (fold)
crude	140	42.00	320.60	0.13	100.00	1.00
20 % (NH ₄) ₂ SO ₄ precipitation	81.0	44.55	277.83	0.16	86.82	1.22
80 % (NH ₄) ₂ SO ₄ precipitation	14.5	16.40	41.11	0.39	12.82	2.97
after passing the Sephadex G-100	21.0	22.99	26.99	0.85	8.43	6.49

Table 2. Relationship between Velocity of Crude Pectinase-catalyzed Reaction and Substrate Concentration

[S]x10 ² (g mL ⁻¹)	-[S] x 10 ² (g mL ⁻¹)	1/[S] (10 ⁻² g ⁻¹ mL)	V x 10 ² (mM min ⁻¹)	1/V (10 ⁻² mM ⁻¹ min)	V/[S] (mM min ⁻¹ g ⁻¹ mL)	[S]/V (g mL ⁻¹ mM ⁻¹ min)
0.2	-0.2	5.00	0.292	3.425	1.460	0.685
0.4	-0.4	2.50	0.397	2.519	0.992	1.007
0.6	-0.6	1.67	0.429	2.331	0.715	1.399
0.8	-0.8	1.25	0.46	2.146	0.582	1.659
1.0	-1.0	1.00	0.482	2.075	0.482	1.988
1.2	-1.2	0.83	0.503	1.988	0.419	2.386
1.4	-1.4	0.71	0.515	1.942	0.368	2.718
1.6	-1.6	0.63	0.523	1.912	0.327	3.059

Table 3. Relationship between Velocity of Partially Purified Pectinase-catalyzed Reaction and Substrate Concentration

[S]× 10 ² (g mL ⁻¹)	-[S] × 10 ² (g mL ⁻¹)	1/[S] (10 ⁻² g ⁻¹ mL)	V x 10 ² (mM min ⁻¹)	1/V (10 ⁻² mM ⁻¹ min)	V/[S] (mM min ⁻¹ g ⁻¹ mL)	[S]/V (g mL ⁻¹ mM ⁻¹ min)
0.2	-0.2	5.00	10.138	0.099	50.693	0.019
0.4	-0.4	2.50	15.005	0.067	37.512	0.027
0.6	-0.6	1.67	17.844	0.056	29.740	0.034
0.8	-0.8	1.25	19.871	0.050	24.839	0.040
1.0	-1.0	1.00	21.088	0.047	21.088	0.047
1.2	-1.2	0.83	21.899	0.046	18.249	0.055
1.4	-1.4	0.71	22.305	0.045	15.932	0.063
1.6	-1.6	0.63	22.710	0.044	14.194	0.070

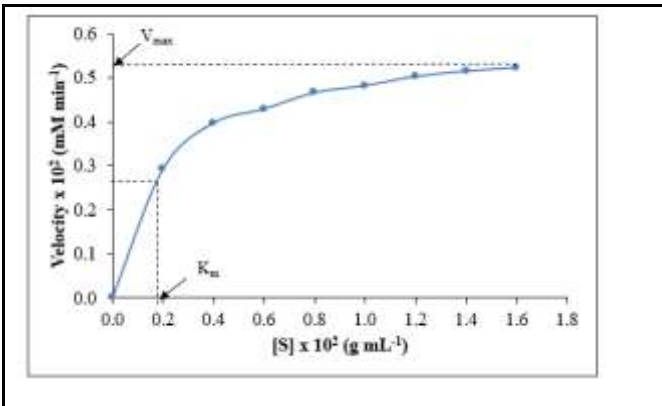


Figure 2. Michaelis-Menten plot of crude pectinase enzyme-catalyzed reaction

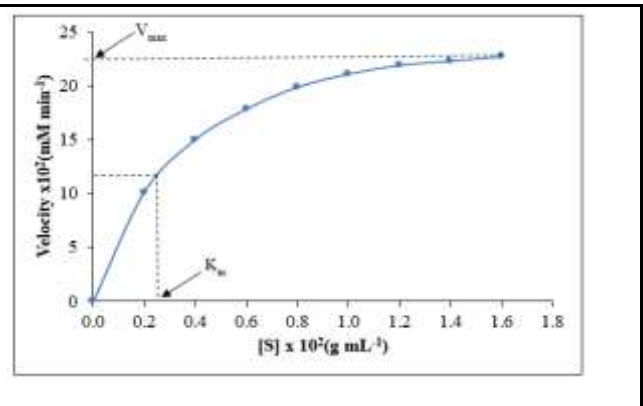


Figure 3. Michaelis-Menten plot of partially purified pectinase enzyme-catalyzed reaction

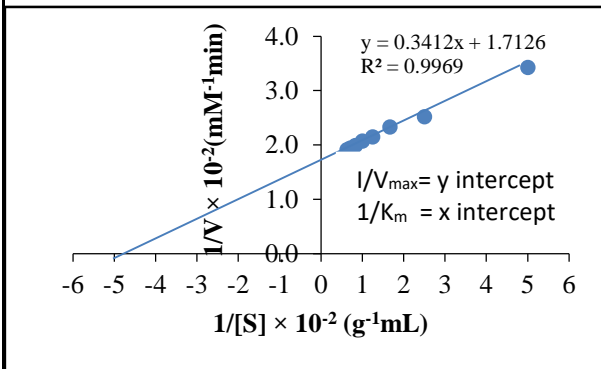


Figure 4. Lineweaver-Burk plot of 1/V vs. 1/[S] for crude pectinase enzyme-catalyzed reaction

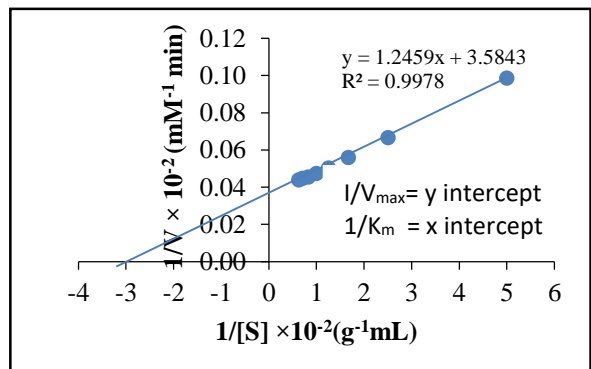


Figure 5. Lineweaver-Burk plot of 1/V vs. 1/[S] for partially purified pectinase enzyme-catalyzed reaction

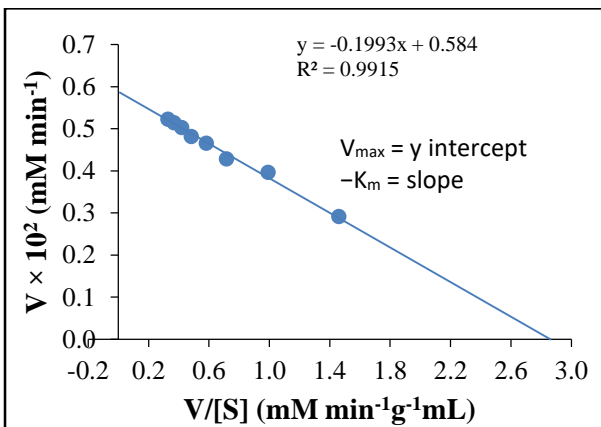


Figure 6. Eadie-Hofstee plot of crude pectinase enzyme-catalyzed reaction

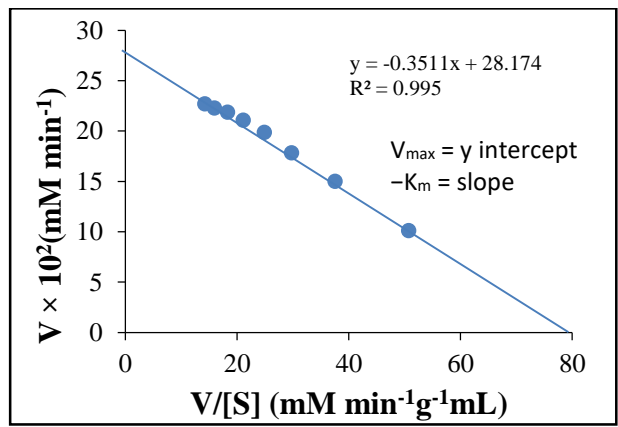


Figure 7. Eadie-Hofstee plot of partially purified pectinase enzyme-catalyzed reaction

Table 4. V_{max} and K_m Values of Crude and Partially Purified Pectinase using Linear Regression and Graphical Methods

Enzyme	Method	Linear regression method		Graphical method	
		$K_m \times 10^2$ (g mL ⁻¹)	$V_{max} \times 10^2$ (mM min ⁻¹)	$K_m \times 10^2$ (g mL ⁻¹)	$V_{max} \times 10^2$ (mM min ⁻¹)
crude pectinase	Michaelis-Menten	-	-	0.199	0.530
	Lineweaver-Burk	0.1992	0.5839	0.200	0.583
	Eadie-Hofstee	0.1993	0.5840	0.194	0.584
partially purified pectinase	Michaelis-Menten	-	-	0.270	22.50
	Lineweaver-Burk	0.3580	28.389	0.333	27.90
	Eadie-Hofstee	0.3510	28.173	0.352	28.20

Table 5. Relationship between $\log V/(V_{max}-V)$ and $\log [S]$ for the Determination of Reaction Order for Crude and Partially Purified Pectinase-catalyzed Reactions

No	Log [S]	Crude enzyme	Partially purified enzyme
		Log $V/(V_{max}-V)$	Log $V/(V_{max}-V)$
1	-2.699	0.0001	-0.246
2	-2.398	0.3272	0.066
3	-2.222	0.4424	0.246
4	-2.097	0.5969	0.396
5	-2.000	0.6749	0.484
6	-1.921	0.7936	0.527
7	-1.854	0.8736	0.563
8	-1.796	0.9339	0.601

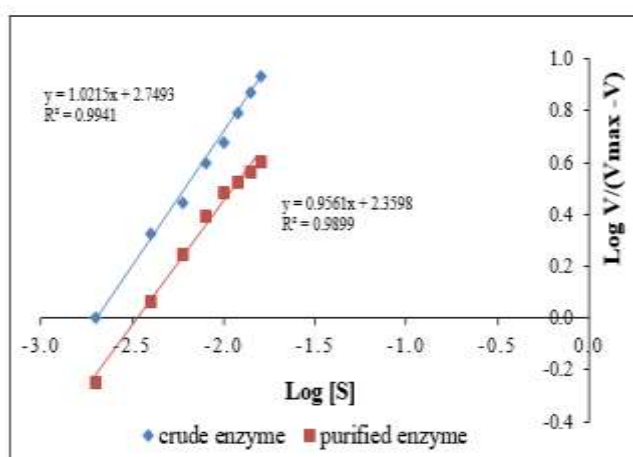
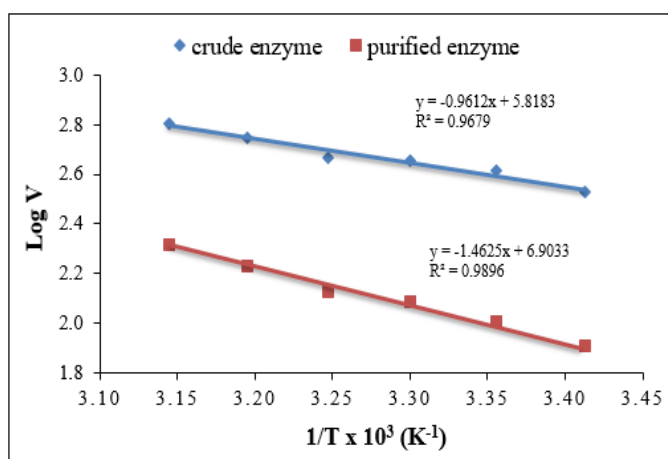


Figure 8. Plot of $\log V/(V_{max}-V)$ as a function of $\log [S]$ of crude and partially purified pectinase-catalyzed reactions

Table 6. Relationship between Velocity of Crude and Partially Purified Pectinase-catalyzed Reactions and Temperature of the Solution at pH 5

Temperature (°C)	1/T × 10 ³ (K ⁻¹)	Crude pectinase		Partially purified pectinase	
		Velocity × 10 ³ (mM min ⁻¹)	Log V	Velocity × 10 ³ (mM min ⁻¹)	Log V
20	3.413	336.664	2.527	81.109	1.909
25	3.356	409.603	2.612	101.387	2.006
30	3.300	454.213	2.657	117.609	2.085
35	3.247	466.379	2.668	125.720	2.126
40	3.195	559.655	2.748	150.053	2.231
45	3.145	783.706	2.894	206.829	2.315

**Figure 9.** A plot of Log V as a function of 1/T for the determination of E_a**Table 7. Transmittance and Absorbance of Crude and Partially Purified Pectinase Enzyme on Apple Juice at 660 nm**

Test	Absorbance	Transmittance (%)	Test	Absorbance	Transmittance (%)
A	0.295	50.69	A	0.303	49.77
B	0.270	53.70	B	0.274	53.21
C (crude)	0.128	74.47	C (partially purified)	0.016	96.38

A = (juice only)

B = (distilled water and juice)

C = (enzyme and juice)

Conclusion

For the extraction and partial purification of pectinase from red dragon fruit peels, the ammonium sulphate precipitation method and gel filtration chromatographic method (Sephadex G-100) were used. The partially purified pectinase increased 6.49 folds compared to crude enzyme extracts. The Michaelis-Menten constant, K_m , of the crude pectinase enzyme was found to be $0.1992 \times 10^{-2} \text{ g mL}^{-1}$, whereas the partially purified enzyme was $0.358 \times 10^{-2} \text{ g mL}^{-1}$. The reaction order (n) of the pectinase-catalyzed reaction was found to be first order. The activation energy values of the crude and purified pectinase-catalyzed reactions were $5.339 \text{ kcal mol}^{-1}$ and $4.12 \text{ kcal mol}^{-1}$, respectively. The crude and purified pectinase enzymes from red dragon fruit peels were used for the clarification of apple juice. The percent transmittance value of apple juice using purified pectinase was found to be higher (96.38 %) compared to crude pectinase (74.74 %). This study shows the efficiency of pectinase in fruit juice clarification.

Acknowledgements

The authors would like to thank the Myanmar Academy of Arts and Science for giving permission to submit this paper and to Professor and Head, Dr Ni Ni Than, Department of Chemistry, University of Yangon, for her kind suggestion. Special thanks are due to the Department of Chemistry, University of Yangon, for providing the research and analytical facilities.

References

- Anisa, S. K. and K. Girish. (2014). "Pectinolytic Activity of *Rhizopus sp.*, and *Trichoderma viridae*". *International Journal of Research in Pure and Applied Microbiology*, vol. 4 (2), pp. 28-31.
- Bergmeyer, H. U. (1983). *Method of Enzymatic Analysis*. New York: Academic Press Inc., pp. 69-78.
- Berutu, C. A. M., F. Fahrurrozi, and A. Meryandini. (2017). "Pectinase Production and Clarification Treatments of Apple (*Malus Domestica*) Juice". *Annales Bogorienses*, vol. 21 (2), pp. 63–68.
- Joshi, V. K., M. Parmar, and N. Rana. (2011). "Purification and Characterization of Pectinase Produced from Apple Pomace and Evaluation of its Efficacy in Fruit Juice Extraction and Clarification". *Indian Journal of Natural Products and Resources*, vol. 2 (2), pp. 189-197.
- Kashyap, D. R., P. K. Vohra, S. Chopra, and R. Tewari. (2001). "Application of Pectinase in the Commercial Sector: A Review". *Bioresource Technology*, vol. 77 (3), pp. 215-227.
- Kumar, S. (2015). "Role of Enzyme in Fruit Juice Processing and its Quality Enhancement". *Advances in Applied Science Research*, vol. 6(6), pp. 114-124.
- Mazlina, M. K. S., L. A. A. Ghani, A.R. N. Aliaa, H. S. Aslina, and O. Rozita. (2008). "Comparison on Optimization of Star Fruit Juice Using RSM between Two Malaysian Star Fruit Varieties (B11 and B10)". *Pertanika J. Sci. & Technol.*, vol.16 (1), pp.1-13.
- Pauldas, K. and A. Jain. (2018). "Optimization of Pectinase Production Kinetics by *Candida tropicalis* and its Applications in Fruit Juice Clarification". *International Journal of Pharmacy and Biological Sciences*, vol. 8(3), pp. 946-958.
- Pawar, H. (2023). "Role of Enzyme Purification Techniques and its Importance". *Enzyme Engineering*, vol. 12(1), p. 1.
- Robinson, P.K. (2015). "Enzyme: Principles and Biotechnological Applications". *Essays in Biochemistry*, vol. 59, pp. 1-41.

STUDIES ON ENZYMATIC PROPERTIES OF PARTIALLY PURIFIED POLYPHENOL OXIDASE IN CABBAGE (*BRASSICA OLERACEA* L.) AND ITS ANTIMICROBIAL ACTIVITY

May Zin Htay¹, Yee Mun Than², Ye Myint Aung³

Abstract

Extraction and purification of polyphenol oxidase from cabbage (*Brassica oleracea* L.) were performed by ammonium sulphate precipitation (35-85 %) and gel filtration chromatography on Sephadex G-100. Polyphenol oxidase activity was determined using catechol as a substrate at 420 nm. The protein content was also determined by the Biuret method, using Bovine Serum Albumin (BSA) at 550 nm. The optimum pH and temperature of both crude and partially purified polyphenol oxidase enzymes were found to be 7.0 and 40 °C, respectively. The activation energy of the crude polyphenol oxidase-catalyzed reaction was -9.33 kcal mol⁻¹ and that of partially purified enzyme was 6.31 kcal mol⁻¹. The K_m (0.052 M) and V_{max} (3.03 × 10⁻⁵ M min⁻¹) of partially purified polyphenol oxidase were determined by using the Lineweaver-Burk plot. The reaction order (n) of the polyphenol oxidase-catalyzed reaction was calculated by using the linear regression method and it was found to be first order for both crude and partially purified polyphenol oxidase. The crude polyphenol oxidase responded the highest antimicrobial activity against the eight microorganisms tested by the agar well diffusion method.

Keywords: cabbage, *Brassica oleracea* L., polyphenol oxidase, ammonium sulphate precipitation, gel filtration chromatography, antimicrobial activity

Introduction

Polyphenol oxidase (EC 1.10.3.1) is a common copper-containing enzyme that is widely distributed in the plant kingdom. and It also known as tyrosinase, catechol oxidase, and monooxygenase. Polyphenol oxidase (PPO) catalyzes the hydroxylation of monophenols to *o*-diphenols, followed by the oxidation of *o*-diphenols to *o*-quinones in the presence of oxygen (Concellon *et al.*, 2004). These enzymes are very prevalent in nature and are in charge of the enzymatic browning of plant products. Polyphenol oxidase is present in most higher plants, but also in animals and fungi (Zhang, 2023). Enzymatic browning is one of the most limiting factors in the shelf life of fresh-cut fruits and vegetables (Wong *et al.*, 2019). Humans have a polyphenol oxidase enzyme that causes skin pigmentation, including the appearance of freckles. Because polyphenol oxidase activity mechanically ruins food, which results in a browning reaction in the presence of oxygen, many fruits and vegetables, including potatoes, cabbage, lettuce, mushrooms, and eggplants, are lost as a result. These fruits and vegetables include peaches, apricots, apples, grapes, bananas, and strawberries (Güven *et al.*, 2017). Numerous researchers have investigated the use of enzymes in the treatment of wastewater (Murniati *et al.*, 2010). The main aim of research is to study the enzymatic properties of partially purified polyphenol oxidase extracted from cabbage and its antimicrobial activity.

¹ Department of Chemistry, University of Yangon

² Department of Chemistry, University of Yangon

³ Department of Chemistry, University of Yangon

Materials and Methods

Cabbage samples were collected from Hledan Market, Kamayut Township, Yangon Region. Then, identification of the sample was done at the Department of Botany, University of Yangon. Sample extraction and purification were performed at the Analytical Chemistry Research Laboratory, Department of Chemistry, University of Yangon. Dipotassium hydrogen phosphate, potassium dihydrogen phosphate from BDH, and ammonium sulphate from Merck were used. The chemicals required and polyphenol oxidase assay reagents were purchased from Sigma-Aldrich, England.

Extraction and Purification of Polyphenol Oxidase

Cabbage (*Brassica oleracea* L.) was washed with distilled water and dried at room temperature. Cabbage was cut into small pieces. Cabbage (200 g) was homogenized for 5 min using a blender with 200 mL of 0.1 M potassium phosphate buffer pH (7.0) and centrifuged at 6000 rpm for 30 min. After centrifugation, solid ammonium sulphate (45.86 g) was added to the supernatant to give 35 % saturation. After settling for 2 h, the precipitate was removed by centrifugation for 30 min at 6000 rpm and was discarded. Additional ammonium sulphate (79.59 g) was then added to achieve 85 % saturation. After being kept overnight, the precipitate containing polyphenol oxidase was collected by centrifugation for 30 min at 6000 rpm. Crude polyphenol oxidase (2 g) was dissolved in 4 mL of potassium phosphate buffer (pH 7.0). This solution was applied to a Sephadex G-100 gel filtration column previously equilibrated with the same buffer. The flow rate was adjusted to 1.5 mL per 5 min. A 1.5 mL fraction was collected in a test tube. Protein content in each tube was checked by measuring the absorbance at 280 nm and polyphenol oxidase activity was also measure at 420 nm. The fractions that had the highest polyphenol oxidase activity were pooled. The pooled polyphenol oxidase fraction was stored at 4 °C.

Polyphenol Oxidase Enzyme Assay

A spectrophotometric method was used to determine polyphenol oxidase activity on the basis of the initial rate of the absorbance increase at 420 nm (Güven *et al.*, 2017). The reaction mixture consisted of 0.5 mL of potassium phosphate buffer (pH 7.0), 2 mL of catechol (substrate), and 0.5 mL of enzyme extract. The mixture was shaken well and incubated at 37 °C for 10 min. One enzyme unit represents the amount of enzyme that produces a rise of 0.001 absorbance in one minute at 420 nm.

Protein Determination

Protein content of the enzyme solution in each purification step was determined by the Biuret method using a spectrophotometer at 550 nm.

Determination of the Optimum pH and Temperature of Polyphenol Oxidase

Polyphenol oxidase activity was determined in a pH range of 6.4-7.6 at 0.2 unit intervals with a 0.1 M phosphate buffer. In this pH range, enzyme activity was measured using the procedure described for the polyphenol oxidase activity enzyme assay.

Furthermore, polyphenol oxidase activity was determined at different reaction temperatures in the range of 20-60 °C using catechol as substrate, and the phosphate buffer (pH 7) was heated to the relevant temperature before the assay.

Kinetic Studies of Crude and Partially Purified Polyphenol Oxidase Enzymes

The Michaelis-Menten constant (K_m), maximum velocity (V_{max}), and reaction order of of crude and partially purified enzymes-catalyzed reactions were determined using catechol as a substrate with a concentration range of 0.005 M to 0.10 M. For the determination of activation energy, the velocities of polyphenol oxidase catalyzed reaction were measured at the temperature range of 20-40 °C at 5 unit intervals. It was then determined from an Arrhenius plot of the initial velocity data.

Screening of the Antimicrobial Activity of Crude Polyphenol Oxidase from Cabbage

The antimicrobial activity of the crude polyphenol oxidase from cabbage was studied by the agar well diffusion method at the Chemistry Department, Patheingyi University. Eight species of microorganisms: *Agrobacterium tumefaciens*, *Bacillus subtilis*, *Staphylococcus aureus*, *Pseudomonas fluorescens*, *Bacillus pumilus*, *Candida albicans*, *Escherichia coli*, and *Micrococcus luteus* were used for this study.

Results and Discussion

Purification of Polyphenol Oxidase Extracted from Cabbage

The polyphenol oxidase was extracted from cabbage by ammonium sulphate precipitation method and the crude enzyme was obtained. Sephadex G-100 was used to partially purify the crude enzyme. Figure 1 shows the stepwise purification of the polyphenol oxidase on Sephadex G-100 gel. The protein content of the eluate was checked spectrophotometrically at 280 nm, and the enzyme activity was determined at 420 nm. The fractions with the highest activity (20-33 fractions) were collected and pooled. The specific activity of the polyphenol oxidase increased about 3.95 folds over that of the crude extract, and the protein recovery was found to be 18.95 %. The degree of purity of polyphenol oxidase in each purification step is described in Table 1.

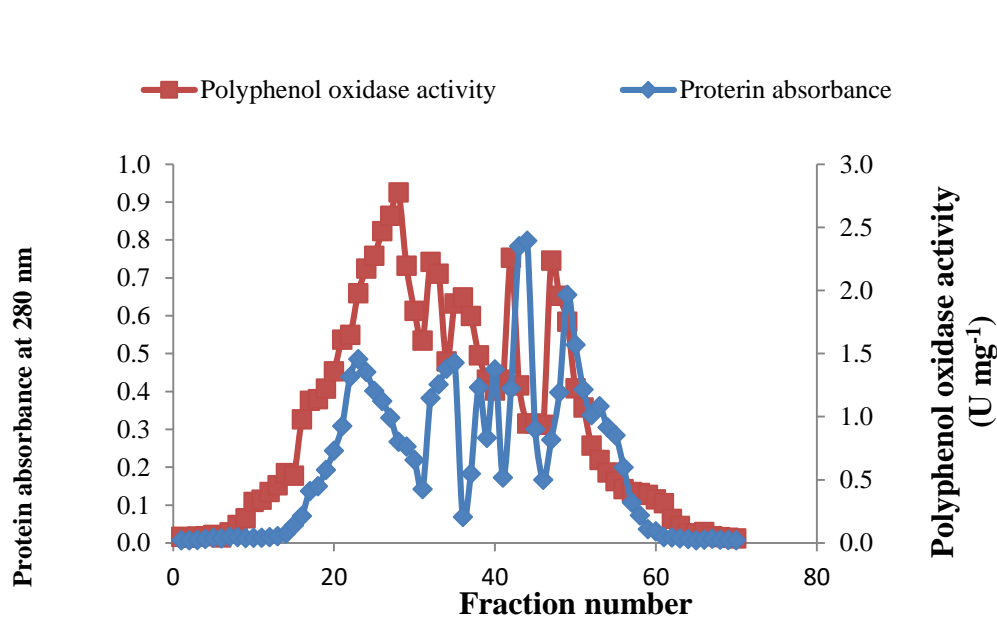


Figure 1. Chromatogram of crude polyphenol oxidase on Sephadex G-100 column

Table 1. Polyphenol Oxidase Activities, Protein Contents and Specific Activities of the Enzyme Solutions at Different Purification Steps

Purification steps	Total volume (mL)	Total protein content (mg)	Total PPO activity (U)	Specific activity (U/mg)	Protein recovery (%)	Degree of purity (fold)
crude	240	530.06	20640	38.94	100.00	1.00
after 35% (NH ₄) ₂ SO ₄	223	400.41	21138	52.79	75.54	1.36
after 85% v(NH ₄) ₂ SO ₄	10	160.33	10600	66.11	30.25	1.69
after passing the Sephadex G-100	20	100.43	15444	153.93	18.95	3.95

Optimum pH and Temperature of Crude and Partially Purified Polyphenol Oxidase

As shown in Figures 2 (a) and (b), optimum pH and temperature of polyphenol oxidase-catalyzed reaction were observed as 7.0 and 40 °C, respectively, using catechol as a substrate. The previous studies also reported that optimum pH was 7.0 for parsley (Lin *et al.*, 2016), artichoke (Dogan *et al.*, 2005), and jackfruit (Tao *et al.*, 2013). Although optimum temperatures of polyphenol oxidase varies among plants depending on the extraction methods and types of substrates used, the optimum temperature is mostly obtained between 30 and 50 °C (Aydin *et al.*, 2015, Sun *et al.*, 2010, Palma-Orozco *et al.*, 2011).

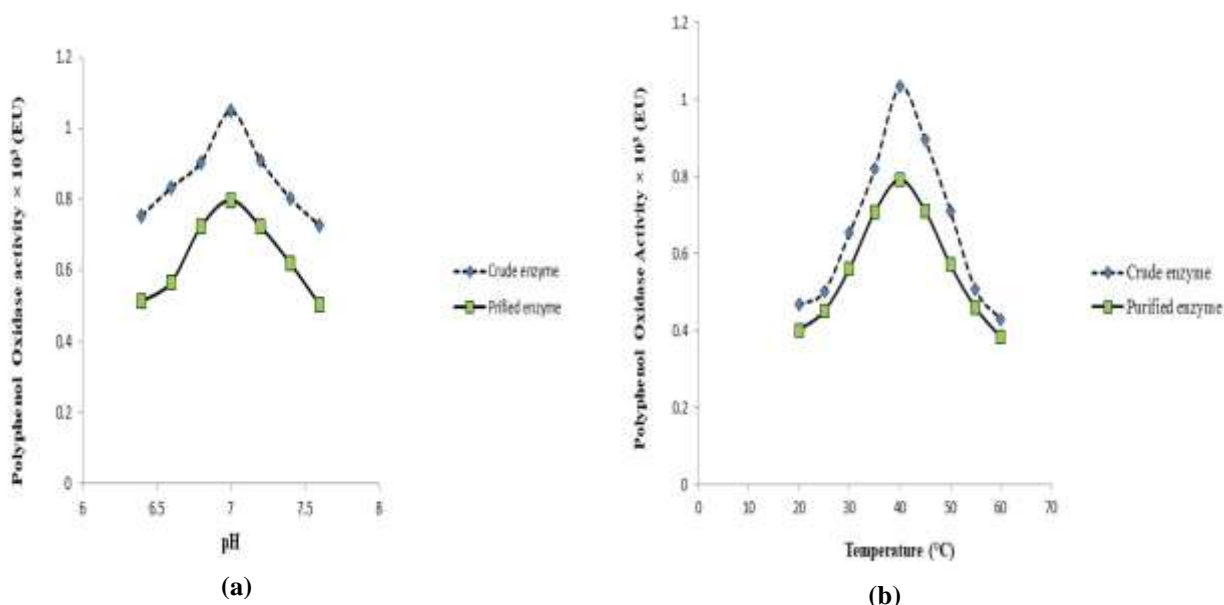


Figure 2. Plots of the crude and partially purified polyphenol oxidase activity as a function of (a) pH and (b) temperature of the solutions

Effect of Substrate Concentration on Polyphenol Oxidase-Catalyzed Reaction

The velocities of crude polyphenol oxidase-catalyzed reactions measured at varying levels of catechol concentration and their reciprocal values are shown in Table 2. In the

Michaelis-Menten plot shown in Figure 3, the velocity of an enzyme-catalyzed reaction is directly proportional to the percentage of the enzymes reacting with the substrate to form an enzyme-substrate complex (Yilmaz., 2020). At this point, the enzyme was said to be saturated with substrate, and further increases in the concentration of the catechol would not increase the velocity of the reaction. The enzyme could have worked no faster, and thus the maximum velocity, V_{max} , can be obtained. The concentration of substrate at which the reaction reaches half its maximum velocity is equal to K_m . For a more accurate estimation of K_m and V_{max} values, these were computed from Lineweaver-Burk (Figure 4) and Eadie-Hofstee plots (Figure 5). Similarly, Table 3 shows the velocities of partially purified polyphenol oxidase-catalyzed reactions at different catechol concentrations. Michaelis-Menten, Lineweaver-Burk, and Eadie-Hofstee plots are depicted in Figures 6, 7, and 8, respectively.

Table 2. Relationship between Velocity of Crude Polyphenol Oxidase-Catalyzed Reaction and Substrate Concentration

[S] (M)	-[S] (M)	1/[S] (M ⁻¹)	V × 10 ⁵ (M min ⁻¹)	1/V × 10 ⁻⁵ (M ⁻¹ min)	V/ [S] × 10 ⁵ (min ⁻¹)	[S]/V × 10 ⁻⁵ (min)
0.005	-0.005	200.0	0.300	3.330	60.00	0.017
0.010	-0.010	100.0	0.550	1.800	55.00	0.018
0.020	-0.020	50.00	0.920	1.086	46.00	0.022
0.030	-0.030	33.33	1.250	0.800	41.60	0.024
0.040	-0.040	25.00	1.490	0.673	37.30	0.027
0.050	-0.050	20.00	1.630	0.613	32.60	0.031
0.060	-0.060	16.64	1.720	0.581	28.60	0.035
0.070	-0.070	14.29	1.760	0.568	25.10	0.039
0.080	-0.080	12.50	1.800	0.555	22.50	0.044
0.090	-0.090	11.11	1.850	0.541	20.55	0.049
0.100	-0.100	10.00	1.870	0.534	18.70	0.053

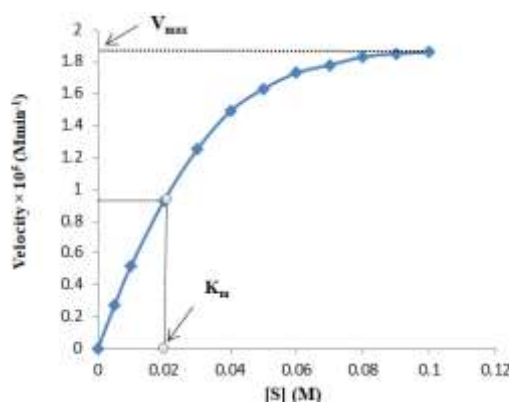


Figure 3. Michaelis-Menten plot of the velocity of crude polyphenol oxidase-catalyzed reaction as a function of substrate concentration

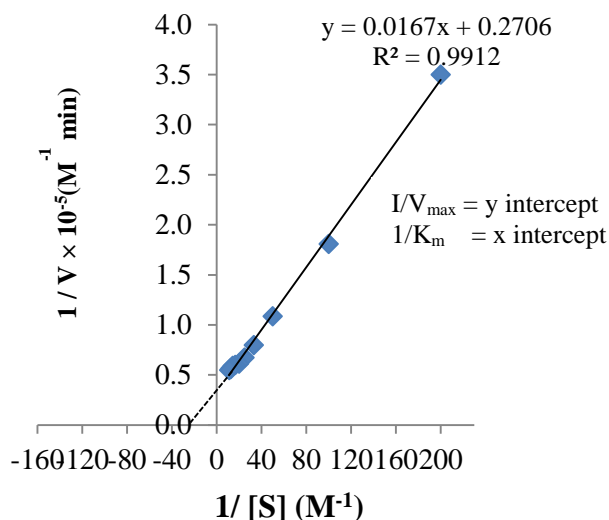


Figure 4. Lineweaver-Burk plot of $1/V$ vs. $1/[S]$ used for graphic evaluation of V_{\max} and K_m for crude polyphenol oxidase

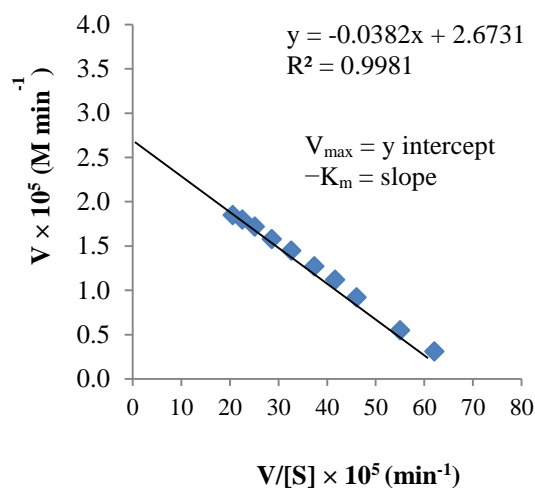


Figure 5. Eadie-Hofstee plot of V vs. $V/[S]$ used for graphic evaluation of V_{\max} and K_m for crude polyphenol oxidase

Table 3. Relationship between Velocity of Partially Purified Polyphenol Oxidase-Catalyzed Reaction and Substrate Concentration

[S] (M)	-[S] (M)	1/[S] (M ⁻¹)	$V \times 10^5$ (M min ⁻¹)	$1/V \times 10^{-5}$ (M ⁻¹ min)	$V/[S] \times 10^5$ (min ⁻¹)	$[S]/V \times 10^{-5}$ (min)
0.005	-0.005	200.0	0.280	3.600	56.00	0.018
0.010	-0.010	100.0	0.510	1.960	51.00	0.020
0.020	-0.020	50.00	0.860	1.160	43.00	0.023
0.030	-0.030	33.33	1.120	0.890	37.33	0.027
0.040	-0.040	25.00	1.340	0.746	33.50	0.030
0.050	-0.050	20.00	1.550	0.650	31.00	0.032
0.060	-0.060	16.64	1.650	0.606	27.33	0.036
0.070	-0.070	14.29	1.740	0.574	24.71	0.040
0.080	-0.080	12.50	1.830	0.546	22.87	0.044
0.090	-0.090	11.11	1.940	0.515	21.56	0.047
0.100	-0.100	10.00	2.030	0.493	20.30	0.049

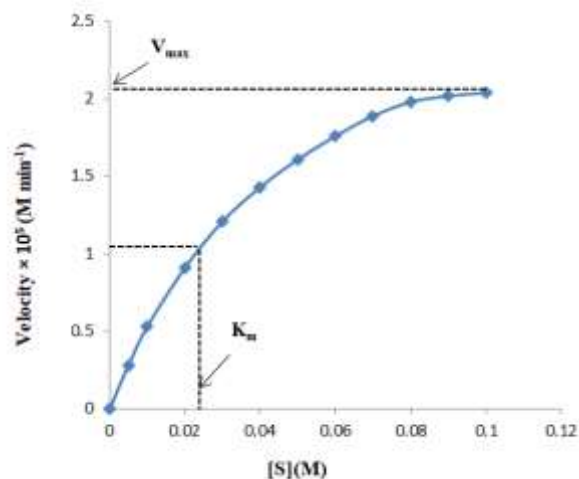


Figure 6. Michaelis-Menten plot of the velocity of partially polyphenol oxidase-catalyzed reaction as a function of substrate concentration

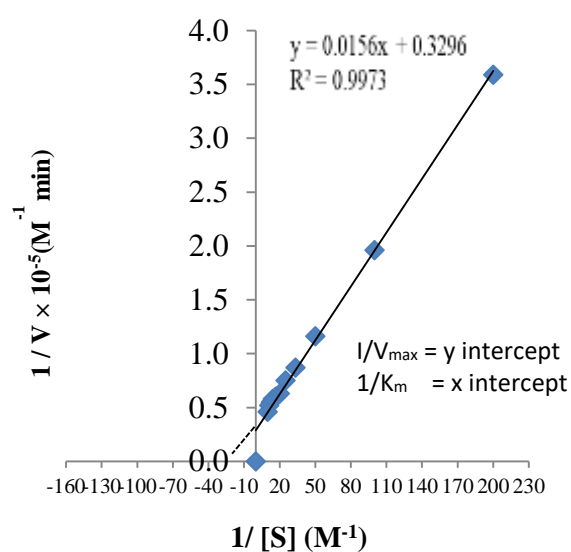


Figure 7. Lineweaver -Burk plot of $1/V$ vs. $1/[S]$ used for graphic evaluation of V_{max} and K_m for partially purified polyphenol oxidase

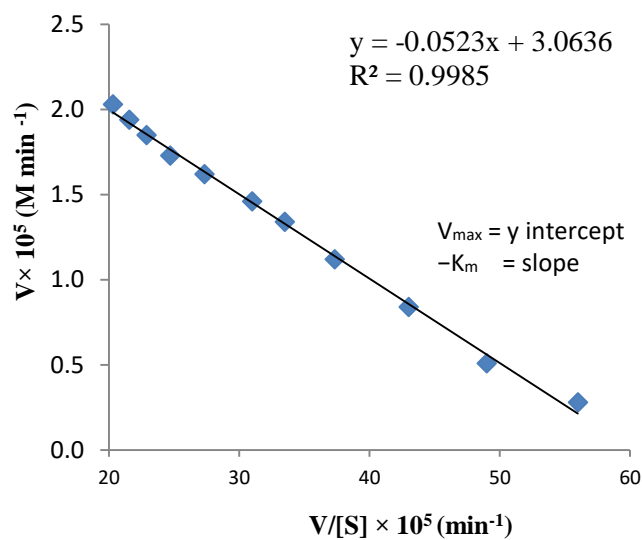


Figure 8. Eadie-Hofstee plot of V vs. $V/[S]$ used for graphic evaluation of V_{max} and K_m for partially purified polyphenol oxidase

Table 4 shows the K_m and V_{max} values of crude and partially purified polyphenol oxidase-catalyzed reactions obtained from graphical methods and linear regression methods.

The K_m and V_{max} values of these two enzymes are not significantly different.

Table 4. Comparison of Kinetic Parameters of Crude and Partially Purified Polyphenol Oxidase from Different Methods

Enzyme	Method	Linear regression method		Graphical method	
		K_m (M)	$V_{max} \times 10^5$ (M min ⁻¹)	K_m (M)	$V_{max} \times 10^5$ (M min ⁻¹)
crude	Michaelis-Menten	-	-	0.020	1.87
	Lineweaver- Burk	0.040	2.77	0.040	2.80
	Eadie-Hofstee	0.040	2.73	0.038	2.67
partially purified	Michaelis-Menten	-	-	0.025	2.03
	Lineweaver- Burk	0.049	3.03	0.052	3.03
	Eadie-Hofstee	0.050	3.03	0.052	3.06

Reaction Order of Polyphenol Oxidase-catalyzed Reaction

Depending on the substrate concentrations, the kinetics of an enzyme-catalyzed reaction may be described by the first-order rate equation (Bergmeyer, 1983). In this study, the 'n' value was determined from the plot of $\text{Log } V/(V_{max} - V)$ vs. $\text{Log } [S]$ for polyphenol oxidase activity using the linear regression method (Table 5 and Figure 9). The reaction order (n) values of crude and purified polyphenol oxidase were calculated to be 0.98 and 1.001, respectively, and thus, it is a first-order reaction.

Table 5. Relationship between $\text{Log } [S]$ and $\text{Log } V/(V_{max}-V)$ for the Determination of Reaction Order of Polyphenol Oxidase-Catalyzed Reaction

[S] (M)	Log [S]	Crude enzyme		Partially purified enzyme	
		$V \times 10^5$ (M min ⁻¹)	Log $V/(V_{max}- V)$	$V \times 10^5$ (M min ⁻¹)	Log $V/(V_{max}- V)$
0.005	-2.301	0.30	-0.908	0.280	-0.979
0.01	-2.000	0.55	-0.607	0.510	-0.714
0.02	-1.700	0.92	-0.304	0.086	-0.402
0.03	-1.520	1.25	-0.085	1.120	-0.232
0.04	-1.400	1.49	-0.065	1.340	-0.100
0.05	-1.301	1.63	0.155	1.550	0.020
0.06	-1.222	1.72	0.214	1.650	0.072
0.07	-1.160	1.76	0.241	1.740	0.124
0.08	-1.110	1.80	0.268	1.830	0.183
0.09	-1.050	1.85	0.303	1.940	0.250
0.10	-1.000	1.87	0.317	2.030	0.307

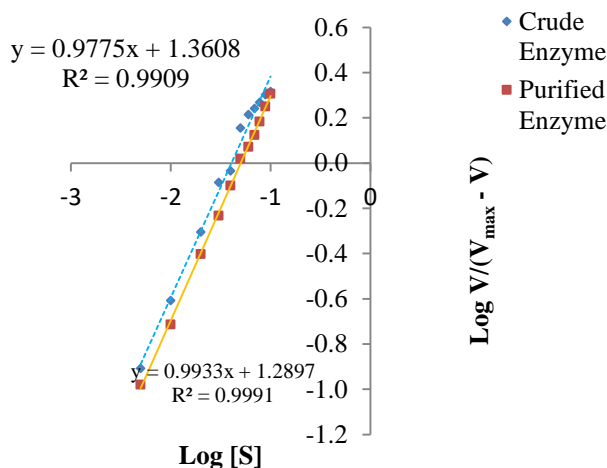


Figure 9. Plot of $\log V/(V_{\max}-V)$ vs $\log [S]$ of polyphenol oxidase- catalyzed reaction

The activation energy (E_a) for enzyme-catalyzed reactions was determined by assaying the enzyme at different temperatures and constructing an Arrhenius plot (Table 6 and Figure 10). The activation energies of crude and partially purified polyphenol oxidase were calculated to be $9.33 \text{ kcal mol}^{-1}$ and $6.31 \text{ kcal mol}^{-1}$, respectively. Moreover, the Arrhenius constants of crude and partially purified polyphenol oxidase were determined to be 3.4824×10^7 and 2.7561×10^5 , respectively.

Table 6. Relationship between Temperature and Velocity of Crude and Purified Polyphenol Oxidase-Catalyzed Reaction

Temperature (°C)	Temperature (K)	$1/T \times 10^3$ (K ⁻¹)	Crude enzyme		Partially purified enzyme	
			Velocity $\times 10^6$	Log V	Velocity $\times 10^6$	Log V
20	293	3.41	5.9	0.750	5.6	0.748
25	298	3.36	6.9	0.830	6.3	0.800
30	303	3.30	9.0	0.950	8.1	0.900
35	308	3.25	11.4	1.056	9.9	0.980
40	313	3.30	14.7	1.166	10.8	1.030

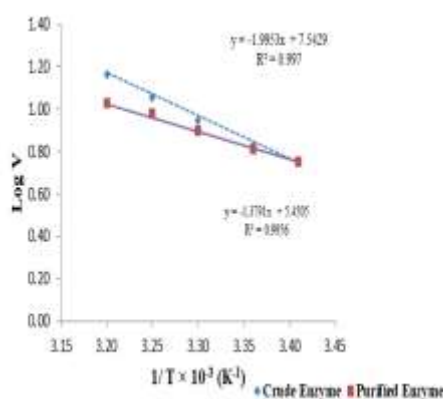


Figure 10. Plot of $\log V$ vs $1/T$ for crude and purified polyphenol oxidase activity

Antimicrobial Activities of the Crude Polyphenol Oxidase Enzyme

The antimicrobial activities were investigated against eight species of microorganisms such as gram-positive bacteria (*Bacillus subtilis*, *Staphylococcus aureus*, *Bacillus pumilus*, and *Micrococcus luteus*), gram-negative bacteria (*Agrobacterium tumefaciens*, *Pseudomonas fluorescens*, and *Escherichia coli*), and gram-positive fungus (*Candida albicans*) by using the agar well diffusion method. In this investigation, the inhibition zone diameters ranged between 26 and 28mm (Figure 10 and Table 7). Crude polyphenol oxidase showed very high antimicrobial activity on all eight microorganisms.

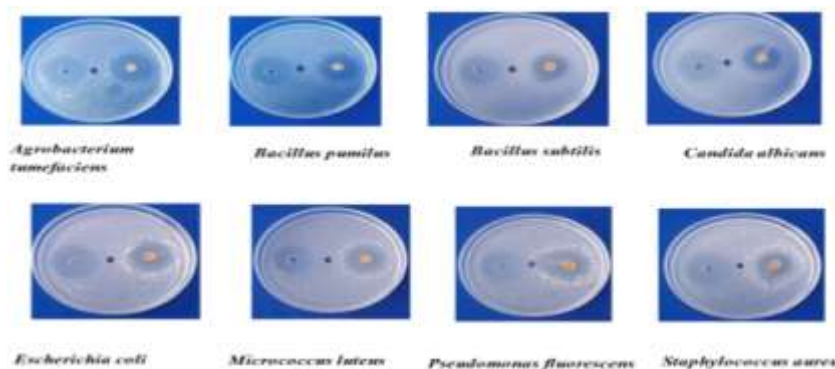


Figure 11. Screening of antimicrobial activity of crude polyphenol oxidase by agar well diffusion method

Table 7. Antimicrobial Activity of Crude Polyphenol Oxidase by Agar Well Diffusion Method

No.	Microorganisms	Inhibition zone diameters (mm)	
		Standard	Enzyme
1	<i>Agrobacterium tumefaciens</i>	28	28
2	<i>Bacillus pumilus</i>	28	27
3	<i>Bacillus subtilis</i>	28	26
4	<i>Escherichia coli</i>	28	26.
5	<i>Micrococcus luteus</i>	29	27
6	<i>Pseudomonas fluorescens</i>	29.	27
7	<i>Staphylococcus aureus</i>	28.	27
8	<i>Candida albicans</i>	29	26

diameter of agar well = 8 mm
 10-14 mm = low activity
 15-19 mm = good activity
 20 mm above = very high activity

standard = chloramphenicol (for bacteria)
 standard = nystatin (for fungus)
 control = potassium phosphate buffer

Conclusion

Polyphenol oxidase from cabbage (*Brassica oleracea* L.) was successfully extracted by using the ammonium sulphate precipitation method (salting out) and partially purified by gel filtration chromatography using Sephadex G-100. The specific activity and relative purity of the enzyme increased by about 3.95 folds. The optimum pH and temperature of polyphenol oxidase were 7 and 40 °C, respectively. The kinetic parameters, K_m and V_{max} of crude and partially purified polyphenol oxidase were determined as 0.040×10^{-5} M and 2.8×10^{-5} M min^{-1} , and 0.052 M and 3.03×10^{-5} M min^{-1} , respectively. The reaction order (n) for both crude and purified polyphenol oxidase was found to be first order. The activation energy of partially purified polyphenol oxidase was lower than that of the crude enzyme. Crude polyphenol oxidase showed very high antimicrobial activity.

Acknowledgements

The authors would like to thank the Myanmar Academy of Arts and Science for giving permission to submit this paper and to Professor and Head, Dr Ni Ni Than, Department of Chemistry, University of Yangon, for her kind suggestion. Special thanks are due to the Department of Chemistry, University of Yangon, for providing the research and analytical facilities.

References

- Aydin, B., I. Gulcin, and S. H. Alwasel. (2015). "Purification and Characterization of Polyphenol Oxidase from Hemşin Apple (*Malus communis* L.)". *International Journal of Food Properties*, vol.18 (12), pp.2735-2745.
- Bergmeyer, H. U. (1983). *Methods of Enzymatic Analysis*. New York: Academic Press Inc., pp. 69-78.
- Concellon, A., M. C. Anon, and A. R. Chaves. (2004). "Characterization and Changes in Polyphenol Oxidase from Eggplant Fruit (*Solanum melongena* L.) during Storage at Low Temperature". *Food Chemistry*, vol. 88 (1), pp. 17-24.
- Dogan, S., Y. Turan, H. Erturk, and O. Arslan. (2005). "Characterization and Purification of Polyphenol Oxidase from Artichoke (*Cynara scolymus* L.)". *Journal of Agricultural and Food Chemistry*, vol.53(3), pp. 776-785.
- Güven, R. G., K. Güven, F. M. Bekler, O. Acer, H. Alkan, and M. Doğru. (2017). "Purification and Characterization of Polyphenol Oxidase from Purslane". *Food Science and Technology*, vol. 37 (3), pp. 356-362.
- Lin, H., A.W.R. Ng, and C. W. Wong. (2016). "Partial Purification and Characterization of Polyphenol Oxidase from Chinese Parsley (*Coriandrum sativum*)". *Food Science and Biotechnology*, vol. 25, pp.91-96.
- Murniati, A., B. Buchari, S. Gandasmita, Z. Nurachman, and N. Nurhanifah. (2010). "Characterization of PPO Application as Phenol Removal in Extracts of Rejected White Oyster Mushrooms (*Pleurotus Ostreatus*)". *Oriental Journal of Chemistry*, vol. 34 (3) , pp. 1457-1468.
- Palma-Orozco, G., A.Ortiz-Moreno, L. Dorantes-Alvarez, J.G. Sampedro, H. and H. Najera. (2011). "Purification and Partial Biochemical Characterization of Polyphenol Oxidase from Mamey (*Pouteria sapota*)". *Phytochemistry*, vol.72 (1), pp.82-88.
- Sun, J. Y., E. G. You, X. Long, and J. Wang. (2010). "Biochemical Properties and Potential Endogenous Substrates of Polyphenol Oxidase from Chufa (*Eleocharis tuberosa*) Corms". *Food Chemistry*, vol.118 (3), pp.799-803.
- Tao, Y. M., Yao, L. Y., Q. Y. Qin, and W. Shen. (2013). "Purification and Characterization of Polyphenol Oxidase from Jackfruit (*Artocarpus heterophyllus*) Bulbs". *Journal of Agricultural and Food Chemistry*, vol.61(51), pp.12662-12669.
- Wong, C. W., K. Y. Ding, and S. V. Anggraeni. (2019). "Aqueous Two-Phase Separation (ATPS) of Polyphenol Oxidase from Lotus Root (*Nelumbo nucifera*) and Its Characterization". vol. 26 (6), pp. 1699-1706.

- Yilmaz, E. (2002). "Kinetics Studies with Crude Tomato Alcohol Dehydrogenase". *Turkish Journal of Agriculture and Forestry*, vol. 26 (3), pp. 141-145.
- Zhang, S. (2023). "Recent Advances of Polyphenol Oxidases in Plants". *College of Food Science and Engineering*, vol. 28 (5), pp. 1-17.

PURIFICATION, BIOLOGICAL PROPERTIES AND PARTIAL STRUCTURAL DETERMINATION OF ANTIBACTERIAL METABOLITES PRODUCED BY *ASPERGILLUS TAMARII*

Moh Moh Htun¹, Zaw Lin Aung², Mar Mar Nyunt³

Abstract

The fungus *Aspergillus tamarii* was isolated from the soil sample of Pone Taung Pone Nyar Area, Magway Region. This fungus showed the antibacterial activity against methicillin resistant *Staphylococcus aureus* (MRSA). The antibacterial metabolites against MRSA were isolated from the toluene extract of the fermented broth by column chromatography. Sephadex LH-20 resin columns were used finally to purify the metabolites. The active fractions eluted from the Sephadex LH-20 column were separately combined and concentrated. These metabolites were checked for purity by thin layer chromatography (TLC), visualized under UV-254 nm and UV-365 nm light. Bioautography on TLC was also carried out to check the retardation factor (R_f) value and purity of the metabolites. From the chromatographic separations, 22.111 mg of metabolite-I and 21.026 mg of metabolite-II were obtained from 0.55 g of the toluene extract of fermented broth. From the physicochemical characterization, UV-vis, and FT IR spectra and comparison with FT IR library, metabolite-I may be a steroid derivative and metabolite-II may be an aromatic derivative compound containing alcohol and carbonyl groups.

Keywords: *Aspergillus tamarii*, metabolites, bioautography, spectroscopy, MRSA

Introduction

Pone Taung Pone Nyar region has been protected under the 1998 law. The fossils in Pone Taung Pone Nyar region are believed to be 4 million years older than the Egyptian counterparts which were thought to be the oldest before (Shwe, 2019). Production of the two antibacterial metabolites from *Aspergillus* was reported in the present research work. This research focuses on the study of the metabolites isolated from the soil sample of Pone Taung Pone Nyar Area. Modern and global healthcare today is facing the problem of multi-resistant bacteria. Many bacterial species have developed resistance mechanisms against several classes of antibiotics in a relatively short period of time after the clinical introduction of antibiotics (Stefan *et al.*, 2011).

From the history of drug discovery from microorganisms, fungal secondary metabolites have provided a number of important drugs (Alberts, 1980). In this study, the isolated soil fungus, *Aspergillus tamarii* of Pone Taung Pone Nyar Area produced antimicrobial substances against methicillin resistant *Staphylococcus aureus* (MRSA). Purifications of antibacterial metabolites were carried out through various chromatography. The functional groups present in the metabolites were studied by FT IR spectroscopic method. The absorption of maximum wavelength of the metabolites was investigated by ultraviolet-visible (UV-vis) spectrophotometry.

¹ Department of Chemistry, Pakokku University

² Department of Botany, Patheingyi University

³ Department of Chemistry, Pakokku University

Materials and Methods

Isolation of Antibacterial Metabolite by Silica Gel Column Chromatography

The silica gel was dissolved in *n*-hexane and column was packed. Concentrated toluene extract (0.55 g) of fermented broth was passed through silica gel column by elution with *n*-hexane and ethyl acetate solvent system in the ratio of (9:1, 4:1 and 7:3, v/v) (Simon and Gray, 1998; Phay, 1999). About 2.5 mL of each fraction was collected individually. One hundred and seven fractions were collected. All these fractions were tested the antibacterial activity against MRSA by paper disc diffusion assay. The active fractions were combined and concentrated separately and named as fraction A and fraction B. The active fractions were then rechromatographed on Sephadex LH-20 column.

Rechromatography of Active Fraction A on Sephadex LH-20 Column

Sephadex LH-20 was dissolved in chloroform and the column was packed. The residue of the active fractions (35-71) which was renamed as fraction A eluted from the silica gel column was transferred on to the Sephadex LH- 20 column and eluted with *n*-hexane. Eleven fractions (1 mL each) were collected. Then methanol was used as eluting solvent and another eleven fractions (1 mL each) were collected. The collected fractions were subjected to assessment of antibacterial activity against MRSA by paper disc diffusion assay.

Rechromatography of Active Fraction B on Sephadex LH-20 Column

The residue of the active fractions (82-94) which was named as fraction B from silica gel column chromatography eluting with *n*-hexane: ethyl acetate (7:3, v/v) solvent system was transferred on to a Sephadex LH- 20 column and eluted with *n*-hexane. Eleven fractions (1 mL each) were collected. Then ethyl acetate was used as another eluting solvent and eleven fractions (1 mL each) were collected. The collected fractions were tested the antibacterial activity by paper disc diffusion assay (Kumar, 2020).

Determination of R_f Value of the Isolated Antibacterial Metabolites

Each dissolved sample (100 μ L) was applied on the TLC plates and allowed to dry. Each TLC plate was developed in the solvent system of benzene: ethyl acetate (4:1, v/v). The TLC plates developed in the solvent systems were allowed to dry and checked under UV (254 nm and 365 nm). Bioautography was also carried out to check the antibacterial activity against MRSA. Each TLC plate was placed on assay agar plates and allowed for 30 min. After 30 minutes, the TLC plates were carefully taken out from the assay plate. Then, the assay plates were incubated for 24 h at 30°C. Clear zones of the active components indicated the presence of bioactive metabolites. The R_f value of active components were measured by localization of spots.

Physicochemical Characterization and Classification of Antibacterial Metabolites

The isolated antibacterial metabolites from the toluene extract of the fermented broth were characterized and classified by determination of their solubility, R_f value, some chemical tests and modern spectroscopic techniques such as UV-visible and FT IR spectrometry.

Determination of Some Chemical Properties of Isolated Metabolites

The isolated antibacterial metabolites were subjected to TLC analysis and then treated with some reagents such as 5% H_2SO_4 , I_2 vapour, Liebermann-Burchard reagent, 5% $FeCl_3$

solution, 2,4-dinitrophenylhydrazine solution and hydroxamic acid test to study their behaviors on TLC and in test tube.

Study on UV-Visible Spectroscopy of Isolated Metabolites

The maximum wavelength of absorption of the metabolites was recorded and examined by UV 1800-UV spectrometer at the Department of Chemistry, Mandalay University and Department of Chemistry, Patheingyi University. UV-Visible spectroscopy of isolated metabolites was studied by the method of Diffey, 2023.

Determination of Functional Groups of Isolated Metabolites by FT IR Spectrometry

The function groups present in the isolated metabolites were studied by Fourier Transform Infrared Spectrophotometer (Perkin Elmer Spectrum Version 10.4.00) at the Department of Chemistry, Mandalay University. Determination of functional groups was studied by the methods of Silverstein *et al.*, 2005; Deng *et al.*, 2014.

Results and Discussion

Isolation of Antibacterial Metabolites by Silica Gel Column Chromatography

According to column chromatography, totally one hundred and seven fractions were collected. Each fraction was subjected to antibacterial activity against MRSA. It was found that fraction numbers (35-71) showed the activity on MRSA. These fractions were combined and renamed as fraction-A. It was also found that fraction numbers (82-94) showed the activity against MRSA. The fractions (82-94) were combined and renamed as fraction-B. The results are tabulated in Table 1 and the antimicrobial activities are shown in Figures 1 and 2. The resultant active fraction-A and B were needed to purify further to produce the bioactive metabolites. These active fractions- A and B were concentrated separately on rotary evaporator and were rechromatographed on Sephadex LH-20 resin column.

Table 1. Activity Against MRSA of the Fractions Eluted from Silica Gel Column Chromatography

Eluting solvent	Fraction No.	Activity
<i>n</i> -Hexane: EtOAc (9:1, v/v)	1-29	No activity
	30-34	No activity
<i>n</i> -Hexane: EtOAc (4:1, v/v)	35-71 (A)	Activity
	72-75	No activity
	76-81	No activity
<i>n</i> -Hexane: EtOAc(7:3, v/v)	82-94 (B)	Activity
	95-107	No activity



Figure 1. Antibacterial activity against MRSA of fractions 1-32 eluted from silica gel column chromatography

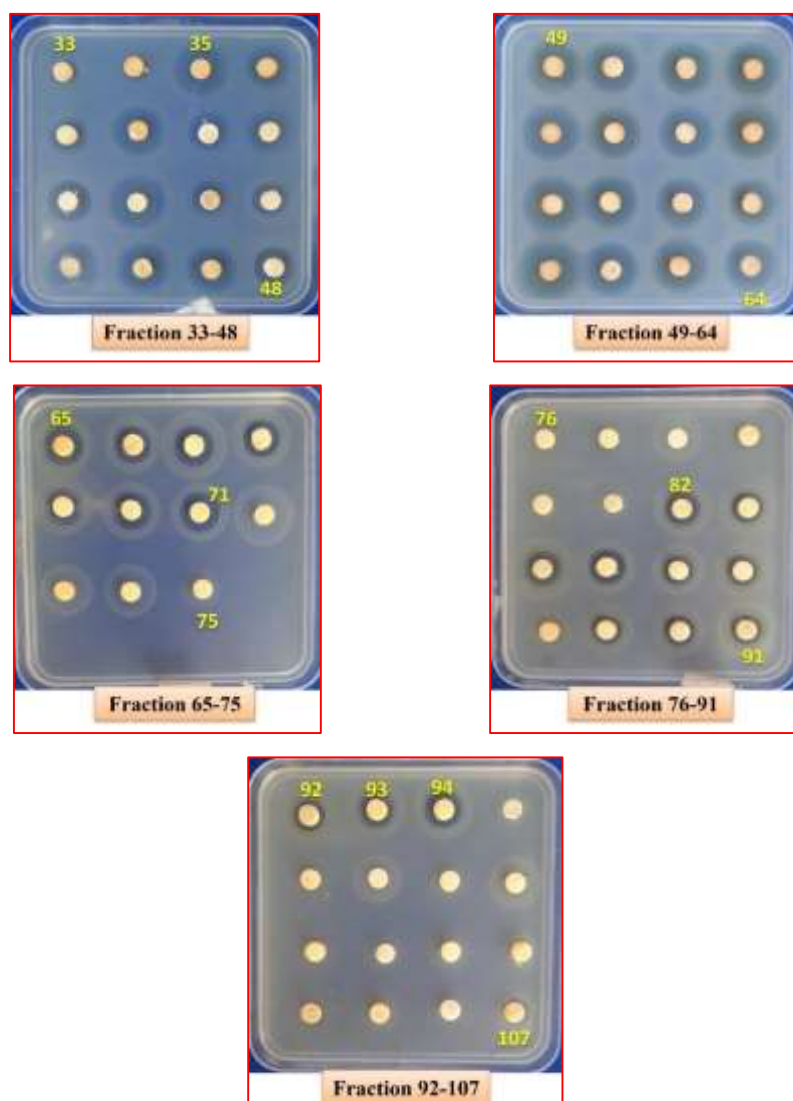


Figure 2. Antibacterial activity against MRSA of fractions 33-107 eluted from silica gel column chromatography

Rechromatography of Active Fraction A on Sephadex LH-20 Column

Active fraction-A was rechromatographed on Sephadex LH-20 using *n*-hexane and methanol as eluting solvent. Twenty two fractions were collected and tested for antibacterial activity against MRSA as shown in Table 2 and Figure 3. Active fractions were combined and concentrated. Then it was crystallized to yield 22.11 mg of metabolite-I.

Table 2. Activity Against MRSA of Fractions Eluted from Re-chromatography of Active Fraction A by Sephadex LH-20 Resin Column

Eluting solvent	Fraction No.	Antibacterial Activity
<i>n</i> -Hexane	1-11	No activity
	12	No activity
Methanol	13-15	Activity
	16-22	No activity



Figure 3. Paper disc diffusion assay for antibacterial activity against MRSA

Rechromatography of Active Fraction B on Sephadex LH-20 Column

Active fraction-B was rechromatographed by Sephadex LH-20 using *n*-hexane and ethyl acetate. Active fractionated compound (13-14) from Sephadex LH-20 column chromatography developed by ethyl acetate was combined and concentrated. It was denoted as Metabolite-II. The results are shown in Table 3 and Figure 4.

Table 3. Activity Against MRSA of Fractions Eluted from Rechromatography of Active Fraction B by Sephadex LH-20 Column

Eluting solvent	Fraction No.	Antibacterial Activity
<i>n</i> -Hexane	1-11	No activity
	12	No activity
Ethyl Acetate	13-14	Activity
	15-22	No activity

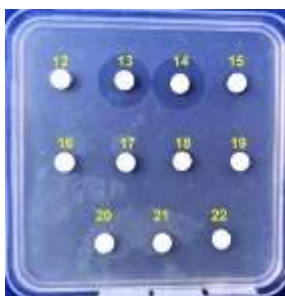


Figure 4. Paper disc diffusion assay for antibacterial activity against MRSA

Determination of R_f Values by Thin Layer Chromatography and Bioautography

In the TLC check of metabolite-I and metabolite-II by UV-254 nm and UV-365 nm, it was found that one active spot for each was found under the short wave and the long wave. The R_f value of metabolite-I was 0.65 and that of the metabolite-II was 0.47 when using the solvent system of benzene: ethyl acetate (4:1, v/v). Bioautography of TLC also showed the activity at the same R_f values with the same eluting solvent system as observed under UV-254 nm and UV-365 nm lights. TLC chromatograms of these purified metabolites are shown in Figures 5 and 6.

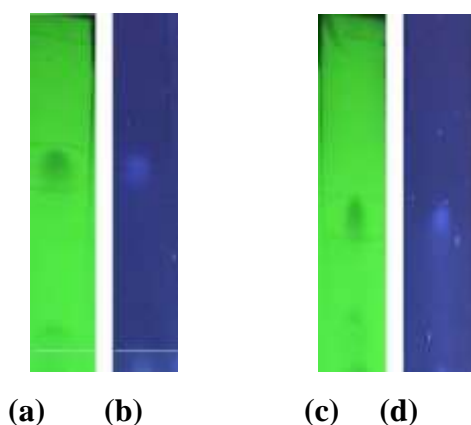


Figure 5. TLC of metabolite-I and metabolite-II under UV light
 (a)metabolite-I under UV 254 nm (b) metabolite-I under UV 365 nm
 (c) metabolite-II under UV 254 nm (d) metabolite-II under UV 365 nm

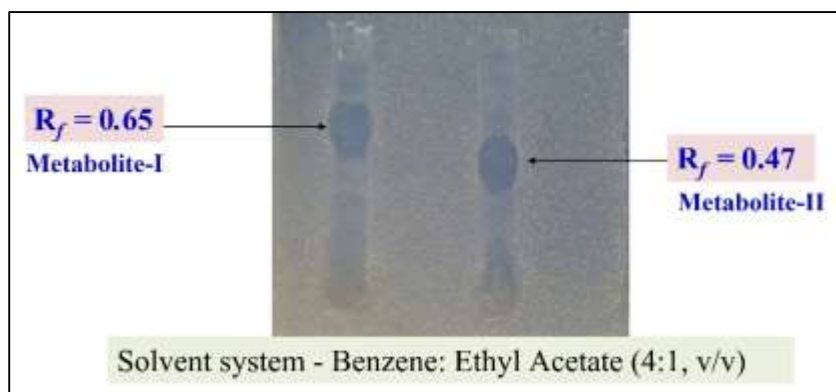


Figure 6. Bioautography of TLC

Physicochemical Characterization and Classification of the Isolated Metabolite-I

The metabolite-1 was firstly characterized by its physical properties such as solubility, R_f value and by some chemical reagent tests. The results for metabolite-I are summarized in Tables 4 and 5 and UV and FT IR spectral data are described in Tables 6 and 7 and Figures 7 and 8.

The solubility of metabolite-I was determined in various solvents. It was found that metabolite-I is soluble in methanol, ethanol, toluene and ethyl acetate; slightly soluble in benzene, dichloromethane and distilled water and insoluble in *n*-hexane and chloroform.

The R_f value of metabolite-I was found to be 0.65 in benzene: ethyl acetate (4:1, v/v) solvent system. According to the results obtained from chemical tests, metabolite-I gave yellow spot on the TLC chromatogram with iodine vapor while spraying with 5% H_2SO_4 followed by heating gave a pink spot. It gave green solution when treated with Liebermann-Burchard reagent, orange yellow precipitates when treated with 2,4-DNP reagent. Therefore, metabolite-I may be classified as a steroidal derivative containing carbonyl group.

In the UV absorption spectrum, maximum absorption bands at λ_{max} 234 nm and 248 nm indicating the $\pi \rightarrow \pi^*$ transition of electrons and at λ_{max} 273 nm was due to $n \rightarrow \pi^*$ transition of the nonbonding electron of carbonyl group.

The functional groups of metabolite-I were assigned by FT IR spectroscopy. According to the FT IR spectrum, physicochemical characterization, UV spectroscopic analysis and comparison with FT IR library, the isolated metabolite-I may be a derivative of steroid.

Table 4. Physical State, Color and R_f Value of Isolated Metabolite-I

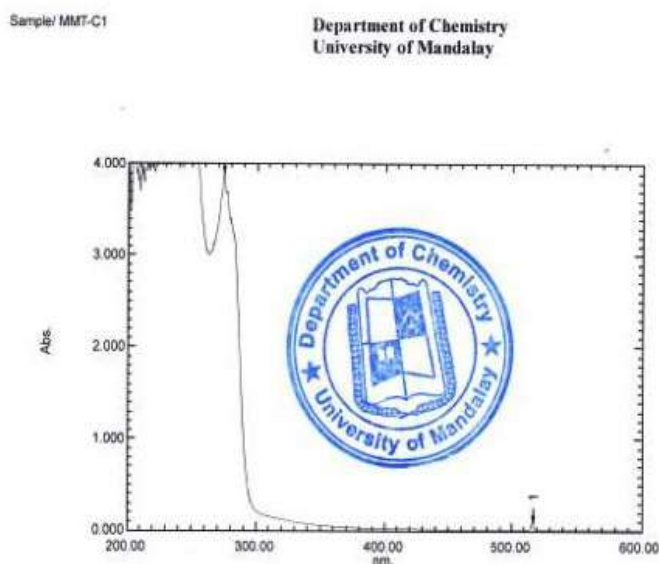
Isolated Metabolite	Physical State	Color	R_f Value	Solvent System
Metabolite-I	Solid	Pale Yellow	0.65	Benzene: EtOAc (4:1, v/v)

Table 5. Some Chemical Reagent Tests of Isolated Metabolite-I

Reagent	Observation	Remark
5% H_2SO_4	pink (on TLC)	C=O present
I_2 vapour	yellow (on TLC)	C=C present
5% $FeCl_3$	no change in colour	Phenolic OH group is absent.
Liebermann-Burchard	green coloration	It may be a steroid.
Hydroxamic acid test	no change in colour	Ester group is absent.
2, 4-DNP	orange yellow precipitate	C=O group of aldehyde or ketone present
Mg, HCl (conc:)	no red coloration	flavonoid absent

Table 6. UV Spectral Data of Isolated Metabolite-I

Solvent Used	Observed λ_{\max} (nm)	Remark
Methanol	234, 248	$\pi \rightarrow \pi^*$ electron transition due to conjugated π bonds
Methanol	274	$n \rightarrow \pi^*$ nonbonding electron transition due to conjugated π system

**Figure 7.** UV-visible spectrum of isolated metabolite-I**Table 7. Interpretation of FTIR Spectra (Metabolite-I)**

No.	Metabolite-I (cm^{-1})	Literature Value*(cm^{-1})	Band Assignment
1	3433.29	3600-3200	-OH stretching vibration of alcohol group
2	3050.27	3100-3000	=C-H stretching vibration of olefinic group
3	2962.66, 2931.80, 2862.36	2962-2840	-C-H asym & sym stretching vibration of -CH ₂ and CH ₃ groups
4	1728.22	1720-1710	-C=O stretching vibration of cyclic ketone
5	1597.06, 1581.63	1600-1450	-C=C stretching vibration of alkenic group
6	1465.90	1475-1445	-C-H asymmetric bending vibration of CH ₃

No.	Metabolite-I (cm ⁻¹)	Literature Value*(cm ⁻¹)	Band Assignment
			group
7	1381.03	1390-1370	-C-H symmetric bending vibration of methylene and methyl group
8	1280.73	1260-1000	-C-C-O asymmetric stretching vibration of alcohol group
9	1126.43, 1072.42	1150-1085	C-F stretching frequency
10	740.67	900-675	-C-H out of plane bending of cis alkenic group

*Silverstein *et al.*,2005

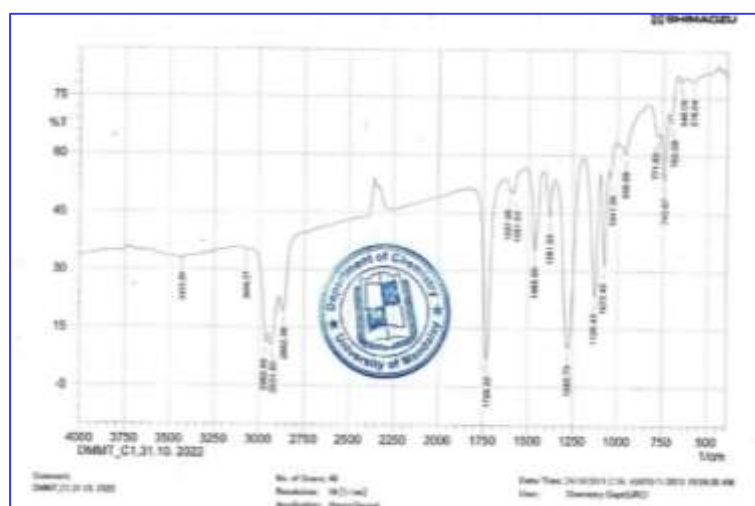


Figure 8. FT IR spectrum of metabolite-I

Physicochemical Characterization and Classification of the Isolated Metabolite-II

Physicochemical characterization and classification of the isolated metabolite-II were also undertaken. The isolated antibacterial metabolite-II from the toluene extract of the fermented broth of *A. tamarii* was firstly characterized by its physical properties such as solubility, R_f values and by some chemical reagent tests. The results for metabolite-II are summarized in Tables 8 and 9 and UV and FT IR spectral data are described in Tables 10 and 11 and Figures 9 and 10.

The solubility of metabolite-II was determined in various solvents. It was found that metabolite-II is soluble in methanol, ethanol, toluene and ethyl acetate; slightly soluble in benzene, dichloromethane and distilled water; and insoluble in *n*-hexane and chloroform.

The R_f value of metabolite-II was found to be 0.47 in benzene: ethyl acetate (4:1, v/v) solvent system. According to the results obtained from chemical tests, metabolite-II gave yellow spot on the TLC chromatogram with iodine vapor while spraying with 5% H_2SO_4 followed by heating gave a pale-yellow spot. There was a change in colour on TLC chromatogram by spraying with 5% $FeCl_3$. This metabolite did not give green solution when treated with

Liebermann-Burchard reagent. Orange yellow precipitates were found when treated with 2, 4-DNP reagent. Therefore, metabolite-II may be classified as aromatic derivative compound.

In the UV absorption spectrum, maximum absorption bands at λ_{\max} 224nm, 232nm and 254 nm indicating the $\pi \rightarrow \pi^*$ transition of electrons due to conjugated π bond.

The functional groups of metabolite-II were assigned by FT IR spectroscopy. Based on the FT IR spectrum, UV spectroscopic analysis and chemical tests, it was suggested that metabolite-II may be classified as aromatic derivative compound containing alcohol group and carbonyl group.

Table 8. Physical State, Colour and R_f Value of Isolated Metabolite-II

Isolated Metabolite	Physical State	Colour	R_f Value	Solvent System
Metabolite-II	Solid	White	0.47	Benzene: Ethyl Acetate (4:1, v/v)

Table 9. Some Chemical Reagent Tests of Isolated Metabolite-II

Reagent	Observation	Remark
5% H ₂ SO ₄	pale yellow (on TLC)	O-H or C=O present
I ₂ vapour	yellow (on TLC)	C=C present
5% FeCl ₃	change in colour	phenolic derivative
Liebermann-Burchard	not detected	It may not a steroid.
Hydroxamic acid test	no change in colour	Ester group is absent.
2, 4-DNP	orange yellow precipitate	C=O group of aldehyde or ketone present
Mg, HCl (conc:)	no red coloration	flavonoid absent

Table 10. UV Spectral Data of Isolated Metabolite-II

Solvent used	Observed λ_{\max} (nm)	Remark
Methanol	224, 232, 254	$\pi \rightarrow \pi^*$ electron transition due to conjugated π bonds

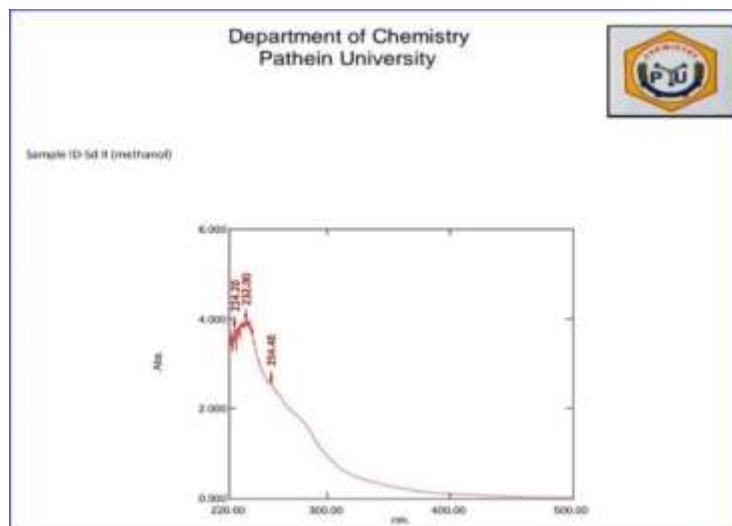


Figure 9. UV-visible spectrum of metabolite-II

Table 11. Interpretation of FTIR Spectra (Metabolite-II)

Sr.	Metabolite-II (cm^{-1})	Literature Value*(cm^{-1})	Band Assignment
1	3433.29	3600-3200	-OH stretching vibration of alcohol group
2	3020.27	3100-3000	=C-H stretching vibration of aromatic ring
3	2924.09, 2854.65	2962-2840	-C-H asym & sym stretching vibration of -CH ₂ and CH ₃ groups
4	1743.65	1810-1715	-C=O stretching vibration of lactone and ester
5	1627.95, 1604.77,	1600-1400	-C=C stretching vibration of alkenic group
6	1465.90, 1411.89	1475-1400	-C-H asymmetric bending vibration of CH ₃ group
7	1381	1390-1370	-C-H symmetric bending vibration of CH ₃ and - CH ₂ group
8	1103.28	1260-1000	-C-C-O asym stretching vibration of alcohol group
9	740.67	900-675	-C-H out of plane bending of aromatic group

*Silverstein *et al.*, 2005

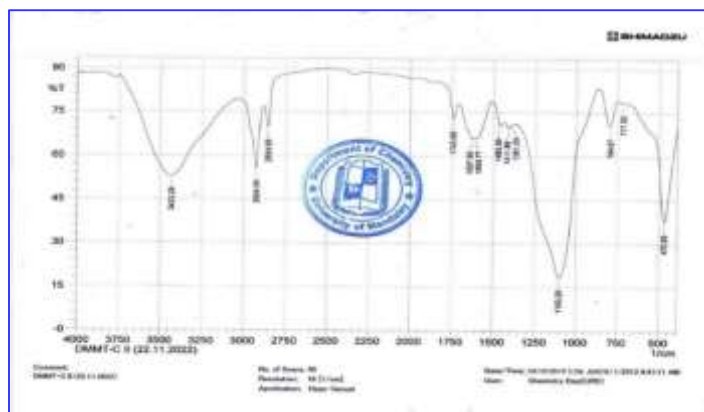


Figure 10. FT IR spectrum of metabolite-II

Conclusion

This study successfully isolated and partially characterized two antibacterial metabolites (metabolite-I and metabolite-II) produced by the soil fungus *Aspergillus tamarii* from Pone Taung Pone Nyar Area, Magway Region. Both metabolites exhibited promising activity against Methicillin-Resistant *Staphylococcus aureus* (MRSA), a multidrug-resistant pathogen posing a significant threat to global health. These findings suggest that *A. tamarii* from this specific region could be a valuable source of novel antibiotics for combating drug-resistant bacteria. Further research on the complete structural elucidation and optimization of these metabolites' potency and selectivity is warranted to translate this discovery into potential therapeutic applications.

Acknowledgements

The authors would like to express our gratitude to the Department of Higher Education, Ministry of Education, Myanmar, for the permission of doing this research and also to the Myanmar Academy of Arts and Science for allowing to present this paper.

References

- Alberts, A. W. (1980). "Mevinolin: A Highly Potent Competitive Inhibitor of Hydroxymethylglutaryl-coenzyme A Reductase and a Cholesterol-lowering agent". *Proc. Natl. Acad. Sci. USA*, vol. **77**, pp. 3957-3961
- Deng Y., Y. Ju, Z. Lu, F. Lu, D. Yan and X. Bie. (2014). "Identification of 4"-isovaleryl-spiramycin III Produced by *Bacillus sp*". *Arch Microbiol*, vol. **196**, pp. 87-95
- Diffey, B. L. (2023). "Sources and Measurement of Ultraviolet Radiation. Methods". vol. **28** (1), pp. 4-13
- Jones, R. J. (2008). "Key Considerations in the Treatment of Complicated Staphylococcal Infections". *Clin Microbiol Infect*, vol. **14**, pp. 3-9
- Kumar, N., R. K. Singh, S. K. Mishra, A. K. Singh and U. C. Pachouri. (2010). "Isolation and Screening of Soil Actinomycetes as Source of Antibiotics Active Against Bacteria". *Inter. J. Microbiology Research*, vol. **2** (2), pp. 12-16
- Phay, N. (1999). "Fistulosin, Antifungal Compound from Welsh onion". *J. Phytochemistry*, vol. **52**, pp. 271-274
- Shwe, K.K. (2019). "Bid for Pone Taung Pone Nyar Heritage Listing". *J. Myanmar Times*. 15th Jan, 2019
- Simon, G., and A. I. Gray. (1998). "Isolation by Planer Chromatography". *Method in Biotechnology*, vol. **4**, pp. 209-245

- Silverstein, R.M., F. X. Webster and D. J. Kiemle. (2005). "Spectrometric Identification of Organic Compounds". Hoboken: 7th Edn, John Wiley & Sons, Inc., New York, pp. 105-119
- Stefan, S. K., G. U If, E. Hesham, B. Lars, L. Joakim, O. Bjorn and C. Erja. (2011). "Antimicrobial Activity of Filamentous Fungi isolated from Highly Antibiotic Contaminated River Sediment". *J. Infection Ecology and Epidemiology*, **14** (7), pp. 344-348

TREATMENT OF LOW QUALITY SOIL WITH PREPARED BIOFERTILIZERS AND CULTIVATION OF CUCUMBER, *CUCUMIS SATIVUS L.*

Ko Ko Aung¹, Sabai Phyu², Su Myat Soe³

Abstract

Fertilizer application is known to increase crop yields and mitigate net soil nutrient mining due to continuous removal. In this paper, the effect of three biofertilizers (C1, C2 and C3) containing (2:1:1), (1:2:1) and (1:1:2) in the ratio of chicken manure, coconut husk powder, rice husk ash and indigenous microorganisms is used as digestion agent. Cultivation of cucumber was carried out with three prepared biofertilizer with the help of fish amino acid as foliar spray and oriental herbal nutrient as insect repellent on low quality soil in Sidi Village, Bago Region. Physicochemical properties of ingredient of natural farming were measured. Field experiments were carried out at Sidi Village in Bago Region from 1st March 2022 to 15th April 2022. The effects of bio-fertilizers (C1, C2, C3 and Control) on growth, yield and plant morphology of cucumber were studied. In this study, the prepared biofertilizer "C1" is the best for cultivation of cucumber in summer. After harvesting, physicochemical properties, texture and nutrient values of the soil before and after cultivation were compared. Soil texture and nutrient values after cultivation were better than before cultivation. Therefore, the prepared biofertilizer C1 was used for treatment of low quality soil. This study concluded that application of biofertilizer significantly increases the yield, biomass production of the soil and was economically efficient.

Keywords: biofertilizer, cultivation, indigenous microorganisms, fish amino acid, oriental herbal nutrient

Introduction

Fertilizer is any organic or inorganic materials of natural or synthetic origin that is added to a soil to supply one or more plant nutrients essential to the growth of plants (Parr *et al.*, 1992). Fertilizer is substance containing some or all of a range of about 20 chemical elements necessary for healthy plant growth, use to compensate for the deficiencies of poor or depleted soil (Rajni *et al.*, 2001). Fertilizers are broadly divided into organic fertilizers (composed of organic matter of plant or animal) or inorganic fertilizers (composed of synthetic chemical and minerals) (Barker and Pileam, 2007). Fertilizer, natural or artificial substance contains the chemical elements that improve growth and productiveness of plants (Audu and Zubairu, 2013).

Fertilizers are applied to crops both as solid and as liquid. About 90% of fertilizers are applied as solids. Solid fertilizer is typically granulated or powdered. Fertilizer burn can occur when too much fertilizer is applied, resulting in damage or even death of the plant (Bhatia, 2010). Fertilizers are able to provide a better growing condition for plants compared to natural soil (Chow, 2002). Fertilizers provide large amount of macronutrients such as nitrogen, phosphorus and potassium while natural soil may not contain sufficient amount of this macronutrients. Fertilizers also provide trace elements such as magnesium, calcium and copper that are crucial in plant growth (Tan, 2015).

In this study, biofertilizers were prepared from organic waste materials (chicken manure, coconut husk powder and rice husk ash). In the first part of this research, some physicochemical

¹ Department of Chemistry, Bago University

² Department of Chemistry, West Yangon University

³ Department of Chemistry, Bago University

properties of raw materials (chicken manure, coconut husk powder and rice husk ash) were determined. The second part was concerned with the preparation of bio-fertilizers from raw materials. The third part dealt with the effect of bio-fertilizers on the growth and yields of cucumber on low quality soil on summer. The last part included the comparison between soil parameters of uncultivated and harvesting soil.

Materials and Methods

The scientific name of *Cucumis sativus* L. (cucumber) belonging to the family cucurbitaceae was identified by authorized botanist at Botany Department, Bago University.

Collection of Samples

Coconut husk powder and rice husk ash were collected from Sidi Village, Bago Region. The chicken manure was collected from Sarkalay Quing Village, Bago Region.

Preparation of chicken manure, coconut husk powder and rice husk ash

Chicken manure, coconut husk powder and rice husk ash were dried in room temperature and ground in grinding machine to obtain chicken manure powder, coconut husk powder and rice husk ash powder. These powders were sieved with 80 mesh size sieve to obtain dry and fine powder. These samples were stored in the air-tight container so that the samples were free from getting molds to prevent moisture as well as other contaminations and were ready to be used for the experimental works.

Preparation of indigenous microorganisms

Indigenous microorganisms (IMO) was prepared using steam rice and brown sugar. Steam rice was mixed with the brown sugar in a ratio of 1:1 and the treatment was left for three weeks. After three weeks, IMO was used as decaying matter for composting processes.

Preparation of chicken manure biofertilizer

Three composted piles were prepared by plastic sheets and the size of each pile was approximately 1.5 meter length, 1.5 meter width and 1.5 meter height. Bio-fertilizers can be prepared with chicken manure, coconut husk powder and rice husk ash in the ratios of 2: 1: 1 (C-1), 1: 2: 1 (C-2), and 1: 1: 2 (C-3) with the addition of indigenous microorganism (IMO) by compost heap layer method. Temperature was key parameter, which determined the success of composting operations. During the composting process temperatures of three different composting piles were measured at 9 am daily. The daily temperature of compost was recorded up to 90 days. After three months later, the compost became ready to use on the field.

Preparation of fish amino acid fertilizer

Fish amino acid (FAA), a liquid organic fertilizer was prepared using the waste product from the fish and brown sugar. A waste product from the fish was mixed with the brown sugar in a ratio of 1:1 and the treatment was left for three weeks. After three weeks, the solution was filtered and FAA was diluted with distilled water in a ratio of 1: 1000. It was used as foliar spray.

Preparation of oriental herbal nutrient

Oriental herbal nutrient (OHN) was prepared using ginger waste and brown sugar. The ginger waste was mixed with the brown sugar with 1:1 weight ratio (g) and the mixture was left for three weeks. After three weeks, equal amount of edible alcohol (v/v) was added in the mixture and stored for two weeks. After two weeks, the solution was filtered and OHN was diluted with distilled water in a ratio of 1: 1000. It was used as insect repellent for plant.

Physicochemical Properties, Nutrient Values of Raw Materials, Prepared BioFertilizer, Soil before and After Cultivation

Physicochemical properties of (chicken manure, coconut husk powder and rice husk ash) raw materials, selected biofertilizer, soil before and after cultivation were studied. Measurement of pH was carried out by a pH meter and the moisture content was determined by a moisture analyzer. The electrical conductivity was determined by a conductivity meter. The nitrogen content was determined by Kjeldahl's method. The potassium content was determined by Flame photometric technique and the phosphorus content was determined by UV-visible spectrophotometric technique. Calcium and magnesium contents were determined by titration method.

Application of Bio-Fertilizer

Field experiments were carried out at Sidi Village in Bago Region from 1st March 2022 to 15th April 2022 and were also studied with the effect of biofertilizers (C-1, C-2, C-3 and control) on growth and yields of cucumber. Foliar spray of FAA and the use of OHN as an insect repellent were employed during the cultivation process.

Determination of plants morphology for field experiment

Plant morphology was measured on 15 days, 30 days and 45 days after cultivation. Plant height, fruit length, number of fruit per plant, root length and total yields were measured for experiment until.

Comparison between Physicochemical Parameters, Nutrient Values and Texture of Selected Soil before and After Cultivation

The original soil was not good for cultivation. After addition of biofertilizer, the quality of soil was suitable for plantation. So, the prepared biofertilizer can be used to treat the low quality soil. Physicochemical parameters, nutrient values and texture of selected soil were determined before cultivation and after harvesting.

Results and Discussion

Some Physicochemical Properties of Chicken Manure, Coconut Husk Powder and Rice Husk Ash

Before preparing biofertilizers, some physicochemical properties and nutrient values of raw materials (chicken manure, coconut husk powder and rice husk ash) were determined. Tables 1 and 2 show some physicochemical properties, N, P, K, Ca and Mg contents of prepared raw materials.

Table 1. Physicochemical Properties of Chicken Manure, Coconut Husk Powder and Rice Husk Ash

Parameters	Physicochemical properties		
	Chicken mnure	Coconut husk powder	Rice husk ash
Moisture (%)	2.00	14.06	2.67
Ash (%)	16.34	5.55	92.65
pH	7.30	7.40	7.60
Bulk density (g/mL)	0.31	0.36	0.27
Organic carbon (%)	48.76	54.60	25.35

Table 2. N, P, K, Ca and Mg Contents of Raw Materials (Chicken Manure, Coconut Husk Powder and Rice Husk Ash)

Parameters	Nutrient Values		
	Chicken manure	Coconut husk powder	Rice husk ash
Nitrogen (%)	2.03	1.31	0.70
Phosphorus P ₂ O ₅ (%)	3.10	2.90	2.10
Potassium K ₂ O (%)	4.48	4.17	5.56
Calcium (ppm)	63.67	21.54	12.3
Magnesium (ppm)	39.18	3.747	2.47

Physicochemical Properties of Indigenous Microorganisms (IMO), Fish Amino Acid (FAA) and Oriental Herbal Nutrient (OHN)

Physicochemical properties of indigenous microorganisms (IMO), fish amino acid (FAA) and oriental herbal nutrient (OHN) are shown in Tables 3-5.

Indigenous microorganism (IMO) had a moisture content of 60.22%, which was high because yeast, fungi, and microorganisms require high humidity for digesting waste materials. The PH value of IMO was 4.48, indicating an acidic nature, as a low PH is required for the

fermentation process. The electrical conductivity was 194.2 $\mu\text{S}/\text{cm}$ due to the presence of exchangeable cations in the sample.

Fish amino acid (FAA) had a viscosity of 84400 m Pa/s, making it a very viscous solution. It was turbid, appearing as dense dark brown. The PH value was of FAA was 5.11, indicating an acidic nature due to the fermentation process involving brown sugar. The electrical conductivity was 194.2 $\mu\text{S}/\text{cm}$.

Oriental herbal nutrient (OHN) was found to have low turbidity of 5.65 NTU. Its PH was 5.36, showing an acidic condition due to the brown sugar fermentation process. The Viscosity was 13550 m Pa/s, which was lower than that of fish amino acid. The electrical conductivity of OHN was 178.5 $\mu\text{S}/\text{cm}$, which was reduced due to the addition of alcohol during fermentation.

Table 3. Physicochemical Properties of Indigenous Microorganisms (IMO)

Parameters	IMO
Moisture (%)	60.22
Ash (%)	0.33
pH	4.48
Conductivity($\mu\text{S}/\text{cm}$)	182.4

Table 4. Physicochemical Properties of Fish Amino Acid (FAA)

Parameters	FAA
Viscosity (mPa/s)	84400
Colour	turbid
pH	5.11
Conductivity($\mu\text{S}/\text{cm}$)	194.2

Table 5. Physicochemical Properties of Oriental Herbal Nutrient (OHN)

Parameters	OHN
Viscosity (mPa/s)	13550
Turbidity(NTU)	5.65
pH	5.36
Conductivity($\mu\text{S}/\text{cm}$)	178.5

On the aspects of preparation of bio-fertilizer

Biofertilizer (C-1, C-2 and C-3) can be prepared with chicken manure, coconut husk powder and rice husk ash in the ratio of (2: 1: 1), (1: 2: 1) and (1: 1: 2) by compost heap layer method. In the composting process, the temperature of compost began at 26 °C and then temperature was gradually increased to approximately 41 °C about 50- 60 days. The increase in

temperature during the composting process was the heat generated from the decomposition of waste materials by IMO. The increment of temperature is a good indicator for digestion. The temperature pattern showed that there was a rapid process for decomposition. The temperature was decreased after 60 days. The change in temperature showed the decomposition of organic matter during 90 days period. The compost processes were occurred between (26-41 °C). After three months, the compost became ready to use in the field. (Figure 1)

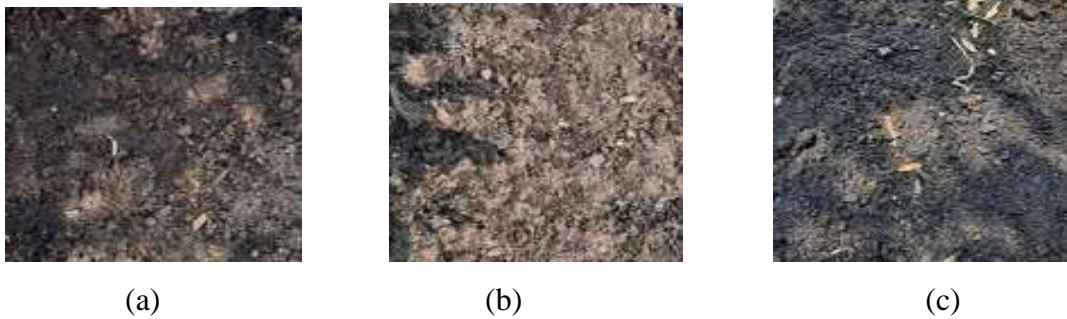


Figure 1. Photograph for prepared bio-fertilizer (a) C-1 (b) C-2 and (c) C-3

Field Experiment

Field experiments were carried out at Sidi Village in Bago Region from 1st March 2022 to 15th April 2022.

Effect of biofertilizer on cucumber

The growth, yields and quality of cucumber depends on nutrient availability in soil which is related to the judicious application of fertilizers. In continuous cropping area, the organic matter supply to the crop field through different maturing practices were made only to a minimum extent. The use of fertilizer may affect either directly or indirectly the availability of soil nutrients.

Effect of biofertilizer on the plant height of cucumber

Table 6 shows a progressive increase in plant height with the age of crop. The plant height of cucumber at (15, 30 and 45) days after cultivation were measured.

Table 6. Effect of Bio-fertilizers on the Height of Plant in Different Life Times

Bio-fertilizers	Plant height of cucumber (cm)		
	15 days	30 days	45 days
C1	70	140	150
C2	65	128	141
C3	50	110	135
Control	43	105	120

Biofertilizer C1 = Chicken manure, coconut husk powder and rice husk ash in ratio of (2:1:1)

Biofertilizer C2 = Chicken manure, coconut husk powder and rice husk ash in ratio of (1:2:1)

Biofertilizer C3 = Chicken manure, coconut husk powder and rice husk ash in ratio of (1:1:2)

Control = Without Bio-fertilizer

Effect of biofertilizers on plant morphology of cucumber

From the field experiment, it was found that the biofertilizers promoted the growth and yields of cucumber. For the life time of cucumber, cultivation to the harvesting was the time frame of 45 days. After harvesting, the plant morphology of cucumber was determined with plant height, fruit length, numbers of fruit per plant, fruit weight per plant, root length and total yields.

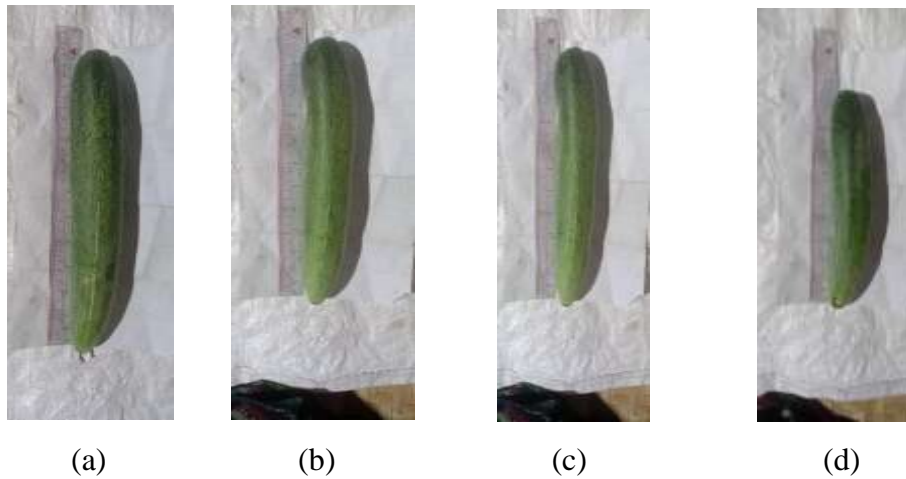


Figure 2. Photographs of cucumber cultivated with (a) C-1 (b) C-2 (c) C-3 and (d) Control

Table 7. Effect of Bio-fertilizers on Plant Morphology of Cucumber

Treatments	Plant morphology					
	Life time (days)	Fruit length (cm)	Number of fruit per plant(mean)	Fruit weight per plant(g)	Root length (cm)	Total yield (kg) (15x15) ft ²
C1	45	28.7	35	560	18	1274.0
C2	45	27.9	30	530	11.5	1033.5
C3	45	26.2	24	450	10	702.0
Control	45	24.4	20	410	9	533.0

Comparison between Physicochemical Parameters, Nutrient Values and Texture of Selected Soil before and After Cultivation

Physicochemical parameter, nutrient values and texture of original soil uncultivated and after harvesting (C1, highest yields farm) are shown in Table 8. Before cultivation, the original soil is sandy loam and it was treated with biofertilizers for the cultivation process. After harvesting, the soil was loam due to the effect of increasing organic carbon content. Nitrogen, phosphorus, potassium calcium and magnesium contents were also increased.

Table 8. Comparison of Physicochemical Parameters, Nutrient Values and Texture of Selected Soil before and after Cultivation

No.	Parameter	Uncultivated Soil	Harvesting Soil (C1)
1	pH	5.61	6.09
2	Moisture (%)	0.26	2.15
3	Sand (%)	56.44	36.42
4	Silt (%)	39.02	49.36
5	Clay (%)	4.54	14.22
6	Texture	Sandy Loam	Loam
7	Organic Carbon (%)	0.48	0.86
8	Humus (%)	0.83	1.48
9	Nitrogen (%)	0.123	1.16
10	Phosphorus (%)	0.01	3.07
11	Potassium (K ₂ O) (%)	0.23	11.4
12	Exchangeable Cation (K ⁺) (meq/100g)	0.21	0.23
13	Calcium (ppm)	9.625	20.4
14	Magnesium (ppm)	1.6	3.27

Conclusion

The research work focused on the preparation of biofertilizers using waste materials such as chicken manure, coconut husk powder, and rice husk ash. The effectiveness of the prepared biofertilizers (C-1, C-2, and C-3) and a control group was evaluated by cultivating cucumber plants in low-quality soil during the summer. The study examined the impact of the biofertilizers and the control group on the morphology of the cucumber plants. After 45 days, the cucumber plants treated with biofertilizer C-1 exhibited the highest plant height (150 cm), fruit length (28.7 cm), fruit weight per plant (560 g), root length per plant (18 cm), and total yield (1244.0 kg in a 15 x 15 ft² area). The study also compared the physicochemical parameters, nutrient values, and soil texture before and after cultivation. The soil parameters of the harvested soil showed improvements in texture, nutrient values, and organic carbon content compared to the uncultivated soil. This improvement was attributed to the effect of the prepared biofertilizer, particularly C-1, which demonstrated the ability to enhance soil fertility. In conclusion, the prepared bio-fertilizer C-1 showed the highest yield and was found to be effective for cucumber cultivation during the summer. The study also indicated that the use of biofertilizers can positively impact soil fertility, as evidenced by the improved soil parameters after harvesting.

Acknowledgement

We would like to express our deep sense of gratitude to Rector Dr. Aye Aye Khaing, Bago University for her kind provision of the research facilities. We also wish to express our profound gratitude to Dr Aye Aye Mon, Professor and Head of Chemistry Department, Bago University for her encouragement and comment without which this work would not have been completed.

References

- Asiamah, R.D. (1998). *Soil and Soil Suitability of Ashanti Region*. Kwadaso Kumari: UNESCO/FAO SRI Technical Report No. 193.
- Audu, M. and A. Zubairu. (2013). "Analysis of Nutrient Content of Some Organic Materials for Soil Amendment in Sokoto Metroplis", *Journal of Biology, Agriculture and Health Care*. vol. 3, (18), pp. 8- 11.
- Barker, A.V. and D.J. Pilbeam. (2007). *Handbook of Plant Nutrition*. Boca Raton, FL: CRC Press
- Bhatia, S.C. (2010). *Environmental Chemistry*. New Delhi: CBS Publisher.
- Chow, J.M. (2002), *Probiotics and Prebiotics: A Brief Overview*: *J. Ren. Nutr.* vol.12 (2), pp.76-86
- Par, J.F; R.I. Papendick, S-B. Hornick, and R.E. Meyer. (1992). "Soil Quality: Attributes and Relationship to Alternative and Sustainable Agriculture". *Am. J. Altern. Agric.*, vol.7, pp. 5-11
- Rajni, R., O. P. Srivastava, and R. Rani. (2001). "Effect of Integration of Organics with Fertilizer N on Rice and N Uptake". *Fertility News*, vol. 46, pp. 63- 65.
- Tan, L. M. (2015). *Production of Fertilizer using Food Wastes of Vegetable and Fruits*. *Malaysia Sarawak University Research Journal*, vol. 12, pp. 8- 14.

EXTRACTION OF ESSENTIAL OIL, SCREENING OF ANTIMICROBIAL AND ANTIOXIDANT ACTIVITIES OF *CITRUS MEDICA* VAR. *ACIDA* BRANDIS (SHAUK THAKWA) LEAF

Su Yi Mon¹, Thandar Aung²

Abstract

Citrus medica var. *acida* Brandis (Shauk thakwa), belonging to the Rutaceae family, has been chosen to investigate phytochemical constituents and some bioactivities. Firstly, preliminary phytochemical tests on *C. medica* leaves revealed the presence of alkaloids, carbohydrates, flavonoids, glycosides, phenolic compounds, reducing sugars, saponins, starch, steroids, tannins, and terpenes. The EDXRF elemental analysis showed that the leaves contained Ca, Al, K, and S as major elements. In the GC-MS analysis of the essential oil extracted by steam distillation method, the thirteen organic compounds detected (2.30 %) were 4-hydroxy-4-methyl-2-pentanone, -3-acetoxy-4-(1-hydroxy-1-methyl ethyl)-1-methyl-cyclohexene, (*R*)-(+)-citronellic acid, 2-(2-hydroxy-2-propyl)-5-methyl cyclohexan-1-ol, (*E*)-3-octadecene, octacosanol, methyl eugenol, benzyl benzoate, *cis*-9, 12-methyl linoleate, methyl (9*E*)-9-octadecenoate, di-isobutyl phthalate, heptadecan-1-ol and methyl stearate. The antimicrobial activity of leaves extracts in various solvents (pet-ether, ethyl acetate, 95 % ethanol, and water) was tested against six species of microorganisms: *Bacillus subtilis*, *Bacillus pumilus*, *Salmonella typhi*, *Pseudomonas aureginosa*, *Escherichia coli*, and *Candida albicans*, by the agar well diffusion method. It was found that the ethyl acetate extract (Inhibition zone diameter, 10–14 mm) and watery extract (10 – 13 mm) exhibited antimicrobial activity against four tested microorganisms except *C. albicans* and *E. coli*. The 95 % ethanol extract exhibited the more potent antimicrobial activity (10 - 18 mm) against all tested microorganisms. In the screening of antioxidant activity, the watery extract (IC₅₀ = 148.58 µg/mL) showed more antioxidant activity than 95 % ethanol extract (IC₅₀ = 636.27 µg/mL).

Keywords: *Citrus medica* var. *acida* Brandis, phytochemical tests, antimicrobial activity, antioxidant activity, essential oil

Introduction

Citrus medica var. *acida* Brandis (Shauk thakwa) is cultivated in many countries all over the world and grows in hot subtropical or tropical regions such as Southern Florida, India, Mexico, Egypt, and West Indies (Onyilofe *et al.*, 2015; Taiwo, 2005). The decoction of pounded leaves is drunk for stomach aches, used as an eyewash, and used to bathe feverish patients. A poultice of leaves is applied to ulcer wounds, and skin disease, and is also applied to the abdomen after childbirth. Crushed leaves are applied to the forehead to treat headaches, and to treat nausea and resuscitate fainting individuals (Khan, 2010). Infusions of *C. medica* leaves have been given to treat fever with jaundice, sore throat, and oral thrush (Kunow, 2003). A decoction of the flower helps induce sleep for those with insomnia. In southwest Nigeria, the roots, bark, stem twigs, leaves, and fruits are used in the treatment of malaria (Khare, 2007).

Scientific Classification of *Citrus medica* var. *acida* Brandis (Shauk thakwa)

Family : Rutaceae
Botanical name: *Citrus medica* var. *acida* Brandis
Myanmar name: Shauk thakwa
Common name: Citron
Synonym name: *Citrus aurantifolia* (Christm)

¹ Department of Chemistry, Meiktila University

² Department of Chemistry, University of Yangon



Figure 1. Photographs of *Citrus medica* var. *acida* Brandis

C. medica juice is used to increase stamina, treat dysfunctional uterine bleeding, be used as a facial wash to rejuvenate the skin and remove stains, be drunk to control epistaxis, and be given in pure form as a remedy for arthralgia, diabetes, and atherosclerosis (Onyilofe *et al.*, 2015). *C. medica* juice is sometimes mixed with oil, used as a vermifuge, and is also incorporated into a weight management diet (Akhtar, 2013). The main aim of the research work is to investigate some phytoconstituents, extract essential oils, and screen the antimicrobial and antioxidant activities of Shauk thakwa leaves (Figure 1).

Materials and Methods

Sampling of Plant Material and Identification

The leaves of *C. medica* (Shauk thakwa) were collected from Meiktila Township, Mandalay Region, Myanmar, in December 2022. The sample was identified as *Citrus medica* var. *acida* Brandis by the authorized botanist from the Department of Botany, Meiktila University. The collected fresh leaves were washed, and air dried at room temperature for one week, ground into powder, and then stored in an air-tight container.

Preliminary Phytochemical Investigation of the Leaves of *C. medica*

To classify the types of organic constituents present in the sample, preliminary phytochemical tests were carried out according to the appropriate reported methods (Trease and Evans, 1978; Marini-Bettolo *et al.*, 1981; M-Tin Wa, 1972; Robinson, 1983; Finar, 1964; Furniss, 1989).

Determination of Elemental Content in Leaf of *C. medica* by EDXRF Method

Some elements present in leaves of *C. medica* powdered samples were semi-quantitatively determined by using EDX-700, Energy Dispersive X-ray Fluorescence Rigaku spectrometer, at the Department of Physics, Meiktila University.

Extraction of Essential Oil from the Fresh Leaf of *C. medica* by Steam Distillation Method

The fresh leaves (500 g) of *C. medica* were cut into small pieces. The essential oil was extracted from the fresh leaves sample with 6 L of distilled water by using the steam distillation method. The essential oil was extracted with *n*-hexane from the distillate. The *n*-hexane layer was dried by adding a small amount of anhydrous sodium sulphate. The dried *n*-hexane layer was then evaporated at 68 °C, and the essential oil was then weighed until it reached a constant weight. Afterward, the essential oil was stored in an air-tight small bottle and placed in the refrigerator for long-term essential oil storage (Hesham, 2016).

To determine the composition of the essential oil and identify the specific compounds responsible for its aroma and potential therapeutic effects, GC-MS analysis of the essential oil was carried out at the Department of Chemistry, University of Mandalay. The National Institute of Standards and Technology (NIST) database was used to analyse the GC-MS spectrum, comparing the unknown and known components. The name, molecular weight, and structure of each component of the test material were identified (Igwe *et al.*, 2015).

Preparation of Various Crude Extracts

The dried powdered sample (50 g) was extracted with 150 mL of petroleum ether (60-80 °C) for 6 h by using a Soxhlet extractor. The filtrate was concentrated by removing the solvent under reduced pressure to give the respective PE crude extract. Similarly, ethyl acetate, 95 % ethanol, and watery extracts were also prepared according to the above procedure. Each extract was dried at normal pressure in a water bath and stored in a refrigerator for screening the antimicrobial and antioxidant activities.

Screening of Some Biological Activities of the Leaf of *C. medica*

(a) Screening of the antimicrobial activity of various crude extracts by agar well diffusion method

The antimicrobial activity of various crude extracts: 95 % ethanol, ethyl acetate, petroleum ether, and watery extracts was studied by the agar well diffusion method (Collins, 1965) at the Department of Chemistry, Loikaw University. The microorganisms used were *Bacillus subtilis*, *Salmonella typhi*, *Pseudomonas aeruginosa*, *Bacillus pumilus*, *Candida albicans*, and *Escherichia coli* from the Department of Chemistry, Loikaw University.

(b) Screening of the antioxidant activity by DPPH assay

In this experiment, the antioxidant activity of ethanol and watery extracts was studied by a DPPH free radical scavenging assay (Patil, 2009). DPPH powder (2 mg) was thoroughly dissolved in 100 mL of 95 % ethanol. The stock solution (1.6 mg/mL) of crude extract was prepared by dissolving the respective crude extract in 10 mL of 95 % ethanol. The stock solution was two-fold diluted serially with 95 % ethanol to get the sample solution with the different concentrations of 1600 µg/mL, 800 µg/mL, 400 µg/mL, 200 µg/mL, and 100 µg/mL.

Phytochemicals of *Citrus medica* var. *acida* Brandis (Shauk thakwa) Leaf

The phytochemical tests revealed that alkaloids, α -amino acids, carbohydrates, flavonoids, glycosides, phenolic compounds, reducing sugars, saponins, starch, steroids, tannins, and terpenes were present in the tested sample. Phenolic compounds, flavonoids, and tannins are major contributors to antioxidant activity. Alkaloids, flavonoids, saponins, steroids, tannins, and terpenes play a major role as anti-inflammatory agents. Alkaloids, flavonoids, glycosides, and tannins have antidiabetic activity (Duthie, 2000).

Elemental Analysis of Sample by EDX RF Technique

According to the EDXRF elemental analysis, *C. medica*-leaves contain Ca, Al, S, and K as major elements. Besides Si and P as minor elements, Mn, Fe, Cu, Zn, Sr, and Ba as trace elements were also detected. The advantages of calcium are strong bones and teeth and the regulation of muscle contraction in the human body. Potassium is used in many foods and as a

supplement. Aluminium is also used to treat muscle and joint pain, fatigue and insomnia, symptoms of colds, and flu. The results are reported in Table 1.

Table 1. Relative Abundance of Elemental Content in *C. medica* Leaf by EDXRF

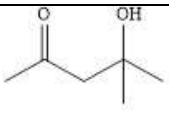
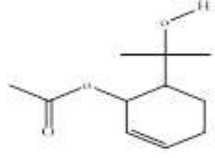
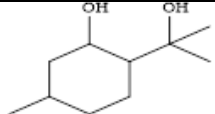
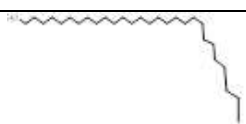
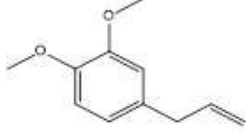
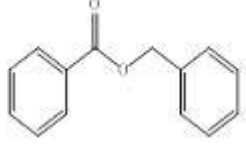
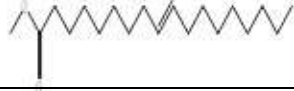
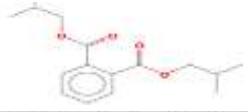
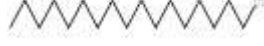
Element	Relative abundance (%)
Ca	38.753
Al	19.813
S	16.953
K	11.392
Si	8.337
P	4.355
Fe	0.102
Cu	0.035
Sr	0.021
Mn	0.019
Zn	0.005
Ba	0.002

Organic Compounds in Essential Oil of the Leaf of *C. medica* by GC-MS

Essential oil from the leaf of *C. medica* was extracted from the fresh leaf samples by steam distillation method (2.30 %). In the GC-MS analysis of the extracted essential oil sample, a total of 13 organic compounds detected are (1) 4-hydroxy-4-methyl-2-pentanone, (2) 3-acetoxy-4-(1-hydroxy-1-methyl ethyl)-1-methyl-cyclohexene, (3) (*R*)-(+)-citronellic acid, (4) 2-(2-hydroxy-2-propyl)-5-methyl cyclohexan-1-ol, (5) (*E*)-3-octadecene, (6) octacosanol, (7) methyl eugenol, (8) benzyl benzoate, (9) *Cis*-9,12-methyl linoleate, (10) methyl (9*E*)-9-octadecenoate, (11) di-isobutyl phthalate, (12) heptadecane-1-ol and (13) methyl stearate.

Citrus species extracts are well-known sources of bio-functional compounds with health-promoting effects. In particular, essential oils are known for their antibacterial activity due to the high content of terpenes. The thirteen compounds identified by GC-MS analysis of the essential oil of *C. medica* leaves matched the NIST library data. These compounds with their respective retention time, together with their structures, molecular weights, and molecular formulae are listed in Table 2.

Table 2. Name of the Compounds, and their Structure, Retention Time, Molecular Weight, and Molecular Formula Detected in the Essential Oil of *Citrus medica* Leaf

No.	Name of Compound	Structure	Retention time (min)	Molecular weight	Molecular formula
1	4-hydroxy- 4-methyl-2-pentanone,		2.972	116	C ₆ H ₁₂ O ₂
2	3-acetoxy-4-(1-hydroxy- 1-methyl ethyl)-1-methyl--cyclohexene		15.197	212	C ₁₂ H ₂₀ O ₃
3	(R)-(+)-citronellic acid		16.319	170	C ₁₀ H ₁₈ O ₂
4	2-(2-hydroxy-2-propyl) - 5-methyl cyclohexan-1- ol		16.543	172	C ₁₀ H ₂₀ O ₂
5	(E)-3-octadecene		17.410	252	C ₁₈ H ₃₆
6	octacosanol		17.567	410	C ₂₈ H ₅₈ O
7	methyl eugenol		17.881	178	C ₁₁ H ₁₄ O ₂
8	benzyl benzoate		36.840	212	C ₁₄ H ₁₂ O ₂
9	Cis-9,12- methyl linoleate		27.580	294	C ₁₉ H ₃₄ O ₂
10	methyl (9E)-9-dctadecenoate		27.790	296	C ₁₉ H ₃₆ O ₂
11	di-isobutyl phthalate		28.426	278	C ₁₆ H ₂₂ O ₄
12	heptadecane-1-ol		28.512	256	C ₁₇ H ₃₆ O
13	methyl stearate		28.639	298	C ₁₉ H ₃₈ O ₂

Screening of Antimicrobial Activity of Different Crude Extracts of *C. medica* Leaf

The crude extracts of *C. medica* leaves (petroleum ether, ethyl acetate, 95 % ethanol, and watery) were tested on six species of microorganisms such as *Bacillus subtilis*, *Salmonella typhi*, *Pseudomonas aeruginosa*, *Bacillus pumilus*, *Candida albicans*, and *Escherichia coli* by using the agar well diffusion method. From the experimental results (Table 3), all the crude extracts except the PE extract showed antimicrobial activity against four of the six tested microorganisms. It was found that EtOAc extract (ID: 10-14 mm) and H₂O extract (ID: 10-3 mm) exhibited antimicrobial activity against four tested microorganisms except *C. albicans* and *E. coli* whereas 95 % EtOH extract exhibited antimicrobial activity against all microorganisms tested (ID: 10-18 mm). In general, since the larger the diameter, the greater is the antimicrobial activity, the polar extracts exhibited higher activity than non-polar extracts. *C. medica* also exhibited more potent antimicrobial activity in the polar extract but was inactive in the non-polar extract.

Table 3. Antimicrobial Activity of Crude Extracts of *C. medica* by Agar Well Diffusion Method

No.	Microorganisms	Inhibition zone diameter (mm)			
		H ₂ O	EtOH	EtOAc	PE
1	<i>B. subtilis</i>	11	16	10	–
2	<i>S. typhi</i>	10	13	10	–
3	<i>P. aeruginosa</i>	13	18	14	–
4	<i>B. pumilus</i>	12	16	11	–
5	<i>C. albicans</i>	–	10	–	–
6	<i>E.coli</i>	–	10	–	–

Agar well diameter- 8mm;

Inhibition zone diameter = 9-14 mm = low activity; 15-20 mm = medium activity
21 mm above = high activity; No zone of inhibition = (-)

Antioxidant Activity of Some Crude Extracts from the Leaf of *C. medica*

The antioxidant activity of 95 % ethanol and watery extracts of the leaves of *Citrus medica* was studied by the DPPH (1,1-diphenyl-2-picrylhydrazyl) free radical scavenging assay method using UV spectrophotometry. This method is based on the reduction of coloured free radical DPPH in ethanolic solution by different concentrations of each sample. The antioxidant activity was expressed as a 50 % oxidative inhibitory concentration (IC₅₀).

From these experimental results (Table 4 and Figure 4), the tested crude extracts were found to have low antioxidant activity. Moreover, the watery extract (IC₅₀ = 148.58 µg/mL) showed higher antioxidant activity than the 95 % ethanol extract (IC₅₀ = 636.27 µg/mL). However, both the watery extract and the ethanol extract were found to have lower antioxidant activity than standard ascorbic acid (IC₅₀ = 4.75 µg/mL) because the lower the IC₅₀ value, the higher the antioxidant activity of the sample.

Table 4. Percent Inhibition and IC₅₀ Values of Crude Extracts from the Leaf of *C. medica*

Extracts	% Inhibition in different concentrations (µg/mL)					IC ₅₀ µg/mL
	100	200	400	800	1600	
ethanol	24.93	27.13	40.82	57.08	81.35	636.27
watery	36.79	63.98	72.59	78.11	84.18	148.58
Standard	1	2	4	8	16	IC50 µg/mL
Ascorbic Acid	16.63	30.63	46.11	74.60	81.73	4.75

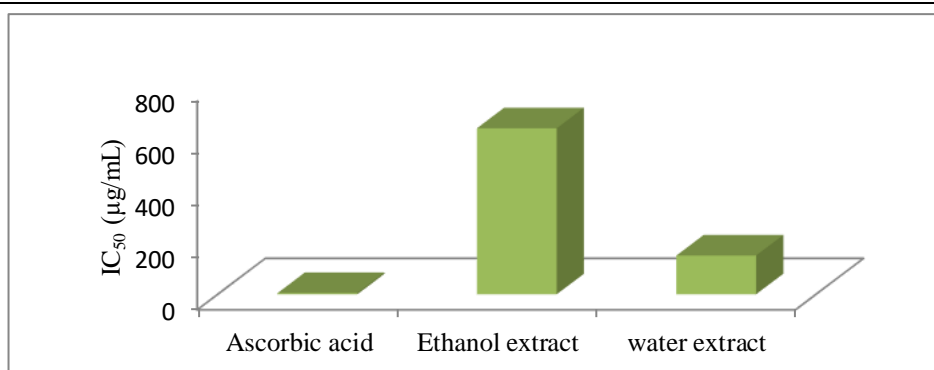


Figure 4. IC₅₀ values of watery and ethanol extracts from *C. medica* leaves compared with standard ascorbic acid

Conclusion

From the overall assessment of the present work, the following inferences could be deduced. The phytochemical investigation showed the presence of phytoconstituents which would be beneficial in understanding the pharmacological importance and health risks. From the EDXRF measurement, it can be found that the leaves of *C. medica* contain the main elements: Ca, Al, S, K, and Si. Among them, the content of calcium is the highest (38.753 %). The GC-MS analysis revealed that the essential oil of *C. medica* leaves contained fatty acid esters, monoterpenoids, and unsaturated fatty acids. Among the chemical composition, methyl eugenol is a major constituent in the leaf, and it is a natural constituent of a large number of essential oils of plant origin. Methyl eugenol also has antioxidant activity. According to the antimicrobial activity of the polar and non-polar extracts, it can be deduced that the polar extract of *C. medica* leaves may be effective for the treatment of some diseases. From the screening of the antioxidant activity, the IC₅₀ values of ethanol and watery extracts were observed at 636.27 µg/mL and 148.58 µg/mL, respectively. Therefore, the antioxidant capacity of the watery extract was higher than that of the ethanol extract. However, these crude extracts possess lower antioxidant activity than the standard ascorbic acid. Moreover, the *C. medica* leaf exhibited low antimicrobial activity.

Acknowledgments

The authors would like to thank the Myanmar Academy of Art and Science, and the Ministry of Education in Myanmar, for giving us to present this research paper. We would like to thank the Department of Higher Education, Ministry of Education in Myanmar, for allowing us to do this research. Our deepest gratitude is expressed to Dr Tin Maung Tun and Dr Ba Han, Rectors of Yangon and Meiktila Universities. We wish to thank Professor Dr Ni Ni Than, Head of the Department of Chemistry, University of Yangon, for her invaluable advice and encouragement. Many thanks are also extended to Dr Sandar Aung (Professor and Head), Department of Chemistry, Meiktila University, for her kind cooperation at the Department of Chemistry.

References

- Akhtar, S. S. (2013). Evaluation of Cardiovascular Effects of *Citrus aurantifolia* Linn. Fruit Social Science Research Network. Retrieved from; <http://ssrn.com/abstract—2279447>.
- Collin, C. H. (1965). *Microbiological Methods*. London: Butterworth and Co., Ltd.
- Duthie, G. G., S. J. Duthie, and J. Kyle. (2000). “Plant Polyphenols in Cancer and Heart Disease: Implications as Nutritional Antioxidants”. *Nutr. Res. Rev.*, vol.13 (1), pp.79-106.
- Finar, I. L. (1964). *Organic Chemistry, Stereochemistry, and Chemistry of Natural Products*. London: 3rd ed., Longman Green and Co. Ltd., pp. 358-420.
- Furniss, B. S., A. J. Hannaford, P. W. G. Smith, and A. R. Tatchell. (1989). *VOGEL's Textbook of Practical Organic Chemistry*. London: 5th ed. Longman Green and Co., Ltd., pp. 131-234.
- Hesham, H. A., R. A. H. Nour, and R. M. Yunus. (2016). “Techniques for Extraction of Essential Oil from Plants: A Review”. *Australian Journal of Basic and Applied Sciences*, vol. 10 (16), pp. 117-127.
- Igwe K. K, P. O. Nwankwo., L. Otuokere, and N. L. Salomon. (2015). “GC-MS Analysis of Phytocomponents in the Methanolic Extract of *Moringa oleifera* Leaves”. *Journal of Research in Pharmaceutical Science*, vol. 2 (11), pp. 2347-2995.
- Khan, I. A. and E. A. Abourashed. (2010). *Legung's Encyclopedia of Common Natura Ingredients*. New Jersey: John Wiley and Sons Publication, pp. 422-423.
- Khare, C. P. (2007). *India Medicinal Plants: An Illustrated Dictionary*. New Dehli: Springer, p.154.
- Kunow, M. A. (2003). *Maya Medicine: Traditional Healing in Yucatan*. New Mexico: p.117.
- M-Tin Wa. (1972). “Phytochemical Screening Methods and Procedures”. *Phytochemical Bulletin of Botanical Society of American*, vol. 5 (3), pp 4-10.
- Marini-Bettolo, G. B., M. Nicolettic, and M. Putamia. (1981). “Plant Screening by Chemical and Chromatographic Procedure under Field Conditions”. *J. Chromato.*, vol. 213, p. 121.
- Onyilofe, S. E., O. O. Ibukan, S. B. Madu, S. O. Isaiah, M. S. Mohammed, and F. A. Suleiman. (2015). “Ethnomedical Importance of *Citrus Aurantifolia* (Christm) Swingle”. *Journal of the Pharma Innovation*, vol. 4 (8), pp. 01- 06.
- Patil A. P., V. V. Patil, and V. R. Patil. (2009). “*In vitro* Free Radicals Scavenging Activity of *Madhuca indica* Gmel.”. *Pharmacology*, vol.2, pp. 1344-1352.
- Robinson, T. (1983). *The Organic Constituents of Higher Plants*. North Amherst: 5thed, Cordus Press, pp. 285-286.
- Taiwo, T. A. (2005). *Production of Fruits, Vegetables, Grains, Legumes, Root Crops in Nigeria, Problems and Prospects*. University Press, Abuja, vol. 1, p. 9.
- Trease, G. E. and W. C. Evans. (1978). *Phytochemistry: Introduction and General Methods*. *Pharmacognosy*. London: Bailliere Tindall, pp. 227-247.

ANTIMICROBIAL AND AMYLASE ACTIVITIES OF ISOLATED SOIL FUNGI FROM TAUNG THAR TOWNSHIP (MANDALAY REGION)

Hnin Nandar Hlaing¹, Moe Pa Pa² and Myint Myint Soe³

Abstract

The soil microorganisms were isolated from the various soils collected from five different places: Yay Kyaw S-1, Thae Taw S-2, Kaing Yar Gyi S-3, Si Sone Kone S-4, and Kone Thar S-5, Taung Thar Township, Mandalay Region. From the analysis of soil textures, sample No.1 was found to be loamy sand, samples No. 2 and No. 3 were sand, and samples No. 4 and No. 5 were sandy loam. In this study, the soil fungi were isolated by using the feeding method and the physical treatment dilution method. Four fungi were isolated from five different soil samples by the feeding method and six fungi were isolated from five different soil samples by the physical treatment dilution method. The morphology of the isolated fungi were studied in PGA medium. These fungi were used for screening the antimicrobial activities against seven tested microorganisms. The first time, after three days of fermentation, the antimicrobial activity was tested against three microorganisms. Among them, only the isolated fungus from soil sample 1 (Yay Kyaw S-1) showed the highest activity in clear zone (27 mm) on *Agrobacterium tumefaciens*, followed by (26 mm) on *Bacillus subtilis* and (25 mm) on *Escherichia coli*, and no activity against the remaining four tested organisms: *Candida albicans*, *Micrococcus luteus*, *Pseudomonas fluorescens* and *Staphylococcus aureus*. In the second time fermentation, the isolate fungus from S-1 (32 mm) was especially active against *Agrobacterium tumefaciens*. This isolated fungus cannot hydrolyze the starch, that is, it did not show the amylase enzyme activity.

Keywords: soil fungi, soil texture, antimicrobial activity, fermentation, amylase enzyme activity

Introduction

Microorganisms live in all parts of the biosphere where there is liquid water, including soil, hot springs, on ocean floor, high in the atmosphere and deep inside rocks within the earth crust. The typical materials for microbial sources are soil, living and fallen leaves, leaf litters, dung, insect, fresh water and marine water. The soil samples are most effective and popular minerals for the isolation of fungi and actinomycetes (Kuntgmen, 1992)(Harayama and Isono, 2002). Soils are the foundation of all terrestrial ecosystems and are home to a vast diversity of bacteria, archaea, fungi, insects, annelids, and other invertebrates as well as plants and algae. These soil dwellers provide food or nutrients that support organisms that live above and below ground. Soils also play critical roles in buffering and filtering freshwater ecosystems. Consequently, soils are extremely important to human societies (Dominati *et al.*, 2010).

Fungi are an important component of the microbiota, typically constituting more of the soil biomass than bacteria, depending on soil depth and nutrient conditions (Cattle *et al.*, 2002). Fungi, bacteria and actinomycetes colonize different habitats and substrates and play substantial role in plant health and productivity besides producing diseases (Aina *et al.*, 2011).

The main aim of this research is to isolate the soil fungi from various soil samples, and to investigate the antimicrobial and amylase activities of the isolated soil fungi.

¹ Department of Chemistry, Meiktila Education Degree college

² Department of Biology, Yangon Education University

³ Department of Chemistry, Patheingyi University

Materials and Methods

Collection of the samples

Microorganisms have different characteristics that define them and different functions in the soil they live in. So, various different soil samples were collected from Taung Thar Township, Mandalay Region, as shown in Figure 1 and listed in Table 1. The five different soil samples were collected from the different places: Yay Kyaw, Thae Taw, Kaing Yar Gyi, Si Sone Kone and Kone Thar. The different soil samples were employed for the isolation of microorganisms. The collected soil samples were washed with water followed by filtration. After cleaning, it was dried at room temperature; the dried powder sample was stored in an air-tight container to prevent moisture changes and other contamination. The dried powder sample was used to investigate the chemical and biological activities.

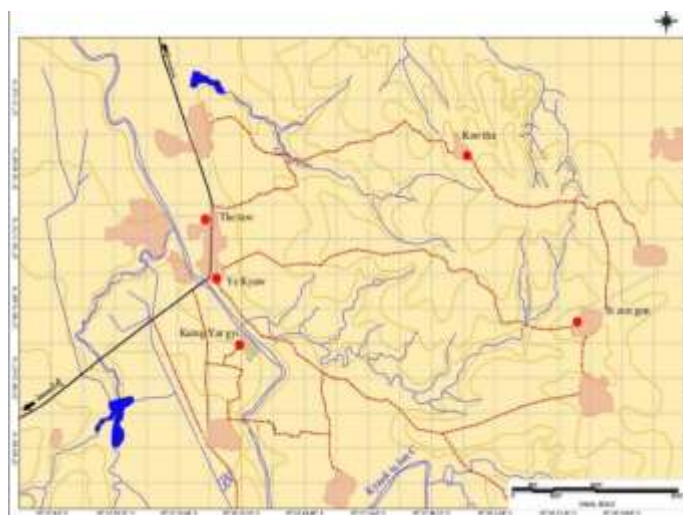


Figure 1. Map of soil samples collected area

Table 1. Five Different Soil Samples Collected from Taung Thar Township, Mandalay Region

Soil No.	Places	Location	Collected date
S-1	Yay Kyaw	N 21° 10' 05" E 95° 26' 21"	8. 6. 2022
S-2	Thae Taw	N 21° 10' 39" E 95° 26' 13"	8. 6. 2022
S-3	Kaing Yar Gyi	N 21° 9' 66" E 95° 26' 36"	8. 6. 2022
S-4	Si Sone Kone	N 21° 9' 80" E 95° 28' 67"	1. 7. 2022
S-5	Kone Thar	N 21° 10' 76" E 95° 27' 92"	1. 7. 2022

Analysis of Collected Soil Sample

Some parameters, such as soil texture, pH, nitrogen, and moisture of the collected samples, were tested at the Department of Agriculture (Land Use), Yezin, and Nay Pyi Taw. Soil textures were analyzed by the triangle method; pH of soil water suspensions was measured using 4A1-1:5; nitrogen content was determined by the Kjeldahl distillation method; and moisture content was determined by the gravimetric method.

Isolation of Fungi from Five Different Soil Samples

Isolation of microorganisms from five different soil samples was carried out by the feeding method (I) and the physical treatment dilution method (II) (Phay & Yama Mura, 2005). Low carbon agar medium (LCA) and potato glucose agar medium (PGA) were used in the procedure for the isolation of soil fungi in this study (Figures 2 & 3).

Method I

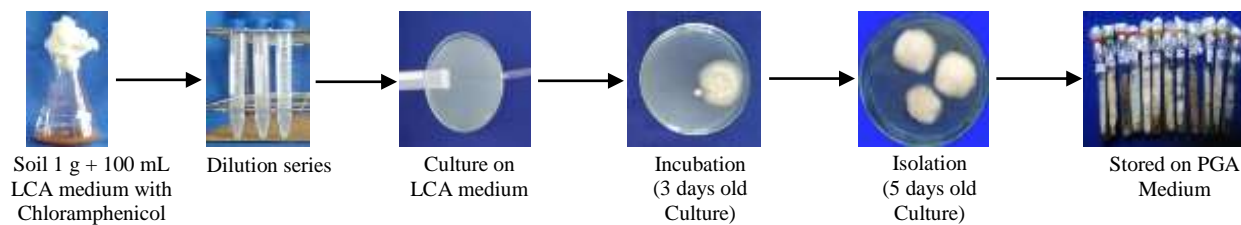


Figure 2. Isolation of soil fungi by the feeding method

Method II

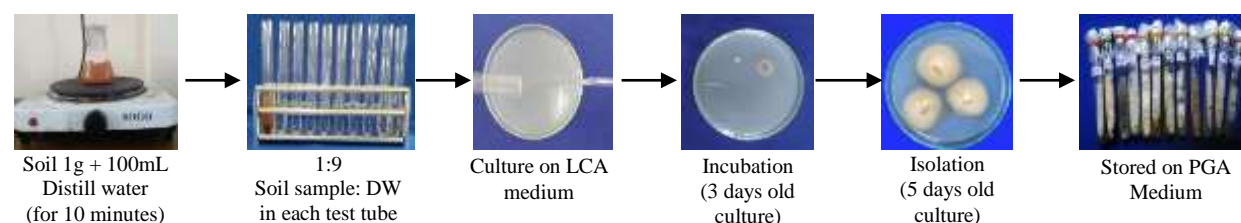


Figure 3. Isolation of soil fungi by the physical treatment dilution method

Medium Used for the Isolation of Fungi, Low Carbon Agar (LCA) Medium (Ando, 2004)

Glucose	2.0 g
Sucrose	2.0 g
K ₂ HPO ₄	1.0 g
KNO ₃	1.0 g
KCl	0.5 g
Agar	18.0 g
D W	1000 mL
pH	6.5

Potato Glucose Agar Medium (PGA) (Ando, 2004)

Potato	200.0 g
Glucose	20.0 g
Agar	18.0 g
DW	1000 mL
pH	6.5

(After autoclaving, chloramphenicol was added to both mediums)

Preliminary Study for Antimicrobial Activity by Paper Disc Diffusion Assay

Antimicrobial activity of isolated fungi was tested at Biological Resource and Biotechnology Development Centre, Botany Department, Patheingyi University. Screening of antimicrobial activity was studied by the Laboratory method of Applied Microbiology, 1992. The assay medium (glucose 10 g, polypeptone 30 g, KNO₃ 10 g, agar 1.8 g, distilled water 1000 mL) was used for the antimicrobial activity test. One percent (1.5 x 10⁸/mL of spore suspension) of the test organism was added to the assay medium and then poured into plates. After

solidification, paper discs (8 mm) impregnated with fermented broth were applied to the agar plates and incubated for 24-36 h at room temperature to examine the inhibitory zones.

Seed and fermentation media were used for screening the antimicrobial activities of isolated fungi against seven tested organisms. The tested organisms used in the paper disc diffusion assay method were *Agrobacterium tumefaciens* NTTE 09678, *Bacillus subtilis* IFO 90571, *Candida albicans* NTTE 09542, *Escherichia coli* AHU 5436, *Micrococcus luteus* NTTE 83297, *Pseudomonas fluorescens* IFO 94307, and *Staphylococcus aureus* AHU 8465 (Table 2). These tested organisms were obtained from the NTTE (National Institute of Technology and Evaluation, Kisarazu, Japan) and sc.

Table 2. Tested Organisms Used in Antimicrobial Activity Screening

No.	Tested organisms (NITE-2004)	Sources	Infections
1	<i>Agrobacterium tumefaciens</i>	NITE 09678	plant disease
2	<i>Bacillus subtilis</i>	IFO 90571	fever
3	<i>Candida albicans</i>	NITE 09542	candidosis
4	<i>Escherichia coli</i>	AHU 5436	diarrhoea
5	<i>Micrococcus luteus</i>	NITE 83297	skin disease
6	<i>Pseudomonas fluorescens</i>	IFO 94307	rice disease
7	<i>Staphylococcus aureus</i>	AHU 8465	boils and food poisoning

BR-BDC-Screening Mediums (2004)

Seed medium		Fermentation medium	
glucose	20.0 g	glucose	20.0 g
polypeptone	3.0 g	yeast extracts	8.0 g
KNO ₃	1.0 g	K ₂ HPO ₄	1.0 g
K ₂ HPO ₄	1.0 g	MgSO ₄	0.1 g
DW	1000 mL	CaCO ₃	1.0 g
pH	6.5	DW	1000 mL
		pH	6.5

Preliminary Study on the Starch Hydrolyzing Activity of Isolated Fungi

The starch hydrolyzing activity was determined by NITE method (NITE, 2005). The preserved fungi were inoculated in 10 mL of liquid medium and incubated for five days at room temperature. Then, the iodine solution was slowly poured into the liquid culture medium. The control was also done. The change of colour was observed After adding iodine solution. If the

colour is still purple, the microorganisms cannot hydrolyze the starch. Conversely, if changes, the microorganisms can hydrolyze the starch. This test was used to determine amylase enzyme activity.

Results and Discussion

The analytical data (pH, soil texture, moisture content and nitrogen content) of the collected soil samples coded as S-1, S-2, S-3, S-4 and S-5 are shown in Table 3.

Table 3. Analytical Data of Five Different Soil Samples

Soil Samples	pH	Soil texture	Moisture (%)	Nitrogen (%)
S-1	8.12	loamy sand	1.7	0.065
S-2	8.82	sand	3.6	0.213
S-3	8.76	sand	0.6	0.013
S-4	7.63	sandy loam	1.9	0.040
S-5	8.86	sandy loam	2.3	0.065

In Table 3, the pH of all tested samples ranged between 7.63 and 8.86. It showed the basic character. The moisture contents were in the range of 0.6 % to 3.6 %. The nitrogen content of all the samples ranged from 0.013 % to 0.213 %. The soil texture of S-1 (Yay Kyaw) was loamy sand whereas S-2 (Thae Thaw) and S-3 (Kaing Yar Gyi) were sand. In addition, the soil samples of S-4 (Si Sone Kone) and S-5 (Kone Thar) were sandy loam.

Isolation of Fungi from Soil Samples

Ten fungi were isolated from five different soil samples in Taung Thar Township, Mandalay Region.

Table 4. Ten Isolated Fungi (ND-01 to ND-10) Isolated from Five Different Soil Samples by Using Two Isolated Methods

Soil samples	Isolated fungi			
	Feeding method	Name of fungi	The physical treatment dilution	Name of fungi
			method	
	Method (I)		(Method II)	
S-1	1	ND-01	1	ND-02
S-2	1	ND-03	1	ND-04
S-3	-		1	ND-05
S-4	1	ND-06	1	ND-07
S-5	1	ND-08	2	ND-09 ND-10
Total	4	-	6	-

In Table 4, four fungi were isolated by method I, and six fungi were isolated by method II. Four isolated fungi: ND-01, ND-03, ND-06, and ND-08 were obtained from soil samples S-1, S-2, S-4, and S-5; six isolated fungi: ND-02, ND-04, ND-05, ND-07, ND-09, and ND-10 were obtained from soil samples S-1, S-2, S-3, S-4, and S-5.

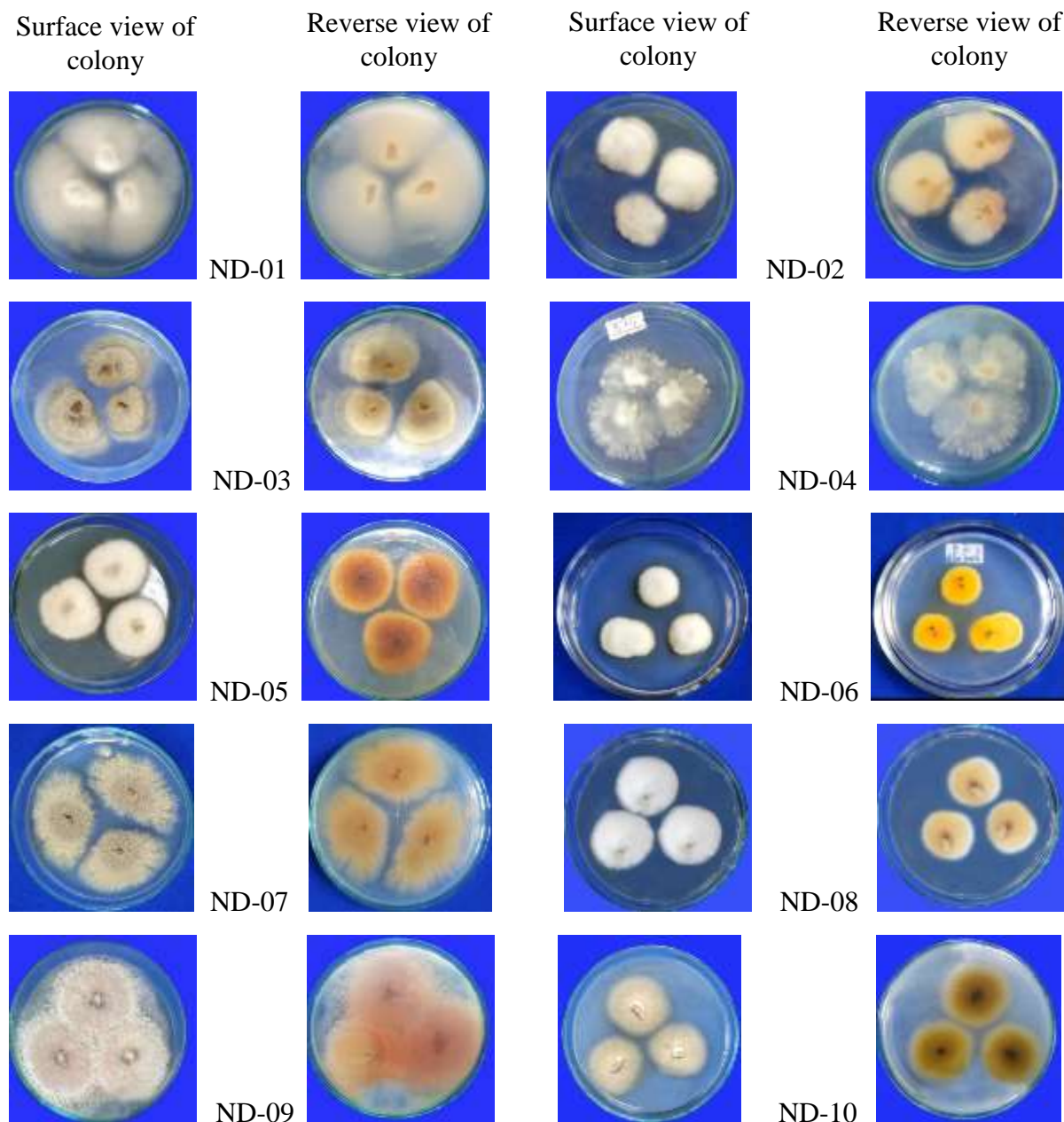


Figure 4. Morphological characters of isolated fungi ND-01 to ND-10 (5-day-old culture) on PGA Medium

In Figure 4, the morphological characters of isolated fungi ND-01 to ND-10 (5-day-old culture) were observed on PGA medium. The surface colour and back (reverse) colour of ND-01 and ND-04 were white. The surface colour and back colour of ND-03 were grey. The surface colours of ND-02, ND-05, ND-06, and ND-08 were white, and their reverse colours were light pale around white, orange, yellow, white in the middle, and light yellow around. The surface colour of ND-07 was pale yellow green and the reverse colour was orange. The surface colour of

ND-09 was centre flower mat and edge white, and the reverse colour was light pink. The surface colour of ND-10 was pale yellow, and the reverse colour was center black around the yellow.

Table 5. Screening of Antimicrobial Activity of Isolated Fungi (3-day-old culture) on Seven Tested Organisms

Isolated fungi	Inhibition zone diameters of tested organisms (mm)		
	<i>Agrobacterium tumefaciens</i>	<i>Bacillus subtilis</i>	<i>Escherichia coli</i>
ND-01	18	22	24
ND-02	27	26	25
ND-03	19	25	23
ND-04	25	22	23
ND-05	26	19	22
ND-06	24	24	23
ND-07	25	22	23
ND-08	24	18	22
ND-09	22	25	18
ND-10	24	22	20

In Table 5, the isolated fungi ND-01 to ND-10 showed the antibacterial activity against *Agrobacterium tumefaciens* inhibition zone diameters ranging between 18 and 27 mm, *Bacillus subtilis* ranging between 18 and 26 mm and *Escherichia coli* ranging between 18 and 25 mm. No activity was found against the remaining four tested organisms: *Candida albicans*, *Micrococcus luteus*, *Pseudomonas fluorescens* and *Staphylococcus aureus*. In Figure 5, the fungus ND-02 showed the highest antibacterial activity against *Agrobacterium tumefaciens* (27 mm), *Bacillus subtilis* (26 mm) and *Escherichia coli* (25 mm) respectively. According to the results, ND-02 fungus showed the highest antibacterial activity out of ten strains.

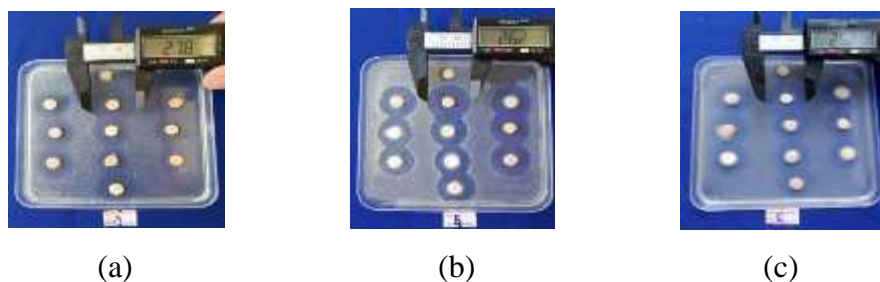


Figure 5. Antibacterial activity of the isolated soil fungi ND-02 (3-day-old culture) against (a) *Agrobacterium tumefaciens*, (b) *Bacillus subtilis* and (c) *Escherichia coli*

Table 6. Inhibition Zone Diameters of Selected ND-02 Fungus (within 3 to 7 days culture) on *Agrobacterium tumefaciens*

Fungus	Inhibition zone diameters of ND-02 fungus (mm) within 3 -7 days				
	3	4	5	6	7
ND – 02	32.61	26.3	26.1	25.3	25.0

The antibacterial activity of ND-02 fungus was determined by paper disc diffusion method. In this study, ND-02 exhibited distinct clear zone against *Agrobacterium tumefaciens* within 3 to 7 days culture as shown in Figure 6 and Table 6.

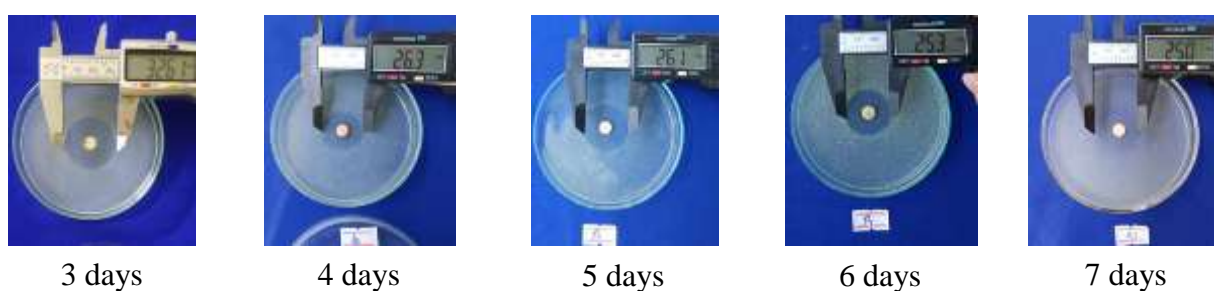


Figure 6. Antibacterial activity of ND-02 fungus (within 3 to 7 days culture) against *Agrobacterium tumefaciens*

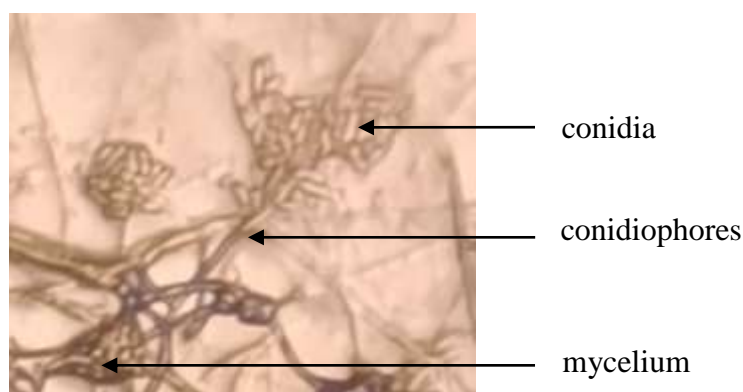


Figure 7. Photomicrograph of isolated fungus ND-02 from the soil (S-1) Yay Kyaw Village, Taung Thar Township (400X)

In Figure 7, photomicrograph of isolated fungus ND-02 consists of conidia, conidiophores and mycelium. The typical fungus character showed that ND-02 was fusarium species, and the surface colour of ND-02 was white and the reverse colour was light pale around white.

The Amylase Enzyme Activity of Isolated Fungi by Iodine Test

The hydrolyzing starch activity of isolated fungi was tested by iodine test (NITE, 2004-2005). Change of iodine colour indicates the action of amylase activity in hydrolysis of starch. After adding iodine solution to the isolated fungi ND-01 to ND-10, all samples except ND-02 showed active with iodine. In this study, ND-01, 03, 04, 05, 06, 07, 08, 09 and 10 can hydrolyze the starch (Figure 8). Therefore, these isolated nine fungi showed that may produce amylase enzyme. But only one fungus ND-02 cannot hydrolyze the starch and not possess amylase enzyme activity.

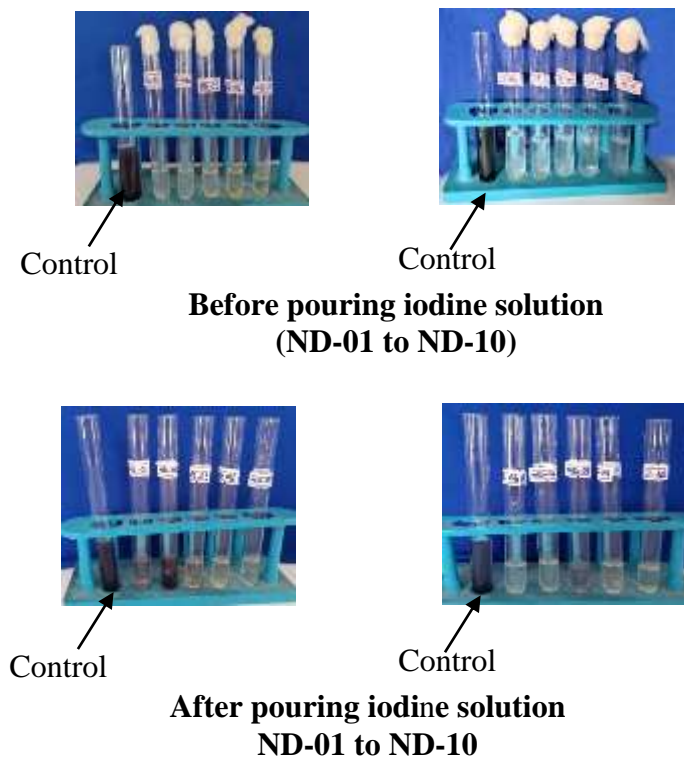


Figure 8. The amylase enzyme activity of isolated fungi

Conclusion

The soil samples (S-1 to S-5) were collected from five different places in Taung Thar Township, Mandalay Region. The soil types of the collected soil samples were loamy sand (S-1), sand (S-2 and S-3), and sandy loam (S-4 and S-5). The pH of all tested soil samples varied from 7.63 to 8.86. Moisture content ranged from 0.6% to 3.6%. Nitrogen content in all samples was between 0.013% and 0.213%. Two fungi, ND-01 and ND-02, were isolated from soil sample S-1; ND-03 and ND-04 from soil sample S-2; ND-05 from soil sample S-3; ND-06 and ND-07 from soil sample S-4; and ND-08, ND-09, and ND-10 from soil sample S-5. Therefore, a total of ten fungus isolates were obtained. A total of ten fungi colonies cultured on LCA medium were transferred to PGA medium by using the feeding method and the physical dilution method. Morphological characters of isolated fungal ND-01 to ND-10 were found to have different shapes, surface colours, and reverse colours significantly. The isolated fungus ND-02 consists of conidia, conidiophores, and mycelium. In this research, after three days of fermentation, ten fungal strains were tested for their antimicrobial activity against seven tested

organisms. ND-01 to ND-10 showed activity only against *Agrobacterium tumefaciens* (27mm), *Bacillus subtilis* (26mm), and *Escherichia coli* (25 mm). The antibacterial activity of ND-02 fungus was found to be higher than the other. All isolated fungi except ND-02 showed amylase enzyme activity by starch hydrolysis test.

Acknowledgements

Firstly, I would like to express our appreciation to Daw Su Latt Htwe, Principal, Meiktila Education Degree College, for her invaluable suggestion and encouragement through the course of this research paper and all required facilities. Finally, I would like to record my deepest advice and thanks to Dr Moe Moe Aye, Professor, Head of Botany Department, Patheingyi University.

References

- Aina, V. O., A. A Adewuni; J. H. Haruna. and Z. Amina. (2011). "Isolation and Identification of Fungi associated with the Deterioration of Painted Wall Surfaces within Daduna Polytechnic". *Asian J. Med. Sci.* vol.3 (6). pp.250-253.
- Ando, K.(2004). *Isolation and Identification of Fungi*. Workshop, BRBDC-Patheingyi University.
- Cattle, J. A., A. B. Mc Branety, and B. K. Minasny. (2002). "Method Evaluation for Assessing the Spatial Distribution of Urban Soil Lead Contamination". *J. Environmental Quality*. vol.31. pp.1576-1588.
- Dominati E., M Patterson, and A. MacKay. (2010). "A Framework for Classifying and Quantifying Natural Capital and Ecosystem Services of Soil, Ecological Uptake in a Boreal Forest". *New Phytologist* vol. 173. pp.611-620.
- Harayama, T., and K. Isono, (2002). "Sources of Microorganisms", *J. Microbiology*, vol.48, pp. 46-50.
- Kurtzman, C.P. (1992). *Impact of Micology on the Needs of the 21st Century, in Proceeding of the Asian Mycological Symposium, Oct 1-4, Seoul Korea*, pp. 1-6.
- Laboratory of Applied Microbiology, (1998). *Screening of Soil Microorganisms*, Faculty of Agriculture, Hokkaido University, Japan.
- NITE (National Institute of Technology and Evaluation), (2005). *Media for Fermentation to Produce the Metabolites*, Hokkaido University, Japan.
- Phay, N. and H. Yamamura, (2005). "Approach Method for Rare Microorganisms from Soil Sources", *J. Microbiol.*, vol.76, pp.237-239.

INVESTIGATION OF SOME BIOLOGICAL ACTIVITIES FROM THE LEAVES OF *CALOTROPIS GIGANTEA* (L.) W.P. AITON (MAYO GYI)

Su Swe Su¹, Suu Suu Win²

Abstract

This research aims to evaluate the phytochemical tests, antioxidant, antimicrobial and cytotoxic activities from the leaves of *Calotropis gigantea* (L.) W.P. Aiton. The total phenol contents of watery extract (47.56 ± 0.1 mg GAE/g) and ethanol extract (64.18 ± 0.7 mg GAE/g) of the sample were tested by using Folin-Ciocalteu method. The total flavonoid contents of watery extract (33.49 ± 0.3 mg QE/g) and ethanol extract (35.47 ± 0.1 mg QE/g) of the sample were determined by aluminum chloride method. In addition, the tannin content (2.1 %) was determined by using titration method. From EDXRF investigation, *C. gigantea* sample contains high concentrations of organic compounds together with trace amounts of some elements. The antioxidant activity was done on the watery extract ($IC_{50} = 42.37$ μ g/mL) and ethanol extract ($IC_{50} = 33.67$ μ g/mL) by using DPPH assay. Then, antimicrobial activities of ethanol and watery extracts of the samples were investigated by agar well diffusion method using pathogenic microorganisms such as *Escherichia coli*, *Saccharomyces cerevisiae*, *Candida albicans*, *Agrobacterium tumefaciens* and *Salmonella typhi* against test microorganisms (13 - 15 mm inhibition zone diameters). Moreover, cytotoxicity of the ethanol extract (LD_{50} value of 1.76 μ g/mL) was higher than watery extract (LD_{50} value of 8.57 μ g/mL) of sample, determined by using brine shrimp lethality bioassay. According to these experimental results, the leaf of *C. gigantea* is safe and suitable to treat various diseases including cancer and aging.

Keywords: *C. gigantea*, antioxidant activity, cytotoxicity and antimicrobial activity

Introduction

Calotropis gigantea (L.) W.P. Aiton is usually called as “crown flower,” and “giant milkweed”. *C. gigantea* is commonly used in medicines such as asthma, colds, hacks and fever. *C. gigantea* is used to treat homeopathic, toothache, erasing, and disgorging. *C. gigantea* leaves has shown cytotoxic activity against human tumor containers. *Calotropin*, which was isolated from its roots, has antitumor activity, cytotoxic activity in leukemia and stomach cancer (Chakre, 2019).

Botanical Description

Botanical name	:	<i>Calotropis gigantea</i> (L.) W.P.Aiton
Genus	:	<i>Calotropis</i>
Species	:	<i>C. gigantea</i>
Family name	:	Apocynaceae
Myanmar name	:	Mayo Gyi
English name	:	Crown flower or giant milkweed
Parts used	:	Leaves
Medicinal uses	:	antitumor activity, cytotoxic activity, antibacterial activity, antioxidant activity, analgesic activity, anti-diarrhea activity, anti-inflammatory activity



Figure 1. *Calotropis gigantea* (L.) W.P. Aiton

¹ Department of Chemistry, Yadanabon University

² Department of Chemistry, Yadanabon University

Materials and Methods

Sample Collection

The leaves of *C. gigantea* were collected from Yadanabon University Campus, Amarapura Township, Mandalay Region.

Phytochemical Screening

The phytochemical investigation of the sample was carried out by standard procedures (Harborne, 1984).

Determination of Mineral Elements

The elemental analysis of powder of *C. gigantea* leaves was determined by Energy Dispersive X-ray fluorescence (EDXRF) spectrometry using EDX-8000 instrument at Monywa University, Sagaing Region.

Determination of Total Phenol, Total Flavonoid and Total Tannin Contents of Ethanol and Watery Extracts from the Leaves of *C. gigantea*

The phenolic contents of watery and ethanol extracts of the leaves sample were determined by utilizing Folin-Ciocalteu reagent (FCR) method according to Song *et al.*, (2010). And the total flavonoid contents of watery and ethanol extracts were estimated by aluminium chloride method. Then, the whole tannin substance in tested sample was evaluated by titrimetric method of watery extract (Atanassova and Christova-Bagdassarian, 2009).

Screening of Antioxidant Activity of Ethanol and Watery Extracts from the Leaves of *C. gigantea*

Diphenyl-1-picrylhydrazyl (DPPH) may be a prevalent, fast, simple, and reasonable approach for the estimation of antioxidant properties that incorporates the utilization of the free radicals for surveying the potential of substances to serve as hydrogen suppliers or free-radical foragers (FRS). DPPH free radical scavenging activity was determined by UV-visible spectrophotometric method.

Screening of Antimicrobial Activity of Crude Extracts from the Leaves of *C. gigantea* by Agar Well Diffusion Method

The screening of antimicrobial activity of crude extracts such as ethanol and watery extracts of the leaves of *C. gigantea* were carried out by agar well diffusion method (Collins *et al.*, 2004) at Department of Botany, Yadanabon University.

Determination of Cytotoxicity of Tested sample from the Leaves of *C. gigantea*

Brine shrimp lethality bioassay could be a quick and comprehensive bioassay for the bioactive compounds. The strategy utilizes *in vivo* lethality in a straight forward zoological living being (*brine nauplii*) as a convenient screen for screening and fractionation within the revelation of unused bioactive normal items (Hassan *et al.*, 2015).

Results and Discussion

Phytochemical Constituents Present in the Leaves of *C. gigantea*

From the research work, the preliminary phytochemical tests, a variety of metabolites such as alkaloids, flavonoids, phenolic compounds, polyphenols, tannins, steroids, α -amino acids, carbohydrates, glycosides, terpenoids and saponins were found in tested sample.

Elemental Analysis of the Leaves of *C. gigantea*

According to EDXRF analysis, some mineral elements required for human beings such as Ca, K, Cu, S, P, Fe, Mn, Sr were observed to be present in plant sample.

Total Phenol, Total Flavonoid, and Total Tannin Contents of the Crude Extracts of *C. gigantea*

In the quantitative analyses of some phytochemical constituents, the total phenol contents of ethanol and watery extracts of *C. gigantea* leaves were found to be 64.18 ± 0.7 and 47.56 ± 0.1 mg GAE/g crude extract, respectively.

In addition, the total flavonoid contents of ethanol and watery extracts of the *C. gigantea* leaves were observed to be 35.47 ± 0.1 and 33.49 ± 0.3 mg QE/g crude extract, respectively. The total phenol and flavonoid contents of ethanol extracts were found to be greater than watery extracts of the sample. Total tannin content was 2.1 % in the tested sample.

Antioxidant Activity of the Leaves of *C. gigantea*

The antioxidant activity was determined in terms of radical scavenging ability of the EtOH and watery extracts of the sample by using the stable radical DPPH assay. These results are shown in Table 1. From these observations, ethanol extract of the *C. gigantea* leaves ($IC_{50} = 33.67 \mu\text{g/mL}$) possessed the better radical scavenging property than the watery extract ($42.37 \mu\text{g/mL}$).

Table 1. Percent Radical Scavenging Activity of Crude Extracts of *C. gigantea*

Tested samples	% RSA (mean \pm SD) in different concentrations ($\mu\text{g/mL}$)					IC_{50} ($\mu\text{g/mL}$)
	6.25	12.5	25	50	100	
ethanol extract	29.97 ± 0.2	36.42 ± 0.2	44.35 ± 0.2	62.22 ± 0.1	94.16 ± 0.1	33.67
watery extract	25.97 ± 0.2	30.57 ± 0.6	41.92 ± 0.6	56.54 ± 0.1	83.89 ± 0.1	42.37
gallic acid (standard)	46.95 ± 0.6	51.78 ± 0.1	55.40 ± 0.2	65.96 ± 0.1	82.98 ± 0.1	10.4

Antimicrobial Activity of Crude Extracts of the Leaves of *C. gigantea*

The antimicrobial activity of ethanol and watery extracts of selected sample was investigated by agar well diffusion against eight microorganisms. The results are described in Table 2.

According to experimental results, ethanol extract of sample showed low activity on four tested organisms and medium activity on *Escherichia coli* (13-15 mm inhibition zone diameters) and then, no activity on *Bacillus subtilis*, *Micrococcus luteus*, and *Pseudomonas fluorescens*.

Furthermore, watery extract of sample responded low activity on *E. coli* and no activity on other organisms. Ethanol extract of sample has higher antimicrobial activity than watery extract of sample. So, the selected sample, *C. gigantea* leaves may be used to treat diseases caused by harmful microorganisms.

Table 2. Antimicrobial Activity of the Ethanol and Watery Extracts of *C. gigantea*

Micro organisms	Inhibition zone diameter (mm)	
	Ethanol extract	Watery extract
<i>A. tumefaciens</i> (NITE 09678)	13	-
<i>B. subtilis</i> (IFO 90571)	-	-
<i>C. albicans</i> (NITE 09542)	13	-
<i>E. coli</i> (AHU 0255)	15	13
<i>M. luteus</i> (NITE 83297)	-	-
<i>P. fluorescens</i> (IFO 94307)	-	-
<i>S. cerevisiae</i> (NITE 52847)	13	-
<i>S. typhi</i> (AHU 9743)	13	-

Agar well – 10 mm; 10 mm–14 mm (low activity); 15 mm–19 mm (medium activity); above 20 mm (high activity); No activity (-),

Cytotoxicity of the Ethanol and Watery Extracts of the Leaves of *C. gigantea*

Brine shrimp cytotoxicity bioassay showed that the ethanol extract of sample was more harmful to brine shrimp than watery extract. The LD₅₀ values of ethanol and watery extracts were 1.76 and 8.57 µg/mL, respectively. These results are indicated in Table 3.

Table 3. Cytotoxicity of Ethanol and Watery Extracts of the Leaves of *C. gigantea*

Sample	Dead % in different concentrations (µg/mL) of samples				LD ₅₀ (µg/mL)
	1	10	100	1000	
ethanol extract	44.7 ± 0.7	73.1 ± 0.1	85.5 ± 0.8	87.9 ± 0.4	1.76
watery extract	36.4 ± 0.7	51.9 ± 0.7	77.6 ± 0.5	80.5 ± 0.4	8.57
*caffeine	0 ± 0	0 ± 0	9.6 ± 0.9	12.7 ± 0.4	>1000
** K ₂ Cr ₂ O ₇	48.6 ± 0.2	73.1 ± 0.5	74.7 ± 0.1	100 ± 0.1	1.58

*Standard caffeine = negative control

**Standard K₂Cr₂O₇ = positive control

Conclusion

According to the preliminary phytochemical tests, different types of metabolites such as alkaloids, flavonoids, phenolic compounds, polyphenols, tannins, steroids, α-amino acids, carbohydrates, glycosides, terpenoids and saponins, were detected and starch, reducing sugar and protein were not detected in the leaves of *C. gigantea*. The total phenol contents and total flavonoid contents were higher in ethanol extract than the watery extract. The ethanol extract had more prominent antioxidant activity than that of the watery extract. Ethanol extract showed medium antimicrobial activity. The leaves of *C. gigantea* may possess strong anticancer activity due to their high cytotoxic effect. Therefore, the tested plant might be valuable in the formulation for the treatment of antitumor.

Acknowledgements

The authors would like to express profound gratitude to the Myanmar Academy of Arts and Science, and Dr Tint Moe Thuzar, Rector, Yadanabon University for their permission to submit this research paper.

References

- Atanassova, M. and V. Christova- Bagdassarian. (2009). "Determination of Tannins Content by Titrimetric Method for Comparison of Different Plant Species". *Journal of the University of Chemical Technology and Metallurgy*, vol.44(4), pp.413-415.
- Chakre, M.B., M. M. Katare, P. N. Gaikwad, K. J. Medpalli, and S. B. Birru. (2019). "Medicinal Properties of *Calotropis gigantea*". *Journal of Research and Analytical*. vol.6(1), pp.175-179.
- Collins, C. H., P. M. Lyne, J. M. Grange, and J. O. Falkinham. (2004). *Microbiological Methods*. New York: 8th ed., CRC Publisher, Oxford University Press Inc., pp.82-90.
- Harborne, J. B. (1984). *Phytochemical Methods, A Guide to Modern Techniques of Plant Analysis*. New York: 2nd ed., Chapman and Hall, pp.120-126.
- Hassan, R., M. Hossain, and D. Nittananda. (2015). "Cytotoxic (Brine Shrimp Lethality Bioassay) and Antioxidant Investigation of *Barringtonia acutangula* (L.)". *Journal of Pharma Sciences and Research*. vol.6(8), pp.1179-1185.
- Song, F. L., R.Y. Gan, Y. Zhang, Q. Xiao, L. Kuang, and H. B. Li. (2010). "Total Phenolic Contents and Antioxidant Capacities of Selected Chinese Medicinal Plants". *Journal of Molecular Science*. vol.11, pp.2367-2372.

COPPER EXTRACTION AND RADON EXAMINATION IN SELECTED MINE SAMPLES

Win Ko¹, Swann Nyein Htet²

Abstract

The main objective of this study was to analyze the elemental composition of three chosen samples, with a specific focus on extracting copper from a rock sample obtained from the Letpadaung copper mine. Additionally, the research investigated the potential health risks for mine workers and assessed radon concentrations in these mine samples using LR-115 Solid State Nuclear Track Detectors (SSNTDs). The LR-115 type II detectors were employed to explore radon in various samples: coal from the Thitchauk coal mine, fly ash from the Tigyit power plant, and rock samples from the Letpadaung copper mine. The tracks observed through an optical microscope, confirmed the presence of radon as an alpha emitter in some samples. The annual effective radiation dose of each sample determined was 0.6531 mSv/y for fly ash sample and 0.4533 mSv/y for coal samples. However, all annual effective doses for the samples were below the international reference level of 3-10 mSv/y recommended by the International Commission on Radiological Protection (ICRP). It is crucial to inform individual working in power plants about the potential health risks associated with radon exposure. Moreover, elemental composition analysis using ED XRF data revealed the presence of various elements in the samples. Furthermore, copper extraction from the rock sample was carried out through a metal displacement reaction and electrolysis, resulting in a copper content of 2.07 %.

Keywords: LR-115 type II detectors, radon, coal, fly ash, rock, and copper

Introduction

Naturally occurring radioactivity is ubiquitous in our environment, with people continuously exposed to various sources such as solar radiation, cosmic radiation, telluric radiation, and internal radiation from within our bodies. Coal contains natural radionuclides primarily from the U-238 and Th-232 decay chains, existing in trace amounts and considered in equilibrium with their parent radionuclides (AboJassim and Shiitake, 2013). Low-quality coal, like lignite, has been reported to contain Ra-226 concentrations ranging from 310 to 350 Bq/kg (Takahashi *et al.*, 2021). When coal is burned and transformed into fly ash, uranium and thorium concentrations can increase by up to 10 times their original levels.

Fly ash disposal in landfills and abandoned sites, including mines and quarries, poses potential risks of groundwater contamination for people residing in those areas (Abojassim and Husain, 2015). Beyond inhalation, solid fallout is an additional radiation hazard, leading to elevated concentrations of natural radionuclides in surface soils around power plants. Uranium leaching from fly ash into soil and water at disposal sites can impact cropland and, consequently, food (Barooah *et al.*, 2011).

Radon, a naturally occurring inert radioactive gas with no taste, colour, or odour and a half-life of 3.83 days, can dissolve in water, enabling its transport over considerable distances through soil. In specific locations, radon concentrations may pose a significant health risk.

Copper, a widely utilized metal in electrical, electronics, construction, and manufacturing sectors, undergoes extraction through two main methods: pyrometallurgy and hydrometallurgy. Pyrometallurgy is primarily employed for sulphide flotation concentrates on an industrial scale, economically viable when dealing with copper-rich ores. In contrast, hydrometallurgy is a widely used method for copper extraction on a global scale.

¹ Department of Chemistry, Monywa University

² General Administration Department, Chaung Oo Township, Sagaing Region

Radon exploration in the building materials by using LR-115 detector has been studied by Win Ko *et al.* (2021). This work focuses on the investigation of the elemental content from three mine samples and the extraction of copper from the Letpadaung copper mine. Furthermore, the examination of the health hazards for mine workers and the radon concentration of these mine samples using LR-115 as Solid-State Nuclear Track Detectors (SSNTDs).

Materials and Methods

Detection of Alpha Particles via Radon in Some Selected Samples

In this work, LR-115 type II Solid State Nuclear Track Detectors were used for measuring alpha particles via radon in coal samples from the Thitchauk coal mine, Kalewa Township, Sagaing Region, fly ash samples from the Tigyit power plant, Shan State, and rock samples from the Letpadaung copper mine, Salingyi Township, Sagaing Region.

Each sample (100 g) was placed in the cylindrical ‘Can’ as shown in Figure 1. The LR-115 type II detector was fixed on the top inside of the ‘Can’ for six months (180 days). The plastic ‘Can’ is 7.5 cm in height and 8.0 cm in diameter. During this time, the alpha particles from radon and its daughter would leave tracks on the detector. The LR-115 type II detector was removed from the plastic ‘Can’ and etched chemically in a 10 % NaOH solution at 60 °C for 90 min in an oven. The etched tracks on the detectors were scanned using an optical microscope at 200 magnifications (Win Ko and Hnin Hnin Than, 2022).

The measured track density was converted into Bq/m^3 by using a calibration factor ($0.21 \text{ tracks/cm}^2\text{d} = \text{Bq/m}^3$) determined by the National Institute of Radiological Science (NIRS), Vietnam (Nguyen *et al.*, 2016).



Figure 1. Detection of alpha particles via radon in the selected sample

Extraction of Copper from Letpadaung Copper Mine Rock Samples

Acid leaching

The copper mine rock samples were crushed into small pieces or powder to increase the surface area for better contact with the acid. Sulphuric acid was commonly used for copper leaching due to its effectiveness and cost-efficiency. A suitable reactor or vessel was set up to conduct the leaching process. The appropriate amount of acid was decanted into the vessel to create the desired concentration of the acid solution. The temperature and time were controlled in the acid-leaching process. Higher temperatures and longer leaching times enhanced copper extraction, but safety considerations should be taken into account. The acid to ore ratio is an essential parameter. The appropriate ratio depends on the ore composition and the desired copper extraction efficiency. It is necessary for good copper extraction to have two days’ percolation. The solid residue (copper-depleted rock) was separated from the liquid solution (leachate) using filtration and centrifugation techniques. The resulting solution, rich in copper sulphate and sulphuric acid, was collected in a beaker. Consequently, the copper sulphate solution was carried out by using displacement reaction and electrolysis.

Displacement reaction of copper (II) sulphate solution

The reactivity between two metals can be compared using displacement reactions in salt solutions of one of the metals. This is easily seen as the more reactive metal slowly disappears from the solution, displacing the less reactive metal. Zinc is a reactive metal and can displace copper from copper (II) sulphate solution. The blue colour of the CuSO_4 solution fades as a colourless zinc sulphate solution is formed.

Electrolysis

Leach liquors (copper (II) sulphate) were used from the acid leaching of the Letpadaung copper mine. During the electrolysis of copper sulphate with copper electrodes, copper was deposited on the cathode and the same amount of copper was removed from the anode. It was done for a good amount of copper to have two days of electrolysis. In this process, a good amount of copper was produced from the Letpadaung copper mine. This result is shown in Table 4.

Results and Discussion

Elemental Analysis of Coal, Fly Ash and Rock Samples by ED XRF

The results of the elemental analysis of coal, fly ash, and rock samples are shown in Table 1. The coal sample contained Fe (51.275 %), Ca (24.727 %), and S (15.192 %). In the fly ash sample, Si (41.027 %), Ca (26.739 %), Al (17.251 %), and U (0.054 %) were detected. The rock sample showed the presence of Si (34.226 %), Cu (27.930 %), S (18.658 %), and Fe (12.072 %).

Table 1. Relative Abundance of Some Elements in Coal, Fly Ash, and Rock Samples by ED XRF

No.	Symbol	Relative Abundance (%)		
		Coal	Fly Ash	Rock
1	Si	-	41.027	34.226
2	Ca	24.727	26.739	0.533
3	Al	-	17.251	-
4	Fe	51.275	7.924	12.072
5	K	0.899	3.620	5.707
6	S	15.192	1.712	18.658
7	Ti	1.155	1.126	0.680
8	V	-	0.128	0.037
9	Mo	-	0.091	-
10	Mn	0.161	0.064	0.032
11	U	-	0.054	-
12	Cr	0.173	0.046	-
13	Zr	-	0.044	0.023
14	As	-	0.042	-
15	Cu	3.484	0.033	27.930
16	Zn	0.258	0.024	-

No.	Symbol	Relative Abundance (%)		
		Coal	Fly Ash	Rock
17	Rb	-	0.023	-
18	Sr	1.629	0.022	0.101
19	Ni	1.048	0.020	-
20	Y	-	0.010	-

From the ED XRF data, uranium was found to be present in the fly ash samples. According to literature, the natural radionuclides present in coal consist mostly of members of the U-238 and Th-232 decay chains. Thus, radon and its decay products will be found in the fly ash samples.

Application of LR-115 Type II Film Detectors for Radon Measurement at Some Selected Samples

The LR-115 type II detector is better at alpha detection. Hence, it was used for the observation of alpha particles via radon-emitting sites such as coal, fly ash, and rock samples. From the study of microscope images, LR-115 type II can detect alpha. An LR-115 type II detector was used for radon level measurement in these selected samples. Radon activity, radon exhalation rate, and radon concentration in some selected samples were measured. Alpha radiation tracks can be detected by using LR-115 type II with an active layer. The photomicrographs for the revelation of alpha particle tracks observed in LR detectors placed at the top of the coal samples are shown in figure 3. The track density, radon activity, radon exhalation rate, radon concentration, and annual effective dose were calculated by a computer Excel program and the results are described in Table 2.

The average track density of coal samples was found to be 105.2542 track/cm²d. The annual effective dose equivalent rate for the Thitchauk coal mine workers lies within the range of 0.1219 to 0.9748 mSv/y, i.e., lies within the intervention limit (3-10 mSv/y) for mine workers. Although the mine workers are safe from health hazards from radon, people staying around the coal mine should be aware of the health risks from radon exposure.

Figure 4 shows the photomicrographs of the revelation of alpha particles tracks observed LR detectors placed at the top of the fly ash samples from Table 3, the average track density of fly ash samples was found 151.6566 tracks/cm²d. The annual effective dose of fly ash samples for the Tigyit power plant workers lies within the range of 0.4265 to 1.0480 mSv/y. According to the ICRP recommendations, the intervention limit for workplaces is 3–10 mSv/y. Therefore, the mean value of annual effective dose (0.6531 mSv/y) of fly ash lies within the intervention limit for workers. People staying around the Tigyit power plant are not at risk of radon exposure.

Figure 5 shows the photomicrographs of the revelation of alpha particles tracks observed LR detectors placed at the top of the rock samples from Table 4, the average track density of rock samples was found 36.2165 tracks/cm²d. Therefore, the mean annual effective dose (0.2418 mSv/y) of rock samples lies within the intervention limit for workers. People staying around the mine are not at risk of radon exposure.

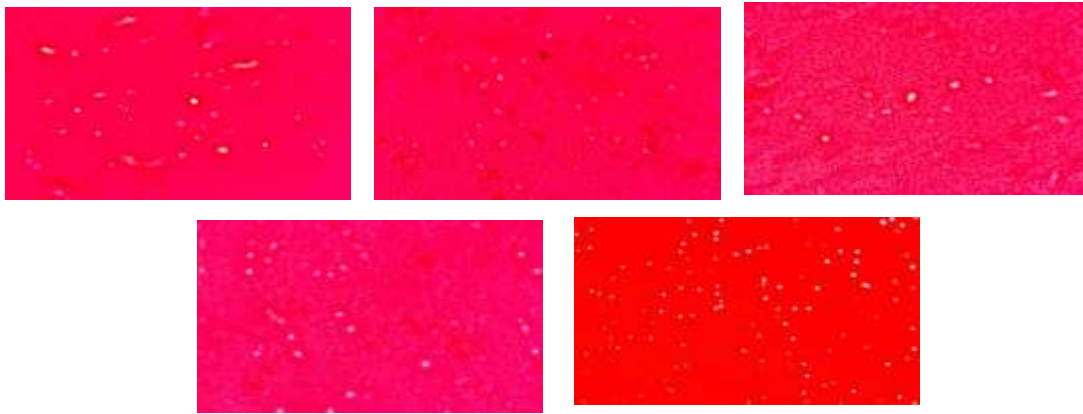


Figure 3. Photomicrographs for the revelation of the alpha particle tracks observed in five LR-115 detectors placed at the top of the coal samples

Table 2. Measurement of Track Density, Radon Activity, Radon Concentration, and Annual Effective Dose in Coal Samples

Detectors	Track Density (tracks/cm ² d)	Radon Activity (Bq/m ³)	Radon Concentration (Bq/m ³)	Annual Effective Dose (mSv/y)
1	28.2941	134.7340	4.3401	0.1219
2	70.7354	336.8351	10.8503	0.3046
3	82.0530	390.7287	12.5864	0.3534
4	118.8354	565.8829	18.2285	0.5118
5	226.3532	1077.8722	34.7210	0.9748
Mean	105.2542	501.2106	16.1453	0.4533
Value ± s	± 75.0035	± 357.1595	± 11.5050	±0.3229

s = standard deviation

* ICRP reference level of radon concentration = 200–600 Bq/m³

** ICRP reference level of annual effective dose = 3–10 mSv/y

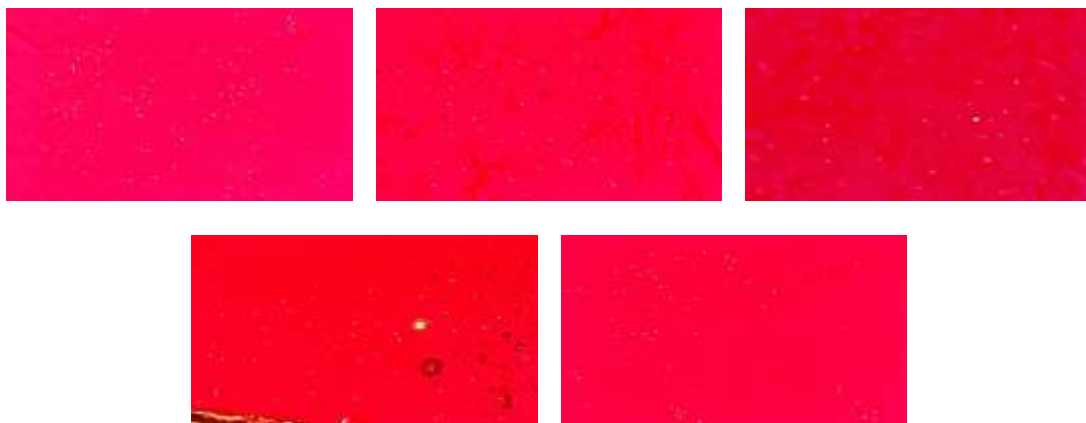


Figure 4. Photomicrographs for the revelation of the alpha particle tracks observed in five LR-115 detectors placed at the top of the fly ash samples

Table 3. Measurement of Track Density, Radon Activity, Radon Concentration, and Annual Effective Dose in Fly Ash Samples

Detectors	Track Density (tracks/cm ² d)	Radon Activity (Bq/m ³)	Radon Concentration (Bq/m ³)	Annual Effective Dose (mSv/y)
1	99.0295	471.5691	15.1904	0.4265
2	127.3237	606.3031	19.5305	0.5484
3	141.4707	673.6701	21.7006	0.6093
4	147.1296	700.6169	22.5686	0.6336
5	243.3297	1158.7126	37.3250	1.0480
Mean	151.6566	722.1744	23.2631	0.6531
Value ± s	±54.5204	±259.6209	±8.3631	±0.2348

s = standard deviation

* ICRP reference level of radon concentration = 200–600 Bq/m³

** ICRP reference level of annual effective dose = 3–10 mSv/y



Figure 5. Photomicrographs for the revelation of the alpha particle tracks observed in five LR-115 detectors placed at the top of the rock samples

Table 4. Measurement of Track Density, Radon Activity, Radon Concentration, and Annual Effective Dose in Rock Samples

Detectors	Track Density (tracks/cm ² d)	Radon Activity (Bq/m ³)	Radon Concentration (Bq/m ³)	Annual Effective Dose (mSv/y)
1	19.8059	94.3138	4.7095	0.1322
2	36.7824	175.1542	8.7463	0.2456
3	42.4412	202.1010	10.0919	0.2833
4	39.6118	188.6276	9.4191	0.2645
5	42.4412	202.1010	10.0919	0.2833
Mean	36.2165	172.4596	8.6117	0.2418
Value ± s	± 9.4690	± 45.0906	± 2.2516	± 0.0632

s = standard deviation

* ICRP reference level of radon concentration = 200–600 Bq/m³

** ICRP reference level of annual effective dose = 3–10 mSv/y

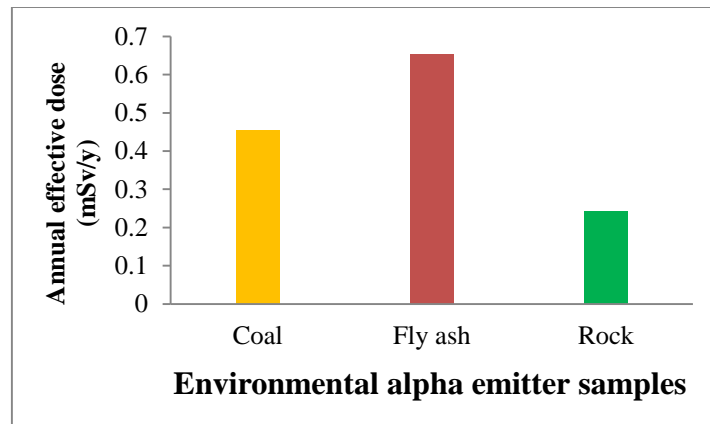
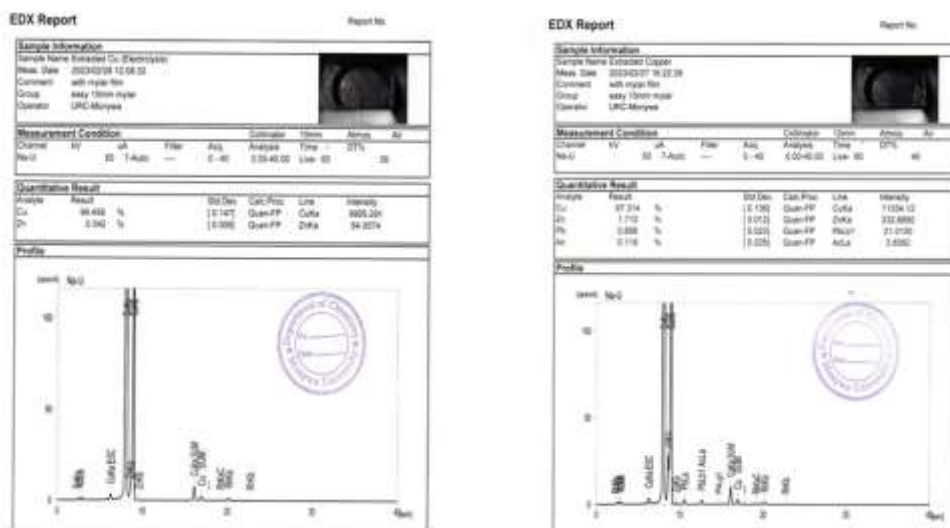


Figure 6. The annual effective doses of environmental alpha-emitter samples

According to Figure 6, the annual effective doses of fly ash samples are higher than the others. The by-products of fly ash from thermal power plants have thus become a subject of worldwide interest in recent years because they can be used in the production of cement, clay ash bricks, and cellular concrete blocks, as well as in the construction of roads and rail embankments and similar applications. Therefore, the workers should be aware of the health risks from radon exposure.

Extraction of Copper from Letpadaung Copper Mine Rock Samples

The copper content (27.930 %) of the rock samples was determined by an ED XRF analysis (Figure 7). Copper extraction (2.6324 g/200g) from the rock ores was successfully carried out after two days of electrolysis. Furthermore, the displacement reaction of metal was used to extract copper (18.100 g/800g from the rock ores). The results from Table 4 shows that a higher copper content (2.07324 %) was obtained in the copper extraction process.



(a) Electrolysis

(b) Displacement reaction of metal

Figure 7. Pure copper content (%) by using ED XRF analysis

Table 5. The Copper Content of the Rock Samples from the Lapadaung Copper Mine

No.	Method	Extracted Copper (g)	Pure copper (%)	Copper content (%)
1.	electrolysis	2.6324	99.458	
2.	displacement reaction of metal	18.100	97.314	2.07324

From ED XRF data, the extracted copper contents by electrolysis and displacement reaction of metal were found to be 99.458% and 97.314%, respectively. During electrolysis, pure copper (99.458 % Cu) was deposited on the cathode plates, along with impurities that are soluble and fall to the bottom of the cell as anode mud or sludge (Figure 8).

**Figure 8.** Extracted copper from the Letpadaung copper mine rock samples

Conclusion

This study concludes that the LR-115 type II film detector successfully detected radon concentration in all samples (coal, fly ash, and rock) due to alpha-emitting radioactive substances. Analysis of ED XRF data revealed the presence of uranium in fly ash samples, indicating the likelihood of radon and its decay products in both coal and fly ash samples. The annual effective doses in coal, fly ash, and rock samples were found to be 0.4533, 0.6531, and 0.2416 mSv/y, respectively, adhering to the international reference level (3–10 mSv/y) set by the ICRP. Despite this, individuals residing in proximity to mines and power plants should remain vigilant regarding potential radon exposure. ED XRF analysis of rock samples identified the presence of copper, sulphur, and iron. Through metal displacement reactions, copper was produced with 97.314 % purity whereas electrolysis produced 99.458% purity. This extracted copper holds potential applications in the production of wires, plates, tubes, and other copper-based products, showcasing the utility of copper displacement reactions for MSMEs (micro, small, and medium-sized enterprises). The insights from this research contribute valuable information to the economic considerations of regional economies.

Acknowledgments

We express our gratitude to Dr Aung Kyaw Thin, the Rector of Monywa University, for granting permission to carry out this research and for his invaluable guidance. Special appreciation is extended to Professor Dr Ni Ni Aung, Head of the Chemistry Department at Monywa University, for her generous assistance and valuable suggestions. Additionally, our thanks go to Professor Dr Hnin Hnin Than, Head of the Chemistry Department at the Dagon University, for her support and contributions to this work.

References

- AboJassim, A. A. and A. R. Shitake. (2013). "Estimated the Mean of Annual Effective Dose of Radon Gases for Drinking Water in Some Locations at Al-Najaf City". *Journal of Kufa-physics*, vol. 5(2), pp. 53-58.
- Abojassim, A. A., and A. A. Husain, (2015). "Radon Concentrations Measurement in Dwellings of Kufa Technical Institute, Iraq using LR-115 Nuclear Track Detector". *Journal of Nuclear Medicine and Radiation Therapy*, (S7), pp.1-6.
- Barooah. D., S. Phukan, and R. Baruah. (2011). "Study of Radon Exhalation Rates using LR-115(II) Nuclear Track Detectors in Coal-mining Area of the Foothills of Mokokchung District, Nagaland". *Indian Journal of Pure and Applied Physics*, vol. 49 (10), pp. 665-668.
- Nguyen, T. T. H., T. V. Giap, and L. D. Cuong. (2016). "Technical Procedure Determination of Thoron Indoor Concentration by LR-115 Type II". *Journal of Environmental Science and Engineering*, vol.5, pp.109-114.
- Takahashi. L. C, T. O. Santos, B.G.Correa, R.M.M.Pinheiro, M.A.B.C. Menezes, and Z. Rocha. (2021). "Calibration of Solid-State Nuclear Track Detectors CR-39 for Radon Study in High Concentration Underground Mines". *Brazilian Journal of Radiation Science*, vol. 9(1A), pp.1-13.
- Win Ko, Toe Toe Lwin, and Hnin Hnin Than. (2021). "Study on Radon Exploration in The Building Materials by Using LR-115 Detector". *J. Myanmar Acad. Arts Sci.* vol. 19, (1A), pp.337-346.
- Win Ko and Hnin Hnin Than (2022). "Comparison of Radon Exploration in Different Environmental Samples by Using LR-115 Type II Detector". *J. Myanmar Acad. Arts Sci.* vol. 20 (1), pp.27-35.

ENZYMIC STUDY ON PECTINASE EXTRACTED FROM WHITE DRAGON FRUIT PEELS

Phyu Phyu Thwin¹, Jue Jue Khin², Myat Kyaw Thu³, Ye Myint Aung⁴

Abstract

Isolation and purification of pectinase enzyme from the peels of white dragon fruit (*Selenicereus undatus*) were performed by 20-80 % ammonium sulphate precipitation followed by gel filtration chromatography on Sephadex G-100. Pectinase enzyme activity was determined using glucose as a standard and pectin as a substrate by a UV-Vis spectrophotometer at 591 nm. The optimum pH and temperature of crude and partially purified pectinase enzymes extracted from the white dragon fruit peels were found as 5 and 30 °C, respectively. The activation energies (E_a) of the crude and purified pectinase-catalyzed reactions were observed as 4.1185 kcal mol⁻¹ and 3.4018 kcal mol⁻¹, respectively. The K_m and V_{max} values were found as 0.300×10^{-2} g mL⁻¹ and 25.380×10^{-2} mM min⁻¹ for crude pectinase enzyme and 0.509×10^{-2} g mL⁻¹ and 26.281×10^{-2} mM min⁻¹ for partially purified pectinase enzyme, using the Lineweaver-Burk plot. The reaction order (n) of the crude and purified pectinase-catalyzed reactions was calculated using the linear regression method, and it was found to be first order. Both crude and partially purified pectinase enzymes were used in the clarification of grape juice and the transmittance percents were 75.49 % and 86.29 %, respectively. The clarity of grape juice can be improved by enzymatic treatment using pectinase.

Keywords: pectinase, white dragon fruit, *Selenicereus undatus*, pectin, grape juice

Introduction

Pectinase alone accounts for about one-quarter of the world's food enzyme production and is among the most important industrial enzymes. Pectinases are enzymes that are responsible for the biological degradation of pectin, a polysaccharide with large molecular weight found in the cell walls of plants. This enzyme splits polygalacturonic acid into monogalacturonic acid by opening glycosidic linkages (Swarnalatha *et al.*, 2021). In plants, pectinases play a diverse role, such as cell-cell adhesion, a source of signaling molecules, and the ripening of fruits (Okonji *et al.*, 2019). Pectinases are used in several conventional industrial processes. They are one of the most widely distributed enzymes in bacteria, fungi, insects, nematodes, and protozoa (Adeyefa and Ebuehi, 2020). They are of great significance, with a wide range of applications in the fruit, beverage, and textile processing industries, in the treatment of wastewater, degumming of plant fibres, pulp and papermaking, and coffee and tea fermentation (Ubani *et al.*, 2015). The current research aims to extract pectinase from white dragon fruit peel, and study its kinetic properties and its efficiency in juice clarification.

Materials and Methods

White dragon fruit (*Selenicereus undatus* (Haw) D. R. Hunt) was collected from Hledan Market, Kamayut Township, Yangon Region. 3,5-Dinitrosalicylic acid (DNS) and all other chemicals were used from Sigma- Aldrich, England. All the chemicals used in this work

¹ Department of Chemistry, University of Yangon

² Department of Chemistry, University of Yangon

³ Department of Chemistry, Mohnyin University

⁴ Department of Chemistry, University of Yangon

were analytical grade. In all procedures, the recommended standard methods and techniques involving both conventional and modern methods were applied.

Isolation of Pectinase Enzyme from White Dragon Fruit Peels

White dragon fruits (*Selenicereus undatus*) was peeled and cut into small pieces. The peels (20 g) were homogenized with 160 mL of 0.1 M sodium acetate buffer (pH 5.0) for 5 min using a blender. After homogenization, the resulting slurry was filtered through cheesecloth. The filtrate was centrifuged for 20 min at 6000 rpm to obtain 82 mL of extract. Solid ammonium sulphate (9.3 g) was added to this extract to obtain 20 % saturation and stirred for 2 h at 4 °C. After standing for 2 h, the suspension was centrifuged for 20 min at 6000 rpm. The supernatant liquid was decanted and brought to 80 % saturation with 23.6 g of solid ammonium sulphate, and stored at 4 °C. After standing overnight, the precipitated protein containing pectinase enzyme was collected by centrifugation for 20 min at 6000 rpm, and the crude pectinase was obtained.

Purification of Pectinase Enzyme by Gel Filtration Chromatography

Gel filtration was carried out in a column (2.0 × 25 cm) packed with pre-swollen Sephadex G-100 using 0.1 M sodium acetate buffer (pH 5.0) and equilibrated with the same buffer (500 mL). The enzyme was eluted from the column with the same equilibrated buffer. The Sephadex column was flushed with the eluent for several hours prior to the addition of the sample.

The crude pectinase enzyme (2 g) was dissolved in 4 mL of sodium acetate buffer (pH 5.0). The solution was applied to a Sephadex G-100 gel filtration column with the flow rate of 1.5 mL per 5 min. A 1.5 mL fraction was collected per tube using a fraction collector. After collection, the protein content of each tube was checked by measuring the absorbance at 280 nm wavelength using a UV-Vis spectrophotometer. Each tube was also measured for pectinase activity at 591 nm using a UV-Vis spectrophotometer. The fractions that had the highest pectinase activity were pooled.

Pectinase Enzyme Assay

For the enzyme assay, 0.5 mL of enzyme solution was incubated with 0.5 mL of 1 % pectin substrate (in 0.1 M sodium acetate buffer of pH 5.0) at 30 °C for 10 min. Then, 1 mL of 1 M of DNS solution was added, and this mixture was boiled at 90 °C for 5 min. Next, 1 mL of 1 M sodium potassium tartrate solution was added to stop the reaction, and then 2 mL of distilled water was added to the mixture. The absorbance of the diluted mixture was measured at 591 nm by a UV-Vis spectrophotometer. For a blank solution, 0.5 mL of distilled water was used instead of 0.5 mL of enzyme solution.

Protein Determination

Protein content in each purification step was determined by Biuret method at 550 nm using bovine serum albumin (BSA) as standard.

Effects of pH, Temperature, and Substrate Concentration on Pectinase Activity

The effect of pH on pectinase activity was determined by varying the pH from 4.4 to 5.8 at intervals of 0.2. The effect of temperature on pectinase activity was determined by varying the temperature from 20 to 50 °C at intervals of 5 °C. The effect of substrate concentration on the pectinase-catalyzed reaction was studied by varying the concentration of substrate (pectin) from 2-16 (mg mL⁻¹). The pectinase activity was assayed as described above using 1% pectin as the substrate. Reaction order of the pectinase-catalyzed reaction was also calculated.

Determination of Activation Energy of the Pectinase-catalyzed Reaction

The velocities of pectinase-catalyzed reaction were measured at the temperature range of 20-50 °C at 5 unit intervals. An Arrhenius plot of the initial velocity data was performed to determine the activation energy.

Application of Pectinase Enzyme in Grape Juice Clarification

In the experiment, 4 mL of grape juice was added to two separate test tubes. Then, 1 mL each of crude and partially purified enzymes was added to the grape juice. The contents of the test tubes were agitated to mix the enzyme throughout the juice and kept for 4 h. After that, the test tubes were heated for 3 min at 40 °C to inactivate the enzyme reaction. Subsequently, the samples were centrifuged for 20 min at 3000 rpm, and the supernatant was filtered. Similarly, the above procedure was carried out without enzymes by using (i) 5 mL of grape juice, and (ii) a mixture of 4 mL of grape juice and 1 mL of distilled water. The clarity of the grape juice obtained was determined by measuring the absorbance of the solution at 660 nm (Ahmed and Sohail, 2020) with a UV-Vis spectrophotometer. The clarity was expressed in percent transmittance.

Results and Discussion

Purification of Pectinase Extracted from White Dragon Fruit Peels

The pectinase enzyme was isolated from a white dragon fruit peel sample and partially purified by the solid ammonium sulphate precipitation method. Figure 1 shows the chromatogram of pectinase on Sephadex G-100 gel. The fraction numbers (30-43) showing the highest pectinase activity were pooled. Table 1 shows the pectinase activities, protein contents, specific activities of the enzyme solutions, and purity of the enzyme. The specific activity of the pectinase increased 3.50 folds over that of crude extract, and the protein recovery was found to be 2.50 %. One unit of enzyme was defined as one micromole of glucose that was liberated per minute.

Optimum pH and Temperature, and Activation Energy of Pectinase-catalyzed Reaction

The optimum pH for pectinase-catalyzed reaction was found to be 5.0 for both crude and partially purified pectinase-catalyzed reactions. It was obvious that the activity of pectinase increased from 4.4 to 5.0 and then decreased from 5.0 to 5.8 as shown in Figure 2. The optimum temperature for pectinase-catalyzed reaction was found to be 30 °C in sodium acetate buffer (pH 5.0) for both enzymes. It was observed that the activity of pectinase increased from 20 to 30 °C and then decreased from 30 to 50 °C as shown in Figure 3.

The activation energy of the pectinase-catalyzed reaction was calculated using the Arrhenius equation. Table 2 shows the relationship between temperature and velocity of pectinase-catalyzed reaction and Figure 4 shows the graph for the determination of activation energy. The partially purified pectinase-catalyzed reaction was found to have a lower activation energy (3.4018 kcal mol⁻¹) compared to crude pectinase-catalyzed reaction (4.1185 kcal mol⁻¹).

Effect of Substrate Concentration on Pectinase-Catalyzed Reaction

The velocities of crude pectinase-catalyzed enzyme reaction measured at different concentrations of substrate and their reciprocal values are shown in Table 3 and the Michaelis-Menten, Lineweaver-Burk, and Eadie-Hofstee plots are depicted in Figures 5, 6, and 7, respectively. In Michaelis-Menten plot, it was found that as the concentration of the substrate was increased while all other factors are kept constant, the velocity increased to a maximum

value, V_{\max} until there was no further increase. The velocity of the reaction at this high substrate concentration is termed as the maximum velocity. The substrate concentration corresponding to half of the maximum velocity is called the Michaelis-Menten constant and is termed as K_m . The Michaelis-Menten plot gives only apparent K_m and V_{\max} values. Table 4 shows the velocities of partially purified pectinase-catalyzed enzyme reaction as a function of concentrations of substrate. In this work, linear regression method was used to obtain K_m and V_{\max} from the experimental results. These values are shown in Table 5 in comparison with K_m and V_{\max} values obtained by Lineweaver-Burk and Eadie-Hofstee plots. K_m for crude pectinase was found to be $0.300 \times 10^{-2} \text{ g mL}^{-1}$ and that of partially purified pectinase was $0.509 \times 10^{-2} \text{ g mL}^{-1}$ from Lineweaver-Burk plot. V_{\max} values were $25.380 \times 10^{-2} \text{ mM min}^{-1}$ and $26.281 \times 10^{-2} \text{ mM min}^{-1}$ for crude and partially purified pectinase enzyme, respectively. K_m and V_{\max} values are not much different between Lineweaver-Burk and Eadie-Hofstee plots. However, the K_m and V_{\max} values of the Michaelis-Menten plot are totally different from those of other plots.

Reaction Order for Pectinase-catalyzed Reaction

Reaction order (n) refers to the number of molecules involved in forming a reaction complex that is required to proceed to the product (s) (Giese, 2004). Depending on the substrate concentrations, the kinetics of an enzyme-catalyzed reaction may be described by a first-order rate equation (Bergmeyer, 1983). In the present work, reaction order (n) values were determined from the plot of $\log V/(V_{\max}-V)$ vs $\log [S]$ using the linear regression method as shown in Table 6 and Figure 11. The reaction order (n) for pectinase was calculated to be ~ 1 , showing that the reaction order is first order.

Application of Pectinase Enzyme in Grape Fruit Juice Clarification

The cloudiness in the juices is due to the presence of polysaccharides such as pectin, cellulose, and starch (Sandri *et al.*, 2011).

In this present work, Table 7 described the clarification of grape juice using pectinase enzyme from white dragon fruit peels. The test tube (A) is only grape juice, the test tube (B) is grape juice and water, and the test tube (C) is the mixture of grape juice and enzyme. The crude and partially purified pectinase showed good activity by clarifying the juices as compared to the control. The pectinase degrades the pectin and increases the clarity of the juice, enhancing its appearance. The clarity in terms of transmittance percent of the grape juice treated with crude pectinase was 75.49 % whereas that of grape juice treated with purified pectinase was 86.29 %. Thus, the partially purified pectinase enzyme has a higher efficiency for clarifying grape juice than crude pectinase enzyme. Thus, pectinase enzyme can be used for the clarification of fruit juice.

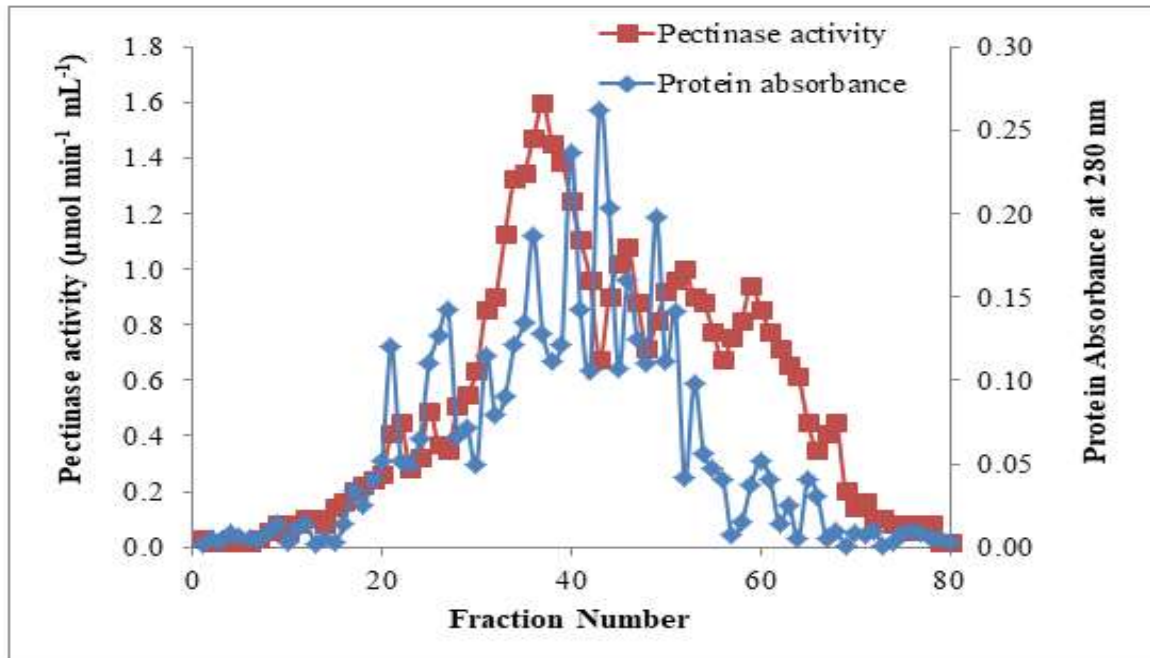


Figure 1. Sephadex G-100 gel filtration chromatogram of crude pectinase enzyme

Table 1. Pectinase Enzyme Activities, Protein Contents and Specific Activities of the Enzyme Solution at Different Purification Steps

Fraction	Total volume (mL)	Total enzyme activity (unit)	Total protein content (mg)	Specific Activity (unit/mg)	Protein recovery (%)	Degree of purity (fold)
crude	145	165.3	749.51	0.22	100	1.00
20 % (NH ₄) ₂ SO ₄ filtrate	90.0	45.00	179.55	0.25	24.0	1.14
80 % (NH ₄) ₂ SO ₄ precipitate	20.0	20.00	60.50	0.33	8.07	1.50
after passing the Sephadex G -100	19.5	14.63	19.11	0.77	2.50	3.50

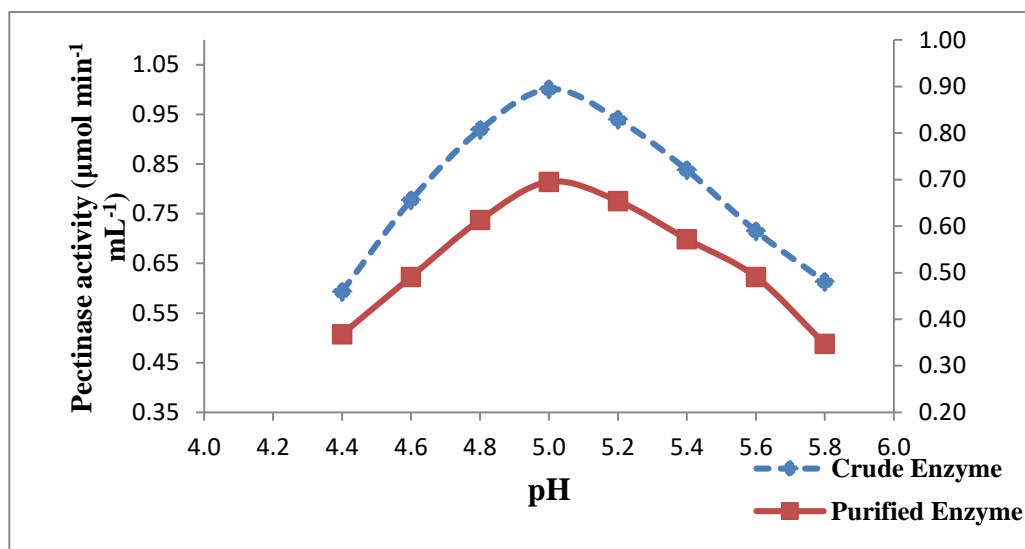


Figure 2. Plot of pectinase activity as a function of pH of the solution

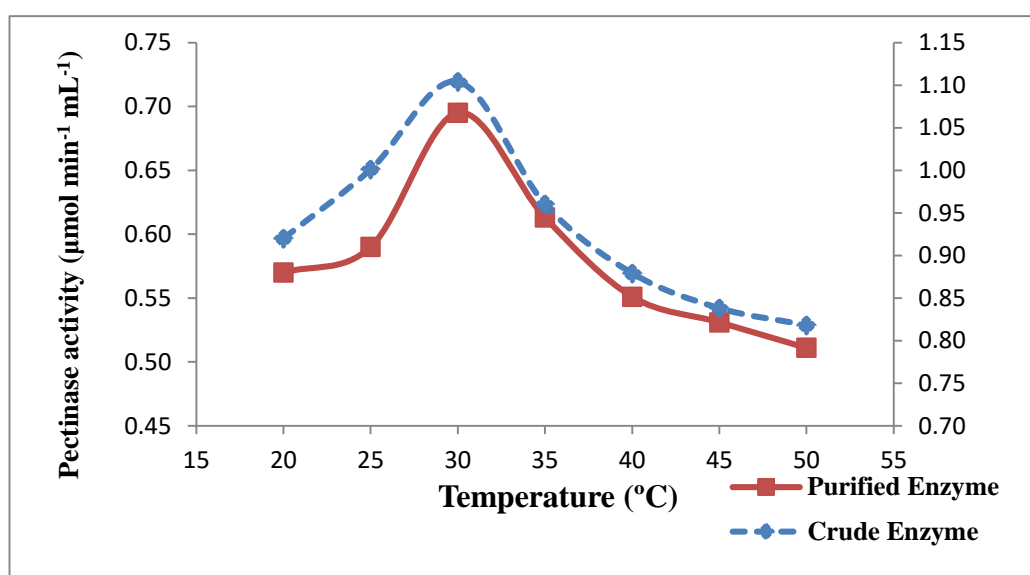


Figure 3. Plot of pectinase activity as a function of temperature of the solution at pH 5

Table 2. Relationship between Temperature and Velocity of Crude and Partially Purified Pectinase-catalyzed Reactions

Temperature (C)	Temperature (K)	1/T × 10 ³ (K ⁻¹)	Crude enzyme		Partially purified enzyme	
			Velocity × 10 ³ (mM min ⁻¹)	Log V	Velocity × 10 ³ (mM min ⁻¹)	Log V
20	293	3.413	174.4	2.241	113.6	2.055
25	298	3.356	198.7	2.298	125.8	2.099
30	303	3.300	214.9	2.340	137.9	2.139
35	308	3.247	190.6	2.280	122.7	2.120
40	313	3.195	174.4	2.241	109.5	1.969
45	318	3.145	166.3	2.220	105.4	1.887
50	323	3.096	162.2	2.210	101.4	1.209

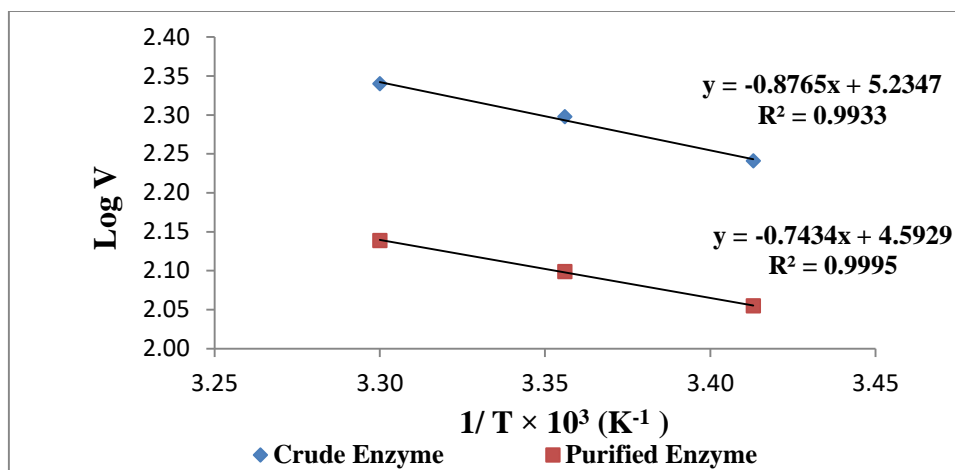


Figure 4. Plot of Log V as a function of 1/T for crude and purified pectinase-catalyzed reactions

Table 3. Relationship between Velocity of Crude Pectinase-Catalyzed Reaction and Substrate Concentration

[S]×10 ² (g mL ⁻¹)	-[S]×10 ² (g mL ⁻¹)	1/[S] (10 ⁻² g ⁻¹ mL)	V × 10 ² (mM min ⁻¹)	1/V (10 ⁻¹ mM ⁻¹ min)	V/[S] (mM min ⁻¹ g ⁻¹ mL)	[S]/V (g mL ⁻¹ mM ⁻¹ min)
0.2	-0.2	5.00	10.10	0.99	50.5	0.019
0.4	-0.4	2.50	14.59	0.685	36.48	0.027
0.6	-0.6	1.67	17.03	0.587	28.38	0.035
0.8	-0.8	1.25	18.65	0.536	23.31	0.043
1	-1	1.00	19.47	0.514	19.47	0.051
1.2	-1.2	0.83	20.28	0.493	16.9	0.059
1.4	-1.4	0.71	20.68	0.484	14.77	0.068
1.6	-1.6	0.63	21.09	0.474	13.18	0.076

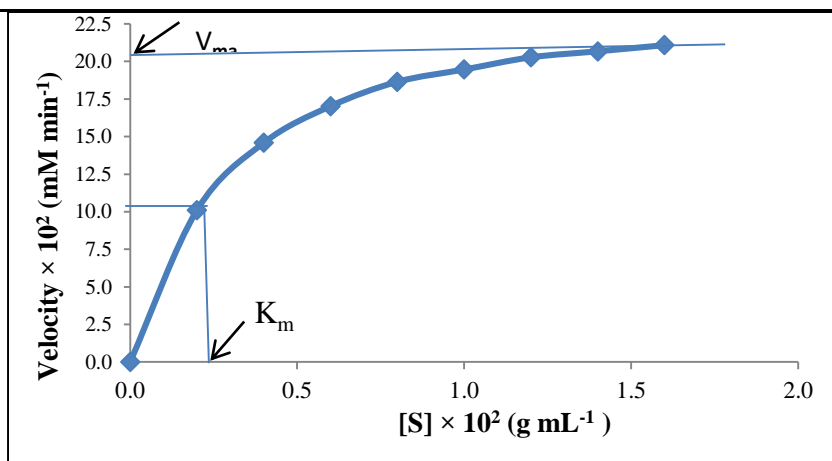


Figure 5. Michaelis-Menten plot of the velocity of crude pectinase-catalyzed reaction as a function of substrate concentration

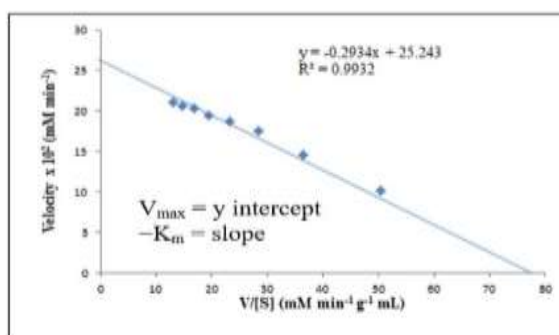
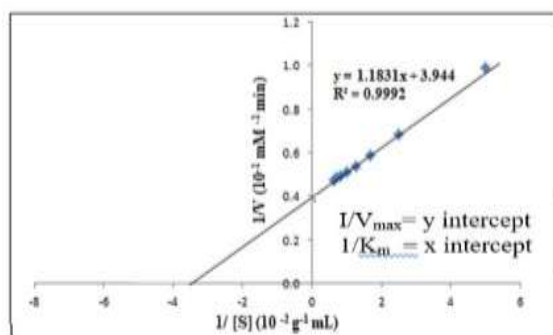
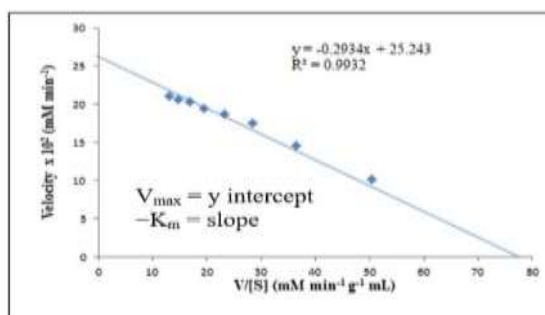
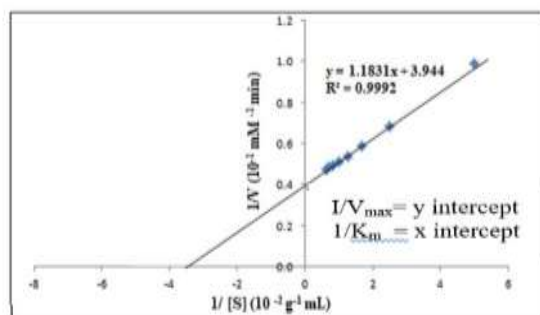


Figure 6. Lineweaver-Burk plot of $1/V$ vs $1/[S]$ used for graphic evaluation of V_{max} and K_m for crude pectinase enzyme

Figure 7. Eadie-Hofstee plot of V vs $V/[S]$ Used for graphic evaluation of V_{max} and K_m for crude pectinase enzyme

Table 4. Relationship between Velocity of Partially Purified Polyphenol Oxidase-Catalyzed Reaction and Substrate Concentration

$[S] \times 10^2$ (g mL ⁻¹)	$-[S] \times 10^2$ (g mL ⁻¹)	$1/[S]$ (10 ⁻² g ⁻¹ mL)	$V \times 10^2$ (mM min ⁻¹)	$1/V$ (10 ⁻¹ mM ⁻¹ min)	$V/[S]$ (mM min ⁻¹ g ⁻¹ mL)	$[S]/V$ (g mL ⁻¹ mM ⁻¹ min)
0.2	-0.2	5.00	7.40	1.351	37	0.027
0.4	-0.4	2.50	11.43	0.874	28.58	0.035
0.6	-0.6	1.67	14.19	0.709	23.65	0.042
0.8	-0.8	1.25	16.22	0.617	2.028	0.049
1.0	-1	1.00	17.84	0.562	17.84	0.056
1.2	-1.2	0.83	18.66	0.536	15.55	0.064
1.4	-1.4	0.71	19.10	0.524	13.64	0.073
1.6	-1.6	0.63	19.46	0.514	12.16	0.082

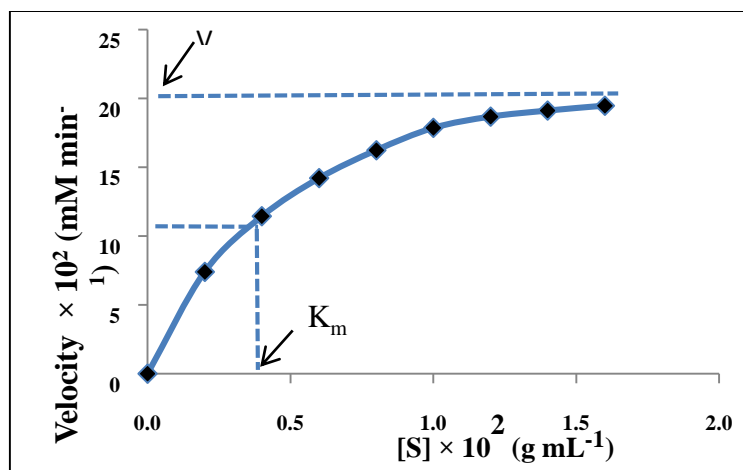


Figure 8. Michaelis-Menten plot of the velocity of partially purified pectinase-catalyzed reaction as a function of substrate concentration

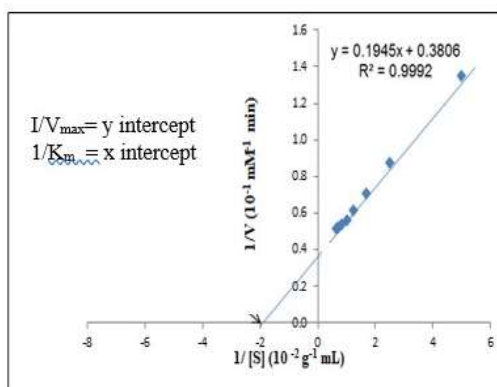


Figure 9. Lineweaver-Burk plot of $1/V$ vs $1/[S]$ used for graphic evaluation of V_{max} and K_m for partially purified pectinase enzyme

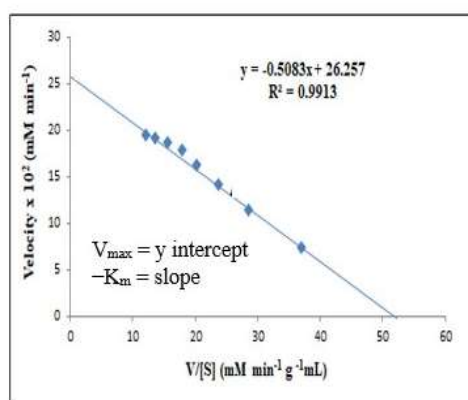


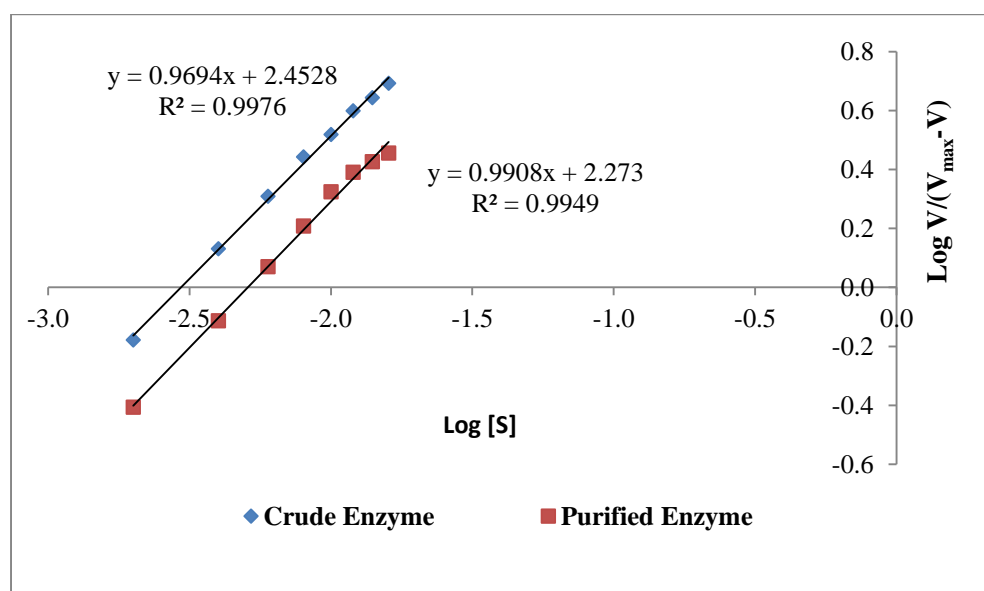
Figure 10. Eadie-Hofstee plot of V vs $V/[S]$ used for graphic evaluation of V_{max} and K_m for partially purified pectinase enzyme

Table 5. Comparison of Kinetic Parameters of Crude and Partially Purified Pectinase from White Dragon Fruit Peels

Enzyme	Method	Linear regression method		Graphical method	
		$K_m \times 10^2$ (g mL ⁻¹)	$V_{max} \times 10^2$ (mM min ⁻¹)	$K_m \times 10^2$ (g mL ⁻¹)	$V_{max} \times 10^2$ (mM min ⁻¹)
crude enzyme	Michaelis-Menten	-	-	0.250	20.02
	Lineweaver-Burk	0.300	25.380	0.330	25.35
	Eadie-Hofstee	0.294	25.196	0.300	25.24
partially purified enzyme	Michaelis-Menten	-	-	0.045	20.05
	Lineweaver-Burk	0.509	26.281	0.500	26.32
	Eadie-Hofstee	0.520	26.503	0.508	26.26

Table 6. Relationship between Velocity of Pectinase-Catalyzed Reaction and Substrate Concentration for the Determination of Reaction Order

[S] (10 ⁻² g mL ⁻¹)	log [S]	Crude enzyme		Partially purified enzyme	
		V × 10 ² (mM min ⁻¹)	Log V/(V _{max} -V)	V × 10 ² (mM min ⁻¹)	Log V/(V _{max} -V)
0.2	-2.699	10.10	-0.179	7.40	-0.407
0.4	-2.398	14.59	0.131	11.93	-0.114
0.6	-2.222	17.03	0.309	14.19	0.070
0.8	-2.097	18.65	0.442	16.22	0.208
1.0	-2.000	19.47	0.518	17.84	0.324
1.2	-1.921	20.28	0.599	18.66	0.390
1.4	-1.854	20.68	0.643	19.10	0.426
1.6	-1.796	21.09	0.692	19.46	0.456

**Figure 11.** Plot of $\text{Log } V/(V_{\text{max}}-V)$ as a function of $\text{log } [S]$ for crude and purified pectinase-catalyzed reaction**Table 7. Grape Juice Clarification at 660 nm by Pectinase**

Test	Absorbance	Transmittance (%)	Test	Absorbance	Transmittance (%)
A	0.186	65.16	A	0.185	65.31
B	0.179	66.22	B	0.178	66.37
C (crude)	0.122	75.49	C (purified)	0.064	86.29

A= control (juice only)

B= grape juice and water

C= grape juice and enzyme

Conclusion

In this research, the pectinase was isolated from white dragon fruit peel by extraction with sodium acetate buffer (pH 5). The specific activity of the enzyme increased about 3.50 folds from crude to the final purification step. The enzymic properties: optimum pH (5.0), optimum temperature (30 °C) and the K_m and V_{max} were determined by the spectrophotometric method. K_m and V_{max} values were calculated to be $0.509 \times 10^{-2} \text{ g mL}^{-1}$ and $26.281 \times 10^{-2} \text{ mM min}^{-1}$ for partially purified pectinase. The reaction order (n) for crude and purified pectinase was a first-order reaction. For the clarification of grape juice, the purified enzyme was found to have a higher efficiency than the crude enzyme. It indicated that the pectinase extracted from peel waste was effective in the clarification of fruit juice. This pectinase needs to be studied more to make sure it works better in the fruit industry.

Acknowledgements

The authors would like to thank the Myanmar Academy of Arts and Science for giving permission to submit this paper and to Professor and Head, Dr Ni Ni Than, Department of Chemistry, University of Yangon, for her kind suggestion. Special thanks are due to the Department of Chemistry, University of Yangon, for providing the research facilities.

References

- Adeyefa, O.M. and O. A.T. Ebuehi. (2020). "Isolation, Identification and Characterization of Pectinase Producers from Agro Wastes (*Citrus sinensis* and *Ananas comosus*)". *World Journal of Agriculture and Soil Science*, vol. 4 (3), pp. 1-6.
- Ahmed, A. and M. Sohail. (2020). "Characterization of Pectinase from *Geotrichum candidum* AA15 and its Potential Application in Orange Juice Clarification". *Journal of King Saud University - Science*, vol.32(1), pp.955-961.
- Bergmeyer, H. U. (1983). *Methods of Enzymatic Analysis*. New York: Academic Press Inc., pp. 69-78.
- Giese, A. C. (2004). *Cell Physiology*. Philadelphia: W. B. Saunders Co., pp.378-386.
- Okonji, R. E., B. O. Itakorode, J. O. Ovumedia, and O. S. Adedeji. (2019). "Purification and Biochemical Characterization of Pectinase Produced by *Aspergillus fumigatus* Isolated from Soil of Decomposing Plant Materials". *Journal of Applied Biology and Biotechnology*, vol. 7 (3), pp. 1-8.
- Sandri, I.G., R. C. Fontana, D. M. Barfknecht, and M. M. da Silveira. (2011). "Clarification of Fruit Juices by Fungal Pectinases". *LWT - Food Science and Technology*, vol.44, pp. 2217-2222.
- Swarnalatha, A., A. Devik, and S. Rishad. (2021). "Isolation and Characterisation of Pectinase Enzyme from Agriculture Waste and its Efficiency in Fruit Juice Clarification". *International Journal of Biology, Pharmacy and Allied Sciences* vol. 10 (11), pp. 335-343.
- Ubani, C. S., A. L. Ezugwu, O. A. Oje, S. C. Gabriel, and A. M. Ekwedigwe. (2015). "Isolation, Partial Purification and Characterization of Pectinase from Water Melon (*Citrullus lanatus*) Rind". *American- Eurasian Journal of Toxicological Sciences*, vol. 7 (2), pp. 110-114.

CONVERSION OF SUGARCANE BAGASSE INTO LEVULINIC ACID BY ACID-CATALYZED HYDROTHERMAL METHOD*

Shunn Lei Nandar¹, Soe Soe Than²

Abstract

Lignocellulosic biomass is a long-term alternative carbon source and could be used as raw material to prepare liquid fuels and valuable chemicals. Among these chemicals, levulinic acid is a valuable platform compound, which is intermediate for preparing alternative petroleum-based chemicals such as plasticizer, coating, and fuel additives. This research work focused on the extraction of levulinic acid from lignocellulosic biomass such as sugarcane bagasse by acid-catalyzed hydrothermal method. The physico-chemical characteristics of sugarcane bagasse such as cellulose, hemicellulose, lignin, extractives, and ash content were analyzed by using TAPPI and AOAC methods. Dilute sulfuric acid pretreatment of sugarcane bagasse was firstly carried out with different variables such as solid to liquid ratio and reaction time for the optimum extraction of cellulose content. Acid-catalyzed hydrothermal treatment of pretreated sugarcane bagasse was performed by controlling reaction temperature, reaction time, concentration of hydrochloric acid (Bronsted acid) and concentration of aluminium chloride (Lewis acid). Central composite design was used to arrange experimental runs to optimize the cellulose content of sugarcane bagasse during dilute sulfuric acid pretreatment and the yield percent of levulinic acid based on concentration during acid-catalyzed hydrothermal method. For calculating the yield percent of levulinic acid based on concentration, the absorbance of levulinic acid was measured by UV-visible spectroscopy at 266 nm (λ_{\max}). The maximum yield percent of levulinic acid based on concentration from sugarcane bagasse (89.64 ± 3.14 %) with the 6.78 % composition of levulinic acid was obtained by synergistic use of 6.4 % (v/v) HCl and 2.3 % (w/v) AlCl₃ at 171 °C for 3 hr and 6 min. The levulinic acid under optimum conditions from pretreated sugarcane bagasse was identified by UV-Visible Spectroscopy for λ_{\max} , FTIR Spectroscopy for functional groups and Gas Chromatography-Mass Spectroscopy (GC-MS) for the presence of levulinic acid.

Keywords: levulinic acid, sugarcane bagasse, bronsted acid, lewis acid

Introduction

Bioenergy and biomass-derived green chemicals have been attracting attention in recent years due to growing concerns about fossil fuel depletion and climate change (Kang *et al.*, 2018). Low-value agro-residues, grasses and energy crops are preferred biomass sources from both a technical and socio-economic point of view, as biomass feedstock does not compete with the food chain (Rackemann & Doherty, 2011).

Due to their complex and specialized structures, biomass such as lignin, cellulose and hemicellulose are difficult to convert directly into desired fuels and chemicals. Therefore, converting biomass to specific platform chemicals and using the platform chemicals to produce various fuels and chemicals would be a viable strategy for biomass utilization (Yang *et al.*, 2013). According to the US Department of Energy, one of the top 12 most promising building materials is levulinic acid, commonly known as 4-oxopentanoic acid or γ -kevaleric acid. It is also known as a promising organic intermediate for synthesizing a wide range of chemicals used in

* Special Award (2023)

¹ Part-time Demonstrator, Department of Industrial Chemistry, University of Yangon

² Professor, Department of Industrial Chemistry, University of Yangon

* Best Paper Award Winning Paper in Industrial Chemistry (2024)

products such as solvents, fragrances, oil additives, pharmaceuticals, and fuel additives (Pileidis & Titirici, 2016).

Significant research is currently underway worldwide to identify attractive pathways for the chemical conversion of lignocellulosic biomass to functional intermediates or platform chemicals. The most widely used method is the hydrolysis of biomass at high temperatures (100–250 °C) using acids as catalysts (Girisuta *et al.*, 2013). In a Chromium (III) Chloride – Hydrochloric acid (CrCl₃-HCl) environment, Choudhary *et al.* (2013) presented a synergistic catalytic method for converting glucose to 5-HMF and LA. Due to their increased activity, Lewis acids are favored over Bronsted acids as isomerization catalysts. A combination of Lewis and Bronsted acids selectively catalyzes the hydrolysis of cellulose, isomerization of glucose, dehydration of fructose, and degradation of 5-hydroxymethyl furfural (5-HMF), ultimately leading to the yield of LA. It may improve the rate and selectivity (Yang *et al.*, 2013).

More studies have been done using Bronsted acids alone than using a combination of Lewis and Bronsted acids to convert lignocellulosic biomass to levulinic acid. Zhang *et al.* (2016) reported the kinetic study of the conversion of levulinic acid from glucose, but not from lignocellulosic biomass, by a combination of HCl and AlCl₃. Therefore, the aim of this study is to apply the synergistic effect of combined Bronsted HCl and Lewis acids AlCl₃ on the conversion of sugarcane bagasse to levulinic acid.

Materials and Methods

Materials

Sugarcane bagasse was collected from Hledan Market, Yangon Region. The analytical grade of hydrochloric acid, aluminium chloride, sodium hydroxide, sulfuric acid, and acetone were purchased from Supershell Store, Pabedan Township, Yangon. **Methods**

Analysis of Composition of Sugarcane Bagasse

Determination of Moisture Content

Moisture content was determined by AOAC 925.09 method (AOAC, 2000).

Determination of Extractives Content

Extractives content was determined following the method (TAPPI T204 cm-97). 2.5 g of dried sample were loaded into the cellulose thimble. With a dry and clean Soxhlet extractor set up, 150 mL of acetone was used as solvent for extraction for 4 hr. After extraction, the sample was air-dried at room temperature for few minutes. Constant weight of the extracted sample was achieved in a hot air oven at 105 °C. Drying, cooling and weighing were repeated until the constant weight was obtained. Then, the extractive content was calculated with the following equation.

Extractives Content, % (w/w) = $\frac{[\text{Weight of raw extractive-laden sample} - \text{Weight of extractive-free sample}]}{\text{Weight of raw extractive-laden sample}} \times 100$

Determination of Hemicellulose Content

Hemicellulose content was determined following (Sluiter *et al.*, 2012). 1 g of extractive-free sample was transferred into a 250 mL Erlenmeyer flask and 150 mL of 0.5 M NaOH was added. The mixture was boiled for 3.5 hr. It was filtered after cooling through vacuum filtration and washed until neutral pH. The residue was dried to constant weight in a hot air oven at 105 °C. Then, the hemicellulose content was calculated with the following equation.

$$\text{Hemicellulose Content, \% (w/w)} = \frac{[\text{Weight of sample before treatment} - \text{Weight of sample after treatment}]}{\text{Weight of sample before treatment}} \times 100$$

Determination of Lignin Content

Lignin content was determined following the method (TAPPI T222 om-11). 0.3 g of extractive-free sample was transferred into a 250 mL Erlenmeyer flask and 3 mL of 72 % H₂SO₄ was added. The sample was kept at room temperature for 2 hr with careful shaking at 30 min intervals in order to allow complete hydrolysis. After initial hydrolysis, 84 mL of distilled water was added. The second step of hydrolysis was made to occur in an autoclave for 1 hr at 121 °C. Then, the slurry was cooled at room temperature and was filtered through vacuum filtration. The residue was dried to constant weight in a hot air oven at 105 °C. Then, the lignin content was calculated with the following equation.

$$\text{Lignin Content, \% (w/w)} = \frac{\text{Weight of sample after treatment}}{\text{Weight of sample before treatment}} \times 100$$

Determination of Cellulose Content

The cellulose content % (w/w) was calculated by difference, assuming that extractives, hemicellulose, lignin, ash, and cellulose are the only components of the entire biomass.

$$\text{Cellulose Content, \% (w/w)} = 100 - [\text{Hemicellulose} + \text{Lignin} + \text{Ash} + \text{Extractives}]$$

Determination of Ash Content

Ash content was determined by AOAC 923 method (AOAC, 2000).

Conversion of Sugarcane Bagasse into Levulinic Acid

The sugarcane bagasse was sun-dried until its moisture content reached below 10 % (w/w). Then, the dried sugarcane bagasse was ground and screened to get suitable particle sizes (- 20 + 40 mesh size). The prepared sugarcane bagasse powder was treated with dilute sulfuric acid 3 % (v/v) at 121 °C to enhance the rupture of biomass. 18 experimental runs were conducted with different process variables such as solid to liquid ratio [1:10 (g : mL) - 1:20 (g : mL)] and reaction time (10 min – 30 min) for the maximum yield of cellulose content. About 3 g of prepared sample were added in a cylindrical stainless steel reactor with polytetrafluoroethylene line inside to resist corrosion by the acid catalyst. The acid catalyzed hydrothermal method was carried out under various process conditions such as acid concentration of Bronsted acid (HCl) and Lewis acid (AlCl₃), reaction temperature and reaction time with a fixed acid ratio (1 (AlCl₃) : 2 (HCl)) and solid to liquid ratio [1:15 (g : mL)] (Chang *et al.*, 2007) in order to optimize the yield of levulinic acid. A preheated air oven was used for heating the reactor to the desired temperature. The reaction was quenched by immersing the reactor in a cool water bath after the desired reaction time. The reaction product was collected and separated from the unreacted residual biomass by filtration. The filtrate was partially neutralized to pH 5 with 1 M NaOH to stabilize levulinic acid and others possibly separated by centrifuge machine with 500 rpm for 5

min. The supernatant was separated by rotary evaporator under vacuum at 120 °C. The distillate residue was detected by UV-visible spectrophotometer at 266 nm for the presence of levulinic acid.

Optimization of Process Variables by Response Surface Methodology

Central Composite Design was chosen for experimental arrangements. Stat-Ease Design-Expert 13 was used. The levels of variables with duplicated samples during dilute sulfuric acid pretreatment are shown in Table 1. The levels of variables for optimization of yield percent of levulinic acid from sugarcane bagasse during acid-catalyzed hydrothermal method are shown in Table 2.

Table 1: Levels of Variables during Dilute Sulfuric Acid Pretreatment of Sugarcane Bagasse

Parameters	Lower Level	Upper Level
Solid to Liquid ratio, g : mL	1 : 10	1 : 20
Reaction Time, min	10	30

Table 2: Levels of Variables during Acid-Catalyzed Hydrothermal Method of Sugarcane Bagasse

Parameters	Lower Level	Upper Level
Temperature, °C	160	180
Reaction Time, hr	2	4
Concentration of HCl, % (v/v)	4	8
Concentration of AlCl ₃ , % (w/v)	1	3

Determination of Yield Percent of Levulinic Acid Produced from Sugarcane Bagasse Based on Concentration

The absorbance of levulinic acid at 266 nm was measured by UV-visible Spectrophotometer (Thermo Fisher Scientific Evolution 201/202 UV-Visible Spectrophotometer). The standard calibration curve for HMF (0 – 0.093 mmol/L) and LA (0 – 64.66 mmol/L) of (Zhang *et al.*, 2013) was applied to calculate the concentration of levulinic acid and yield percent of levulinic acid based on concentration by using the equation; $A_{LA, 266} = 0.0096 + 0.023C$.

Yield percent of Levulinic Acid Based on Concentration =

$$\frac{\text{Concentration of Levulinic Acid } \left(\frac{\text{g}}{\text{L}}\right) \times \text{Dilution Factor} \times \text{Volume of Acid Catalyst (L)} \times 100}{\text{Amount of Biomass Used (g)}}$$

Where, $A_{LA, 266}$ = Absorbance of Levulinic Acid at 266 nm, C = Concentration of Levulinic Acid

Identification of Levulinic Acid Produced from Sugarcane Bagasse by UV-Visible Spectroscopy, FTIR Spectroscopy and Gas Chromatography-Mass Spectroscopy (GC-MS)

The λ_{\max} of levulinic acid was identified by UV-visible Spectrophotometer (Thermo Fisher Scientific GENESYS 10S UV-Visible Spectrophotometer) at the Department of Chemistry, University of Yangon.

The functional groups of levulinic acid were identified by FTIR Spectrometer (PerkinElmer Spectrum Two FT-IR spectrometer) at the Department of Chemistry, University of Yangon.

The levulinic acid produced from sugarcane bagasse was identified by Gas chromatography-mass spectroscopy (GC-MS), (Shimadzu GC-MS QP2010 Ultra) at the Department of Chemistry, University of Mandalay.

Results and Discussion

The chemical composition of sugarcane bagasse powder was presented in Table 3. The cellulose content of sugarcane bagasse was 46.7 % (w/w). Sugarcane bagasse had 24.79 % (w/w) of hemicellulose. The lignin content of sugarcane bagasse was 21.25 % (w/w). Below 10 % (w/w) moisture content gave suitable condition for further processing. Neureiter *et al.* (2002) reported that sugarcane bagasse is composed of 40.2 % (w/w) cellulose, 26.4 % (w/w) hemicellulose, 25.5 % (w/w) lignin and 8.2 % (w/w) others.

Table 3: Composition of Sugarcane Bagasse

Sr. No.	Components of Sugarcane Bagasse	Percent Composition, % (w/w)
1	Moisture content	8.0
2	Extractives	2.2
3	Hemicellulose content	24.79
4	Lignin content	21.25
5	Cellulose content	46.7
6	Ash content	5.06

Dilute sulfuric acid pretreatment was performed to enhance the rupture of sugarcane bagasse for the maximum yield of cellulose content. The 3D surface plots of the effect of solid to liquid ratio and reaction time on the yield percent of cellulose content, hemicellulose content and lignin content are shown in Figure 1 (a, b, c) respectively. The maximum cellulose content 56.15 ± 0.35 , % (w/w), the minimum hemicellulose content 8.63 ± 0.35 , % (w/w) and lignin content 28.76 ± 0.35 , % (w/w) for sugarcane bagasse has resulted by 3 % (v/v) dilute sulfuric acid pretreatment with 1:14 (g:mL) solid to liquid ratio and 24 min reaction time at 121 °C. It was indicated that dilute acid pretreatment of sugarcane bagasse was related to produce maximum cellulose content. According to Mosier *et al.* (2005) and according to Zheng *et al.* (2009), a pretreatment procedure using dilute acid can dissolve virtually all hemicellulose and disrupt lignin-cellulose bonds, thus increasing the digestibility of enzymes/catalysts in the hydrolysis process. During dilute acid pretreatment, increasing solid to liquid ratio and increasing reaction

time resulted increasing in cellulose and lignin and decreasing in hemicellulose content. After increasing the reaction time beyond the optimum conditions, it was found that the slight decrease in cellulose content because of the further degradation products such as furfural and 5-HMF. A dilute sulfuric acid pretreatment is used, which can practically fully dissolve the hemicellulose component (80-90 %), increase the sensitivity of the cellulose, but only marginally break down the lignin component (Yang & Wyman, 2008). Almost all hemicellulose can be dissolved during the pretreatment process using dilute acid, but the lignin component cannot be dissolved. The process can be performed at a temperature range from 120-180 °C and residence times ranging from 15-60 min (Zheng *et al.*, 2009).

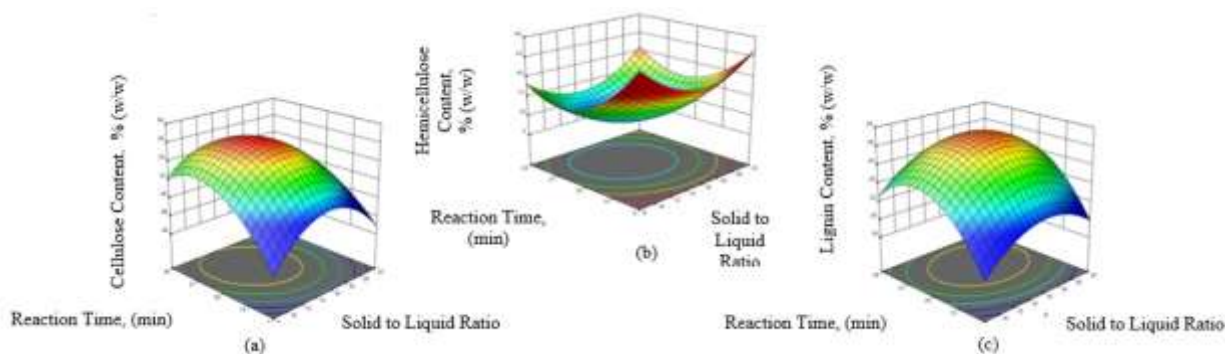


Figure 1: 3D Surface Plots of the Effect of Solid to Liquid Ratio and Reaction Time on the Yield Percent of (a) Cellulose Content (b) Hemicellulose Content (c) Lignin Content during Dilute Sulfuric Acid Pretreatment

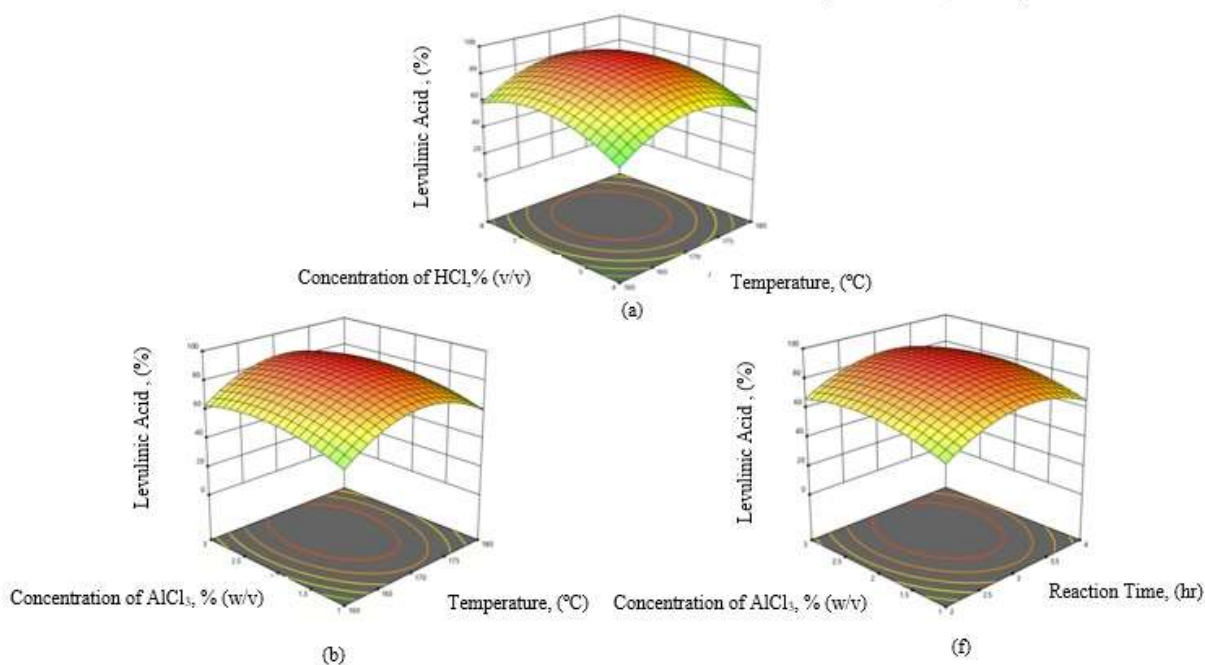
The observed yield percent of levulinic acid produced from sugarcane bagasse due to the effect of temperature, reaction time, concentration of HCl and concentration of AlCl_3 are presented with three-dimensional surface plots for plotting to explore the interactions between variables and determine the optimum conditions for each factor for maximum yield percent of levulinic acid from sugarcane bagasse are shown in Figure 2. The coded equation for the quadratic model describing responses such as yield percent of levulinic acid from sugarcane bagasse based on concentration as a function of temperature, reaction time, concentration of HCl and concentration of AlCl_3 are shown in equation 1.

$$\begin{aligned} \text{Yield Percent of Levulinic Acid Produced from Sugarcane Bagasse} = & \\ & +88.55+3.13A+3.81B+5.94C+4.3D+0.2325AB+0.3313AC-0.0387AD+1.19BC \\ & -0.0837BD+0.6275CD-19.32A^2-14.37B^2-14.17C^2-8.08D^2 \text{ -----(1)} \end{aligned}$$

By solving equation in Microsoft Excel, the predicted value for the optimum variables and yield percent of levulinic acid from sugarcane bagasse are obtained. The maximum yield percent of levulinic acid from sugarcane bagasse (89.64 ± 3.14 %) has resulted with optimum variables such as 171 °C of temperature, 3 hr and 6 min of reaction time, 6.4 % (v/v) of concentration of HCl and 2.3 % (w/v) of concentration of AlCl_3 . It was observed that as HCl and AlCl_3 concentrations increased, the production of levulinic acid increased significantly. However, increasing the concentrations of HCl and AlCl_3 above the optimum conditions resulted in no further increase in levulinic acid yield. Kuznetsov *et al.* (2013) noted that the following activity order might be used to categorize inorganic acids capacity to hydrolyze carbohydrate into LA: $\text{HCl} > \text{H}_2\text{SO}_4 > \text{H}_3\text{PO}_4$. Higher concentrations of mineral acid also severely corroded the

reactor (Chang *et al.*, 2007). According to Signoretto *et al.* (2019), Lewis acid catalysts are used in this procedure because not all Lewis acid sites are active for glucose isomerization, but they also act as a catalyst for side reactions involving soluble polymers and insoluble humins. In this study, the more AlCl_3 was utilized in levulinic acid production from biomass beyond the optimum condition, the lower the percentage of levulinic acid produced due to the formation of undesirable side reactions. One undesirable side reaction is the formation of humins as a result of polymerization processes from a number of intermediate products. The synthesis of humins during the conversion of C6 carbohydrates to levulinic acid is also said to be more evident under harsh reaction circumstances (Sevilla & Fuertes, 2009a, 2009b; Sweygers *et al.*, 2018; Van Zandvoort *et al.*, 2013). The effect of reaction temperature on levulinic acid yield from sugarcane bagasse was investigated in the temperature range of 160–180 °C. Regarding the temperature, it can be seen that the yield of levulinic acid was sufficiently improved as the reaction temperature increased. This clearly indicates that the conversion of biomass to levulinic acid is endothermic in nature, so high temperatures are advantageous for effective conversion (Liu *et al.*, 2017). However, the production of levulinic acid decreased above 180 °C. High temperatures can accelerate the conversion of carbohydrates to levulinic acid, but also cause undesirable side effects (Chang *et al.*, 2007). The effect of reaction time on levulinic acid yield from sugarcane bagasse was investigated in the range of 2 hr to 4 hr. Regarding the reaction time; a decrease in the yield of levulinic acid was observed when the reaction was performed beyond the optimal conditions. This decrease in levulinic acid yield is due to the fact that the dehydrated product is unstable and can undergo decomposition upon prolonged exposure to high temperatures. In addition, prolonged hydrolysis of biomass may promote side reactions and generate chars and humins (Joshi *et al.*, 2014; Patil & Lund, 2011).

Furthermore, if the reaction is prolonged, decomposition of levulinic acid may occur, resulting in a decrease in the yield of levulinic acid (Liu *et al.*, 2017).



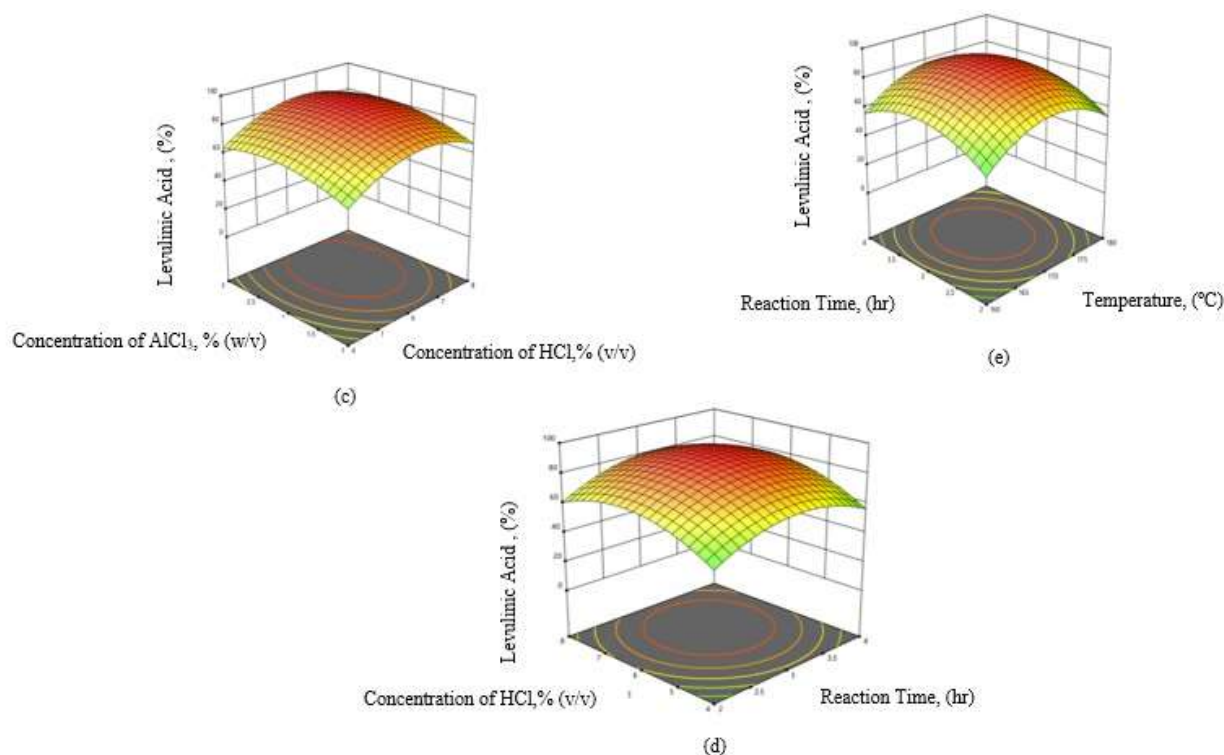


Figure 2: 3D Surface Plots of the Effect of (a) Temperature and Concentration of HCl (b) Temperature and Concentration of AlCl₃ (c) Concentration of HCl and Concentration of AlCl₃ (d) Reaction Time and Concentration of HCl (e) Temperature and Reaction Time (f) Reaction Time and Concentration of AlCl₃ on the Yield of Levulinic Acid Produced from Pretreated Sugarcane Bagasse

Identification of Levulinic Acid Produced from Sugarcane Bagasse

UV-Vis Spectrum of levulinic acid from sugarcane bagasse was shown in Figure 3. For interpretation of UV-Vis spectrum, the more easily an electron can be excited, the greater the wavelength that is absorbed, and the more electrons will be excited, the higher the absorbance. Compounds such as ketones, acids, esters, amides, and other compounds that contain the system π and lone pair shows two absorption: the transition $n \rightarrow \pi^*$ at wavelengths longer (> 300 nm, low intensity) and the transition $\pi \rightarrow \pi^*$ at wavelengths lower (< 250 nm high intensity with their conjugations), λ_{\max} ribbon $\pi \rightarrow \pi^*$ shifted to wavelengths greater and predictable with the Rules of Woodward (Pratiwi & Nandiyanto, 2022). Levulinic acid is keto-carboxylic acid containing keto carbonyl group and carboxylic acid group. Based on the observation of the absorption bands and the identification of the possible chromophore, it can be inferred that the chromophore absorption band at 266 nm appearing in Figure 3 is levulinic acid.

To identify the functional groups of levulinic acid produced from sugarcane bagasse, FTIR analysis was conducted. Figure 4 show the results of the FTIR spectrum of levulinic acid produced from sugarcane bagasse. Mthembu (2016) reported that the O-H ($3300-2500$ cm^{-1}) stretching of carboxyl groups, the C=O (1715 cm^{-1}) stretching of ketone and carboxyl groups, and the C-H ($3000-2850$ cm^{-1}) stretching of alkanes groups are essential vibrations of levulinic acid. For sugarcane bagasse, the FTIR spectrum contains all of the important vibrations of LA,

including O-H (3289 cm^{-1}) stretching for the carboxylic group, a very strong absorption of C=O at 1698 cm^{-1} stretching for the carboxylic ketone group, C-H (2928 cm^{-1}) stretching for alkane and the sp^2 hybridized C-O vibration stretching for carboxylic groups at 1209 cm^{-1} .

Levulinic acid was detected using the Gas chromatography-mass spectroscopy (GC-MS), as indicated in Figure 5. The GC chromatogram for sugarcane bagasse revealed the presence of two main products in the sample taken from the reaction mixture. The components were identified by comparing with the GC libraries (NIST14.lib) and literature. 4-oxo-pentanoic acid, methyl ester (levulinic acid, methyl ester) is present in the sample at a concentration of 0.62 peak area % with the similarity index 94 %, as indicated by the peak that emerged at 4.854 retention time. Levulinic acid, with a 6.16 peak area % with the similarity index 98 %, is the primary component of the second peak with a retention time of 7.663. For sugarcane bagasse, the mass spectrum of levulinic acid, methyl ester is depicted in Figure 5a. The first bar found has an m/z ratio of 130, which is identical to the relative molecular mass of methyl ester of levulinic acid. The subsequent fragmented isotopes found are 115, 99, 88, 71, 57, 43, and so on. This particular fragment or ion may be the most abundant and have the highest intensity among all the observed ions because m/z 43 is the base peak in this mass spectrum. For sugarcane bagasse, there is another peak for confirmation of the presence of levulinic acid. Figure 5b shows the mass spectrum of levulinic acid. The first bar found has an m/z ratio of 116, which is identical to the relative molecular mass of levulinic acid. Following that, fragmented isotopes 96, 73, 56, 43, and so on are discovered. The pattern is extremely similar to the data retrieved from the NIST library, as illustrated in Figure 5. The fact that m/z 43 is the base peak in this mass spectrum indicates that this particular fragment or ion is the most abundant and has the highest intensity of all the observed ions. According to the peak area %, the composition of levulinic acid was 6.78 % with similarity index 98 % from sugarcane bagasse. The yield percent of 6.78 % composition of levulinic acid from sugarcane bagasse based on concentration ($89.64 \pm 3.14\%$) was obtained.

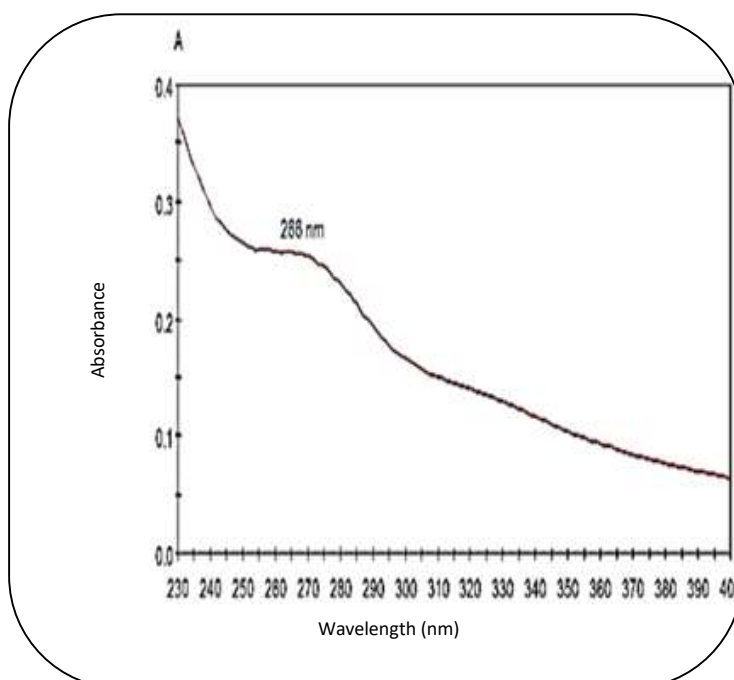


Figure 3: UV-Visible Spectrum of Levulinic Acid from Sugarcane Bagasse

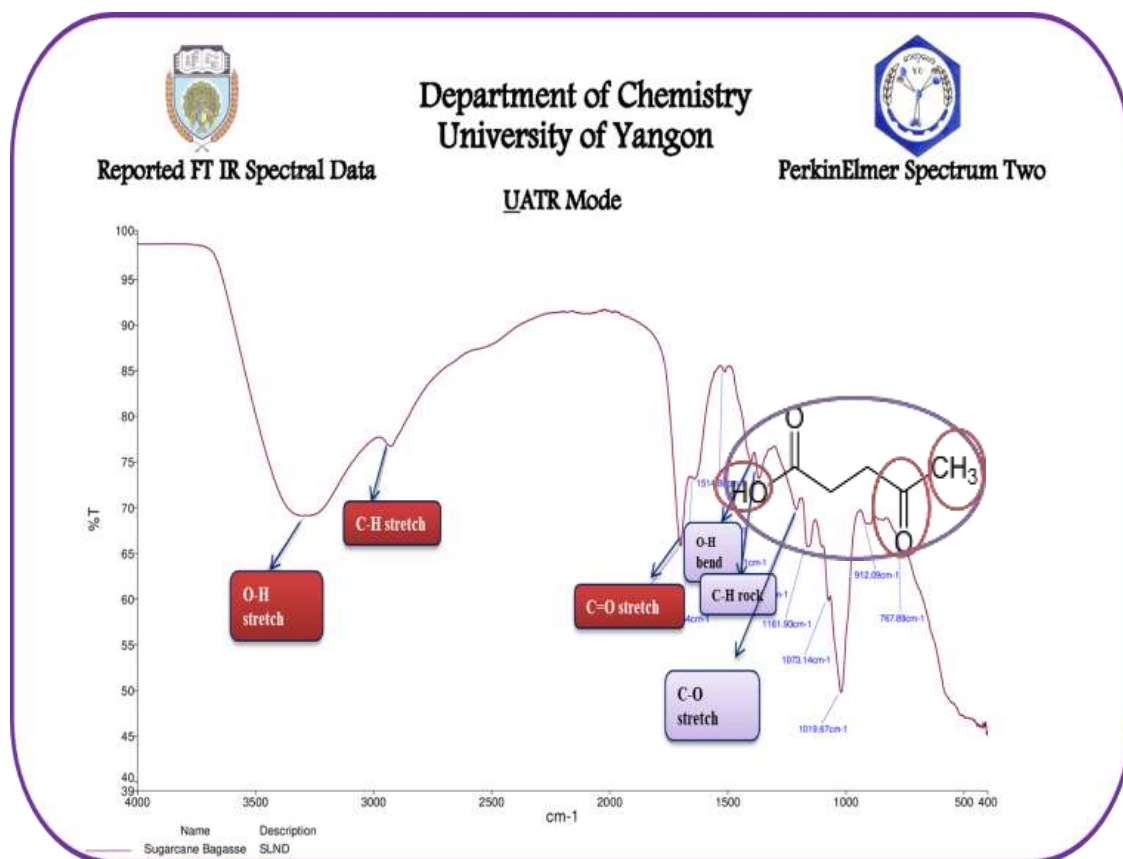
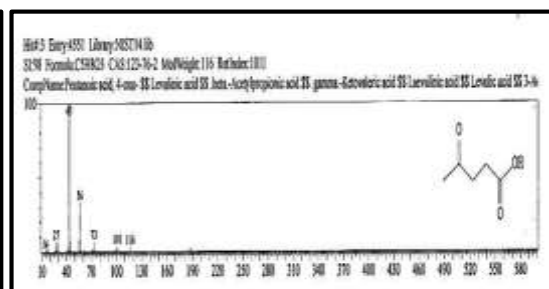
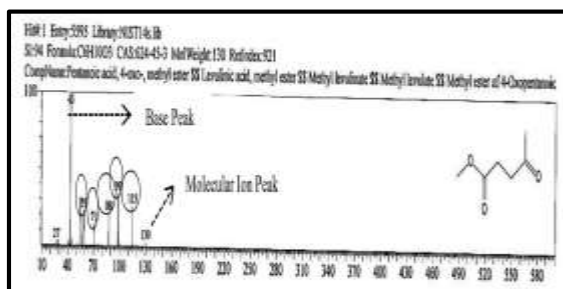
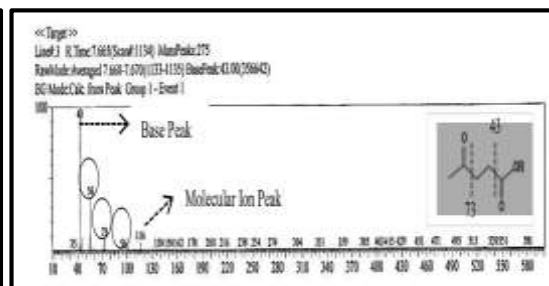
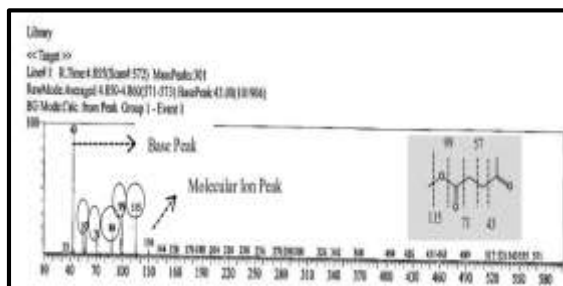
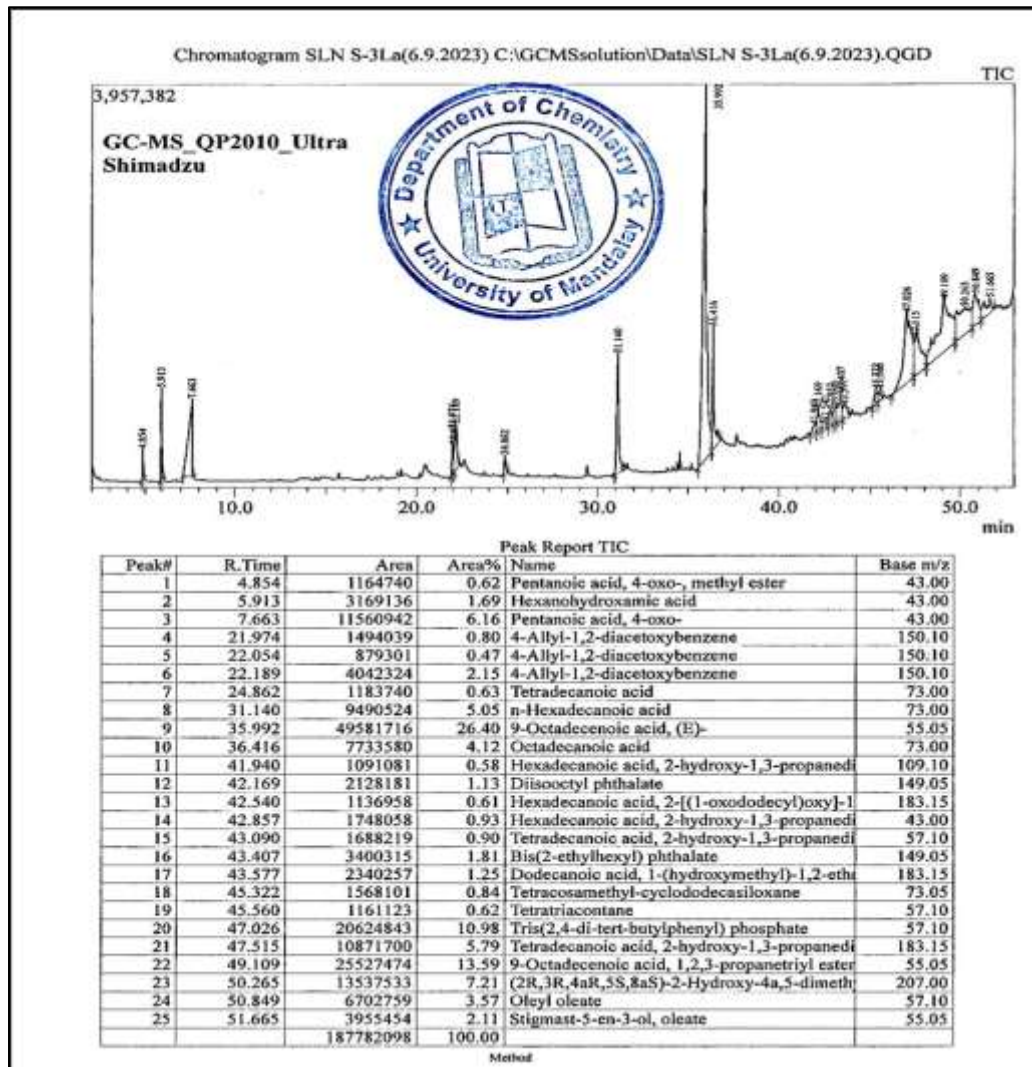


Figure 4: FTIR Spectrum of Levulinic Acid from Sugarcane Bagasse



(a) (b)
Figure 5: Gas Chromatogram and Mass Spectra of (a) Levulinic Acid, Methyl Ester and (b) Levulinic Acid from Sugarcane Bagasse

Conclusion

This research work aimed to undertake the conversion of sugarcane bagasse into levulinic acid by acid-catalyzed hydrothermal method. The reaction pathways for conversion of sugarcane bagasse into levulinic acid are (1) hydrolysis of cellulose to glucose, (2) isomerization of glucose to fructose, (3) dehydration of fructose to 5-hydroxy methyl furfural and (4) rehydration of 5-hydroxy methyl furfural to levulinic acid. Only the isomerization process is catalyzed with Lewis acid AlCl_3 . The Lewis acid was used in this research because the direct conversion of glucose to 5-HMF is slow and fructose is high selectivity to form levulinic acid. In this research, the purity of levulinic acid from sugarcane bagasse was low because of complex structure of sugarcane bagasse, the necessary for pretreatment process of sugarcane bagasse to achieve pure cellulose and the necessary for further purification process to achieve high purity levulinic acid.

Acknowledgements

I would like to express my gratitude to Dr Soe Soe Than, Professor and Head, Department of Industrial Chemistry, University of Yangon, for allowing me to conduct this research at the department and to submit this article.

References

- Chang, C., Chen, P., & Ma, X. (2007). Levulinic acid production from wheat straw. *Bioresource Technology*, 98(7), 1448–1453.
- Choudhary, V., Mushrif, S. H., Ho, C. R., Anderko, A., Nikolakis, V., Marinkovic, N., Frenkel, A. I., Sandler, S. I., & Vlachos, D. G. (2013). Insights into the Interplay of Lewis and Brønsted Acid Catalysts in Glucose and Fructose Conversion to 5-(Hydroxymethyl)furfural and Levulinic Acid in Aqueous Media. *Journal of the American Chemical Society*, 135(10), 3997–4006.
- Girisuta, B., Dussan, K., Haverty, D., Leahy, J. P., & Hayes, M. G. (2013). A kinetic study of acid catalysed hydrolysis of sugar cane bagasse to levulinic acid. *Chemical Engineering Journal*, 217, 61–70.
- Joshi, S. S., Zodge, A., Pandare, K., & Kulkarni, B. D. (2014). Efficient conversion of cellulose to levulinic acid by hydrothermal treatment using zirconium dioxide as a recyclable solid acid catalyst. *Industrial & Engineering Chemistry Research*, 53(49), 18796–18805.
- Kang, S., Fu, J., & Zhang, G. (2018). From lignocellulosic biomass to levulinic acid: A review on acid-catalyzed hydrolysis. *Renewable & Sustainable Energy Reviews*, 94, 340–362.
- Kuznetsov, B. N., Sharypov, V. I., Grishechko, L. I., & Celzard, A. (2013). Integrated catalytic process for obtaining liquid fuels from renewable lignocellulosic biomass. *Kinetics and Catalysis*, 54(3), 344–352.
- Liu, Y., Li, H., He, J., Zhao, W., Yang, T., & Yang, S. (2017). Catalytic conversion of carbohydrates to levulinic acid with mesoporous niobium-containing oxides. *Catalysis Communications*, 93, 20–24.
- Mosier, N. S., Wyman, C. E., Dale, B. E., Elander, R. T., Lee, Y., Holtzapple, M. T., & Ladisch, M. R. (2005). Features of promising technologies for pretreatment of lignocellulosic biomass. *Bioresource Technology*, 96(6), 673–686.
- Mthembu, L. D. (2016). *Production of levulinic acid from sugarcane bagasse*.
- Neureiter, M., Danner, H., Thomasser, C., Saidi, B., & Braun, R. (2002). Dilute-Acid hydrolysis of sugarcane bagasse at varying conditions. *Applied Biochemistry and Biotechnology*, 98–100(1–9), 49–58.
- Patil, S. K. R., & Lund, C. (2011). Formation and Growth of Humins via Aldol Addition and Condensation during Acid-Catalyzed Conversion of 5-Hydroxymethylfurfural. *Energy & Fuels*, 25(10), 4745–4755.
- Pileidis, F. D., & Titirici, M. (2016). Levulinic Acid Biorefineries: New Challenges for Efficient Utilization of Biomass. *Chemsuschem*, 9(6), 562–582.

- Pratiwi, R. A., & Nandiyanto, A. B. D. (2022). How to read and interpret UV-VIS spectrophotometric results in determining the structure of chemical compounds. *Indonesian Journal of Educational Research and Technology*, 2(1), 1–20.
- Rackemann, D. W., & Doherty, W. J. (2011). The conversion of lignocellulosics to levulinic acid. *Biofuels, Bioproducts and Biorefining*, 5(2), 198–214.
- Sevilla, M., & Fuertes, A. B. (2009a). Chemical and structural properties of carbonaceous products obtained by hydrothermal carbonization of saccharides. *Chemistry: A European Journal*, 15(16), 4195–4203.
- Sevilla, M., & Fuertes, A. B. (2009b). The production of carbon materials by hydrothermal carbonization of cellulose. *Carbon*, 47(9), 2281–2289.
- Signoretto, M., Taghavi, S. S., Ghedini, E., & Menegazzo, F. (2019). Catalytic Production of Levulinic Acid (LA) from Actual Biomass. *Molecules*, 24(15), 2760.
- Sluiter, A., Hames, B. R., Ruiz, R., Scarlata, C. J., Sluiter, J., Templeton, D. W., & Crocker, D. P. (2012). Determination of Structural Carbohydrates and Lignin in Biomass. *NREL Laboratory Analytical Procedures for Standard Biomass Analysis*.
- Sweygers, N., Harrer, J., Dewil, R., & Appels, L. (2018). A microwave-assisted process for the in-situ production of 5-hydroxymethylfurfural and furfural from lignocellulosic polysaccharides in a biphasic reaction system. *Journal of Cleaner Production*, 187, 1014–1024.
- Van Zandvoort, I., Wang, Y., Rasrendra, C. B., Van Eck, E. R. H., Bruijninx, P. C. A., Heeres, H. J., & Weckhuysen, B. M. (2013). Formation, molecular structure, and morphology of humins in biomass conversion: influence of feedstock and processing conditions. *Chemsuschem*, 6(9), 1745–1758.
- Yang, B., & Wyman, C. E. (2008). Pretreatment: the key to unlocking low-cost cellulosic ethanol. *Biofuels, Bioproducts and Biorefining*, 2(1), 26–40.
- Yang, F., Fu, J., Mo, J., & Lu, X. (2013). Synergy of Lewis and Brønsted Acids on Catalytic Hydrothermal Decomposition of Hexose to Levulinic Acid. *Energy & Fuels*, 27(11), 6973–6978.
- Zhang, J., Li, J., Tang, Y., & Xue, G. (2013). Rapid method for the determination of 5-Hydroxymethylfurfural and levulinic acid using a Double-Wavelength UV spectroscopy. *The Scientific World Journal*, 2013, 1–6.
- Zhang, X., Murria, P., Jiang, Y., Xiao, W., Kenttämaa, H. I., Abu-Omar, M. M., & Mosier, N. S. (2016). Maleic acid and aluminum chloride catalyzed conversion of glucose to 5-(hydroxymethyl) furfural and levulinic acid in aqueous media. *Green Chemistry*, 18(19), 5219–5229.
- Zheng, Y., Pan, Z., & Zhang, R. (2009). Overview of biomass pretreatment for cellulosic ethanol production. *International Journal of Agricultural and Biological Engineering*, 2(3), 51–68.

EXTRACTION AND UTILIZATION OF WATER-SOLUBLE DIETARY FIBRE (SDF) FROM BANANA PEEL

Seinn Lei Lei Phyu¹

Abstract

Development of food supplement plays an important role in functional food processing and it becomes a challenge among people and manufacturers. In this research, water-soluble dietary fibre (SDF) was extracted from banana peels of Hpi Kyam (*Musa chiliocarpa* Backer) and Thi Hmwe (*Musa acuminata* Colla). The extracted SDF was included in wheat noodle formulation. This makes not only innovation but also gets new beneficial products. Cellulase enzyme was utilized in the extraction of SDF. Conventional acid treatment method was also carried out in SDF extraction. The functional properties of extracted SDFs were evaluated. The SDF obtained from banana peel (Hpi Kyam) by cellulase treatment had better characteristics and higher yield percent than that of the banana peel (Thi Hmwe) by acid treatment method. Both SDFs contained minerals such as iron and manganese. The FTIR results showed that SDFs composed of the functional groups which held to enhance the solubility of food. The physico-chemical characteristics of SDF supplemented wheat noodle were determined. In the formulation of noodle making, among the sixteen formulations, a formula of 86.5 % of wheat, 10 % of potato starch, 1.5 % of SDF, 1 % of sodium chloride and 1 % of sodium bicarbonate gave the best results and its characteristics and these nutritional properties were superior than those of the others.

Keywords: water-soluble dietary fibre, acid treatment, cellulase enzyme treatment, noodle formulation

Introduction

Nowadays, consumers become interested in the nutrition and health benefit from the food they eat. This has led to new detections about the linkage between food and health. The basic tendency of human beings has always been to prefer natural foods. Ready-to-eat foods have now moved into the essential point and onto the interest of modern consumers and new living style of people. Banana is one of the most common crops grown in almost all tropical countries, including Myanmar. Banana normally has a short shelf life and starts deteriorating just after plucking. The most widely used part of banana is the flesh of the fruit; meanwhile, the outer skin is only used for animal feed and organic fertilizer. Plantain and unripe banana are cooked as vegetable, chips, snacks, powder etc., whereas, banana is eaten raw. In recent years, banana peel has been utilized for various industrial applications including bio-fuel production, bio-sorbents, pulp and paper, cosmetics, energy related activities, organic fertilizer, environmental cleanup and biotechnology related processes (Benjamin and Ugye, 2008). The banana peel is richer in phytochemical compounds than its pulp. The antifungal, antibiotic properties of banana peel can be put to good use. The banana peels are waste and normally disposed to municipal landfills, which contributes to the existing environmental problems. The best way to solve the waste problem for banana peels is to produce value added compounds, including the dietary fibre fraction that has a great potential in the preparation of functional foods (Prashanthi, 2020). Dietary fibre has shown beneficial effects in the prevention of several diseases, such as cardiovascular diseases, diverticulosis, constipation, irritable colon, colon cancer, and diabetes (Rodriguez et al., 2006). The fruit fibre has a better quality than other fibre sources due to its

¹ Department of Industrial Chemistry, University of Yangon

high total and soluble fibre content, water and oil holding capacities (Figuerola et al., 2005). A high dietary fibre content of banana peel (0.5 g)

is indicative of a good source of dietary fibre. Happi Emaga et al. (2007) found that the maturation of banana fruits has shown its impact on the dietary fibre composition of banana peels.

This research was objected to extract SDF by cellulase enzyme and acid treatment methods. The resulting SDFs were incorporated in the formulation of wheat noodle. Functional groups and mineral contents of SDFs were analyzed by FTIR (Fourier-transform Infrared Spectroscopy) and AAS (Atomic Absorption Spectroscopy). Nutritional properties of processed noodle were also evaluated.

Materials and Methods

Raw Materials

Banana peels were collected from banana-based product shops. They were cleaned and dried in an oven at 70 °C for 6 h. The dried peels were ground by using a grinder and screened with 20 mesh sieve to obtain banana peel powder (+20 mesh). In this research, two types of banana varieties (Hpi Kyam, *Musa chiliocarpa* Backer) and Thi Hmwe, *Musa acuminata* Colla) were used for the extraction of water-soluble dietary fibre. The enzyme *Aspergillus niger*, was purchased from Baodeli Inc. (Henan, China) and other required chemicals were purchased from Empire chemical shop, Pabedan Township, Yangon Region.

Acid Treatment Extraction of Soluble Dietary Fibre (SDF)

20 g of banana peel powder were subjected to extraction by adding 400 mL of distilled water, and pH was adjusted to pH 3.5 with 98 % (36.8 N) sulfuric acid solution by using pH meter (Consort C1010). The mixture was heated at 80 °C for 4 h with magnetic stirring, and then filtered. The filtrate was concentrated to half of it, and cooled to room temperature. The concentrate was precipitated into 70 % ethanol solution. The ethanol precipitation process lasted for 1 h, and SDF was collected after filtration, and then dried at room temperature. The yield was calculated as a percentage of the obtained SDF to banana peel powder used. The effects of pH on SDF yield were studied by varying the pH of (1.5, 2.5, 3.5, 4.5 and 5.5) and the resulting yield % of SDFs were recorded.

Enzymatic Extraction of Soluble Dietary Fibre (SDF)

In this research work, the cellulase enzyme from *Aspergillus niger*, was used to extracted both SDFs. The enzymatic hydrolysis of banana peel powder was conducted by preparing (4 % w/v) sodium acetate solution to which 0.02 % (based on peel powder weight) cellulase enzyme was added. The hydrolysis was carried out at 50 °C for 3 h with magnetic stirring, and then filtered. The filtrate was concentrated to become half of its volume, and cooled to room temperature. The concentrate was precipitated into 70 % ethanol solution. The ethanol precipitation process was taken for 1 h, and SDF was collected after filtration, and then dried at room temperature. The yield was calculated as a percentage. The effects of cellulase enzyme

concentration on SDF yield were also studied by using (0.005, 0.01, 0.02, 0.03, 0.04) % of cellulase enzyme and the resulting yield % of SDFs were recorded.

Formulations for Wheat Noodle Including SDF

Sixteen experimental runs were conducted for the formulation of noodle processing according to the design arrangement. Design expert version 11 (Analysis of Variance, ANOVA) was applied for the formulation of noodle processing.

About 86.5 % of wheat flour, 10 % of potato starch powder, 1.5 % of SDF, 1 % of salt, and 1 % of sodium bicarbonate were mixed in a container. Then, 55 mL of water was added for making dough. The constituents were mixed at room temperature, and the mixing time was 15-20 min. The dough produced in this process was composed of a fine mesh structure and formed the glutinous dough. The dough was placed into the noodle extruder. Before the dough was extruded, the dough was sometimes aged for a period of time. In this process, the dough was made strong, and uniform. The dough was extruded directly into the boiling water. The noodles were boiled in water for 10 min. The resulting wet noodle were filtered with stainless steel screen, and then dried in an oven at 70 °C for 4 h.

Observation of Surface Morphology

Surface morphology of banana peel powder and SDFs were observed by using Scanning Electron Microscopy (SEM), (JSM- 5610 LV) at the Universities' Research Center, University of Yangon.

Analysis of Functional Groups in SDF by FTIR

FTIR analysis was carried out to qualitatively examine the functional groups of SDFs by using FTIR (PerkinElmer Spectrum, Version 10.5.2) at the National Analytical Laboratory, Department of Research and Innovation, No.6 KabaAye Pagoda Road, Yankin, Yangon Region.

Determination of Mineral Contents in SDF by Atomic Absorption Spectroscopy

The concentrations of individual mineral contents were determined by Atomic Absorption Spectroscopy (AAS, PerkinElmer, PinAAcle 900F) at the National Analytical Laboratory, Department of Research and Innovation, No.6 KabaAye Pagoda Road, Yankin, Yangon Region.

Sensory Evaluation of Processed Wheat Noodle Including SDF

The sensory evaluation was carried out to assess the overall acceptability of the SDF powder enriched noodles. The sample noodles were cooked in boiling water for 15 min and the quality attributes (Colour, Taste and Texture) of prepared noodles were evaluated for overall liking of the samples by 10 well trained persons using a nine-point hedonic scale.

Statistical Analysis

By using D-optimal mixture design, the optimum amount of ingredients used in noodle formulations was determined based on the most acceptable like on taste, colour and texture of the resulting noodles.

Determination of Nutritional Characteristics of Noodle

The nutritional characteristics such as the protein, fat, crude fibre, carbohydrate, sugar, moisture, ash content, cooking weight, cooking loss of resulting Noodle including SDF and without SDF were determined. The energy value of resulting noodle was also determined by using the following formula.

$$\text{Energy Value} = (4 \text{ kcal/g} \times \text{Protein}) + (4 \text{ kcal/g} \times \text{Carbohydrate}) + (9 \text{ kcal/g} \times \text{Fat})$$

The resulting noodle was stored in air-tied plastic bag and stored in room temperature and there was no change in conditions (colour, odor and texture) of both SDFs and noodle during 6 months.

Results and Discussion

Figure 1 shows the resulting values of acid treatment extraction method. The effect of pH on the yield percent of SDF was conducted by varying pH. The optimum pH that gave the maximum amount of yield was 3.5, and beyond this pH the yield percent became lower. The yield percent was not significantly lower but the higher concentration of acid gave the odor of SDF with pungent smell. Below pH 3.5, the treatment was not enough for disruption of walls of banana peels.

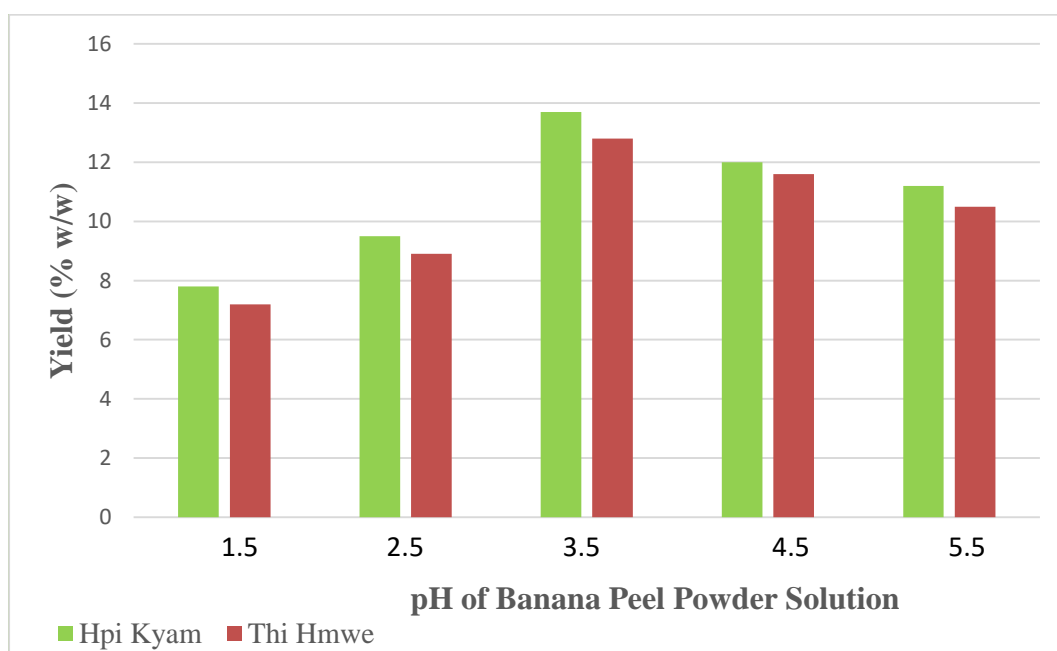


Figure 1: Effect of pH on the Yield Percent of SDFs by Acid Treatment

The effect of cellulase concentration on the yield percent of SDF was studied. As shown in Figure 2, it was found that the maximum amount of SDF was obtained at 0.02 % of cellulase, and the lower amount of enzyme gave the lower amount of SDF. The enzyme action was found

to be optimum in 0.02 %, and it gave the yield percent of 13.7 % in Hpi Kyam, and 12.4 % in Thi Hmwe respectively. 0.02 % of cellulase enzyme concentration was effective substrate to enzyme ratio to obtain the maximum SDF extraction.

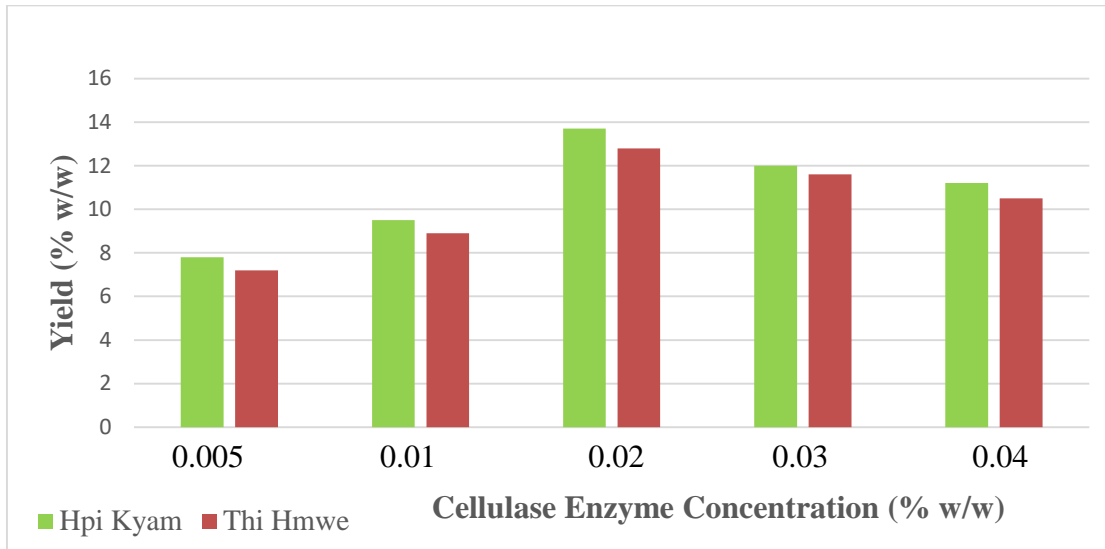
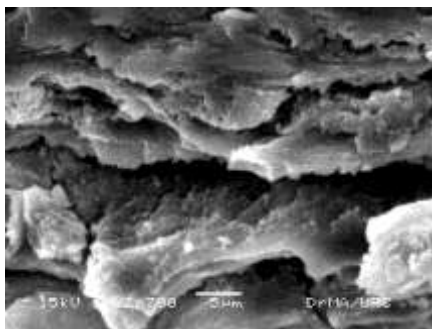
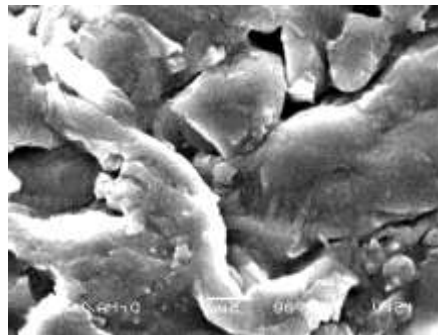


Figure 2: Effect of Cellulase Concentration on the Yield Percent of SDFs by Enzyme Treatment

Surface morphology of raw banana peel powder, and its products SDFs were observed by scanning electron microscope (SEM) and the results are shown in Figures 3 and 4. The surface morphology was highly influenced by the presence of cellulose materials in the banana peel. According to the SEM images, the heterogeneous nature was observed at the surface of which indicate the amorphous structure of materials.



(a)



(b)

Figure 3: Surface Morphology of Raw Banana Peel Powders

(a) Hpi Kyam (b) Thi Hmwe



Figure 4: Surface Morphology of Extracted SDFs from
(a) Hpi Kyam (b) Thi Hmwe

FTIR spectrum of SDFs are shown in Figures 5 and 6 and their band assignments are tabulated in Table 1. It was found that the sharp intense band at 3330 cm^{-1} and 3329 cm^{-1} indicates C-H stretching, and it will be the hydrogen bonded O-H stretching vibration. The medium intensity C=C stretching bend occurred near 1639 cm^{-1} and 1640 cm^{-1} . The observed pattern of finger-like bands further suggested disubstituted or trisubstituted groups that were present in the resulting SDF. There was also a weak absorption at 1413 cm^{-1} , and it was constituent with C=C-H in plane bending vibration of the terminal $=\text{CH}_2$ group. The conjunction with aliphatic asymmetric, and symmetric C-H in plane banding vibration at 1450 cm^{-1} , and 1552 cm^{-1} indicated the presence of alkyl group. There was also C-O stretching vibration at 1020 cm^{-1} and 1021 cm^{-1} indicates the ester and amines groups presence in both SDFs. The FTIR analysis of both SDFs show the presence of 4-(2,3-Dihydroxypropyl), 2-Isononenylsuccinate and Pama Dendrimer compounds that can enhance the solubility of resulting products.

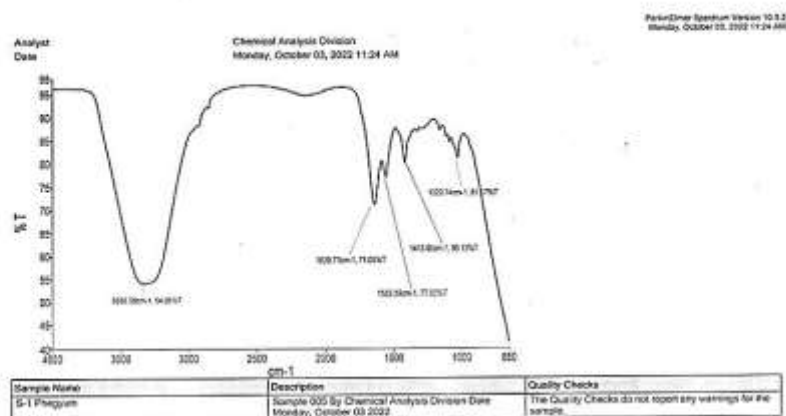


Figure 5: FTIR Spectrum of SDF (Hpi Kyam)

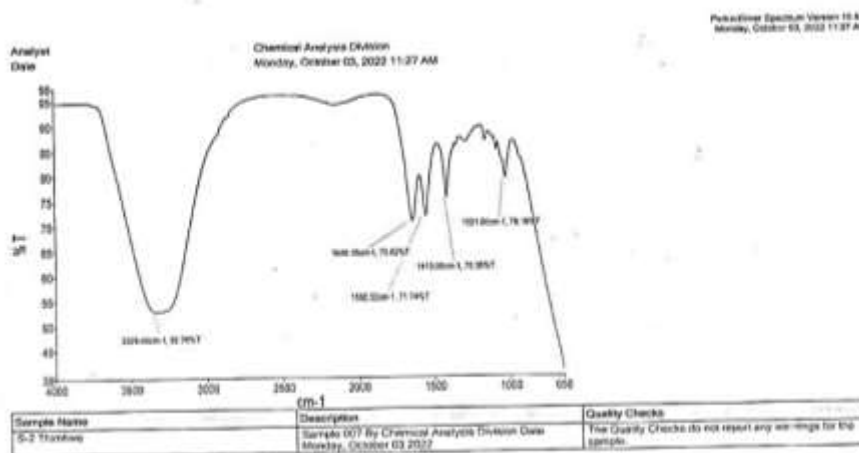


Figure 6: FTIR Spectrum of SDF (Thi Hmwe)

Table 1: FTIR Absorption Bands and Assignments of Extracted SDFs

Sr. No.	Experimental Frequency (cm ⁻¹)		Literature Frequency (cm ⁻¹)	Band Assignments	Types of Identified Functional Groups
	Hpi Kyam	Thi Hmwe			
1	3330.58	3329.45	3500-3200	O-H stretch, C=O stretch	Alcohol , Phenol
2	1639.77	1640.15	1670-1620	C=C stretch, C=O stretch	Trisubstituted Groups
3	1563.59	1552.32	1800-1260	C=CH stretch,	Asymmetric and Symmetric Alkyl Group,
4	1413.86	1413.08		=CH stretch	
5	1020.74	1021.60	1260-1000	C=C stretch, O-H bends, C-N stretch	Ester, Aliphatic amines, Aromatic ring, Alcohol, Phenol
The identical compounds found in Extracted SDF 4-(2,3-Dihydroxypropyl) 2-Isononenylsuccinate, Pama Dendrimer					

(Noh *et al.*, 2017), (Maobe M.A.G. *et al.*, 2013)

Table 2 shows that the mineral contents of SDFs and it was found that both SDFs contained high amount of iron (Fe) content, and manganese content. When compared, SDF from Thi Hmwe contained a little high mineral contents than that of Hpi Kyam. This agreed with the findings of Akinyosoye (1991), and Anhwange *et al*, (2009) that pointed as banana peel can serve as one of the major source of iron and manganese ions.

Table 2: Mineral Contents of Extracted SDFs by Atomic Absorption Spectroscopy

Elements	Concentrations (mg/g)	
	SDF (Hpi Kyam)	SDF (Thi Hmwe)
Calcium	0.09	0.19
Iron	16.85	19.24
Manganese	7.01	9.37
Potassium	0.20	0.21
Sodium	0.99	1.39

Table 3 shows the experimental runs and sensory scores of formulated 16 samples of SDF enriched noodle. It was found that the taste, colour and texture of sample with 86.5 % of wheat flour, 10 % of potato starch, 1.5 % of extracted SDF, 1 % of NaCl and 1 % of NaHCO₃ were superior to the others. The amount of SDF in best formulation was 1.5 % (w/w) and it was in acceptable range for human diet.

Table 3: Sensory Scores of Formulated Noodle Including SDF

Run	Ingredients						Sensory Score		
	Wheat Flour (%)	Potato Starch (%)	SDF (%)	NaHCO ₃ (%)	NaCl (%)	Distilled Water (mL)	Taste R ₁	Colour R ₂	Texture R ₃
1	77.875	19.125	1	1	1	55	6.5	6.45	6.2
2	50	47.5	0.5	1	1	55	5.8	6.4	4.8
3	87.5	10	0.5	1	1	55	6.7	5.92	6.4
4	85.5	10	2.5	1	1	55	6.9	5.68	6.5
5*	86.5	10	1.5	1	1	55	7.2	7.81	6.9
6	50	45.5	2.5	1	1	55	5.7	6.12	5.2
7	59.125	36.875	2	1	1	55	5.7	6.65	4.9
8	68.75	28.75	0.5	1	1	55	6.4	6.5	5.4
9	68.75	28.75	0.5	1	1	55	6.4	6.5	5.4
10	87.5	10	0.5	1	1	55	6.9	5.9	5.9
11	50	46.5	1.5	1	1	55	5.5	4.89	4.5
12	85.5	10	2.5	1	1	55	6.4	5.7	6.4
13	50	45.5	2.5	1	1	55	5.9	6.2	4.9

Run	Ingredients						Sensory Score		
	Wheat Flour (%)	Potato Starch (%)	SDF (%)	NaHCO ₃ (%)	NaCl (%)	Distilled Water (mL)	Taste R ₁	Colour R ₂	Texture R ₃
14	50	47.5	0.5	1	1	55	5.8	6.4	4.8
15	67.75	27.75	2.5	1	1	55	6.2	6.3	5.9
16	59.125	37.875	1	1	1	55	6.1	6.53	5.2

* = the optimum formulation

R₁, R₂, R₃ = Responds for sensory evaluation (Taste, Colour, Texture)

Table 4 shows the predicted and experimental values of sensory scores for the optimized formulation. From the results of Table 4, there were no significant differences between the predicted and experimental scores of the responses for optimized formulation of SDF enriched noodle and also good agreement with the model used.

Table 4: Optimum Composition of Noodle Including SDF

Sr. No.	Ingredients	Composition (g)	Taste		Colour		Texture	
			P	E	P	E	P	E
1	Wheat Flour	86.5	6.8	7.2	7.8	7.81	6.4	6.9
2	Potato Starch	10						
3	SDF	1.5						
4	Water	55						
5	NaCl	1.0						
6	NaHCO ₃	1.0						

P = Predicted value

E = Experimental value

Table 5 shows the characteristics of SDF enriched noodle. It was found that the resulting noodle had higher protein content, carbohydrate content, energy value, and cooking weight. These characteristics are very good for human health, and there was a little cooking loss in noodle. The extracted SDFs were stored in airtight bottles in refrigerated storage. The resulting noodle was stored in airtight plastic bag and stored at room temperature. There was no change in colour, odor and texture of both SDFs and processed noodle during 6 months. From the results the noodle including SDF had high energy value and no fat content. The nutritional values of prepared noodle including SDF were high and achieved good organoleptic quality. Moreover, the SDF enriched noodle makes enhance lowering fat absorption and weight management. It promotes digestibility, lowering cholesterol and stabilizing blood sugar level than the normal noodle.

Table 5: Characteristics of Wheat Noodle Including SDF and Without SDF

Sr. No.	Characteristics	Wheat Noodle Including SDF	Wheat Noodle Without SDF	Literature Value*
1.	Protein (% w/w)	15.8	10.5	4.5
2.	Fat (% w/w)	N. D	0.94	2.06
3.	Crude Fibre (% w/w)	1.7	0.36	1.19
4.	Carbohydrate (% w/w)	76.6	74.88	25
5.	Sugar (% w/w)	3.29	3.0	0.375
6.	Moisture (% w/w)	5.9	< 14	5.6
7.	Ash (% w/w)	0.92	0.94	1.4
8.	Energy Value (kcal/100 g)	370	192	140
9.	Cooking Weight (% w/w)	200.0	189.0	-
10.	Cooking Loss (% w/w)	1.49	1.4	-
11.	Shelf Life (Months)	6	6	6

* (Kawaljit S.S, 2010)



(a)



(b)



(c)

Figure 7: (a) Solid SDF (b) Wet Noodle (c) Dry Noodle

Conclusion

Physical modification of foods is very important in several industries. Since the well proved nutritional benefits of dietary fibers, many efforts are being put in the improvement of their functionality by physical means. Banana peel was observed to be an excellent source of dietary fibre, and it was concluded that the waste banana peel could be used as a potential source of fibre. The characteristics of SDFs showed a drastic efficiency, and enzyme treatment provided the higher SDF yield than the acid method. The present study showed that extracted SDF from banana peel (Hpi Kyam) by cellulase enzyme treated method was a promising material for the development of noodle formulation. The studies on cooking quality such as colour, taste and texture revealed that the noodle incorporated with 1.5 % of SDF was the most acceptable in terms of both palatability and nutritional compositions. There were no significant differences between the predicted and experimental values of the responses for optimized formulation of SDF enriched noodle by statistical analysis. Formulation of such type of functional foods can impart positive results against many diseases like cancer, cardiovascular diseases, obesity, heart problems etc. So, these noodles can be a good source of nutraceuticals containing functional food from byproduct of banana food industries.

Acknowledgements

I would like to express my gratitude to the Department of Higher Education, Ministry of Education for research grant of (2022-2023). I also would like to express my thanks to the Myanmar Academy of Arts and Science for allowing me to submit this article. I would like to express my special thanks to Rector Dr. Tin Maung Tun, University of Yangon and Pro-Rectors Dr. Khin Chit Chit, Dr. Cho Cho and Dr. Thida Aye, University of Yangon, for giving their permission to submit this research paper. I also gave special thanks to Dr. Soe Soe Than, Professor and Head and my colleagues at Industrial Chemistry Department for their help and support in carrying out this present research.

References

- Benjamin, A and J.T. Ugye, (2008). "Chemical Composition of *Musa sapientum* (Banana) Peels, J, Food technol., 6 (6), 263-266
- Anhwange, B.A., Ugye, T.J. and Nyiaatagher, T.D. (2009). Chemical Composition of *Musa Sapientum* Banana Peels. *Electronic Journal of Environmental, Agricultural and Food Chemistry*, 8(6), 437-442
- AOAC. (2000). Official Methods of Analysis of AOAC International. Washington, DC, USA: AOAC
- AOAC. (2006). Official Methods of Analysis Minerals Analysis Flame Atomic Absorption Spectroscopy (FAAS). 17th ed. Gaithersburg, USA: AOAC
- Tsai, A *et.al.*, (2003). A Shape-based Approach to the Segmentation of Medical Imagery Using Level Sets, *IEEE Transactions on Medical Imaging*, 22, 137-154
- Figuerola, F., Hurtado, M.L., Estevez, A.M., Chiffelle, I., Asenjo, F. (2005). Fibre Concentrate from Apple Pomace and Citrus Peel as Potential Fibre Sources for Food Chemistry, 395-401
- Kawaljit S.S, Maninder, K., Mukesh (2010). Studies on Noodle Quality of Potato and Rice Starches and Their Blends in Relation to their Physicochemical, Pasting and Gel Textural Properties, *LWT-Food Science Technology*, 43, 1289-1293
- Maobe, M.A.G., & Nyarango, M.R. (2013). Fourier Transformer Infra-Red Spectrophotometer Analysis of *Warburgia ugandensis* Medicinal Herb Used for the treatment of Diabetes, Malaria and Pneumonia in Kisii Region, Southwest Kenya, *Global Journal of Pharmacology*, 7(1), 61-68

- Noh,C.H.C., Azmin, N.F.M., & Amide, A. (2017). Principal Component Analysis Application on Flavonoids Characterization, *Advance in Science, Technology and Engineering Systems Journal*, 2(3), 435-440
- Prashanthi D, M.C., (2020). A Review on Multiple Uses of Banana Peel
- Rodriguez, R., Jimenez, A., Fernandez-Bolanos, J., Guillen, R. and Heredia, A. Extrution (2006). Dietary Fibre from Vegetable Products as Source of Functional Ingredients. *Trends in Food Science and Technology*. 17, 3-15
- Thomas Happi Emaga, Rado H.A, Bernard W, Jean T.T, Michel P., (2007). Effects of Stage of Maturation and Varieties n the Chemical Compositon of Banana and Plantain Peels, *Food Chemistry*, 103,590-600
- Akinyosoye, V.O., (1991). "Tropical Agriculture, Macmillan Publishers Limited, Ibadan, 65-68

EXTRACTION OF FERULIC ACID FROM DEFATTED WHEAT BRAN FOR IMPROVING ANTIOXIDANT ACTIVITY

Naw Zar Htwe¹

Abstract

Ferulic acid (4-hydroxy-3-methoxycinnamic acid) is one of the most significant natural bioactive phenolic acids generally found in the seeds as well as leaves, both in its free form and covalently conjugated with the plant cell wall materials. The extraction of ferulic acid has been found much attention nowadays due to the fact that it exhibits a wide variety of biological activities. In the present study, the extraction of ferulic acid from wheat bran was carried out by alkaline hydrolysis using NaOH and later purified by precipitating hemicellulose and glucomannans with ethanol. Optimization of antioxidant activity in ferulic acid from defatted wheat bran was conducted using response surface methodology (RSM). The conditions investigated were 0.5, 1.0 and 1.5 M of NaOH concentration (x_1), 2, 4 and 6 hr of extraction time (x_2), and 40, 50 and 60 °C for the extraction temperature (x_3). Box-Behnken design indicated that the model can significantly ($p < 0.05$) express more than 80 % (> 0.80) of the response variation. The optimal extract condition for maximum antioxidant activity was 0.5 M of NaOH concentration, 2 hr of extraction time, and 50 °C for extraction temperature. The antioxidant activity of extracted ferulic acid was determined by DPPH (2, 2-diphenyl-1-picryl-hydrazyl) radical photometric scavenging method. According to these results, ferulic acid from wheat bran possesses high antioxidant activity.

Keywords: ferulic acid, wheat bran, extraction, response surface methodology, antioxidant activity

Introduction

Wheat bran is a by-product from the roller milling of the wheat grain to produce wheat flour (Apprich *et al.*, 2014). One of the functional compounds extracted from agricultural by-product is ferulic acid, the most abundant hydroxycinnamic acid found in plant cell wall is covalently linked to polysaccharides and lignin (Masoomeh *et al.*, 2008). Ferulic acid was exhibited several physiological benefits such as anti-microbial, anti-oxidants, anti-inflammatory and anti-cancer activities (Buranov & Mazza, 2009).

There are many different extraction techniques from natural plants. They are acid hydrolysis, alkaline hydrolysis and enzymatic hydrolysis. Acid hydrolysis can be used for the determination of bound phenolic acids, hydrolysable tannins or non-extractable proanthocyanidins (NEPA) remaining in the residue. White and coworkers (2010) described alkaline hydrolysis to be the best extraction option in order to release bound procyanidins from cranberry pomace matrix. Using this method there was a significant release of cell wall bound or insoluble ferulic acids. The treatment time, temperature, and the concentration of the base are parameters that were tested. They also found optimized conditions of 2 M NaOH, 60°C and 15 min, in order to release the highest amount of bound procyanidins from cranberry pomace (White *et al.*, 2010). Enzymatic hydrolysis can also be performed by carbohydrases such as cellulases, amylases, hemicellulose or proteases. These are helpful in the release of cell wall bound phenolic acids or NEPA, because they break down the plant. Enzymes are specific, water-soluble, not toxic, biodegradable, but also expensive and rather unstable. Factors that can be optimized in order to increase the hydrolysis efficiency are the hydrolysis extraction time and the dosage of enzyme (Navarro *et al.*, 2011). In order to optimize the extraction conditions, response surface

¹ Department of Industrial Chemistry, Yadanabon University

methodology (RSM) has been widely used. The most common designs, such as Central Composite Design (CCD) and Box-Behnken design (BBD).

In present study, antioxidant capacity was considered as response value while extraction times, concentration of NaOH and extraction temperature were considered for optimization parameters. The experiments were done in triplicate. The results are given as mean standard deviation (SD). One-way Analysis of Variance (ANOVA) was used for comparison of more than two means. A difference was considered statistically significant when $p < 0.05$ (Barberousse *et al.*, 2009).

Antioxidant is a molecule that inhibits the oxidation of other molecules. Antioxidants terminate these chain reactions by removing free radical intermediate and reducing other oxidative reactions (Ames *et al.*, 1993 and Shenoy & Shirwaiker, 2002). Antioxidants are often reducing agents such as, thiols, ascorbic acid or polyphenols (Sies, 1997). The main function of antioxidants is to protect the body against the destructive effects of free radicals damage (Marques *et al.*, 2014). Antioxidant activity of ferulic acid from wheat bran was measured by using the DPPH (2, 2-diphenyl-1-picryl-hydrazyl) radical photometric assay in a process guided by its discoloration (Xiong *et al.*, 1996). The antioxidant activity of these extracts was compared with standard Ascorbic acid (Ascorbic acid Equivalent Antioxidant Capacity (AEAC)). The main purpose of this research is to develop useful chemicals made from agricultural by-product.

Materials and Methods

Sample Collection

Raw material (Wheat Bran) was collected from Yaykyi Village, Patheingyi Township, Mandalay Region. The chemicals used for this research were n-hexane, sodium hydroxide, hydrochloric acid and 95% ethanol. These were purchased from Able and Golden Lady Chemical shops, Chan Aye Thar Zan Township, Mandalay Region.

Defatting of Wheat Bran

Wheat bran was initially cleaned and dried at room temperature for 24 hr. It was sieved on an 80 mesh screen for the removal of husk, grits and other impurities. Wheat bran was degreased with n-hexane in 1:3 ratio (w/v) at 50°C for 3 hr on a water-bath shaker. The mixture was filtrated to remove n-hexane from wheat bran. Wet wheat bran was dried at about 105 °C for 2 hr in an oven. After drying, the wheat bran was sieved again on a 100 mesh screen. Finally, defatted wheat bran was obtained.

Extraction and Purification of Ferulic Acid

Extraction process was carried out according to the method described by Buranov and Mazza (2009). To optimize the extraction process, different extraction time, concentration of NaOH and extraction temperature were tested. 5 g of defatted wheat bran and 150 mL of sodium hydroxide were added in Erlenmeyer flask. The flask was kept on a water-bath shaker and boiled at 60 °C and 1.5 M NaOH concentration with different extraction time (2, 4 and 6 hr) at 200 rpm. The extraction was repeated as described above but at varying extraction temperature, namely

(40, 50 and 60°C) and at different NaOH concentration (0.5, 1.0 and 1.5 M) for ensuring total hydrolysis. After cooling down, the hydrolysate was filtered and then neutralized by using 6 M hydrochloric acid. The hemicelluloses and glucomannans were precipitated by adding 95 % ethanol. The amount of added ethanol corresponded to three times of the original volume of wheat bran. The precipitate was separated by using a centrifuge machine. After decanting the supernatant extract, excess ethanol was removed from the extract by using a rotary vacuum evaporator. This led to the formation of a brown extract which contained ferulic acid. The extract was finally passed through a 0.45 µm filter before analysis. The yield percent of extracted ferulic acid was 6.95 ± 0.28 mg/g.

The extraction procedure of the experiment arranged by 'Box-Behnken design' was set up as follows; Three factors including sodium hydroxide concentration (x_1), extraction time (x_2) and extraction temperature (x_3) were chosen. The antioxidant activity of ferulic acid (y) was determined using optimization method Table 1. Each experiment was carried out in triplicate.

Experimental Design

A Box-Behnken experimental design was used to investigate the effects of three independent variables, namely NaOH concentration (x_1), extraction time (x_2) and extraction temperature (x_3). Three levels of each variable were coded as -1, 0 and 1 based on the results of preliminary single factor experiments according to the following equation.

$$x = (x_1 - x_0) / \Delta x$$

When x is the code value, x_1 is the corresponding actual value, x_0 is the actual value in the center of the domain and Δx is the increment of x_1 corresponding to a variable of 1 unit of x . The experimental design consists of 12 factorial experiments and three replicates of the central point that were given in Table 2. Ascorbic acid equivalent antioxidant capacity (AEAC) was selected as the responses for the combination of the independent variables using DPPH radical scavenging method. Experiment runs were randomized, to minimize the effects of unexpected variability in the observed responses.

Table 1: Coded and Actual Levels of Three Variables

Variables	Factors	Coded Levels of Variables		
		-1	0	1
Concentration of NaOH (M)	x_1	0.5	1	1.5
Extraction Time (hr)	x_2	2	4	6
Extraction Temperature (°C)	x_3	40	50	60

Determination of Antioxidant Activity Using DPPH Radical Scavenging Method

The antioxidant activities of the samples were determined by the DPPH free radical scavenging assay according to (Lee *et al.*, 2004). The samples were diluted with 50% ethanol for various concentrations. Briefly, the reaction mixture containing 50 µL of diluted test sample of

various concentrations and 50 μL of DPPH (300 μmol) dissolved in methanol, was taken in a 96-well micro-titer plate and kept standing at 37 $^{\circ}\text{C}$ for 30 min. The absorbance was measured at 517 nm by using 96 well micro plate readers (Spectrostar Nano, BMG Labtech Microplate reader). Ascorbic acid was used as a standard. 50% ethanol was used as the control and added to the 96-well plate instead of the sample. Percent Radical Scavenging Activity (% RSA) was calculated by using the following formula:

$$\% \text{ RSA} = [(A_c - A_s) / A_c] \times 100$$

where,

% RSA= % Radical Scavenging Activity

A_c = Absorbance of Control

A_s = Absorbance of Sample

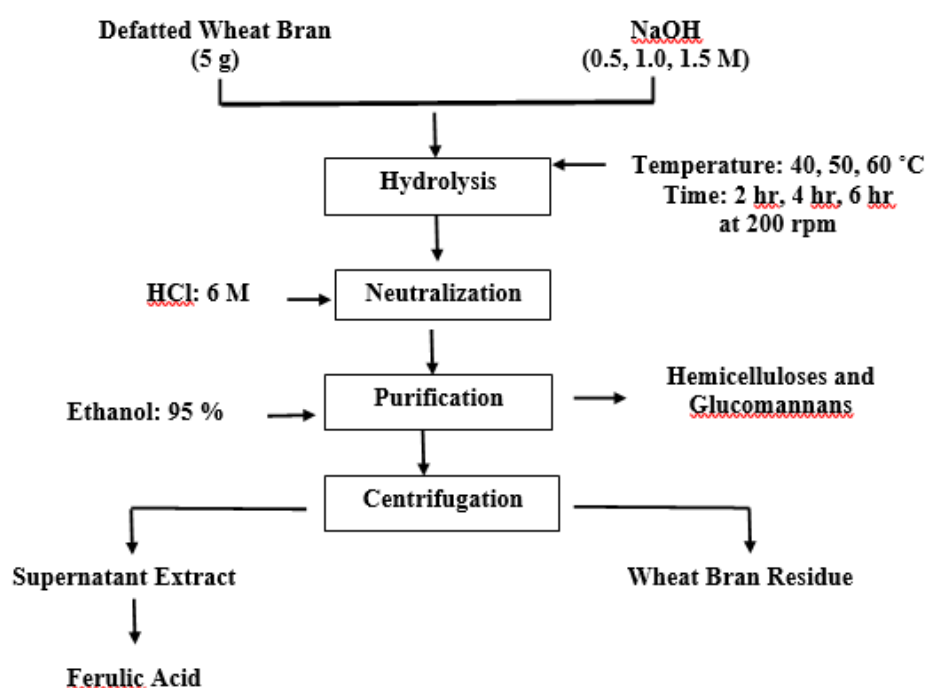


Figure 1: Process Flow Diagram for the Extraction of Ferulic Acid from Defatted Wheat Bran

Preparation of Whitening Scrub

Coffee powder (2 g), baking soda (1 g) and (2 mL) of coconut oil were placed in a cleaned, dried and weighed steel bowl. And then it was stirred at room temperature for about 15 min. When the ingredients had completely melted, (0.1 mL) of prepared extracted ferulic acid and (0.1 mL) of olive oil were added into the above mixture with constant stirring at room temperature for 15 min. The resulting mixture was poured into sterilized airtight container, labeled and stored in a cool and dry place. It was kept for up to 6 months.

Evaluation of Whitening Effect

In evaluation, seven women who were about fifty years old were tested with samples. Before testing with the samples, the face skin of tested women was initially photographed. And then, the face area was divided into two parts: the left part and the right part. The left part was no treatment (control) position. The right part was utilized with samples. After one week, face area

with samples of tested women was checked. The result was clear in these faces. And then two weeks later, their face became tight and very clear skin. In the last step, the right parts of seven women were totally white and got the sort of skin in three weeks.



Figure 2: Extracted Ferulic Acid

Results and Discussion

In this research work, the extraction of ferulic acid from wheat bran was done by using sodium hydroxide. Hemicellulose was removed by using ethanol as a solvent. The waxy materials from the biomass were removed by using hexane prior to the NaOH extraction which enhances the quality of the extracted ferulic acid. Conventional solvent extraction in this study has produced extracts with high antioxidant activities.

The extraction conditions for improving antioxidant activity in ferulic acid were optimized through the RSM approach (Box-Behnken design). The coded and actual levels of the three variables as shown in Table 1 were chosen to optimize the antioxidant activities. Each experiment was carried out in triplicate. From the results of a single factor, the maximum antioxidant activity of each factor was defined as the center of domain (x_0). The actual level of -1, 0 and 1 were calculated as described in experimental part. Treatments with coded levels of variables and experimental results of antioxidant activity of ferulic acid from wheat bran are also represented in Table 2. The treatments with coded levels ranged from 37.39 ± 8.87 mg to 76.64 ± 3.88 mg AEAC. The highest AEAC value 76.64 ± 3.88 mg AEAC was obtained under experiment condition of 0.5 M of NaOH concentration and 2 hr extraction time and 50 °C extraction temperature. The process flow diagram for the extraction of ferulic acid from defatted wheat bran was indicated in Figure 1. The extracted ferulic acid was shown in Figure 2.

By applying multiple regression analysis on the experimental data, the response variable (antioxidant activity) and the test variables are related by the following polynomial equation (in terms of coded factors).

$$\begin{aligned} \% \text{ RSA} = & 72.89 - 3.50875 X_1 - 5.1975 X_2 + 2.70875 X_3 - 0.665 X_1^2 X_2 + 0.225 X_2^2 X_3 \\ & + 10.9425 X_1^2 X_3 - 0.40625 X_2^2 X_2 - 9.09875 X_1^2 X_1 - 11.5588 X_3^2 X_3 \end{aligned}$$

The analysis of variance (ANOVA) for the regression equation by Minitab 14 Software is presented in Table 3. The quality of fit to the second-order polynomial models was confirmed based on the coefficient of determination, $R^2 = 0.917$. The result indicated that models can significantly ($p < 0.05$) express more than 80 % (> 0.80) of the response variation. The lack of fit ($p < 0.05$) was significant suggesting that the model was suitable to represent the actual situation, reflecting the relationship between the antioxidant activity and extraction parameters. In addition, the obtained regression equation can predict well the extraction condition for high antioxidant

activity. The terms of square ($p = 0.020$), interaction ($p=0.048$) and regression model ($p = 0.030$) indicating that the relationship between response and the test variable were significant as shown in Table 3.

The DPPH radical has been extensively applied to assess the antioxidant potential of food items, such as vegetables, olive oils, fruits, juices and wines etc. Stable organic radical DPPH has been utilized in determination of the antioxidant activity of ferulic acid as well as purification compounds. The ability of antioxidants for DPPH radical scavenging is supposed to be free radicals due to their hydrogen donating property. After acceptance of an electron or a hydrogen atom, a stable diamagnetic molecule will emerge which will result in vanishing the absorption band at 517 nm. The radical scavenging activity of the sample corresponds to the remaining DPPH in an inverse manner. The antioxidant potential of wheat bran extracts to scavenge free radical varied from ($37.39 \pm 8.87 \%$) to ($76.64 \pm 3.88 \%$). Highest antioxidant potential of ferulic acid in present study ($76.64 \pm 3.88 \%$) was found in agreement with standard ferulic acid (78 %) (Alanon *et al.*, 2011), however, it was lower than that reported for ascorbic acid (91.42 %). The DPPH assay for antioxidant activity of extracted ferulic acid is shown in Figure 3.

Three-dimensional response surface plots are presented in Figure 4-A to 4-C. These types of plots reflected the effects of two factors on the response at a constant agitation (200 rpm). As shown in Figure 4-A, the highest antioxidant activity of ferulic acid was observed at 1.0 M of NaOH concentration and 2 hr of extraction time, further increase of NaOH concentration with time significantly decreases the activity. The results as shown in Figure 4-B, the antioxidant activity of ferulic acid increases with increase in temperature. However, at 4 hr extraction time the activity decrease with increase in temperature. After 4 hr, the activity was significantly increase using highest extraction temperature. In Figure 4-C, the optimum condition was observed at mid-level of NaOH concentration and extraction temperature. By applying increased concentration with high temperature, the antioxidant activity will also decrease. The effects of extraction temperature had a more significant effect on the antioxidant activity than NaOH concentration and extraction time.

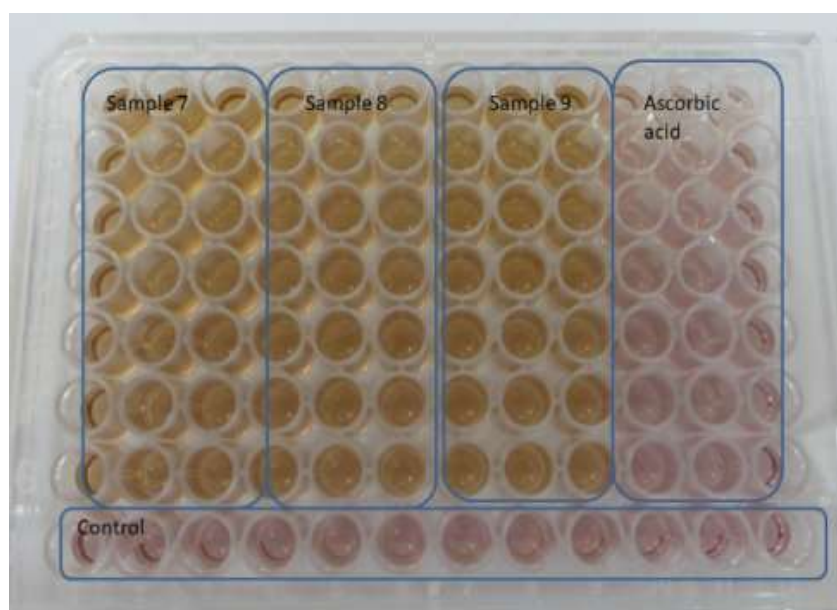


Figure 3: DPPH Assay for Antioxidant Activity of Extracted Ferulic Acid

Table 2: Experimental Designs Using Box-Behnken Design and Results

Run Order	Natural Variables			% RSA
	Concentration of NaOH (M)	Extraction Time (hr)	Extraction Temperature (°C)	
1.	0.5	4	60	45.19±6.13
2.	1	2	60	65.708±3.59
3.	1	6	60	63.61±4.24
4.	0.5	4	40	63.71±10.97
5.	1	4	50	72.89±7.64
6.	1	2	40	58.69±5.47
7.	1	4	50	72.89±7.64
8.	1.5	4	40	37.39±8.87
9.	0.5	6	50	59.73±5.7
10.	0.5	2	50	76.64±3.88
11.	1.5	4	60	62.64±6.33
12.	1.5	2	50	68.37±3.90
13.	1.5	6	50	48.8±5.03
14.	1	6	40	55.59±5.72
15.	1	4	50	72.89±7.64

Table 3: Analysis of Variance (ANOVA) for the Regression Equation

SD	SS	DF	MS	F Value	P Value	S
Model	1602.14	9	178.015	6.14	0.030	*
Linear	373.30	3	124.434	4.30	0.075	-
Square	747.91	3	249.304	8.61	0.020	*
Interaction	480.92	3	160.308	5.53	0.048	*
Residual Error	144.85	5	28.97	-	-	-
Lack-of-Fit	144.85	3	48.28	-	-	-
Pure Error	0.00	2	0.000	-	-	-
Total	1746.99	14	-	-	-	-

Note: SD= source of deviation, SS= sum of square, DF= degree of freedom, MS= mean square, S= significant, p* = 0.05

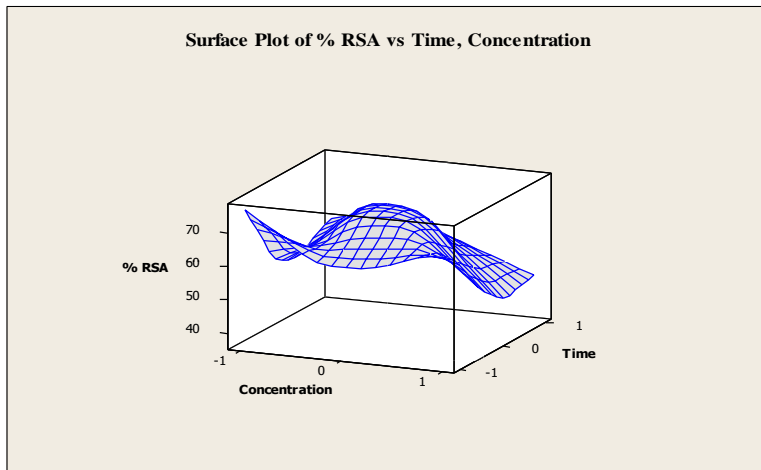


Figure 4-A: Three-dimensional Response Surface Plot of Antioxidant Activity of Ferulic Acid Showing the Influence of NaOH Concentration (x_1) vs. Extraction Time (x_2)

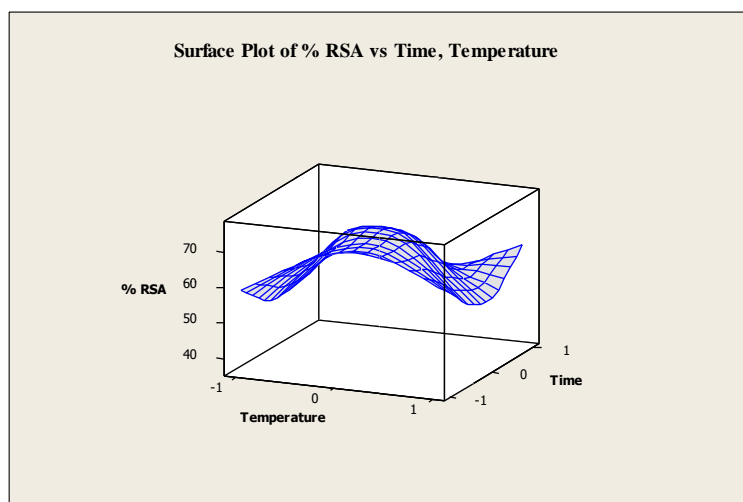


Figure 4-B: Three-dimensional Response Surface Plot of Antioxidant Activity of Ferulic Acid Showing the Influence of Extraction Time (x_2) vs. Extraction Temperature (x_3)

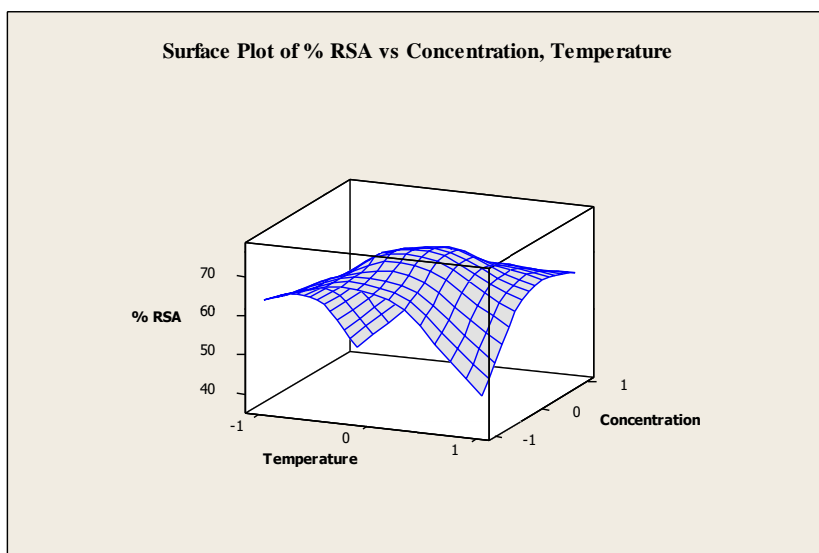


Figure 4-C: Three-dimensional Response Surface Plot of Antioxidant Activity of Ferulic Acid Showing the Influence of NaOH Concentration (x_1) vs. Extraction Temperature (x_3)

Conclusion

The response surface methodology (RSM) was used to optimize the extraction condition for antioxidant activity in ferulic acid from defatted wheat bran using Box-Benken design. According to the ANOVA analysis, the optimal condition was 0.5 M of sodium hydroxide concentration, 2 hr of extraction time and 50 °C for the extraction temperature. Moreover, p-value is less than the significant level. Therefore, it can be concluded that there is a statistically significant association between response variables and the terms. Conventional solvent extraction in this study has produced the extract having high antioxidant activities. Despite being agricultural by-product produced in the food supply chain, the enormous availability of ferulic acid could be beneficial for the production of value added products in line with green technology.

Acknowledgements

The author would like to express my greatest appreciation to the members of Myanmar Academy of Arts and Science. I also wish to acknowledge my gratitude to Dr Tint Moe Thu Zar, Rector, Dr Thwe Linn Ko, Dr U Khin Myoe, Dr Myint Myint Oo, Dr Khin Maw Maw Soe and Dr Win Naing, Pro-rectors of Yadanabon University for their permission to present this paper. I would like to express my greatest appreciation to Dr Aye Pa Pa Win, Professor and Head of Industrial Chemistry Department, Yadanabon University for her invaluable help in preparing this research and permission to submit this research paper.

References

- Apprich, S., Tirpanalan, O., Hell, J., Reisinger, M., Bohrdorfer, S., Siebenhandl, S., Novalin, S., & Kneifel, W., (2014). Wheat bran-based biorefinery 2: Valorization of products. *LWT – Food Science and Technology*, 56(2), pp. 222-231.
- Alanon, M. E., Castro, I., Diaz, M.C., Cordon, M. H., & Perez, M. S., (2011). A study of the antioxidant capacity of oak wood used in wine aging and the correlation with polyphenol composition. *Food Chemistry* 128, pp. 997-1002.
- Ames. B.N, Shigenag, M.K & Hagen T.M, (1993). “Oxidants, antioxidant and the degenerative diseases of aging. *Processing of the National Academic Science*, 90: 7915-22
- Buranov, A. U., & Mazza, G., (2009). Extraction and purification of ferulic acid from flax shives, wheat and corn bran by alkaline hydrolysis and pressurized solvents. *Food Chemistry*, 115(4), pp. 1542-1548.
- Barberousse, H., Kamoun, A., Chaabouni, M., Giet, Roiseux, O., Paquot, M., Deroanne, C., & Blecker, C., (2009). Optimization of enzymatic extraction of ferulic acid from wheat bran, using response surface methodology, and characterization of the resulting fractions. *Journal of the Science of Food and Agriculture*, 89(10), pp. 1634-1641.
- Lee, S., Son, D., Ryu, J., Lee, Y. S., Jung, S. H., Lee, S. Y., Shin, K. H., (2004). Antioxidant activities of *Acanthopanax senticosus* stems and their lignan components. *Archives of Pharmacal Research*, 27, 106–110.
- Marques, S. S., Magalhaes, L. M., Toth, I. V., & Segundo, M. A., (2014). Insights on antioxidant assays for biological samples based on the reduction of copper complexes-the importance of analytical conditions. *Int F Mol Sci*. 2014; 15:11387-402. Doi: 10.3390/ijms 150711387.
- Masoomeh, S., Jamshid, L. M., and Abolghasem, J., (2008). “Determination of total phenols in tea infusions, tomato and apple juice by terbium sensitized fluorescence method as an alternative approach to the Folin-Ciocalteu spectrophotometric method”, *Food Chemistry*, 108, 15. May 2008, pp. 695-701.

- Navarro, I., García, V., García, J., & Periago, M. J., (2011). Chemical profile, functional and antioxidant properties of tomato peel fiber. *Food Research International*; 44(5), pp. 1528-1535.
- Shenoy K., & Shirwaiker, A., (2002). Anti-inflammatory and free radical scavenging studies of *Hyptis suaveolens*. *Indian drug*, 39: 574-577
- Sies, H. (1997). Oxidative stress, oxidants and antioxidants. *Experimental physiology* 82: 291- 295.
- Siriwardhana, N., Jeon, Y. J., Kim, S. H., Ha, J. H., Heo, S. J., & Lee, K. W. (2004). Enzymatic hydrolysis for effective extraction of antioxidative compounds from *Hizikia fusiformis*. *Algae-Inchon*; 19(1), pp. 59-68.
- White, B. L., Howard, L. R., & Prior, R. L., (2010). Release of bound procyanidins from cranberry pomace by alkaline hydrolysis. *Journal of agricultural and food chemistry*; 58(13), pp. 7572-7579.
- Xiong Q, Kodata S., Tani T, Namba T. (1996). Antioxidative effects of phenylethanoids from *Castanhe deserticola*. *Bio Pharm Bull* 19; 1580-1585

Websites

<http://www.en.m.wikipedia.com>.

<http://www.sciencedirect.com>

<http://www.agriculturejournals.cz.com>.

<http://onlinelibrary.wiley.com>.

PHYSICOCHEMICAL PROPERTIES AND SENSORY EVALUATION OF PROCESSED COGNAC (GRAPE BRANDY)

Mon Mon Maung¹, Thwe Linn Ko², Khin Thet Ni³

Abstract

Cognac (Grape Brandy) is a portable spirit by distilling of grape wine and aging in oak cask. This research work is concerned with the preparation of cognac (grape brandy) from locally available table grapes. Firstly, the characteristics of table grape were studied and wine was made by fermenting clarified juice of table grapes. The highest alcohol content 10 % v/v in prepared wine was formed with 1:0.2 juice to sugar ratio after twenty weeks fermentation period. The main constituent and fusel oils in prepared wine were firmly resolved by gas chromatography. For higher alcohol content in processed cognac (grape brandy), most fine brandies (35 % v/v- 65 % v/v alcohol) were taken into double distillation. Prepared wines were distilled to obtain cognac (grape brandy) and properties of cognac (grape brandy) were also studied. It was observed that alcohol content of the first distillate from wine was 36 % v/v and the second distillate contained 76 % v/v of alcohol content. The main constituent (ethanol) and fusel oils were observed in these distillates by gas chromatography. Processed cognac (grape brandy) was aged in oak cask to improve colour, taste and odour. Moreover, caramel colour was prepared by heating brown sugar and white sugar and effect of prepared caramel colour on the characteristics of cognac (grape brandy) without aging in the oak cask was evaluated.

Keywords: table grapes, white wine, grape brandy, distillation

Introduction

Table grapes are grown for production of juice, production of wine or for drying into raisins. Table grapes may be either seeded or non-seeded varieties in terms of colour, size, sweetness and are the deciduous woody vines of the botanical genus *Vitis vinifera*. White wine is specially made from "white" (table) grapes, which are green, yellow, straw-yellow, yellow green, or yellow-gold in colour. White wine is a wine that is fermented except for the skin and is not produced by the alcoholic fermentation of the non-coloured pulp of grapes (Reisch, Peterson and Martens, 2008).

Grape brandy is a spirit processed by means of distilling wine and the alcohol content of brandy is generally 35–60 % by volume. Grape brandy are mostly aged in wooden casks and some are coloured with caramel colouring to affect aging and some are produced using a combination of both aging and colouring. While grape brandies are usually produced from wine or various fermented fruit juices, it can be distilled from any liquid that consists of sugar (Blue, 2004).

Wine is made by crushing and pressing the grapes to extract the juice. This juice is then fermented, which means that the sugar contained within the juice turns to alcohol. In the method of making grape brandy, the grapes are picked, crushed and pressed, after which fermented. The fermented wine is then distilled twice in pot stills. Within these stills the liquid is heated, and the various volatile components within the liquid are separated and eliminated and the alcohol is concentrated. The process is carried out twice, which is one of the unique aspects of grape brandy making. This is referred to as "double distilled" (Eisenman, 1998).

¹ Department of Industrial Chemistry, University of Mandalay

² Yadanabon University

³ Department of Industrial Chemistry, University of Yangon

Distillation is usually used for purifying beverages and separating mixtures of liquids into their individual components. In practice, distillation may be carried out by way of either of two principal methods. After distillation, the aging of brandy is made in oak casks for 3 to 15 years or more. At the time of aging, some of the ethanol and water ooze through the oak and evaporate, so brandy is filled to substitute for this loss. Caramel coloring is introduced to offer the brandy a dark brown color. Brandy may be mixed and/or flavored, and then chilled, filtered, and bottled after aging (McCabe, 2005).

The main objective of this research was to make a study on processing of grape brandy from locally available table grapes. The specific objectives of this study were to study the characteristics of table grape, physicochemical properties of prepared wines and to analyze the properties of distillates for processing of grape brandy, to determine the main constituent and fusel oils in prepared wine, distillate and grape brandy by gas chromatography, and to study the effect of aging in the oak cask and the effect of caramel colour on the processed grape brandy.

Materials and Methods

Materials

Raw materials for processing of grape brandy, table grapes were collected from Saebauk Grape Farm, Kyaukpadung Township, Mandalay Region. Sugar was purchased from City Mart supermarket, 8 miles, Mayangone Township, Yangon Region. Yeast (*Saccharomyces cerevisiae*), ascorbic acid, potassium metabisulphite and potassium sorbate (Analar grade, England) were purchased from KEMIKO chemical shop, 28th Street, Pabedan Township, Yangon Region.

Methods

Processing of Grape Brandy

Selected table grapes were washed with water and seeds were removed. And then the grapes were crushed and pressed immediately to separate the juice from the table grapes. After pressing, the skins, stems and seeds were discarded and juice was collected and allowed to stand for 2 hr, and the clear juice was again collected and residue was discarded. Various ratios of grape juice and sugar were used (1:0, 1:0.01, 1:0.1, 1:0.2 and 1:0.3 v/w) to obtain high yield of wine. Sugar was added in the form of syrup and water was added to it. After that yeast (*Saccharomyces cerevisiae*) was added to enhance fermentation and the content stirred two times day by day for three weeks of fermentation time. On the sugar fermentation that kept for three weeks, the liquid was separated from the stable substances through racking. After racking, prepared white wines were obtained and stored in the wine pot.

Prepared wine was placed into a one-necked round bottomed flask. The distillation column, condenser and distillate collector were attached. Heating was applied to the round bottomed flask. The column top temperature was at 78 °C as the first distillate was being produced and the quantity of first distillate which was collected, and the final volume of first distillate was recorded.

After the first distillation which took about two hours, wine had been converted to the concentrated liquid (not yet grape brandy) with an alcohol content of 36 % v/v. Second distillation was conducted similarly and the second distillate was collected and amount of

volume obtained was recorded. The product of the second distillation had an alcohol content of around 76 % v/v. The grape brandy so produced was not yet ready for drinking after the second distillation was placed in oak casks and allowed to age for three years. As the grape brandy ages, it absorbed flavors from the oak while its own structure softens, becoming less astringent, and curing to be an acceptable brandy.

Preparation of Caramel Colour

Caramel colour was prepared by heating either brown sugar or white sugar. Sugar and water were mixed in a pan and strongly heated until the sugar was dissolved. Then, ammonium chloride was added to it and heating was continued. When it reached the point of almost being burnt, it became foaming and smoking. Then it was removed from heat immediately. The lumps left were strained out. The caramel was cooled and stored in airtight bottle.

Characterization

Physicochemical characteristics of table grapes, wine and grape brandy were determined. Main constituent (ethanol) and fusel oils of wine, first distillate, second distillate, grape brandy aged three years in oak cask were examined separately by gas chromatography at the Scientific and Technological Instrument Centers (STIC), Mae Fah Luang University, Chiang Rai, Thailand. In determining alcohol content, firstly specific gravity of sample was determined and then specific gravity of sample was converted to respective alcohol percent (%v/v) by reading Standard Alcohol Density Table. Colours (absorbance) were measured by UV spectrophotometer (UV-1800 SHIMADZU). Sensory evaluation (organoleptic properties) of grape brandy with caramel colour and aged three years in oak cask were also carried out based on colour, taste, odour and overall acceptability were analyzed on the basis of 15 semi-trained panelists. For sensory evaluation, the scoring was based on a 9-point Hedonic Scale: 9 - like extremely, 8 - like very much, 7 - like moderately, 6 - like slightly, 5 - neither like nor dislike, 4 - dislike slightly, 3 - dislike moderately, 2 - dislike very much, 1- dislike extremely. The overall acceptability was taken as the average score of all these organoleptic properties.

Results and Discussion

Grapes are planted in very dry areas of Central Myanmar. As table grape possesses thin skin and soft texture, it has lower fiber content than wine grape, 0.33 %. pH value of table grape was 2.69 with acidity 1.21 and reducing sugar content was 1.73 mg/g for table grape. The right proportion of acid in grape (acid balance) could provide to produce good wine because good acid balance was important in wine making. These properties would be varied depending on the grape variety and climatic conditions of grape growing areas and ideal grape varieties should be chosen to get good wine and related beverages.

As wine was prepared with different amounts of sugar, it was observed that alcohol content of wines depended upon the quantity of sugar to a certain limit. Sucrose inverts into glucose and fructose and then turns into alcohol and carbon dioxide. Colour of prepared wines had a straw yellow due to oxidation during storage.

The highest alcohol content 10 % v/v (wine) was found in grape juices to sugar ratio of 1:02 v/w. Alcohol content of wines gradually increased till a certain fermentation period of twenty weeks (five months).

Effect of fermentation period on the yield of alcohol in wines was studied. The results are shown in Table 1. It was found that five months fermentation period to complete fermentation to produce wine. Several different fermentation parameters such as period, temperature, skin contact time, pressing technique could manage fermentation were studied. After complete fermentation period, yield of alcohol in wine was 10 % v/v.

pH value of prepared wine was 3.3, which can distinctly affect on the wines' flavor, such as aroma, colour, and stability. The acidity value was 0.65 for prepared wine. It was the practical value for expression of the organic acid concentration within wine. Sugar content in wine was measured as soluble solids. A soluble solid ($^{\circ}$ Brix) of prepared wine was 2.7 and alcohol content was 10 % v/v. The reducing sugar content was displayed by the conversion of sugars in the grape juice to alcohol by yeast.

The colour of wine had 0.05 colour (absorbance) in the visible region (wavelength-520 nm) and were clear and transparent, without sediments or cloudiness. There is an extra absorption band in the ultraviolet region (500-524 nm) for wine. The colour also indicates the age and evolution of the wine.

Table 1: Effect of Fermentation Period on the Yield of Alcohol in Wines

Wine (Grape Juice: Sugar Ratio) (v/w)	Yield of Alcohol (% v/v)					
	FP 1	FP 2	FP 3	FP 4	FP 5	FP 6
1 : 0	2.0	3.0	3.0	4.0	5.0	5.0
1 : 0.01	2.0	4.0	5.0	6.0	7.0	7.0
1 : 0.1	3.0	5.0	7.0	8.0	9.0	9.0
1 : 0.2*	4.0	6.0	8.0	9.0	10.0	10.0
1 : 0.3	3.0	5.0	6.0	7.0	8.0	8.0

FP = Fermentation Period (month)

Main constituent and fusel oils content of wine, first and second distillates from wine were analyzed by gas chromatography. The spectra are shown in Figures 1, 2, and 3 and their respective data are also presented in Tables 2, 3 and 4. From analysis by gas chromatography, it could be confirmed that the main organic compound in first and second distillates were ethanol. Minute trace amount of other organic compounds were contained in the distillates. The other compounds were acetaldehyde 1,1-dioxyethane, isoamyl alcohol, propyl alcohol, ethyl acetate, 1,3-dioxolane, 2,4,5-trimethyl alcohol, 2-methyl-n-butyl etc.

Volatile fatty acids, ethyl acetate and acetaldehyde were contributed to the flavor and aroma of wine. The aroma of wines was represented by a complex of volatile compounds coming from several sources. These may be by products of alcoholic fermentation and the composition can vary widely depending on the raw materials used. It was observed that alcohol content of

first distillate and second distillate of white wine were 36 % v/v and 76 % v/v respectively. The alcohol content was drastically increased after second distillation.

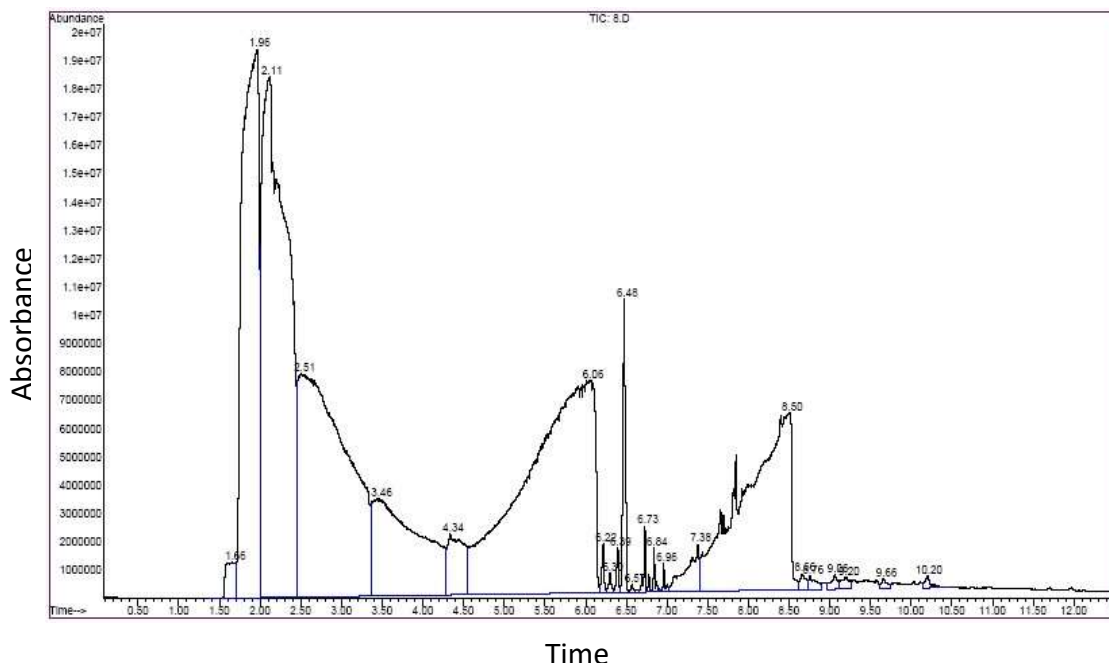


Figure 1: Gas Chromatography Spectrum of Main Constituent and Fusel Oils in Prepared Wine

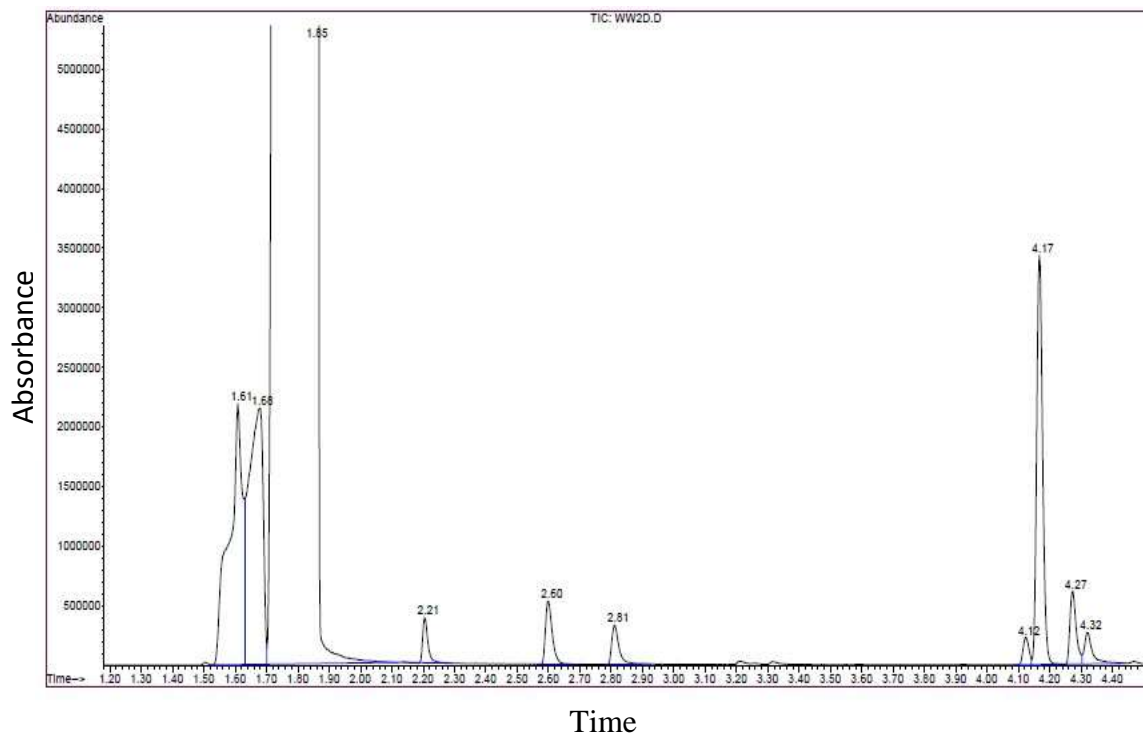


Figure 2: Gas Chromatography Spectrum of Main Constituent and Fusel Oils in First Distillate from Wine

Table 2: Main Constituent and Fusel Oils in Prepared Wine Analyzed by Gas Chromatography

Peak No.	Retention Time (min)	Area (%)	Compound Name	Quality	Total (%)
1	1.66	0.52	Not detected: Value of quality less than 60%	2	0.522
2	1.96	14.05	Ethanol \$\$ Ethyl alcohol	91	14.046
3	2.11	20.17	Ethanol \$\$ Ethyl alcohol	91	20.168
4	2.51	17.21	Ethanol \$\$ Ethyl alcohol	90	17.212
5	3.46	7.24	Ethanol \$\$ Ethyl alcohol	90	7.242
6	4.34	1.55	Not detected: Value of quality less than 60%	4	1.551
7	6.06	22.75	Not detected: Value of quality less than 60%	2	22.746
8	6.21	0.18	Acetic acid \$\$ Ethylic acid	91	0.175
9	6.30	0.08	Not Report: Value of quality less than 80%	47	0.082
10	6.39	0.14	1,2-Propanediol \$\$ Propylene glycol	91	0.145
11	6.48	1.17	2,3-Butanediol	90	1.169
12	6.57	0.04	Not detected: Value of quality less than 60%	47	0.039
13	6.73	0.21	Not detected: Value of quality less than 60%	56	0.211
14	6.84	0.12	Butyrolactone \$\$ Butyryl lactone	64	0.118
15	6.96	0.08	cis-5-hydroxy-2-methyl-1,3-dioxane	87	0.076
16	7.38	0.92	Not Report: Value of quality less than 60%	43	0.921
17	8.50	12.77	Glycerin \$\$ Glycyl alcohol	83	12.771
18	8.66	0.14	Not detected: Value of quality less than 60%	47	0.142
19	8.76	0.16	Not detected: Value of quality less than 60%	38	0.158
20	9.06	0.15	Not detected: Value of quality less than 60%	46	0.148
21	9.20	0.15	Not detected: Value of quality less than 60%	35	-
22	9.66	0.09	Not detected: Value of quality less than 60%	50	-
23	10.20	0.11	Benzene ethanol, 4-hydroxy-	74	-

Table 3: Main Constituent and Fusel Oils in First Distillate from Wine Analyzed by Gas Chromatography

Peak No.	Retention Time (min)	Area (%)	Compound Name	Quality	Total (%)
1.	1.61	2.27	*Acetaldehyde	86	2.27
2.	1.85	92.43	Ethyl alcohol	86	92.43
3.	2.21	0.16	*Propyl alcohol	90	0.16
4.	2.60	0.28	*Ethyl acetate	91	0.28
5.	2.81	0.19	*Isobutyl alcohol	90	0.19
6.	4.12	0.10	*1,3-dioxolane,2,4,5-trimethyl alcohol	83	0.10
7.	4.17	1.63	*1,1-diethoxyethane	83	1.63
8.	4.27	0.30	*Isoamyl alcohol	86	0.30
9.	4.32	0.17	*2-methyl butyl alcohol	87	0.17

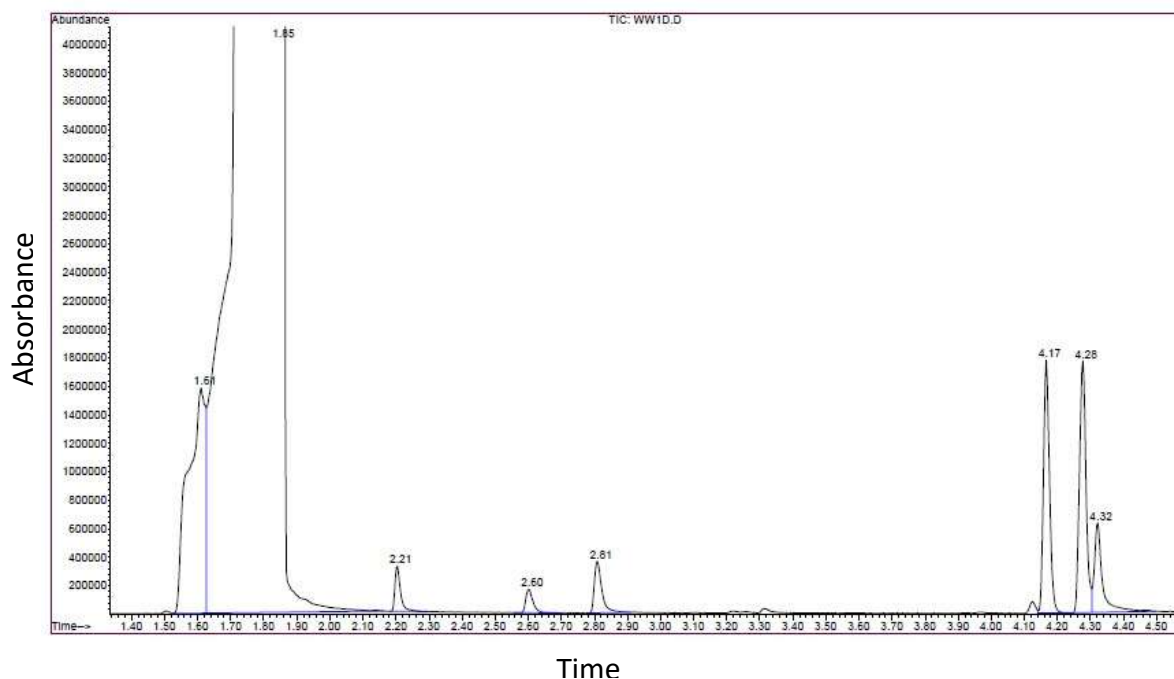


Figure 3: Gas Chromatography Spectrum of Main Constituent and Fusel Oils in Second Distillate from Wine

Table 4: Main Constituent and Fusel Oils in Second Distillate from Wine Analyzed by Gas Chromatography

Peak No.	Retention Time (min)	Area (%)	Compound Name	Quality	Total (%)
1.	1.84	95.47	Ethyl alcohol	86	95.47
2.	2.20	0.14	*Propyl alcohol	91	0.14
3.	2.60	0.09	*Ethyl acetate	91	0.09
4.	2.81	0.21	*Isobutyl alcohol	91	0.21
5.	4.17	0.81	*1,1-diethoxyethane	83	0.81
6.	4.28	0.88	*Isoamyl alcohol	90	0.88
7.	4.32	0.39	*2-methyl butyl alcohol	91	0.39

Processed grape brandy from wine was aged in the toasted oak cask at 18°C. Aged grape brandy (aged for three years in the oak cask) contains ethanol as main constituent with no fusel oils according to the result of Gas Chromatography, as described in Figure 4 and Table 5. Thus, aging in the oak cask supported the brandy to improve the taste, colour, and odour and also excluded the fusel oils.

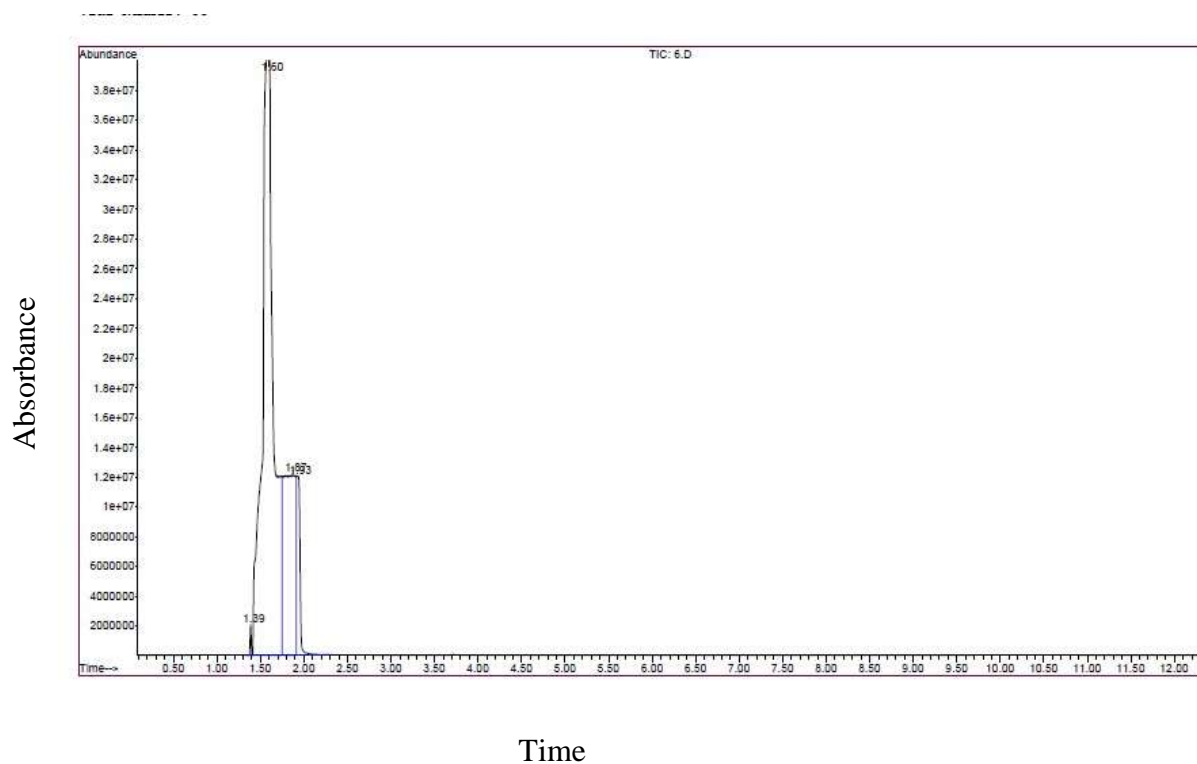
**Figure 4: Gas Chromatography Spectrum of Main Constituent and Fusel Oils in Three Years Aged Grape Brandy in Oak Cask**

Table 5: Main Constituent in Three Years Aged Grape Brandy in Oak Cask Analyzed by Gas Chromatography

Peak No.	Retention Time (min)	Area (%)	Compound Name	Quality (Grade)	Total (%)
1.	1.58	70	Ethyl alcohol	83	76.45

Colour (absorbance) of prepared caramel colour from brown sugar and white sugar was 4.992 and 4.978. Colour (absorbance) of commercial caramel colour was 5.457. It was observed that prepared caramel colour had rather higher absorbance than that of commercial product colour. The effect of caramel colour on the colour of grape brandy to match the effect of aging in the oak cask is shown in Table 6. The suitable amounts of added caramel colour were 0.03 g from brown sugar and 0.04 g from white sugar for processed grape brandy. Since these amount could provide the absorbance nearly the same as commercial brandy.

Sensory evaluation (organoleptic properties) of grape brandy was similar to wine tasting that includes appearance, colour, taste and aroma. Grape brandy contained lower quantities of acids and a much higher quantity of ethyl alcohol. The organoleptic properties of grape brandy with added caramel colour (sample 1), grape brandy aged three years in oak cask (sample 2), and also commercial brandy (sample 3) were studied and these results are shown in Table 7. Panelists gave the highest preference for all sensory attributes of sample (2) followed by sample (3) and sample (1). Sample (2) was recorded the highest overall acceptance of sensory evaluation (7.08) and mean scores for appearance (7.15), colour (6.98), taste (6.86) and aroma (7.32). The least preference for all sensory attributes sample recorded the least overall acceptance of sensory evaluation (5.77). The overall acceptability of grape brandy depended on the organoleptic properties of processed grape brandy.

Table 6: Effect of Caramel Colour on the Colour of Grape Brandy

Sr. No.	Colour (absorbance) of Grape Brandy without Caramel	Amount of Caramel Colour Added (g)	Colour (absorbance) of Prepared Grape Brandy from Wine using Caramel			Colour (absorbance) of Commercial Brandy
			Caramel Colour (Brown Sugar)	Caramel Colour (White Sugar)	Commercial Caramel Colour	
1	1.112	0.01	2.912	3.654	1.345	5.389
2		0.02	4.229	3.792	2.476	
3		0.03	*4.922	4.092	3.891	
4		0.04	5.788	*4.978	5.342	
5		0.05	6.865	4.108	*5.457	

Table 7: Sensory Evaluation (Organoleptic Properties) of Grape Brandy

Organoleptic Properties	Panelist Hedonic Rating		
	Sample (1)	*Sample (2)	Sample (3)
Appearance	5.53	7.15	6.91
Colour	5.74	6.98	6.75
Taste	5.92	6.86	6.67
Aroma	5.87	7.32	7.11
Overall Acceptance	5.77	7.08	6.86

Sample (1) = Prepared Grape Brandy processed with caramel color

Sample (2) = Prepared Grape Brandy aged two years in oak cask

Sample (3) = Commercial Brandy

Conclusion

Grape brandy is a wine spirit processed by distillation of wine and is aged in oak casks. This research was emphasized mainly on alcoholic fermentation, distillation, aging and to study the characteristics that may affect grape brandy quality, according to their composition to promote quality and to provide a dissimilar aroma and a smooth taste to the finished product. It was found that the alcohol content of wine depended upon the certain limit of the quantity of sugar and fermentation period. Double distillation sharply increased ethanol concentration. Grape brandy from wine was colourless and odourless, thus needs to study the effect of aging. The addition of caramel was rather common in the processing of aged grape brandy since it has given an attractive amber coloration to the consumer. To obtain fine brandy, concentrated alcohol must be placed in oak casks and allowed to age for at least three years, an important step in the production process. Compounds released from wood into brandy depend on the factors such as type of wood and time of contact. Aging in the oak cask could support not only to improve the taste, colour and odour of finished grape brandy but also to eliminate the fusel oils. Moreover, by aging in the oak cask, grape brandy could also have interacting with air and oak barrel in which evaporation can take place and concentration would be dropped from 76 % v/v to about 65 % v/v. Processing of grape brandy could be conducted from locally available table grapes which provides value-added product for Myanmar grapes cultivators and communities.

Acknowledgements

I am grateful to Dr Tin Tun, Rector, University of Mandalay and Pro-Rectors, University of Mandalay, for their permission to submit this article. I would like to express my greatest appreciation to Dr Soe Win, Professor and Head, Department of Industrial Chemistry, University of Mandalay for his permission to submit this research paper, reviewing the manuscript and suggestions.

References

- Anderson, F., and Hull, R., (1970). "The Art of Wine Making", New York.
- Blue, Anthony, (2004). "The Complete Book of Spirits". New York: HarperCollins. p. 239. ISBN 978-0-06-054218-4.
- Eisenman, L., (1998), "The Home Winemakers Manual".
- Green Don W. & Perry Robert H., (1997). "Perry's Chemical Engineers' Handbook, 8th Edition, McGraw-Hill, Inc., New York.
- McCabe Warren L., Smith Julian C. & Harriott Peter, (2002). "Unit Operations of Chemical Engineering", 5th Edition, McGraw-Hill Chemical Engineering Series, New York.
- McCabe Warren L., Smith Julian C. & Harriott Peter, (2005). "Unit Operations of Chemical Engineering", 7th Edition, McGraw-Hill Chemical Engineering Series, New York.
- Reisch B. I., Peterson D. V. & Martens M-H., (2008). "Seedless Grapes Breeding for Disease Resistance by Using Embryo Rescue" Archived 2008-06-19.
- Reisch Bruce I., Peterson David V. & Martens Mary-Howell, (1993). "Table Grape Varieties for Cool Climates", Information Bulletin 234, Cornell University, New York State Agricultural Experiment Station